

Contents

Monday 18 June		Page Number
Session 1: Keynote Speakers		
Keynote speech <i>L Thomsen, CEO, Future Matters</i>		Paper not included
The galvanizing industry in Germany <i>M Huckshold, Industrieverband Feuerverzinken e. V.</i>		7
The zinc supply/demand outlook <i>Dr R Cochrane, CRU International Ltd (UK)</i>		15
Session 2: Galvanizing in Bridge Construction		
Hot-dip galvanizing for steel and composite bridges – New research for application of hot-dip galvanizing with dowel strips <i>Prof. Dr.-Ing. D Ungermann, S Holtkamp; TU Dortmund University – Institute of Steel Construction (Germany)</i>		21
Galvanized bridges in Japan <i>H Shibayama, Japan Galvanizers Association (Japan)</i>		29
Hot-rolled sections and hot-dip-galvanizing – a perfect combination for efficiency and sustainability of bridges <i>Dr.-Ing. D Rademacher, ArcelorMittal Europe – Long Products (Luxembourg); T Pinger, Zinq Technologie (Germany)</i>		41
Session 3: Innovative Applications of Galvanizing in Steel Construction		
Fire resistance of galvanized structures <i>Prof. Dr.-Ing. M Mensinger, M.Sc. C Gaigl, Technical University of Munich, Chair of Metal Structures, Munich (Germany)</i>		53
Steel Hybrid Onshore Wind Towers Installed with Minimum Effort ('SHOWTIME') <i>Prof C Rebello, Institute for Sustainability and Innovation in Structural Engineering, University of Coimbra (Portugal)</i>		61
Galvanized steel expansion joints for bridges <i>S Adam, mageba GmbH (Switzerland)</i>		71
Session 4: Design of Bolted Steel Structures with Galvanizing		
Galvanized Steel Slip Factor Investigation – Part 2 <i>T J Langill, American Galvanizers Association (USA)</i>		81
Slip-resistant connections made of hot-dip galvanized steel – The EU Sirocco Project <i>Prof. Dr.-Ing. N Stranghöner, N. Afzali, Institute for Metal and Lightweight Structures, University of Duisburg Essen (Germany)</i>		87
Examination of influencing factors on the coating quality of hot dip galvanized high strength fasteners for construction purposes <i>Dr.-Ing. H Hoche, M Lander, Prof. Dr.-Ing. M Oechsner, Center for Engineering Materials MPA-IfW, Technische Universität Darmstadt S Six, Dr. S Friedrich, Institut für Korrosionsschutz Dresden GmbH (Germany)</i>		101
Slip-resistant connections in hot-dip galvanized steel bridge constructions <i>A Schudlich, Dr.-Ing. M Klein, Prof. Dr.-Ing. M Oechsner; State Materials Testing Institute (MPA) and Chair and Institute for Materials Technology (IfW) Darmstadt, (Germany) Prof. Dr.-Ing. D Ungermann, J Grote; TU Dortmund University – Institute of Steel Construction (Germany)</i>		115

Tuesday 19 June		Page Number
Session 5: Process Optimisation		
The myth of steel hydrogenation during pre-treatment for hot dip galvanizing – dogma versus reality <i>V Kuklík, J Kudlacek, M Zoubek, Czech Technical University in Prague; S Węgrzynkiewicz, BELOS-PLP S.A (Czech Republic)</i>		129
Chemical pre-treatment of steel in the hot dip galvanizing process with focus on flux and drying conditions <i>F Schmelz, RAM Engineering + Anlagenbau GmbH (Germany)</i>		137
Controlling LMAC occurrence at drain holes during hot-dip galvanizing <i>Dr H Asada, Y Fujiwara & T Tanaka, Kobe University, T Yamashita, Kakuto Corporation, Y Kitano, Tanaka Galvanizing Co.,Ltd, T Watarai, Yokohama Galvanizing Co., Ltd, Y Murakami, Galva Kogyo Co. Ltd (Japan)</i>		149
Effect of geometric configuration on high-mast illumination pole demands during galvanizing process <i>R Nasouri, A Montoya & A Matamoros, University of Texas at San Antonio; K Nguyen, C Bennett & J Li, University of Kansas; T Kinstler, GalvaScience LLC (USA)</i>		163
Session 6: Bath Alloy Technology		
Influence of alloying elements on galvanizing abnormalities with a special view on surface defects <i>R Pankert, Boliden (Sweden)</i>		181
Bismuth influence in different concentrations in thickness and coating morphology for hot-dip galvanizing process <i>R Cavalcanti de Albuquerque Tozin & I Rezende, Nexa Resources (Brazil)</i>		191
Lead-free and bismuth-containing zinc melts and kettles in hot-dip galvanizing <i>Dr. J Triebert, Institut für Korrosionsschutz Dresden GmbH (Germany)</i>		201
New zinc-aluminium-magnesium alloy galvanizing technology <i>Y Kiyokawa, Komagata Galvanizing Co. LTD (Japan)</i>		213
Session 8: Global Galvanizing Awards (Sponsored by International Zinc Association)		Not included
Session 7: Insights in Galvanizing for Architecture and Construction		
Global structural steel projects in developing countries <i>M Lechner, Waagner-Biro AG (Austria)</i>		Paper not included
Modern application of batch galvanized steel facades in architecture <i>Prof. Hachul & D Ridder, Fachhochschule Dortmund (Germany)</i>		221
A bright future for hot dip galvanized steel in the circular economy <i>B Dursin, Zink Info Benelux (Benelux)</i>		233
Wednesday 20 June		
Session 9: Galvanizing Meets Market Demands		
Utility tunnels in China <i>Prof Z Qifu (China)</i>		253
Galvanizing for solar applications <i>J Tundidor, ATEG (Spain)</i>		Paper not included
Beyond construction – galvanizing in transport and other applications <i>H Glinde, Industrieverband Feuerverzinken (Germany)</i>		261
After 50 years of protection for the Sydney Opera House – time to develop a practical model for the durability of concrete structures using galvanized rebar <i>F Papworth, Building & Construction Research & Consultancy & P Golding, Galvanizers Association of Australia (Australia)</i>		267

Session 10: Practical Experience & Market Opportunities with Galvanized Rebar	
Galvanized reinforcing steel – better perspectives in application in Germany <i>Prof. Dr.-Ing. W Breit & R Adams, Technische Universität Kaiserslautern (Germany)</i>	283
Corrosion behaviour of galvanized reinforcement in chloride containing mortar and carbonated mortar <i>G Ebell, Bundesanstalt für Materialforschung und -prüfung (Germany)</i>	301
Session 11: Sustainability and Environment	
Integration of a kettle cover in the zinc bath enclosure <i>F Nerat, KVK KOERNER Chemieanlagenbau G.m.b.H (Austria)</i>	313
Reducing emissions and imissions in pre-treatment plants caused by hydrochloric acid <i>J Kader, Stockmeier Chemie GmbH & Co. KG (Germany)</i>	319
Effective recovery of HCl and metals from pickling solutions by cutting-edge membrane technologies <i>R. Gueccia, S. Randazzo, A. Culcasi, A. Cipollina, G. Micale, Dipartimento dell'Innovazione Industriale e Digitale, Università di Palermo (Italy)</i>	327
Session 12: Corrosion protection performance of zinc and zinc alloy coatings	
Duplex systems at an oil & gas company – Brazil: Performance assessment <i>R Suplicy de Araujo Goes, ICZ – Instituto de Metais não Ferrosos; M Schultz, Petrobras; R Yuriko Ogura, Armco Staco; P Cesar Maziero Tiano, Marangoni Maretti; C Gnecco, Sherwin-Williams Paint Company; Prof. I Vieira Aoki, Polytechnic School of the University of São Paulo (Brazil)</i>	341
Durability determination of bridge constructions protected by hot dip galvanized coatings <i>P Lebelt & J Gehrke, Institut für Korrosionsschutz Dresden GmbH (Germany)</i>	375
Monitoring and mapping of corrosion of zinc coatings in some climatic zones of Italy <i>Prof. R Fratesi, Università Politecnica delle Marche (Italy)</i>	Paper not included
Corrosion investigations on zinc coatings by using gel-type electrolytes <i>M Babutzka, Bundesanstalt für Materialforschung und -prüfung (BAM) (Germany)</i>	385
Corrosion behaviour of zinc-chromium alloys for batch hot dip galvanizing <i>Prof. R. Feser, University of Applied Sciences, Iserlohn (Germany)</i>	393

Session 1:

Keynote Speakers

THE GALVANIZING INDUSTRY IN GERMANY

M Huckshold (Industrieverband Feuerverzinken, Germany)

THE GALVANIZING SECTOR

The German galvanizing industry is a typical medium sized service sector with a long history. The members operate as specialists in the field of corrosion protection of steel applications and provide additional services to their customer's, e. g. organic painting, logistics etc.

In 2017, around 1.9 million tonnes of steel were batch galvanized in Germany. About 80 percent of that volume is done by sub-contact 'jobbing' galvanizing. There are about 147 galvanizing plants in Germany - with a total kettle volume of 5,500 cubic meters. The industry employs approximately 4800 employees and has a turnover of around 760 million euros. For those people interested in zinc demand, 110,000 tonnes of zinc are used in 2017 by the German batch galvanizing industry.

If we look back over a longer period, the development of the galvanizing business since the last 20 years has been very positive due to a wide variety of activities. The batch galvanizing tonnage could be increased from 1,43 Mill. tonnes in year 2000 (last INTERGALVA in Berlin) to 1.9 Mill tonnes in 2017 which is more than 30 percent. Within the European General Galvanizers Association (EGGA) Germany is also an important member from an economic point of view. One quarter of the total batch galvanized steel tonnage of the 23 EGGA member states is hot dip galvanized in Germany.

THE MARKET

The galvanizing industry provides services to many customers and sectors. Corrosion prevention is increasingly becoming a job for specialists. For economic and ecological reasons, corrosion prevention is generally increasingly supplied works, and galvanizers are bearing this development in mind.

Even though the construction industry is by far the biggest customer, other sectors (energy, transport engineering, metal trades, etc are also very strongly represented, though the picture varies very greatly from one region to another. With about 49 per cent, the construction industry (structural engineering) takes the lead. Industrial equipment registers 12,5 percent, and transport/vehicles is in third place with about 11 percent. These three construction branches put together represent more than 70 per cent of all the applications for galvanizing.

Germany is unique in Europe in having open borders with nine neighbouring countries, and galvanizing works from most of them seek customers in the German market and vice versa.

The largest batch galvanizing plants in Germany have kettles with a length of 19.5 m. The wide variety of sizes and locations of galvanizing kettles serves a very diverse range of customers that is dominated by the construction sector. The market segments of the German galvanizing industry in terms of galvanized tonnage are shown in Figure 1.

Typical products of the German batch galvanizing industry include highway safety barriers balcony railings, stairways, car trailers, truck semi-trailers, steel constructions, modern steel and glass architecture and parking garages.

Due to a strategic planned market development programme in recent years, innovative architectural applications such as use of batch galvanized plates for facades have contributed to some interesting new applications for the industry (Figure 2).

Other new market initiative started with basic research work on cyclic load behaviour of galvanized steel and now aimed in expanding the use of batch galvanizing for highway bridges (Figure 3)

MODERN SERVICE PROVIDERS FOR THEIR CUSTOMERS

The majority of the German batch galvanizers understand themselves as modern service providers. In addition to the core business of galvanizing, the German galvanizing industry offers a lot of additional services before and after galvanizing.

- Consulting, design and process optimization

Consulting and design optimization is one of the typical services of a hot-dip galvanizing plant in Germany. Even with complicated steel components there are good galvanizing solutions possible. For major industrial customers, smooth integration of galvanizing into the value chain is crucial. Just in time production, which requires maximum adherence to deadlines and accuracy, is a typical logistics service provided by German galvanizing plants.

- Painting services

After galvanizing, it is not uncommon for customers to wish a wet or powder coating for reasons of design or to improve the corrosion protection properties. Galvanizers are happy to take over the painting of the galvanized steel parts for their customers (Figure 4). Depending on the philosophy, this is done in the own coating line or through cooperations with partner companies.

- Warehousing, assembly and logistics

Whether packaging of galvanized products, installation on the construction site or delivery to the customer's end customers - warehousing, assembly and logistics are services that modern galvanizing companies increasingly offer and take over. All parties benefit from this. Customers and their end customers save costs, the galvanizer increases its added value. Transport-services by delivery and pick-up from and to the customer or deliveries to the construction site are also part of the standard offer of most German galvanizers.

- Specialists at work - containers, small parts and others

There are products that can only be galvanized in specialized companies. These include, for example, the high-temperature galvanizing, centrifugal galvanizing, the historical pliers galvanizing of smaller bins and cans or the "outside only" galvanizing of tanks and containers. For these and many other special applications, there are specialists who have the necessary technical equipment and knowledge.

- The best of all industries

The galvanizing industry galvanizes a variety of products for a variety of industries. This includes for example truck trailer chassis and chassis components for the automotive industry or gratings, crash barriers, balconies and structures for the construction industry. Galvanizers have by doing this the opportunity to learn from the best industries the best practices. This creates benefits for all customers.

THE ASSOCIATION

The German galvanizers association was founded in 1958, so it has its 60th anniversary in 2018. With its 107 members, Industrieverband Feuerverzinken is a strong sector association; it covers approximately 50 per cent of the industry capacity, representing a relatively high degree of organisation. The members of the German Association are widely distributed throughout the country, but naturally with concentrations in the conurbations.

A total of 11 people is employed by the Industrieverband Feuerverzinken and its associated organisations.

Industrieverband Feuerverzinken e.V. and its associated organizations

The Industrieverband Feuerverzinken e.V. (IFV) is the galvanizers association that represents the German batch galvanizing industry. It is based in Düsseldorf in the western part of Germany. The association represents the economic and technical interests of the German hot dip galvanizing industry to the public, politicians, authorities, process users, consumers and scientific institutions. The duties of the organisations include:

- Lobbying
- Research and Development
- Members Support
- Public relations and process marketing
- Technical support for users
- Training for members and process users
- Standardization
- Representation of the industry within EGGA and other associations

The Institut Feuerverzinken GmbH (IFG), as 100 percent subsidiary and service organization of the industry association is active for the hot dip galvanizing industry in the areas of marketing and technology.

The Gemeinschaftsausschuss Verzinken e. V. (GAV) is the research organisation of German galvanizing industry. The main task of GAV is organizing and coordinating joint research in the product, process and application technology for hot dip galvanizing. This is done in cooperation with leading universities in Germany.

In order to carry out its tasks and to make use of synergies, the Industrieverband Feuerverzinken is a member of several organisations, which are concerned with the metal zinc, with steel or with galvanizing.

These include:

- The Non Ferrous-Metals Industrial Association (WV Metalle)
- The Steel Industrial Association (WV Stahl)
- The German Steel Construction Association (bauforumstahl)
- European General Galvanizers Association (EGGA)

MAIN ACTIVITIES

The main activities from the association and their organisations are orientated towards strategic goals. Among the most important areas of activity are:

- Technical advice for potential demand-side representatives (planners, architects, engineers, authorities).
- Communication with interested parties and groups of interested parties in a wide range of different media (Print, Internet, social media etc.)
- Disseminating information through talks, seminars and events.

Technical advice and providing information for architects and engineers form the core of these aspects of the Institute's work.

Providing information for architects and engineers in good time

Direct contact with architects, engineers, planners and those who issue requests for tenders is an essential component of marketing. By evaluating planning data for construction projects, the Institute is able to contact decision makers at a very early stage -by telephone or letter, or in person - and to provide them with information on corrosion prevention.

One important information path involves providing architects and engineers with information in good time during their training (students). Knowledge of galvanizing can be transmitted through seminars in colleges and universities. In 2017, more than 1,000 consultations were organised for architects, engineers, authorities and members on galvanizing.

Presentations, seminars, training courses

The technical and marketing engineers give presentations in technical schools, colleges and universities to disseminate information about galvanizing. This provides an opportunity to reach interested target groups directly and at an early stage. In 2017 alone, our specialist engineers were responsible for a total of 101 presentations and seminars, with audiences totalling more than 4,400.

Fairs and conferences

One important instrument for disseminating information is attendance at fairs and technical events. In this connection, Industrieverband Feuerverzinken is for instance represented at

- The 'BAU': the leading Trade Fair for Architecture, Materials and Systems, is held every two years. It sets standards and is the industry's most important gathering (80,000 of the more than 250,000 visitors were from abroad, 2,120 exhibitors from 45 countries gave the fair top marks)
- International Architecture Congress in Essen with about more than 800 participants is held every two years (Figure 5)

We also exhibit at technical gatherings and symposia which are of individual interest to us.

The magazine 'Hot Dip Galvanizing', press work and the Internet

Since its first appearance in 1972, the magazine 'Hot Dip Galvanizing' has developed into a recognised technical periodical in the field of corrosion prevention (Figure 6). It is an important instrument for information and identification purposes. Main target group are steel fabricators and corrosion protection decision makers like architects and engineers. Today the magazine is published by the so called magazine group, which is a partnership of the German, English and Spanish batch galvanizers association. In addition to that the Italian and the Czech batch galvanizers association are offering license versions of the magazine. So the hot dip magazine is available in five languages. Since 2012 it is available the magazine is in addition to the print version available in an iPad-Version and an Online-version.

The German galvanizers association does a lot of Press work and gets by doing this topic-related reaches of up to 550 publications and more than 10 million readers per year. The digital marketing activities of the German galvanizers association stands for high-reach digital presences in the form of own websites, social media activities and apps. More than 200.000 persons per year visit the websites of the association. The associations Youtube channel has more than 34.000 views per year, the twitter account has more than 30.000 impressions per year and the Pinterest account has yearly reach of more than 60.000 viewers. In addition to that the association is editing Wikipedia articles to

improve them with facts to corrosion protection. These articles have a reach of more than 1 million views per year.

Awards of the association

Since 1989, the association is praising the Verzinkerpreis, which is the German galvanizers award for Architecture and Metal Design in odd years (Figure 7). The prize is awarded for outstanding structures, objects and products, which are largely galvanized or contain important hot-dip galvanized details. Architects, engineers, steel and metal workers, locksmiths, blacksmiths, designers, builders can take part. The galvanizer price is endowed with 15,000 euros. Other European countries have recently also made use of a galvanizers' prize as a marketing device.

In 2003, the association awarded for the first time the innovation award for hot dip galvanizing. The prize is aimed at companies, planners, researchers and inventors. It is awarded for innovative products and research services that open up new fields of application for hot-dip galvanizing.

The future in Europe

European markets are becoming ever more closely interconnected and, if the policies laid down in Brussels do not always meet with our approval, we still have to recognise that political developments affect us and that we have to respond to them.

As the Association representing the German galvanizing industry, Industrieverband Feuerverzinken likewise sees the future in European terms. In this context, EGGA is an important instrument for successful European cooperation. Industrieverband Feuerverzinken as one of the strongest association within EGGA plays a special role and by that have a special responsibility for the future development of our industry.

We see it as an important task to form part of a Europe which is working together. By co-operating with other national galvanizing organisations and associations, we wish to use synergies to achieve success for the galvanizing process and to be able to face challenges and threats together.

Opening to the rest of the World: Offering Official Partnership for galvanizers from outside Germany

In the past there were often request from galvanizers outside Germany who asked for support. It is now possible for galvanizers from outside Germany to become an Official Partner of the Institut Feuerverzinken (Figure 8). Official Partners can benefit from a wide range of services:

- Exclusive specialist information on galvanizing
- Use of our advertising material on galvanizing
- Participation in assemblies and events
- Participation in seminars/workshops on galvanizing topics
- Professional advice on technical/business topics
- In-house training on technical topics
- Company presentation on the association website
- Certificate confirming the official partnership

More Information about the Official Partnership is available on request at: info@feuerverzinken.com

SUMMARY

The main tasks of Industrieverband Feuerverzinken and its subsidiary, Institut Feuerverzinken, and the Research organisation GAV are the successful development of galvanizing sector in Germany.

The galvanizing industry has a well-established position in the field of corrosion prevention, but it is necessary to defend this and build on it in order to continue to be successful in the long term. A wide range of concepts, instruments and activities were used to bring this forward in the history of the last 60 years.

As part of an overall strategy, many full-time employees, and many people working in an honorary capacity, are working for success in the board and on the various committees.

Author

Mark Huckshold

- studied Environmental Technology at Technical University Berlin, 1999 degree as Diplom-Ingenieur (Dipl.-Ing.)
- 1999 – 2002 scientific researcher at Technical University Berlin, working on optimisation technologies for pre-treatment processes in electroplating and hot dip galvanizing industry
- 2002 technical manager Institut Feuerverzinken GmbH
- 2008 managing director Industrieverband Feuerverzinken e.V.

Figures:

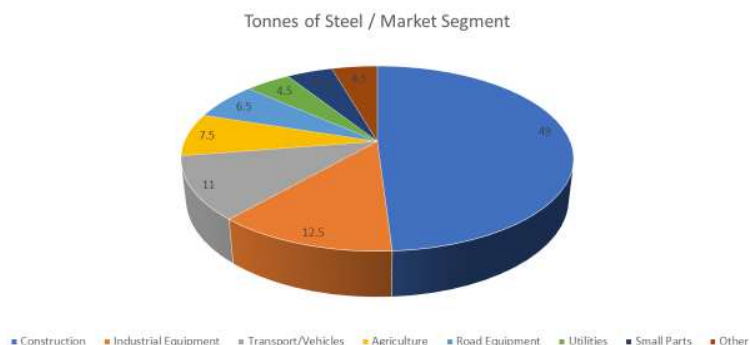


Figure 1: Markets for Batch Galvanized Steel in Germany

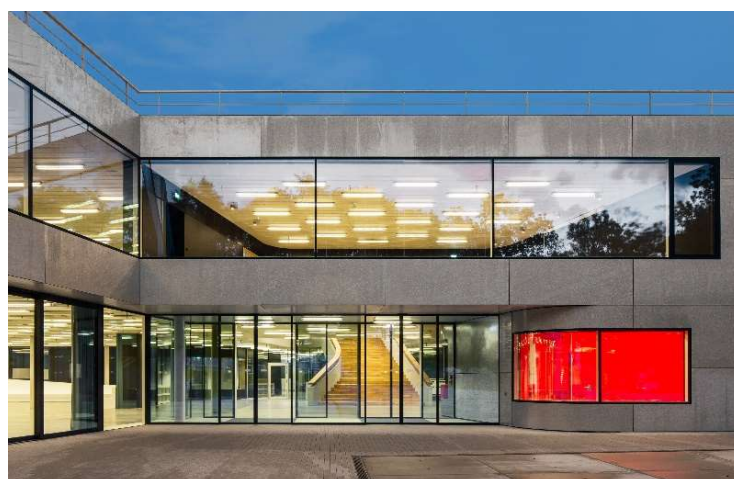


Figure 2: Facades are an increasing market for batch galvanizing.



Figure 3: Another new market is galvanizing of highway bridges in Germany.

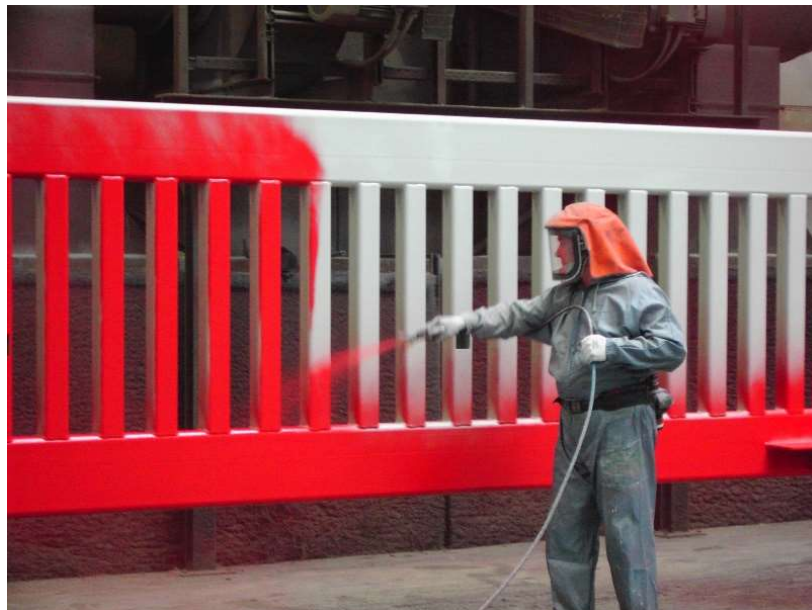


Figure 4: German galvanizers offer additional services like painting to their costumers.



Figure 5: More than 800 participants are usually coming to the architects congresses organized by Industrieverband Feuerverzinken.



Figure 6: The hot dip galvanizing magazine is targeting steel fabricators, architects and engineers.

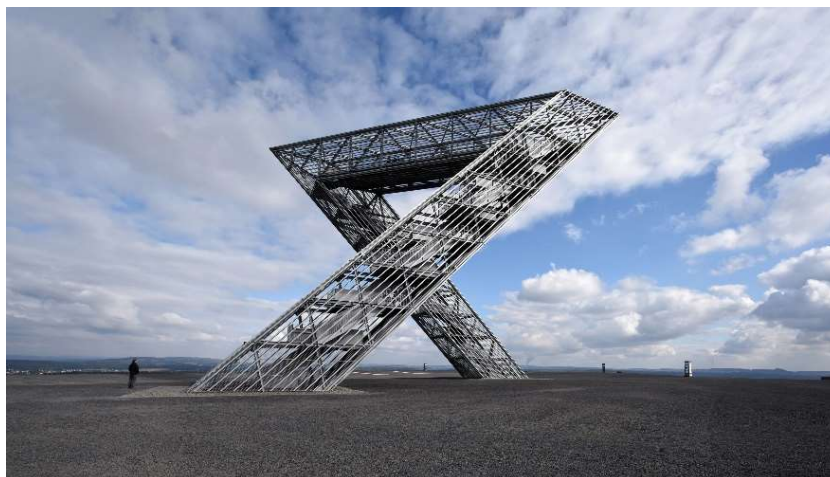


Figure 7: The Saarpolygon had been the winner of the Verzinkerpreis 2017.



Figure 8: Galvanizers from outside Germany can benefit from the German association service by becoming an official partner.

THE ZINC SUPPLY/DEMAND OUTLOOK: SUPPLY GROWTH WILL DRIVE AN INEVITABLE PRICE RESPONSE

R Cochrane, CRU Group (United Kingdom)

ABSTRACT

Zinc's price got off to a bullish start to the year on positive investor sentiment and a weak US dollar, lifting prices above \$3,600/t in mid-February. However, the mood has cooled somewhat since as several factors - reported stock gains on the LME, USA-China trade war rhetoric and rumours of SRB selling - sent prices tumbling to the low \$3,000s by early May 2018.

The recent correction has likely been overdone given market fundamentals and we still expect the year be characterised by concentrate tightness in 2018 H1, relatively depressed smelter utilisation rates and sizeable metal deficits. This will draw reported metal stocks down to critical levels through the middle of the year and should support a rebound in prices.

Significant ex-China supply-side developments have led us to upgrade several new projects to committed, suggesting the next wave of zinc mines is well and truly upon us. While concentrate availability in 2018 H2 will improve, much of the extra supply will be absorbed through raised smelter utilisation rates. Over the balance of our forecast period, we expect concentrate stocks to build, driving up smelter utilisation, TCs and ultimately smelter investment, and this should be more than adequate to also tip the metal market into surplus.

HIGH PRICES ARE CONSTRAINING DEMAND GROWTH

In addition to high prices, there are several factors in the current market which we believe will hinder demand growth over our forecast period in the absence of any significant new applications for zinc.

China will continue to add the most to demand in absolute tonnage terms over the next five years, despite expected constraints from the rebalancing of the economy and at least another three years of environmental protection measures. We have consumption growth slowing this year and next and averaging just under 2% per annum over our forecast period. We are already seeing a slowdown in China's galvanised sheet output and are forecasting zero growth over our forecast period. Galvanised sheet net exports have already fallen, excluded from several markets by trade tariffs, and efforts to close surplus steel sector capacity are ongoing. China's small-scale fabricators in all sectors are still vulnerable to forced cutbacks and closures for environmental reasons, due to the Chinese authorities' ongoing commitment to reducing air pollution. Even after the end of the coal-intensive winter heating season there were temporary closures in Tianjin and Hebei, and we expect demand to continue to be disrupted by environmental protection measures. Demand will not necessarily be lost as large-scale consumers and those outside the most polluted industrial areas may benefit, but over time we expect increasing costs to encourage the relocation of some of China's fabricators to lower cost countries in the Asiatic region. This has already been the case for some die casting capacity.

We expect demand to grow only marginally in the world ex-China this year and next as high prices take their toll, and for demand to grow by around 1% over our forecast period. Within these figures India is a bright spot, with urbanisation and the potential for greater use of galvanised steel in the automotive sector supporting demand. We expect demand there to grow by an average of just under 4% per year, lifting it from 2017's 680,000 tonnes to 810,000 tonnes in 2022. New galvanising capacity in Mexico should also lift demand there, if the renegotiated NAFTA agreement does not hinder trade with the USA. We are also watching developments on US trade tariffs, with US galvanisers potentially lifting output should the 25% duty on steel products have the desired effect.

GLOBAL MINE SUPPLY CONTINUES TO RISE

The period of high prices since the second half of 2017 through the time of writing has supported a raft of project advancements. Our forecast of committed world-ex China production for 2022 is 8.74 Mt zinc (see Figure 2). Somewhat offsetting this, in China we have completed our 2017 roundup of mines and projects and have reduced our Inner Mongolian production capacity forecast by 192,000 tonnes. Global mine supply is now forecast to reach 14.34 Mt by 2022.

CHINA - MARGIN EXPANSION AND CONSOLIDATION TO DRIVE MINE CAPACITY GROWTH

Chinese mine production underwhelmed in 2017. Despite higher prices, particularly during the second half of the year, output remained constrained as a continued trend of environmental inspections and non-compliance left many operations shuttered. Official NBS statistics listed full year production of 3.27 Mt, which was reportedly down by 8.6% on a heavily revised 2016 estimate. We believe these figures grossly underestimate Chinese mine supply in 2017. Based on our roundup for 2017, CRU estimates that full-year production increased by 2% with mine supply totalling 4.17 Mt.

While the potential for capacity additions in 2018 is greater than at any other period in recent history, there is a lot of uncertainty as to how much will materialise into actual production. Therefore, the degree of slippage to plans will be key to determining production levels. Our current production forecast for 2018 allows for 250,000 t/y (or 5 %) of slippage on 4.72 Mt of potential capacity. While we don't expect a repeat to the levels of slippage seen in 2017 (some 8.4%), high prices and margins should continue to support investment in environmental compliance and drive a meaningful return to production growth in the Chinese mining sector. In contrast to our longer-term view, in which we see progressive consolidation and increased average capacities driving growth, 2018 may be characterised by the potential for relatively large project (>10Kt/y) gains as well as numerous small (<5Kt/y) gains translating into a material rise in production.

EX-CHINA MINERS RESPOND SWIFTLY TO HIGH PRICES

In the world-ex China we have identified 1.4 Mt of potential capacity gains (excluding redevelopments). This is made up of 907,000 tonnes of new mines and 528,000 tonnes from increased output at existing mines. If we include our assessment of probable and possible developments, mine supply in world-ex China has the potential to reach 9.03 Mt by 2022 (some 1.3 Mt higher than 2017 levels). The key factor accounting for the increase in our forecast compared to three months ago is that positive new mine project developments have led us to upgrade some projects from probable to committed (and from possible to probable) and add some new projects which have recently been announced. For example, Hindustan Zinc, who are currently expanding mined zinc and lead production to 1.2 Mt by 2020, announced they had approved an expansion to 1.35 Mt by 2021. We calculate the 1.35 Mt equates to 1.09 Mt of zinc and 265,000 tonnes of lead, with smelting capacity to increase in line. This means additional refined metal production of around 135,000 tonnes of zinc compared to our latest forecast. Vedanta have also announced that they are undertaking a feasibility study on construction of a greenfield smelter at Gamsberg. Production at the mine is due to start in the middle of this year at 250,000 t/y of zinc in concentrates, and the smelter would initially be matched to this at a capital cost of \$700-800M. Phase II of Gamsberg is an expansion to 450,000 t/y, so potentially adding another 200,000 t/y to the pipeline around the same time as their Indian mines ramp-up.

Idled capacity is considered unlikely to come on stream given the outlook for mine supply – we now count just five remaining idled assets. Volcan's Cerro De Pasco saw production levels in 2017 that were substantially higher than our idled capacity estimates due to processing of stockpiles, and we have moved this asset into our firm category. Additional potential production from reactivations has been reduced, to 225,000t by 2022. Mines still partly or wholly curtailed include: Glencore's McArthur River and Iscay Cruz, Toho Zinc's Endeavor and EMR's Golden Grove. CRU believes that there is now little potential for these operations to be reopened during our forecast, given the already large tonnage of committed production due on stream.

SMELTING CAPACITY GROWTH CONTINUES TO LAG MINE SUPPLY

Overall global capacity is expected to reach 16.635 Mt by 2022, from 15.08Mt in 2017.

Capacity growth in China is expected to reach 7.79 Mt by 2022, although there have been a handful of delays to smelter development in 2018 – for example, Baiyin has delayed a planned April 2018 start at its new 120,000 t/y smelter until May 2018 citing concentrate shortages. In the world ex-China, capacity is expected to rise only modestly, from 8.43M t/y to 8.56M t/y by 2022. The largest committed addition to smelter capacity outside China is Peñoles' \$327M, 120,000 t/y expansion of Torreon. In its 2017 Q4 results the company reported that the project would start up in 2018 Q3, which is up to six months later than previously reported.

Rising concentrate availability in 2018 H2 is expected to be absorbed almost entirely by rising smelter utilisation rates. Conditions are still not favourable for investment in smelting capacity and require i) a counter-cyclical investment approach and/or ii) Chinese state support of a more integrated mine to smelter chain. Ultimately, the market will need to move decisively into surplus to encourage additional investment, and with global concentrate supply increasing, we still believe that smelting capacity will be something of a cap on refined supply.

BOTH CONCENTRATE AND METAL INVENTORIES TO RISE OVER FORECAST

The first quarter of this year saw near record imports of zinc in concentrates into China, which helped offset depressed seasonal mine supply and supported better smelter utilisation rates than in 2017 Q1. While this drew down already critical levels of concentrate inventories in the world-ex China, several Chinese smelters began maintenance shut downs in March and April.

- In 2018 H2, we expect rising concentrate supplies to begin to alleviate some of the tightness (see Figure 4). The likely effect of this, however, will be for smelters to lift utilisation rates and absorb virtually all fresh supply.
- While we expect this will bring the metal market to balance by 2018 H2 (see Figure 5), it is unlikely that we will see any material recovery in concentrate inventories through the balance of the year. Increased utilisation rates may coincide with a return to modestly rising spot TCs – a development we view as important in determining the peak of the current zinc price cycle.

By 2019, concentrate availability should exceed that of smelting capacity, even at record utilisation rates, and concentrate inventories will start to recover. With demand growing only marginally, the metal market will also return to surplus. Sharp gains in concentrate inventories will be accompanied by rising TCs and modestly rising metal stocks over the balance of our forecast period.

AUTHOR BIOGRAPHY

Ryan joined CRU in 2017 and oversees Lead, Zinc and Precious Metals research. Ryan has over ten years of experience as a metals analyst and geologist and has worked on gold and polymetallic projects in South Africa, Western China, Armenia and the Northern Andes.

Prior to joining CRU, Ryan worked at Wood Mackenzie where he led gold mine cost research and contributed to base metal coverage along with new product development initiatives. Before this, he covered gold, silver and, to a lesser extent, PGMs at Thomson Reuters GFMS. Ryan has frequently presented at international conferences geared to industry and academia and has presented at numerous investor briefings.

Ryan holds a PhD in geochemistry, geochronology and thermochronology from the University of Geneva, Switzerland

Figure 1: Global demand growth will average less than 2% per annum in 2017-2022
Source: CRU

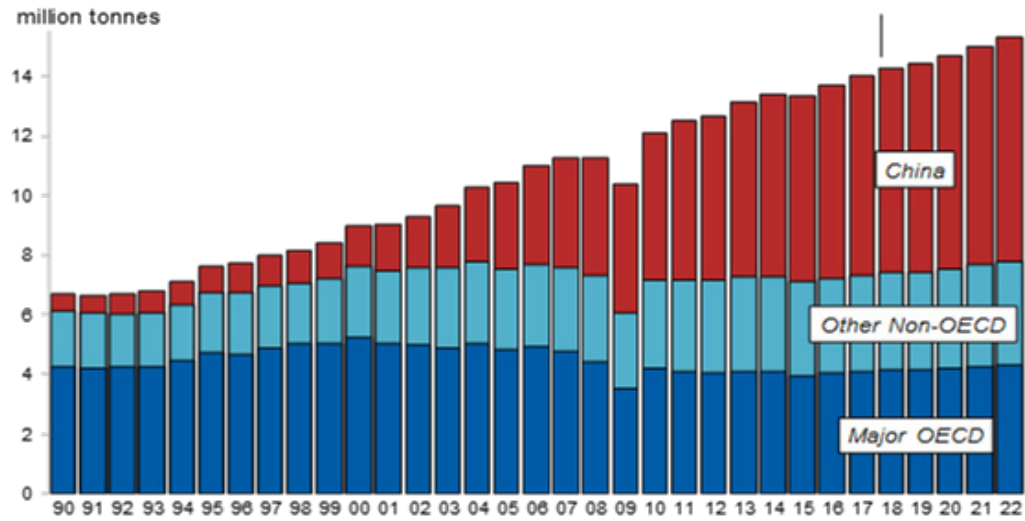


Figure 2: Total world mine production is now forecast to reach 14.35 Mt by 2022.
Source: CRU

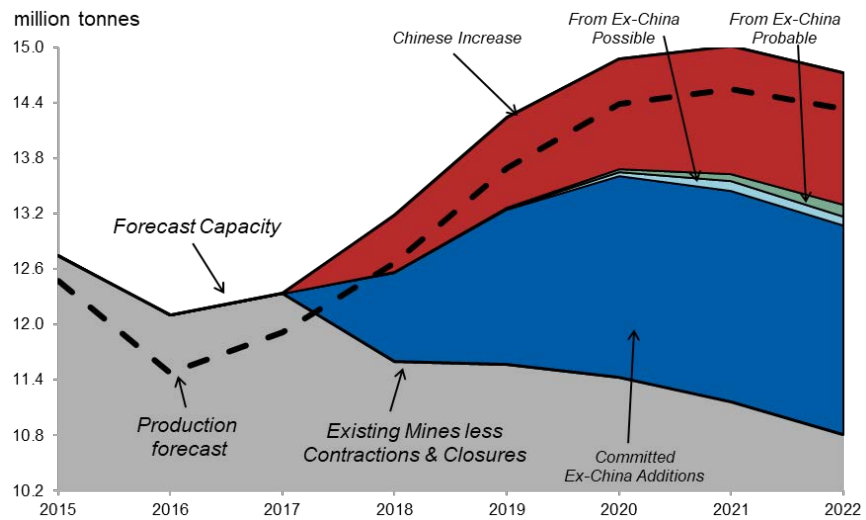


Figure 3: The next generation of zinc mines set to supply

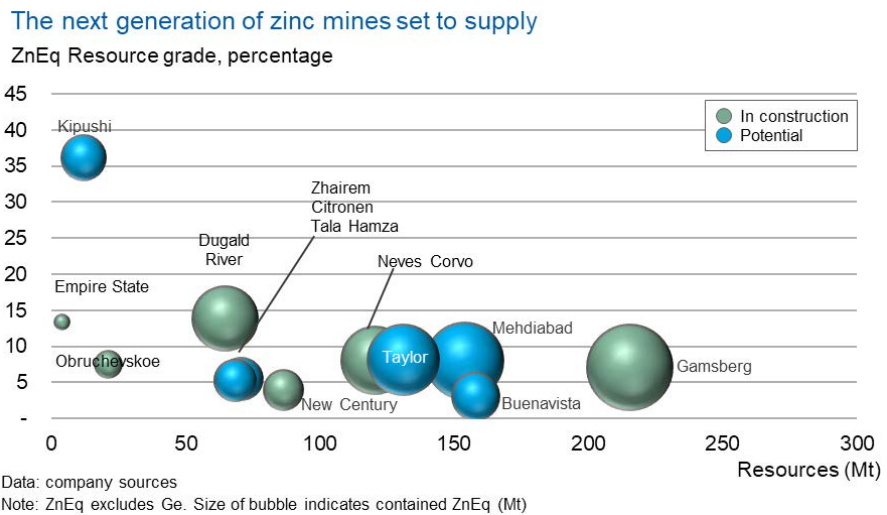


Figure 4: Concentrate inventories will start to recover in 2018 H2

Source: CRU

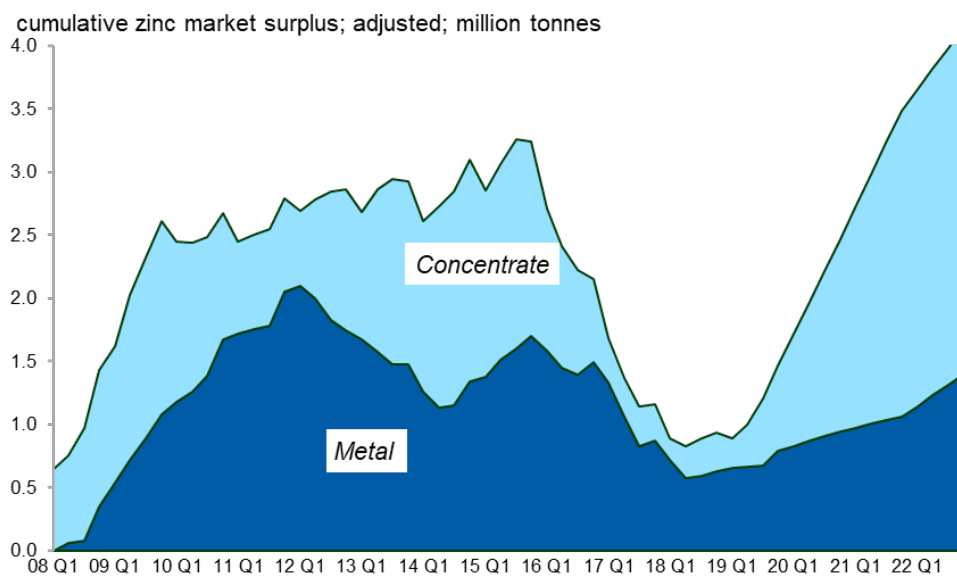
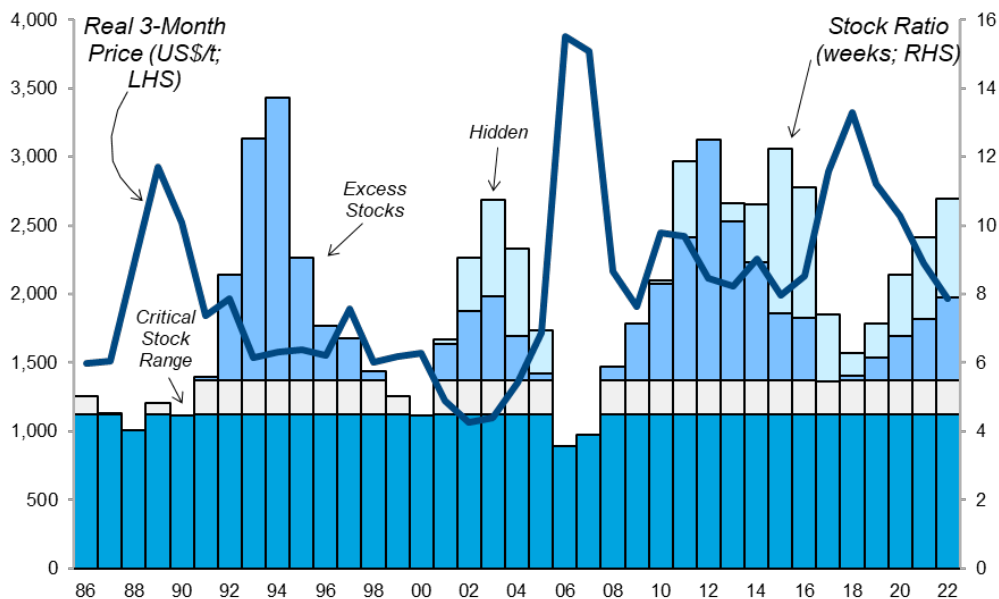


Figure 5: Stocks to hit low point of cycle in 2018

Source: CRU



Session 2:

Galvanizing in Bridge Construction

Hot-dip galvanizing for steel and composite bridges – New research for application of hot-dip galvanizing with composite dowel strips

Dieter Ungermann & Svenja Holtkamp, TU Dortmund University, Institute of Steel Construction (Germany)

Abstract

This paper presents an additional potential for the future economic development of composite dowel strips in composite bridge construction using hot-dip galvanizing. Hot-dip galvanizing offers a long-lasting and permanent corrosion protection for the bridge's design life of about 100 years [1] even in an environment with high corrosivity, so that no major maintenance measures of the corrosion protection are necessary. As part of current research [2] the influence of hot-dip galvanizing on the fatigue strength of the composite dowel strips is examined by experimental and numerical investigations. The results of these fatigue tests shall enable the safe and scientifically proven application of hot-dip galvanizing with composite dowel strips in composite bridge construction.

Introduction

In composite bridge construction the shear connection between steel beams and concrete slab usually is realized using headed studs. The headed studs welded to the upper flange of the steel girders achieve an interaction of the steel beam and the concrete slab as a total cross-section. This optimal utilization as total cross-sections enables composite beams with high load-bearing capacity and bending stiffness at small section height and less material. A high degree of prefabrication allows short construction times, especially with additional use of prefabricated concrete slabs.

Composite bridges with the use of composite dowel strips are one of the most economic variants for bridges with small and medium spans, compared to other construction options with headed stud, due to their simple fabrication and great bearing capacity. Generally, hot rolled sections are cut in the middle of the web by autogenous flame-cutting or a method which is equivalent in terms of load bearing capacity and fatigue resistance, producing two beams with composite dowels necessary for transferring the longitudinal shear forces (see Figure 2a). By the elimination of the upper steel flange and thus the reduction of steel consumption in areas which contribute only slightly to stiffness and load-bearing capacity, the great economic and product-technical advantages of the composite dowel strip become apparent (compare Figure 2b). Furthermore, they can also be used with T-beam cross-sections with external dowel strips functioning as external reinforcement, as used at Elster bridge Osendorf, presented in [3]. A less beneficial application of composite dowel strips in composite bridge construction are conventional composite girders, in which composite dowel strips, flame-cut from heavy plate, are welded onto the upper flange of the steel girders. This application is comparable in terms of load-bearing capacity to composite beams with headed studs.

Based on numerous studies within various research projects, the composite dowel strips were introduced by the building authorities in the form of a general technical approval (abZ) Z-26.4-56 [4] in 2013. Since then it has been applied to various bridge structures in Germany and Europe. The technical approval regulates the geometry, the production and design principles as well as the determination of load-bearing capacity and the fatigue check for non-galvanized composite dowel strips with clothoid and puzzle shape.

The calculation of composite beams with composite dowel strips is carried out according to the limit state design of concrete (EN 1992), steel (EN 1993) and composite steel and concrete structures (EN 1994) supplemented by the general technical approval. For composite construction exposed to cyclic loading, as is the case with composite bridges, the fatigue strength has to be verified for both steel and concrete and a rigid shear connection has to be ensured, whereby the individual components influence each other. The procedure for the fatigue check of steel dowels is given in the abZ in accordance with the local stress concept of EN 1993-1-9 (EC3-1-9) [5], compare equation 1 in Figure 3.

The local stress (L) resulting from the transmission of the longitudinal shear force of the considered dowel (clothoid = CL or puzzle = PZ) and the global stress (G) from the bending action of the composite beam determine the stress amplitude at the maximum point. These stresses are calculated from the nominal stresses (taking account of both the local and global stress effect) by stress concentration factors. These stress concentration factors were derived from finite element calculations and verified by strain measurements in push-out and beam tests [6]. For clothoid shape the stress concentration factors were set to 7.3 for local and 1.5 for global stress, for puzzle shape to 8.6 (L) and 1.9 (G). Depending on the cutting quality of the flame-cut surfaces, detail category 125 or 140 according to EC3-1-9 applies on the resistance side.

However, the regulations and design bases of the general technical approval [4] currently do not permit an application of hot-dip galvanized composite dowel strips. The hot-dip galvanization is a very long lasting and durable alternative to organic coatings and has been used for corrosion protection in steel building constructions for many decades. Its excellent properties in corrosion protection can provide a lifetime durability [1] and additionally minimizes weaknesses of protection in contact joints of steel and concrete. However, the influence of the hot-dip galvanizing on the fatigue strength of composite dowel strips has not yet been scientifically studied.

For typically used bridge details of steel and composite bridge construction the effects of hot-dip galvanization on fatigue behaviour have been analyzed in the finished research project P835 "Hot-dip galvanizing in steel and composite bridge construction" [1]. Therefore, various fatigue tests of large and small-scale tests of non-galvanized and hot-dip galvanized components, including component-like, batch galvanized test samples with geometrical and structural imperfections as manufacturing tolerances or residual welding stresses, corresponding to notch details according to EC3-1-9 were carried out at TU Dortmund University and MPA Darmstadt.

In a direct comparison of non-galvanized to hot-dip galvanized samples, a reduced fatigue strength was observed for all examined details, which is also presented in [3]. The results of all fatigue tests, evaluated according to the background document of EC3-1-9 [5], have been compiled and published in form of a detailed table for hot-dip galvanized steel details [1] complementary to the standard of EC3-1-9. In some cases, a reduction of the notch detail by 1 detail category is required, in some cases the detail category has been confirmed. Table 1 shows a section of the table for hot-dip galvanized details, with the two new details for flame-cut hot-dip galvanized metal plates.

In principle, it would be possible to carry out the fatigue check of hot-dip galvanized composite dowel strips using this table of new detail categories for hot-dip galvanized steel [1]. However, the specific influences from complex geometry, production-induced residual stresses and the load-bearing behavior of the dowel strip were not considered in the underlying tests. In order to reliably exploit the economic advantages of hot-dip galvanizing for composite bridges with composite dowel strips and to provide a fatigue check by means of extended scientific certifications the influence of hot-dip galvanizing on the fatigue strength of composite dowel strips is analyzed in the current research project P1042 "Fatigue strength of hot-dip galvanized composite dowel strips in composite bridge construction" [2] carried out by the Institutes of Steel Construction of RWTH Aachen University and TU Dortmund University, including extensive experimental and numerical studies.

Experimental investigations

Experimental test program

The main issue of the experimental research work in P1042 is to investigate the influence of hot-dip galvanizing on the fatigue strength of composite dowel strips. Numerous comparative (galvanized / non-galvanized), small- and large-scale fatigue tests are carried out to determine new notch details for the fatigue check of hot-dip galvanized composite dowel strip or to confirm the existing classification of hot dip-galvanized notch details (see Table 1). These tests consider the specific influences of the complex geometry, the residual stresses due to production and galvanizing process and the special load bearing behaviour of the composite dowel strips.

The different series of tests are based on the design concept of steel fatigue of the technical approval abZ [4] using the structural stress concept of EC3-1-9 [5]. The nominal stresses are calculated from two load carrying effects, the local and the global contact ratio of the composite beam, extrapolated to the hot-spot at the dowel curvature by stress concentration factors. To determine the influence of hot-dip galvanizing on both contact ratios separately, two different small-scale test series are carried out. For comparison, both galvanized and non-galvanized samples are examined. The first series includes cyclic tests on "naked" composite dowel strips (without the concrete slab) with a bending load corresponding

to the global contact ratio. Based on these fatigue tests with different parameter configurations, a preliminary S/N-curve, basis for the notch detail of EC3-1-9, should be determined. In order to take into account the interaction between the steel dowel and the concrete slab and to investigate a possible interference or influence of the zinc layer to the composite effect, the second test series, includes additional cyclic push-out tests, similar to the standard test set-up according to EN 1994-1-1, appendix B [7]. Thereby the specimens' stresses correspond to the "local" bearing behaviour of the composite beams. For the final verification of the preliminary S/N curve, large four-point bending tests on long composite beams with welded composite dowel strips and halved rolled sections with component-like dimension are carried out. Thereby previously excluded effects of the real load-bearing behavior can be taken into consideration.

As far as possible, all geometry parameters of the small-scale series and the large composite beams were chosen with real dimensions. The distance of the dowels was set to $e_x = 250\text{mm}$, as usual in bridge construction. Considering the DASt-Guideline 022 [8] the galvanizing process of the small-scale specimens and the large beams was controlled so a targeted pre-load of the test specimens was obtained, which corresponds to the most unfavorable stress from the galvanizing process of real beams with composite dowel strips. Therefore, numerous numerical studies on the galvanizing process were carried out at the research partner at RTWH Aachen University, compared and verified with strain measurements during the hot-dip galvanizing process, performed by the Institute of Steel Construction of the TU Dortmund University with the support of two galvanizing plants. Based on these calculations, long, flame-cut dowel strips with one-sided clothoid steel dowels were galvanized horizontally (dowels first) and at lowest dipping speed (Figure 4). These long, hot-dip galvanized dowel strips are then shortened to small-scale samples.

Small Scale tests

In the small-scale series of the "naked" dowel strip, small specimens with two steel dowels, cut of the long hot-dip galvanized dowel strip, are fixed upright (dowels out) in a servo-hydraulic test machine by means of a hydraulic flat-plate clamping, compare Figure 6a. They are then tested in the fatigue test with tensile stress. Three different configurations of samples with steel S355 or S460 and a surface treatment of the flame-cut edges according to detail category 125 or detail category 140 are investigated comparatively in galvanized and non-galvanized state.

A double-symmetrical model of the composite dowel strip with two steel dowels was generated for a numerical preliminary investigation of the small-scale tests. In order to exclude an influence of the contact pressure on the stress at the relevant point, the clamping jaws were modeled, and the load was applied in two separate load steps, first the contact pressure followed by the tensile, see Figure 4a. Thus, the required off-center position of the sample and the size of the tensile force were determined which result in a bending stress of the sample causing specified stresses at the hot spot in the dowel curvature, as Figure 5b shows. For the first comparative tests, the stress was determined to correspond stress range for the non-galvanized detail categories of 125 or 140 according to EC3-1-9 at 200,000 load cycles.

The numerical model could be verified in the first experiments by means of strain measurements in the areas of the hotspots. In addition, the fatigue cracks on the galvanized samples occurred at the numerically determined hot spot, as shown in Figure 6b compared with Figure 5b.

The strains are measured with strain gauges closed to the dowel curvature and on both sides of the dowel strip and extrapolated to the hot spots by factors derived by the numerical investigations. In addition, the expansion between the two dowels is measured to be able to determine the formation of a crack by increasing dowel deformations and to define the point of failure.

Some results of small-scale samples from S460, with flame-cut edges grounded according to notch case 140, are shown in Figure 6. These results of fatigue tests at one stress level show a decrease in the fatigue strength of the hot-dip galvanized samples compared to the non-galvanized samples. Since all results currently lie above the S/N-curve according to EC3-1-9, no major reduction in detail class is expected for this configuration. At present, however, no statement can be made about a classification into a defined notch details.

Currently fatigue tests of small-scale samples with different configurations are running. With the results of these test and the following extended tests of the most unfavorable configuration at different load levels a preliminary S/N-line can be deduced. But only in consideration of the push-out tests, in which a load transfer into the concrete is taken into account, and the final composite beam tests, considering the interaction of both contact ratios, a final definition of the S/N-curve can be derived.

Summary

Several investigations in recent years have contributed to an innovative shear connector, the composite dowel strip, which is regulated in a general technical approval [4] in Germany. Furthermore, the finished research project P835 [1] showed that hot-dip galvanizing has great advantages with regards to life cycle costs and durability of steel and composite bridges and can easily be applied with moderate modifications, amongst others due to the reduction of fatigue strength for hot-dip galvanized details.

To combine and take advantage of both developments, the influence of hot-dip galvanizing on the fatigue strength of composite dowel strips is investigated in the current research project P1042 [2] by numerous fatigue tests. While maintaining the design concept based on the general technical approval of composite dowel strips, the possibly new S/N curve and the subsequent defined detail category of the flame-cut, hot-dip galvanized composite dowel strips for the fatigue check according to EC3-1-9 or the confirmed classification according to the newly derived table of detail categories [1] will permit a scientifically verified application of hot-dip galvanizing for composite dowel strips in future composite bridge constructions. In addition, the numerical parametric studies of RWTH Aachen University are intended to classify a detail class according to the DAST-Guideline 022 [8] for the hot-dip galvanized composite dowel strips.

Acknowledgement

The FOSTA research projects P835 (IGF-No. 351/ZBG) [1] and P1042 (IGF-No. 18624N) [2] was/is carried out with the financial support of the Arbeitsgemeinschaft industrieller Forschungsvereinigungen „Otto von Guericke“ e. V. (AiF) Cologne, Germany and funding from the German Federal Ministry for Economy. Many thanks to these supporting committees. Also many thanks to Forschungsvereinigung Stahlanwendung e. V. (FOSTA) and Gemeinschaftsausschuss Verzinken e. V. (GAV) for their supervision and support. Furthermore, many thanks to the project partners, the involved industry companies and the project support committee of all projects for their support.

References

- [1] Ungermann, D, Rademacher, D, Oechsner, M, Landgrebe, R, Adelman, J, Simonsen, F, Friedrich, S and Lebelt, P (2014) *Feuerverzinken im Stahl- und Verbundbrückenbau*, IGF-No. 351/ZBG, research report FOSTA P835 (Düsseldorf)
- [2] Feldmann, M, Kühne, R, Kopp, M, Ungermann, D and Holtkamp, S (expected release 2019) *Ermüdungsfestigkeit feuerverzinkter Verbunddübelleisten im Verbundbrückenbau* IGF-No. 18624N, FOSTA P1042
- [3] Rademacher, D, Pinger, T (2018) Hot-rolled sections and hot-dip-galvanizing – a perfect combination for efficiency and sustainability of bridges, *Intergalva 2018*, Berlin
- [4] Deutsches Institut für Bautechnik (DIBt) (2013) Allgemeine bauaufsichtliche Zulassung Z-26.4-56: Verbunddübelleisten (composite dowel strips)
- [5] European Committee for Standardization (CEN) (2010) Design of steel structures; Fatigue *Eurocode 3, Part 1-9 (EN 1993-1-9)*
- [6] Gündel, M, Kopp, M, Feldmann, M, Hegger, J, Gallwoszus, J and Seidl, G (2014) Die Bemessung von Verbunddübelleisten nach neuer Allgemeiner bauaufsichtlicher Zulassung *Stahlbau* 83(2)
- [7] European Committee for Standardization (CEN) (2010) Design of composite steel and concrete structures; General rules and rules for buildings *Eurocode 4, Part 1-1 (EN 1994-1-1)*
- [8] Deutscher Ausschuss für Stahlbau DAST (2016) Guideline for hot-dip-zinc-coating of prefabricated loadbearing steel components *DAST-Richtlinie 022*

Figures



Figure 1. First hot-dip galvanized composite bridge near Kassel, Germany with headed stud for shear connection

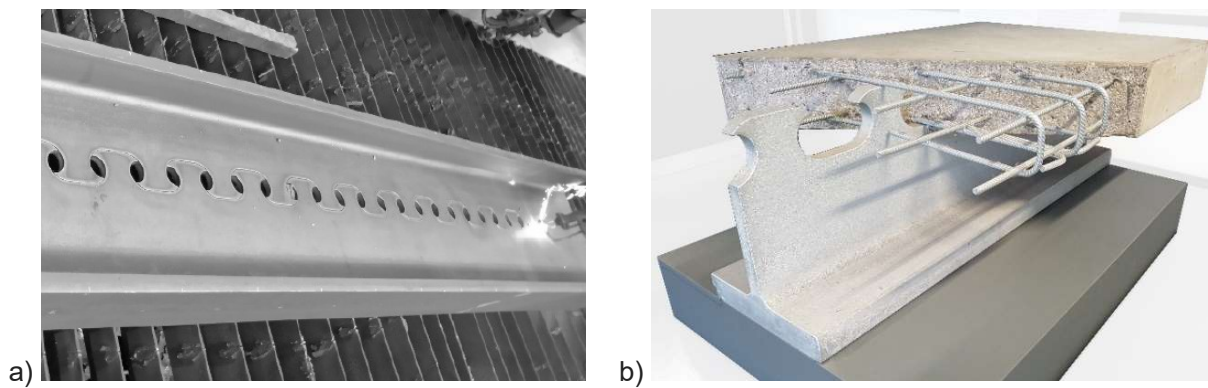
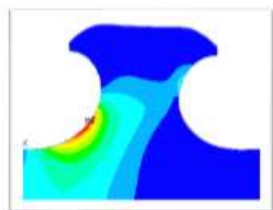


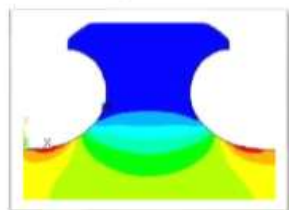
Figure 2. a) Flame-cut process for obtaining two beams with composite dowel strips, b) Exhibit of a composite structure with hot-dip galvanized composite dowel strip, here additionally with hot-dip galvanized reinforcement

Figure 3. Fatigue check of composite dowel strip according to general technical approval [4]

$$\Delta\sigma = \left| k_{f,l} \cdot \frac{\Delta V \cdot S_y}{I_y \cdot t_w} \right| + \left| k_{f,g} \cdot \left(\frac{\Delta N}{A} + \frac{\Delta M}{I_y} \cdot z_D \right) \right| \quad (1)$$



Local stress concentration



Global stress concentration



Figure 4. Long sheets of composite dowel strips after hot dip galvanizing

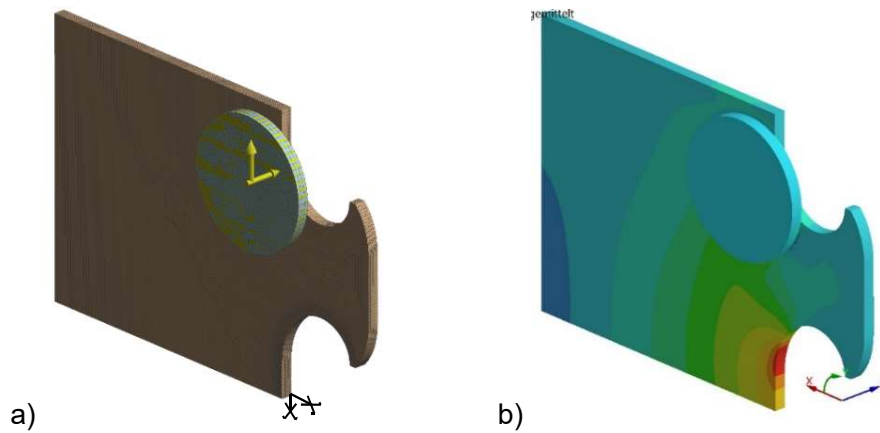


Figure 5. (a) Double-symmetrical model of the dowel strip with clamping jaws, (b) Normal stress distribution (local y) with hot-spot in dowel curvature

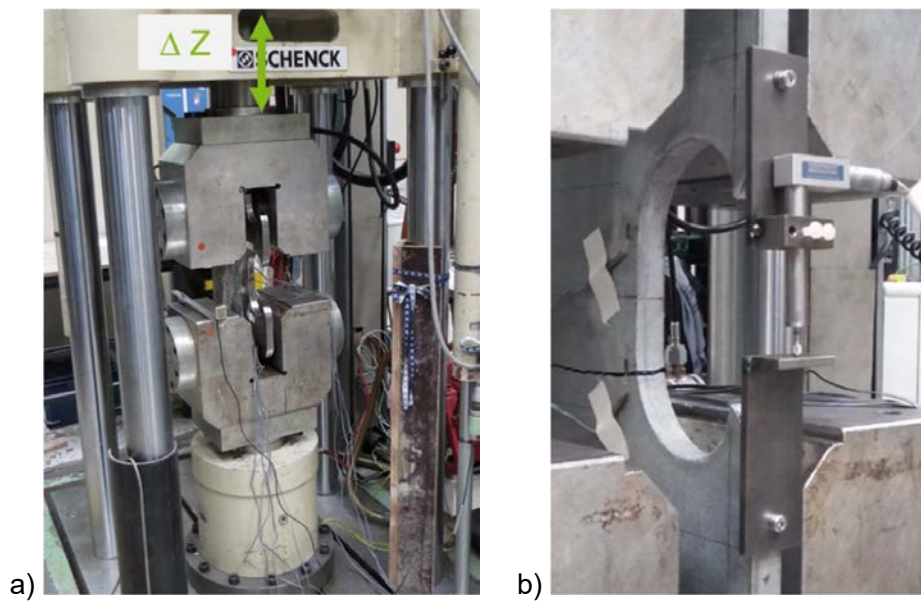


Figure 6. a) Test setup for a fatigue small-scale test with "global" bending, b) Failed small scale sample of a composite dowel strip

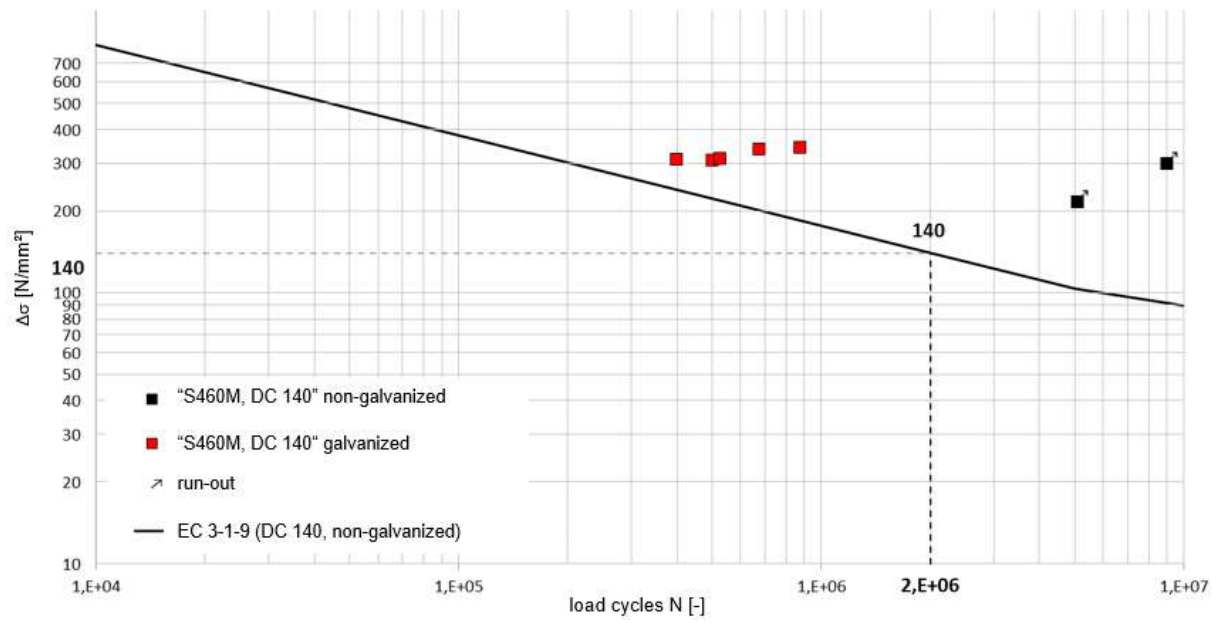


Figure 7. Comparison of non-galvanized (detail category 140) to hot-dip galvanized small-scale samples

Tables

Table 1. Extract of detail categories for tested hot-dip galvanized construction details [1]

Detail category	Construction detail	Description	Requirements
140		Plates, flats and rolled sections with rolled or milled edges NOTE: The fatigue strength curve associated with category 140 is the highest. No detail can reach a better fatigue strength at any number of cycles	Sharp edges, surface and rolling defects must be removed by grinding and a seamless transition is to be made.
112		Material with machine flame- or water jet cut edges with shallow and regular drag lines Machine flame- or water jet cut with cut quality according to EN 1090	Internal corners must be machined by grinding (inclination $\leq 1/4$) or considered by a corresponding stress concentration factor No repairs by filling with weld metal

Author Biographies

Prof. Dr.-Ing. Dieter Ungermann

See extra biography

Svenja Holtkamp M.Sc.

University degree in civil engineering

Research Associate at Institute of Steel Construction, TU Dortmund University

Focus on research on hot-dip galvanized composite dowel strips

Galvanized Bridges in Japan

Hiroshi Shibayama , Yoshikazu Takedomi, Japan Galvanizers Association

Abstract

Total road length in Japan is more than 1,200,000 km and it is the 6th longest in the world. Because of the topographical feature of Japan, there are a lot of bridges and tunnels and the number of bridges is well over 15,000. (bridges over 15m length) About one-third of these bridges are steel bridges.

As the weight of a steel bridge is lighter than a concrete bridge, it is suitable for a relatively long span bridge. Also in a place where the bridge construction requires hard work, over a river or in urban area for example, a steel bridge should be the best choice. On the other hand, weak point of steel is rust. To increase reliability of a steel bridge, rust prevention is essential.

Hot dip galvanizing is durable corrosion protection and has been widely used since it was first used 150 years ago. In Japan, the first hot dip galvanized bridge was Ryusogawa Bridge, constructed in Yatsushiro City, Kumamoto in 1963. The bridge is H girder type with 13m length, 9.5m width and 27tons weight. Since then, more than 1,000 galvanized bridges have been built all over Japan. Although most of the hot dip galvanized bridges are road bridges, 29 railway bridges were built in 1980's and 1990's, also all over Japan. The type of galvanized bridges is shown in figure 1¹. More than 80 % are H girder type and plate girder type bridges, but hot dip galvanizing is also applied to other type of bridges, such as box girder, steel floor slab and truss bridge. More than a half century has passed since the first galvanized bridge was built, all hot dip galvanized bridges are still in sound condition and it proves that hot dip galvanizing provide strong corrosion protection without disturbing other property of steel. This paper reports technical problems and the solutions when hot dip galvanizing is applied to steel bridges, points of attention on design and manufacturing and the results of site survey of some hot dip galvanized bridges.

Technical problems

For maintenance work of bridges, the traffic has to be fully or partially shut off. In addition to that, as there is the sea, river, road or railway under the bridges, the maintenance work of bridges is problematic. Therefore, maintenance free technology is required for bridge management. Hot dip galvanizing is widely used for corrosion protection of steel and can be suitable for a steel bridge. But to apply it to a steel bridge, some technical problems has to be solved.

- (1) Not to deteriorate mechanical property.
- (2) All parts of bridges should be galvanized not to make weak points.

Details are as follows

Mechanical properties of steel

To investigate the influence of galvanizing on mechanical properties of base steel, material tests were carried out before and after galvanizing. The samples for the test are made of SM41A and SM58Q, JIS specification of rolled steel for welded structure. The results are shown in figure 2² and 3³. Figure 2 is for non-weld zone and figure 3 is for weld zone. It is proved that galvanizing does not affect mechanical properties of steel.

Behavior of thermal stress and its influence

In galvanizing process, the steel article is dipped in molten zinc bath at temperature 430 to 450 °C and cooled down immediately after galvanizing. This rapid heating and cooling make thermal stress in the steel article. Sometime magnitude of the thermal stress becomes close to the yield point of the steel material and it may cause problems such as buckle of web and torsion of girder. To alleviate the problems, following points should be considered at design of a steel bridge.

- (1) Make members symmetric as much as possible and avoid big change of cross section and material
- (2) For H section steel, thickness of flange should be less than three times of web thickness (e.g. if the web thickness is 10 mm, flange thickness should be less than 30 mm).
- (3) Stiffeners should be arranged as indicated in figure 4, that is, horizontal stiffener and vertical stiffener should be attached in opposite side.

Residual stress at weld zone

Figure 5 shows residual stress at weld zone before and after galvanizing⁴. In higher stress range, the stress tends to be reduced after galvanizing. This is assumed to be an annealing effect during galvanizing.

Fatigue characteristics of weld joint

As shown in figure 6, fatigue strength of galvanized weld joint is better than non-galvanized one, when the joint is water cooled after galvanizing⁵. The reason of the improvement is reduction of residual stress by galvanizing. This is regarded as one of the advantages of galvanizing.

However, when the joint is air cooled after galvanizing, fatigue strength is reduced. The reason is assumed that when the joint is air cooled after galvanizing, brittle alloy layer grows up to the surface of the coating and increases roughness of the surface. Therefore, to assure better fatigue characteristic of galvanized steel, it is important to water cool immediately after galvanizing and prevent burning.

Galvanizing of splicing parts

Generally speaking, surface of galvanized steel has smaller slip factor than non-galvanized steel and does not satisfy current criterion for slip factor (0.4) as it is. To obtain specified slip factor, some surface treatment is necessary. At first, blasting was mostly used, but phosphating⁶ has become more common and the load of surface treatment work is reduced.

High strength bolt

High strength bolt is made of quenched and tempered high tensile strength steel and its tempering temperature is 400 to 600 °C. On the other hand, galvanizing temperature is 430 to 450 °C and when the tempering temperature of high strength bolt is lower than galvanizing temperature, the mechanical properties may be changed after galvanizing. JIS specifies F8T(tensile strength 800 to 1000 N/mm²) and F10T(1000 to 1200 N/mm²) as fastener for friction joint. The tempering temperature of F10T is lower than usual galvanizing temperature and it causes problems. At this moment, high strength bolts which can be used for galvanizing is F8T only.

Another problem is hydrogen embrittlement caused by pickling before galvanizing. It was confirmed that blast treatment, instead of pickling, practically causes no problem.

Follow-up survey of galvanized bridges⁷

JGA surveyed 14 galvanized bridges which were constructed 15 to 37 years before and examined the condition of the bridges. The bridges are located in different corrosive environment all over Japan.

General visual examination

The results of visual examination are shown in table 1.

Surroundings in which the bridges are located are classified into 6 zones, rural area, urban area, industrial area, mountainous area, coastal area and extremely corrosive area, according to its corrosiveness. The feature of each area is as follows.

Rural area : more than 2 km from the sea, less traffic, less air pollution

Urban area : commercial, residential, densely populated area

Industrial area : lot of factories, exhaust pollutants (Recently, due to antipollution measures, the corrosiveness of this area is close to urban area.)

Mountainous area : more than 10 km from the sea, less building, less traffic.

Coastal area : less than 2 km from the sea

Extremely corrosive area : coastal area with floating salinity of more than 100mg/m²/day

As shown in table 1, the results of visual examination in the same area are similar.

(1) In rural, urban and industrial area, most of the parts of the bridges are in sound condition. In some places around expansion joints, degradation of coating due to water leakage was observed.

(2) In mountainous area with snow fall in winter, degradation of coating caused by snow melting agent flew down at the end of the girder was observed.

(3) In coastal area, white rust caused by sea salt grain stick on the surface was observed on some parts. However, major components were in sound condition. On some bolts and nuts with light zinc coating, tarnished alloy layer which looked red was observed.

(4) In extremely corrosive area, lot of bulky corrosion products were observed and on some bolts and nuts, steel base was exposed.

Note

N bridge in the extremely corrosive area is located in the area on the sea front, northern part of central Japan. In this area, intense seasonal wind blows from the ocean in winter and the salinity is 125 mg/m²/day, which is far higher than average coast in other part of Japan. The salinity on the average coast is 10 to 30 mg/m²/day at about 200m from the sea. In average rural area, it is 1 to 5 mg/m²/day.

Corrosion rate of galvanized coating and its service life

Measurement the coating thickness on main girders of the bridges

The coating thickness of main girders was measured for bridge A, C in rural area, H, I in industrial area and J in mountainous area regularly and corrosion rate was calculated to estimate service life of galvanized coating. The results are shown in table 2. As for bridges A, C, H, I, J, corrosion loss of the coating is 0.64 to 1.57 μm/year and the order of corrosion loss is industrial<mountainous<rural. Rational reason of this order has not been found. In any case, it is estimated that the service life of galvanized coating is more than 100 years. It can be said that galvanizing is the technology which contribute to the maintenance free of steel bridges.

For bridges M and N, which are in coastal area and extremely corrosive area, thickness measurement was tried but it did not go well. The measured thickness of coating was thicker than previous measurement in most of the portion. This is due to corrosion product made by sea salt grain stick tightly on the surface of the coating and could not be removed when the thickness was measured. It made measurement inaccurate.

Measurement of corrosion loss of exposure test samples

As explained in the last section, coating thickness of main girders was measured and corrosion

loss was calculated, and then the service life was estimated. However, in the coastal area with high salinity, bulky corrosion product is accumulated on the coating surface and it makes coating thickness measurement difficult. To estimate the service life of galvanized coating in this kind of area, exposure test is useful. JGA conducted exposure test for 15 years with exposure samples set in the inspection passage of the bridge near the bridge N. The results are shown in Table 3. To estimate the service life, initial coating thickness is assumed to be 220 μm , which is the average initial coating thickness of the bridge C, H, I, J. and the following formula was used.

$$\text{Service life (year)} = [\text{initial coating thickness}(\mu\text{m}) / \text{corrosion loss}(\mu\text{m}/\text{year})] \times 0.9$$

Data for average coastal area and rural area, which were obtained by another exposure tests, are put in the table as a comparison. The service life in average coastal area is estimated as 73 years and in rural area, 324 years. On the other hand, in the extremely corrosive area, the service life is estimated as 30 years. In this kind of area, duplex system, painting on galvanized coating, for main component and zinc-aluminum alloy coating for small parts are recommended to extend the service life.

Maintenance of galvanized bridge

The results of the follow-up survey indicate that degradation of galvanized bridges is localized and it was caused by water leakage or flow-down of snow melting agent etc. in most of the cases. The examples of localized degradation are shown in figure 7 and 8. Figure 7 shows locally accumulated white rust caused by water leak from piping system. Figure 8 shows degradation of coating on bridge shoe caused by water leakage through expansion joint. To make performance of galvanizing maximum, it is important to find out those kind of localized degradation as early as possible and take appropriate measures to prevent further degradation or restore the performance.

JGA published "Manual for maintenance of galvanized bridge" jointly with Japan Bridge Association in 2004. In this manual, judgement of degradation of coating and repair work are explained.

Degradation level

There are two methods to judge degradation level of galvanized coating, one is visual inspection and the other one is coating thickness measurement. Table 4 shows the visual inspection criteria used in the manual. The coating thickness is measured with magnetic coating thickness gauge. When the thickness is measured, corrosion product on the surface of coating should be completely removed.

Repair work

The coating should be repaired when the surface condition is judged as grade 4 usually, or grade 3 to take the at most care. Coating should be repaired with painting or thermal spraying. Prior to

the repair work, rust or other foreign material on the surface of coating or base steel must be completely removed, but this work requires care not to remove effective coating.

Conclusion

Since the first galvanized bridge in Japan was constructed in 1963, more than thousand galvanized bridges have been built and there have been no major problem up to now. JGA conducted follow-up survey of 14 galvanized bridges 15 to 37 years after construction and the results show that the bridges are in sound condition in general and can be expected to be in the same condition for several decades or even hundred years. However, localized degradation of coating was observed in some places and it was due to water leakage through expansion joint in most of the cases. To keep the performance of galvanizing best, it is important to find out localized degradation and take appropriate measures to prevent further degradation or restore the performance. For this purpose, JGA published the manual specialized for maintenance of galvanized bridge to provide better bridge management.

Regarding railway bridges, no survey has been conducted yet due to access difficulty. However, there has been no report of problem due to galvanizing and it can be regarded that the galvanized railway bridges in Japan are all in sound condition same as galvanized road bridges. Despite its excellent durability, the number of galvanized bridges built in this decade is limited. The reason is that a galvanized steel bridge requires special care for its design and fabrication. However, it deserves the additional burden. Galvanizing is strongly recommended for the durability, the reliability and the safety of the social infrastructures.

Acknowledgment

The authors would like to thank West Nippon Expressway Company Limited for their professional advices.

References

1. Japan Bridge Association Inc., Japan Galvanizers Association Inc., 1999 Youyu aen mekkikyō jissekihyō (List of galvanized Bridges)
2. Japan Galvanizers Association Inc., Musashi Institute of technology, 1976 Teigoukin kouchouryokukou no kikaitekiseisitu ni youyuu aen mekki no oyobosu eikyo (Influence of galvanizing on mechanical properties of low alloy steel) Lead and zinc, vol.74.11, 1976
3. Japan Bridge Association Inc. 1973 Kouhanngeta no youyuu aen mekki (Galvanizing

of plate girder)

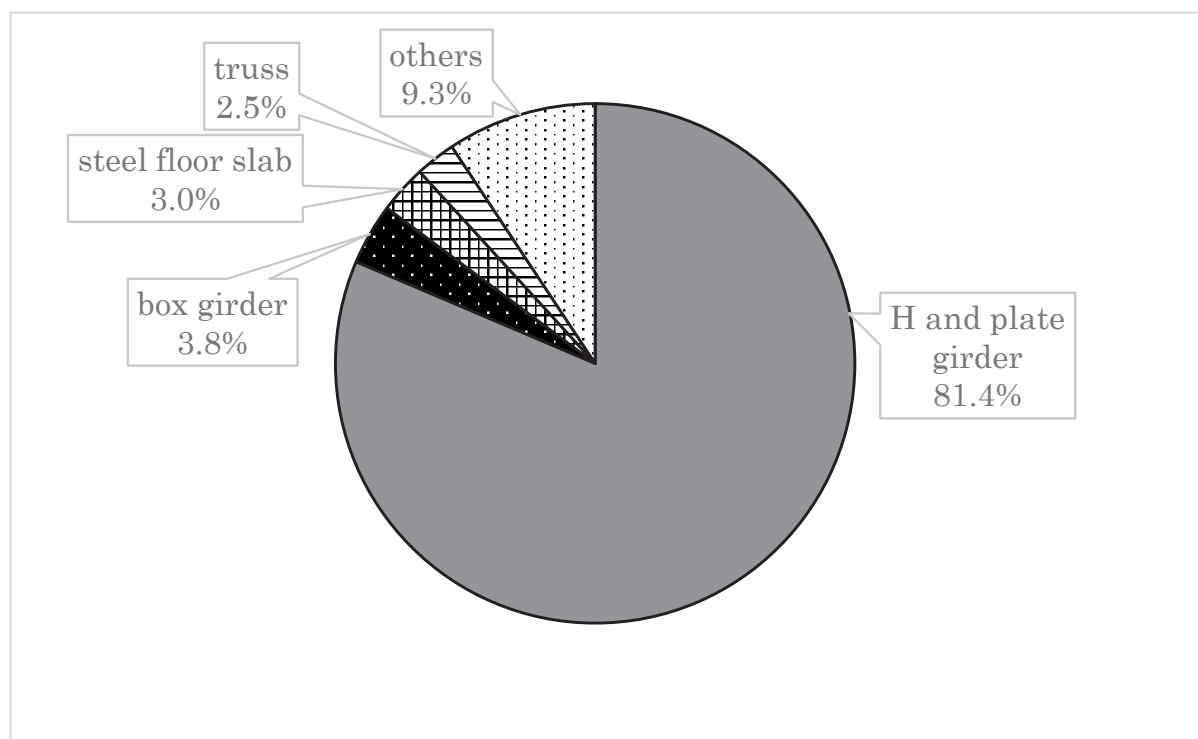
4. S.Kanazawa, et.al, ” Study on Hot-Dip Galvanizing Steel Bridge-Behavior of Stress in Molten Zinc Galvanizing” 1988, Tomoe Corporation Technical Report No.1

5. Isao Soya et al. 1988 Fatigue strength of galvanized weld joints for steel bridges – A study of high strength steels for hot dip galvanized bridge 3 -, Current Advances in Materials and Processes, Vol 1, No.2, 1988.3

6. T.Kohashi 1996 et al. Investigation on Application of Phosphate Treatment to Friction Surface of Hot Dip Galvanized Coatings, Ajigawa Annual Research Review Vol.12 1996

7. Japan Bridge Association Inc., Japan Galvanizers Association Inc., 2001 Aen mekki kyouryou no tuisseki chousa(Follow-up survey of galvanized bridges)

Figures:



Bridge type		
	H and plate girder	81.4%
	box girder	3.8%
	steel floor slab	3.0%
	truss	2.5%
	others	9.3%

Figure 1 Type of Galvanized Bridges

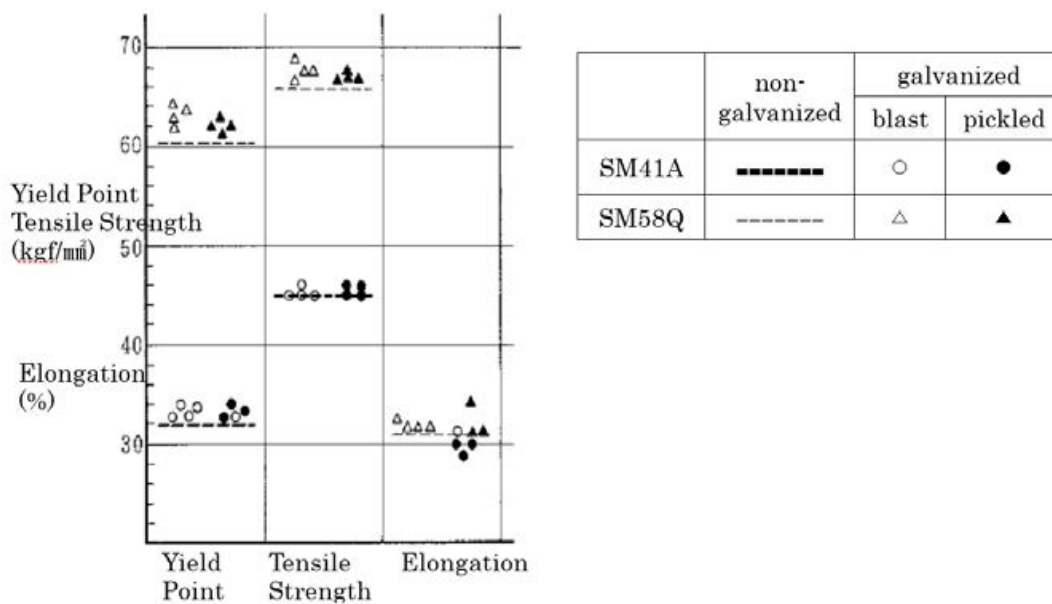


Figure 2 Mechanical property change by galvanizing (non-weld zone)

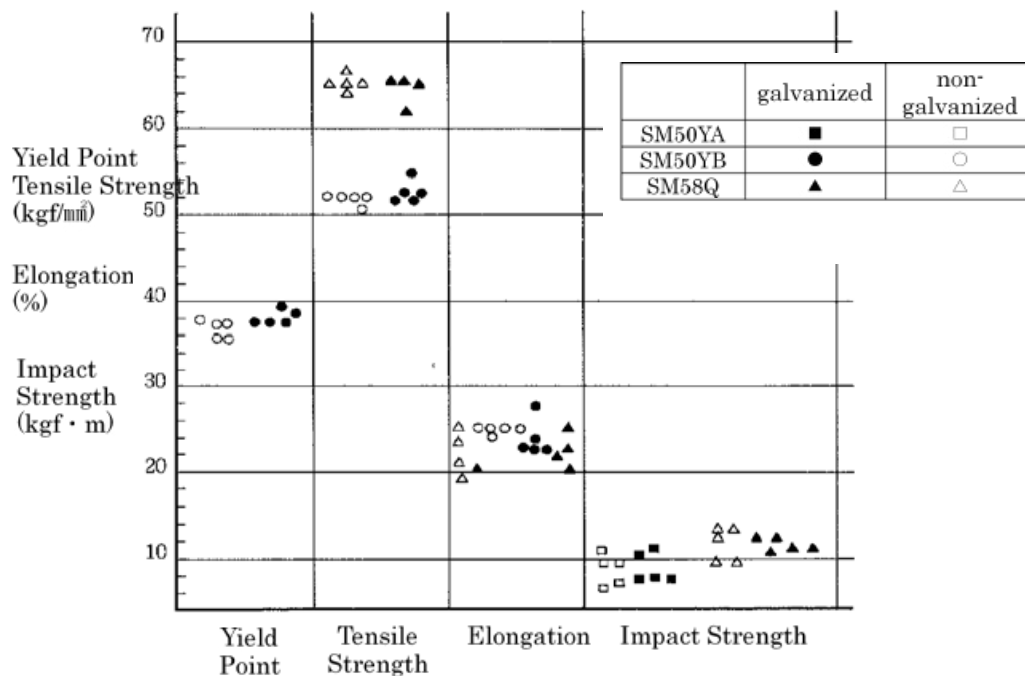


Figure 3 Mechanical property change by galvanizing (weld zone)

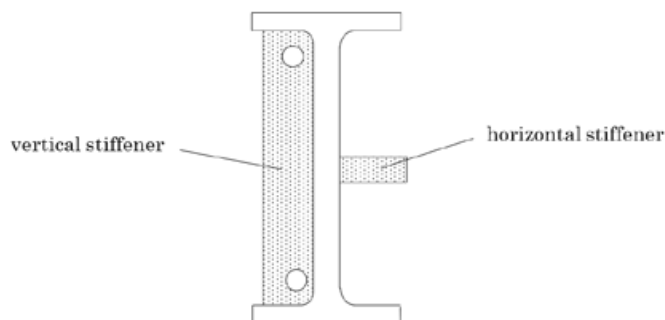


Figure 4 Arrangement of stiffeners

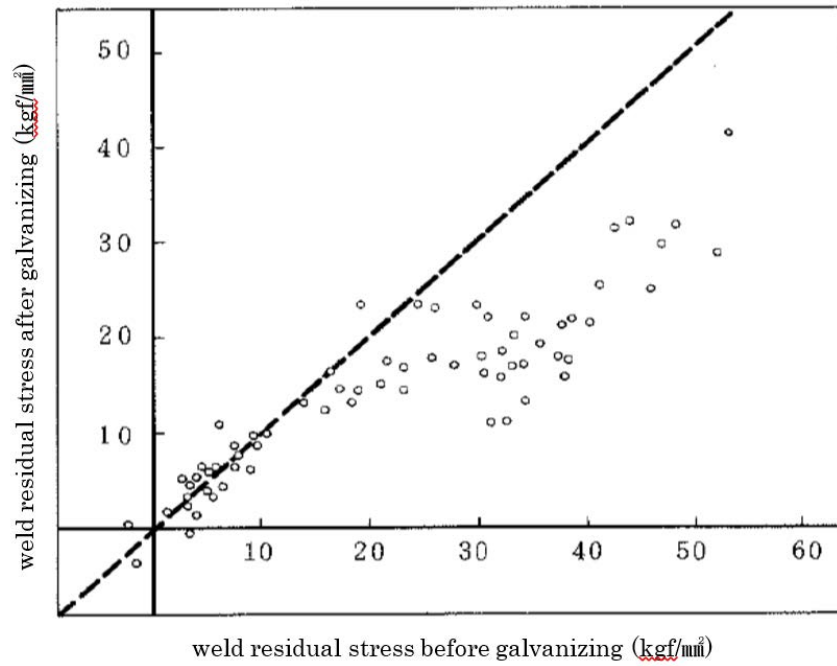


Figure 5 Change of weld residual stress by galvanizing

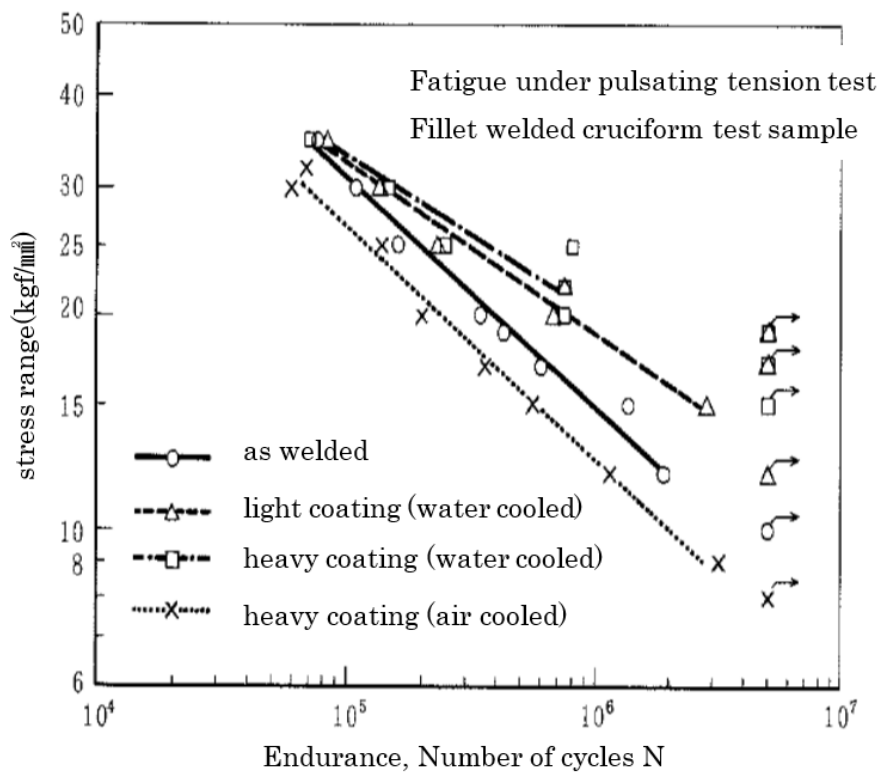


Figure 6 Effect of galvanizing on fatigue stress of fillet welded cruciform joint



Figure 7 White rust due to water leak



Figure 8 Degraded shoe at girder end

Tables:

Table 1 Results of follow-up survey of galvanized bridges

zone	bridge	year built	year surveyed	years since built	visual examination
rural	A	1964	2000	36	Generally the bridges are in sound condition. White rust due to water leakage was found around expansion joints. On some bolts and nuts, tarnished alloy layer was observed.
	B	1964	2000	36	
	C	1965	2003	38	
	D	1976	2013	37	
urban	E	1978	2003	25	Generally the bridges are in sound condition. White rust due to water leakage was found around expansion joints. On some bolts and nuts, tarnished alloy layer was observed.
	F	1984	2003	19	
	G	1988	2017	29	
industrial	H	1964	2000	36	Generally the bridges are in sound condition. White rust due to water leakage was found around expansion joints. On some bolts and nuts, tarnished alloy layer was observed.
	I	1973	2000	27	
mountainous (snow fall in winter)	J	1974	2000	26	In some part, red rust probably causes by snow melting agent was observed. Other portion was in sound condition.
	K	1983	2000	17	
coastal	L	1983	2000	17	White rust caused by sea salt was observed on most of the parts. On some bolts and nuts, tarnished alloy layer was observed. Other than that, the bridges were in sound condition and protected from corrosion.
	M	1984	2000	16	
coastal (very corrosive)	N	1987	2002	15	In many parts, bulky corrosion product was found. Tarnished alloy layer was found on the portion of thin coating. Some bolts and nuts lost zinc coating and red rust of steel was observed.

Table 2 Coating measurement results

zone	bridge	initial coating thickness (μm)	corrosion loss ($\mu\text{m}/\text{year}$)	service life (year)
rural	A	204	1.57	117
	C	216	1.57	124
industrial	H	253	0.64	356
	I	254	0.75	305
mountainous	J	183	1.01	163

Table 3 Exposure test results

zone	salt amount (in winter) $\text{mg}/\text{m}^2/\text{day}$	corrosion loss ($\mu\text{m}/\text{year}$)	service life (year)
coastal(very corrosive)	125	6.45	30
coastal(general)	10~30	2.72	73
rural	1~5	0.61	324

Table 4 Inspection criteria

grade	condition
I	Zinc layer is remained and no abnormality is observed
II	Zinc layer is partially lost and alloy layer ζ is observed
III	Zinc layer is lost and alloy layer ζ is observed on entire surface
IV	Alloy layer ζ is lost and alloy layer δ_1 is observed
V	Galvanized coating is totally lost and base steel is exposed

Hot-rolled sections and hot-dip-galvanizing – a perfect combination for efficiency and sustainability of bridges

Dennis Rademacher¹⁾, Thomas Pinger²⁾

¹⁾ArcelorMittal Europe – Long Products, 66, rue de Luxembourg, 4221 Esch-sur-Alzette Luxemburg, dennis.rademacher@arcelormittal.com

²⁾ZINQ Technologie GmbH, An den Schleusen 6, 45881 Gelsenkirchen, Germany, thomas.pinger@zinq.com

Summary

Increasingly problems in terms of damages on bridges in Germany correlated with partly massive long-term impacts on road traffic have shown how essential it is to ensure the durability of the infrastructure and thus the mobility of people as well as the exchange of goods, both nationally and internationally. Based on latest investigations on the fatigue behavior of galvanized steel components and the resulting in-depth understanding of design and execution, hot-dip galvanizing of steel and steel composite bridges offer a robust and maintenance-free corrosion protection for the bridge's design life of 100 years and therefore an excellent alternative to conventional construction methods. Particularly economical and sustainable solutions can be created in the field of short and medium spans using hot-rolled sections, which offer a high variety of applications. Standard higher strengths with steel grade S460 allow for more economical cross-sections with weight savings in steel construction of often 20-30% over welded sections in S355. In addition, the production effort is significantly lower due to the longer delivery lengths from the rolling mill (up to 40 m) and the elimination of the assembly of the webs and flanges.

The combination of hot-dip galvanizing with rolled sections in bridge applications offers significant advantages. Over all the very high quality and efficiency in the execution of the structure is to be emphasized, based on the use of industrially produced and standardized profiles and hot-dip galvanizing as full shop application method. Due to the uniform chemical composition throughout the steel profile a homogeneous appearance and zinc layer thickness is achieved. There is no need for grinding of cut surfaces as necessary in case of welded built-up sections from plates, resulting in high efficiency in the production. Finally, the robustness of the zinc layer withstands the loading during transport and assembly so that extensive renovation work on site, as common in case of organic coating systems, is avoided, meaning relevant savings in time and money.

1. Introduction

1.1 Status of bridges in Germany

A detailed survey on the condition of bridges in Germany reveals a negative situation. About 20-25% of the municipal road bridges in steel and composite construction bridges require replacements by new constructions. The annual investment, required only for replacements of these bridges without (partial) repair, is estimated at 630 million euro [1]. The poor condition of bridges in Germany correlated with partly massive long-term impacts on road traffic have shown how essential it is to ensure the durability of the infrastructure and thus the mobility of people as well as the exchange of goods, both nationally and internationally.

Elements of a bridge are exposed to atmospheric influences and to other additional corrosive loads, e.g. caused by using de-icing salts on the roads during the winter months. All bridge components must withstand these corrosive influences for decades to ensure their long-term use. Thus, a key aspect of the permanent function of bridges is the durable protection against corrosion damage during the

intended 100-year service life. Recent studies [1] show that corrosion damage is often responsible for the poor condition of a bridge (see Figure 1). This can be observed independently of the main construction materials on concrete, steel and composite bridges. In about 68% of all cases corrosion is the reason for the requirement of replacing a composite bridge [1], this value corresponds approximately to that of the concrete bridges. For steel bridges with a share of 94% corrosion is the decisive cause. Hence, an improvement in the general condition of the bridges would be achievable using a more durable corrosion protection system in steel and composite bridges. Therefore, a clear need regarding more durable and sustainable solutions could be derived, including both technical as well as economical aspects, e.g. high quality in fabrication combined with high robustness during utilization phase, resource efficient use of material, potential of reusing material according to the principles of circular economy, competitiveness in terms of initial costs as well as costs over the life cycle.

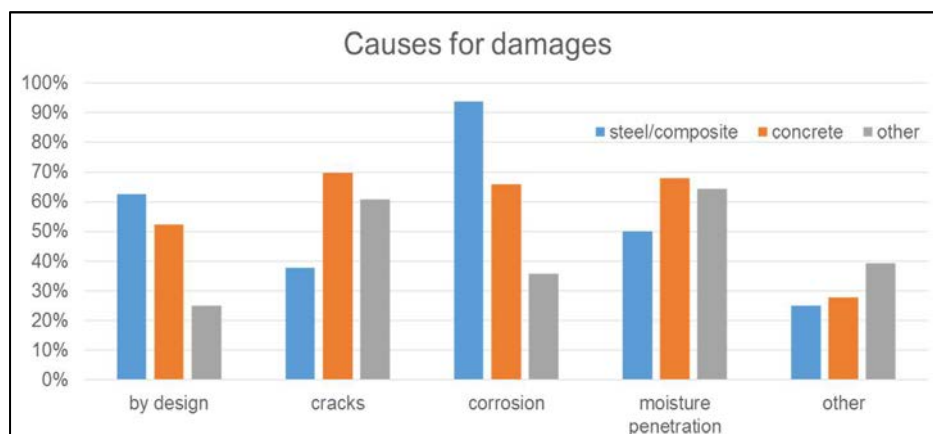


Figure 1: Causes for damages at German municipal bridges

1.2 Current corrosion loads

In Europe, environmental pollution has been systematically reduced in recent decades through stricter legislation on emission limits. The lower pollution in the atmosphere reduces the atmospheric corrosivity and can therefore have a positive effect on a longer corrosion protection period. In outdoor exposure investigations at selected locations and road bridges in Germany, the atmospheric corrosivity [2] was determined over a period of 5 years beginning in 2011. By comparison with results of a study of the Federal Highway Research Institute (BASt) from 1983 [3] at four identical bridge locations, a reduction of the atmospheric corrosivity by one or two categories could be observed.

1.3 Corrosion protection for bridges

There are several technologies for corrosion protection for the steel members in bridges. Traditionally, multilayer organic coating systems are applied. Advantages of this method are the ease of use, high degree of experience and the option of color design. However, these systems have the distinct disadvantage that they have to be renewed after 25-30 years. In addition, they are still prone to damages during transport and assembly.

Against this background, the use of hot dip galvanizing (HDG) as state of the art corrosion protection method with more than 120 years of positive experience in the long-term protection of steel in a wide range of application would have been an obvious approach. Based on recent measurements (see chapter 1.2), it was found that a coating thickness of only 200 μm can be sufficient to provide corrosion protection over the entire life cycle without renewal. On a closer look, however, it became apparent that, despite the advantages and the principle feasibility from a technical point of view, the necessary conditions for immediate implementation in practice were not met. Relevant obstacles were:

- HDG is not foreseen for load-bearing structures of bridges in the relevant standards (Eurocode 3 [4]) and guidelines (such as ZTV-ING in Germany [5]) as the basic documents for the authorities
- lack of basic knowledge regarding the behavior of HDG components under cyclic loading

- little motivation within the regulating authorities to change existing rules for corrosion protection systems
- prejudices regarding the pricing (initial and life cycle costs) in comparison with organic coating systems
- prejudices against galvanizers regarding the execution quality, process control and documentation on a technical very high level as an indispensable requirement for suppliers in the bridge industry, especially against the background of cracking problems on large steel structures related with HDG in the early 2000s.
- bridge market is strongly ruled by concrete solutions over the last decades
- weak lobby for steel and no lobby for HDG in the bridge market
- non-affinity of current national steel bridge construction principles (e.g. welding of complete steel structure) with HDG construction principles (HDG of pre-fabricated components and bolting them together)

Now, in recent years the galvanizing industry woke up, faced the challenges and started creating solutions in close cooperation with the steel industry to enter the bridge market. As part of a research project [2], the technical basics of the behavior of hot-dip galvanized components under cyclic loading were examined on the basis of typical, bridge relevant notch details and appropriate solutions for the fatigue design of galvanized bridge components were created. Comparative cost and sustainability analyzes have demonstrated the competitiveness and even superiority of hot-dip galvanizing over existing corrosion protection systems, counteracting prevailing prejudices. In a guideline, these results, together with practical instructions and recommendations, have been prepared in such a way that they serve both the authorities and the planning engineers as a valuable basis for future applications [6].

Table 1. Distribution of bridges in Germany

	Road Bridges	Railway Bridges	Pedestrian/Cycling Bridges
Quantity	~ 118,000	~ 25,000	~ 90,000
• under local authority	~ 67,000		
• under federal and states authority	~ 51,000		
Short and mid span	~ 80%	~ 90%	~ 100%
Steel / composite structure	~ 15% (ascending trend for new constructions)	~ 50 %	unknown

Market experience shows that the focus on small and medium span bridges is effective for the application of hot dip galvanizing, especially in combination with hot-rolled sections:

- biggest market segment concerning the quantity of bridges (see Table 1),
- good compliance of geometrical limitation of HDG with components' dimensions (no need or very limited need of site welding leads to cost efficient solutions),
- smaller projects which are easier to handle,
- simple geometries lead to good, easy and quick handling resulting in high economic competitiveness,
- typified construction methods in this market segment including HDG offer the potential for a broad dissemination based on successful initial projects.

2. Conception for the design of hot-dip galvanized bridge components

2.1 Fatigue design

Hot dip galvanizing has been known in building construction for decades as a high performing, permanent corrosion protection. The decisive difference between bridge construction and predominantly static loaded building construction lies in the cyclic loading of bridges caused by traffic loads, which may require fatigue checks according to EC 3-2 (EN 1993-2 [7]) in combination with EC 3-1-9 (EN 1993-1-9 [4]). This check is performed by a classification of the construction into detail categories, which are assigned in the standard corresponding notch cases. Although the standard does not provide a distinction between the surface conditions (galvanized or non-galvanized) of the design details, the fatigue tests on which the standard is based have generally been carried out with non-galvanized specimens. Thus, the scientifically secured assessment basis for the execution of galvanized bridge structures was missing so far. To provide proof for hot-dip galvanized components, research projects have been carried out in recent years and the results of detail categories on common construction details for bridges of small and medium spans were derived [2] [8]. These were obtained by experimental tests on small-scale specimens in a direct comparison with zinc-free specimens and on component-like test specimens as well. The test results were statistically evaluated according to the methods and background information of Eurocodes 3.

The comparison of the experimental results of hot-dip galvanized and non-galvanized specimens shows that hot-dip galvanization has an influence on the fatigue resistance of the details investigated. Exemplary, the results of comparative fatigue tests of small samples, classified to the detail category 125, according to EN 1993-1-9 [4] in non-galvanized state, are shown in Fig. 2. The evaluation of the test results according to the background document of EN 1993-1-9 [4] proofed the detail category of 125 for the non-galvanized specimens, represented as black dots, but the hot-dip galvanized samples, shown as red triangles, had to be classified one detail category lower at category 112.

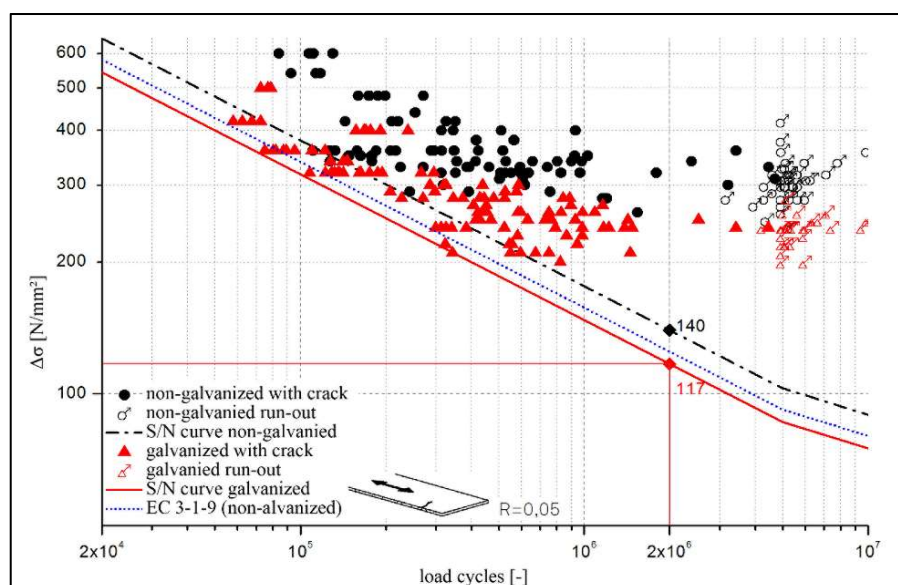


Figure 2: Comparison of non-galvanized (detail category 125) to hot-dip galvanized small-scale specimens [2]

Summarizing the assessment of these results, it can be concluded as a rule of thumb that the detail categories for low notched details ($> \text{FAT } 80$) of galvanized members must be reduced by one category. For details in categories lower than 80 the results indicate that the metallurgical and geometrical imperfections generally dominate the fatigue resistance and the galvanization might lose impact on the fatigue strength.

2.2 Structural design

Regarding the galvanizing of bridge components HDG-process-specific aspects have to be taken into account and constructional adjustments are necessary. Basically, the construction must be designed to withstand the galvanizing process to guarantee a good galvanizing quality, using the principles given in EN ISO 14713 [9]. For instance, draining and ventilations holes have to be provided in sufficient number and size. To avoid unwanted warping by the interaction of fabrication-related and thermal residual stress states the recommendations of [9] and [10] have to be considered as well as the rules and recommendations to avoid critical states with regard to liquid metal-induced stress corrosion cracking [11] [12].

Further, it should be noted that the application of the zinc coating is carried out by immersing discrete members in a zinc melt. Accordingly, the size and weight of the segments have to match with the zinc bath size and the crane capacity of the HDG facility. Currently, segment lengths of 16 m would be possible to handle in many shop galvanizing facilities in Europe, up to 19 m as single dip in few facilities. Against this background, in the target market of small and medium span bridges regular site joints might be necessary.

2.3 Choice of steel and zinc layer thickness

To ensure the durability of the structure over the life time, appropriate measures have to be provided. In the case of hot dip galvanizing the reduction of the zinc layer thickness, which is caused by the active reaction of zinc with the atmosphere which leads to a minimal but steadily erosion of the zinc layer, must be taken into consideration. The theoretical calculation of the durability of the zinc layer, mainly depending on the zinc layer thickness, the zinc alloy and atmosphere specific corrosion rate, could be carried out by using the non-linear approach acc. to ISO 9223 [13]. Based on this method, the durability of a 200 μm thick zinc layer in C4-atmosphere is more than 83 years, when calculating with the maximum zinc loss rate of 4.2 $\mu\text{m/a}$ and more than 116 years, when calculating with the mean zinc loss rate for C4 of 3.15 $\mu\text{m/a}$.

$$\sqrt[b]{\frac{D_{tZn}}{r_{\text{corr,tZn}}}} = t = {}^{0,873}\sqrt{\frac{200\mu\text{m}}{3.15\mu\text{m/a}}} = 116.1 \text{ years}$$

Based on this theoretical approach and taking into account that air pollution has decreased significantly over the last decades and will further do in the context of ongoing measures of environment protection, a zinc layer thickness of 200 μm is considered to be the target value to reach a maintenance-free bridge service life of 100 years. Therefore, a steel should be used with a silicon content in the range of $0.14 \leq \text{Si} \leq 0.35\%$ and a phosphorus content $\text{P} \leq 0.035\%$. Aluminum should be limited to $\text{Al} \leq 0.035\%$. Not only theoretical calculations, but already implemented projects, especially in North America and Japan and few in Europe, confirm the maintenance-free, long-term service life of galvanized bridges as well.

3. Selection of most economical steel profile

Common practice is to optimize the steel sections depending on the loads and construction phases, resulting in composite bridges with asymmetric steel sections with narrower and thinner upper flanges and wider thicker lower flanges. Occasionally, the cross-sectional height also changes due to variation of the web height. In this way, the amount of steel used is kept minimal. In rolled sections, changes in cross section along the longitudinal axis can generally only be achieved by adding reinforcing plates on the flanges or welding plates into the web. In general, however, the designer is bound to the geometric properties of the rolled standard products. But due to its maximum height of up to 1,138 mm, it makes sense to use rolled sections for bridges with span lengths up to about 40-45 m (slenderness $L / 30$). In this case, rolled sections may be a few percent heavier than optimized built-up sections, if the same steel grade is used.

In Europe, welded beams for small and medium span bridges are usually made from standard plates in steel grade S355. The use of plates with higher strength is not common for small and medium span bridges. On the other hand, the use of hot-rolled sections in S460 is well established in European practice and is advantageous for road bridges since the high strength can lead to weight savings in the construction of the structure. Further, when the higher strength profiles are thermo-mechanically rolled and optionally produced by the QST-process-(Quenching and Self-Tempering) [14] [15], the low carbon equivalent of the steel components results in improved weldability of the material. For welded beams, in addition to the fillet welds between the flanges and the web, every 12-18 m butt weld joints of the plates or plated beams are required (either in the workshop or on the construction site). For long products such as rolled sections, neither fillet welds nor butt weld joints up to a component length of up to 40 m are required. In addition to the reduction in processing costs, any capacity bottlenecks in steel fabricators' workshops can be circumvented and thereby delivery times can be shortened. Because of the benefits of weight savings and simplified manufacturing, rolled sections in high strength steel grade (HSS) are being used more and more frequently as the more economical alternative to welded built-up sections.

4. Beneficial combination of hot-rolled sections with hot dip galvanizing

In particular in combination with hot-dip galvanizing hot-rolled sections offer additional advantages that further enhance the benefits of both technologies. Regarding the process-sided handling, the homogeneous hot-rolled profiles fit very well to the galvanizing process, where they are completely and uniformly coated with zinc by immersion into the liquid-hot zinc melt. Hot dip galvanized hot-rolled sections have an optically homogeneous appearance due to uniform layer growth, since the chemical composition in the web and in the flanges is uniform. In the case of welded built-up sections the unavoidable use of different materials may lead to differences in appearance and zinc layer thickness. In contrast to applications of coating material by means of spraying or painting, this full shop application method offers by far higher quality of execution and safety, matching the corresponding quality of the profiles. In addition, since rolled beams are produced without welding work, there are no residual welding stresses and the risk of welding-induced distortion, both in steel construction production and galvanizing, is excluded per se. From an economic point of view, not only the elimination of welding costs, but also of straightening work which could be necessary to correct for possible distortion effects, is beneficial in case of hot-rolled sections.

Before hot-dip galvanizing, the structure should be prepared according to preparation grade P3 in accordance with EN ISO 8501-3 [16]. For example, untreated thermally cut edges and surfaces are inadmissible and all cut edges must be rounded with a minimum radius of 2 mm. In addition, thermally cut surfaces must be removed mechanically a few tenths of a millimeter (at least 0.5 mm), otherwise the zinc deposit on the cut surfaces is defective. This means that all cut surfaces in the longitudinal direction on the flanges of welded built-up sections must be ground. Additional blasting of the cut surfaces can improve zinc deposit. The rounding and grinding of edges and surfaces of rolled sections is not necessary. For this, the preparation grade P2 is sufficient. This eliminates a costly grinding when using rolled sections as main girders, which hereby sets an ideal combination. If the load-bearing steel structure for a bridge is to be hot-dip galvanized, the use of rolled sections for production and cost reasons is to be preferred.

For the project realization in bridge construction, the system "hot dip galvanized hot-rolled sections" benefits that the engineers and executing companies already gained experience from applications in building construction with the material as well as the planning and processing principles, e.g. are familiar with the aspects of galvanizing design. This aspect is also helpful regarding the necessary persuasive work with authorities for the new combination in bridge projects. Here, the high planning and implementation safety, which is based on simple design principles and normatively clear rules, e.g. defined and proven detail categories, is of advantage, so that potential changes compared to the original

planning without galvanized components are limited and fewer problems with authorities are to be expected.

In terms of the assembly process, the very high robustness and resistance of the galvanizing is highly beneficial. The zinc coating resists the mechanical stresses which usually occur during transport and assembly without damage to the coating. In contrast, transport and assembly-related damage are inevitable in organic coating systems. The resulting repair work leads to sometimes very high additional financial costs as well as to time delay. Thus, the use of galvanized components saves time and costs and is therefore in line with the principles of steel and composite construction in terms of short construction times.

5. Elster bridge Osendorf – example of a new bridge type using galvanized hot-rolled sections

Although hot dip galvanizing as corrosion protection for load-bearing bridge components is currently not included in the German specification standards such as ZTV-ING [5] as a generally approved system, the first successfully executed bridge projects show the feasibility. The Elster-Bridge Osendorf is the worldwide first “PreCoBeam” bridge with hot-dip galvanized steel structure. This bridge combines the economic and ecological advantages of prefabricated composite beams (PreCoBeams) with composite dowel strips with those of hot-dip galvanizing. It therefore results in an extremely economic construction, both in production and in service life. The bridge is located in Saxony-Anhalt (D) southeast of Halle in the district Osendorf and transfers a rural road across the Weisse Elster to a nature reserve. The single-span frame bridge with twin-girder cross-section and a span length of 21 m (see Figure 3) replaces an old three-span structure that was damaged by a flood.

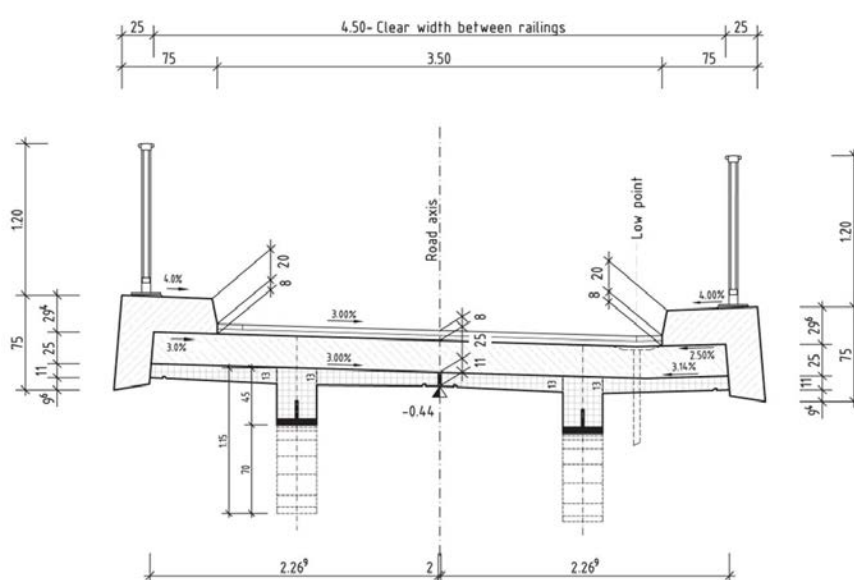


Figure 3: Cross-section with two PreCoBeams and in-situ concrete (© SSF Ingenieure AG) [17]

The rolled sections (HD320x300, steel grade S355ML) cut into halves with the typical modified clothoid dowel shape [18] are used as an external reinforcement of the T-beams. After flame cutting in the ArcelorMittal beam finishing center “Eurostructures” the edges and surfaces of the steel teeth were ground. The halved beams were subsequently cambered by cold forming with a depth gauge of 1.08 m, which could still be measured without changing after galvanization. The construction depth is 0.70 m in mid-span and 1.40 m at the abutments of the bridge, resulting in a slenderness of $l/30$ respectively $l/15$.

For reasons of transport and because of the limited length of the zinc kettle, the 20.38 m long halved beams were divided in length, resulting in a total of four T-shaped sections. Each profile received two holes $\varnothing 25$ mm in the steel dowels as a suspension option for galvanizing. The galvanizing was carried

out according to EN ISO 1461 [19] and DAST-Guideline 022 [11] close to the construction site at the ZINQ Group's galvanizing facility in Landsberg/Halle. The necessary length of immersion time was derived from preliminary tests, so that finally a mean layer thicknesses of at least 350 μm could be measured on the flange bottoms of the four rolled profiles (see Figure 4). These thicknesses ensure a theoretical corrosion protection period of > 100 years (see 2.3). The cut surfaces of the dowel geometry gained significantly lower layer thicknesses. As they are finally completely enclosed in concrete, this has no adverse effects in terms of durability (corrosion), but has a positive effect on the fatigue behavior. The thicker the zinc layer thickness the more the negative influence on the fatigue strength.



Figure 4: Cooling of galvanized beams [17]

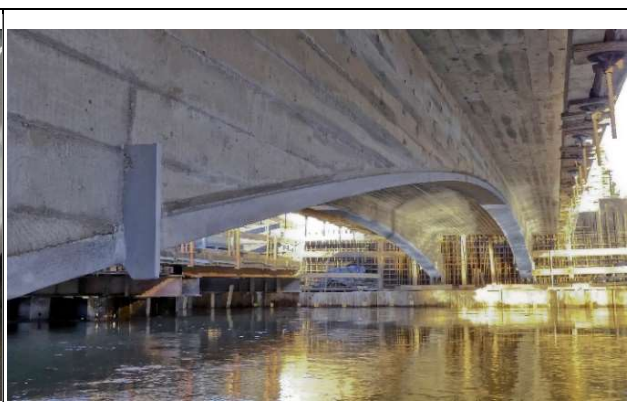


Figure 5: PreCoBeam in final position before adding in-situ concrete for the slab (© SSF Ingenieure AG) [17]

After hot-dip galvanizing each two 10.2 m long pieces had to be connected again to one beam by welding. To avoid high efforts to remove zinc around the intended site joints, the areas close to the weld preparation were protected by a special lacquer before galvanizing. Thus, zinc deposit could be prevented. According to the procedure [6] [20], which was developed for site joints of galvanized bridge components, at first residues of the lacquer at the beam ends were removed, subsequently the joints were welded and the weld seams ground flush. The areas around the joint were blasted, spray-galvanized with ZnAl15 and sealed.

After pouring the concrete of the PreCoBeam into the prepared formwork and hardening of the concrete, the prefabricated beams with external reinforcement were lifted in place. Finally, the deck slab was completed by in-situ concrete (Figure 5). The bridge construction was completed in 2017 and released for traffic.

References

- [1] Deutsches Institut für Urbanistik (DIfU), „Ersatzneubau Kommunale Straßenbrücken,“ Berlin, 2013.
- [2] D. Ungermann, D. Rademacher, M. Oechsner, R. Landgrebe, J. Adelman, F. Simonsen, S. Friedrich und P. Lebelt, „Hot-dip galvanizing for steel and composite bridges , IGF-No. 351/ZBG, FOSTA P835,“ Düsseldorf, 2014.
- [3] BAST – Bundesanstalt für Straßenwesen, „Salzablagerungen auf Korrosionsschutzbeschichtungen an Brückenuntersichten,“ Bergisch Gladbach, 1983.
- [4] EN 1993-1-9, *Eurocode 3: Design of steel structures - Part 1-9: Fatigue*, Brussels: European Committee for Standardisation, 2010.
- [5] BAST – Bundesanstalt für Straßenwesen, „ZTV-ING Stahlbauten: Zusätzliche Technische Vertragsbedingungen und Richtlinien für Ingenieurbauten - Teil 4: Stahlbau, Stahlverbundbau

- (ZTV-ING),“ Verkehrsblatt-Verlag, Dortmund, 2017.
- [6] D. Ungermann, D. Rademacher, T. Pinger und O. Hechler, „Guideline for Hot-Dip Galvanized Components in Steel and Composite Bridge Constructions,“ bauforumstahl e.V., Düsseldorf, 2017.
- [7] EN 1993-2, *Eurocode 3: Design of steel structures - Part 2: Steel bridges*, Brussels: European Committee for Standardisation, 2010.
- [8] D. Rademacher, „Zur sicheren Anwendung feuerverzinkter Bauteile im Stahl- und Verbundbrückenbau (On the safe application of hot-dip galvanized components in steel and composite bridges),“ Dissertation, Lehrstuhl Stahlbau, TU Dortmund, 2017.
- [9] EN ISO 14713, *Zinc coatings - Guidelines and recommendations for the protection against corrosion of iron and steel in structures*, Brussels: European Committee for Standardisation, 2009.
- [10] T. Pinger, „Thermodynamische Effekte beim Feuerverzinken und deren Beherrschung (Thermodynamic effects during hot-dip galvanizing and their control),“ *Konstruktion*, pp. 62-67, 6 2013.
- [11] Deutscher Ausschuss für Stahlbau, *DAST-Richtlinie 022: Feuerverzinken von tragenden Stahlbauteilen*, Düsseldorf: Stahlbau Verlags- und Service GmbH, 2016.
- [12] T. Pinger, „Zur Vermeidung der Rissbildung an Stahlkonstruktionen beim Feuerverzinken unter besonderer Berücksichtigung der flüssigmetallinduzierten Spannungsrisskorrosion (On the avoidance of cracking in steel structures due to LME during hot-dip galvanizing),“ Dissertation, Institute of Steel Structures, RWTH Aachen University, 2009.
- [13] EN ISO 9223, *Corrosion of metals and alloys – Corrosivity of atmospheres – Classification, determination and estimation*, Brussels: European Committee for Standardisation, 2012.
- [14] ArcelorMittal Europe - Long Products, „HISTAR product brochure,“ 2017. [Online]. Available: <http://sections.arcelormittal.com/library/product-catalogues.html>.
- [15] DIBt - Deutsches Institut für Bautechnik, *ETA-10/0156 Long products made of HISTAR 355/355L und HISTAR 460/460L*, Berlin, 2015.
- [16] EN ISO 8501-3, *Preparation of steel substrates before application of paints and related products - Visual assessment of surface cleanliness - Part 3: Preparation grades of welds, edges and other areas with surface imperfections*, Brussels: European Committee for Standardisation, 2007.
- [17] G. Seidl, A. Danders, F. Gunkel, D. Rademacher und T. Pinger, „Elster bridge Osendorf - a hot-dip galvanized composite bridge with external reinforcement,“ *Stahlbau*, 2 2017.
- [18] DIBt - Deutsches Institut für Bautechnik, „Allgemeine Bauaufsichtliche Zulassung (AbZ) Z-26.4-56: Verbunddübelleisten (composite dowel strips),“ Berlin, 2013.
- [19] EN ISO 1461, *Hot dip galvanized coatings on fabricated iron and steel articles - Specifications and test methods*, Brussels: European Committee for Standardisation, 2009.
- [20] P. Lebelt und J. Gehrke, „Korrosionsschutztechnologie für Montageschweißstöße einer feuerverzinkten Stahlbrücke,“ *Stahlbau*, Bd. 86, Nr. 2, pp. 191-196, 02 2017.

Author Biographies

Dr.-Ing. Dennis Rademacher, SFI/IWE

University degree in civil engineering

Research Associate at TU Dortmund University

Focus on research on hot-dip galvanized bridge structures

International Welding Engineer

PhD at TU Dortmund University

Since 2015 Head of Development and Technical Advisory – Bridges at ArcelorMittal Europe – Long Products, Luxemburg. Focus on application of hot-rolled sections in bridges.

Dr.-Ing. Thomas Pinger, SFI/IWE

University degree in civil engineering

Research Associate at University of Kaiserslautern and RWTH Aachen University

Focus on research on LME related cracking of hot dip galvanized structures

International Welding Engineer

PhD at RWTH Aachen University

Since 2008 at ZINQ-Group in Gelsenkirchen, Germany, since 2013 Head of R&D, dealing with the full range of HDG related topics, especially focus on optimization of zinc layer performance, application techniques and fields of applications.

Session 3:

Innovative Applications of Galvanizing in Steel Construction

Fire resistance of galvanized structures

C. Gaigl & M. Mensinger, Chair of Metal Structures, Technical University of Munich, Munich, Germany

ABSTRACT:

Once a fire resistance rating is necessary, it has to be proofed that the load bearing behaviour of a steel construction under the exposure of fire still fits the static demands. High costs of passive fire protection can be avoided by determination of the critical failure temperature of the steel structure according to the Eurocode DIN EN 1993-1-2.

For this purpose, positive effects of hot dip galvanized surface layers on the temperature development of steel members in the accidental situation of fire exposure has been investigated. The test results show a significant better heating behaviour of hot dip galvanized steel components compared to steel specimen without galvanization. This leads in many cases to a R30 fire resistance of the unprotected steel sections, which means that the hot dip galvanized members are able to withstand 30 minutes of ISO-fire according to EN 13501-2 without failure.

Economic relevance

The high costs of passive fire precautions, for example, intumescent paints, are a huge economic disadvantage of steel and composite structures compared to simple concrete constructions. Hot dip galvanization constitutes an economic and efficient way to permanently protect steel members from corrosion. It has been used successfully for many decades, especially in the area of steel buildings and recently in steel bridge constructions. When hot dip galvanization additionally can contribute beneficially to the fire resistance of unprotected steel members, it will be a huge economic advantage.

Fire scenario & ISO fire curve

The typical development of a fire is given in Figure 1. The vertical axis represents the temperature whereas the horizontal axis represents the different phases of a fire. At the beginning, there is the slow ignition and smoldering phase. Subsequently, the full fire phase is transited, accompanied by a sudden flashover and a corresponding increase of temperature. Afterwards, the cooling phase begins and the fire subsides. The intensity and duration of each phase vary strongly and depend on several influence factors like the type, quantity, and distribution of the fire loads in the surrounding.

To simplify, unify and to compare the fire behaviour of building materials and components, the standard temperature-time curve was introduced (Figure 1). The curve itself starts just before the full fire phase. Hence, the temperature rises rapidly within a few minutes. For example: after 30 minutes of the normative fire, a room temperature of about 842°C is reached.

Heat transport mechanisms

The exchange of thermal energy between objects depends on their temperatures and the properties of the intervening transportation medium.

Within a fire, the heat is distributed by three transport mechanisms: conduction, convection, and radiation. Heat conduction depends on molecular activities and is the energy flow without particle transport, for example, the heat transfer in a solid body. The second mechanism is the convection. The heat is thereby distributed by a flow respectively a particle transport in fluids (e.g. liquids, gases). The third one is electromagnetic radiation, which is the most important mechanism for this research (Figure 2).

Radiation

The heat transfer by conduction and convection is bound to matter. In contrast, solid and liquid bodies, as well as a number of gases emit heat also by radiation, which is not bound to matter. The same applies

to the heat absorption. Heat rays appear as electromagnetic waves, which are different from light beams only by their mostly larger wavelength. While the electromagnetic waves of visible light include a wavelength range from 0.35 to 0.75 μm , the wavelength range of the heat radiation extends from 0.3 to 100 μm and are therefore in the infrared region.

Emissivity

Any object with a temperature above absolute zero emits thermal radiation and therefore exchanges heat with its environment. The emissivity ϵ is a measure of how much a material emits and absorbs the heat radiation in and of its environment. According to Kirchhoff's radiation law, from the second law of thermodynamics on the emissivity of a radiating body, the ratio of the emittance to the absorbance at a given wavelength and temperature for any radiant heater is equal. This can be expressed in a simplified way by the sentence: A good absorber of heat radiation is also a good emitter.

The emissivity of an arbitrary body indicates how much radiation it emits in comparison to an ideal thermal radiator, a so-called black body. A black body radiator absorbs any electromagnetic radiation and thereby also emits maximally at any temperature and for each wavelength. The maximum value of the emissivity is thus $\epsilon = 1.0$.

The radiation emitted by a body is generally spread over a wide wavelength range. Following characteristics can be distinguished with regard to the intensity of the emitted radiation. For this purpose a body can be called:

- | | |
|-----------|--|
| Black | if the body emits the maximum possible radiation energy at his temperature at any wavelength |
| Grey | if the body emits the same fraction of the maximum amount in all wavelengths (= value of emissivity) |
| Selective | if the body only radiates in some wavelength ranges, but not in others. |

In figure 4 one can see this coherence.

Fire behaviour of building components

Building materials are assessed by their influence on a fire due to their decomposition and therefore their flammability. Steel and concrete are non-combustible materials. Even when they do not burn, their material properties change with an increasing temperature. As early as about 100 $^{\circ}\text{C}$, the modulus of elasticity of steel starts to decrease and from about 400 $^{\circ}\text{C}$, the yield point decreases as well. Concrete loses its strength at lower temperatures. However, due to steel's higher thermal conductivity, steel structures heat up much faster.

Building components, respectively structures, have to maintain certain functions over a prescribed period in the event of a fire. A number of criteria are defined in DIN 13501-2. For load-bearing members the following three criteria are of interest:

- *R* – Load-bearing capacity (The period of time that structural elements are able to carry its loadings)
- *E* – Integrity (The duration that the structural element retains its integrity against flames or/and hot gases in a fire)
- *I* – Insulation (The time it takes to engender an increase in temperature on the other side of the structural element)

The Eurocode DIN EN 13501 defines different levels of fire protection requirements. Many office buildings in Germany have usually a minimum requirement of *R30*, which means that the load bearing structures have to resist 30 minutes of fire.

Structural fire design of steel structures according to Eurocode

Three levels are available in the Eurocodes for the fire design to prove the criteria R (load-bearing capacity) of a component. The project focus on the second level, which is a calculation method with two different ways to prove the remaining load bearing capacity.

One way is to determine the load-bearing capacity at a specific time in this undesirable event. This design format basically corresponds to the usual approach of the Eurocode at ambient temperature. The design value of the governing loads in the event of fire must be at any time not greater than the corresponding design value of the capacity of the steel members in a fire situation. Alternatively, it can be shown that the steel temperature of the member during the fire does not exceed the critical temperature. This is the temperature in the member, wherein the strength (or stiffness) of the steel dropped to a point where the ultimate limit state is reached. This approach is shown in the following.

For an equivalent uniform temperature distribution in the steel cross-section, the increase of temperature $\Delta\theta_{a,t}$ during a fire in an unprotected steel member within a time interval Δt can be determined by following equation of the Eurocode:

$$\Delta\theta_{a,t} = k_{sh} \frac{A_M/V}{c_a \rho_a} \dot{h}_{net} \Delta t \quad (1)$$

On the one hand, the heating is strongly influenced by the section factor (A_M/V -value), which means the relation of the surface to the volume of the member, and on the other hand by the value of the net heat flux.

As mentioned, the heating of unprotected steel members in fire depends on energy transfer by convection and radiation. Both are included in the net heat flux \dot{h}_{net} :

$$\dot{h}_{net} = \dot{h}_{net,c} + \dot{h}_{net,r} \quad (2)$$

$$\dot{h}_{net,c} = \alpha_c (\theta_g - \theta_a) \quad (3)$$

$$\dot{h}_{net,r} = \phi \cdot \epsilon_m \cdot \epsilon_f \cdot \sigma \cdot [(\theta_g + 273)^4 - (\theta_a + 273)^4] \quad (4)$$

By analysing the last two equations, radiation dominates the heating process due to the fourth power in case of a large difference between the gas and the steel member temperature and convection dominates the heating in case of a small difference. It can be seen that the values of the emissivity of the flames ϵ_f and more important, of the surface ϵ_m are an important variable with a large influence on the radiation part of the net heat flux.

For a member with the $R30$ requirement and a small A_M/V -value, it is thus of interest, when a lower value of emissivity of the section surface offers some benefits to the fire design of the member.

Fire resistance of hot-dip galvanized steel members

The heat flux from radiation highly depends on the hemispherical emissivity of the member. The bigger the difference between the temperature of the fire and the member, the larger is the influence of the emissivity (Equation 4). Therefore the emissivity has a large influence on the heating of a steel member at the beginning of a fire and this especially applies to members with small section factors (A_M/V -values), due to their slower heating. At later stages of a fire the structural members are mainly heated by convection and thus the influence of the emissivity of a member's surface is of minor importance.

As a consequence, the smaller the emissivity of the surface, the slower the heating develops. At this point, galvanisation can help to influence the emissivity of a steel member.

Radiation of metal surfaces is based on atomic and molecular vibrations, depending on the chemical composition in a small layer with a thickness of about 0 to 10^{-10} m [Sala (1986)]. The radiation behaviour of galvanized surfaces, with a thickness of 50 to $200 \cdot 10^{-6}$ m, is hence almost exclusively provided by the zinc layer.

The emissivity depends on several surface characteristics and thereby to a decisive extent on the chemical composition, the roughness and as well on the degree of oxidization. It is thus a variable depending on the temperature. With respect to this, different galvanized surfaces with different weathering conditions had to be tested to gain an optimized statement of realistic values of the emissivity of such surfaces.

Emissivity measurements of HDG steel at elevated temperatures

For this research, samples ($d=50$ mm; $t=10$ mm) with two different types of steel categories: category A, the lower silicon content range ($\leq 0,04\%$ Si), and category D, a higher silicon content ($> 0,25\%$ Si) have been tested, as shown in Figure 3. The resulting thickness of the different zinc layers are given in the Table 1. The measured values coincide with the different layer structures and agree with the known iron-zinc layers in literature [Schulz & Thiele (2012)]:

In this approach, the temperature dependent emissivity was determined by comparing the temperature of the specimen, measured with thermocouples (TC), with the measured temperature by infrared sensors and simultaneously adjusting their emissivity. To get a precise statement of the behaviour of HDG-steel at elevated temperatures a range of 20°C (room temperature) till 850°C was observed. The exact setup of the so-called "small-scale tests" is described in [Gaihl & Mensinger (2017)].

As mentioned before, emissivity depends on several surface characteristics and thereby to a decisive extent on the surface texture, the chemical composition and as well on the degree of oxidization. All these factors had to be considered to make reliable statements about hot-dip galvanized steel specimen under the impact of elevated temperatures.

As shown in Figure 5 and Figure 6, the zinc-iron alloy layers have a big influence on the emissivity value. Looking at Figure 5 one can see, that the emissivity values (≈ 0.35) at lower temperatures are smaller than the given emissivity value of 0.7 by the Eurocode (red line). The curve increases two times, first at about 419°C (resistance level of the η -phase / melting point of the pure zinc) and second at about 530°C (resistance level of the ζ -phase). In the end, the emissivity $\varepsilon = 0.65$ and therefore still smaller than the comparative value. The exact emissivity values at different temperature stages depend on the specific surface texture. The specimens, which have been stored outside exhibit about 5-10% higher values than "indoor" samples of the same category. Nevertheless, each emissivity value from ambient room temperature till 750°C of the steel sample is better than $\varepsilon_{\text{EC}} = 0.7$, given by the Eurocode. A reason for the different values can be found, on the roughness of each surface. Surfaces with a higher level of white rust exhibit a higher roughness and as a consequence higher emissivity values.

Comparing the results of category A specimen (Figure 5) with category D (Figure) at about 530°C , the same effect, at the resistance level of the ζ -Phase, can be recognized. Nevertheless, one can see that the behaviour of the latter is worse but still better than the normative emissivity of 0.7. These different emissivity values can be led back to the various surfaces. The roughness-effect, for example, is again one reason why the values of the emissivity of category D surfaces are greater than the values of category A surfaces.

The influence of the thermal exposure can be seen on the surface and layer structure. It is an ongoing process during the heating, which transforms the different layers. The η -phase of category A, for example, coalesce with the surrounding oxygen and builds zinc oxide, but with increasing temperatures, further processes like diffusion as well as exchanges on molecular level take place in between the different alloy layers. After a temperature of 850°C , the known layer structure is transformed. With its new appearance and a distinct higher roughness on the surface, an increasing emissivity is accompanied.

Full-scale fire tests

To double check the findings of the small-scale tests, some full-scale fire tests have been made at the Technical University of Munich. Therefore various test specimen with different surfaces, like rusted, hot-dip-galvanized (category A & D) as well as blanc steel, were taken into account. The furnace test was performed according to the defined standard temperature-time curve of the Eurocode.

By comparing the heating of each specimen in the furnace with implemented thermocouples, with the forecasted temperature-time-curves, calculated with the different emissivity values of the small-scale tests for each specimen, the results could be confirmed. For each surface, a different heating behaviour was quantified. Because of this, it was possible to show that on the one hand the rusted surface behaved like the forecast of the Eurocode ($\epsilon_{EC} = 0.7$) and on the other hand each other surface with a different heating rate can be assigned to other emissivity curves.

Conclusion

The results show a much better behaviour of hot-dip galvanized (according to EN ISO 1461) steel elements in comparison to the given emissivity value of $\epsilon_{EC} = 0.7$ for carbon steel in the Eurocode EN 1993-1-2. Especially for steel members with a composition according to category A of EN ISO 14713-2 and for temperatures up to 530°C. The favourable effect influences the fire resistance positively and, depending on the steel section and the steel category, an R30 fire resistance requirement can be reached without additional passive fire protection.

ACKNOWLEDGEMENTS:

Special thanks to our supporters, especially: GAV, Kopf Holding, W. Pilling, Acelor Mittal, Max Bögl

REFERENCES

A. Sala, Radiant properties of materials: Tables of radiant values for black bodies and real materials, Elsevier; PWN Polish Scientific Publishers; distribution for the U.S.A. and Canada, Elsevier Science Pub. Co, Amsterdam, New York, Warsaw, New York, N.Y., 1986.

C. Gaigl and M. Mensinger, "Hot dip galvanized steel constructions under fire exposure," in IFireSS 2017, E. Nigro and A. Bilotta, Eds., pp. 557–564, Doppiavoce, Napoli, 2017.

C. Gaigl and M. Mensinger, "Thermal impact on HDG construction," TU München - Lehrstuhl für Metallbau, 2018.

DIN Deutsches Institut für Normung e. V., "DIN EN 1993-1-2:2010-12; Eurocode 3: Bemessung und Konstruktion von Stahlbauten – Teil 1-2: Allgemeine Regeln – Tragwerksbemessung für den Brandfall Deutsche Fassung EN 1993-1-2:2005 + AC:2009," 2010-12, DIN EN 1993-1-2:2010-12.

DIN Deutsches Institut für Normung e. V., "DIN EN 13501-2 Klassifizierung von Bauprodukten und Bauarten zu ihrem Brandverhalten – Teil 2: Klassifizierung mit den Ergebnissen aus den Feuerwiderstandsprüfungen, mit Ausnahme von Lüftungsanlagen; Deutsche Fassung EN 13501-2: 2016," 2016-12.

W.-D. Schulz and M. Thiele, Feuerverzinken von Stückgut: Werkstoffe - Technologien - Schichtbildung - Eigenschaften - Fehler, Leuze, Bad Saulgau, 2012.

FIGURES & TABLES

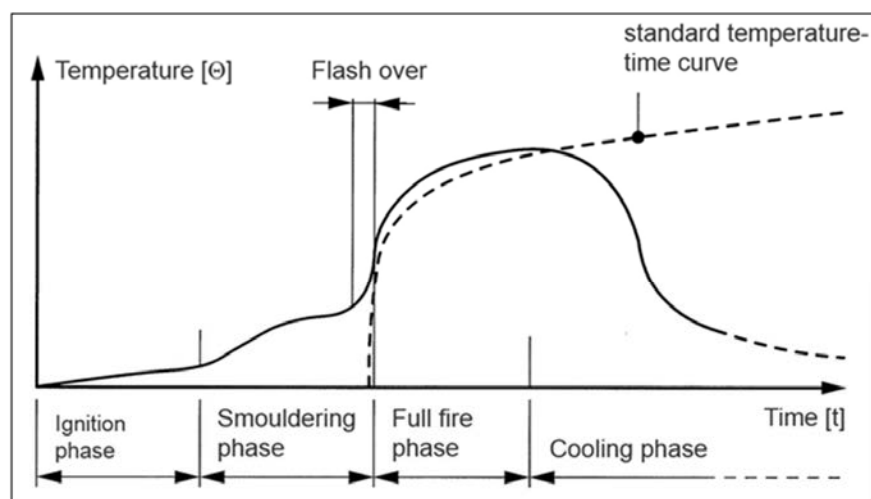


Figure 1: Typical fire progress & standard temperature-time curve according to EN 13501-2

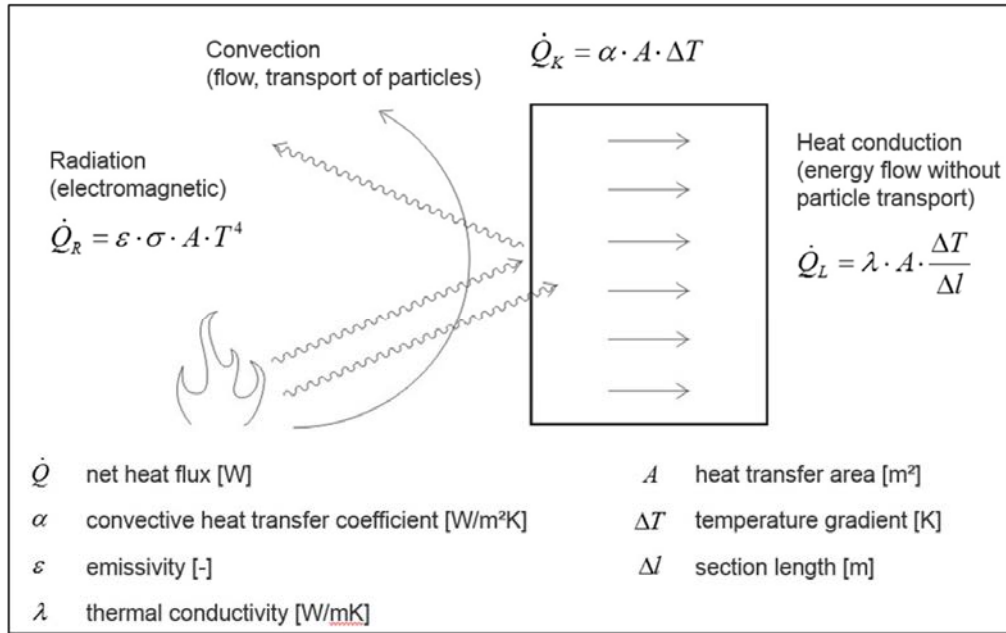


Figure 2: Heat transport mechanisms

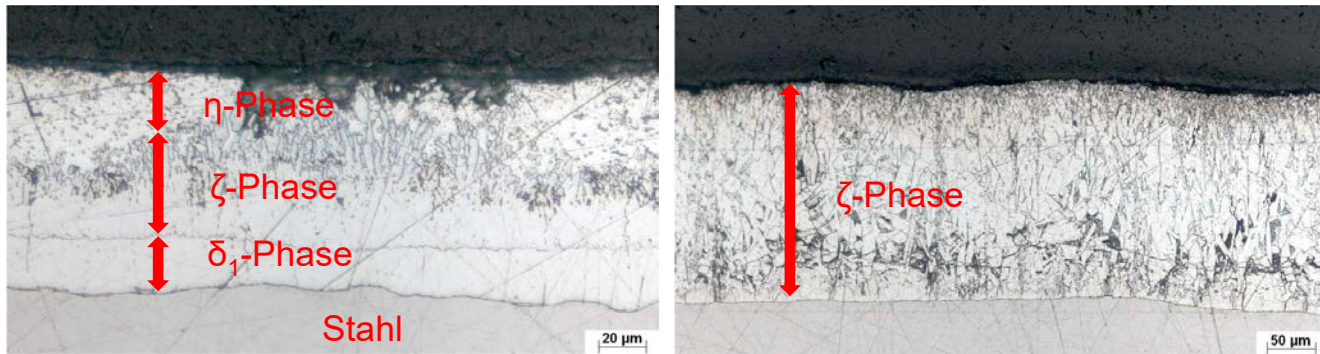


Figure 3: Micrographs of HDG alloy layers. Left: Category A; Right: Category D [Gaijl & Mensinger (2018)]

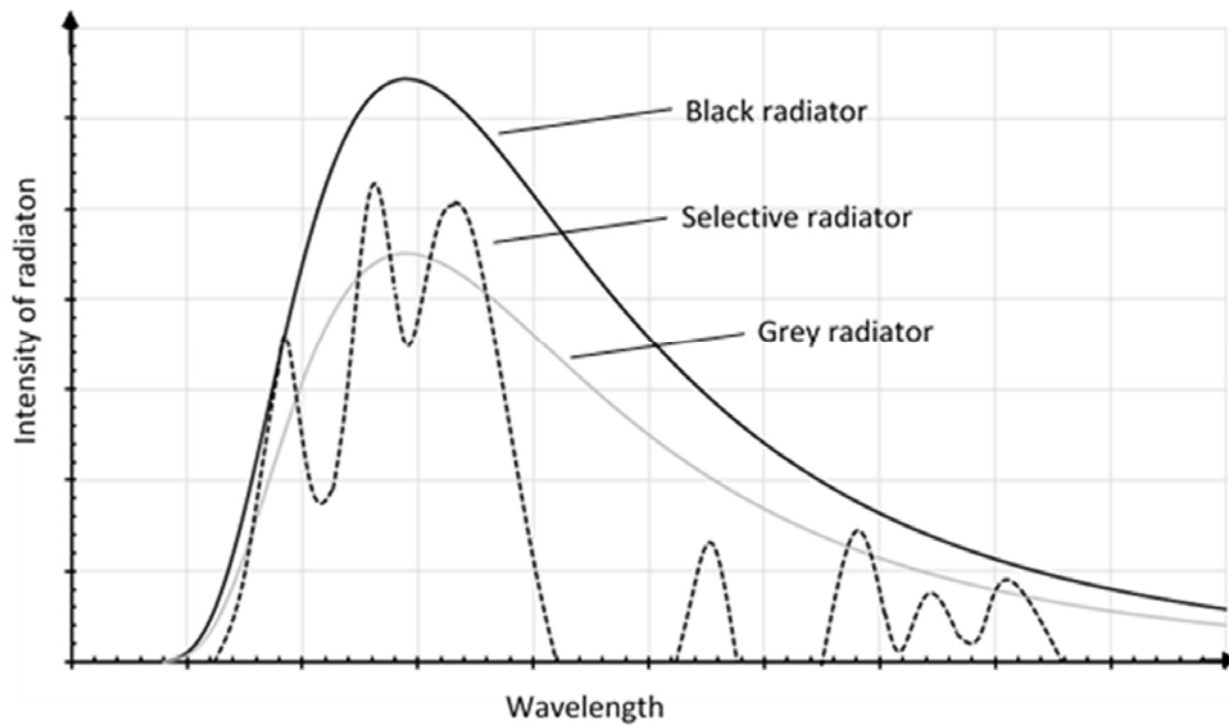


Figure 4: Radiation behaviour of different objects

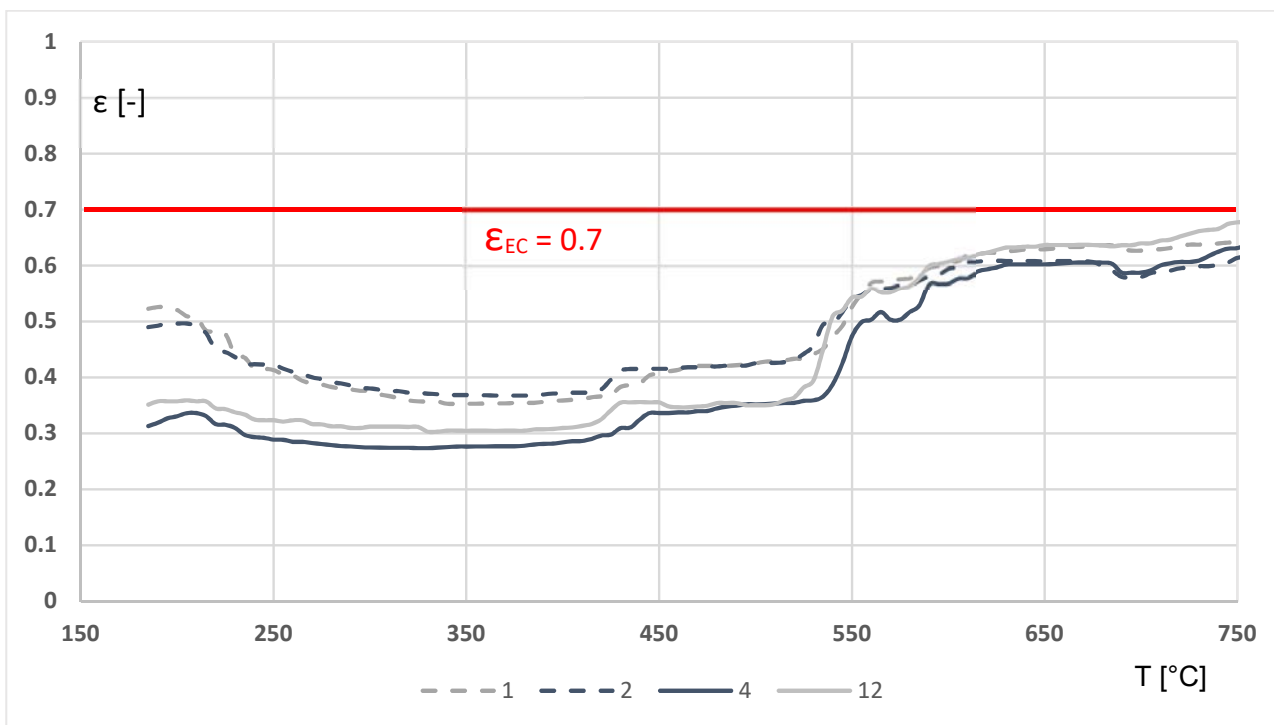


Figure 5: Emissivity curves – Category A (dashed: stored outside; lines: stored inside)

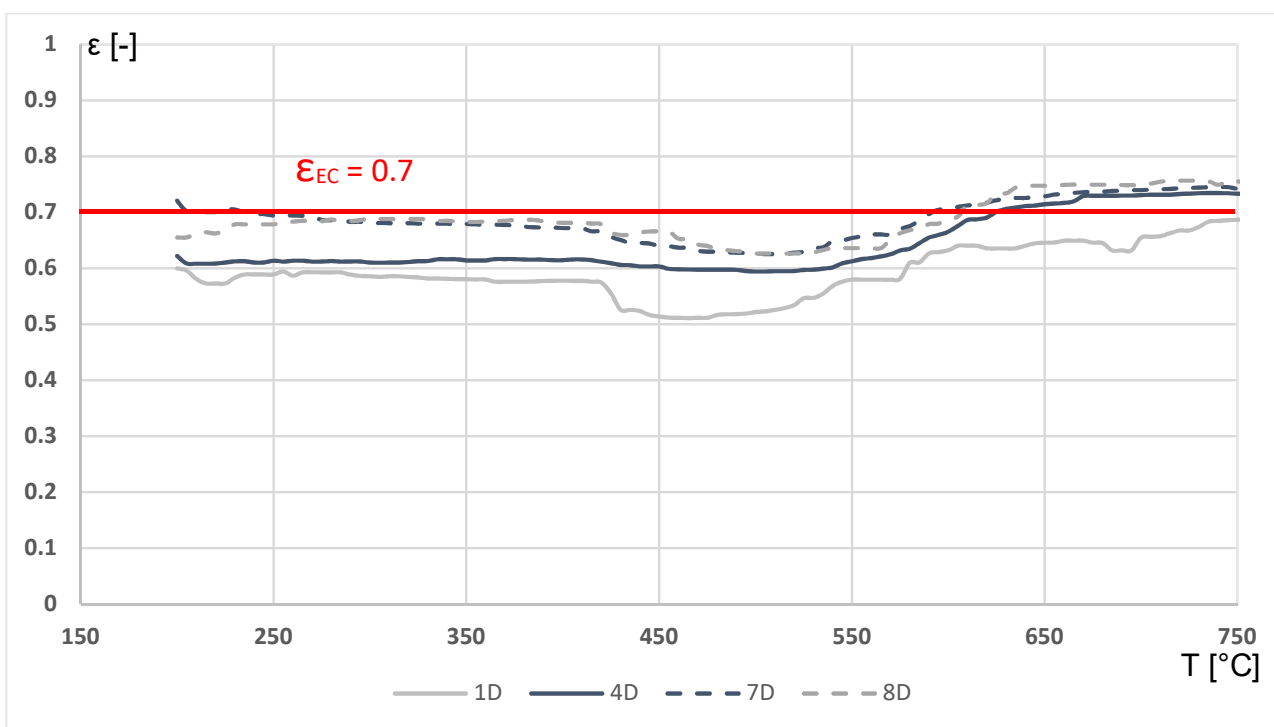


Figure 6: Emissivity curves – Category D (dashed: stored outside; line: stored inside)

Table 1: Thickness of the zinc coating of different specimen

Specimen Category	Average Thickness [μm]	Roughness (stored inside/outside) [μm]
A	88.0	9,85 / 12,28
D	179.3	15,12 / 17,03

Table 2: Thermal impact on HDG-steel specimen [Gaigl & Mensinger (2018)]

Category	Before thermal impact	After thermal impact
A		
D		

Author biography

Christian Gaigl, M.Sc. (TUM)

Christian Gaigl (* 1987) is a doctoral candidate at the chair of metal structures of Prof. Mensinger at the Technical University of Munich (TUM). He was awarded a B.Sc. and an M.Sc. degree from the TUM and graduated as a civil engineer in 2012. From 2012 until 2016, he worked as a structural engineer at Zilch + Müller Ingenieure in Munich. Afterwards, he started to do his doctorate at the chair of Prof. Mensinger in the area of fire design in steel structures.

Prof. Dr.-Ing. Martin Mensinger

Prof. Mensinger (* 1967) deals with questions of extreme influences on steel structures such as fire and explosion, with the robustness and stability of steel and aluminium structure, with questions of glass building and with the topic of the sustainable use of metallic materials in the construction industry.

After studying civil engineering at the Technical University of Karlsruhe and working as a structural engineer at the Phillip Holzmann AG, Neu-Isenburg, Prof. Mensinger did his doctorate at the chair of Prof. Bode at the University of Kaiserslautern about fatigue problems in composite bridges. At the same time, he was also active as a structural engineer in the systems and power plant construction at the Voss u. Kamb Partner GmbH in Kaiserslautern.

In 2001 he joined as a member of the Executive Board of the H. Wetter AG in Switzerland. From 2003, he worked as a lecturer and as a Director of the Institute for Building Technology at the Lucerne University of Applied Sciences and Arts. In 2006, he followed the call to the chair of metal structures at the Technical University of Munich.

He is a registered inspector and testing engineer for metal construction and after being a member of the board in the engineering office Büchting Streit AG in Munich, he founded his own engineering firm, Mensinger Stadler Ingenieure in Munich.

Steel Hybrid Onshore Wind Towers Installed with Minimum Effort

Slobodanka Jovašević, Mohammad Reza Shah Mohammadi, Carlos Rebelo

ISISE, Department of Civil Engineering, University of Coimbra, P-3004 516 Coimbra, Portugal

Abstract

With the increase for renewable energies demand, namely wind energy, the construction of more powerful wind energy converters (WEC) is a matter of great importance. More powerful converters require higher supporting towers. Height of the most commonly used steel tubular towers is limited by manufacturing and transportation logistics. The lattice tower instead of tubular steel towers appears as a possible solution. To overcome a large number of bolts as the major disadvantage of the lattice tower a new solution, which uses steel hybrid tower by assembling a lattice structure for the lower portion and a tubular tower for the upper portion is under investigation. The erection process for this type of towers is assessed and the viability of the hybrid support structure is investigated in respect to ultimate limit states and structural dynamic behaviour as part of the requirements in exploring the feasibility of the proposed concept. The cross sections are designed and optimized based on an iterative procedure, in which the aero-servo-dynamic loading was obtained in subsequent structural solutions aiming the minimization of total mass and number of joints. The lattice structure was designed using low-maintenance preloaded bolted connections and, for the members, new types of cross-sections. In this sense, the most effective geometry of the lattice portion of the tower is investigated in order to decrease number of connections and bolts. The sections used in lattice structure are built-up polygonal sections composed of cold-formed pieces connected together with preloaded bolts and gusset plates. Furthermore, the steel hybrid towers require a transition piece to establish a connection between lattice and tubular parts. The transition piece is transferring the loads from the tubular segment at higher elevation to the lattice structure which is fixed to the foundation. It is critical component to design, because non-standardized solution is necessary to resist cyclic loading in a cost-effective solution. Well-designed transition pieces with optimized resistance and feasible for manufacturing and execution on site is important for the market acceptance of a new type of onshore wind towers. This research focuses on development of optimal geometry for the lattice structure, detail investigation of low-maintenance preloaded bolted connection between polygonal members and transition piece design considering ultimate limit load and fatigue load.

Introduction

As the land based wind turbine installations started in early 90's, most of the wind turbine towers aged and the owners are faced with the high maintenance, low efficiency and the risk of failure. Additionally, the technological advancements suggest repowering the old wind parks with higher power capacity wind converter [1], [2]. Two types of full and partial repowering were proposed by National Renewable Energy Laboratory (NREL) [1]. The full repowering means the replacement of the whole tower and the converter with a new structure and higher capacity converter. The partial repowering means replacing only the rotor nacelle assembly. The first active repowering started in Denmark in 2007 and followed by Germany and limited number of cases in India and Netherlands [1]. German repowering share during the last four years was close to 20% of the total installed power associated to hub height average of 128 meters [23].

According to [3] only 2.5 MW and 80 m to 120 m hub height for onshore wind turbines are economical to be installed. However, due to the wind potential of some wind parks' locations, higher WEC capacity of more than 5 MW can be used, which imposes the use of longer blades and require higher hub height to take advantage of less turbulent wind and higher wind speeds. Therefore, higher support structure is necessary, which puts new challenges to the well-established technology based on steel tubular wind tower concept [4].

Nowadays, the most commonly used type of tower for WEC is steel, concrete or hybrid tubular tower. One of the tallest steel tubular tower installed is Vestas 3MW wind turbine with 166m hub height. The diameter of this WEC tower model reaches 6.5m in the base. Tower base segments are built in several pieces in order to satisfy public road transport limitations. However, this has resulted in increasing transportation and installation costs [5]. For heights beyond 130 meters GE proposed new enclosed lattice space frame assembled onsite [6]. This new solution makes the tower cost effective and utilizes standard logistic. Ruukki uses lattice structure for 2.5MW turbine to reach 160m height [7]. Moreover, Suzlon designed 120m hybrid wind turbine tower with 2.1MW of rated power. Suzlon tower is 4-legged lattice structure with "L" shape cross-sections. Instability of compressed members is overcome using intermediate struts [6]. Contrarily, Ruukki proposed a new type of open 6 corner polygonal sections to improve stability of members in lattice towers.

A new concept of steel hybrid tower using lattice and tubular approach is being developed within SHOWTIME research project, in which the lower part of the tower is lattice structure and the upper part is tubular tower connected to the lattice structure with a transition piece. The aim in this approach is to keep the base diameter of the tubular segment in order to make possible the transportation on roads. The use of tubular tower for upper portion takes all the advantages of optimized technology for tubular steel towers with the diameters within public road transportation limitations, while the lattice portion enables the required extension of height [8], [9]. Another advantage is that the lattice portion can be used to facilitate installation of the upper tubular portion and the turbine, therefore avoiding the need for very high cranes. Although several similar lattice tubular supporting structures were proposed as an onshore wind turbine supporting structure, one of the objectives in this research is to use new type of bolted polygonal built-up cross sections introduced by Ruukki [7]. In this type of structure, members are composed from built-up open cross-sections connected together with preloaded bolts (Figure). Polygonal sections with number of sides lower than 12 were chosen for the members in lattice structure. For the pylon nonagonal section is adopted and for diagonal section hexagonal sections (Figure). Parametric study on the geometry of the lattice portion of the tower was done in order to determine the geometry and the cross-sections in the lattice structure.

The design of the transition piece might be different in every project due to material, geometry and the loading conditions. A complex topology might meet all the requirements but it would make the manufacturing process and the transportation rather expensive. Recent jacket supporting structure for offshore wind turbines have applied this design concept. In addition, there are several industrial R&D projects and registered patents in the research stage. For example, Geodome LTD has developed an offshore transition piece for 6MW wind turbines. The aim of the design was to fulfil requirements of the fatigue life at least 25 years and to reduce the fabrication costs [10]. SeaPlace Company did a full scope study on jacket structures and related areas like lifting, life cycle assessment and transition piece design [11]. The Repower wind turbine concept consists of a conical shell and combines the clinging legs to the main body. In comparison with previous shell frame structure, a reduction of material cost might be achieved through the elimination of the bracing legs[12]. Furthermore, AMBAU GmbH [13] constructed a 14 m high cone-shaped shell transition piece with 200 tonnes weight for the "Baltic2" wind farm . The 120 m hybrid lattice-tubular tower installed by Suzlon Energy also uses a conical transition piece, which constitutes the basis for the design of innovative transition pieces. The transition piece was developed by Türme-Unlimited [14]. They use a hexagon concept which arranges six instead of four legs. The transition piece is connected to the lattice structure with bolts.

Behaviour of the joint is an important parameter in structural global behaviour. The codes in practice rely on effective length method to assess the stability of structures [15]. The compressed member effective length factors (pylon as well as brace elements) are derived considering the effects of the non-linear moment-rotation characteristics of the joints. Considering that current design codes lack information on this type of joints, and intensive study is carried out.

New concept for the Steel Hybrid Wind Tower

A set of structural solutions was designed for Ultimate Limit States in order to assess different geometries of the lattice structure. Parameters chosen in the study are mainly targeting the balance between the height of tubular and lattice parts, the balance of base width to height and the number of connections/bolts to be used. Defined case studies have following parameters:

- wind turbine power: 5MW
- lattice part height: 120m
- tubular part height: 100m
- number of 'Legs': 4 and 6
- height/spread ratio of lattice part: $H/L=1/1$ to $6/1$

In order to determine optimal geometry for the face of the lattice part, four different solutions (Figure) were analysed. For each case the angle of the brace from horizontal plane was varied between 30° and 50° (35° and 55° for 6 "legs" towers) with the increment of 5° [16].

Figure shows that optimum solution regarding the ratio between the weight and the number of connections of the structure, can be obtained with the 2nd solution and 45° . This solution was chosen for further parametric study. In case of the lattice with 6 "legs" two solutions were considered, one chosen for 4 "legs" lattice towers and one with K braces (Figure). Solution chosen for further investigation was with K braces. In both cases (4 and 6 "legs") the parametric study was carried out with the brace angle of 45° .

For the next stage of the analysis, the 3D model of the lattice structure was created with varying braces' cross sections along the height, while the columns' cross section was considered constant. The weight and the number of connections of 120 m lattice models were compared for different H/S ratios of 4-legged and 6-legged lattice structures in Figure .

Parameters considered in the comparison of proposed solutions were:

- weight of the lattice structure
- number of the connections in the structure
- estimated number of the bolts (designed for axial load N_{Ed} in brace elements)
- reaction force in the foundation

Parametric study results for 4 and 6 "legs" structures are shown in Figure . Comparison is made for mass of the structure, number of the connections and estimated number of the bolts. In the Figure (left) only lattice portion of the tower was considered in analysis. The lowest mass of the structure was obtained for height/spread ratios 3/1 to 5/1. These three ratios were chosen for further investigation in which the tubular portion is included. The number of the bolts was estimated by designing the connections for each solution. The lowest number of the bolts was obtained for lattice tower with 6 "legs" and K braces without horizontal bracing.

The height over spread (H/S) ratios of 3/1 to 5/1 show more promising results, therefore, further analysis is performed on 120 m lattice with the mentioned H/S ratio.

The 6-legged lattice without horizontal braces is investigated. The 4-legged design optimization without horizontal bracing was not considered as elimination of any horizontal bracing causes an out of plane deformation at X-braces cross points. In order to compare the 6-legged structures with and without horizontals and the 4-legged lattice structure, the same set of results were obtained and compared for all the designed structures. Moreover, the mass and estimated number of bolts for 4 and 6-legged structures with and without horizontal bracing are compared in Figure (right)..

Furthermore, it can be seen in Table 1 that with the increase of H/S ratio the maximum tensile force is increasing as well. Between two compared models the tensile force for heavier transition piece is less due to the increase of the structural weight with which leads to less overturning moment.

Taking into account that with the increase of height/spread ratio the reaction forces are increasing, the solution that was chosen as the most optimal one between the proposed cases is for ratio 4/1.

Design and Modelling of Transition Piece

Design and numerical analysis of the transition piece were done corresponding the lattice and the tubular tower geometry of the wind energy converter. The design validation was based on the structural Eurocodes. In the preliminary analysis, a plate are modelled at the bottom of the transition piece and at the top of the lattice tower. The model includes the upper part of the lattice structure to assure the load transfer from the tubular part to the lattice structure. The transition piece diameter is defined by the size of the bottom diameter of the tubular segment and the top dimension of the lattice segment [17].

Three different case studies based on different mechanical and functional requirements were investigated:

- cylindrical transition piece made of S355
- cylindrical transition piece made of S690
- influence of stiffeners in the FEA

The ultimate limit state analysis was performed and stress concentrations were identified. The stress concentration occurs in the welded connection between chord and transition piece shell, and might be possible fatigue hot spots. In comparison of two case studies, the normal strength steel piece is approximately 40% heavier comparing to the high strength steel solution. This is a crucial parameter concerning transportation of the structure and assembling so application of high strength steel is effective in design of transition piece [17].

The fatigue analysis was conducted using two S-N curve and FEM model in Fe-safe module of ABAQUS. The time series of 25m/s wind speed is chosen as the highest possible load on the wind turbine. There was no damage detected using cyclic counting based on rain flow counting and compering to the S-N curve. However, the damage was detected using elastic FE model with multiaxial loads using strain life equations. Table 2 summarizes the multiaxial fatigue life for transition piece case studies. The most loaded element, where a potential crack initiation may happen is shown in Figure for both case studies.

FEA of the transition piece which contains “stiffened walls” shows reduction of the stress level in the area where the stress concentration spots are the biggest. The additional plate is made of S690. The S690 transition piece showed better elastic behaviour and the life time was increased to more than 12 years using stiffener. Although, the same life time can be achieved with increasing the overall thickness of the transition pieces shell by 10mm, due to current difficulties in high strength still rolling and part manufacturing the thinner plate is favourable.

In-situ Bolted Connections in Lattice Part of the Tower

The joint analysed in this work has the geometry depicted in Figure . The secondary member of the connection (horizontal or with 45° angle in Figure (right)) is called brace, and the main member (vertical in Figure (right)) is the pylon. Connection with gusset plates and preloaded bolts is used in order to maintain simplicity of the connection bolted in-situ.

The cross-sections proposed for lattice structure are composed of cold formed pieces connected together along the length with preloaded bolts creating polygonal cross-sections. For the pylon three pieces are bolted together forming nonagonal, while for the brace two pieces are bolted together forming hexagonal cross-section (Figure) [18]. Polygonal built-up cross-section are to be used instead of CHS in order to use advantages of polygonal over circular sections, as well as to improve fatigue life of the connections and members considering that the fatigue behaviour of preloaded high strength bolted joints under shear or friction loads can bear higher fatigue loads than welded joints [19].

These types of polygonal cross-sections are very sensitive to the corrosion taking into account that are open cross-sections. The gap between the elements of which the cross-sections are composed exposes the interior of the cross-section to the environmental conditions but on the other hand it is not possible to do maintenance of the inside part of the members. Therefore, hot dip galvanizing is proposed as corrosion protection of these sections. Galvanizing is one of the most widely used to methods for protecting metal from corrosion. It involves applying a thin coating of zinc to a thicker base metal, helping to shield it from the surrounding environment. Hot dip galvanizing offers coverage both externally and internally, it is environmentally sustainable and has a maintenance-free life of 50 years or more. Galvanizing can also protect metal through a process called “galvanic corrosion”.

Connection behaviour is represented by the moment-rotation curve. In this work this curve was used to validate FE model by comparing the obtained ultimate resistance with the results obtained using EC3 [20]. This curve describes the relation between the bending moment ratio M_j/M_y and the corresponding rotation ratio θ_j/θ_y . Bending moment M_j is moment applied to a joint and the rotation θ_j is corresponding rotation between the connected members. Bending moment M_y is plastic resistance of brace and rotation θ_y is yield rotation of the brace calculated according to FEMA 356 [21] using following expression:

$$\theta_y = \frac{W_{pl} \cdot f_y \cdot L_b}{6 \cdot E \cdot I_b} \quad (1)$$

The bending moment acting on connection corresponds to applied load ($R3_{RP3}$ - reaction force of the brace end) multiplied by the distance between centre of the pylon and end of the brace (L_{load}).

Moment and rotation of the connection are computed using following expressions:

$$M = R3_{RP3} \cdot L_{load} \quad (2)$$

Displacement values in the reference points (P_1, P_2, B_1, B_2) of Figure are used to determine rotational deformation of the joint:

$$\theta = \frac{u_{1(B1)} - u_{1(B2)}}{h_{br}} - \frac{u_{1(P1)} - u_{1(P2)}}{h_{gp}} \quad (3)$$

where:

u_1 is the horizontal displacement

h_{br} is the distance between points B_1 and B_2

h_{gp} is the distance between points P_1 and P_2

The results from FE models were compared with simplified design models based on EN 1993-1-8 rules. Two observations can be made, which are: (i) the ultimate resistance obtained from FE models is slightly higher comparing with EC3. This is due to more conservative approach of Eurocode (ii) the failure modes suggested by Von Mises plastic strain correlated with EC3 and are: Gusset plate nest section failure, Gusset plate buckling, Brace section failure and Brace block tearing (Figure **Error! Reference source not found.**).

Experimental testing on connection is being carried out at the moment and FE model validation. In addition, a new hand-calculation method taking into account the influence of the joint tolerances for assembly is to be developed.

Erection process

The erection process procedure is inspired by the assembly of a lattice tower from Donges Steeltec [22]. Thereby, first the lattice tower is mounted on site in several pieces and the pieces are put together by a mobile crane afterwards. For the hybrid tower, the tubular parts are assembled on the ground in the inside of the lattice tower. In the final state a transition piece which is located at the top of the lattice tower connects the lattice and the tubular part. During the assembly process, the transition piece serves as a supporting area for four strand jacks which lift the tubular part from the ground to its final position. To prevent an overturning during the assembly of the tubular parts on the ground and also during the lifting, the tubular tower should be fixed by strand jacks from the bottom as well. Therefore, a pedestal with four strand jacks is installed to the foundation. Additionally, hydraulic pressure rollers or springs are installed on the inside of the transition piece as a horizontal support and guidance during the lifting of the tubular tower. These horizontal holding devices have to be positioned in at least two height levels to enable a release of the device in one level when the flange of the last tubular segment passes by..

These erection procedure was discussed with the company HebeTec, from which the strand jacks and equipment are being used for the prototype.

Conclusions

Future investments in onshore wind turbine installations are highly required in order to decrease the cost for repowering and new installation based on new supporting structure. Therefore, the analysis of several support structure types is an important step to identify the potential in cost reduction by an optimized design. The hybrid lattice/tubular tower is an alternative design solution. The parametric study presented in this paper shows optimal solutions based on the realistic optimization criteria. The hybrid lattice-tubular structure was proposed as a 185 m supporting structure for the 5 MW onshore wind turbine. It can be claimed that the 185 m hybrid solution, has similar cost for the transportation and the foundation as 125 m tubular tower and the cost of the tower and the lifting is between the 125 and 150 m tubular solutions. Therefore, the hybrid solution is better solution rather than tubular solutions for the height above 150 m.

The proposed hybrid solution relies on two important assumptions, which are the feasibility of installation, erecting the tubular part from the lattice lower structure and economic solutions for the transition piece between lattice and tube and the connections between members in lattice structure.

The analysis of a new concept of the transition piece for steel hybrid lattice-tubular tower is presented as well. This includes the detailed design of a transition piece considering different steel grades, investigation of different stability criteria with ultimate limit state and calculating fatigue life time. It was shown that the design with mild steel grade leads to very large dimensions. The high strength steel reduces the dimensions but introduce lower life time which causes additional external stiffeners. The influence of the internal stiffener was shown. The high strength steel concept led to smaller dimensions, however, an increase of the thickness is required in order to have the standard 25 years' life time.

Additionally, behaviour of gusset plate connection between polygonal built-up members is investigated more in detail. The finite element results were compared with analytical calculation according to EC3-1-8. The comparison revealed that FE models are able to accurately predict the failure mode of the joint, while overestimating the design moment resistance. These difference can be attributed to more conservative approach of Eurocode. Different failure modes were observed. The experimental testing is being carried out in order to validate the results obtained from FE models. Parametric study will follow and hand calculation model that takes into account joint tolerances for assembly will be developed.

Finally, the erection procedure was developed focusing on decreasing the installation costs of WEC.

Acknowledgements

The authors acknowledge with thanks the support of the European Commission's Framework Programs "Horizon 2020" program through the Marie Skłodowska-Curie Innovative Training Networks (ITN) "AEOLUS4FUTURE – Efficient harvesting of the wind energy" (H2020-MSCA-ITN-2014: Grant agreement no. 643167), the RFCS – Research Fund for Coal and Steel program through the Grant Agreement RFSR-CT-2015-00021 and the Regional Operational Programme CENTRO2020 within the scope of the project CENTRO-01-0145-FEDER-000006.

References

- [1] E. Lantz, M. Leventhal, and I. Baring-gould, "Wind Power Project Repowering : Financial Feasibility , Decision Drivers , and Supply Chain Effects," 2013.
- [2] S. Lüers, K. Segelken, and K. Rehfeldt, "Status of land-based wind energy development in Germany - Year 2015," 2015.
- [3] E. W. E. A. (EWEA), "The European offshore wind industry key 2015 trends and statistics," 2015.
- [4] R. McKenna, P. Ostman v.d. Leye, and W. Fichtner, "Key challenges and prospects for large wind turbines," *Renew. Sustain. Energy Rev.*, vol. 53, pp. 1212–1221, Jan. 2016.
- [5] Vestas Wind Systems A/S, "Large Diameter Steel Flanges (LDST)," 2016.
- [6] General Electric, "Space Frame Tower," p. 2, 2014.
- [7] Ruukki, "Ruukki wind towers: Reaching the heights with Ruukki," 2011.
- [8] E. Hau, "Wind turbines: fundamentals, technologies, application, economics," *Springer Berlin, Ger.*, 2014.
- [9] G. Figueiredo and R. Carlos, "Structural behaviour of hybrid lattice – tubular steel wind tower," Univesity of Coimbra, Portugal, 2013.
- [10] "Development of Jackets and Transition Pieces for Wind-Turbine Installations." [Online]. Available: <http://www.geodome.co.uk/www.geodome.co.uk/applications/off-shore.html>.
- [11] "Jacket for 5MW Wind Turbines. Seamar Project." [Online]. Available: <http://www.seaplace.es/projects/offshore-renewable-energy/proyecto-seamar/>.
- [12] M. Seidel, "Jacket substructures for the REpower5 M wind turbine," i," *Proc. Eur. offshore Wind energy Conf. Exhib.*, 2007.
- [13] "AMBAU Press information." GmbH, Ambau, 2013.
- [14] W. Meiners, *Bolt connection between lattice and tube in a steel hybrid tower*. 2015.
- [15] A. Webber, J. J. Orr, P. Shepherd, and K. Crothers, "The effective lenght of columns in multi-storey frames," *J. Eng. Struct.*, vol. 102, pp. 132–143, 2015.
- [16] S. Jovašević, M. R. Shah Mohammadi, C. Rebelo, M. Pavlović, and M. Veljkovic, "New Lattice-Tubular Tower for Onshore WEC – Part 1: Structural Optimization," in *Procedia Engineering 199*, 2017, pp. 3236–3241.
- [17] M. R. Shah Mohammadi, M. Farhan, C. Rebelo, and M. Veljkovic, "Preliminary transition piece design for an onshore wind turbine," in *EUROSTEEL 2017*, 2017, pp. 4400–4409.
- [18] S. Jovašević, C. Rebelo, M. Pavlović, and M. Veljković, "Numerical investigation of preloaded gusset plate connections between polygonal built-up members," in *EUROSTEEL 2017*, 2017, pp. 292–297.
- [19] J. P. Jaspart and K. Weynand, *Design of Joints in Steel and Composite Structures*. ECCS - European Convention for Constructional Steelwork, 2016.
- [20] European Committee for Standardisation (CEN), "EN 1993-1-8:2005 Eurocode 3: Design of steel structures - Part 1-8 : Design of joints," vol. 3, 2010.
- [21] 5.5.2.2.2 Nonlinear Static Procedure, "FEMA 356." .
- [22] P. Schäfer, "'Lattice Towers for Wind Turbines', information brochure Donges STEELTEC, received 22.09.2016 from P. Schäfer.
- [23] Deutsche WindGuard GmbH, www.windguard.com, assessed 12/04/2018

Figures and tables

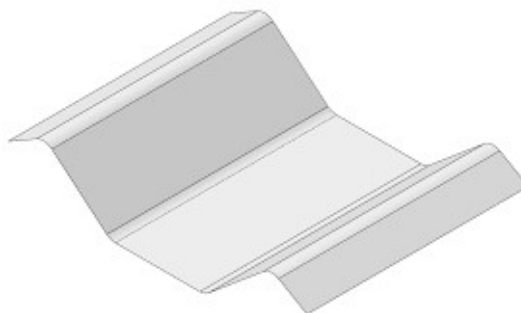


Figure 1: Lattice tower with built-up polygonal sections (left), polygonal section segment (right)

Pylon members		Brace members	
bolted built-up pylon		bolted built-up brace	
Joint detail	Cross-section	Joint detail	Cross-section

Figure 2: Proposed cross-sections and joint details

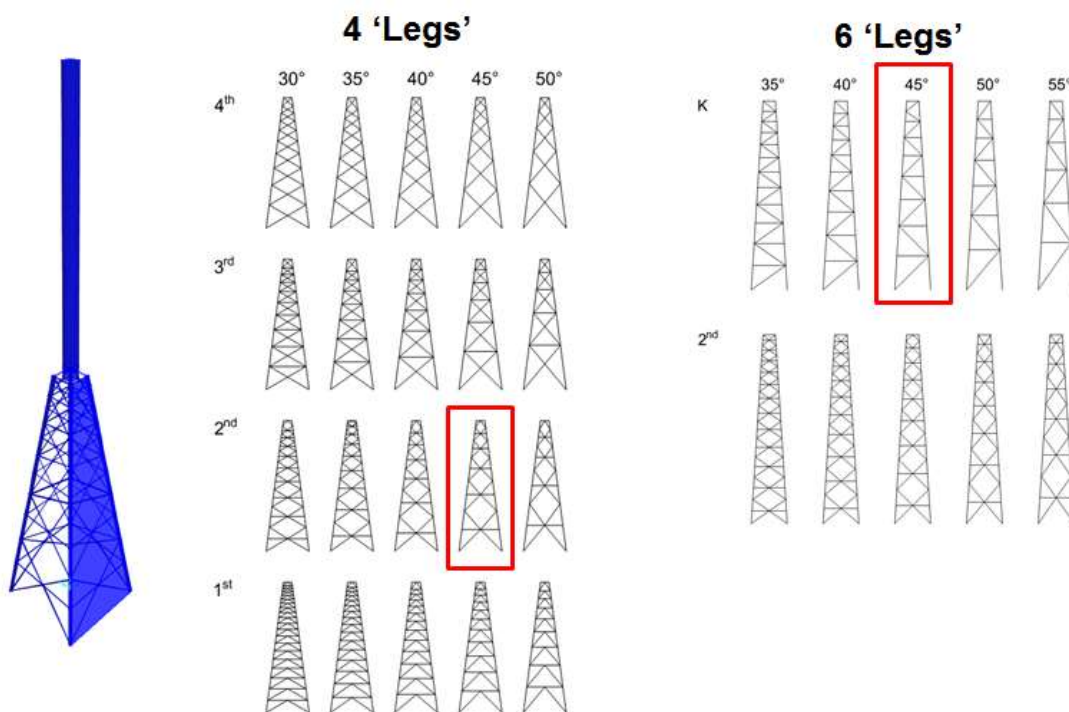


Figure 3: Parametric study – brace geometry

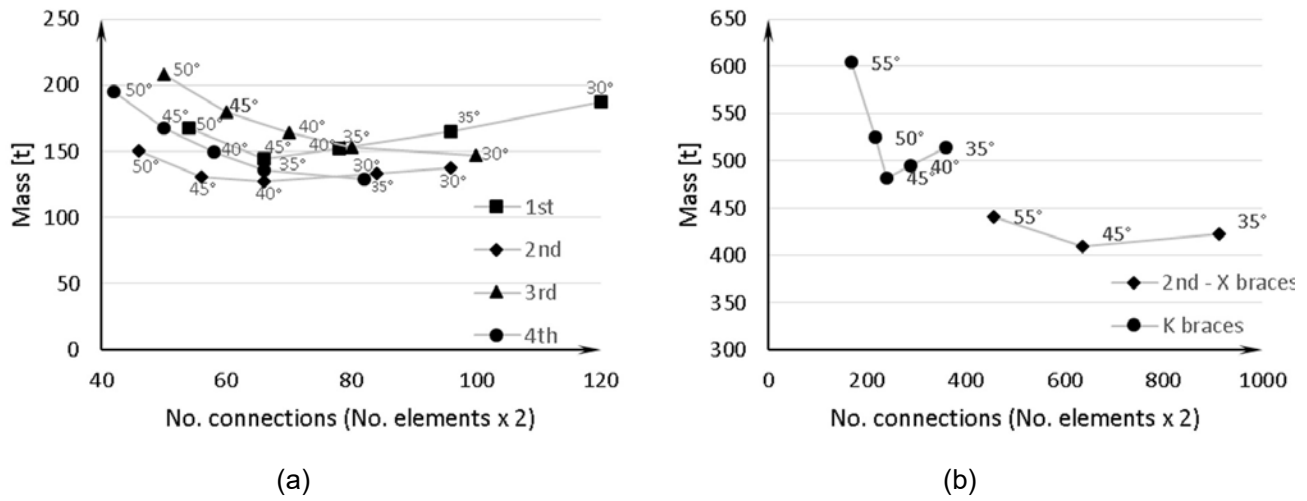


Figure 4: Comparison of 2D models for (a) 4-legged, and (b) 6-legged models.

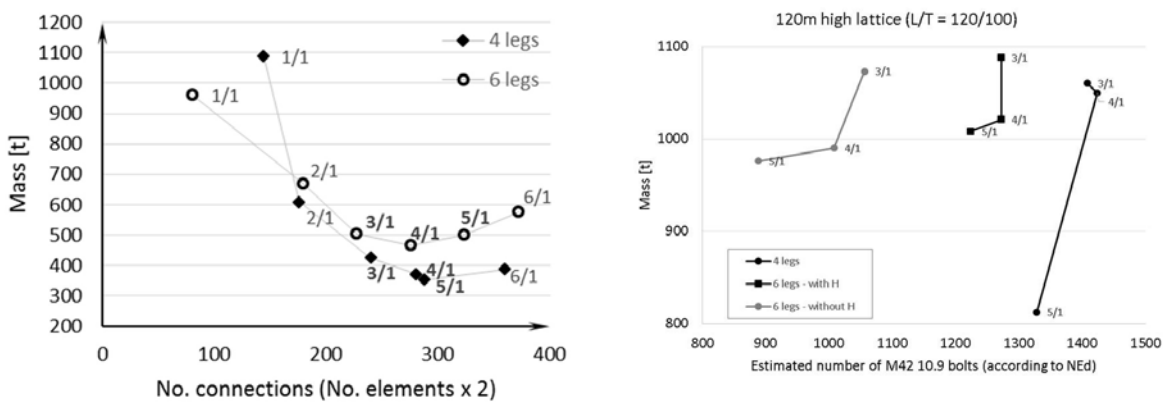


Figure 5: The weight and number of the connections (estimated number of the bolts) for chosen geometries

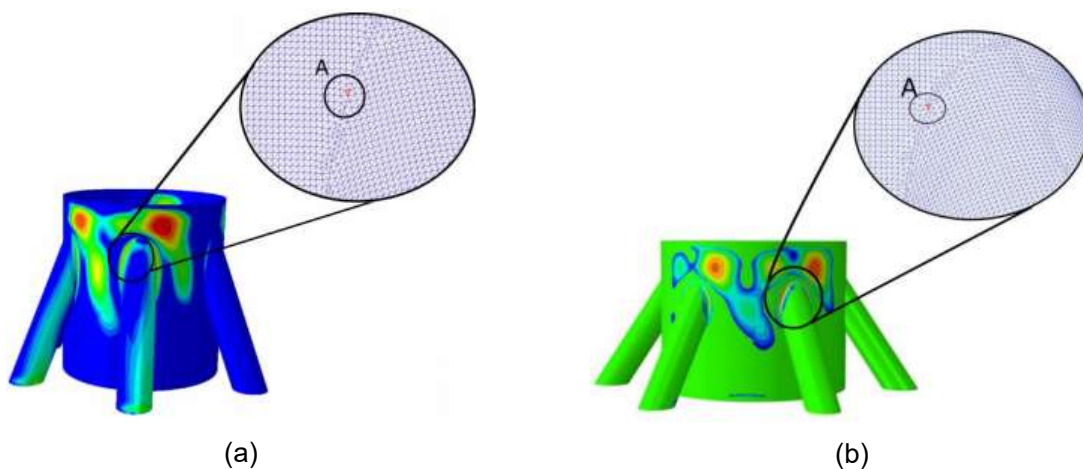


Figure 6: Contours of fatigue life in transition piece and the worse element, a) S355 steel, b) S690 steel

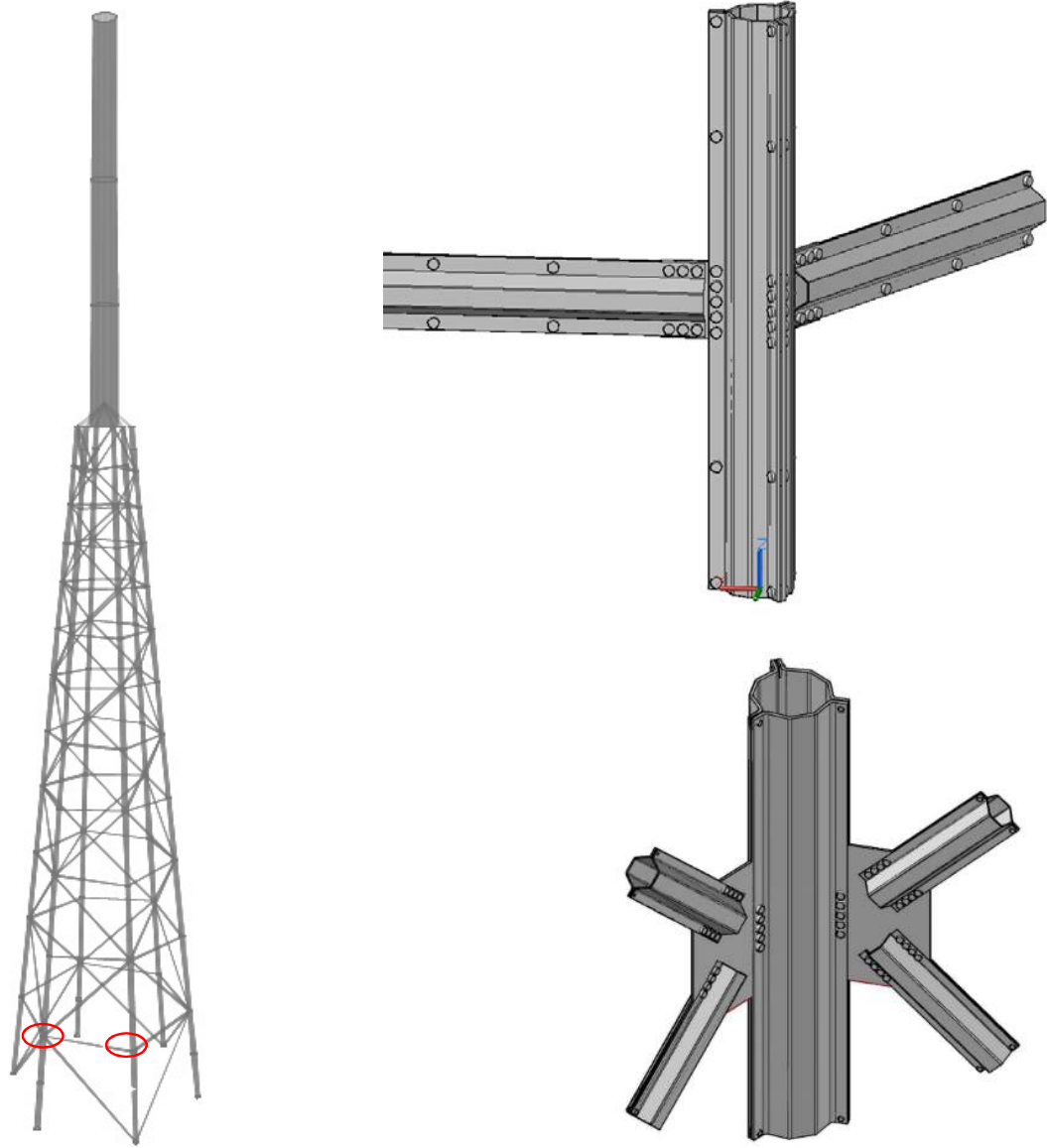


Figure 7: Joint between pylon and brace members

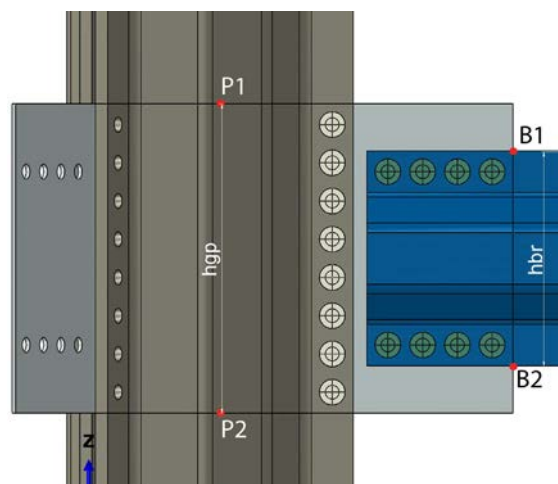
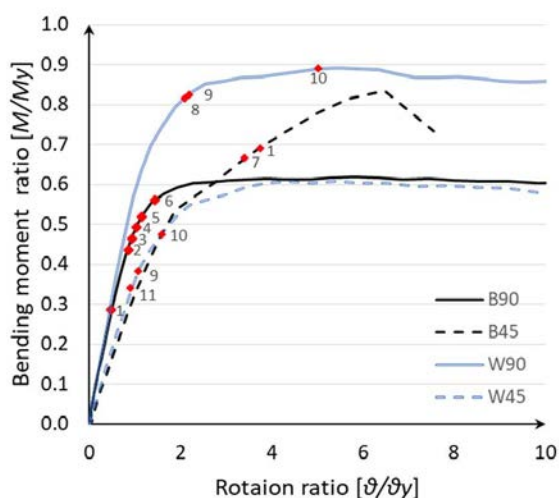


Figure 8: Moment and rotation calculation parameters



- Analytical results
1. Gusset plate bearing resistance – pylon bolts
 2. Pylon 1st bolt slip (end bolt)
 3. Gusset plate net-section in bending
 4. Gusset plate block tearing
 5. Pylon 2nd bolt slip
 6. Pylon 3rd bolt slip
 7. Gusset plate buckling
 8. Brace net section in bending
 9. Brace block tearing
 10. Brace bearing resistance
 11. Brace bolts slip resistance

Figure 9. Moment-rotation curves

Table 1: Maximal tensile force in the foundation

		Model 1	Model 2
	H/S	R ₃ [kN]	R ₃ [kN]
4 legs	3/1	10001	9281
	4/1	16031	15423
	5/1	23617	22847
6 legs	3/1	10947	10514
Without	4/1	14823	14403
HB	5/1	20967	20572

Table 2: Summary for fatigue life using multiaxial loading

	S355	S690
Worst Life-Hours	17.3 years	2.3 years
Largest SMAX	423.7 MPa	848.2 MPa
Largest Damage	6.6e-6	5e-5

Author Biography

Slobodanka Jovašević is a PhD student at the Institute for Sustainability and Innovation in Structural Engineering (ISISE) and a Marie Skłodowska-Curie research fellow.

Mohammad Reza Shah Mohammadi is a PhD student at the Institute for Sustainability and Innovation in Structural Engineering (ISISE) and a Marie Skłodowska-Curie research fellow.

Carlos Rebelo is Associate Professor in the Civil Engineering Department of the University of Coimbra, Portugal and senior researcher at the Institute for Sustainability and Innovation in Structural Engineering (ISISE).

Galvanized steel expansion joints for bridges

Mr Stefan Adam, mageba GmbH (Germany)

The importance of reliable, long-lasting corrosion protection

The annual direct costs of corrosion have been estimated to amount to approximately 3 % of GDP, both in the context of the United States and on a global scale. Including also indirect costs, this number is even greater. In the case of critical bridge components such as bearings and expansion joints, the impacts of corrosion are especially strongly felt, because the performance, serviceability and even safety of a bridge depends on the proper functioning of these key components. Repair works on bearings and expansion joints can be very expensive and have a significant impact on traffic, and the impacts are likely to be much greater when a component needs to be fully replaced, as it may arise when corrosion damage has become very serious. (see Image 1, 2)

The life to first major maintenance depends strongly on the environment in which the structure is located, and particularly on the corrosivity of that environment. For example: temperate zones, atmospheric environment with high pollution or substantial effect of chlorides, e.g. polluted urban areas, industrial areas, coastal areas without spray of salt water, exposure to strong effect of de-icing salts and subtropical zones with atmosphere with medium pollution, are far more corrosive to steel and to corrosion protection systems than inland, rural environments. Therefore, it is critically important that the environment is considered in selecting and designing any corrosion protection solution.

In the following, I would like to describe our galvanizing system, the hot dip galvanizing (HDG).

Hot dip galvanizing (HDG)

Introduction

Hot dip galvanizing (HDG) consists of the application of a protective zinc / zinc alloy coating to a steel element, by dipping it into a bath of molten zinc, where a reaction occurs between the steel and the zinc. As a result of a diffusion reaction, the galvanized coating “grows” perpendicularly to all surfaces at a uniform rate – not as a “separate” coating, but as part of the structure.

Therefore, the coating will be as thick at corners and edges as on flat surfaces, providing uniform protection against corrosion – an important characteristic, since a corrosion protection system might be considered to have failed completely as soon as it has failed to a significant extent, regardless of the precise location on the structure.

German guidelines

In Germany, guidelines published by the country's Federal Environmental Agency (see Figure 1) show that the corrosion rate in most of the country is between 0.5 and 0.8 microns per year (approx. 0.02 to 0.032 mils). At that rate, across most of Germany, a zinc coating of thickness 85 µm can be expected to provide protection for a period of between 106 and 170 years.

American guidelines

In the United States, the American Galvanizers Association, using decades of corrosion rate data from all over the world, provides guidance for how service life (defined as the time to 5 % rusting of the steel surface) can be related to environment – see Figure 2.

International guidelines

The international standard ISO 14713-1 defines the expected life of a hot dip galvanized corrosion protection system as presented in Figure 3.

mageba's HDG systems and benefits

As a conservative approach – ensuring that the durability of corrosion protection is not over-estimated – mageba's HDG corrosion protection solutions are based on ISO 14713-1.

C4 – Hot dip galvanized: Corrosion protection according to EN ISO 14713-1. Corrosivity category C4, expected durability VH (very high). Steel components (with specific exceptions, depending on the product) are hot dip galvanized (per EN ISO 1461) with a minimum zinc coating of 85 µm.

C5 – Hot dip galvanized: Corrosion protection according to EN ISO 14713-1. Corrosivity category C5, expected durability VH (very high). Steel components (with specific exceptions, depending on the product) are hot dip galvanized (per EN ISO 1461) with a minimum zinc coating of 140 µm.

Long life to first major maintenance

100 years or more can be expected in very many cases, even for a relatively modest thickness of 85 microns – and performance can be yet further improved by using high-temperature hot dip galvanizing.

Ease of repair of minor damage

By brush, e.g. using a suitable zinc primer, following cleaning as necessary. To some extent, zinc coatings are self-repairing, with thin cracks effectively sealing themselves.

Resistance to further deterioration once damage occurs

Water cannot spread underneath the zinc coating, causing flaking (unlike for a painted coating), since this is integral with the underlying steel.

Hardness - Very high.

Abrasion resistance - Very high.

Appearance

Where choice of colour is not important, hot dip galvanized surfaces have a very good appearance – particularly after many years of service due to their excellent durability and long-term ability to prevent corrosion.

Particular limitations

- Size of parts which can be galvanized is limited by the size of the galvanizing bath
- Care must be taken to ensure that steel parts will not deform unacceptably due to the high heat during galvanizing
- Can generally only be done by a specialist HDG supplier
- Depends on availability of a suitable HDG supplier – geographically and time-wise
- Requires transport to and from the HDG supplier

Particular advantages

- Corrosion protection work is done by corrosion protection specialists, ensuring quality
- Not particularly susceptible to environmental conditions during application process

High-temperature galvanizing

Normal-temperature galvanizing, with molten zinc at a temperature of approx. 450 °C (840 °F), produces a zinc coating which varies in characteristics and performance from the inside (steel substrate) to the outside

(exposed surface). The so-called η -, ζ - and δ -phases (see Figure 4) have hardness values, on the Vickers scale, ranging between approx. 40 HV and 150 HV (with the lowest hardness at the exposed surface).

High-temperature galvanizing is a more advanced hot dip metal coating process, in which steel components are coated in a ceramic-lined, induction-heated pot at temperatures of 560 °C to 630 °C (1040 °F to 1166 °F).

This process produces only a δ -phase (see Figure 5), with a hardness value throughout the coating of approx. 150 HV – greatly increasing abrasion resistance and stone-impact resistance, and clearly far superior to normal-temperature galvanizing.

Sinus plates

For these reasons, mageba uses high-temperature galvanizing to provide corrosion protection for the noise-reducing surface plates of modular and single-gap expansion joints, which are subjected to continual abrasion from vehicle wheels. At the driving surface of a steel expansion joint, mechanical damage is generally the main cause of corrosion protection failure, so the higher the abrasion resistance, the better the durability.

For this application, high-temperature galvanizing also improves slip resistance in wet conditions, and the more uniform thickness achieved maximizes the durability of the pre-stressed bolted connections even further.

Conclusions

- 100 years or more can often be expected regarding the first maintenance – minimizing life-cycle costs
- In case of minor damage self-repairing, to some extent, saving the need for manual application of e.g. a zinc primer by brush
- Water cannot spread underneath zinc coating since this is integral with the steel base
- Roughly 20 times harder than a typical painted system
- Roughly 10 times more abrasion resistant than a typical painted system
- No choice of colours but good, even after many years of service due to their excellent durability and long-term ability to prevent corrosion
- Requires transport to/from HDG supplier. Care must be taken to ensure that steel parts will not deform unacceptably due to the high heat during galvanizing
- Improved quality control due to well-defined process and lower susceptibility to environmental conditions during application

Worldwide references:



Naab Bridge | Germany



Waikato River Bridge | New Zealand



Aizhai Bridge | China



Port Mann Bridge | Canada



Golden Ears Bridge | Canada



Mackays to Peka Peka Expressway | New Zealand



Image 1 - When a bridge bearing requires to be replaced, the costs (including for lifting of the bridge deck) can be substantial



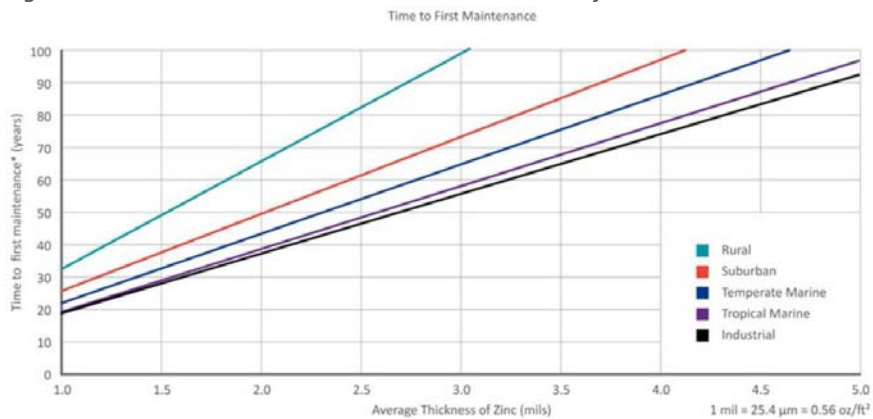
Image 2 - Corrosion of expansion joints, and at their moving / sliding interfaces in particular, can cause severe deterioration, often necessitating complete replacement of the joint which causes severe cost impact on traffic

Figures and tables:



Figure 1. German Federal Environmental Agency "Zinc Corrosion Rate Map"

Figure 2. American Galvanizers Association – "Time to first maintenance"



AGA's Time to First Maintenance Chart for Hot-Dip Galvanized Coatings
 *Time to first maintenance is defined as the time to 5% rusting of the steel surface.

Figure 3. ISO 14713-1, Table 2 – Life to first maintenance for a selection of zinc coating systems in a range of corrosivity categories

3

System	Reference Standard	Minimum thickness	Selected corrosivity category (ISO 9223) life min./max. (years) and durability class (VL, L, M, H, VH)							
			μm	C3		C4		C5		CX
Hot dip galvanizing	ISO 1464	85	40/>100	VH	20/40	VH	10/20	H	3/10	M
		140	67/>100	VH	33/67	VH	17/33	VH	6/17	H
		200	95/>100	VH	48/95	VH	24/48	VH	8/24	H

Figure 4. Hardness of high-temperature HDG δ -Phase (only): approx. 150 HV

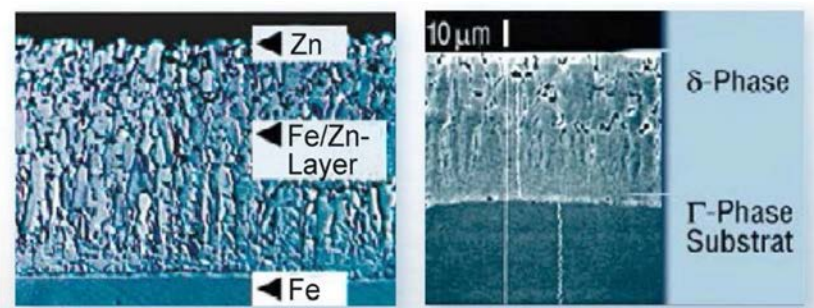
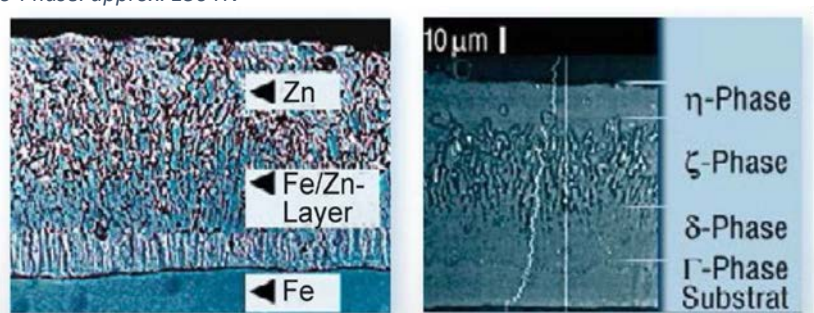


Figure 5. Hardness of normal-temperature HDG

η -Phase: approx. 40–60 HV
 ζ -Phase: approx. 60–120 HV
 δ -Phase: approx. 150 HV



Author Biography

Mr Stefan Adam was born on 4th October 1965. He studied structural engineering in Holzminden, Germany and industrial engineering in Bielefeld. From 1990 he was executive partner of the company "Adam Bauunternehmungen" und from 2001 department chief at "Ing. Holzbau Cordes". Since 2008 he works as CEO at mageba GmbH in Göttingen, Germany. He has a daughter and a son and celebrates the silver wedding anniversary with his wife this year.

Session 4:

Design of Bolted Steel Structures with Galvanizing

Galvanized Steel Slip Factor Investigation – Part 2

Alana Hochstein and Thomas J Langill

American Galvanizers Association

Abstract

The American Galvanizers Association's (AGA) Slip Factor Study attempts to qualify the slip coefficient of a slip critical joint of faying surfaces made up of hot-dip galvanized steel, metallized steel and paint over hot-dip galvanized steel. The American Institute of Steel Construction's (AISC) Specification for Structural Joints Using High Strength Bolts classifies mean slip coefficient values as either Class A ($\mu = 0.30$), Class B ($\mu = 0.50$), Class C ($\mu = 0.30$) or Class D ($\mu = 0.45$). Currently, hot-dip galvanized steel achieves only a Class C slip coefficient value. Designing with a Class C slip coefficient limits the design freedom of an engineer or architect designing a steel construct; such as a bridge. Therefore, it is advantageous to the hot-dip galvanizing industry to find a surface treatment method which increases the slip coefficient of hot-dip galvanized faying surfaces from a Class C rating to a Class B or D rating under the AASHTO LRFD standard. This study uses zinc-rich paints in combination with a galvanized coating to raise the slip coefficient. Further work has been performed on unpainted galvanized steel to find the slip factor of galvanized coatings in their various surface states. New classes have been added to the acceptable slip coefficients. This paper will describe the new classes and the results of creep testing of various combinations of coatings.

Background

In the construction of bolted steel structures, hot-dip galvanized (HDG) structural connections offer many advantages such as durability, cathodic protection, and suitability for corrosive or extreme temperature environments. Although the hot-dip galvanized coating does not affect design strength considerations for bearing type connections, the design of slip critical connections is affected by the slip coefficient of the hot-dip galvanized faying surfaces. Traditionally, industry standards^{1,2,3} denote newly hot-dip galvanized steel has a lower mean slip coefficient ($\mu = 0.30$) than blast cleaned bare steel ($\mu = 0.50$) or bare steel painted with Class B coatings ($\mu = 0.50$). As a result, design freedom and cost can be affected when specifying hot-dip galvanizing for corrosion protection, as more bolts, holes, and joints are required in the design of high-strength structural connections. Several studies conducted by the American Galvanizers Association (AGA) in collaboration with other research organizations indicate consistently obtaining a higher slip coefficient through control of processing parameters, roughening, or other surface treatments is not possible⁷. However, it was determined applying Class B or D zinc-rich paints (ZRP) over HDG faying surfaces can significantly increase the slip coefficient and provide a greater variety of coating options to the specifier/designer without affecting long-term corrosion protection^{4,5}.

Recent slip factor and tension creep testing^{4,5} performed by the AGA indicate higher slip coefficients ($\mu = 0.45$ or $\mu = 0.50$) can be achieved by applying Class B or D zinc-rich paints to hot-dip galvanized faying surfaces which have been prepared with a chemical pre-treatment/conversion coating. Based on these findings, the 8th edition of the AASHTO Load Resistance Factor (LRFD) Bridge Design Specification includes updated class definitions to include any blast-cleaned surfaces coated with zinc-rich paints (Class D, $\mu = 0.45$).

Specifying HDG + ZRP for bridges, highways, and buildings

The AASHTO Load Resistance Factor (LRFD) Bridge Design Specifications are intended for use in the design, evaluation, and rehabilitation of bridges, and are mandated by the Federal Highway Administration (FHWA) for use on all bridges using federal funding. The Technical Committee for Structural Steel Design (T14) recently passed changes to Section 6 (Steel Structures) of the document and the revised language appears in the new 8th revision. The revised language of Section 6 reflects the need within the industry to re-define the available surface condition classes and associated values for slip coefficients used to calculate the nominal slip resistance of a high-strength bolt in slip-critical connections.

Class definitions within the 11th paragraph of Article C6.13.2.8 were updated to revise the class for hot-dip galvanized faying surfaces shown in Figure 1, and include options for metallized faying surfaces and blast-cleaned surfaces coated with zinc-rich paints:

- **Class A:** Unpainted clean mill scale and blast-cleaned surfaces with Class A coatings. The value for a Class A surface condition is reduced from 0.33 to 0.30 to better align with the value provided in the latest RCSC specification corresponding to the median of available historical data.
- **Class B:** Unpainted blast-cleaned surfaces to SSPC-SP 6 or better, blast-cleaned surfaces with Class B coatings, or unsealed (pure zinc or 85/15 zinc/aluminum) thermal-sprayed coatings with a thickness less than or equal to 16 mils. Unsealed thermal-spray coatings were not previously addressed by the specification² but are now included within Class B based on recent research data.
- **Class C:** Hot-dip galvanized surfaces. Based on recent industry research, the value for a Class C surface conditions is reduced from 0.33 to 0.30, and subsequent treatment (wire brushing) of the galvanized surface is no longer required.
- **Class D:** Blast-cleaned surfaces with Class D coatings. Added to increase the options for zinc-rich coatings over any blast cleaned surface (including HDG).

Updated slip coefficient values for each class are reflected in Figure 1, and a summary of the overall changes are as follows:

Eventually, specifications related to structural connections used in other industries may be similarly revised. Meanwhile, for the galvanizer involved in any federal highway and transportation projects, wire brushing of the HDG faying surface is no longer required. Doing so will only lead to increased cost, as industry research determined wire brushing does not increase slip properties⁷.

For the FHWA/bridge customer, the revisions allow a greater variety of coating systems that can be used for the design of high strength slip critical connections. Specifically, it will become easier and more economical for the specifier to select hot-dip galvanizing and metallizing for corrosion protection. Although the slip coefficient for hot-dip galvanized surfaces are reduced from 0.33 to 0.30 in this revision, it is anticipated the new value will have minimal impact on design. However, there is a potential for a small increase in the number of bolts used in connections with HDG fasteners. Regardless, customers will benefit from the removal of additional labor previously required to roughen HDG faying surfaces. For the new Class D ($\mu = 0.45$) surface condition, a slightly lower slip coefficient value is provided than for Class B ($\mu = 0.50$), but the value will not cause a significant impact in the overall number of bolts required for most high-strength bolted connections. Therefore, the addition of Class D simply provides a greater variety of coating options to the specifier/designer, including the use of HDG surfaces with zinc-rich paints.

Available Slip and Tension Creep Testing Results for HDG/ZRP Faying Surfaces

The American Institute of Steel Construction (AISC) and the Research Council on Structural Connections (RCSC) publish the *Specification for Structural Joints Using High Strength Bolts*². Appendix A, "Testing Method to Determine the Slip Coefficient for Coatings Used in Bolted Joints" contains procedures relating to coating testing which must be performed to obtain a slip coefficient for use in the connection design.

The AGA performed sample design, preparation, slip tests, and tension creep tests in accordance with Appendix A of the RCSC specification², in order to obtain faying surface classifications for the coating systems below. Preparation and results from the slip testing⁴ and tension creep testing⁵ are provided in Figure 2.

- HDG & Sherwin-Williams Zinc Clad II Plus with a slip factor $\mu = 0.45$
- HDG & PPG Dimetcote® 9/Sigmazinc™ 9 with a slip factor $\mu = 0.50$

The HDG surfaces were prepared for painting using a chemical surface treatment (Picklex® 20)⁶, and both of the paint systems were brush-applied (no thinner used) and cured in accordance with cure schedules provided within each manufacturer's technical data sheet.

The result of this testing indicates the above coating systems and application method can be used to successfully achieve increased slip factors for HDG faying surfaces without need for further testing. Other paint systems were spot tested and have the potential to be Class D or B coatings through a complete series of testing. Two other systems that were tested include International's Interzinc 2 and Tnemec's Series 394.

Recommendations for Consistent Faying Surface Preparation

The following recommendations for surface preparation and paint application are provided for achieving consistent and repeatable results for using zinc-rich paints over hot-dip galvanized faying surfaces, whether for classification testing or eventual field application.

HDG Surface Preparation

To begin preparation of the HDG faying surface for successful application of zinc-rich paint, avoid any post-treatment process such as chromate quenching or water quenching, as these processes are known to interfere with adhesion of the paint. If there is uncertainty regarding whether the steel was chromate quenched, allow the surface to weather naturally in the environment for at least six weeks, or test the HDG surface for the presence of passivation agents per the procedure described in ASTM B201, *Standard Practice for Testing Chromate Coatings on Zinc and Cadmium Surfaces*, and remedy according to methods outlined in Appendix X1.3 of ASTM D6386, *Standard Practice for Preparation of Zinc (Hot-Dip Galvanized) Coated Iron and Steel Product and Hardware Surfaces for Painting*.

Upon withdrawal from the zinc bath, sometimes excess zinc is present in small bumps, runs, or drips. These imperfections will be visible and can affect the slip factor of the galvanized coating as well as the adhesion of the zinc-rich paint and must, therefore, be removed prior to painting the part. Runs, drips, or bumps can be removed by grinding or filing the surface smooth and flat, taking care to not remove excess coating thickness.

Once the galvanized surface imperfections have been removed, eliminate organic contaminants by performing solvent cleaning using clean rags according to SSPC SP 1, *Solvent Cleaning*. After cleaning, rinse thoroughly and allow to dry completely.

Profiling the HDG Surface with Chemical Pretreatment

Next, the surface must be profiled to promote adhesion of the zinc-rich paint. Various methods for preparing and profiling the HDG surface prior to paint application were studied⁷, and it was determined chemical pretreatments provided the most accurate and consistent results with maximized slip properties. Additionally, a chemical pretreatment provides cost savings as opposed to other surface preparation methods such as brush-off blasting.

Picklex® 20⁶ is a chemical treatment that removes surface oxides and deposits a pre-treatment conversion coating. Picklex® 20 should be spray or brush applied liberally and uniformly to wet the surface. Let sit for one minute, then wipe off excess chemical completely from the surface down to the metal using a clean rag and then fully air dry. Sometimes a brownish yellow tint may be noticed on the surface; this coloring is a thickness variation of the conversion coating.

Application of Zinc-Rich Paint

Since the testing of the coating during the acceptance procedure uses an applied coating thickness of 2 mils over the recommended thickness², the zinc-rich paint should be applied to the recommended thickness from the manufacturers guidelines. As inorganic zinc-rich paints are susceptible to mud cracking at thicknesses beyond 4-5 mils, be sure the intended thicknesses for both testing and field use are in line with the manufacturer's recommendations regarding maximum coating thickness.

Although spray application is often recommended by the manufacturer, brush-on application can be successfully utilized to minimize application time and costs. Roller application should not be utilized, as it is difficult to obtain a uniform coating thickness and there is increased risk for excessive coating thickness. Follow the manufacturer's recommendations regarding mixing, thinning, over-coating, and curing. Faying surfaces should be fully cured prior to fit-up of the connection.

Classification of Additional HDG/Zinc-Rich Paint Faying Surfaces

Although two different zinc-rich paint formulations applied over hot-dip galvanizing have been successfully classified with a higher slip factor, there are many other zinc-rich paints available on the market, as well as other preparation and application methods for providing similar results. To determine whether application of an alternate zinc-rich paint product, alternate paint application method, and/or surface preparation method will provide Class D ($\mu = 0.45$) or Class B ($\mu = 0.50$) slip properties when applied over HDG, additional slip and tension creep testing will be required before use. Design and preparation of the test plates along with slip testing, and tension creep testing should be performed in accordance with Appendix A of the RCSC specification, *Specification for Structural Joints Using High Strength Bolts*².

When looking to obtain test data which will accurately describe the slip properties of the connection after installation, be sure to apply the zinc-rich paint in a manner which can and will be replicated closely in the field. This includes specifying the HDG surface preparation method (chemical pretreatment, brush-off blasting, etc.), paint application method (brush or spray), and paint dry-film thickness (test thickness minus two mils). Further recommended practices include selecting a cure schedule for testing which represents the intended or worst-case environment for paint application whether at the job site, shop, or other controlled environment. Additionally, as minimum cure time is an essential variable that affects slip performance, testing should be performed immediately upon full cure of the paint to eliminate additional wait time before fit-up of the connection can be performed.

Acknowledgements

The authors would like to acknowledge the contributions of Bernardo Duran, AZZ Metal Coatings; Sean Donahue, Todd Helwig, and Joseph Yura, University of Texas – Austin; Carly McGee, KTA-Tator; and Justin Ocel, FHWA.

References

1. American Institute of Steel Construction, *Code of Standard Practice for Steel Buildings and Bridges*. AISC, Chicago, October 17, 2016.
2. Research Council on Structural Connections, *Specification for Structural Joints Using High-Strength Bolts*. RCSC, August 1, 2014 (includes April 2015 Errata).
3. AASHTO, *LRFD Bridge Design Specifications*, 8th edition. American Association of State Highway and Transportation Officials, Washington, D.C., 2017.
4. Helwig, Todd, Joseph Yura, Michael Engelhardt, and Sean Donahue. *Final Report for Study: Slip Coefficients for Galvanized Surfaces With Paint Coatings and Metalized Surfaces*. Tech. Austin, Texas: U of Texas at Austin, Sponsored by The American Galvanizers Association, 2017.
5. *Results of Tension Creep Testing of Galvanized, Metalized, and Painted Specimens*. Rep. no. 360758. Pittsburgh, PA: KTA-Tator, 2017.
6. Picklex® 20, International Chemical Products, Inc., 1209 Meadow Park Drive SE, Huntsville, AL 35803. rsen@icpi.net, (256) 650-0088, <https://picklex20.com>.
7. Helwig, Todd, Joseph Yura, and Sean Donahue. *Final Report for Study: Slip Coefficients for Galvanized Surfaces*. Tech. Austin, Texas: U of Texas at Austin, Sponsored by The American Institute of Steel Construction and the Research Council on Structural Connections, 2014.

Figures and Tables

Figure 1. Table 6.13.2.8-3 AASHTO LRFD Bridge Design Specification

Surface Condition	Definition	Ks (Slip Coefficient)
Class A	<ul style="list-style-type: none"> • unpainted clean mill scale • blast-cleaned surfaces with Class A coatings 	0.30
Class B	<ul style="list-style-type: none"> • unpainted blast-cleaned surfaces to SSPC-SP 6 or better • blast-cleaned surfaces with Class B coatings • unsealed (pure Zn or 85/15 Zn/Al) thermal-sprayed coatings with a thickness \leq 16 mils 	0.50
Class C	<ul style="list-style-type: none"> • hot-dip galvanized surfaces (roughening by wire brushing no longer required) 	0.30
Class D	<ul style="list-style-type: none"> • blast-cleaned surfaces (including HDG) painted with Class D coatings 	0.45

Figure 2: Results of Slip and Tension Creep Testing for HDG/ZRP Faying Surfaces

HDG (ASTM A123)	HDG Surface Preparation	Zinc-Rich Paint	Slip Test ⁴	Tension Creep Test ⁵	Classification
			Mean Slip Coefficient	1000-hr Creep Deformation	
6 mils HDG	No Quenching, SSPC SP 1, Picklex® 20	3 mils SHW Zinc Clad II Plus (5 mils test thickness)	0.49	Assembly 1 0.0026"	$\mu = 0.45$
				Assembly 2 0.0035"	
				Assembly 3 -0.0014"	
6 mils HDG	No Quenching, SSPC SP 1, Picklex® 20	2 mils PPG Dimetcote® 9 / Sigmazinc™ 9 (2-4 mils test thickness)	0.50	Assembly 1 -0.0002"	$\mu = 0.50$
				Assembly 2 0.0019"	
				Assembly 3 0.0024"	

Biographies

Alana Hochstein is the corrosion engineer for the American Galvanizers Association (AGA). She provides assistance to architects, engineers, fabricators, owners, and other specifiers regarding technical issues and the processing of hot-dip galvanized steel. She also manages AGA studies and research on performance, application, and processing of hot-dip galvanized steel. Hochstein can be reached via email at ahochstein@galvanizeit.org.

Dr. Thomas J Langill has been with the American Galvanizers Association for 24 years as its Technical Director. He has been active in helping shape the research programs for galvanizing programs. He has provided technical support for many specifiers and engineers who have technical questions about galvanized steel or its use in the environment. He writes a regular feature in the American Galvanizers Association Magazine on problems related to hot dip galvanizing. He has authored and presents a seminar series on Processing Details in the Hot Dip Galvanizing Industry. He is the Chairman of the ASTM Subcommittee A05.13 that authors and edits specifications on hot-dip galvanizing of steel articles. He is a member of NACE, ASM, SSPC, ASCE, SME, ISS, and AWS. He is active in presenting papers on hot-dip galvanized steel as well as editing reference articles in ASM volumes and NACE publications on the galvanizing process. He has designed and written a course in training inspectors of hot-dip galvanized articles.

Slip-resistant connections made of hot-dip galvanized steel – The EU SIROCO Project

Natalie Stranghöner, Nariman Afzali

University of Duisburg-Essen, Institute for Metal and Lightweight Structures, Essen, Germany

Abstract

The application of hot dip galvanized steel is an efficient method of corrosion protection. Previously reported friction coefficients in hot-dip galvanized plates show large variations, e.g. from 0.15 to 0.5. In practice, this results in the use of the lower values in design. It is understood that the causes of the variations are the thickness and structure of the coating which can vary dependent on factors such as the chemical composition of the steel (some promote a stronger reaction between zinc and iron than other compositions), the thermal mass of the steel component and other process variables. For structural sections, steel with a content of silicon from 0.14 to 0.25 % (Category B steels according to EN ISO 14713-2 [1]) and, to a lesser extent, more than 0.25 % (Category D steels according to EN ISO 14713-2) are used. The influence of the steel composition may, to some extent, be controlled by the composition of the zinc melt during processing. The extent to which a softer, outer zinc-phase is present on the coating surface is reported to be the main determinant of slip resistance although if small amounts of slip can be tolerated, this phase will experience a 'cold welding' upon loading. However, when small amounts of initial slip cannot be tolerated, this layer can be easily removed by abrasive sweep blast cleaning or other techniques to modify the surface. Therefore, a comprehensive investigation was carried out within the scope of the European research project SIROCO in order to investigate the influence of surface preparation and post treatment on the slip-resistant behaviour of preloaded bolted connections with hot-dip galvanized faying surfaces.

Keywords

Hot-dip galvanized steel, slip-resistant connections, preloaded bolted connections, slip factor test, EN 1090-2.

1 Introduction

Slip-resistant connections are required, when deformations in bolted connections must be limited either for serviceability or ultimate limit reasons. Typical applications can be found in bridges, cranes, radio masts and towers of wind turbines, which are loaded by alternate loading and/or fatigue or where functional requirements make slip-resistant connections necessary. In general, the resistance to slip in a slip-resistant connection mainly depends on the condition of the faying surfaces and the total clamping force in the bolts.

The exposed elements in slip-resistant connections may be subjected to different environmental conditions. This may cause corrosion of the surfaces of the components, which might reduce the slip resistance of the connections. Covering the faying surfaces with a protective layer is a common way to protect the slip-resistant connection components against corrosion. For this reason, the slip factor of such connections has to be determined by experimental testing applying one of the testing procedures according to various standards/recommendations.

A common coating system for protecting carbon steel surfaces is hot-dip galvanizing (HDG) according to EN ISO 1461. Previous studies on hot-dip galvanized faying surfaces show a large scattering in slip factors for galvanized surfaces with/without post treatments on the surfaces, see [2], [3], [4], [5], [6], [7] and [8]. For this reason, in the frame of European research project SIROCO the influence of the surface preparation and post

treatment on the slip-resistant behaviour of HDG-coated surfaces was investigated. The relaxation behaviour of HDG-coated surfaces with different surface treatments was also investigated. However, these results are not presented in frame of this contribution.

2 Experimental investigations

2.1 Test procedure according to Annex G of EN 1090-2

EN 1090-2 prescribes a generalized experimental procedure to obtain the slip factor. The test procedure consists of a three step test procedure. In the frame of the presented investigations, the test specimen geometry was chosen to the test specimen with M20 bolts as shown in Figure 1 according to EN 1090-2. Four tests must be conducted under an incremental tensile loading condition at normal speed. The duration of the tests shall be 10 min to 15 min.

The individual slip value μ_i , the mean value μ_m and the standard deviation S_μ shall be derived from the following equations:

$$\mu_i = \frac{F_{Si}}{4F_{p,C}}, \quad \mu_m = \frac{\sum \mu_i}{n}, \quad S_\mu = \sqrt{\frac{\sum (\mu_i - \mu_m)^2}{n-1}} \quad (1), (2), (3)$$

The slip loads F_{Si} are defined as the load at which a slip of 0.15 mm is observed. In the presented investigations, the slip load was determined at the maximum load corresponding to a slip deformation lower than or equal to 0.15 mm. With the fifth test specimen, a creep test has to be carried out with 90% of the mean slip load F_{sm} from the first four tests. The test shall last 3 hours to investigate the behaviour of the joint under sustained loads. If the difference between the recorded slip at the end of 5 min and 3 hours after the full load application does not exceed 0.002 mm, the slip load for the specimen under long term condition must be specified as for the previous four tests.

If the difference between the slips exceeds 0.002 mm, at least three extended creep tests must be performed. The standard deviation S_{Fs} of the ten slip load values which are obtained from the five specimens should not exceed 8% of the mean value, otherwise additional specimens have to be tested.

The slip displacements were measured in the centre bolts group (CBG) of the specimens (LVDTs 1-8), as shown in Figure 2. The slip was measured also on the upper and lower edges of the cover plates (PE: LVDTs 9-12). In this report, the slip factors are evaluated based on the measured slip displacement in CBG position for all four sliding planes.

2.2 Test programme

In order to investigate the influence of different post treatments on the slip-resistant behaviour of the HDG surfaces, ten different test series according to Annex G of EN 1090-2 were conducted, see Table 1. Four test series were conducted for HDG surfaces without any further surface treatment considering different clamping length and galvanizing conditions. The galvanizing procedure for HDG-Ref test series was conducted to ensure that the outer zinc layer was present. Combined with a less reactive steel chemistry, this ensured a worse-case substrate for slip resistance prior to further modification of the surface in the other test series.

The faying surfaces of two test series were treated with needle gun with 9 bar air pressure and two different angles to the coated surfaces (45° (HDG_NG-I) and 90° (HDG_NG-II)). The needle gun contained 50 needles and each needle had a diameter of Ø 2 mm. Two test series were sweep blasted with air pressure of 2.5 bar at an angle of 30° to the zinc surface but with two different particle sizes. Both series were blasted with corundum particles of size between 0.2 mm to 0.5 mm (HDG_SB-I) and 0.5 mm to 1.0 mm (HDG_SB-II). The distance between nozzle and zinc surface was about 200 mm for both test series. Two more series were also

sweep blasted using an identical blasting procedure as for series HDG_SB-I and then coated with alkali-zinc silicate (ASI) coating (HDG-ASI) and ethyl-zinc silicate (ESI) coating (HDG-ESI). All post treatments were conducted at the Institute for Corrosion Protection (IKS) Dresden GmbH, Germany.

Test series HDG-I and HDG-II were subjected to extended immersion times during galvanizing and were centrifuged after galvanizing to remove a large proportion of the outer zinc layer prior to solidification. This is a galvanizing procedure used for small components (in this case, sample sets) and not for larger components. The test samples for test series HDG-III were stripped and re-galvanized from Series HDG-I and HDG-II, see Table 2.

The roughness measurement was carried out with a stylus instrument, conforming to the description in ISO 3274 [10] and equipped with a diamond stylus. Processing with the needle gun yielded to roughnesses between 30 and 40 μm . Sweep blasting with fine grain yielded to a roughness of approx. 30 μm and sweep cleaning with coarser grain to values between 50 and 60 μm .

The zinc coating was measured randomly by means of magnetic induction in accordance with EN ISO 2808 [11]. The calibration was performed on a smooth steel sheet with foils of known thickness. Magnetic induction means that nonmagnetic films (e. g. zinc) are measured on steel. The thicknesses of the coatings were measured prior to and after mechanical processing on selected test specimens. During these measurements it was detected that the thicknesses of the zinc films were partially higher after mechanical processing than before surface preparation. The reason for this is presumably the roughness distorting the results. For this reason, the zinc film thicknesses were determined on metallographic cross sections.

All specimens were made of S355. However, the plate material was ordered from different batches with two different chemical compositions. For HDG-I, HDG-II and HDG-III test series, the steel was more reactive (Si 0.03 % and P 0.024 % by mass) in comparison to the other test series (Si 0.01 % and P 0.018 % by mass). The silicon and/or phosphorous content (as well as the thickness of the steel) have an influence on the morphology of the galvanized coating and its thickness. For this reason, it is notable that the plate material was delivered from different batches with two different chemical compositions of the steel. Furthermore, the galvanizing conditions were adjusted between the test series in order to optimise the sample set preparation. This included centrifuging of the sample sets used in HDG-I and HDG-II test series. These differing steel chemistries and sample conditions are reflective of real variations in the galvanized coating but are also important for the interpretation of the results. The main influencing factors for interpretation of the results of each test series are summarized in Table 2.

In practice, non-galvanized steel is sold based on its mechanical properties. In this case, the content of reactive elements is insignificant. Therefore, it is problematic to order steel with defined silicon and phosphorous content from a supplier.

Almost all different test series were selected with the same clamping length ($\Sigma t = 48 \text{ mm}$) in order to eliminate the effect of clamping length on the loss of preload, see also [12]. Only for the HDG-I test series, a different clamping length was considered ($\Sigma t = 152 \text{ mm}$) in order to investigate the influence of the clamping length.

For each test specimen, four M20 HV bolts, property class 10.9 were instrumented with a strain gauge, see Figure 3 and Figure 4. For HDG-I test series, four load cells with a capacity of 180 kN and a relatively long length (100 mm) were prepared in the Stevin lab of TU Delft (TUD), The Netherlands, as an additional measurement method to measure the preload level.

All slip factor tests have been carried out at the Institute for Metal and Lightweight Structures of the University of Duisburg-Essen (UDE), Germany, except two extended creep tests for HDG-II test series, which have been

performed at Fraunhofer Research Institution for Large Structures in Production Engineering IGP, Rostock, Germany [13].

2.3 Results and discussions

The aim of the study was to investigate the influence of different post treatments on the determination of the static slip factor. The results of the static and creep tests are summarized in Table 3 separately for the static tests only and for the combined evaluation of the static and creep tests (in case that the creep test was passed). Extended creep tests have only been performed for some tests series but not for all.

Table 3 presents the calculated slip factors as mean values considering the nominal preload in the bolts $\mu_{nom,mean}$, the initial preload when the tests started $\mu_{ini,mean}$ and the actual preload at slip $\mu_{act,mean}$. The final slip factor for test series (HDG-II) is presented as the result of passed extended creep test. Further extended creep tests for HDG-ASI and HDG-ESI test series were carried out as well. But as these tests were not passed on the applied load levels and further test samples were not available to perform additional extended creep tests on lower load levels, final slip factors could not be determined for these test series. Figure 5 shows the influence of different surface treatments/preparations on the slip-load behaviour and initial slip factors for hot-dip galvanized surfaces. Each test is presented by two graphs, which represent the behaviour of the upper and lower part of the connection.

As it can be seen in Table 3, the influence of the clamping length is negligible for HDG-I and HDG-II test series. In fact, having a high coefficient of variation for HDG-II (about 15 %) and HDG-I (about 9 %) prevents to see the influence of the clamping length on the static slip factor clearly.

Using needle gun results into a slightly improved slip-resistance behaviour of the galvanized specimens, see Figure 5 and Figure 6. The results show that the sweep blasted surfaces achieved higher static slip factors compared to needle gun treated surfaces. Figure 6 shows that better results can be achieved by using a bigger particle size for sweep blasting of the surfaces. The results show that the highest static slip factor for test specimens is achieved for the sweep blasted and ASI-coated (HDG-ASI) test series followed by the sweep blasted test series with ESI coating (HDG-ESI). The slip factors achieved after sweep blasting showed higher coefficient of variations than for other post treated test series. A closer examination of the test results indicated that for both test series HDG_SB-I and HDG_SB-II, higher slip factors were achieved on sample sets of higher steel reactivity, see Table 2 within each test series. Assuming that (i) the sample sets with a more reactive steel have a thinner outer layer of zinc and (ii) blasting conditions are constant within the test series, this indicates that increased exposure of the Fe-Zn layers will yield to higher slip factors. This also indicates that the average slip factors resulting from test series HDG_SB-I and HDG_SB-II can be considered as conservative for the moderately reactive steels encountered in practice for typical structural steels. This hypothesis is confirmed by considering that the highest measured slip factors achieved for test series HDG_SB-II (larger blast media combined with thinner outer zinc layer) approach those measured for test series HDG_II (the same steel chemistry with the outer zinc layer largely removed during the centrifuging process).

Figure 7 shows the metallographic cross-section of the HDG specimens before any post-treatment which were conducted at the Institute for Corrosion Protection (IKS) Dresden GmbH. The typical zinc-phase system of steel with low silicon content is visible. In the upper area, the outer layer of pure zinc can be observed. The preparation of the surface with needle gun and sweep blasting may lead to breaks in the zinc layer, see Figure 8 and Figure 9, although the blasting distance used in these tests was lower than recommended in practice to avoid such effects on the coating. As it can be seen in Figure 10, the galvanized surfaces with ASI or ESI coating show areas with large-scale detachment of the coating. Partially detached coating residues from the

opposite contact area are visible. Zinc-dust particles are visible as white particles. Generally, it can be observed that during preparation of cross-sections zinc-dust particles can break out. These areas appear dark in the image.

For each post treated test series, one creep test was carried out with 90% of the mean slip load F_{sm} from the first four tests. The test shall last 3 hours to investigate the behaviour of the joint under sustained loads. If the difference between the recorded slip at the end of 5 min and 3 hours after the full load application does not exceed 0.002 mm, the slip load for the specimen under long term condition must be specified as for the previous four tests. If the difference between the slips exceeds 0.002 mm, at least three extended creep tests must be performed.

The creep tests failed for all test series for both upper and lower part of the specimens, see Figure 11, thus it is necessary to perform extended creep tests to determine the final slip factor.

Evaluating the slip displacement – log time curve based on the results of the creep tests is a valuable way to estimate the suitable load level for performing extended creep tests for the coated surfaces. Figure 12 shows that $0.9 F_{sm}$ is a high load level for performing the extended creep test for all treated and untreated surfaces and the constant load level has to be reduced for further investigations. For HDG-ASI coated surface one extended creep test was performed with a lower constant load level of $0.8 F_{sm} = 341.4$ kN. As it can be seen in Figure 12 (b), the slip suddenly increased and the extrapolation was not possible. For this reason, the test cannot be considered as a passed extended creep test. Furthermore, one extended creep test was conducted for HDG-ESI coated surfaces with a constant load level of $0.83 F_{sm} = 272.4$ kN. The result shows that the extended creep test was also failed for both parts of the test specimen, see Figure 12 (c). This means the load level is still high and further investigations are needed to achieve the final slip factor. Herewith, the achieved extended creep test results for the HDG-ASI and HDG-ESI coated surfaces do not allow a conclusion regarding the final slip factor for these test series. At least it can be concluded, that the final slip factor will be smaller than 0.5 and 0.4 for HDG-ASI and HDG-ESI test series respectively.

3 Conclusions

A hot-dip galvanized coating will typically comprise a series of Fe-Zn alloy layers covered with an outer layer of zinc. This typical coating structure yielded to relatively low static slip factors (0.12- 0.14). The Fe-Zn alloy layers are harder than the outer zinc layer and are often harder than the steel substrate. The results showed that higher static slip factors in the range of 0.35 - 0.40 for hot-dip galvanized surfaces can be achieved when the outer zinc layer is sufficiently removed by a light blasting procedure (sweep blasting), so that the Fe-Zn layers control the slip behaviour. Higher levels of zinc layer removal will lead to higher slip factors, but the extent of blasting required may depend on the proportion of outer zinc layer within the original coating. The effectiveness of blasting may be adjusted through the size and type of blast media, but can also be adjusted by other blasting parameters.

Modification of the surface with a needle gun does not remove the outer layer of zinc and, for the typical coating structure used as a basis for these tests, will only increase slip factors in the range of 0.20- 0.24 through an increase in surface roughness.

Sweep blasting of a hot-dip galvanized surface combined with the application of an alkali-zinc silicate (ASI) paint produces the highest static slip factors observed in these tests ($\mu_{ini,mean} = 0.62$). Although ASI paints have limitations in terms of overcoating, this would not normally be necessary as the underlying galvanized coating will provide the required corrosion protection.

For all test series, the creep tests failed for both upper and lower part of the specimens and thus extended creep tests are necessary to determine the final slip factors. However, the extended creep test results achieved by a limited number of available test samples for the HDG-ASI and HDG-ESI coated surfaces do not allow a conclusion regarding the final slip factor for these test series up to now. Further investigations are planned.

Acknowledgements

The authors wish to express thanks to the Research Fund for Coal and Steel (RFCS)/European Commission for funding the research project "Execution and reliability of slip resistant connections for steel structures using CS and SS" SIROCO (RFSR-CT-2014-00024).

References

- [1] EN ISO 14713-2 (2009) Zinc coatings - Guidelines and recommendations for the protection against corrosion of iron and steel in structures - Part 2: Hot dip galvanizing (ISO 14713-2:2009).
- [2] Valtinat, G., Albrecht, F. & Dangelmaier, P. (1993) Gleitfeste Verbindungen mit feuerverzinkten Stahlteilen und Reibfesten Beschichtungen oder anderen reibbeiwert erhöhenden Maßnahmen, Gemeinschaftsausschuss Verzinken e.V., Technische Universität Hamburg-Harburg, Deutschland, Forschungsbericht, Heft 3, Bericht Nr. 22.
- [3] Valtinat, G. (1996) Gleitfeste Vorgespannte Verbindungen mit Langlöchern bei feuerverzinkten Stahlbauteilen für Fassaden-Unterkonstruktionen, Gemeinschaftsausschuss Verzinken e.V., Forschungsvorhaben GAV-Nr. FG 25, Technische Universität Hamburg-Harburg, Deutschland, Bericht Nr. 132.
- [4] Kammel, C., Sedlacek, G. (2001) Dauerverhalten von GV-Verbindungen bei verzinkten Konstruktionen im Freileitungs-, Mast- und Kaminbau, Studiengesellschaft Stahlanwendung e.V., Düsseldorf, Lehrstuhl für Stahlbau, RWTH Aachen, Deutschland, Forschungsbericht P409.
- [5] Cruz, A., Simões, R., Alves, R. (2012) Slip factor in slip resistant joints with high strength steel, Journal of Constructional Steel Research 70, H. 3, S. 280–288.
- [6] Heistermann, C., Veljkovic M., Simões, R., Rebelo, C., Simões da Silva, L. (2013) Design of slip resistant lap joints with long open slotted holes, Journal of Constructional Steel Research 82, Elsevier Ltd, Iulea University of Technology, Sweden, University of Coimbra, Portugal.
- [7] Annan, C.-D., Chiza, A. (2013) Characterization of Slip resistance of high strength bolted connections with zinc-based metallized faying surfaces, Engineering Structures 56, Department of Civil and Water Engineering, université Laval, Canada.
- [8] Annan, C.-D., Chiza, A. (2014) Slip resistance of metalized galvanized faying surfaces in steel bridge constructions, Journal of Constructional Steel Research 95, Elsevier Ltd, Department of Civil and Water Engineering, université Laval, Canada.
- [9] EN 1090-2:2008+A1 (2011) Execution of steel structures and aluminium structures — Part 2: Technical requirements for steel structures.
- [10] ISO 3274 (1996) Geometrical Product Specifications (GPS) - Surface texture: Profile method - Nominal characteristics of contact (stylus) instruments.
- [11] EN ISO 2808 (2007) Paints and varnishes – Determination of film thickness.
- [12] Stranghöner, N., Afzali, N., de Vries, P., Glienke, R., Ebert, A. (2017) Optimization of the test procedure for slip factor tests according to EN 1090-2, Steel Construction 10, Issue 4, p. 267-281.
- [13] Stranghöner et al. (2018) Execution and reliability of slip resistant connections for steel structures using CS and SS, RFCS Research project SIROCO (RFSR-CT-2014-00024), 29 March 2018 (not published yet).

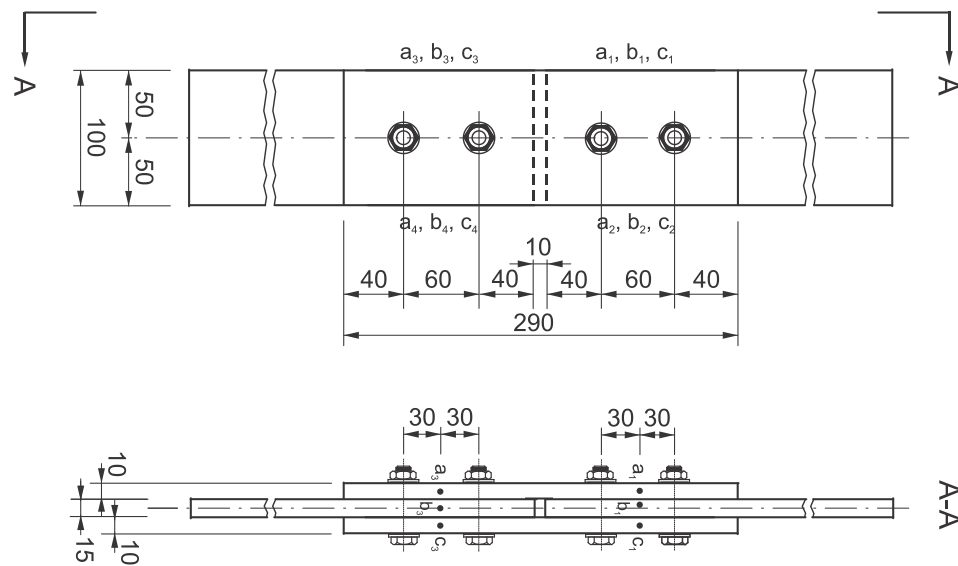


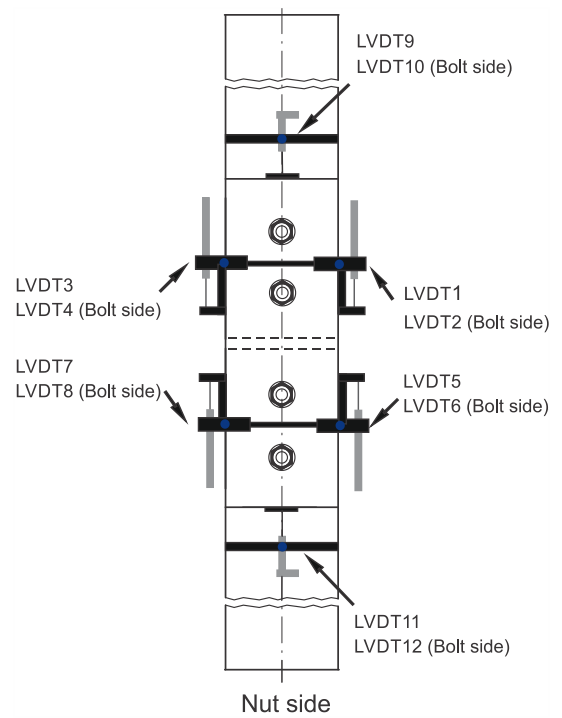
Figure 1 Chosen test specimen geometry for the determination of the slip factor according to EN 1090-2, Annex G, test specimens for M20 bolts



(a) Test setup (Instrumented bolt for application combined with the long-load cell (SG + LC))



(b) Test setup (Instrumented bolt for application without any adapter (SG))



CBG (Centre Bolt Group): → LVDTs 1-8

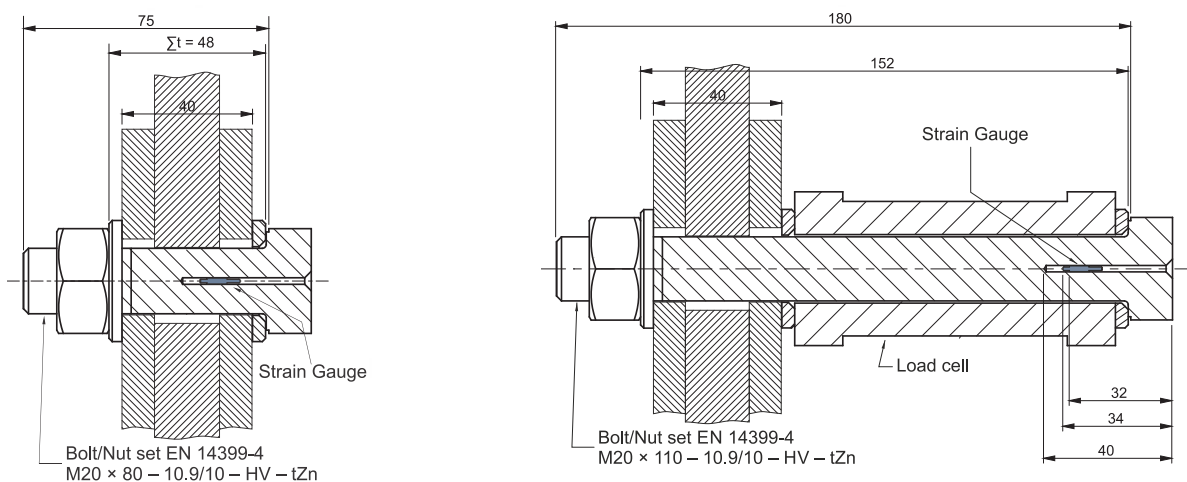
PE (Plate Edge): → LVDTs 9-12

(c) Positions of LVDTs

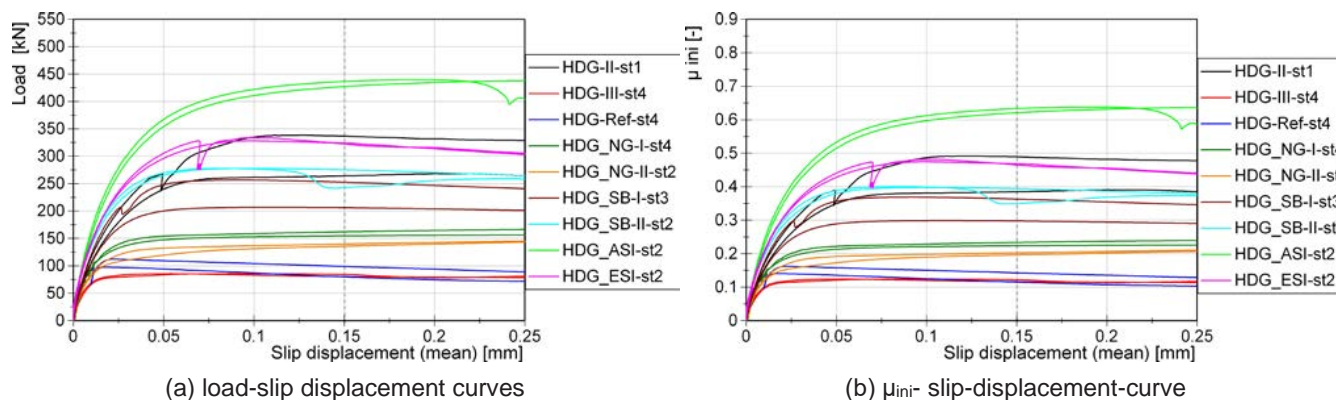
Figure 2 Test setup, positions of displacement transducers (LVDTs)



a) production process of the instrumented bolts
 b) production process of the load cells (© TUD)
Figure 3 Production of the bolts with implanted strain gauges at UDE and load cells at TUD



a) Instrumented bolt for application without any adapter (SG)
 b) Instrumented bolt for application combined with the long-load cell (SG + LC)
Figure 4 Clamped plates of the specimen including an instrumented bolt



(a) load-slip displacement curves
 (b) μ_{ini} - slip-displacement-curve
Figure 5 Influence of different surface treatment/preparation on the slip-load behaviour and initial slip factors

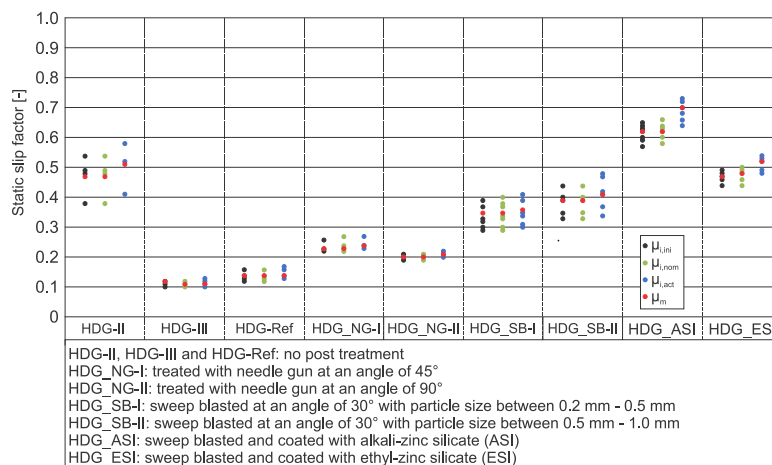
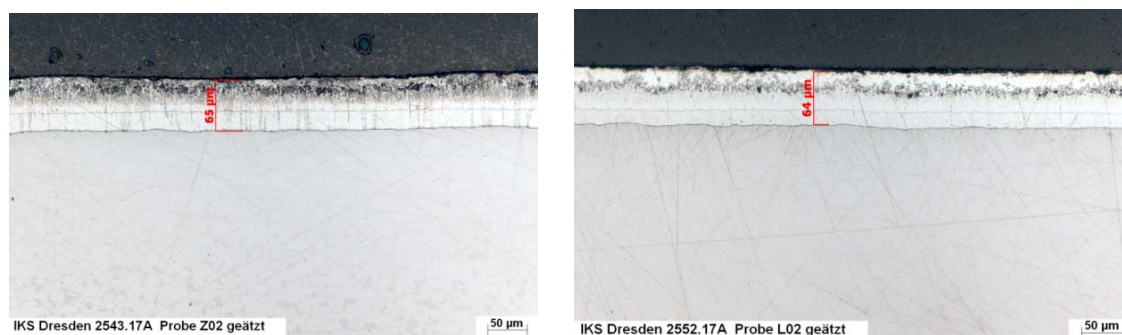
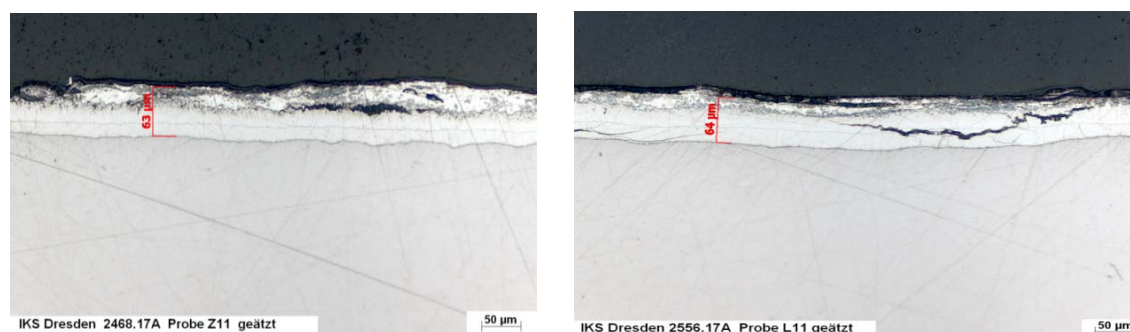


Figure 6 Influence of different post treatments on the static slip factors

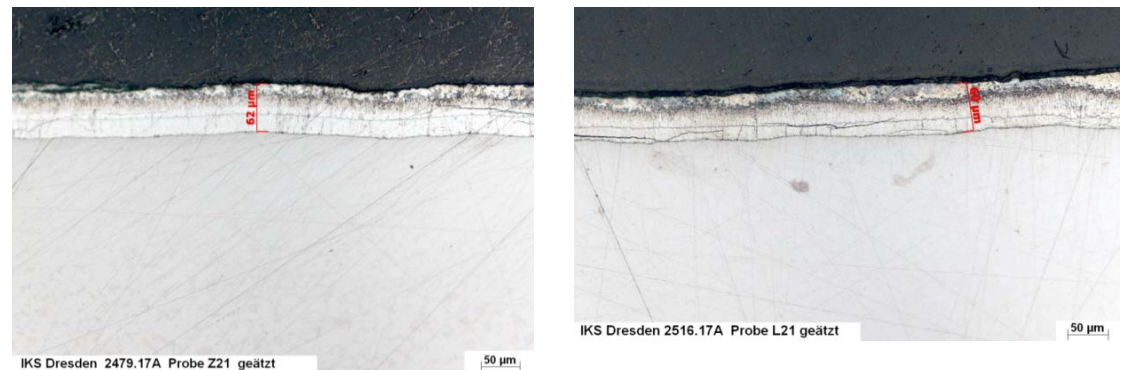


(a) without surface preparation - inner plate (b) without surface preparation - outer plate

Figure 7 Metallographic cross-section of the HDG specimens without any further treatments (© IKS)

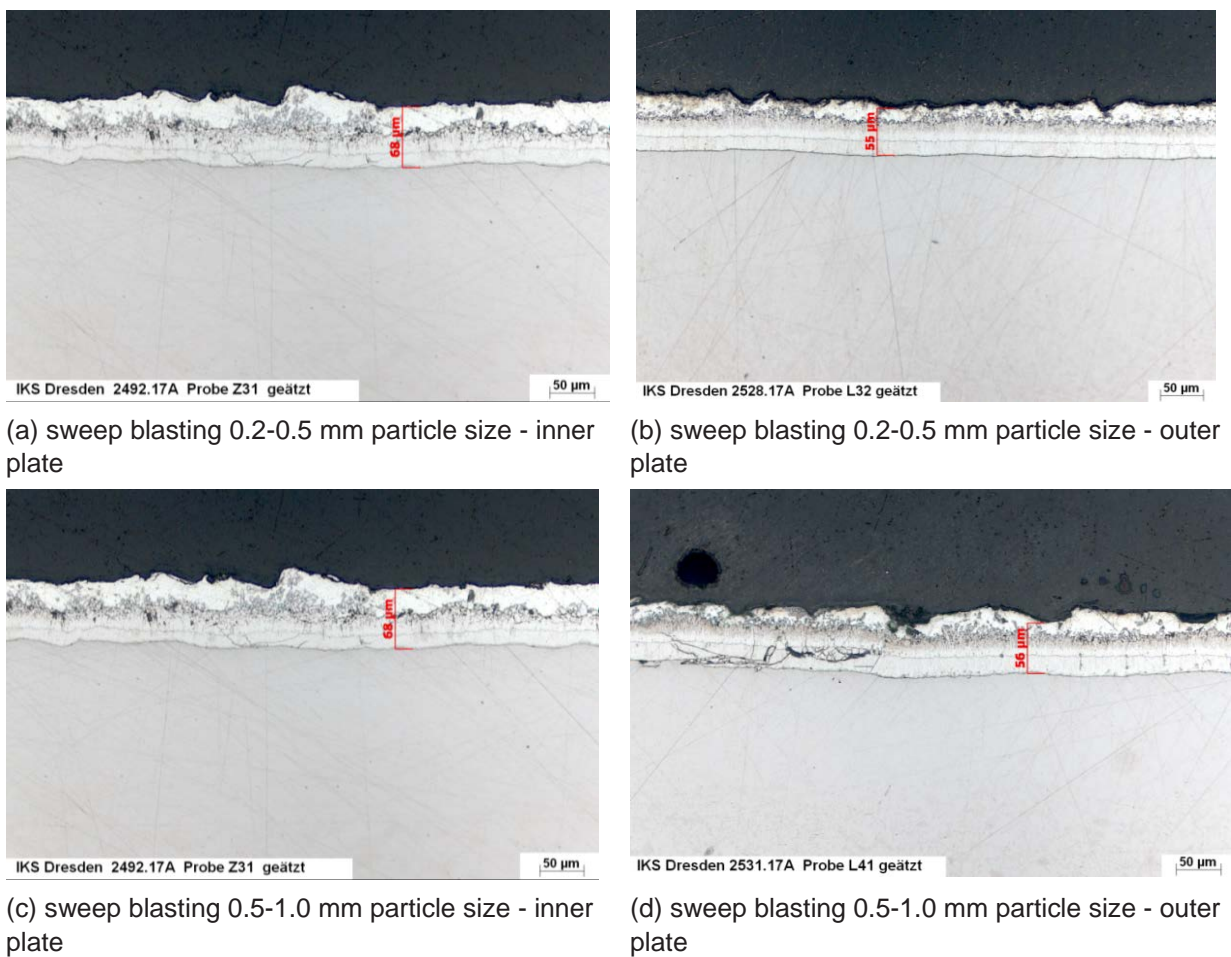


(a) needle gun at angle of 45° - inner plate (b) needle gun at angle of 45° - outer plate



(c) needle gun at angle of 90° - inner plate (d) needle gun at angle of 90° - outer plate

Figure 8 Metallographic cross-section of the HDG specimens treated with needle gun (© IKS)



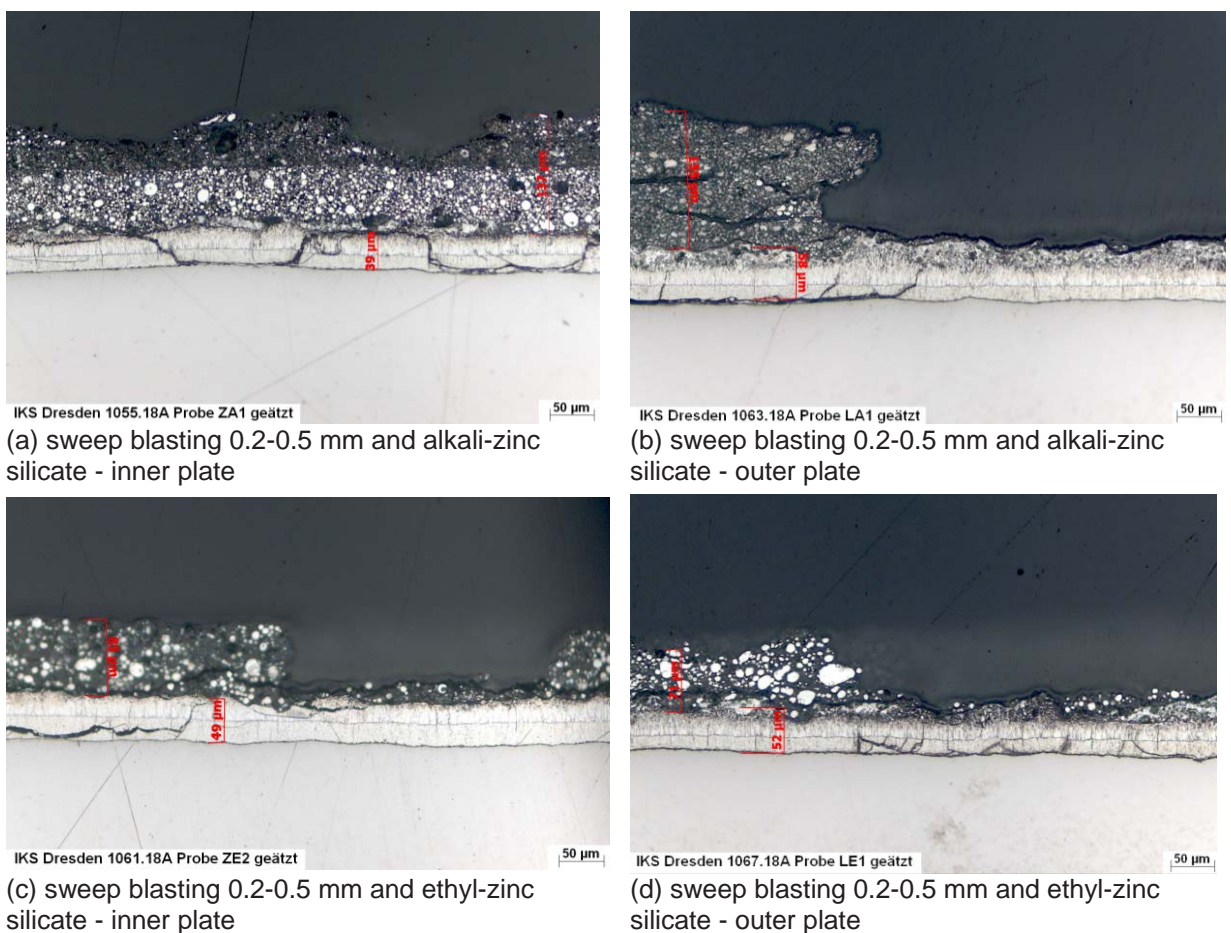
(a) sweep blasting 0.2-0.5 mm particle size - inner plate

(b) sweep blasting 0.2-0.5 mm particle size - outer plate

(c) sweep blasting 0.5-1.0 mm particle size - inner plate

(d) sweep blasting 0.5-1.0 mm particle size - outer plate

Figure 9 Metallographic cross-section of the HDG specimens with sweep blasted surfaces (© IKS)



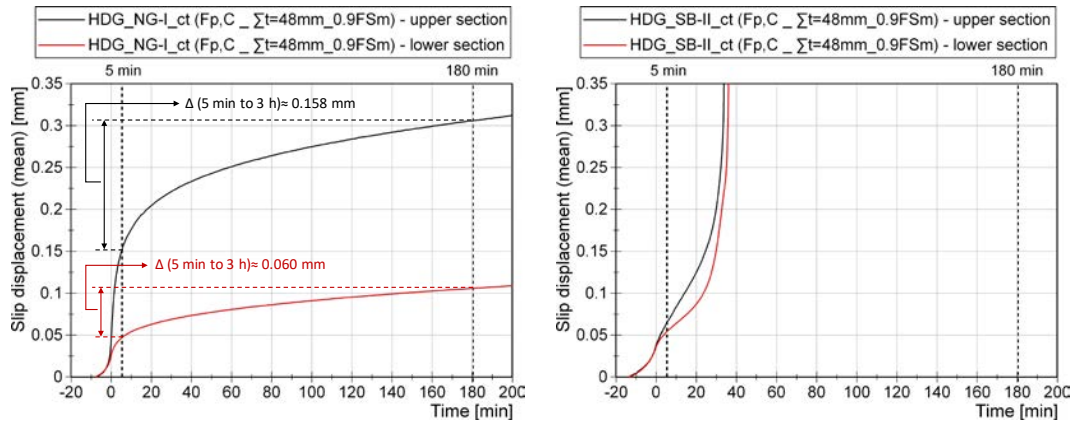
(a) sweep blasting 0.2-0.5 mm and alkali-zinc silicate - inner plate

(b) sweep blasting 0.2-0.5 mm and alkali-zinc silicate - outer plate

(c) sweep blasting 0.2-0.5 mm and ethyl-zinc silicate - inner plate

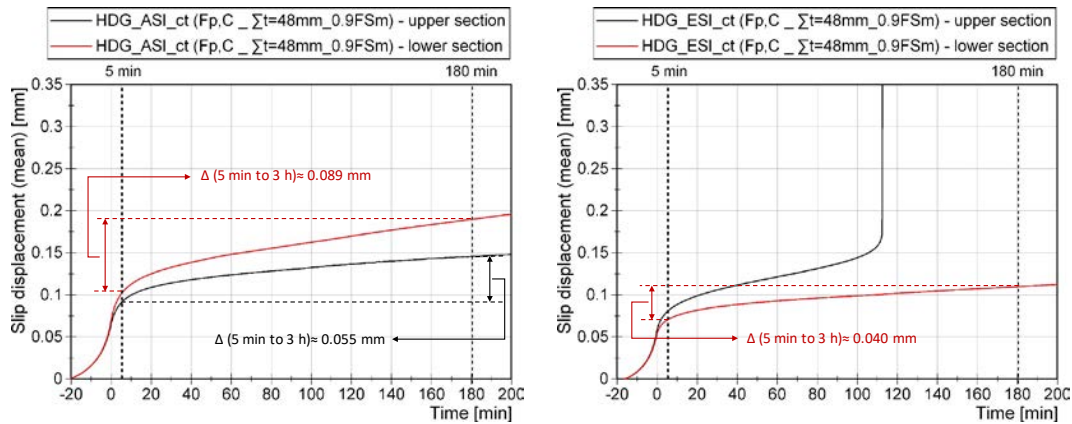
(d) sweep blasting 0.2-0.5 mm and ethyl-zinc silicate - outer plate

Figure 10 Metallographic cross-section of the HDG_ASI and HDG_ESI specimens (© IKS)



(a) treated with needle gun at an angle of 45°

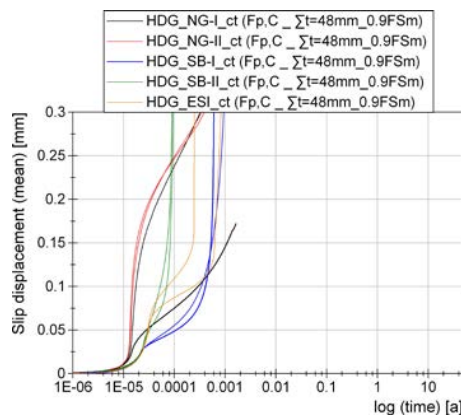
(b) sweep blasted at an angle of 30° with particle size 0.5 - 1.0 mm



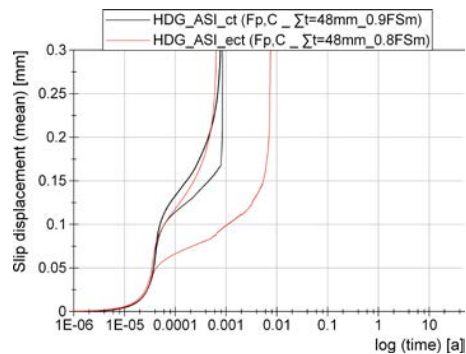
(c) sweep blasted and coated with alkali-zinc silicate (ASI)

(d) sweep blasted and coated with ethyl-zinc silicate (ESI)

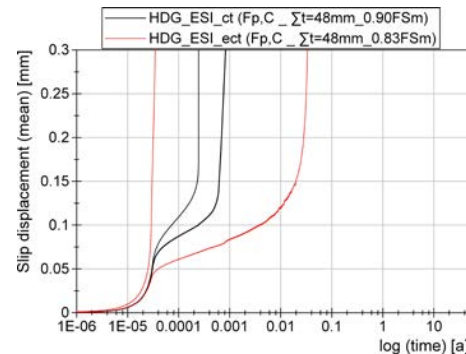
Figure 11 Exemplary results of creep tests considering different post treatment for galvanized specimens



(a) different surface treatments



(b) sweep blasted and coated with alkali-zinc silicate (ASI)



(c) sweep blasted and coated with ethyl-zinc silicate (ESI)

Figure 12 Evaluating the slip displacement – log time curves based on the results of the creep and extended creep tests

Table 1 Test specimens and surface conditions

Series ID	Steel grade	Surface condition								
		Before coating	Main coating			Additional coating				
			Type	Post treatment	Rz ¹⁾ [μm]		t ²⁾ [μm]	Type		
HDG-I	S355 ⁴⁾	Chemically cleaned	Hot dip galvanized	-	-	105	-			
HDG-II					-	105				
HDG-III					-	80				
HDG-Ref					-	71				
HDG_NG-I	S355 ⁵⁾			Hot dip galvanized	sweep blasted at an angle of 30° with particle size 0.2 - 0.5 mm	30		60-70	-	
HDG_NG-II						40		60-70		
HDG_SB-I						30		60-70		
HDG_SB-II						50		60-70		
HDG-ASI						30		60-70		ASI ⁶⁾
HDG-ESI						30		60-70		ESI ⁷⁾

¹⁾ surface roughness | ²⁾ average HDG coating thickness | ³⁾ DFT: dry film thickness (coating thickness) | ⁴⁾ moderately reactive Steel (S) | ⁵⁾ low-reactive steel chemistry for galvanizing | ⁶⁾ alkali-zinc silicate (ASI) coating | ⁷⁾ ethyl-zinc silicate (ESI) coating
 All bolts were preloaded with a preloaded level of F_{p,c} = 172 kN.

Table 2 Parameters of importance with regard to the interpretation of the test results

Series ID	Galvanizing conditions	Steel Chemistry of relevance to reactivity during galvanizing					
		Si (%)		P (%)		Si + 2.5 P	
		10 mm plate	20 mm plate	10 mm plate	20 mm plate	10 mm plate	20 mm plate
HDG-I HDG-II	Centrifuged; Conventional galvanizing temperature; extended immersion time to ensure EN ISO 1461 coating thickness achieved.	Supplier Cert: <0.030	Supplier Cert: 0.016	Supplier Cert: <0.025	Supplier Cert: 0.020	0.0915	0.0825
HDG-III	Conventional dipping procedure; Conventional galvanizing temperature; immersion time and withdrawal optimised to achieve smooth coating for slip test procedure. Sample sets were stripped and re-galvanized from Series HDG-I and HDG-II.	Analysis 1: 0.0290 Analysis 2: 0.0290	0.030	Analysis 1: 0.0240 Analysis 2: 0.0260	0.0210		
HDG-Ref	Conventional dipping procedure; Conventional galvanizing temperature; immersion time and withdrawal optimised to achieve smooth coating for slip test procedure.	Analysis 1: 0.010 Analysis 2: 0.009	Analysis 1: 0.0110 Analysis 2: 0.0110	Analysis 1: 0.018 Analysis 2: 0.019	Analysis 1: 0.0160 Analysis 2: 0.0170	0.0558	0.0523
HDG_NG-I HDG_NG-II HDG_SB-I HDG_SB-II HDG-ASI HDG-ESI		The steel chemistry of sample sets used in these test series were a mixture of those employed in Series HDG-II and HDG-Ref.					
NOTES	<p>1. Both Si and P levels in steel have influence on the reaction between molten zinc and iron during hot dip galvanizing. EN ISO 14713-2 identifies that steels with chemistries satisfying the formula $Si+2.5P \leq 0.09\%$ will have lower reactivity during galvanizing. Steels used for sample sets in test series HDG-II and HDG-III are at the upper boundary of this general rule and therefore exhibit higher reactivity than the sample sets used for HDG-Ref.</p> <p>2. A more reactive steel used in a sample set can be expected to produce a higher proportion of Fe-Zn alloy layer within the galvanized coating structure.</p> <p>3. Centrifuging of a sample set will remove a large amount of the outer zinc layer before freezing and thus increases the presence of Fe-Zn alloy at the surface.</p>						

Table 3 Test programme, mean slip factors based on static and creep tests only ($\mu_{ini,mean}$ and $\mu_{act,mean}$) as well as final slip factors calculated as 5% fractile or determined in the extended creep test ($\mu_{5\%}$ or μ_{ect})

Series ID	Final surface condition			$\Sigma t^{(3)}$ [mm]	Number of tests st/ct/ect ⁽⁴⁾	$\mu_{ini,mean}^{(5)}$ st/st+ct [-]	$\mu_{act,mean}^{(6)}$ st/st+ct [-]	V (μ_{act}) ⁽⁷⁾ st/st+ct [%]	Final slip factor [-] $\mu_{5\%}^{(8)} / \mu_{ect}^{(9)}$
	Post treatment	Rz ⁽¹⁾ [μ m]	DFT ⁽²⁾ [μ m]						
HDG-I	no post treatment	-	105 ⁽¹⁰⁾	152	4/1/-	0.47/-	0.48/-	9.2/-	-/-
HDG-II		-	80 ⁽¹⁰⁾	48	2/-/2	0.47/-	0.51/-	14.6/-	-/0.35 ⁽¹¹⁾
HDG-III		-	80 ⁽¹⁰⁾	48	4/-/-	0.12/-	0.12/-	6.6/-	-/-
HDG-Ref		-	71 ⁽¹⁰⁾	48	4/-/-	0.14/-	0.14/-	11.6/-	-/-
HDG_NG-I	needle gun (45°)	30	60-70	48	4/1/-	0.23/-	0.24/-	6.2/-	-/-
HDG_NG-II	needle gun (90°)	40	60-70	48	4/1/-	0.20/-	0.21/-	3.7/-	-/-
HDG_SB-I	sweep blasted particle size 0.2 - 0.5 mm	30	60-70	48	4/1/-	0.35/-	0.36/-	11.9/-	-/-
HDG_SB-II	sweep blasted particle size 0.5 - 1.0 mm	50	60-70	48	4/1/-	0.39/-	0.41/-	11.8/-	-/-
HDG-ASI	sweep blasted + ASI ⁽¹²⁾	30	120-130	48	4/1/1	0.62/-	0.70/-	5.1/-	-/-
HDG-ESI	sweep blasted + ESI ⁽¹³⁾	30	120-130	48	4/1/1	0.47/-	0.52/-	4.3/-	-/-

⁽¹⁾ surface roughness | ⁽²⁾ dry film thickness (total coating thickness) | ⁽³⁾ Σt : clamping length | ⁽⁴⁾ st: static test/ct: creep-/ect: extended creep test | ⁽⁵⁾ $\mu_{ini,mean}$: calculated slip factors as mean values considering the initial preload when the tests start | ⁽⁶⁾ $\mu_{act,mean}$: calculated slip factors as mean values considering the actual preload at slip | ⁽⁷⁾ V: coefficient of variation for $\mu_{act,mean}$ | ⁽⁸⁾ $\mu_{5\%}$: slip factors as 5 % fractile calculated based on the static tests and the passed creep test | ⁽⁹⁾ μ_{ect} : slip factor resulting from the extended creep test passed | ⁽¹⁰⁾ average HDG coating thickness | ⁽¹¹⁾ see [13] | ⁽¹²⁾ alkali-zinc silicate (ASI) coating | ⁽¹³⁾ ethyl-zinc silicate (ESI) coating.
All bolts were preloaded with a preloaded level of $F_{p,C} = 172$ kN.

Biographies

Prof. Dr.-Ing. Natalie Stranghöner

Professor Natalie Stranghöner is full professor and head of the Institute for Metal and Lightweight Structures of the University of Duisburg-Essen since 2008. She was project co-ordinator of the European RFCS research project SIROCO with in total 11 partners in which frame the presented research activities were carried out. Her research focuses are the execution and load bearing capacity of non-preloaded and preloaded bolted connections made of carbon and stainless steel, fatigue, shell structures, and textile membrane and foils for textile architecture. Professor Stranghöner is member of several European and German national standardization committees for steel structures (e.g. EN 1090-2, EN 1993-1-1, -1-4, -1-6, -1-7, 4-1, 4-2) and membrane structures.

Nariman Afzali, M.Sc.

Nariman Afzali is research assistant at the Institute for Metal and Lightweight Structures of the University of Duisburg-Essen since 2014. His main research activities lie in the field of slip-resistant connections made of carbon and stainless steel. Nariman Afzali was deeply involved in the European RFCS research project SIROCO which he co-ordinated together with Professor Stranghöner.

Examination of influencing factors on the coating quality of hot dip galvanized high strength fasteners for construction purposes

Holger Hoche, Miro Lander, Matthias Oechsner, TU Darmstadt, State Materials Testing Institute (MPA) and Chair and Institute for Materials Technology (IfW), Darmstadt (Germany)

Grafenstraße 2, 64283 Darmstadt
+496151 1625074
hoche@mpa-ifw.tu-darmstadt.de

Steffen Six, Susanne Friedrich, Institut für Korrosionsschutz Dresden GmbH, Dresden (Germany) – Institute of Steel Construction (Germany)

Abstract

Insbesondere bei den im Hochtemperatur (HT)-Verfahren erzeugten Zinkschichten stellt derzeit die Sicherstellung der Haftfestigkeit ein maßgebliches technologisches Problem für die Verzinkungsbetriebe dar. Die Schichten platzen zum Teil ab und / oder es ist eine erhöhte Brüchigkeit mit einer deutlichen Reduktion der Schlagfestigkeit zu beobachten.

Gerade bei der Feuerverzinkung hochfester Schraubengarnituren kommt es immer wieder zu Fehlverzinkungen durch mangelnde Schichthaftung. Aufgrund der geringeren Verbreitung ist die HT-Verzinkung anteilmäßig stärker betroffen als die Normaltemperatur (NT)-Verzinkung.

Eine Beschreibung der Ursachen dieser Fehlverzinkungen gibt es heute nicht, weil die gesamte Prozesskette, vom Vormaterial über die Herstellung bis zur Verzinkung des fertigen Bauteils bezüglich der Zusammenhänge und Einflussfaktoren auf das Verzinkungsergebnis noch unberücksichtigt geblieben ist. Aufgrund der nicht ausreichend spezifizierten Prozessführung sind gute Verzinkungsergebnisse heute oft das Resultat von Empirie.

Daher wurden verschiedene Einflussfaktoren bezüglich der Werkstoffeinflüsse und der Verzinkungsparameter systematisch im Hinblick auf die Überzugsqualität für die HT-Feuerverzinkung untersucht. Die aktuellen Ergebnisse werden auszugsweise zusammengefasst.

Especially in the case of high temperature (HT) hot-dip galvanizing, the securing of the adhesive strength is currently a significant technological problem for galvanizers. Typical failures are chipping or cracking of the coatings, which often leads to increased brittleness and a reduced impact strength of the layers.

Especially hot-dip galvanized high-strength bolts, nuts and washers suffer from these failures, thus and additional pickling off the layer and a subsequent galvanizing is necessary. Due to the lower prevalence, HT galvanizing is proportionately more affected than normal temperature (NT) galvanizing.

To this day, the reasons for the occasionally occurring adhesion problems is still not known entirely. The lack of knowledge can be attributed to the fact that the entire process chain, i.e. the raw material, the production of the components and the galvanizing process itself, is not put in context regarding the influencing factors and the galvanizing result. Due to insufficiently specified process control, good galvanizing results are still often the result of empiricism.

Therefore, various influencing factors with regard to material influences and galvanizing parameters were systematically investigated with regard to the layer quality for HT hot-dip galvanizing. The current results are summarized in extracts.

Einleitung / Introduction

Bisher durchgeführte wissenschaftliche Untersuchungen zur Haftfestigkeit beschränken sich schwerpunktmäßig auf die NT-Verzinkung von Baustählen niedriger Festigkeiten ohne Vergütungsbehandlung. Sowohl für die HT-Verzinkung als auch für die Verzinkung von Vergütungsstählen existieren bis dato nur wenige Forschungsergebnisse. Verfügbare wissenschaftliche Daten stammen bis heute zum großen Teil aus den 70er bis 90er Jahren des vergangenen Jahrhunderts und sind aufgrund neuer Werkstoffentwicklungen nicht mehr aktuell. Die gesamte Prozesskette, vom Vormaterial über die Herstellung bis hin zur Feuerverzinkung des fertigen Bauteils ist bezüglich der Zusammenhänge und Einflussfaktoren auf das Verzinkungsergebnis von Schraubengarnituren bis heute unberücksichtigt. Dies betrifft sowohl die HT- als auch die NT-Verzinkung, wobei aufgrund der mangelnden Kenntnisse der Gesamtzusammenhänge zur Erzielung hafter Zinküberzüge

insbesondere die HT-Verzinkung heute starken Streuungen in der Schichtqualität und der Prozesssicherheit unterliegt.

Für die NT-Verzinkung von Baustählen wurden die Prozessschritte der Vorbehandlung vor dem Verzinken, der Verzinkungsprozess selbst und der Abkühlung nach dem Verzinken weitgehend untersucht [1, 2, 3]. Für Vergütungsstähle besteht dagegen noch Untersuchungsbedarf.

So beeinflusst z.B. für die NT-Verzinkung der Oberflächenzustand die Phasenausbildung des Zinküberzugs [4]. Generell beeinflussen unterschiedliche Oberflächenzustände (z.B. Randoxidation, gewalzte, gestrahlte Oberflächen) die Haftfestigkeit von NT-Verzinkungen.

Bezüglich des Werkstoffeinflusses wurden in [5] über eine Häufung von Haftungsproblemen bei höherfesten Vergütungsstählen berichtet, während sich allgemeine Baustähle normalerweise relativ problemlos verzinken lassen. Eine Erklärung für die Ursache wurde jedoch nicht geliefert.

Die Abkühlbedingungen beeinflussen entscheidend die Schichtqualität. Bei sehr schroffer Abkühlung NT-verzinkter Schrauben in Wasser wurden Risse in der Schicht beobachtet, während bei etwas sanfterer Abkühlung mittels einer Brause keine Risse festgestellt wurden [6]. Die abkühlbedingte Rissbildung in den Schichten wird durch spröde Phasen (δ_1 und Γ) begünstigt. Unter Beanspruchung wurden auch Delamination bzw. Rissbildung innerhalb der Phasen beobachtet, die auf deren Unterschiede in den mechanischen Eigenschaften zurückzuführen sind, indem in der Grenzfläche vorhandene Schubspannungen die Rissbildung bewirken [7].

In HT-Zinküberzügen soll die Rissbildung mit Eigenspannungen bei der Abkühlung aufgrund unterschiedlicher thermischer Ausdehnungskoeffizienten zwischen Schicht und Stahl sowie aufgrund der Volumendifferenzen und Eigenspannungen innerhalb der an der Schichtbildung beteiligten Phasen zusammenhängen [8]. Erste empirische Untersuchungen zur Haftfestigkeit von HT-Zinküberzügen [9] zeigten, dass mit einer schnellen Abkühlung (Abschrecken in Wasser) bessere Haftfestigkeiten erzielt werden als mit langsamer Abkühlung (Luft). Die die Haftfestigkeit begünstigende schnelle Abkühlung beim HT-Verzinken (Abschrecken im Wasserbad), sowie die aufgrund einer langsamen Abkühlung an Luft hervorgerufenen Phasenumwandlungsprozesse mit rissigen und porigen Überzügen wurden in [6, 10] auf Basis phänomenologischer Untersuchungen ebenfalls bestätigt.

Aufgrund der mangelnden Kenntnisse der Zusammenhänge und der Einflussfaktoren auf das Verzinkungsergebnis unter Berücksichtigung der gesamten Prozesskette, vom Vormaterial über die Fertigung bis hin zur Feuerverzinkung des fertigen Bauteils, unterliegt insbesondere die HT-Verzinkung heute starken Streuungen in der Schichtqualität und der Prozesssicherheit.

Die existierenden offenen technologischen Fragestellungen zur Sicherstellung der Qualität der Zinküberzüge stellen zur Zeit ein Hemmnis dar, die HT-Verzinkung für hochbeanspruchte, hochfeste Schraubengarnituren breiter anzuwenden.

Vor diesem Hintergrund werden in dem Forschungsvorhaben IGF 18389 BG „Optimierung feuerverzinkter Überzüge für hochfeste Schrauben“ die Einflüsse der Verzinkungsbedingungen sowie des vorgelagerten Herstellungsprozesses auf das Verzinkungsergebnis systematisch untersucht. Die Ergebnisse sind im Folgenden auszugsweise dargestellt.

Ergebnisse / Results

Einfluss des Oberflächenzustands

Influence of the materials surface condition

Zur Untersuchung des Oberflächeneinflusses wurden Schrauben, Muttern und Scheiben unterschiedlicher Abmessungen, Festigkeitsklassen, Werkstoffe und Oberflächenzustände bei einem Verzinkungsbetrieb in Standardprozessen für das NT- und das HT-Verfahren feuerverzinkt und anschließend im Hinblick auf Schichtausbildung und Schichthaftung untersucht. Das Parameterscreening umfasste 9 Werkstoffe, 8 Abmessungen, 5 Oberflächenzustände und 3 Festigkeitsklassen.

Hinsichtlich der Werkstoffe, der Festigkeitsklassen und der Abmessungen wurden keine das Verzinkungsergebnis beeinflussende signifikante Einflussfaktoren festgestellt. Als einziger signifikanter Einflussfaktor stellte sich der Oberflächenzustand heraus. Hier konnten drei Einflüsse abgeleitet werden:

- a) *Verzunderung der Oberfläche*: Anhäufungen von Zunder infolge des Vergütungsprozesses bewirken ein ungleichmäßiges Beizergebnis im Rahmen der Vorbehandlung. Dies ist insbesondere bei hochfesten 10.9-Schrauben problematisch, weil hier gemäß DSV-GAV-Richtlinie [11] die Beizdauer auf max. 15 Minuten beschränkt ist. Unvollständig entzunderte Oberflächen bewirken dann Fehlstellen des Zinküberzugs (**Bild 1**).
- b) *Randoxidation und Randentkohlung*: Die Scheiben werden im Regelfall aus einfachen, unlegierten Vergütungsstählen gefertigt. Weil diese in Bezug auf die Dauerhaltbarkeit und die Bauteilsicherheit eine vergleichsweise geringe Rolle spielen, kommt diesen Komponenten der Schraubengarnitur oft nur eine untergeordnete Bedeutung zu. Allerdings werden neben den prozessbedingten Klebern auch oft Beschichtungsfehler beobachtet. Untersuchungen zeigten, dass Wärmebehandlungsartefakte in Form von Randentkohlung und Randoxidation schlechte Verzinkungsergebnisse bewirken (**Bild 2**).
- c) *Deltaferrit (δ -Ferrit)*: Gemäß DSV-GAV-Richtlinie müssen Schrauben der Festigkeitsklasse 10.9 frei von δ -Ferrit sein, um die Anfälligkeit für wasserstoffinduzierte Spannungsrisskorrosion zu reduzieren. Für niederfestere Schrauben ist δ -Ferrit nicht explizit verboten. δ -Ferrit bildet sich, wenn die Schrauben vor der Vergütung nicht entphosphatiert werden. Der Phosphor diffundiert beim Härten in den Randbereich und inhibiert dort die martensitische Umwandlung.

Bild 3 zeigt lichtmikroskopische Aufnahmen des Randgefüges vor dem Feuerverzinken sowie Aufnahmen der Zinküberzüge nach dem Verzinken in verschiedenen Bereichen einer M20, 10.9-Schraube. Bei dieser Schraube wurde bewusst auf die Entphosphatierung verzichtet, um den Einfluss des δ -Ferrit zu untersuchen. Aufgrund der sehr geringen Umformung im Schaftbereich liegt praktisch die ursprüngliche Drahtoberfläche vor, und der δ -Ferrit ist dort stark ausgeprägt. Der Zinküberzug ist dort brüchig und zeigt partiell Abplatzungen. Aufgrund der starken Gefügeverformung durch das Anstauchen des Kopfes ist der δ -Ferrit dort deutlich schwächer ausgebildet, und der Zinküberzug zeigt in diesem Bereich weniger Risse. Die Schlüsselflächen wurden durch Scherschneiden hergestellt und weisen demnach kein δ -Ferrit auf. Hier ist der Zinküberzug frei von Fehlstellen.

Auch bei Schadensfällen im Zusammenhang mit Haftungsproblemen des Zinküberzugs wurde ein Einfluss von δ -Ferrit nachgewiesen (**Bild 4**). Während der Zinküberzug in der Mitte des Kopfes gut haftet, weil dort infolge der Schnittkante kein δ -Ferrit vorhanden ist, kommt es im Randbereich zu Abplatzungen. Dort wurden mittels Rasterelektronenmikroskop (REM) und energiedispersiver Röntgenmikroanalyse (EDX) Reste von Phosphor nachgewiesen sowie ein sehr feiner δ -Ferrit im metallographischen Schliff.

In diesem Zusammenhang ist darauf hinzuweisen, dass durch δ -Ferrit bedingte Haftungsprobleme bei fertig verzinkten Schrauben oft nicht nachweisbar sind, weil die oft nur wenige Mikrometer dünnen δ -Ferrit Schichten infolge der Fe-Zn-Legierungsschichtbildung nicht mehr erkennbar sind.

Einfluss der Abkühlbedingungen und der Verzinkungstemperatur ***Influence of the cooling conditions and the galvanizing temperature***

Bezüglich der Verzinkungsbedingungen wurde der Einfluss der Verzinkungstemperatur und der Abkühlbedingungen untersucht. Dazu wurden Verzinkungen in einem Laborkessel durchgeführt, der bereits in [12] zum Einsatz kam. Die Erfassung der Zeit-Temperaturverläufe erfolgte mittels Thermoelementen, die im Rand- und im Kernbereich von M24x160-Schrauben in mittels Erodieren eingebrachten Kanälen positioniert wurden. Für die Versuche wurde eine Halterung für zwei Schrauben konstruiert, wobei eine Schraube zur Messung der Zeit-Temperaturverläufe genutzt wurde und an der anderen Schraube die Bestimmung der Schichthaftung und -ausbildung im metallographischen Schliff erfolgte.

Die am Kessel eingestellte Schmelzetemperatur wurde von 540°C bis 600°C in 20°C-Schritten erhöht. Die Abkühlbedingungen wurden wie in **Tabelle 1** zusammengefasst variiert. Bei allen Versuchen waren die Tauchdauer im Kessel 120s sowie eine Haltedauer von 90s nach der Entnahme aus dem Kessel jeweils konstant. Erst nach Anlauf der Haltedauer nach der Entnahme wurden die in Tabelle 1 dargestellten Abkühlparameter angewendet. Die Haltedauer von 90s wurde auf Basis eines durch den Gemeinschaftsausschuss Verzinken e.V. durchgeführten Screenings in verschiedenen Verzinkungsbetrieben gewählt, weil dies die minimale Dauer zwischen Entnahme des Korbs aus dem

Kessel, dem Schleudern und dem Abschrecken der Bauteile darstellt. Die weiteren Haltedauern an Luft (60s - WL6 und 90s - WL9) wurden ebenfalls auf Basis des Screenings festgelegt. Die Abkühlungen an stehender Luft bzw. im Luftstrom sollen den Einfluss verzögerter Abkühlung, z.B. bei behinderter Wärmeabfuhr im Fall mittig im Korb positionierter Bauteile, abbilden.

Beispielhafte Abkühlkurven für eine Kesseltemperatur von 560°C sowie die korrespondierenden Schichtausbildungen im metallographischen Schliiff sind in **Bild 5** dargestellt. Bei allen im Rahmen der Parametervariationen gemäß Tabelle 1 durchgeführten Versuche ergibt sich eine systematische Differenz zwischen des zur Temperaturregelung des Kessels verwendeten Thermoelements sowie der in die Schrauben eingebachten Thermoelemente von ca. 10°C. Dabei zeigt sich, dass die an Luft bzw. im Luftstrom abgeschreckten Bauteile rissbehaftete bzw. brüchige Überzüge aufweisen. Neben mitunter ausgeprägten Querrissen sind horizontale Trennungen sowohl innerhalb des Überzugs als auch in der Grenzfläche zum Stahl vorhanden. Bei den in Wasser abgeschreckten Schrauben sind dagegen nur die typischen, leichten Querrisse in den Überzügen erkennbar. Unabhängig von den Abkühlbedingungen zeigen alle Überzüge eine Mikrostruktur aus kompakter δ_1 -Phase. Da die nach der Entnahme aus dem Laborkessel anhaftende Schmelze nicht abgeschleudert werden konnte, sondern lediglich abgeschlagen wurde, kommt es auf den kompakten δ_1 -Schichten teilweise zur Ausbildung aufgelockerter Strukturen durch auskristallisierende Restschmelze (z.B. obere Bildhälften der Schriffe von 56WL6 und 56W in Bild 5), die bei der Beurteilung der Schichtqualität allerdings nicht berücksichtigt werden.

Um die Grenze zu bestimmen, bis zu der ein Abschrecken im Wasserbad erfolgt sein muss, um Fehlverzinkungen bzw. Schichthafffestigkeitsprobleme zu vermeiden, wurde gezielt bis zu Temperaturen zwischen 450°C und 350°C an Luft abgekühlt, bevor die Proben im Wasserbad abgeschreckt wurden. Die Ergebnisse sind in **Bild 6** zusammengefasst. Es konnte dabei gezeigt werden, dass langsam / verzögert abgekühlte Proben Schichthafffestigkeitsprobleme aufweisen, wenn eine Abschreckung später als etwa 4 Minuten nach der Entnahme aus dem Zinkbad erfolgte. Proben, die entsprechend früher abgeschreckt wurden, zeigten dagegen keine Haftungsprobleme. Ebenso ist aus den Ergebnissen ersichtlich, dass die Abkühlgeschwindigkeit und die Temperatur, ab der abgeschreckt wird, offensichtlich eine untergeordnete Rolle auf die Schichtqualität ausüben. Die durchgeführten Versuche zeigen ausschließlich die Existenz einer „Zeitbarriere“, nach deren Überschreiten es zu Haftungsproblemen kommen kann.

Eine Ursache für die Existenz der „Zeitbarriere“ kann die Ausbildung von Eigenspannungen infolge der verzögerten Abkühlung und der damit einhergehenden Nachlegierungseffekte und der Ausbildung mehrphasiger Überzüge sein.

Die Untersuchungen bezüglich der „Zeitbarriere“ wurden aufgrund des großen Versuchsumfangs bisher nur bei der typischerweise in der Industrie genutzten Kesseltemperatur von 560°C durchgeführt. Versuche mit den Parametervariationen gemäß **Tabelle 1** zeigen allerdings eine Verbesserung der Schichtqualität mit steigender Verzinkungstemperatur (**Bild 7**). Der positive Einfluss der Verzinkungstemperatur wird insbesondere bei Luftabkühlung deutlich. Bereits eine Erhöhung der Kesseltemperatur von 560°C auf 580°C bewirkt ein geringes Ausmaß an horizontalen Rissen in der Schicht. Bei 600°C ist die Schichthftung vergleichbar mit Wasserabschreckung. Die Erhöhung der Verzinkungstemperatur führt auch zu einer Verdichtung der auf der kompakten δ_1 -Phase auskristallisierenden Restschmelze. Dieser Verdichtungseffekt ist gleichermaßen ausgeprägt bei Abkühlung an Luft und bei Abschreckung in Wasser.

Praxisverzinkungen von Schrauben in unterschiedlichen Betrieben

Hot dip galvanizing of bolts in plants for series production

Neben den vorgenannten Parameterstudien wurden zwei Schraubenvarianten in vier verschiedenen Betrieben im Hochtemperaturverfahren feuerverzinkt. Die Proben durchliefen dabei jeweils die betriebsüblichen Standardprozesse in Serienanlagen, um anschließend auf Verzinkungsergebnis und Schichthftung hin untersucht zu werden. Dazu kamen Schrauben M16x30 - 8.8 aus dem Werkstoff 28B8 (0.28 C, 0.079 Si, 0.85 Mn, 0.012 P, 0.009 S, 0.26 Cr, 0.011 Cu, 0.004 B) und M24x95 - 10.9 aus dem Werkstoff 32CrB4 (0.34 C, 0.14 Si, 0.86 Mn, 0.014 P, 0.009 S, 1.15 Cr, 0.023 Cu, 0.003 B) zum Einsatz. Die von den Betrieben mitgeteilten Verzinkungsparameter sind in **Tabelle 2** zusammengefasst. Die Verzinkungstemperaturen variieren dabei im für die HT-Verzinkung praxisüblichen Bereich zwischen 550°C und 560°C und auch die Tauchzeiten liegen bis auf Verzinkerei 1 mit rund 90s in einem

engen Streuband. Bedingt durch die unterschiedliche Auslegung der Serienanlagen unterscheiden sich jedoch die Zeiträume zwischen der Entnahme des Korbs aus der Schmelze und dem Abschrecken signifikant.

Es konnte in den metallographischen Schlifften jedoch bereits festgestellt werden, dass es in allen Verzinkungen in den Serienanlagen zu starken Abweichungen des Verzinkungsergebnisses kommt. unter Berücksichtigung der Laborversuche (Bild 6) liegt auch die maximale Dauer von drei Minuten immer noch unterhalb der festgestellten „Zeitbarriere“, deren Überschreiten zu Haftungsproblemen führt.

Aus den Praxisversuchen wurden Schrauben sowohl in der Mitte des Korbs als auch am Rand positioniert. Es wurden Schliffe im Bereich Schraubenkopf, Schaft und Gewinde angefertigt und metallographisch untersucht. Insgesamt zeigen die Befunde für den Schraubentyp bzw. die Verzinkerei gute Übereinstimmung miteinander, so dass diese beispielhaft in **Bild 8** dargestellt sind.

Wie die Ergebnisse der metallographischen Analysen zeigen, sind die Verzinkungsergebnisse trotz scheinbar ähnlicher Verzinkungsparameter sehr heterogen. Dies betrifft sowohl die Schichtdicken, als auch die Rissbildung in den Überzügen. Für die beiden verwendeten Werkstoffe sind die erzielten Überzugsdicken innerhalb eines Betriebs ähnlich ausgebildet. Die Schichtqualitäten sind dabei unterschiedlich. Während beim 28B2 in den Verzinkereien 1 und 4 gute Schichtqualitäten erzielt werden, kommt es beim 32CrB4 zu brüchigen Schichten und ausgeprägten horizontalen Trennungen. Bei Verzinkerei 3 sind die Befunde genau umgekehrt, indem beim 32CrB4 gute und beim 28B2 schlechte Schichtqualitäten erzeugt wurden.

Demnach lässt sich hinsichtlich der zur Verfügung stehenden Verzinkungsparameter und der resultierenden Schichtqualitäten für die beiden betrachteten Werkstoffe keine Systematik ableiten.

Zusammenfassung / Summary

In umfangreichen Labor- und Praxisversuchen wurde der Einfluss von Werkstoffen und Verzinkungsparametern hinsichtlich Überzugsqualität für die HT-Feuerverzinkung untersucht.

Dabei zeigt sich, dass die Oberflächen der zu verzinkenden Bauteile für den nachfolgenden Verzinkungsprozess einschließlich der Vorbehandlungsprozesse geeignet sein müssen. Insbesondere für die Feuerverzinkung hochfester Schrauben der Festigkeitsklasse 10.9 muss sichergestellt sein, dass die durch den vorgeschalteten Vergütungsprozess entstehenden Zunderbeläge innerhalb der nach GAV-DSV-Richtlinie [11] vorgeschriebenen Beizdauern vollständig entfernt werden können.

Auch wirken sich eine Randoxidation, einhergehend mit einer Randentkohlung und insbesondere Deltaferritbildung infolge ungenügender bzw. nicht durchgeführter Entphosphatierung negativ auf das Verzinkungsergebnis aus.

Randartefakte mit geringer bzw. schwacher Ausprägung, wie z.B. Deltaferrit, können bei Fehlverzinkungen allerdings nicht oder nur schwer nachgewiesen werden, weil die dünnen Randschichten infolge der Legierungsbildung in die Fe-Zn-Legierungsschichten umgewandelt werden. Mittels metallographischer Methoden wird daher oft kein Befund erzielt, und aufgrund des hohen Analyseaufwands und der damit verbundenen Kosten werden keine weiteren Analysen durchgeführt. Neben dem Oberflächenzustand wird das Verzinkungsergebnis sowohl durch die Verzinkungstemperatur, als auch durch die Abkühlbedingungen beeinflusst. Generell bewirken höhere Verzinkungstemperaturen und schnellere Abkühlung bessere Überzugsqualitäten. Weiterhin wurde in den Versuchsreihen festgestellt, dass bei der Dauer zwischen der Entnahme des Korbs aus dem Kessel und dem Abschrecken eine „Zeitbarriere“ existiert, nach deren Überschreiten es zu Haftfestigkeitsproblemen kommen kann.

Praxisverzinkungen von zwei Schraubenvarianten in vier unterschiedlichen Betrieben zeigen, dass die Verzinkungsergebnisse trotz scheinbar ähnlicher Verzinkungsparameter sehr heterogen ausfallen. Dies betrifft sowohl die erzielten Schichtdicken, als auch die Rissbildung in den Überzügen.

Auf Basis der Labor- und Praxisversuche sowie der vom GAV durchgeführten Screening-Studien sollen in einem nächsten Schritt weitere Verzinkereien in das Praxis-Screening sowie die Prozessschritte bei der Vorbehandlung einschließlich der Überwachung und Analyse der Betriebsstoffe einbezogen werden. Aus einer solchen umfassenden Analyse lassen sich mittels statistischer Versuchsauswertung signifikante Einflussfaktoren bezüglich des Verzinkungsergebnisses ableiten. Aufgrund der in den Serienanlagen oft nur eingeschränkten Möglichkeiten zur Beeinflussung der Verzinkungsparameter ist jedoch nicht sichergestellt, dass alle notwendigen Maßnahmen umgesetzt werden können.

In extensive laboratory and practical experiments, the influence of the materials and the galvanizing parameters on the coating quality for high temperature hot-dip galvanizing was investigated.

Regarding the materials, the surface condition significantly determines the success of the galvanizing process. The surfaces of the components to be galvanized must be suitable for the subsequent galvanizing process, including the pretreatment processes by degreasing, pickling and fluxing. In particular, for the hot-dip galvanizing of high-strength fasteners grade 10.9, it must be ensured that the scale deposits resulting from the foregoing tempering process can be completely removed within the pickling periods as prescribed in the GAV-DSV guideline [11].

Also, an edge oxidation along with a decarburization and in particular phosphor induced deltaferrite formation due to insufficient or not carried out de-phosphating prior to the heat treatment have a negative effect on the coating quality.

Surface artefacts of low thickness (only few micrometres), e.g. phosphor induced deltaferrite, however, often cannot or only with great effort be detected in the case of defective zinc plating because the thin surface layers are converted as a result of the Fe-Zn alloying during hot dip galvanizing (HDG). Therefore, in most cases, no findings are obtained by means of standard metallographic methods and no further analyses are carried out because of the high analysis effort and the associated costs.

In addition to the surface condition, the coating quality is influenced both by the galvanizing temperature and by the cooling conditions. In general, higher galvanizing temperatures and faster cooling result in better coating qualities. Furthermore, it was found, that there is a "time barrier" between the removal of the basket from the vessel and quenching. Exceeding this "time barrier", coating adhesion problems may arise.

Hot dip galvanizing of two bolt types in four different galvanizing plants shows, that the qualities of the zinc platings are very heterogeneous despite apparently similar galvanizing parameters. This applies both to the layer thicknesses and to the formation of cracks in the coatings.

On the basis of the laboratory and practical experiments as well as the screening studies carried out by the GAV, in a next step more data should be acquired by extending the studies on further galvanizing plants as well as considering the pre-treatment steps including the monitoring and analysis of the operating supplies. From such a comprehensive analysis, methods of statistical test evaluation can be applied to identify significant influencing factors relating to the galvanizing result. However, due to the often limited possibilities in the plants for series production to influence the galvanizing parameters, it is not ensured that all necessary measures can be implemented.

Danksagung / Acknowledgement

Das IGF-Vorhaben 18389BG des GAV (Gemeinschaftsausschuss Verzinken e.V.) und des DSV (Deutscher Schraubenverband e.V.) wurde über die AiF im Rahmen des Programms zur Förderung der industriellen Gemeinschaftsforschung (IGF) vom Bundesministerium für Wirtschaft und Energie (BMWi) aufgrund eines Beschlusses des Deutschen Bundestags gefördert.

The IGF Project 18389BG of the GAV (Gemeinschaftsausschuss Verzinken) and the DSV (German Fastener Association - Deutscher Schraubenverband) was supported via AiF within the programme for promoting the Industrial Collective Research (IGF) of the German Ministry of Economic Affairs and Energy (BMWi), based on a resolution of the German Parliament.

Literatur / References

- [1] Thiele M.: Die Schichtbildung beim Feuerverzinken und die Eigenschaften der Zinküberzüge, Dissertation 2010 Freiberg.
- [2] Etoh G., Funami K., Yamamoto Y., Shimizu H., Sugita H., Kikuchi S, Journal of the Society of Materials Science, v 40, n 452,(1991) p 595-600
- [3] Zraggen M., Trzebietowski O. v.: Lasergeschnittene Bauteile-Eine Herausforderung für Verzinker, Sonderdruck aus JOT 4/01 von Galva Suisse.
- [4] Norden M., Blumenau M., Schönberg R., AISTech - Iron and Steel Technology Conference Proceedings (2012) p 1791-1797
- [5] Nieth F., Hofmann A., Kolb U., Blech Rohre Profile 37 (1990) S. 471-473

- [6] Etoh G., Funami K., Shimizu H., Yamamoto Y., Sugita H., Kikuchi S, Journal of the Society of Materials Science, v 43, n 492, (1994) p 1120-1126
- [7] Di Cocco V., Iacoviello F., Natali S.: Cracking mechanisms in a hot-dip zinc coated steel 11th International Conference on Fracture 2005, ICF11, v 6, p 4076-4080, 2005, 1.
- [8] Tzimas E., Papadimitriou G., Surface and Coatings Technology 145 (2001) S. 176-185
- [9] IGF16245BR: Verfahrensoptimierung bei der HT-Verzinkung von Kleinteilen, Abschlussbericht IKS Dresden, 2012.
- [10] Schütz A., Thiele M., Six S.: Verfahrensoptimierung bei der HT-Verzinkung von Kleinteilen, Bericht Nr. 162 Gemeinschaftsausschuss Verzinken e.V. FD 25 2012.
- [11] GAV-DSV-Richtlinie für die Herstellung feuerverzinkter Schrauben, Deutscher Schraubenverband e.V. und Gemeinschaftsausschuss Verzinken e.V., 2009
- [12] Körber D, Adelman J, Landgrebe R, Berger C, MP Materials Testing 52,9 (2010), S. 578–587.

Tabellen / Tables

Tabelle 1: Zusammenfassung der Parameter bezüglich der Verzinkungstemperaturen und der Abkühlbedingungen. Konstant waren jeweils die Tauchdauer von 120s sowie eine Haltezeit von 90s an Luft nach Entnahme der Proben aus dem Zink-Kessel. Nach der Haltezeit wurden die aufgelisteten Abkühlbedingungen angewendet

Table 1: Parameter variation regarding the set point temperature of the Zn kettle and the cooling conditions. Immersion time for HDG was 120s, followed by a holding period of 9s after extraction from the kettle. After the holding period, the listed cooling parameters were applied

Parameter	Label
<i>Set Point Temperature of the Zn-Kettle</i>	
Set point temperature 540 °C	54
Set point temperature 560 °C	56
Set point temperature 580 °C	58
Set point temperature 600 °C	60
<i>Cooling Parameters</i>	
Cooling in air to ambient temperature (aprox. 25 °C)	L
Cooling in air stream to ambient temperature (aprox. 25 °C)	Lv
Quenching in water (aprox. 35°C)	W
Cooling in air 60s , then quenching in water (aprox. 35°C)	WL6
Cooling in air 90s , then quenching in water (aprox. 35°C)	WL9

Tabelle 2: Zusammenfassung der Verzinkungsparameter für vergleichende HT-Verzinkungen von M16 und M24 Schrauben in Serienanlagen von insgesamt vier Verzinkungsbetrieben. T_{Kettle} : Verzinkungstemperatur, t_{HDG} : Tauchdauer, t_{Quench} : Dauer zwischen Entnahme des Korbs aus der Schmelze und Abschrecken

Table 2: Screening tests of four galvanizing plants for HT-HDG of M16 and M24 bolts: Galvanizing parameters were submitted by the plants. T_{Kettle} : Set point temperature of the Zn-Kettle, t_{HDG} : immersion time in the melt, t_{Quench} : Time between extraction from the kettle and quenching

Plant	T_{Kettle} in °C	t_{HDG} in s	t_{Quench} in s	Melt Composition in %m/m					
				Pb	Bi	Ni	Al	Sn	Fe
1	550°C	120	110	0,35	0,0001	0,0008	0,0042	0,13	0,24
2	560°C	95	85	1,15	---	0,0221	0,0012	---	0,0395
3	562°C	99	180	0,28	---	0,0013	0,0032	---	0,32
4	540-560°C	90	65	Class 1 acc. DAST 022					

Bilder / Figures

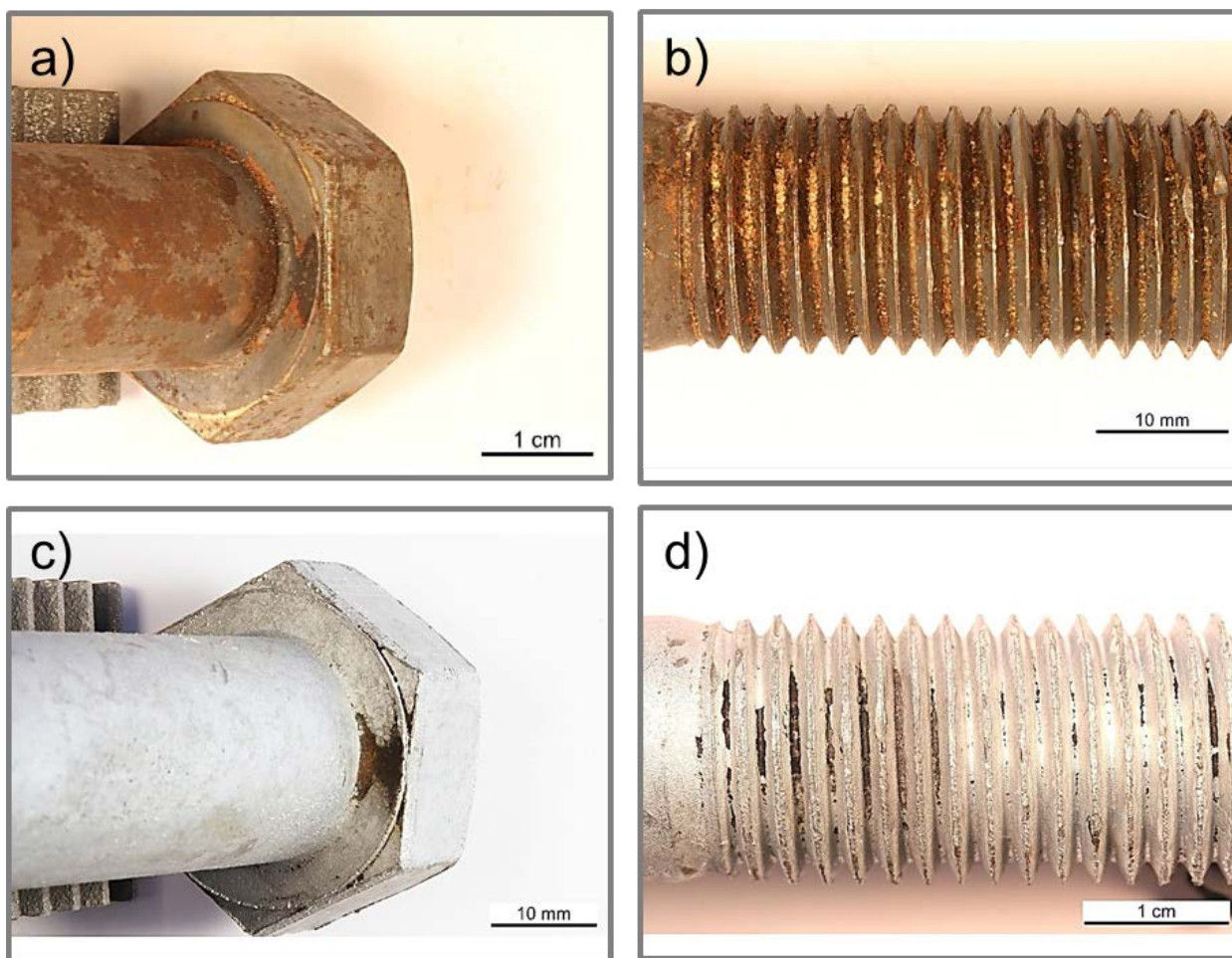


Bild 1: M20 10.9 Schraube: a, b) Oberflächenzustand nach der Vorbehandlung (Entfetten, Beizen) gemäß GAV-DSV-Richtlinie [11], c,d) Verzinkungsfehler

Figure 1: M20 10.9 bolt: a, b) Surface after pre-treatment (degreasing and pickling) acc. to GAV-DSV guideline [11], c, d) defective zinc coating

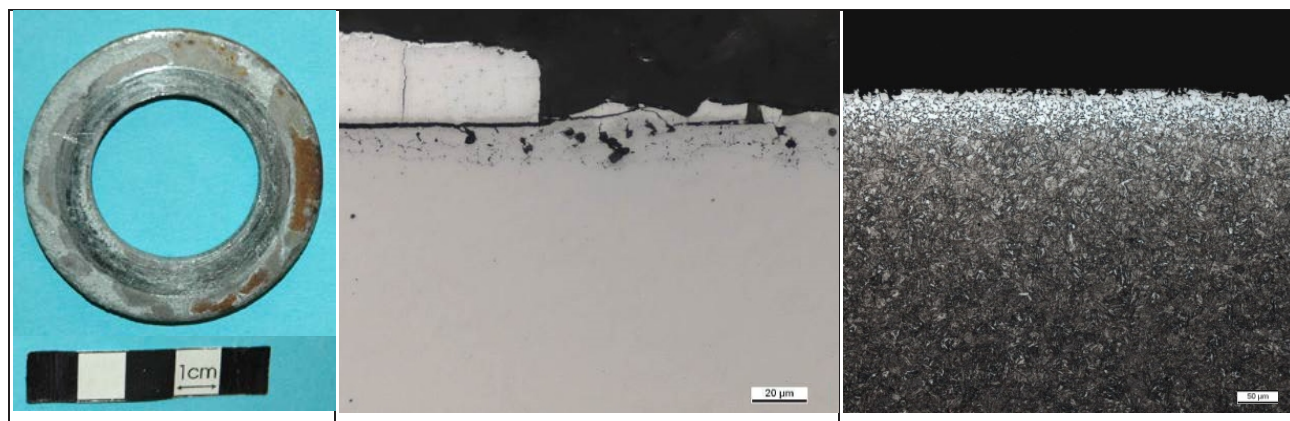


Bild 2: a) Abplatzungen eines NT-Zinküberzugs einer Scheibe au seiner HV-Garnitur. Die Abplatzungen entstanden infolge der mechanischen Beanspruchungen während der Montage, b) Schliff, ungeätzt: Randoxidation und Schichtabplatzungen, c) Schliff, geätzt: Randentkohlung

Figure 2: a) Spallation of a NT-HDG coating on a washer of a HV-bolt set. The failure was caused by the mechanical stresses during on site installation, b) microspecimen, unetched: Oxidation in the surface near area and spallation of the coating, c) microspecimen, etched: decarburization

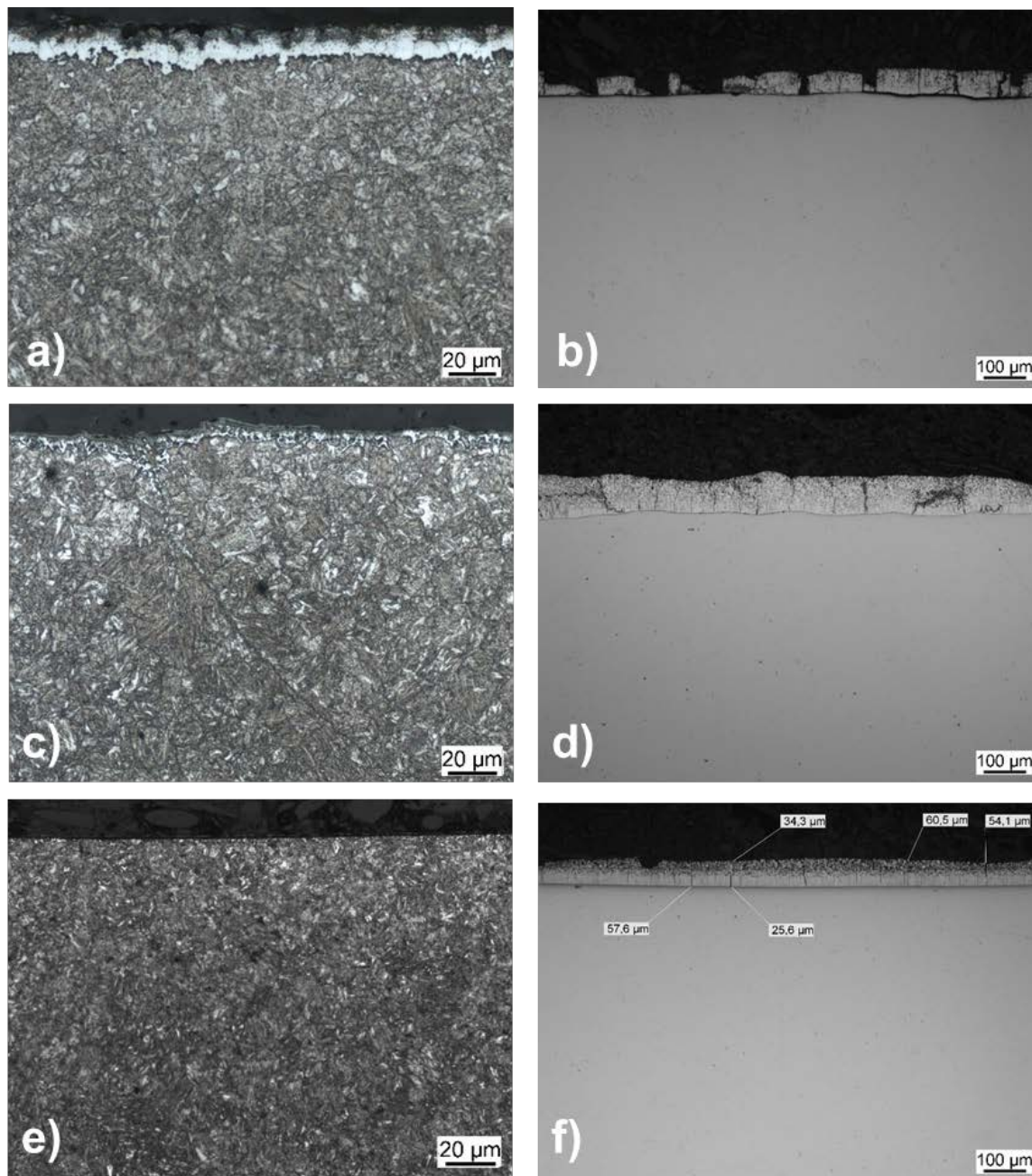


Bild 3: Einfluss des phosphorinduzierten δ -Ferrits auf die Schichtausbildung. Links: Schliffbilder der Randgefüge VOR dem Feuerverzinken, rechts: Randgefüge NACH dem Feuerverzinken (Zn-Überzug abgeätzt). a, b) Schaftbereich mit ausgeprägter δ -Ferritbildung und stark rissbehaftetem Überzug, c, d) Stirnseite des Schraubenkopfes mit schwacher Ausprägung des δ -Ferrits und wenigen horizontalen Rissen, e, f) Schlüsselfläche ohne δ -Ferrit und guter Schichtqualität

Figure 3: Influence of phosphorus induced δ -ferrite on the zinc coating quality. Left handed figures: surface microstructure before HDG, microspecimens etched with 3% HNO_3 , right handed figures: zinc coating after HDG. a, b) shaft area with pronounced δ -ferrite and cracked coating; c, d) face side of the bolt head with slight δ -ferrite and only some coating cracks and e, f) spanner flat without δ -ferrite and good coating quality

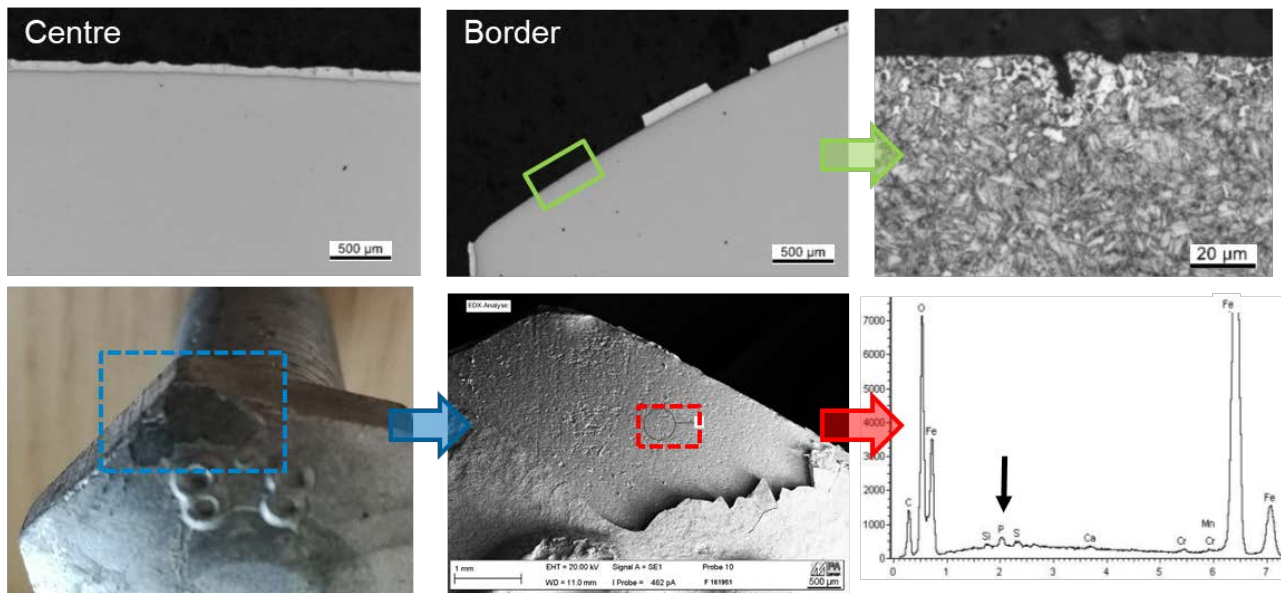


Bild 4: Schichtabplatzungen eines HT-Zinküberzugs im Randbereich des Schraubenkopfes an einer M16 8.8-Schraube. Im Bereich der Schichtabplatzungen zeigen Schliffbilder Hinweise auf phosphor-induzierten δ -Ferrit. Phosphor konnte mittels EDX im Bereich der Abplatzungen nachgewiesen werden.

Figure 4: Spallation of a HT-HDG coating on the head area of a M16 8.8 bolt. The sites with spallation show remains of phosphor induced δ -ferrite in the metallographic analysis. P could also be detected by EDX

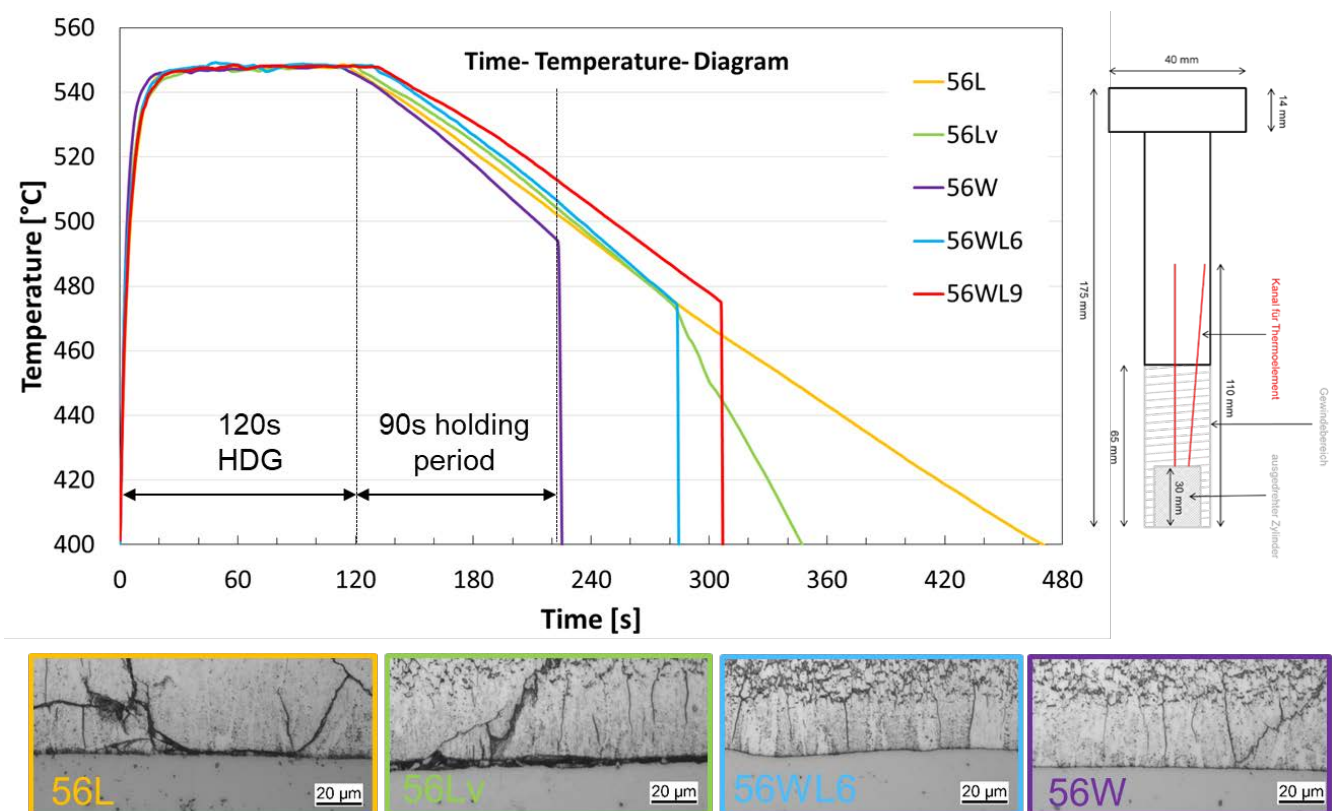


Bild 5: Beispielhafte Abkühlkuren für HT-Verzinkung bei einer Kesseltemperatur von 560°C sowie Einfluss der Abkühlbedingungen (siehe Tabelle 1) auf die Ausbildung des Zinküberzugs.

Figure 5: Exemplary time-temperature curves after HDG at 560°C to visualize the variation of the cooling parameters and the influence on the coating quality. Labeling of the curves see table 1.

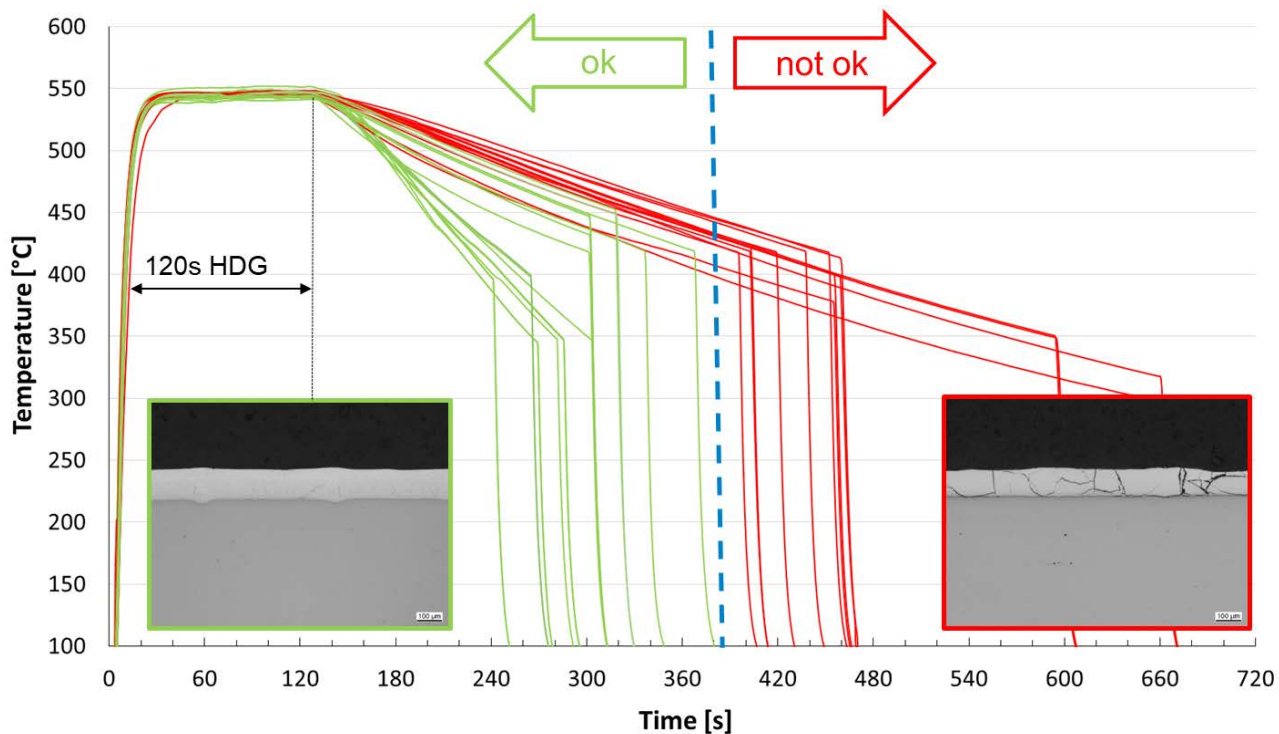


Bild 6: Zeit-Temperatur-Verläufe bei unterschiedlichen Abkühlbedingungen. Nach dem Erreichen der Zieltemperaturen zwischen 350°C und 450°C wurden die Schrauben in Wasser (ca. 35°C) abgeschreckt.

Figure 6: Time-temperature curves by variation of the cooling rate until reaching the set temperatures between 350°C and 450°C. After reaching the set temperature, the bolts were quenched in water (T 35°C)

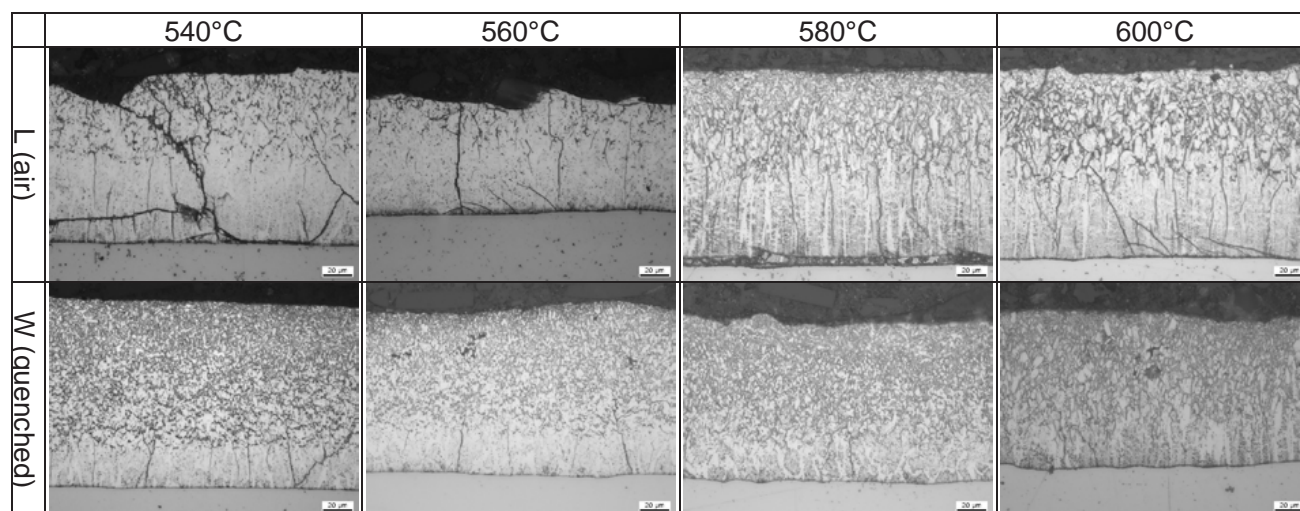


Bild 7: Ausbildung der Zinküberzüge in Abhängigkeit der Verzinkungstemperatur für Luftabkühlung (oben) und Wasserabschreckung (unten)

Figure 7: Coating morphologies of different galvanizing temperatures for air cooling (upper row) and water quenching (lower row)

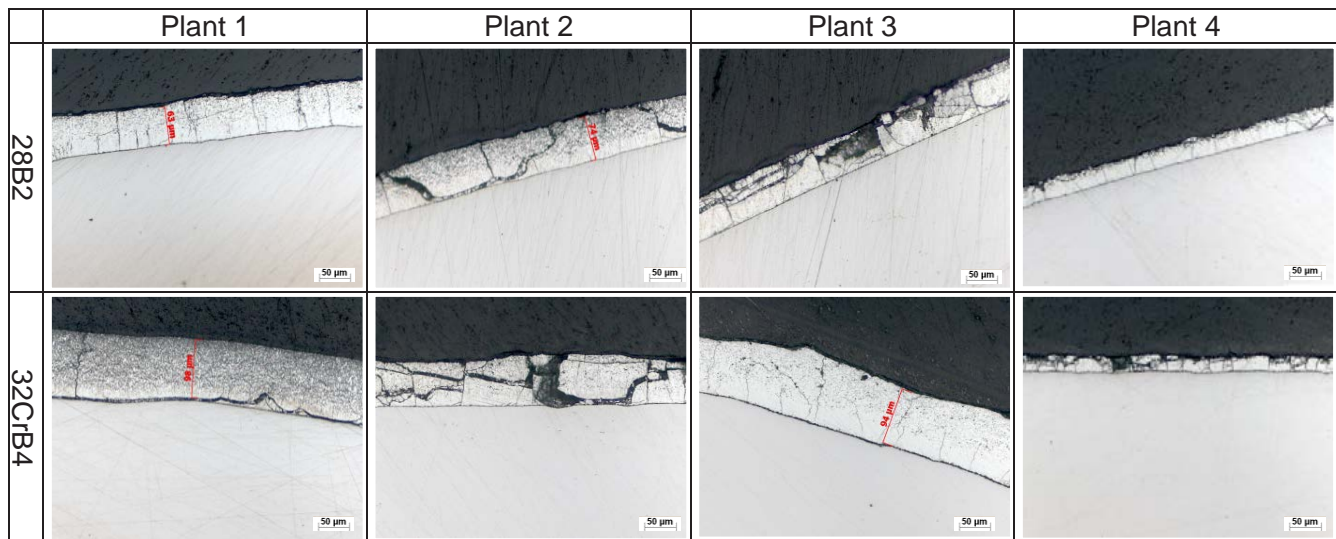


Bild 8: Ausbildung der Zn-Überzüge für zwei Schraubenwerkstoffe, die in vier verschiedenen Betrieben im HT-Verfahren feuerverzinkt wurden (Parameter siehe Tabelle 2)

Figure 8: Coating morphologies of two bolt materials, which were HT-HDG in four different plants according to the parameters listed in table 2.

Author Biography

Dr.-Ing. Holger Hoche

studied Material Science and Engineering at the Technische Universität Darmstadt (TU) and was issued his doctorate at the Center for Engineering Materials (State Materials Testing Institute (MPA) and Chair and Institute for Materials Technology (IfW)) in 2004.

Since 2012 he has been head of the department Material Analysis. His research focuses on materials development and characterization and failure analysis.

Dipl.-Ing. Steffen Six

studied manufacturing engineering at the TU Dresden. After working at a planning office and as a research assistant at the TU Dresden he has been working at the Institut für Korrosionsschutz Dresden GmbH as research assistant since 2011. The focus of his research work is especially on layer-forming reactions from interactions of steel, zinc melts and technological boundary conditions.

Slip-resistant connections in hot-dip galvanized steel bridge constructions

Anna Schudlich, Marcus Klein, Matthias Oechsner, TU Darmstadt, State Materials Testing Institute (MPA) and Chair and Institute for Materials Technology (IfW) Darmstadt, (Germany)

Grafenstraße 2, 64283 Darmstadt

+496151 1625106

schudlich@mpa-ifw.tu-darmstadt.de

Johannes Grote, Dieter Ungermann, TU Dortmund University – Institute of Steel Construction (Germany)

August-Schmidt-Str. 6, 44227 Dortmund

+49231 7554769

johannes.grote@tu-dortmund.de

Abstract

Wirtschaftlichkeit und Nachhaltigkeit im Brückenbau sind neben den Neubaukosten insbesondere von den während der Lebensdauer anfallenden Unterhaltungskosten bestimmt. Ein erfolgreich abgeschlossenes Forschungsvorhaben zeigt, dass die Feuerverzinkung als Korrosionsschutz grundlegend und vorteilhaft einsetzbar ist. Feuerverzinkte Brückenkonstruktionen können eine Korrosionsschutzdauer in der Größenordnung der Lebensdauer einer Brücke (≥ 100 Jahre) erreichen. Die Ausführung von feuerverzinkten Stahlbauten hat sich im Hochbau etabliert und gehört zum Stand der Technik. Die Ergebnisse des Forschungsprojektes zeigten im Bereich der Ermüdungsfestigkeit der feuerverzinkten Bauteile kaum Einbußen gegenüber nicht verzinkten Stahlbauteilen. Geschweißte Montagestöße an feuerverzinkten Bauteilen ziehen eine aufwändige Vor- und Nachbearbeitung des Korrosionsschutzes mit sich. Der nachträglich aufgebrachte Korrosionsschutz erreicht nicht die Schutzdauer einer Feuerverzinkung. Diese technologische Einschränkung kann vermieden werden, wenn die Ausführung der Montagestöße durch feuerverzinkte, geschraubte Anschlüsse erfolgt. Im Stahlbrückenbau hat sich der Einsatz von gleitfest vorgespannten (GV-) Verbindungen bewährt. Für eine Anwendung von GV-Verbindungen bei feuerverzinkten Montagestößen fehlen bislang wesentliche wissenschaftliche Untersuchungen. Technische und wissenschaftliche Grundlagen zum Einsatz von feuerverzinkten Schraubanschlüssen zyklisch beanspruchter Stahl- und Verbundbrückenkonstruktionen auf Basis des Eurocode 3 werden erarbeitet und Berechnungsnachweise sowie Konstruktionsempfehlungen bereitgestellt. Die aktuellen Ergebnisse werden vorgestellt und ein Ausblick auf die geplanten Versuche wird gegeben.

Abstract

Economic efficiency and sustainability in bridge construction are, in addition to the construction costs, determined by the incurred maintenance costs during lifetime. A successfully completed research project shows that hot-dip galvanizing is a basic and suitable applicable corrosion protection. Hot-dip galvanized bridge constructions can achieve a corrosion protection period in the magnitude of the lifetime of a bridge (≥ 100 years). Hot-dip galvanized steel structures are well established and state of the art for public and industrial buildings. Various research projects demonstrate hardly any reduction of the fatigue strength of the hot-dip galvanized components compared to the non-galvanized steel components. Welded site joints of hot-dip galvanized components require a complex pre- and post-treatment of the corrosion protection. Nevertheless, on-site applied corrosion protection cannot reach the protection durability of a hot-dip galvanized component. This technological restriction can be avoided when utilizing hot-dip galvanized bolt connections. The application of slip-resistant pre-stressed connections was proved successful in steel bridge construction. However, relevant scientific investigations are not available for the use of slip-resistant connections for hot-dip galvanized site joints. Technical and scientific basics for the application of hot-dip galvanized bolted connections in cyclically loaded steel and composite bridge constructions, based on the European standard for steel constructions (Eurocode 3), will be investigated within the scope of this research project. The provision of construction and design recommendations is the goal of this project. The current results are presented and an outlook concerning the upcoming experiments is given in this paper.

Introduction

Bridge constructions are dimensioned for a lifetime of at least 100 years. The economic efficiency and sustainability are affected by the construction costs and especially by the incurred maintenance costs during lifetime. Steel bridge constructions need a coating as a corrosion protection, which is typically to be renewed after several years. Besides the actual cost for maintaining and renewing the coating, this process often requires lane blocking and thus a substantial impact on traffic.

The hot-dip galvanizing of steel constructions can achieve a corrosion protection period in the magnitude of the bridge's lifetime. The research project "Hot dip galvanizing in steel and composite bridge construction" [1] verified the hot-dip galvanizing as a basic and suitably applicable corrosion protection. The investigations show only a slightly lower fatigue resistance. Therefore the costs during lifetime can be reduced significantly. A hot-dip galvanized bridge, shown in fig. 1, was built as result of [1].

State of the art

Hot-dip galvanized steel structures are well established and state of the art for public and industrial buildings. The research project [1] demonstrated on a scientific basis that hot-dip galvanizing of steel in bridge constructions is feasible. Experiments on hot-dip galvanized components of the significant detail categories were performed. The result was a slightly decreased fatigue resistance compared to non-galvanized specimens, leading to minor significance in dimensioning. The hot-dip galvanized details could mainly be classified into the detail categories of DIN EN 1993-1-9 [2], only some of them were classified in a lower detail category for the proof against fatigue. This knowledge allows economic, efficient and sustainable bridge constructions. The maximum length for steel beams in hot-dip galvanizing depends on the zinc bath length - currently up to 18 m. Because of this limitation, it is necessary to build steel bridges with site joints. DIN EN 1090-2 [4] specifies that hot-dip galvanized steel parts must not be welded. Welded site joints require a complex pre- and posttreatment regarding the corrosion protection. Nevertheless, on-site applied corrosion protection cannot reach the protection durability of a hot-dip galvanizing. This restriction can be avoided by using hot-dip galvanized bolted connections.

Up until now, there are limited studies of bolted connections of hot-dip galvanized steel. Especially the slip-resistant pre-stressed connections according to DIN EN 1993-1-8 [3] are suitable for load reversal and fatigue (figure 2). The preload level and the surface texture of the contact areas influence the slip resistance behaviour of the connection. DIN EN 1993-1-8 (short EC 3) gives a fixed preload level for slip limitation during service. Slip factors for hot-dip galvanized surfaces are not covered in DIN EN 1090-2, but it is possible to determine the factor experimentally according to Annex G of [4]. Over the last years, some scientific studies report on slip factor tests on hot-dip galvanized surfaces. The results fall in a large range of slip factors from $\mu = 0.2$ up to 0.4. The roughening of the zinc surface as a subsequent treatment has caused an increase of the slip factor. However, a thicker zinc coat might also have a significant influence on preload relaxation, outbalancing the increase in slip factor.

Experimental investigations

Reliable predictions of slip factors of hot-dip galvanized steel connections are rather difficult to achieve and not covered by the current design standards. Scientific studies are necessary to provide reliable slip factors. In addition, the fatigue behavior of steel components, especially the slip-resistant connections of hot-dip galvanized steel, is an influencing factor of the sustainability. The detail categories of EC 3 give no information for galvanized bolted connections. There are contradictory statements on the fatigue strength of hot-dip galvanized steel. However, it is necessary to ensure the design. As part of this research project, a promising combination of the essential parameters (chemical composition, surface treatment, galvanizing, post treatment, preload, etc.) should be identified to guarantee a high fatigue strength and at the same time an economic manufacturing.

Slip factor tests

The slip factor can be determined experimentally according to Annex G of DIN EN 1090-2 for a particular surface treatment [4]. The given specimen size is similar to real components and is used as standard specimen in this project. It is a two-shear connection with a single-row of bolts, figure 3. Tension rod (S355J2+N, $t=20\text{mm}$), joint plate (S355J2+N, $t=10\text{mm}$) and bolts M20 10.9 HV are detailed according to Annex G.

Different mechanical surface treatments before and after the hot-dip galvanizing are chosen. Table 1 lists the combinations for the slip factor tests. Figure 4 shows exemplarily the blasted and milled surface condition.

In a second step, after the two best combinations are identified, the influence of the thickness of the zinc coat will be determined (table 2). The effect of three different thicknesses for each type of tension rod will be investigated.

Regarding the testing and evaluation of the standard specimens in accordance to DIN EN 1090-2 a high fidelity displacement measurement device including eight transducers, will be applied. The preload loss of the bolts will be measured during the whole experiment. For the preload measurements, an ultrasonic and a strain change based system will be applied with the intention to compare their effort, accuracy and applicability. The ultrasonic based system is an easy-to-prepare and easy-to-use tool. Its measuring procedure as well as the glued piezo ceramic transducer, which is necessary to send the signal, are shown in fig. 5. The second method is based on a strain change measurement of the bolt by using an applied strain gauge in the middle of the bolt (figure 5).

The first investigations should determine the slip factor of slip-resistant connections between tension rods made of sebigy steel with a natural zinc surface and all types of joint plates (table 1). As preparatory work of the slip factor tests, the thickness of the zinc coatings was measured. The coatings of the normal temperature (NT) galvanized tension rods and joint plates exhibit a thickness of about $140\ \mu\text{m}$, the thickness of the coatings of the high temperature (HT) galvanized joint plates is about $125\ \mu\text{m}$. The surfaces of the galvanized tension rods and joint plates show a grey and matt finished colour, this indicates that a Fe-Zn-alloy forms the top of the zinc coating. This is confirmed by micrographs of the zinc coatings (figure 6). Blasted surfaces show a mean roughness of $R_z=117.5\ \mu\text{m}$, after HT galvanizing the roughness decreases to $R_z=89.5\ \mu\text{m}$. The milling was executed under 45° , depth of $1\ \text{mm}$ and distance of $2\ \text{mm}$.

In addition to the slip-factor tests, the preload loss for each combination of the connection was measured over a period of up to 18 hours (figure 7). In this case, the preload was determined by applied strain gauges inside the bolts. Connections with normal or high temperature galvanized and natural zinc surfaces reduce the preload of the bolts to 95.1 % of the initial preload level of $172\ \text{kN}$. NT galvanized joint plates, which were milled after the galvanizing, showed a reduction to 87.5 % of the initial preload level. HT galvanized joint plates with a milled structure (before galvanizing) revealed a reduction to 78.2 %. Acceptable preload losses according to DIN EN 1090-2, Annex G [4] are limited to 5 %. If necessary, the preload of the bolts was increased to the required level afterwards in order to comply with the guidelines for the slip factor tests.

The results of the slip-factor tests are given in table 3. The slip-factor tests show slip factors between $\mu_m = 0.30$ and $\mu_m = 0.57$. Untreated, NT galvanized surfaces lead to a higher slip factor ($\mu_m = 0.36$), compared to untreated, HT galvanized surfaces ($\mu_m = 0.30$). Joint plates with blasted and HT galvanized surfaces show a slip factor of $\mu_m = 0.38$, only a small improvement compared to the untreated NT galvanized surfaces. The comparison of the ungalvanized and HT galvanized milled joint plates shows a reduction of the slip factor from $\mu_m = 0.57$ to $\mu_m = 0.44$. Figure 8 shows the shear force-slip-relationship of a HT galvanized blasted and HT galvanized milled surface. The individual slip load is defined as the load at $0.15\ \text{mm}$ displacement [4].

The creep tests of the combination failed. The determined difference in slip after 5 min and 3 h after application under the constant load (90 % of the mean slip load F_{sm}) exceeded the maximum allowance of $0.002\ \text{mm}$. At least three extended creep tests according to EN 1090-2, Annex G are required and will be performed in future work.

Fatigue tests

Due to contradictory statements on the fatigue strength of NT galvanized slip-resistant connections and due to a lack of scientific knowledge about the fatigue strength of HT galvanizing, fatigue tests on hot-dip galvanized specimens will be performed. Table 4 shows the testing program of standard specimens and large-scale experiments. Different surface treatments and further connection types are taken into account for comparison reasons. The analysis of the results offers the possibility to determine the fatigue strength of the structural details. S-N curves will be generated in order to classify into the details according to standard DIN EN 1993-1-9. In the experimental process, the mounting of the bolts will be performed preload controlled using applied strain gauges with additional torque and angle control. In addition, the ultrasonic measuring technology will be used determine the bolt preload and to allow a comparison of the two measurement techniques. With that, it will be possible to adjust a reproducible preload level for the evaluation of the fatigue resistance, regardless of the variations of the slip factors.

The results of the fatigue tests on the standard specimens will be validated by means of large-scale experiments. Figure 9 shows the chosen dimensions following a characteristic bridge girder. The specimens will be fatigue tested with constant stress amplitudes. During the fatigue tests of the standard specimens the load, the number of cycles and the displacement will be measured continuously.

Summary

Slip-resistant connections according to DIN EN 1993-1-8 are used for bridge constructions due to their good fatigue resistance and simple installation. The slip has to be minimized to comply with the EC3 requirements. DIN EN 1090-2 specifies different slip factors, though a hot-dip galvanized surface is missing. The test results described above show that it is possible to generate slip-resistant connections of galvanized surfaces with slip factors up to 0.57. The specimen surfaces are normal temperature (NT) and high temperature (HT) galvanized. The HT galvanized surfaces offered the option to treat the joint plate surfaces before the galvanizing process. The slip factor was increased by blasting or milling the surfaces. A milled surface has an impact on the preload loss of the bolts. Extended creep tests are necessary to accomplish a nominal friction coefficient for the tested surfaces.

Fatigue testing is still in progress but will be completed prior to the termination of the project in October 2019.

Acknowledgements

The Gemeinschaftsausschuss Verzinken (GAV) research project 19444N is funded through the AiF within the program in cooperative industrial research (IGF) of the Bundesministerium für Wirtschaft und Energie. We would like to thank the mentioned institutions for their support and funding and voestalpine AG for supplying the testing material.

References

- [1] D. Ungermann, D. Rademacher, M. Oechsner, R. Landgrebe, A. Adelman, F. Simonsen, S. Friedrich, P. Lebelt, "Hot dip galvanizing in steel and composite bridge construction", ZUTECH Forschungsprojekt P 835, IGF Nr. 351, Düsseldorf, FOSTA, Verl. und Vertriebsges. mbH, 2014
- [2] DIN EN 1993-1-9, Eurocode 3: Design of steel structures Part 1-9: Fatigue, German version, Beuth, Berlin, 2010
- [3] DIN EN 1993-1-8, Eurocode 3: Design of steel structures Part 1-8: Design of joints, German version, Beuth, Berlin, 2010
- [4] DIN EN 1090-2, with Annex G, Execution of steel structures and aluminium structures Part 2: Technical requirements for steel structures, Beuth, Berlin, 2015
- [5] Voigt & Schweitzer GmbH & Co. KG, Gelsenkirchen, Germany, www.zinq.com
- [6] ZSE Electronic GmbH, Bietigheim-Bissingen, Germany, www.zse.de

- [7] Intellifast GmbH, Speyer, Germany www.intellifast.de
 [8] Institut für Korrosionsschutz Dresden GmbH, Internal Report, Dresden, Germany

Tables

Table 1 static strength tests on standard specimens according to EN 1090-2, annex G

Slip-resistant connection between		Joint plate with surface treatment after normal temperature galvanizing		Joint plate with surface treatment before high temperature galvanizing		
Tension rod with normal temperature galvanizing	steel / zinc surface	natural zinc surface	milling	natural zinc surface	blasting	milling
	Sebisty natural zinc surface	5 (1 creep test of it)	5 (1)	5 (1)	5 (1)	5 (1)
	Sebisty zinc surface sweeping	5 (1)	5 (1)	5 (1)	5 (1)	5 (1)
	Silicon steel natural zinc surface	5 (1)	5 (1)	5 (1)	5 (1)	5 (1)
	Silicon steel zinc surface sweeping	5 (1)	5 (1)	5 (1)	5 (1)	5 (1)

Table 2 static strength tests on standard specimens with different hot-dip galvanized thickness

Slip-resistant connection between		Joint plate with surface treatment	
Tension rod with normal temperature galvanizing	steel / zinc surface	First optimized treatment	Second optimized treatment
	Sebisty 3 thicknesses of zinc	5 x 3 = 15 (3 creep tests)	15 (3)
	Silicon steel 3 thicknesses of zinc	15 (3)	15 (3)

Table 3 Results of the slip-factor test: Mean slip loads and friction coefficients

Slip-resistant connection between		Joint plate with surface treatment after normal temperature (NT) galvanizing		Joint plate with surface treatment before high temperature (HT) galvanizing		
Tension rod with normal temperature (NT) galvanizing	steel / zinc surface	natural zinc surface	milling	natural zinc surface	blasting	milling
	Sebisty natural zinc surface	$F_{sm} = 248.2 \text{ kN} / \mu_m = 0.36$	388.8 kN / 0.57	205.8 kN / 0.30	262.2 kN / 0.38	299.7 kN / 0.44

Table 4 fatigue tests on standard specimens and large-scale experiments

Slip-resistant connection between		Joint plate with surface treatment	
Tension rod with normal temperature galvanizing	steel / zinc surface	First optimized treatment	Second optimized treatment
	Sebisty 2 thicknesses of zinc	5x2x5=50 (5 cycles)	5x2x5=50 (5 cycles)
Sum		100	
		no	Normal temperature galvanizing
Tension rod with	Sebisty no zinc	5x5 =25 (5 cycles) REF 1	

normal temperature galvanizing	Sebisty Normal temperature galvanizing		5x5 =25 (5 cycles)
Sum			50

Shear connection between		Joint plate	
Tension rod with normal temperature galvanizing	steel / zinc surface	Normal temperature galvanizing	
	Sebisty Normal temperature galvanizing	5x5 =25 (5 different cycles) REF 2	
Sum			25

Joint plate with hole					
No zinc	surface treatment after normal temperature galvanizing		surface treatment before high temperature galvanizing		
	Natural zinc surface	milling	Natural zinc surface	blasting	milling
5x5 =25 (5 cycles)	5x5 =25 (5 cycles)	5x5 =25 (5 cycles)	5x5 =25 (5 cycles)	5x5 =25 (5 cycles)	5x5 =25 (5 cycles)
Sum 125					

Site joint with slip-resistant connection between		Joint plate	
Tension rod with normal temperature galvanizing	steel / zinc surface	First optimized treatment	Second optimized treatment
	Sebisty 2 thicknesses of zinc	2x2x5=10 (5 cycles)	2x2x5=10 (5 cycles)

Figures



Figure 1 hot-dip galvanized steel bridge across A44 close to Kassel (Germany) within [1]



Figure 2 two-shear connection of the main girders of a composite construction in Belgium [5]

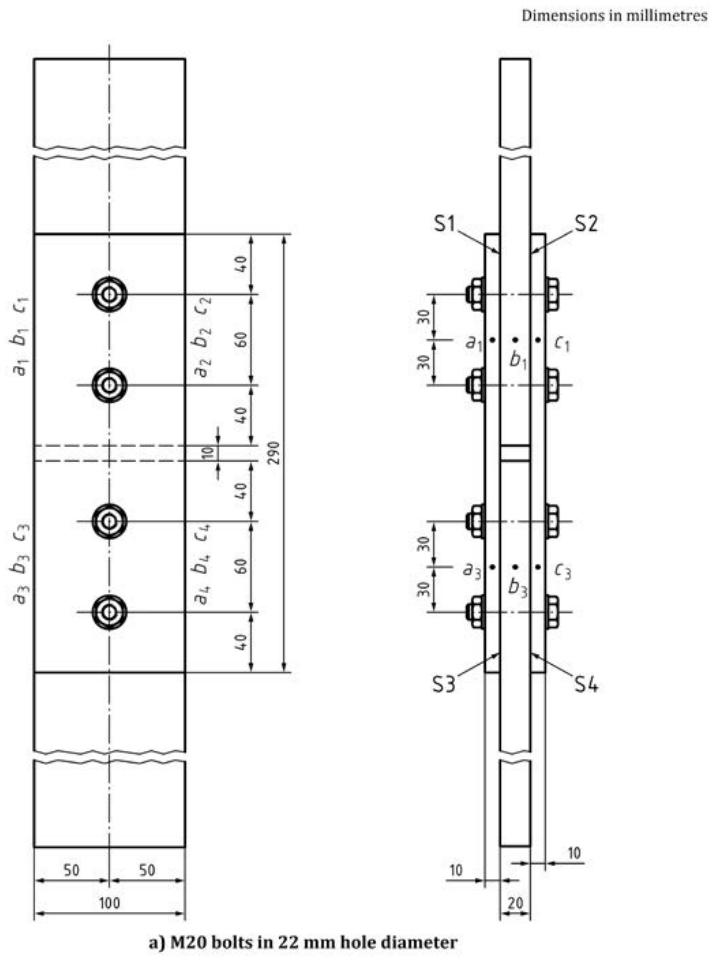


Figure 3 standard specimen to determine the slip factor [4]

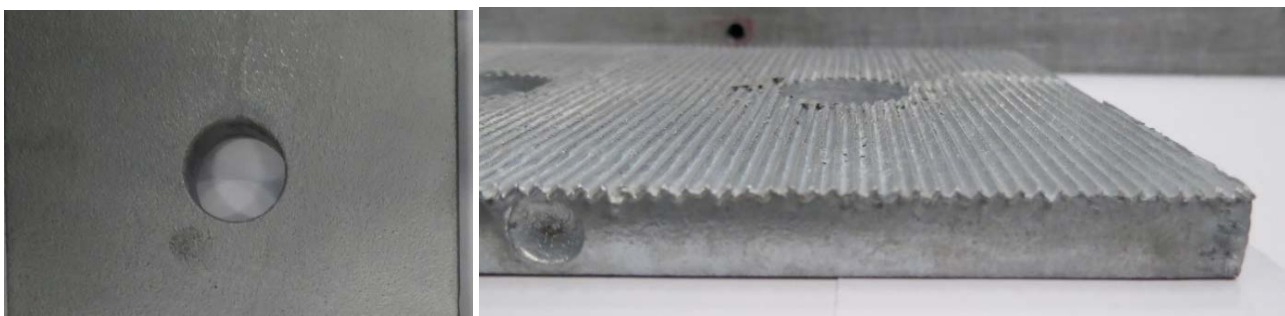


Figure 4 mechanical surface treatment before high temperature galvanizing – blast (left) and milled surface (right)

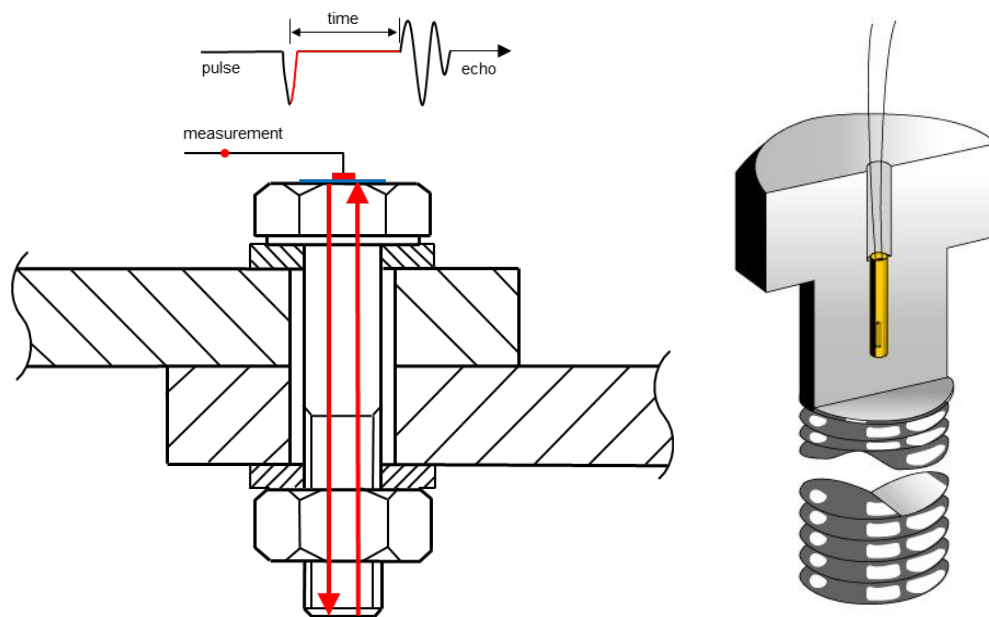


Figure 5 preload measuring systems: ultrasonic based measuring technology (left) [6] and applied strain gauges inside the bolt (right) [7]

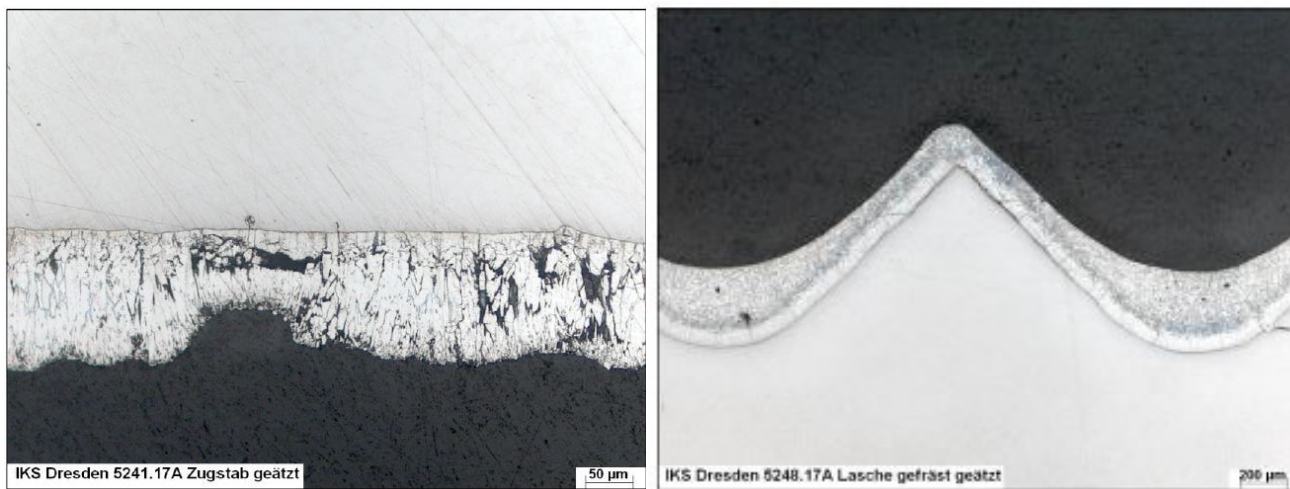


Figure 6 Micrographs of the zinc coatings: NT galvanized (left) [8] and HT galvanized milled surface (right) [8]

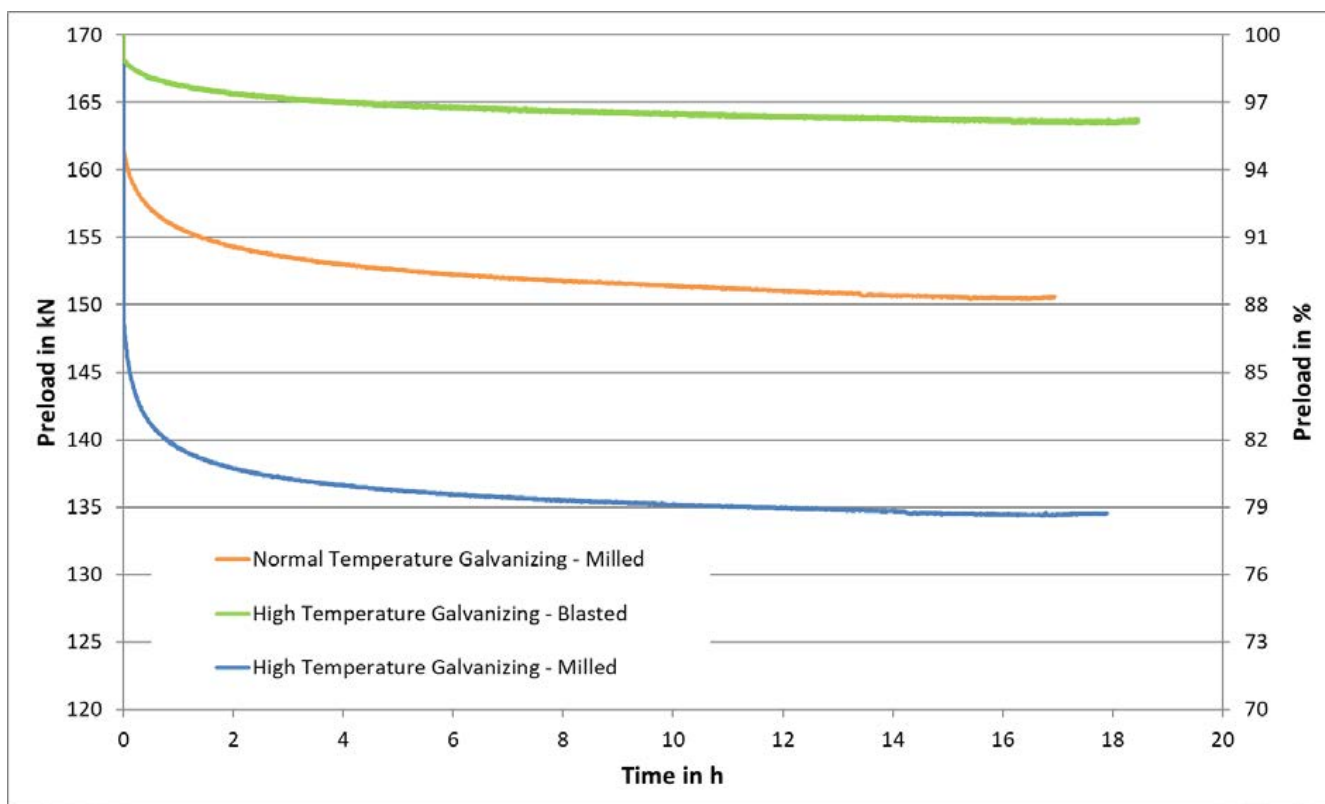


Figure 7 Preload-time-curves of hot-dip galvanized specimens with different surfaces treatments

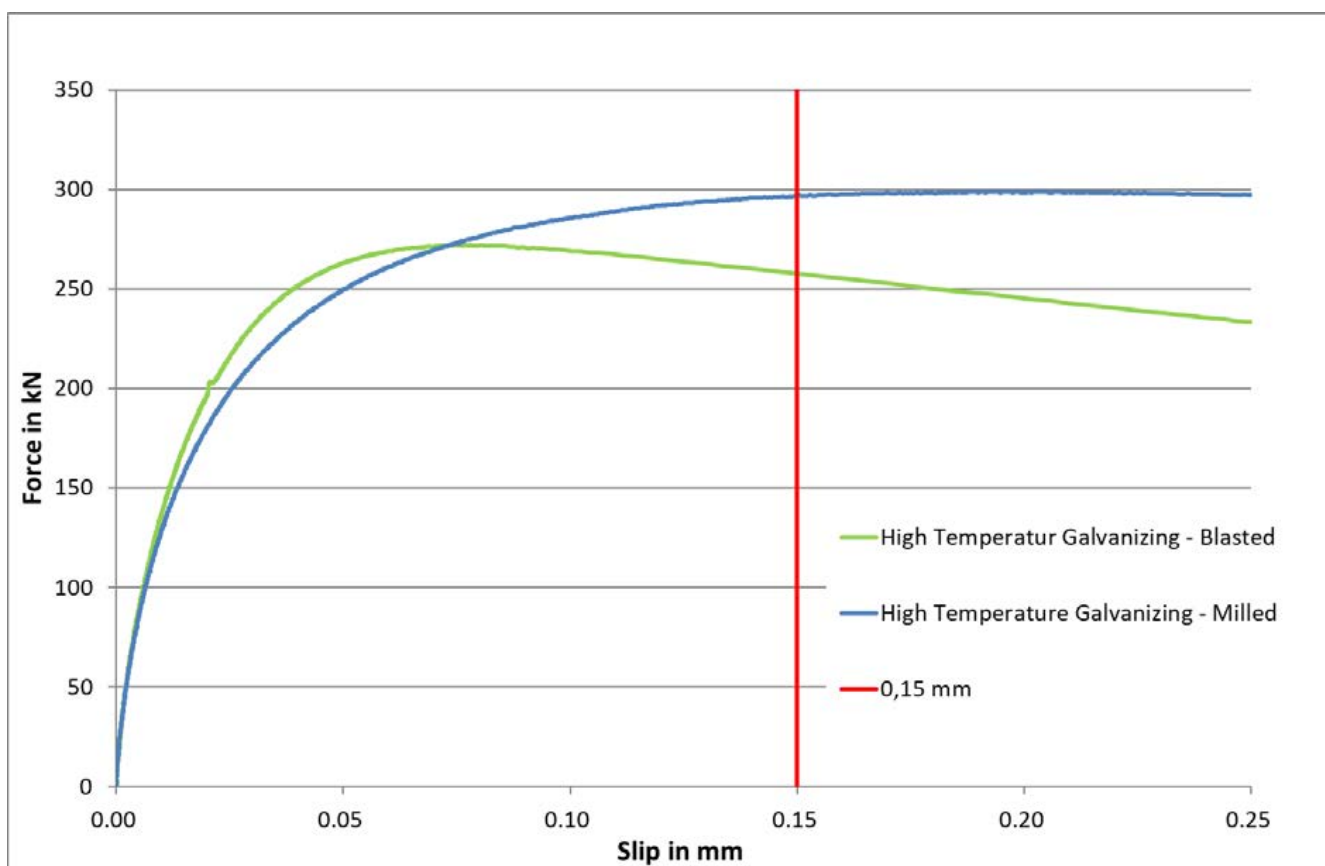


Figure 8 Shear force-slip-relationship of hot-dip galvanized specimens with different surface treatments

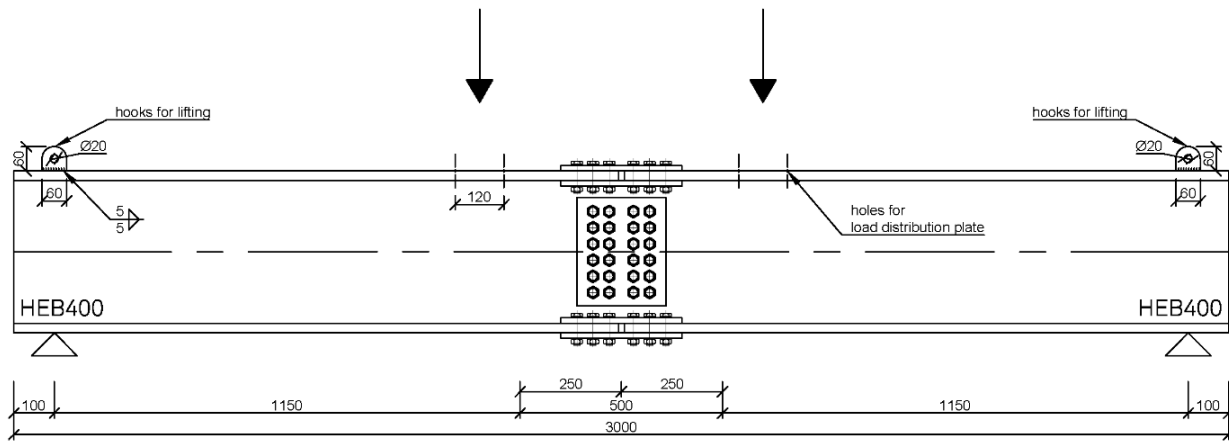


Figure 9 experimental setup with dimensions of large-scale experiments

Author Biography

Johannes Grote, B.Sc.

Johannes Grote studied civil engineering at the TU Dortmund University through the years 2011 to 2018. During his bachelor thesis at the Institute for steel construction, he followed up with the topic "Construction of a Test Setup to Determine the Shear Stiffness of a Frame in High Rack Storages Based on DIN EN 15512". He deepened the studies of structural engineering during the master, steel and solid constructions and their application to individual building assignments were the main subjects. His master thesis "Experimental Investigations of Load-Bearing Capacity of High-Strength Friction Grip Fastening of Hot-Dip Galvanized Construction Steel with Different Surface Preparation under Particular Consideration of EN 1090-2, Annex G, for Testing and Determining Slip Factor" was based on the idea of the mentioned research project.

In addition to his studies, he worked from 2016 until 2017 as an engineer assistant at Ingenieurbüro v.Spiess & Partner mbB, Dortmund and was involved in various projects of steel and solid construction. Since 2018 he is working at the Institute of Steel-Construction, TU Dortmund. He supervises the AiF GAV research project "Slip-resistant connections in hot-dip galvanizing steel bridge constructions".

Dipl.-Ing. Anna Schudlich

Anna Schudlich studied civil engineering at the Technische Universität Darmstadt in the years 2006 to 2012. The specializations during her study, steel construction, solid construction and geotechnics, formed the classical basis of a constructive study of civil engineering. During the studies she spent half a year at Virginia Tech, USA, working at her research project "Experiments on cold-formed steel C-section joists". Her diploma thesis, back at the Institute for steel construction TU Darmstadt, was about the topic "Design of steel bolts under combined stress according to DIN 18800 and DIN EN 1993-1-8". After completing her studies, A. Schudlich worked as a project engineer at KREBS+KIEFER Ingenieure GmbH in Darmstadt until 2017. She was responsible for various projects of different sizes in the fields of steel and solid construction as well as geotechnics.

Since 2017 she is working at the State Materials Testing Institute (MPA) and Chair and Institute for Materials Technology (IfW), TU Darmstadt in the field of component integrity. Among the daily responsibilities of the Institute (e.g. testing, consulting and failure analysis), she supervises the AiF GAV research project "Slip-resistant connections in hot-dip galvanizing steel bridge constructions".

Session 5:

Process Optimisation

The myth of steel hydrogenation during pre-treatment for HDG - dogma versus reality

Vlastimil Kuklík, Jan Kudlacek, Michal Zoubek, Czech Technical University in Prague, Sylwia Węgrzynkiewicz, BELOS-PLP S.A.

1. Annotation

It is generally assumed that pickling of steel parts in hydrochloric acid for HDG (hot-dip galvanizing) leads to saturation of the substrate with hydrogen, which may lead to hydrogen embrittlement. Therefore, for hot-dip galvanizing of parts made of high-strength steels, various measures are adopted for the prevention of hydrogen charging in the course of chemical pre-treatment. There are standards stipulating restrictions for pickling processes. However, are such restrictions justified? Not every brittle fracture is induced by the hydrogen embrittlement. High-strength steels are supersaturated solid solutions. Due to the elevated temperature during hot-dip galvanizing, the process of their disintegration is significantly accelerated and the precipitates along the grain boundaries of the material cause the decohesion.

2. Introduction

The impulse for our project was an investigation by BELOS-PLP S.A., a Polish company, conducted because of a lattice tower breakdown in the South African Republic, where BELOS-PLP S.A. had supplied fixtures for this structure. In the tower decries, a broken U-bolt made of 41Cr4 steel was found and the investor came to the conclusion that the reason for the bolt brittle fracture was the material hydrogen embrittlement allegedly caused by the fixture manufacturer because of a negligent approach in the pre-treatment process, where sandblasting of parts and very short pickling was required. However, BELOS-PLP S.A. rejects any lapse on its side. In order to support their point, they have carried out tests to show that pickling of steel parts in hydrochloric acid does not lead to any increase of the hydrogen content in the substrate. Consequently, the BELOS-PLP S.A. representatives turned to our university and asked us to verify their experimental results through an independent research.

3. Steel hydrogen charging during the chemical pre-treatment process for HDG

The most common materials processed by hot-dip galvanizing are ferritic or ferrite-pearlite warranted weldable structural steel types with a low carbon content. During the hot-dip galvanizing process, the utmost purity of the surface of parts is essential for the formation of a good-quality coating. In practice, this is achieved by pickling in hydrochloric acid. In the pickling process, hydrogen ions (protons) are released.



Owing to its small dimensions, the nascent hydrogen easily penetrates the steel material interstitially and vaporise off again in a short time, unless it is stuck in the hydrogen trap. The hydrogen trap is a disorder in the steel crystal structure (e.g. substitutions, lattice vacancies, precipitates, inclusions, etc.). In such places, the nascent hydrogen may recombine to hydrogen molecules that – due to their large dimensions – are not able to move further. In such case, the recombined hydrogen cannot be expelled from the solid material by any heat-treatment (annealing) process. In the point of such disturbance, the molecular hydrogen causes pressure effects in the order of hundreds of megapascals, which counteract against cohesion forces within the metal [1].

Exposed parts are manufactured of alloyed or compound steels, where the alloying elements form with iron solid solutions that increasingly suffer from deviations in the metal crystal structure. Therefore,

high-strength steels are more susceptible to hydrogen embrittlement. Practical experience shows that an increased risk of hydrogen charging occurs with steel types with strength limit over 1,000 MPa.

The objective of our research consisted in the verification to what extent may be endangered with hydrogen embrittlement the steel parts made of construction steel and pickled in hydrochloric acid before the hot-dip galvanizing process.

4. Research conducted by BELOS-PLP S.A. [2]

The concentration of hydrogen in samples from different stages of production was determined. The fittings are made of 41Cr4 steel with chemical composition according to Tab. 1. In order to perform research the samples- bars were prepared (Fig. 1). The material as delivered (SD), after rolling (W), shot blasting (S), shot blasting and pickling (ST) and HDG was analyzed.

Before HDG, the material was divided into three groups: 0, 1 and 2. The crucial criterion for the division was the surface preparation before HDG. Division of material for testing with the characteristics preparation of surface is shown in Table 2. All samples were galvanized in a single production batch.

Then, a determination of the hydrogen content of the samples prepared in this way was made by a LECO ONH836 elemental analyser.

The results of the hydrogen content in samples taken from different stages of production, i.e. from the material as delivered, after rolling, shot blasting, shot blasting and pickling and with Zn coating are presented in Table 3.

5. Methodology of research conducted at Czech Technical University in Prague

Within the framework of our research, we have conducted hydrogen content measurements, in steel samples made of M8 threaded rods (Fig. 2) of two quality grades: "V" thread-rod sample series in the quality grade of 5.8 with a guaranteed strength limit of 500 MPa and "X" thread-rod sample series in the quality grade of 10.9 with a guaranteed strength limit of 1000 MPa (steel chemical composition according to Tab. 4). The samples of 5 mm diameter and the cylinder length of 5 mm (Fig. 3) were tested for the hydrogen content by the Inert Gas Fusion Method, the Bruker equipment, and with G8 Galileo ONH Elementary Analyser (Fig 4).

The aim of the project was to verify the conclusions that are declared in the evaluation of the research carried out in BELOS-PLP S.A., especially the effect of the flux. According to equation (2), the thermal decomposition of the flux results in superheated steam. Hydrogen ions are formed by the reaction of water vapor with iron. Insufficiently dried flux is a source of excess water vapor and, consequently, an increase in partial pressure of the nascent hydrogen. The effects of the wet flux were verified on a sample "V" prepared from a thread-rod of quality 5.8.

The samples were tested in their degreased natural form and this after the pickling process with the exposure time of 2 hours, others with exposure time of 24 hours and further specimens after 2 hour of pickling and burning of the flux applied. The specimen size was deliberately chosen for the direct testing with the Bruker equipment without any necessity of parting so that cutting effects were eliminated. Instead of zinc, a lead bath heated up to 450 °C was used for the flux burning in order to avoid coat forming. The same delay of 60 minutes between the sample preparation and the testing was maintained.

6. Experimental part

At the beginning, all the samples were degreased and rinsed with water. The pickling process was conducted in a pickling bath containing 140.3 g/l of free HCl and 76 g/l of Fe; then they were rinsed with water again. After the selected samples were coated with the flux by immersion into the bath for 10 minutes, the samples "F-V-2-D" and „F-X-2-D“ were dried in the stream of hot air while "F-V-2-

W" and "F-X-2-W" were left in the wet state. The test results are shown in graph on Fig. 5 and in Table 5.

Our research has proven that after usual pickling in hydrochloric acid, the increase in the hydrogen content in steel is insignificant; the decisive aspect of the hydrogen charging is the flux burning. In its thermal decomposition, hydrogen chloride is generated necessary for additional, intensive cleaning of the surface of the charge as well as the zinc bath level from oxides, and ammonia, which is oxidised by atmospheric oxygen producing nitrogen gas and water steam.



The resulting water vapours are decomposed over the iron according to the equations (3) and (4).



In order to prove the influence of surplus water in the flux, the "F-V-2-W" specimen made of the 5.8 grade thread-rod (pickled for two hours) was immersed, after the flux coating, into the liquid lead only after simple dripping off. The experiment has proven the assumption that if the flux-drying step is skipped before the batch is immersed into molten metal, it would result in a dramatic increase of hydrogen content in the substrate.

The relatively high hydrogen content found with the samples in their condition after degreasing before the pickling process is caused by the presence of iron corrosion products on the surface (hydrated iron oxide $Fe_2O_3 \cdot nH_2O$). This is surface contamination only. Samples were stored in a water bath for 24 hours after degreasing. Through this result was verified the surface contamination effect before Inert Gas Fusion Testing on its result.

7. Conclusions

The results of our experiments prove that the usual pickling process in hydrochloric acid does not increase the hydrogen content in construction steels. Hydrogen values of up to 2 ppm in the natural state of steel are nothing extraordinary. An increased risk of hydrogen charging should be expected in case of high-strength steels over 1,000 MPa and, in particular, due to insufficient drying of flux in the dry process galvanizing.

Acknowledgement

The research was supported by SGS16/217/OHK2/12. Sustainable Research and Development in the Field of Manufacturing Technology.

References:

- [1] Kuklik, V, Kudlacek, J. (Elsevier 2016) Hot Dip Galvanizing of Steel Structures, ISBN 978-0-08-100753-2
- [2] Węgrzynkiewicz, S, Kiełbus, A, Hajduga, M, Piecha, I, Sozańska, M, Waś-Solipivo, J, (Hot Dip Galvanizing Conference Mikulov 2016) The Influence of the surface preparation of elements made of steel grade 41Cr4 on the structure of zinc coating and hydrogen content, ISBN 978-80-905298-54

Figures



Fig. 1: The object of the research in stage II- bar threaded at one end; X-1, X-2 sampling points for the hydrogen content test; X - stages of production i.e. SD- the material as delivered, W- after rolling, S- after shot blasting, ST- after shot blasting and pickling, 0,1,2- after HDG



Fig. 2: M8 thread-rods (quality grade of 5.8 blue, quality grade of 10.9 white)



Fig. 3: Specimens for the hydrogen content analysis by the Inert Gas Fusion Method



Fig. 4: G8 Galileo ONH Elementary Analyser

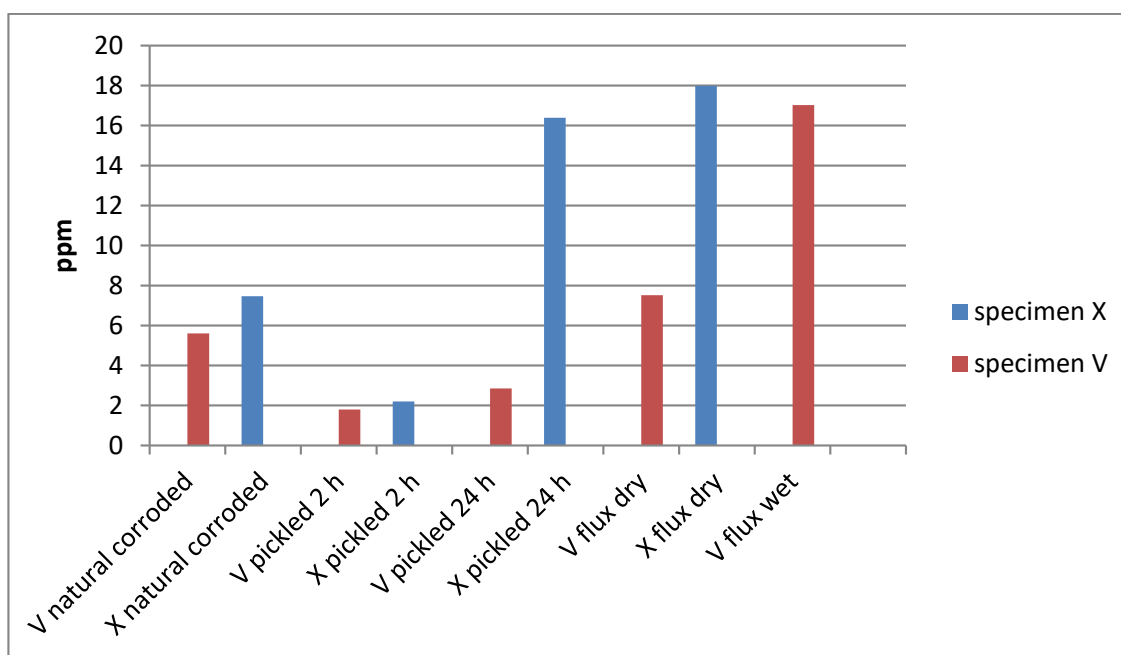


Fig 5: Graph with test results

Tables

Table 1: Chemical composition of 41Cr4 steel

C	Mn	Si	P	S	Cr	Ni	Mo	W	V	Cu
0,36 ÷ 0,45	0,6 ÷ 0,9	0,17 ÷ 0,37	0,035 max	0,035 max	0,8 ÷ 0,12	0,3 max	0,1 max	0,2 max	0,05 max	0,25 max

Table 2: An overview of tested samples

Material designation	Process data	Remarks
0	- Steel shot, GL40 - TIBFLUX 60, pH 4,65 - HDG in temp. 457 °C and centrifuging	Bars galvanized in accordance with the customer's guidelines and expectations- pickling in HCl was eliminated.
1	- Steel shot, GL40 - HCl (14%) + inhibitor, 10min. - TIBFLUX 60 (pH 4.65) - HDG in temp. 457 °C and centrifuging	Bars shot-blasted and short pickling. This kind of surface preparation is used in the production of power network fittings.
2	- Steel shot, GL40 - HCl (14%) + inhibitor, 10min - TIBFLUX 60 (pH 4.65) - HDG temp. 457 °C and centrifuging - removing of Zn coating in HCl (6 %) + inhibitor, 3 hrs. - TIBFLUX 60 (pH 4.65) - HDG in temp. 457 °C and centrifuging	Dezincification of bars and re-galvanizing. Treatments repeated twice before applying the final zinc coating. The purpose of this procedure was to evaluate the effect of intensive chemical treatment, especially on the hydrogen content.

Table 3: Concentration of hydrogen in the tested samples

Description	X	Concentration of hydrogen, ppm	
		Threaded part X-1	Non-threaded part X-2
Material as delivered	SD	-	1,03 ±0,57
After rolling	W	1,08 ±0,53	0,82 ±0,18
After shot blasting	S	0,98 ±0,18	0,66 ±0,44
After shot blasting and pickling	ST	6,38 ±1,44	2,05 ±0,42
After HDG "0"	0	13,47 ±9,75	2,79 ±1,17
After HDG "1"	1	7,82 ±1,55	7,77 ±1,73
After HDG "2"	2	5,38 ±0,79	3,77 ±1,28

Table 4: Chemical composition of specimens V (steel grade 5.8) and X (steel grade 10.9)

Specimen	C	Si	Mn	S	P	Al	Cr	Mo	Ni
V (5.8)	0,157	0,271	1,340	0,029	0,025	0,039	0,050	0,010	0,028
X (10.9)	0,371	0,501	0,792	0,025	0,010	0,019	1,133	0,201	0,120

Table 5 Survey of specimens, tests and their results

Steel and type of testing	V – steel 5.8	X – steel 10.9
	IGF	IGF
Specimen state	[ppm]	[ppm]
Specimen natural	F – V	F – X
	5,6024	7,4623
Specimen pickled 2 hours	F – V – 2	F – X – 2
	1,7960	2,2024
Specimen pickled 24 hours	F – V – 24	F – X – 24
	2,8490	16,3901
Specimen pickled 2 hours, flux dried, immersed in lead	F – V – 2 – D	F – X – 2 – D
	7,5168	17,9876
Specimen pickled 2 hours, flux wet, immersed in lead	F – V – 2 – W	F – X – 2 – W
	17,0217	

Author biography

Vlastimil Kuklik studied at the Faculty of Mechanical Engineering of CTU in Prague the Management Engineering with a degree MSc first. Later, he passed additional education in post-graduate studies in the field of finishes and qualifying as a corrosion engineer. Finally he completed his studies defending his dissertation in the field of engineering technology, focusing on finishes and awarded Doctor Degree. He deals with a hot-dip galvanizing for long time. He was employed at the METALEUROP S.A., the ZINKPOWER Kopf Holding GmbH and the WIEGEL GROUP in this field. Vlastimil Kuklik currently lectures technology of Hot Dip Galvanizing on the Faculty of Mechanical Engineering of the Czech Technical University in Prague. As a Corrosion Engineer and a Judge Advocate in Hot Dip Galvanizing he carries out the quality assessment of zinc coatings. The results of his work are often published in expert magazines and he regularly supplies contributions to the expert program of conferences on metal coatings. Vlastimil Kuklik is an author of the monograph Hot Dip Galvanizing of Steel Structures.

Chemical pre-treatment of steel in the hot dip galvanizing process

with focus on flux and drying conditions

Dr. Frank Schmelz,
RAM Engineering + Anlagenbau GmbH,

1. Abstract

The hot dip galvanizing process is based on a wet- chemical pre- treatment of the material prior to the galvanizing process itself. The degreasing, rinsing, pickling, fluxing and drying of the steel determines the result of the galvanizing process in the kettle. Every deviation from the optimal process parameters results in a loss of quality of the galvanizing process. An insufficient degreasing results both in an extended pickling duration and in an extended usage of pickling acid and also in an increased carry-over of organic material in the following process steps. This increases the overall costs for pre-treatment and leads to an increased rate of emissions. Maintaining adequate conditions of the pickling liquids decreases the carry-over of dissolved iron into the rinse and flux bath. Separating the dezincification pickle from the iron pickle decreases the costs for the disposal of spent pickling liquids noteworthy. The adjustment of the salt content, the salt ratio as well as the pH value of the flux influences the drying process and the galvanizing process. Not keeping the flux conditions in the optimal ranges result in many disadvantages as increased costs and in a decrease of quality. This paper shows that an insufficient degreasing of material can lead to +10 times higher pickling acid consumption and pickling times. The cost for disposal of spent acid liquids increase up to +100% in dependence on the iron and zinc content of the liquids. The heating of bathes with waste heat of the furnace can decrease the energy costs for heating up to 60%. The influence of well-conditioned flux in matters of cost savings varies in ranges between 5% and +10% zinc savings.

2. Introduction

Within this presentation the economic influences of keeping and leaving the optimum working parameters at a wet-chemical pre-treatment area of a hot dip galvanizing plant are shown. A standard pre-treatment area consist of one degreasing bath, several pickling baths, two rinses in front and behind the pickling baths, one fluxbath and a dryer. The pre-treatment is the basis for the galvanizing process, most importantly the wettability of cold rolled steel and the absence of scale of hot rolled steel. Inefficiencies of process steps, for instance inefficient Degreasing, pickling or rinsing, influences the following process in a negative way. As well as inefficiencies the carry-over of liquids in downstream processes increases the overall operation costs, the safety of work, the quality of galvanizing and the environmental impact.

3. The wet chemical pre-treatment of hot dip galvanizing process

3.1. The degreasing process

The surface of steel material often shows superficial contamination with grease, oil, oxides, dust and dirt. If the contaminants are not removed, they disturb the next process steps and lead to poor galvanizing quality, higher ash seizure and black spots on the galvanized surface. The superficial contamination can be eliminated by

- chemical / physical processes which emulsify oils and fats
- dispersion / suspension of dirt particles
- saponification of many oils and fats
- dissolving / complexing metals, oxides and metal salts.

The amount of contamination per m² varies around average values of app. 500..1000 mg C/m², both on cold- and hot rolled steel. For zero- defect galvanizing C- contents of

- <50mg/m² (CRS)
- <130mg/m² (HRS)

are required [1].

The degreasing process is mainly divided into two different types, the alkaline- and the acid dip degrease. The alkaline degrease is operated at higher temperatures than the acid degreasing, but the effectiveness of degreasing and the lifetime of the chemicals are higher, the costs for the chemicals are lower than for acid degreasing [2].

The degreasing effect of acid degrease and alkaline degrease is higher on cold rolled steel than on hot rolled steel. The dip degreasing both of CRS and HRS does not lead to C- contents below 50mg/m² without rinsing after degreasing.

An insufficient degrease of the steel leads to significant increases both in pickling time and acid consumption, see Fig.2 and Fig.3.

For a surface with >500mgC/m² in comparison to a surface with <50mgC/m²

- The pickling time is up to +100 times longer and
- The acid consumption is up to +20 times higher.

With a pickling acid of 10% HCl and 50 g/l Fe, the pickling time increases from 15 minutes to 27 hours and the acid consumption increases from 5 g/m² to >100g/m², for instance.

These figures show, that the degreasing of steel products in the first pre-treatment step influences the economic data of the galvanizing process in total. If the inefficient degreasing is not covered in the pickling bath (with increased time and acid consumption) the contamination leads to poor galvanizing results and may lead to a dezincification and with this to an increase of costs.

The effectiveness of the degreasing can be increased by:

- Higher temperatures (do not exceed over the cloud point)
- Increased mass transfer by motion
 - Pumping
 - Ultrasound
 - Air agitation
 - Movement of the work
- Longer dipping times
- Higher concentration of effective ingredients.

3.2. The rinsing process

The use of alkaline degrease baths makes it necessary to rinse the metal in order to avoid the (acid) pickling from undesired carry-over of liquids into the pickling bath. Even for acid degreasing baths a rinse might be reasonable to increase the degreasing effectiveness and to decrease the carryover of liquids. The limit concentration of ingredients in the rinse (g/l) is dependant from the rinsing criterion. The rinsing criterion is the dilution ratio of the concentration in the processing bath and the last rinsing bath. Exceeding the concentration in the liquid increases the carryover of ingredients at constant carryover ratios. A second rinse in series increases the effectiveness of rinsing. Shortages in rinse bath should be balanced with fresh water, spent rinsing should be used for balancing shortages in pickling bathes.

3.2.1. Carryover of liquids

In general, the total amount of fluids which are carried over from one bath to the following one depends on (a.o.)

- The (related) surface of the material
- The surface finish (roughness)
- The type of part (corners, scooping parts)
- The dripping time
- Liquid properties (density, surface tension, viscosity, temperature).

A brief overview of quantities is given in Fig. 5.

These dependencies result into some unavoidable amounts of liquid input in the next process step and- bath. The total liquid carryover can be reduced by

- Longer dripping time
- Reduced viscosity and surface tension (higher temperatures, additives)
- Appropriate constructions for galvanizing (vent holes, dead zones)
- Appropriate wiring, steep dipping angles.

By increasing the dripping time after degreasing from 4 sec to 10 sec the carryover is reduced by 30% [3].

3.3. The pickling process

The pickling process is a process to remove the native impurities (i.e. rust and scale) from the surface of the steel, see. Fig.4. The most common process is the acid pickling with hydrochloric acid. The effectiveness of the pickling is based on the chemical reaction of HCl and ferric oxides. The main reactions are:

- $\text{Fe}_3\text{O}_4 + 8\text{HCl} \rightarrow \text{FeCl}_2 + 2\text{FeCl}_3 + 4\text{H}_2\text{O}$
- $\text{Fe} + 2\text{HCl} \rightarrow \text{FeCl}_2 + \text{H}_2$
- $2\text{FeCl}_3 + \text{Fe} \rightarrow 3\text{FeCl}_2$
- $2\text{FeCl}_3 + 2\text{H} \rightarrow 2\text{FeCl}_2 + 2\text{HCl}$

Even with a brand new bath you have Iron salts as they help the pickling process to be much more efficient. During the pickling process the dissolved Iron accumulates as Ferrous Chloride and the acid concentration decreases. This increasing iron concentration and decreasing acid concentration decreases the pickle effectively.

To compensate the decrease in effectiveness,

- the dipping time has to be increased or
- the effectiveness has to be re-increased by
 - recharging of the pickle with HCl or
 - increasing the temperature.

Higher temperatures lead to higher evaporation rates and acid emissions. Therefore the heating of pickle is not recommended in HDG plants without encapsulated pre- treatment areas.

With respect to minimize the HCl consumption per ton, some aspects should be regarded:

- do not exceed the amount recharged HCl
- do not overheat the pickle (according to concentration)
- use inhibitors
- avoid overpickling
- increase the dripping time
- use rinse liquids to recharge pickling baths
- avoid the pickle from zinc and ammonium (increased disposal costs)

The pickling solution should be disposed, when the required time for pickling exceeds the economic dividing line. This line is given by the dipping time that exceeds the critical time (pickling is the bottleneck of the process), and by increased disposal costs. In most countries the disposal costs for waste pickle liquids are related to the content of Iron and zinc. The comparison of costs for the disposal of mixed pickling solutions and separated iron- and zinc pickling solutions in Fig.6. shows, that the dezincification in a separated pickling bath (instead of dezincification in any pickling bath) leads to significant savings (basis: disposal costs in Germany (average)). In this example the savings for disposal of spent pickling are +50% by separating iron pickling from dezincification.

3.4. The fluxing process

The fluxing process usually consists of three steps: rinsing of the pickled work, dipping it into the flux solution and drying the work.

3.4.1. The physical properties of the flux solution

The majority of fluxes are based on the binary system Zinc / Ammonia chloride. These standard fluxes are all Eutectic mixture with 1 mol of Zinc chloride and either 2 or 3 mol's of Ammonium chloride. This includes all the usual fluxes and some for specialist applications such as continual HDG or high levels of Al in the zinc. Also much more complex formulations are used for special applications.

The melting point of these mixtures is lower than the individual melting points of the ingredients. Zinc and ammonium chlorides both have as individual substances melting points well above 300°C, Zinc-Ammonium based fluxes have melting points of around 150°C.

3.4.2. The flux function

The fluxing of work prior to HDG leads to

- a dissolution of Fe-salts by immersion into the flux agent
- a fine- pickling caused by the formation of hydroxo zinc acids (acid pickling effect) while drying
- protection against oxidation of the metal while transport into the zinc bath
- a fine- pickling during dipping into the zinc melt due to thermal dissociation of zinc and ammonium chloride and resultant HCl in the zinc melt
- dissolving of zinc oxide at the surface while immersion into the zinc melt.

The first fine pickling takes place during the drying process by evaporation of water and with this an increase of the salt concentration above 600g/l. Exceeding this concentration leads to the formation of complex chlor- zinc acids which support the removal of left oxides on the surface and they prevent the surface from re- rusting.

The second fine pickling takes place during the dipping into the molten zinc. While the work is being lowered into the zinc, the dried flux layer is already melting (melting point app. 150°C) and lowering the surface tension of the zinc, allowing a much greater contact area between the work and zinc (Fig. 7). While the temperature exceeds 180°C the flux begins to thermally dissociate building hydrochloric acid, ammonia gas and zinc metal. These phase- changes result in a huge expansion of the volume. This "explosion" produces a cleaning effect that removes any contaminants left on the surface and the hydrogen chloride dissolves any oxides that were picked up at the surface.

With rising temperature the galvanizing reaction starts and due to the flux process and fine pickling effects the work and the zinc form the desired layers on the surface.

3.4.3. Flux parameters

The correct and economical function of flux depends on the process parameters density, pH value, temperature and iron content (a.o.).

3.4.3.1. Density

The density is given by the salt content of the flux. For regular galvanizing a salt content of approx. 400 to 425 g/l is recommended, at least 350 to a maximum of 500 g/l. A low salt content leads to insufficient drying of the salt layer and with this to a transfer of moisture into the zinc. There is also the danger of not fully forming a salt layer on the surface of the work, so there is no protection against a renewed rusting. The density can be adjusted either by adding flux salt or water.

3.4.3.2. pH value

The pH value should be kept between $3,5 < \text{pH} < 5,5$. A pH value $< 3,5$, leads to pickling in the flux and with this to an increasing iron content in the flux. A pH value $> 5,5$ can lead to an increased amount of ash being produced. To avoid the flux from low pH values the rinse waters should be returned to the pickles and fresh water should be added. The pH value can be raised by adding buffered fluxes or by ammoniac (which causes a readjustment of flux chemistry).

3.4.3.3. Temperature

The temperature of the flux solution has no influence on the layer formation itself, but heated fluxes reduce the drying time and therefore the heat quantity in the dryer. A temperature of 50°C is recommended.

3.4.3.4. Iron content

The iron content in the flux results from pickling processes in the flux (at low pH values) and from carryover of rinsing liquids with high iron contents. The iron content in the flux should be kept to lower than 5g/l. Higher Fe contents in the flux result in increased dross formation (1 gram of Iron reacts with app. 25 grams of Zinc (20 – 33 g) to form bottom and floating dross), longer drying times, more ash (wet) and lower galvanizing quality. The input of iron into the zinc-melt results from the contained ferric chloride of the flux.

The influencing parameters of the carryover of liquids are described in 3.2.1. For a throughput performance of 10.000 tons Fig. 8 shows the quantities of iron input into the flux. For an average material mix at a total amount of 10.000tons of galvanized steel the amount of 900kg iron is carried over into the flux and with this into the zincbath.

The methods to reduce the iron content in the flux are to

- rinse with 2 rinses (cascade)
- rinse with cleaner water
- rinse longer
- extend the dripping time (the dripped volume of zinc electrolytes doubles when increasing the dripping time from 4 sec. to 10 sec.!))
- keep the pH value on >3,5
- treat the flux (batch wise or continual).

3.4.4. The flux treatment

In order to keep the flux-parameters in the optimum range means to maintain the salt content and composition, the pH value and the iron content as well as the content of undesired organic in optimum ranges. To reduce the iron content in the flux the classical chemical reactions are:

- Oxidation from Ferric to Ferrous Iron with Hydrogen Peroxide:
 - $2\text{Fe}^{2+} + \text{H}_2\text{O}_2 + 2\text{H}^+ \rightarrow 2\text{Fe}^{3+} + 2\text{H}_2\text{O}$
- Precipitation of Ferrous Iron as Iron Hydroxide with Ammonium hydroxide:
 - $2\text{FeCl}_2 + 6\text{NH}_4^+ + 6\text{OH}^- \rightarrow 2\text{Fe}(\text{OH})_3 + 6\text{NH}_4\text{Cl}$

Another kind of chemistry of reducing the iron contamination is:

- Oxidation of Ferric to Ferrous Iron and precipitation in 1 step:
 - $3\text{FeCl}_2 + \text{KMnO}_4 + 7\text{H}_2\text{O} \rightarrow 2\text{Fe}(\text{OH})_3 + \text{MnO}_2 + \text{KCl} + 5\text{HCl}$
 - $2\text{HCl} + \text{ZnO} \rightarrow \text{ZnCl}_2 + \text{H}_2\text{O}$

Further methods are (not common) [2]:

- Oxidation of Ferric to Ferrous Iron with Ozone
- Oxidation of Ferric to Ferrous Iron with Boron doped Diamond electrodes
- Oxidation of Ferric to Ferrous Iron with Ultra Violet light and an O₂ source

For flux treatment/ iron removal some aspects have to be kept in mind [2;4;5]:

- pH <3.5: incomplete iron precipitation
- pH <2.5: no iron precipitation
- pH <2 : creation of toxic chlorine gas
- H₂O₂ decay is an exothermic reaction (when H₂O₂ comes into contact with iron salts, ie when no Fe (II) ions are present), plant should be T_{max}-protected
- Optimal results are expressed by continuous flux conditioning
- Discontinues treatment leads to "sawtooth" effect that may cause un- consistent qualities of galvanizing
- Using TIB Ferrokill® reduces the amount of chemicals and maintenance needed
- Too low pH values in the flux increase the Fe input and degrade the desired effects of the flux
- Flux treatment is only economical if the rest of the process works optimally
- elimination of organics from carryovers by flux conditioning is only possible to a very limited extent

- Flux additives can lead to foam formation (restriction of plant performance conditioning), additive manufacturers can provide Anti-Foam's

In general, three modes of iron removal/ flux treatment are applicable:

- discontinuous removal directly in the bath by decanting and filtration,
- treatment in *discontinuous* (batch wise) treatment systems
- treatment in *continuous* treatment systems.

Fig. 9 shows the overall apparatus of the 3 systems and the characteristic properties of the systems as well as advantages/ disadvantages.

The financial benefits of a continuous flux treatment result from:

- Lower flux consumption
- 5 – 8% reduction in the zinc consumption (references)
- up to 50% less dross
- up to 24% less ash
- Less reworking / stripping.

References show savings directly connected to flux conditioning systems of 5% to 18% [2; 5]. These savings correlate with results of several investigations, which showed a direct dependency between pH Value and iron content with the overall zinc consumption in HDG process. For instance, the zinc consumption overall decreases from 809g/m² to 733g/m², 10% respectively, while reducing the iron content from 60g/l to 0g/l and increasing the pH value from 1,1 to 4,5 [6].

3.5. The drying process

The drying process of fluxed work is driven at temperatures $80^{\circ}\text{C} < T < 120^{\circ}\text{C}$, the average drying time is 20 minutes. The drying air flows through the dryer in one direction, therefore the wiring at the traverse should consider this flow direction in order to minimize dead zones and scooping areas. The volume flow can be calculated by $750 \times \text{volume of the drying chamber}$. Increasing the volume flow has major influence on the drying process than higher temperatures. At least 10 % of the volume flow should be fresh air in order to reduce the humidity of the drying airflow. The heating of the drying air with "waste heat" from the kettle furnace by using a heat exchanger is most common. It is not expedient to use furnace exhaust gases, because of their humidity and content of soot particles. If the heat energy content of the kettle furnace is not sufficient or not available, a separate heater with a heat exchanger can be implemented into the plant.

„Wrong drying“ at wrong temperatures or insufficient rates of convection can influence the positive effect of the dried flux agent negatively.

- Too low temperature:
 - water - bounded as hydrates at the zinc chloride – flakes off in the zincbath (perhaps surface defects),
 - increased pickling effect in this temperature range caused by hydroxo zinc acids results in additional occurrence of hard zinc
- too high temperature:
 - melting point of the flux agent is exceeded, thermal dissociation of zinc ammonium chloride in the dryer (additional hard zinc).

Cold dryers or drying by infrared dryers are options as well as microwave caused drying, but they are not very common.

An inefficient drying process prior to the galvanizing process causes zinc losses through splashes of boiled flux liquid and decreases the fine pickling effect of a melting flux layer.

4. Heating of baths in the pre-treatment process

Almost every pre- treatment process in the HDG process can be enhanced by temperature increase:

- heating the degreasing bath (even acid degreasing) increases the efficiency of the process
- heating the pickle reduces the dipping time/ increases the activity of pickle

- heating the flux reduces the surface tension/ reduces the dripping time.

The desired temperatures in the different areas of pre- treatment are typically 60°C (alkaline degrease), 50°C (flux), 20°C (pickle and rinse). The heat quantities to achieve these temperatures depend on the size of the baths and the amount of steel processed. For a reference plant with a 7m kettle the quantities of heat are calculated as shown in Fig. 10.

The heat demand depends from:

- amount of processed steel (small influence!)
- temperature of the liquids (medium influence)
- ambient air temperature (big influence)
- size of surface area (very big influence!)
- temperature of the liquid (very big influence)

Fig. 11 shows the quantitative influence of the different parameters on the heat demand (for the given example Fig.10)

The amount of waste heat from a furnace of 900kW combustion performance is 180kW without air pre-heater, and 90kW with air pre- heater [7]. This heat amount is available for heating water as a heat storage. Since the flow temperature should be limited to 85°C in order to prevent the apparatus and the liquids from improper temperatures, this heat amount comes to 108kW of effective heat usage. Using cascades for the centralized heat exchange in extern heat exchangers leads to usage of to 80% of this waste heat amount, see Fig.12. The usage of extern heat exchangers increases the heat transfer significantly because of app. 3 times increased heat transfer coefficients (in Wm^2/K) in comparison to immersion heat exchangers. The application of this centralized, extern heat management allows the usage of high efficient heat exchangers. Even in the case of a pipe burst of the heat exchanger almost no liquid contamination occurs.

With the waste heat recovery unit shown in Fig. 12 almost 50% of the demanded heat amount is covered. For standard German energy prices these 50% are +55.000€/annum. Dependant from the kind and size of heat recovery unit this leads to returns on investment of app. 1 year.

4.1. Measurements for heat energy reduction (a.o.)

The energy consumption in a HDG plant is related to the temperatures of the heated baths:

- Zinc kettle
- Degreasing bath
- Flux bath
- Pickling bathes
- Rinse bathes

(in descending order). As shown in Fig. 11 the temperature and the size of surface area have big influences on the heat consumption. In order to reduce the heating energy consumption the bathes should be operated at the lowest possible temperatures. The increase of temperature leads to a quadratic increase in heat consumption. Beside the energy saving potentials by lower operating temperatures the amount of emissions from evaporation and vaporization decrease on a noteworthy scale.

During all "non- productive" periods (night shifts, weekends etc.) the covering of surface areas leads to remarkable energy savings. The zinc kettle can be covered with a solid coverage which can be handled with the kettle´s crane facility.

All other surfaces should be covered by plastic spheres or solid caps and the temperature of the bathes should be optimized with regard to the balance between efficiency and heat consumption.

5. Remarks on pre-treatment and efficiency in HDG plant

The efficiency and the economic data of the pre- treatment process can be increased by:

- Clean surfaces (no grease, no oil)
- Good rinsing conditions (keep the content of oil and grease low), good rinsing and dripping
- Rust- free surfaces (proper pickling)
- Good rinsing conditions (reduced iron content, pH > 5, long dripping periods)
- Good flux conditions (low iron content, correct pH value, salt content and – composition)
- Adequate drying (no wet surfaces, no fluid accumulations)
- High dipping angles (better dripping behaviour)
- Reasonable temperatures in all baths

References

[1] Stieglitz & Schulz, Metalloberfläche 47. Jahrg. 1993/12
 [2] TIB Chemicals
 [3] Johannes Fresner, Thomas Bürki, Henning H. Sittel, Ressourceneffizienz in der Produktion: Kosten senken durch Cleaner Production
 [4] Peter Peißker, Mark Huckshold, Handbuch Feuerverzinken, 4. Auflage 2016
 [5] Dr. Frank Schmelz, RAM Engineering + Anlagenbau GmbH, Workshops 2016 for member companies of the Industrieverband Feuerverzinken e.V.: Flux agent de-ironing and processing - an overview of causes, impacts and effects of (i.a.) ferric chloride in flux agent –
 [6] W. Katzung, R. Rittig, Metall: 52. Jahrgang Nr. 5/1998
 [7] Zink Koerner, Hagen, Germany

Figures and tables

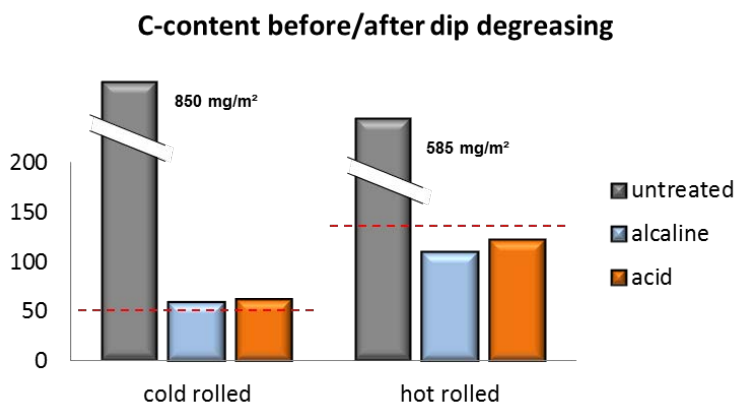


Fig. 1: Grease layer on the surface of cold and hot rolled steel before and after dip degreasing in alkaline/ acid degrease. The red lines show the critical values for zero-defect galvanizing.

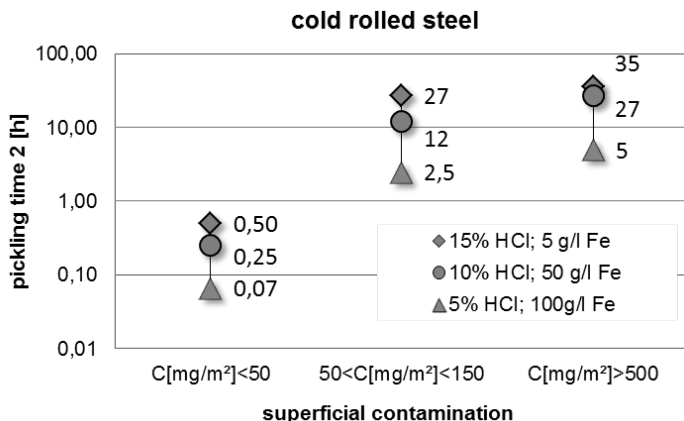


Fig. 2: Average pickling time [h] of cold rolled steel as a function of superficial contamination with oil/grease (C in mg/m²), pickling time 2 stands for total wettability of the surface. The pickling time is shown as a function of different acid compositions, [data from 1].

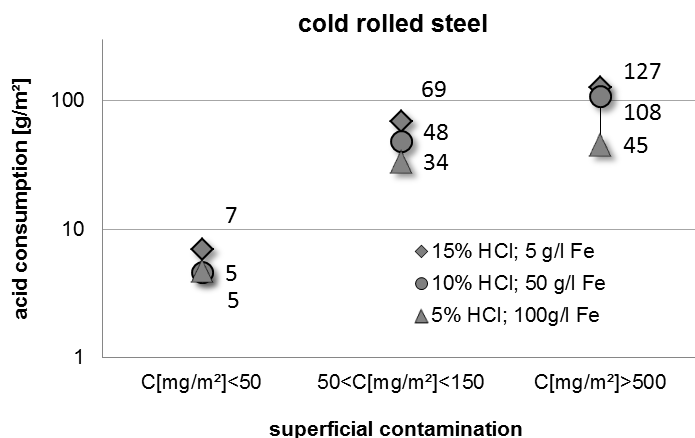


Fig. 3: Average pickling acid consumption [g/m²] for cold rolled steel as a function of superficial contamination with oil/grease (C in mg/m²). The pickling acid consumption is shown as a function of different acid compositions, [data from 1].

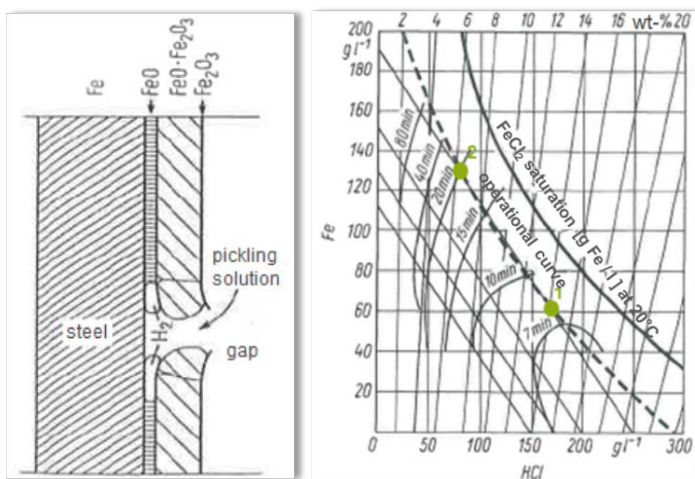


Fig. 4: The pickling process and the origin of iron chloride; the figure (right) shows the decreasing pickle efficiency (1 -> 2) parallel to an increasing iron content and a decreasing acid content [4]

Rate of carryover pro/m ² of surface		
Large / smooth components	0.04-0.08	l/m ³
Lightly textured components	0.08-0.12	l/m ³
Textured / rough components	0.12-0.2	l/m ³

Surface area of the components		
Heavy steel construction	20 - 30	m ² /t
Forgings	80 - 90	m ² /t
Gratings, light constructions	90	m ² /t

Carryover of liquid		
Liquid per ton	6,4 .. 10,8	l/t

Fig. 5: Calculation of carryover of liquids in a HDG plant (example)

Steel processed 10.000 t/a ; pickling usage 30kg HCl/t ; 300t/a pickling liquid			
	Zn+Fe pickling	Zn pickling + Fe pickling	
cost [€/t]	165€/t	50€/t	70€/t
content [g/l]	30 g/l Zn 120 g/l Fe	160 g/l Zn 20 g/l Fe	5 g/l Zn 130 g/l Fe
amount [t/a]	300 t/a	100 t/a	200 t/a
cost [€/a]	49.500 €/a	5.000 €/a	14.000 €/a
total cost [€/a]	49.500 €/a	19.000 €/a	

Fig. 6: Comparison of disposal costs for 10.000 tons processed steel and usage of 30kg/t pickling solution. The costs for disposal of separated Zn and Fe pickling solution decrease to <40% of disposal costs for mixed pickling solutions. For this example (Germany 2017) the savings are 30.500€ for 10.000 tons processed steel.

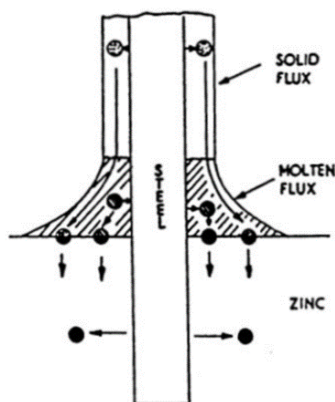


Fig. 7: Melting of the dried flux layer while dipping the work into the molten zinc leads to reduced surface tensions and a better contact between steel and zinc [2].

Assessment of the amount of Iron in the Flux per 10000 tons of work									
Fe-amount in the rinsing		5 g/l	10 g/l	20 g/l	5 g/l	10 g/l	20 g/l		
Material mix parameter	Liquid Volume	Iron accumulation in the flux			Wasted zinc due to reaction with iron				
Best case: 0,04l/m ² ; 20m ² /t	8.000 l/a	40 kg/a	80 kg/a	160 kg/a	1 t/a	2 t/a	4 t/a		
Av. case: 0,1l/m ² ; 90m ² /t	90.000 l/a	450 kg/a	900 kg/a	1800 kg/a	11 t/a	22 t/a	45 t/a		
Worst case: 0,2l/m ² ; 150m ² /t	300.000 l/a	1500 kg/a	3000 kg/a	6000 kg/a	38 t/a	76 t/a	152 t/a		

Fig. 8: The total carryover of iron from the rinse into the flux depends on the amount of processed steel (10000t/a), material mix parameters (related surface, carryover rate per m²) and the iron content in the rinse. In this example the iron accumulation of 900kg/a result in a calculated amount of 22 tons of wasted zinc due to reaction with iron.

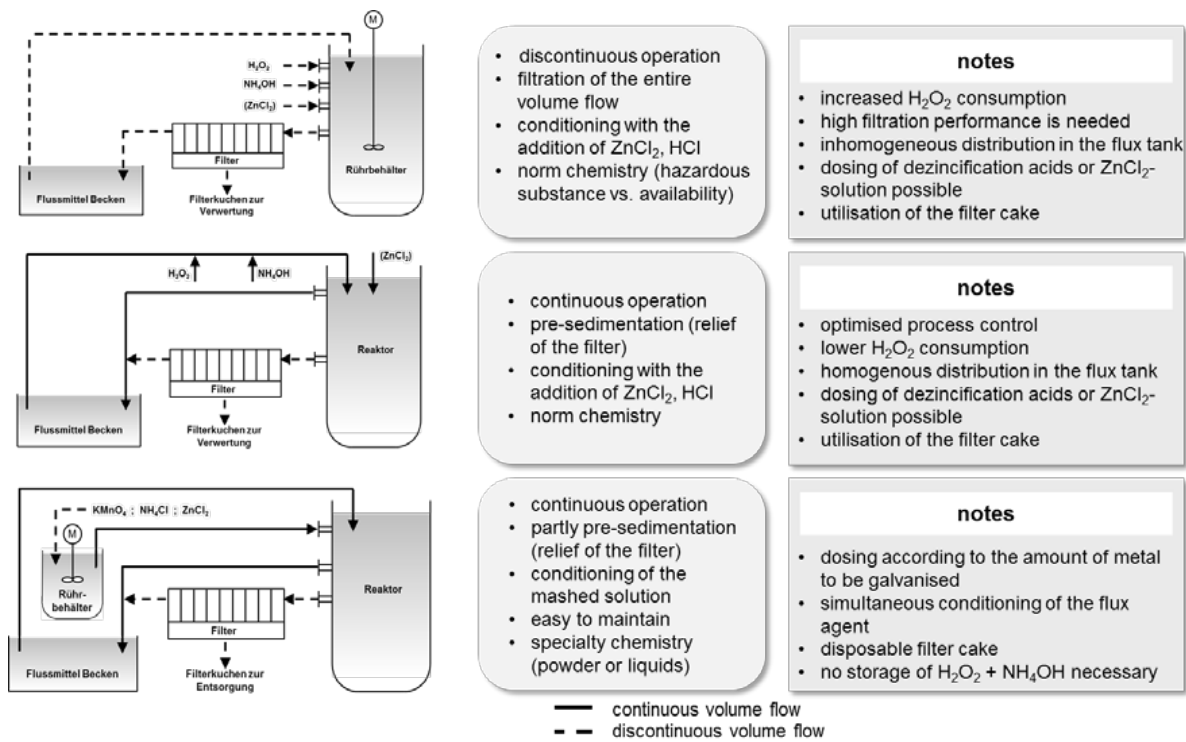


Fig. 9: overall apparatus of the 3 flux treatment systems and the characteristic properties of the systems as well as advantages/ disadvantages [5]

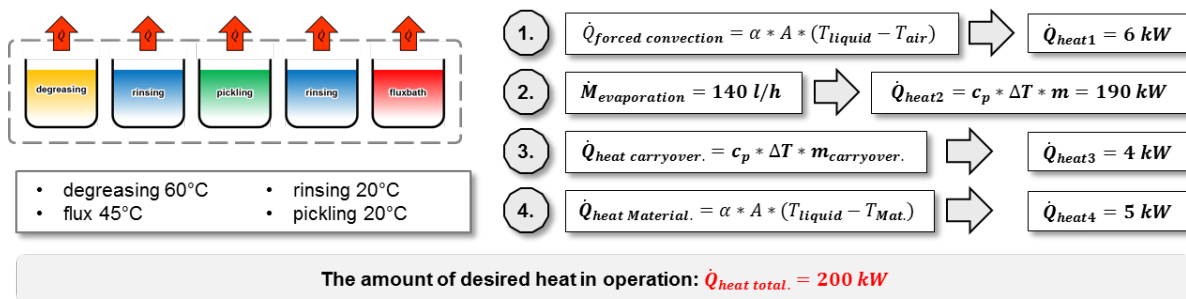


Fig. 10: Calculation of heat quantities for an example plant with bath dimensions of 7m x 2,2m x 1,4m (L x W x H), 1 degreasing-, 2 rinse-, 6 pickling-, 1 fluxbath. The heat quantities mainly result from convection, evaporation (encapsulated area), carry over, heating of material. Commissioning processes are not considered.

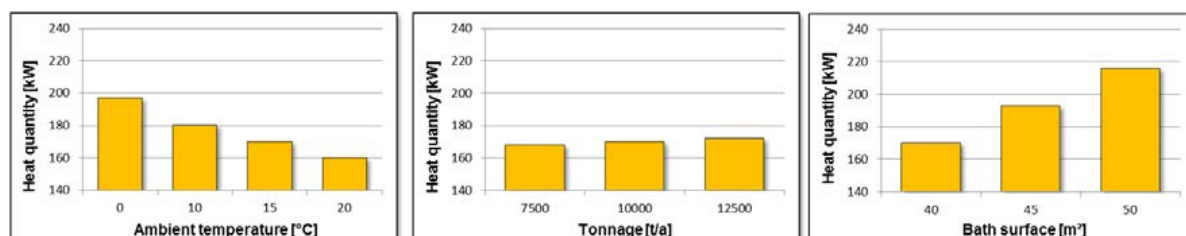


Fig.11: The influence of the ambient temperature, the amount of processed steel and of the surface area of a bath is shown. The high impact of surface area on the overall heat consumption results from the evaporation enthalpy of the liquid. This shows that a covering of liquid surface areas during non-operating periods decreases the energy consumption noteworthy.

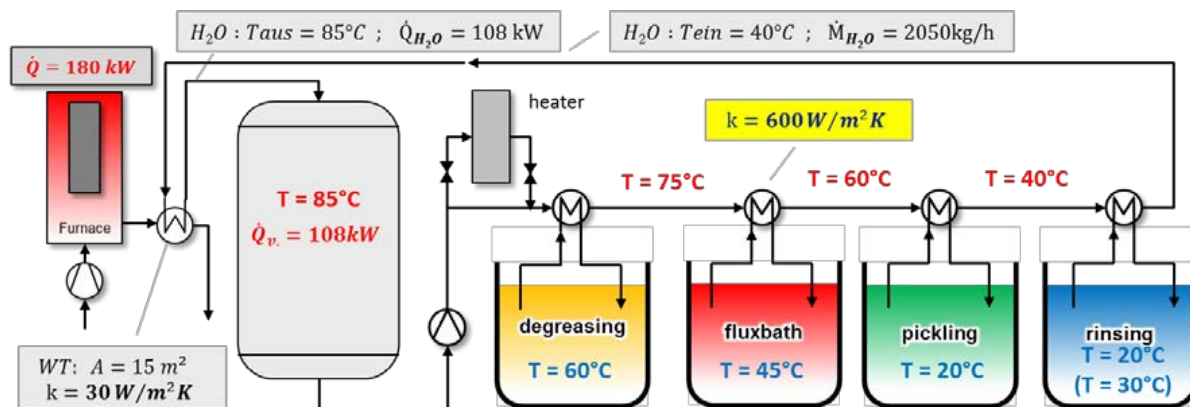


Fig. 12: For an example kettle (7m length) the resulting waste heat of 180kW from the exhaust temperature of the furnace is stored in a hot water buffer vessel. The resulting 108kW are uses in a cascade of heat exchangers to heat different bathes. The advantage of this centralized system in comparison to a heating system with immersion heat exchangers is the higher jeat transfer rate k.

Authors biography

	Dr. Frank Schmelz	Education Graduate Engineer (Mechanical and Process Engineering), University Essen PhD Engineering, TU Dortmund University PMP certified Project Management Professional since 2005 HAZOP study leader since 2010
	Work Experience	25 years work experience 3 years F+E Fluid Mechanics, >20 publications, TU Dortmund University 2 years Head of Process Engineering, SABIC Polyolefine, Gelsenkirchen 18 years CEO RAM Engineering GmbH, Gelsenkirchen 5 years CEO OORAM Russia, Moscow
	Project References	E.ON, Gazprom, Rosneft, SABIC, Evonik, Ineos Phenol, BASF, Bayer, BP, MiRO, Esso, Exxonmobil, Petrom, Arcelor Mittal, ThyssenKrupp, Goldschmidt, Basell Polyolefins, Degussa, Rüttgers, Sachtleben, Coperion, Babcock, RAG, HKM, Infracore, Gelsenwasser Lurgi, MAN, Open Grid Europe, Saria, Aker, Uhde (selection of companies)
	Industry Focus	Power plants, refinery, chemical and petrochemical industry, natural gas and gas transport, plant engineering, project management, steelworks, metallurgical plants and rolling, HDG plants
	Functional Focus	strategy, technology, engineering, project management, organisation, project execution

membership/ honorary office of several organisations (Rotary, employers' association, VDI (association of German engineers), PMI (project management institute), IHK (chamber of industry and commerce), different industry associations)

Liquid metal assisted cracking initiated at drain holes during hot-dip galvanizing

Yuki Fujiwara*, Hayato Asada*, Tsuyoshi Tanaka*, Tatsuo Yamashita**, Yuji Kitano***, Takeshi Watarai****, Yoshihiro Murakami*****

* Department of Architecture, Kobe University, 1-1 Rokko-dai Nada, Kobe, 657-8501, Japan

** Kakuto Corporation, 51 Minami-Yashima, Nagano, 381-8686, Japan

*** Tanaka Galvanizing Co., Ltd., 5-1-1 Mitejima Nishi-Yodogawa, Osaka, 555-0012, Japan

**** Yokohama Galvanizing Co., Ltd., 1838-1 Shimotsuboyama, Shimono, Tochigi, Japan

***** Galva Kogyo Co., Ltd., Japan

Abstract

Hot-dipped zinc coating is well recognized as a standard method of long-term protection from corrosion and is widely applied to heavy steel products such as building structures in Japan. In this process, liquid metal assisted cracking (LMAC) has sometimes occurred at drain holes which were located at corner of welded beam-to-column connection during hot-dip galvanizing. However, the mechanism of the phenomenon has not been well understood. To develop the understanding of the phenomenon, this paper focused on the effect of geometric parameters including web thickness, the ratio of web-flange thickness, location, and size of drain holes on the strain concentration and resulting occurrence of cracking. Immersion tests and corresponding finite element analysis were performed with small scale specimens to investigate the thermal history and strains due to the thermal expansion and contraction in hot-dip galvanizing process. The specimens were composed of web plate surrounded by flange plates with drain holes drilled at corners. All specimens were fabricated from mild steel (SN490B) with nominal yield strength of 325MPa which are commonly used for building structures in Japan. From the investigation, it was found that the magnitude of tensile strain occurred at cracking points increased as flange-web thickness ratio increased, and as web thickness decreased, expanding diameter of drain hole somehow reduced strain concentration. Based on correlation between magnitude of tensile strain and occurrence of cracking, tensile strain could be considered as helpful index to evaluate the effect of geometric parameters on LMAC.

1. Introduction

In hot-dip galvanizing of steel products, vent and drain holes (hereafter referred to as drain holes) must be placed close to the corners of the steel products in order to avoid the formation of pools of molten zinc and uncoated spots due to air pockets at the corners. When the weld access holes called "scallop" that allows for welding of the beam flange is alternative for venting and drainage, as shown in Fig. 1(a), It has been recognized that the impact of the stress and strain concentration due to its shape, as well as the impact of the residual stress due to the welding lead to significant occurrence of liquid metal assisted cracking (LMAC) [1-4]. Therefore, the Structural Steelwork Specification for Building Construction (JASS6) specified by the Architectural Institute of Japan recommends that non-weld access hole type beam-to-column connections

should be used for galvanized structures, and that circular holes should be placed in corners to serve as vent and drain holes, as shown in Fig. 1(b) [5, 6]. However, although the use of circular holes is able to reduce the frequency of occurrence of LMAC, LMACs still do occur in some cases.

The Previous researches on LMAC of steel conducted by Japanese researchers primarily have focused on LMAC in the heat-affected zone of welded connections made of 590 N/mm² grade high-strength steel. These researches [7-10] reported that LMAC occurs as a result of the decreased grain boundary strength due to the infiltration of the coating into the prior austenite grain boundaries, and that this phenomenon is highly correlated with the chemical composition of the steel, particularly with the amount of boron. These investigations led to the establishment of the Carbon Equivalent for Zinc induced Cracking (CEZ) and its allowable thresholds in the Japan Industrial Standard (JIS) for high strength steel used for tower structures. It is also well-known that the residual stress due to the forming process of steel and welding is one of considerable factors for LMAC. In Japan, cold-formed square steel tubes are commonly-used for columns in building structures. A few researches undertaken for LMAC of cold-formed steel tubes indicated that as the tensile residual stress induced by cold-forming increases, the occurrence of LMAC significantly increases, and suggested that partial masking at the corners of tube for preventing adhesion of zinc is an effective way to prevent LMAC [11].

In contrast, the focus of this research is on LMAC that initiated from circular holes for venting and drainage. It is hypothesized that this type of LMAC occurs due to the equivalent position of the circular holes in the base metal rather than in the heat affected zone which has been primarily focused by previous studies. Also, as long as the circular vent holes are not placed excessively close to the weld, the residual stress due to the welding, would not be significant.

This study focuses on the effect of geometric parameters such as the flange-to-web thickness ratio, the web thickness, the diameter of the circular holes, and their position on LMAC to develop the understanding of the mechanisms through which LMAC that initiated from circular holes and seek to identify effective way for preventing them in practice. As the pilot study, Immersion tests were performed with a scale test specimens to investigate the thermal history, and strains due to the thermal expansion and contraction in hot-dip galvanizing process. A companion analytical model, which is capable of simulating the test results was developed. The verified numerical model was used to develop the helpful index for evaluating the effect of geometric parameters on LMAC, in term of the tensile strain at the point corresponding to LMAC occurrence. The paper briefly summarized test results and companion numerical results.

2. Immersion testing and heat transfer and thermal stress analysis

2.1 Test specimen

Immersion tests were performed on a scale model test specimens that reproduced a section of a welded web connection. The strain and temperature history properties of the test specimens were investigated while it was immersed and investigated the reproducibility of heat transfer and heat stress FEA based on the test results. The Configuration of scale model test specimen is shown in Fig. 2. The test specimen consists of a steel plate (SN490B) that resembles a web surrounded on four sides of its perimeter by steel plates (SN490B) that

resemble column flange and beam flanges. The web thickness (t_w) was 9 mm in all cases, and the flange thickness (t_f) was 19 mm and 32 mm in the two types of models that were used (T19 and T32, respectively). Drain holes of diameter 24 mm were drilled into the four corners of the web. The fillet welds on the T joints were created through carbon dioxide gas shielded arc welding using 1.4 mm diameter flux-cored wires. The target size for the web side of the fillet welds between the web and the flanges was set at 6 mm. Welding was performed with the welding input heat controlled to remain within the range of 14-15 kJ/cm. An example of the appearance of the corners after welding is shown in Fig. 2(c). Measurements of the distance between the weld toes on the web side of the welds and the hole edges showed that the distances were in the range of 3-5 mm (the dimension was 4 mm in the design). The results of coupon tests and chemical component analyses of the steel material used for the web are shown in Table 1. PL-12 and PL-14 refer to the material that was used for the web of the test specimen in the immersion testing in the parametric study, which will be described later. Since PL-9 contains a large amount of boron at 4.8 ppm, the carbon equivalent for zinc induced cracking (CEZ) of PL-9 exceeded the allowable threshold ($\leq 0.44\%$) specified in JIS G3138 because the CEZ is heavily affected by the boron content.

In order to produce large temperature gradients in this experiment, severe process conditions were selected. Therefore, the temperature of the zinc bath was set to a relatively high temperature of 445°C (actual measured temperature: 446°C), the immersion speed and the withdrawal speed were set to 0.5 m/min, which is the slowest speed within the range over which the process can be carried out, and the immersion time was set to 8 minutes. Immersion and withdrawal were performed with the test specimen maintained in a horizontal state in order to reduce the impact of factors that affect temperature changes. The locations at which the temperature and strain were measured are shown in Fig. 3. The temperature measurements were taken using type K thermocouples. The thermocouple tips were inserted into holes that were created in the plates up to the center of the plate thickness. Strain was measured at two locations, which consisted of a location in the vicinity of the drain hole along the 45-degree line that is orthogonal to the direction in which the crack is anticipated to grow (s1) and a location that was 35 mm away from the center of the web (s2). LMAC detection after hot-dip galvanizing was performed through visual testing and magnetic particle testing.

2.2 Numerical model

The FE model is shown in Fig. 4. The FE model was constructed using 3-dimensional solid elements. A 1/4 model was used, considering the temperature boundary conditions and symmetry of the shape of the specimens. The temperature boundary conditions in the heat transfer analysis were set to 446°C for the molten zinc temperature and 40°C for the steel temperature. The immersion speed was considered, as shown in Fig. 5. The heat transfer coefficient between the molten zinc and steel during immersion was selected by referring to the reference [12]. The temperature dependence of the specific heat and the heat transfer coefficient was considered, in accordance with the AIJ Recommendations for Fire Resistant Design of Steel Structures [13]. The temperature dependence of Young's modulus, the strength, and the strain hardening coefficient of the steel material used in the heat stress analysis was implemented according to Lie's method [14]. The coefficient of linear expansion and the Poisson ratio of steel were assumed to be independent of temperature and were set to 1.2×10^{-5} ($1/^\circ\text{C}$) and 0.3, respectively. A bilinear plastic material model with kinematic hardening was

employed to simulate strain and stress reversals in the immersion process. Material properties of the steel used in the analyses were based upon measured stress-strain relationships obtained from the coupon test results shown in Table 1. The FEA was conducted using a general-purpose finite element analysis software program, ABAQUS ver. 6.11-2.

2.3. Test and numerical results

2.3.1 Observation of cracks

An example of LMAC occurrence is shown in Fig. 6. LMAC occurred in T32, in which the flange thickness was 32 mm, at the two circular holes on the top of specimens, while not in T19. The observation results from a scanning-electron microscope (SEM) of the crack tip and a zinc mapping are shown in Fig. 7. The results show that the crack propagated along the crystal boundaries in the steel and that zinc infiltrated into the crack. These results indicate that the cracks that observed in this test were due to molten zinc embrittlement cracking, which is a type of LMAC that happens during hot-dip galvanizing process similar to the LMAC that occurred in the heat-affected zone that was observed in previous studies.

2.3.2 Temperature and strain history

The temperature history during immersion in molten zinc is shown in Fig. 8. The time (t) is measured with respect to time 0, which is defined as the moment at which immersion of the test specimen in the zinc bath began. In the figures, the interval until the entire test specimen is immersed in the bath is referred to as A, and the interval after the entire test specimen is immersed in the bath is referred to as B. First, we will focus on the temperature histories of the flanges and the web, which are immersed in the molten zinc bath at almost the same instant. The temperature rise of the flange (t_9) is more gradual compared to the temperature rise of the web (t_1 and t_2) regardless of the flange thickness. Next, we will focus on the temperature histories at the web center (t_5) and in the vicinity of the circular holes. The temperature rise in the vicinity of the circular holes (t_1 and t_2) is more gradual compared to the temperature rise at the web center. Since the corners are surrounded by the flanges, which are thicker than the web, the temperature of the molten zinc decreases, which causes a decrease in the heat transfer due to adhesion of solid zinc. This phenomenon is also thought to be caused by deprivation of heat due to re-melting of the zinc. The FEA reproduces the temperature history of the experiments in all locations for the most part, regardless of the flange thickness with quite good accuracy.

The strain histories in the vicinity of the circular holes (s_1) and at the center of the web (s_2) are shown in Fig. 9. The strain that occurs in the vicinity of the circular holes (s_1) is much larger than the strain at the web center (s_2), regardless of the flange thickness. Comparisons of the temperature histories shown in Fig. 8 shows that the temperature difference between the flanges and the web reaches a maximum approximately 50 seconds after immersion begins and that the compressive strain reaches a maximum at the same instant. As the temperature difference between the web and the flanges decreases afterwards, the strain progresses towards the tensile direction. A comparison between T19 and T32, focusing on the area in the vicinity of the circular holes, shows that the maximum compressive strain that occurs during immersion is larger for T32 than for T19. Furthermore, in T32, the strain suddenly increased in the compressive direction during the process in which the strain progressed towards the tensile direction accompanying the decrease in the temperature difference within

the steel. This change is thought to be due to the release of the tensile strain due to the occurrence of LMAC at this point in time during immersion.

The Numerical results capture the trends in the behavior of the strain propagation, at both the center of the web and in the vicinity of the circular holes. However, the FEA results for the maximum compressive strain that occurs in the vicinity of the circular holes were larger than in the tests. Also, the behavior of the strain propagation in the tensile direction accompanying the decrease in the temperature difference afterwards was more gradual in the numerical results than in the test results. This difference is thought to be due to the fact that the FEA was unable to accurately reproduce the progress of the plastic strain in the tensile direction after compressive yield under changing temperatures, or in other words, the behavior in the Bauschinger region. As the results, the FEA tended to underestimate the magnitude of the tensile strain difference $\Delta\varepsilon_t$ that occurs during immersion, which is defined as the difference between the maximum compressive strain and the strain during constant temperature measured in the tests. However, The increase in the strain due to increasing the flange thickness from 19 mm to 32 mm was 50% in the FEA and was 46% in the tests. Therefore, the FEA was able to successfully qualitatively capture the impact of the flange thickness on the behavior of the strain.

The equivalent plastic strain distribution obtained by the FEA at the locations where cracks occurred (at the circular holes at the top of the test specimen) is shown in Fig. 10. Strain concentration can be seen in the vicinity of the circular holes, corresponding to the occurrence of cracks as shown in Fig. 6. The stress-strain relationship in the 45-degree direction that was extracted from the element at the hole edge at which the strain reaches a maximum is shown in Fig. 11. A comparison of the tensile strain $\Delta\varepsilon_t$ derived from this stress-strain relationship between T19 and T32 shows that this value is approximately 50% larger in T32 than in T19, similar to the values at the locations where the strain gauges were attached. The comparison also shows that as the flange thickness increases, the strain concentration at the hole edges increases as well, which is thought to have induced the cracks.

3. Parametric study

3.1 Parameters

In order to investigate the correlation between the impact of the various geometric parameters on the strain properties at the circular hole edge and the occurrence of cracks, a parametric study through FEA and immersion testing were conducted. A summary of the details of the test specimen and results is shown in Table 2. The test results for the number of locations at which LMAC occurred are included in the table. The number of locations at which cracks occurred is counted in terms of the number of circular holes at which the cracks occurred. The parameters that were considered in this investigation include the flange-to-web thickness ratio t_f / t_w , the web thickness, the diameter of the circular holes, and the distance between the circular holes and the weld toe. The web thickness was set to the three values of 9 mm, 12 mm, and 14 mm; the flange thickness was varied in the range of 12 - 56 mm, the circular hole diameter was set to the two values of 24 mm and 40 mm, and the minimum distance L between the circular hole and the weld toe was set to the three values of 9 mm, 14 mm, and 40 mm. For $L = 40$ mm, only FEA was performed. The tests to investigate the effect of the flange thickness were performed in advance, with the web thickness set to 9 mm. These tests showed that the

occurrence of cracks increased significantly when the flange thickness was around 20 mm. Although the tests that were performed afterwards did not include cases with such large flange thicknesses, the FE models were added to the investigation in order to include test cases in which the effects of the various parameters were considered with t_f / t_w varied from 1.33-4.00, since the flange-to-web thickness ratio was one of the main parameters.

3.2 Effect of geometric parameters

The effect of the geometric parameters was analyzed based on the tensile strain $\Delta\varepsilon_t$ at the edge of the circular holes. The relationship between each factor and $\Delta\varepsilon_t$ is shown in Fig. 12.

(a) Effect of flange-to-web thickness ratio:

As t_f / t_w increases, $\Delta\varepsilon_t$ also increases significantly. Once t_f / t_w is sufficiently large, the rise in the value of $\Delta\varepsilon_t$ becomes more gradual. When the web thickness was 9 mm, LMAC occurred at four locations at the circular holes whenever t_f / t_w was larger than 2.78 in all cases.

(b) Effect of web thickness:

A comparison between cases with the same flange-to-web thickness ratio t_f / t_w shows that as the web thickness t_w increases, $\Delta\varepsilon_t$ becomes smaller. Furthermore, for all values of t_f / t_w , the value of $\Delta\varepsilon_t$ becomes smaller in proportion to the web thickness. When the web thickness was 9 mm, LMAC occurred whenever t_f / t_w was larger than 2.78 in all cases. However, when the web thickness was 12 mm or 14 mm, LMAC did not occur even when the t_f / t_w was larger than 2.78.

(c) Effect of distance L between the circular holes and the weld toe

Depending on t_f / t_w , the effect of the drain hole location L with respect to $\Delta\varepsilon_t$ is different. Even when L was varied within the range 4 - 14 mm, almost no decrease in $\Delta\varepsilon_t$ was observed. When L = 9 mm, LMAC occurred at one location, when t_f / t_w was 2.44, and at two locations when t_f / t_w was 2.78. When L = 14 mm, LMAC occurred at one location when t_f / t_w was 2.11. Conversely, when L was 40 mm, $\Delta\varepsilon_t$ was greatly reduced for all t_f / t_w . However, when L was 40 mm, the holes did not function well as drain holes any longer. Therefore, increasing L, while assuring that the hole still functions as a drain hole, is not anticipated to have a large effect on reducing the strain. However, in cases in which the hole is close to the weld toe, increasing L is thought to be somewhat effective, since it reduces the effect of the residual stress accompanying welding, which is significant in this case.

(d) The effect of hole diameter

Increasing the diameter of the drain holes decreases $\Delta\varepsilon_t$ for all t_f / t_w . Furthermore, increasing the hole diameter by a factor of two results in a reduction of approximately 20% of the strain, regardless of the flange-to-web thickness ratio. Although experiments were only performed for flange-to-web thickness ratios below 2.44, LMAC did not occur in any of the cases.

3.3 Correlation between occurrence of LMAC and tensile strain

In order to consider the correlation between the occurrence of LMAC and the tensile strain, the relationship between $\Delta\varepsilon_t$ and the flange-to-thickness ratio t_f / t_w is shown in Fig. 12. As $\Delta\varepsilon_t$ increases, the occurrence of

cracks also increases significantly, regardless of the other parameters. In other words, the value of $\Delta\epsilon$ that occurs at the hole edges is an effective indicator for quantitatively evaluating the effect of the other parameters on the occurrence of cracks.

4. Conclusion

In this paper, in order to evaluate the effect of various geometric parameters on the occurrence of LMAC initiated from circular holes, immersion testing using a simple scale model test specimen and heat transfer and heat stress analyses were conducted. The following conclusions were drawn.

- Immersion testing with the flange thickness as the test parameter showed that as the flange thickness increases, the strain at the circular hole edges also increases. For a web thickness of 9 mm, LMAC occurred at two locations at the top of the test specimen when 32 mm flanges were attached. Furthermore, microscope images (SEM) of the cracks and the behavior of the strain in the vicinity of the circular holes showed that the LMAC occurred while the test specimen was immersed in the molten zinc.
- Increases in the tensile strain, which is defined as the difference between the maximum compressive strain at the strain concentration point at the edge of the circular holes during immersion in molten zinc and the strain at steady state, cause significant increases in LMAC.
- As the flange-to-web thickness ratio increases, the tensile stress that occurs at the hole edges increases as well, and the occurrence of cracking also increases significantly. However, even for cases in which the flange-to-web thickness ratio is the same, it is possible to reduce the tensile strain by increasing the web thickness. Therefore, increasing the web thickness, as well as reducing the flange-to-web thickness ratio, is effective in preventing cracking.
- Increasing the diameter of the circular holes by a factor of 2 results in an approximately 20% reduction in the tensile strain. Increasing the distance between the circular hole edges and the weld toes within the range over which the holes still function as drain holes ($L = 4\text{-}14$ mm) has small effects on reducing the tensile strain.

Acknowledgments

The authors would like to thank Takemi Furudate at Just Corporation, Fumio Kashimoto and Yuji Ohnishi at Nippon steel & Sumikin Technology for technical assistance with the experimental works. We also thank to Masayuki Takakura, former graduate student at Kobe University for conducting tests and numerical simulations.

References

- [1] Koyama, A., Iwasaki, M., Nagata, S., Jikihara, A. (2004), QUARTERLY JOURNAL OF THE JAPAN WELDING SOCIETY, 22(3), 435-442 (in Japanese)
- [2] Mori, M., Nakagomi, T., Suzuki, I., Kim, C. (2009) QUARTERLY JOURNAL OF THE JAPAN WELDING SOCIETY, 27(1), 41-47 (in Japanese)

- [3] Nishio, Y., Iwasaki, S., Deto, H., Onishi, H. (2013) Journal of Japan Society of Civil Engineers, Ser. A2 (Applied Mechanics (AM)), 69(2), I_615-I_624 (in Japanese)
- [4] Yamashita, T., Nishizawa, J., Tanaka, T., Asada, H., Takakura, M., Furudate, T. (2015) Papers of Annual Meeting, Architectural Institute of Japan, 1147-1154, (in Japanese)
- [5] Architectural Institute of Japan (2018) Japanese Architectural Standard Specification, (JASS 6), 2018.
- [6] Architectural Institute of Japan(2018) Technical Recommendation for Steel Construction for Buildings (Part 1 Guide to Steel-rib Fabrications), 2018. 4. (in Japanese)
- [7] Takeda, T., Kanaya, K., Yamato, K., Eiro, K., Chano Z., Kanazawa, S., Hiroki, T., Iezawa, T. (1984), Tetsu-to-Hagane, 70(6), 596-602, 1984. (in Japanese)
- [8] Fujimoto, M., Kanazawa, S. (1985), JSSC, 21(221), 11-45 (in Japanese)
- [9] Iezawa, T., Inoue, N., Hirano, K., Okazawa T., Ozeki, T. (1993), Transactions of the Iron and Steel Institute of Japan, 79(9), 1108-1114 (in Japanese)
- [10] Takeda T.: Evaluation Method of Zinc Induced Cracking, Quarterly Journal of The Japan Welding Society, Vol.71, Issue 4, pp.32-38, 2002. (in Japanese)
- [11] Mori, M., Nakagomi, T., Suzuki, I., Kim, C.: Proposal of Prevention Method on Cracks at Hot-Dipped Galvanization of Rectangular Hollow Section Steel Pipes by Cold Forming, Journal of Structural and Construction Engineering (Transactions of AIJ), Volume 74, No. 638, pp.739-746, 2009. (in Japanese)
- [12] Nagano, M., Mikami, Y., Miyazawa T., Kanaya, K., Yoshida, K., Shinniwa Y.: Prediction and Prevention of Liquid Zinc Induced Cracking in Tubular Structures of 590MPa Steel Based on Elastic-Plastic-Thermal Stress Analysis, Journal of High Pressure Institute of Japan, Vol. 41, Issue 1 pp.17-27, 2003. (in Japanese)
- [13] Architectural Institute of Japan: Recommendations for Fire Resistant Design of Steel Structures, The Second Edition, 2017. 6 (in Japanese)
- [14] Lie T.T.: Structural Fire Protection, ASCE, 1992.

AUTHORS BIOGRAPHY

Ms. Yuki Fujiwara received the B. E degrees in engineering from Kobe University, Kobe Japan, in 2016.

She is now a graduate student of Kobe University.

Dr. Hayato Asada received doctor degree in engineering from Tokyo Institute of Technology, Tokyo Japan, in 2011. He is now assistant professor at Kobe University. His research primary focuses on seismic performance of steel building structures, performance-based seismic design and rationalization of steel fabrication in high seismicity region.

Dr. Tsuyoshi Tanaka received doctor degree in engineering from Kobe University Kobe Japan, in 1994. He is now professor at Kobe University. He has served as chair of the technical committee on steel fabrication in Architectural Institute of Japan from 2013. He has performed a wide range of research on steel and composite buildings.

FIGURES

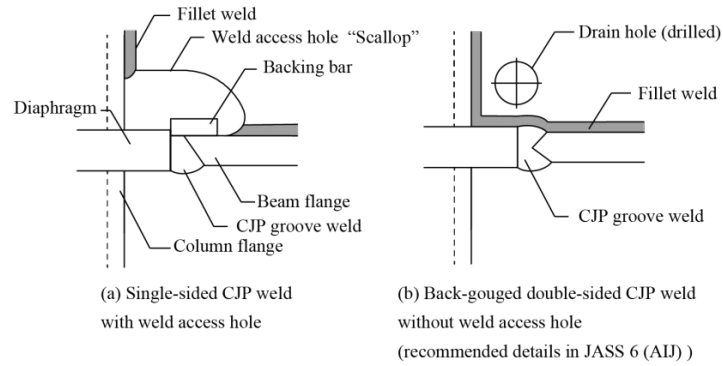


Fig.1 Connection details of beam-to-column connection with consideration of venting and drainage of air and molten zinc commonly used in Japan

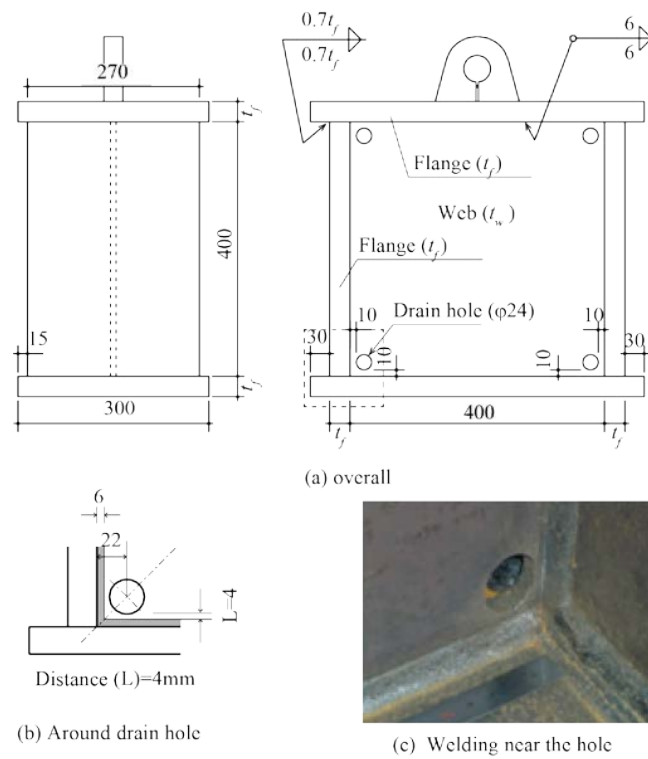


Fig. 2 Test specimen

Table 1 Material properties of steel

Thickness	Steel Grade	Coupon test results			Chemical composition wt (%)								
		Yield strength N/mm ²	Tensile strength N/mm ²	Elongation %	C	Si	Mn	Ni	Cr	Mo	V	B	CEZ
PL-9	SN490B	375	524	29	0.17	0.34	1.39	0.01	0.00	0.01	0.005	0.00048	0.58
PL-12	SN490B	372	533	26	0.17	0.37	1.41	0.01	0.02	0.01	0.002	0.00010	0.43
PL-14	SN490B	402	549	26	0.17	0.32	1.33	0.02	0.03	0.01	0.00	0.00010	0.42

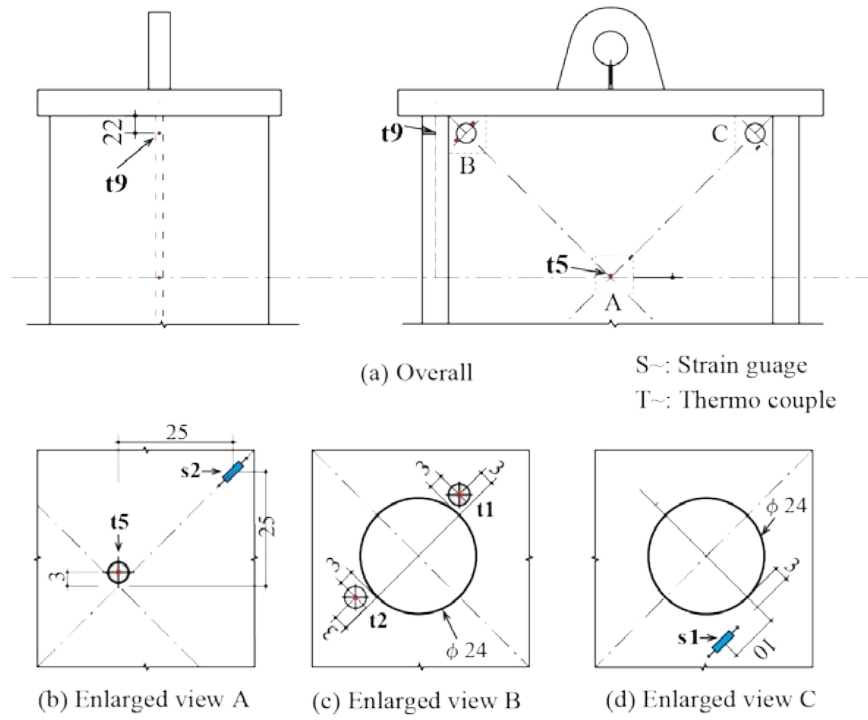


Fig. 3 The position of strain gauges and thermocouples

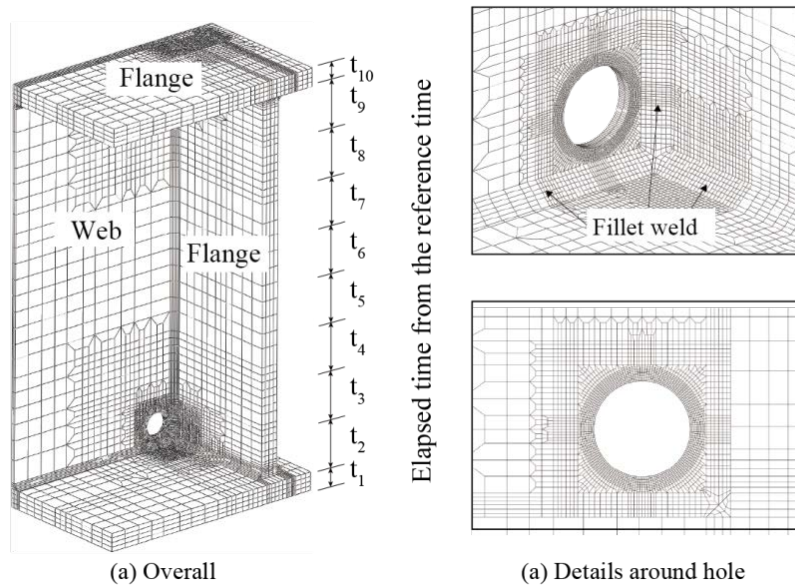


Fig.4 FE model

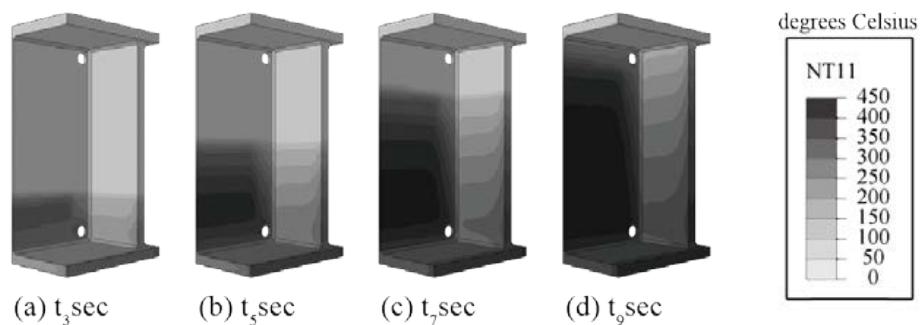


Fig.5 Temperature distributions in hot-dip galvanizing process reproduced by FEA

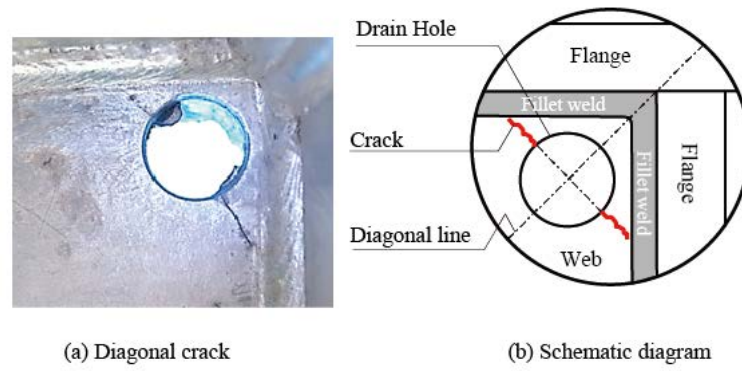


Fig. 6 Diagonal cracking initiated from the toe of drain hole

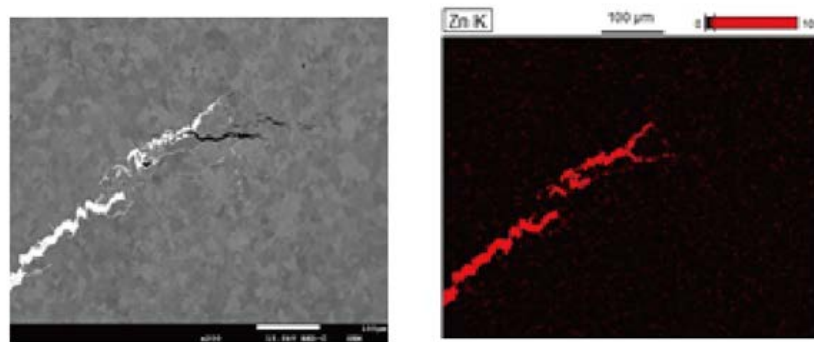


Fig. 7 Zinc diffused into cracking (Microphotograph and Zinc mapping)

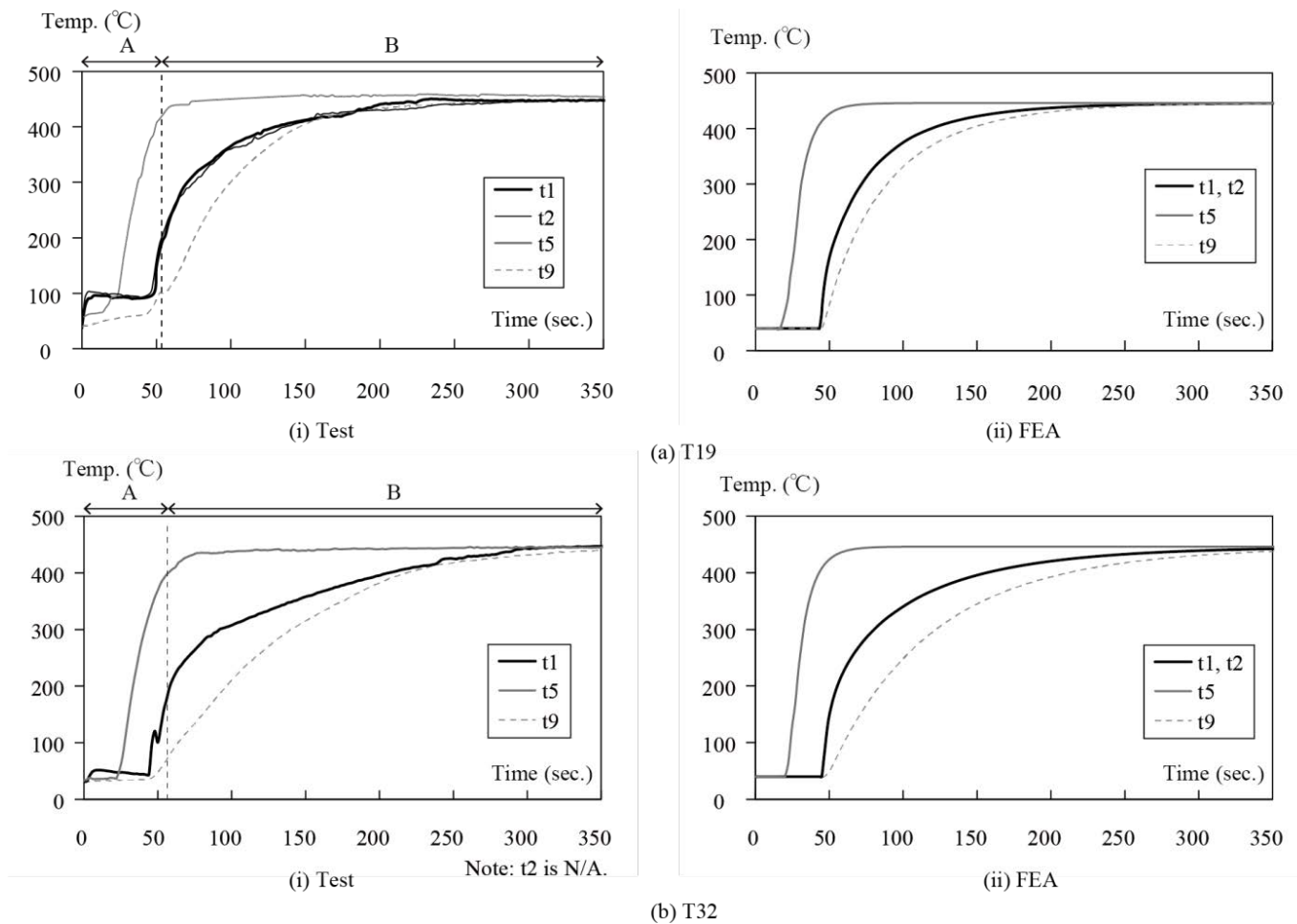


Fig. 8 Temperature histories obtained from Tests and FEA

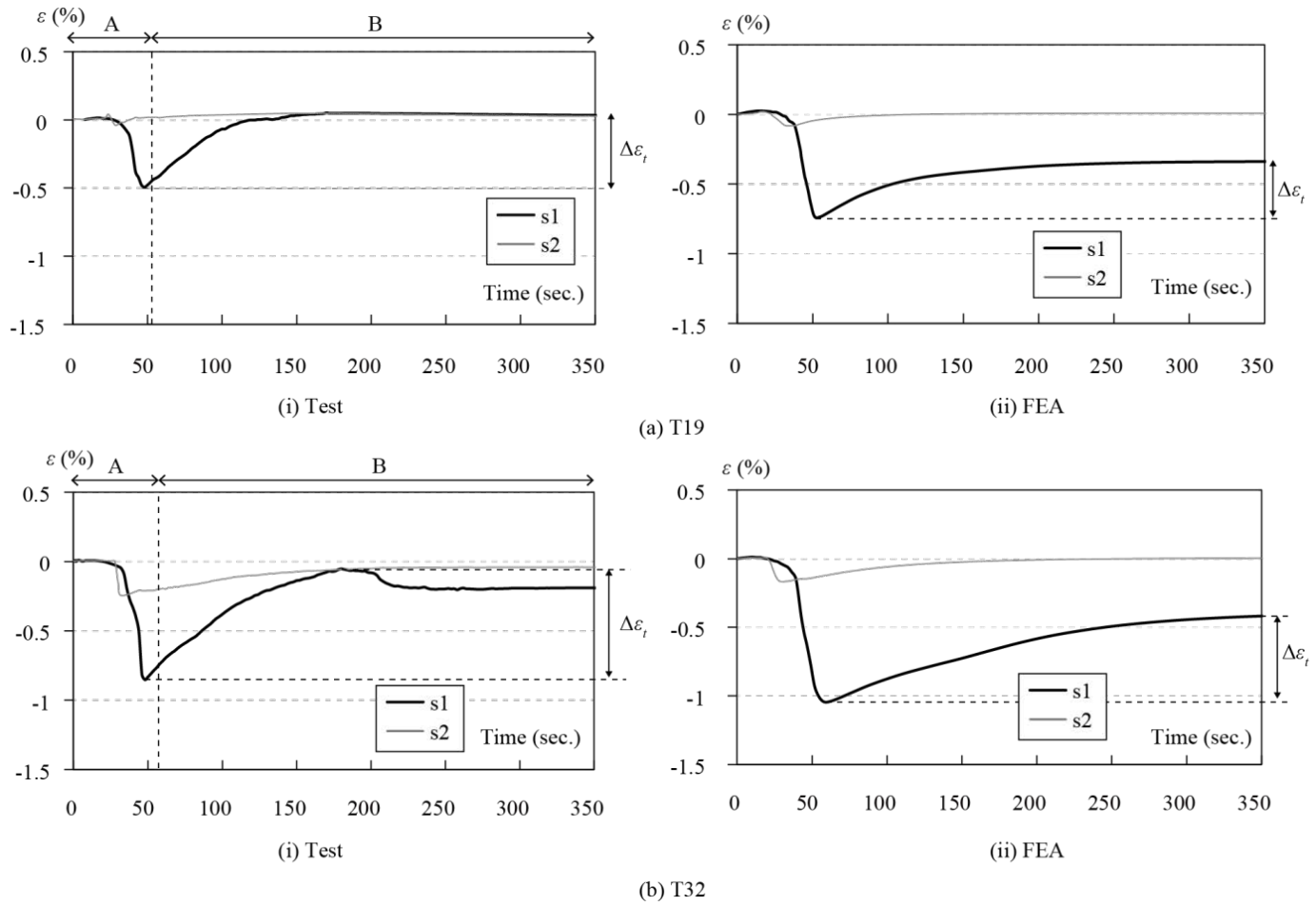


Fig. 9 Strain histories obtained from Tests and FEA

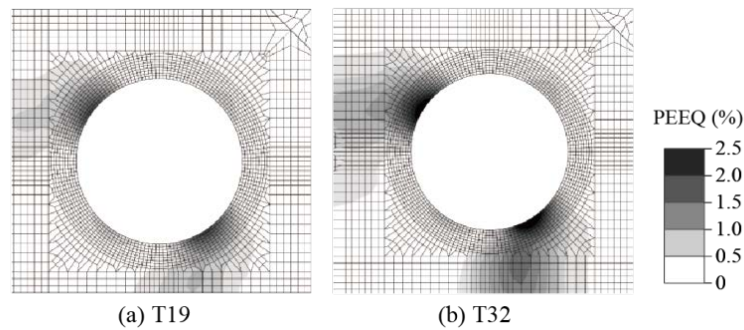


Fig. 10 Plastic strain distributions around drain hole on upper side

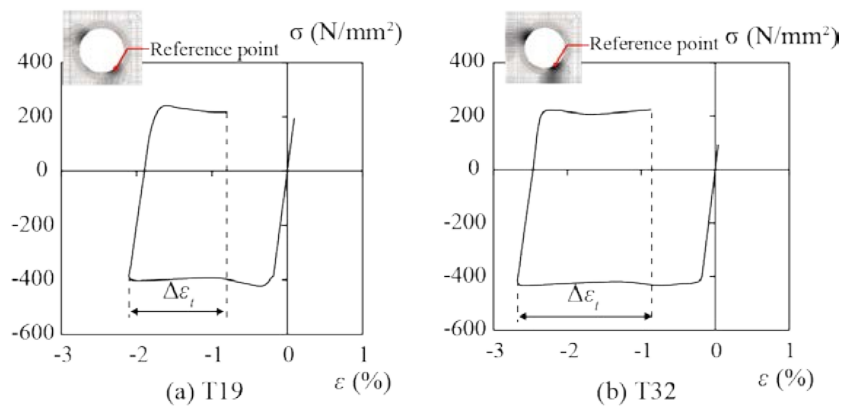
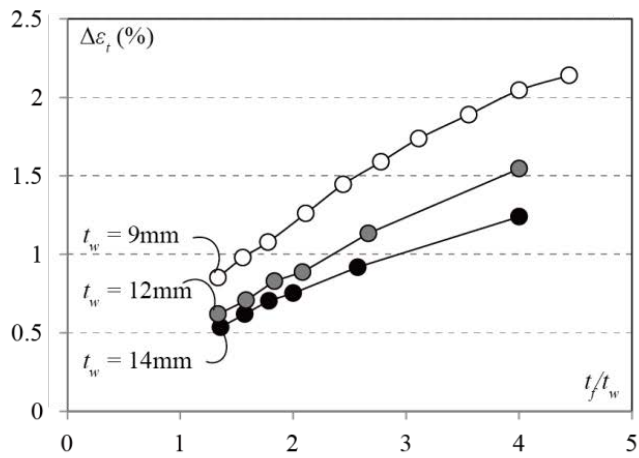


Fig. 11 45-degree stress versus strain relationships at the point of strain concentration

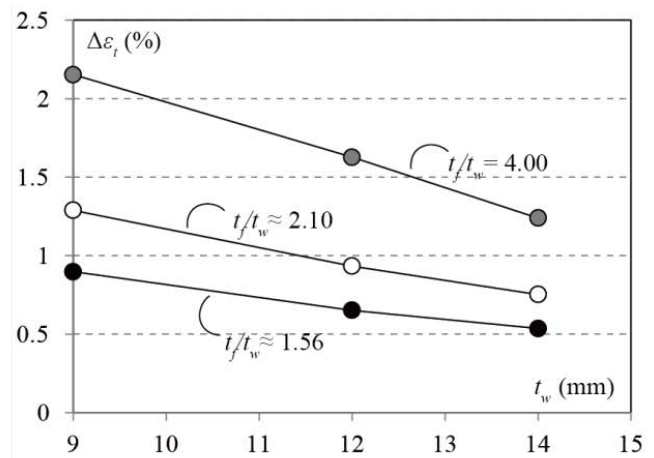
Table 2 Parameter matrix and summary of test results

Parameter	ID	t_w [mm]	t_f [mm]	t_f/t_w	Drain hole		Num. of D H Cracked
					L* [mm]	D [mm]	
Thickness of Flange	1-1	9	12	1.33	4	24	0
	1-2		14	1.56			0
	1-3		16	1.78			1
	1-4		19	2.11			1
	1-5		22	2.44			0
	1-6		25	2.78			4
	1-7		28	3.11			4
	1-8		32	3.56			4
	1-9		36	4.00			4
	1-10		40	4.44			4
Thickness of Web	2-1	12	16	1.33	4	24	0
	2-2		19	1.58			0
	2-3		22	1.83			0
	2-4		25	2.08			0
	2-5		32	2.67			0
	2-6		48	4.00			-
	3-1	14	19	1.36			0
	3-2		22	1.57			0
	3-3		25	1.79			0
	3-4		28	2.00			0
	3-5		36	2.57			0
	3-6		56	4.00			-
Position of Drain Hole	4-1	9	16	1.78	9	24	0
	4-2		19	2.11			0
	4-3		22	2.44			1
	4-4		25	2.78			2
	4-5		32	3.56			-
	5-1		19	2.11	14		1
	5-2		22	2.44			0
	5-3		25	2.78			0
	5-4		28	3.11			0
	5-5		32	3.56			0
	40-1		16	1.78	40		-
	40-2		22	2.44			-
	40-3		32	3.56			-
	Diameter of Drain Hole		10-1	9	14		1.56
10-2		16	1.78		0		
10-3		19	2.11		0		
10-4		22	2.44		0		
10-5		32	3.56		-		
10-6		40	4.00		-		

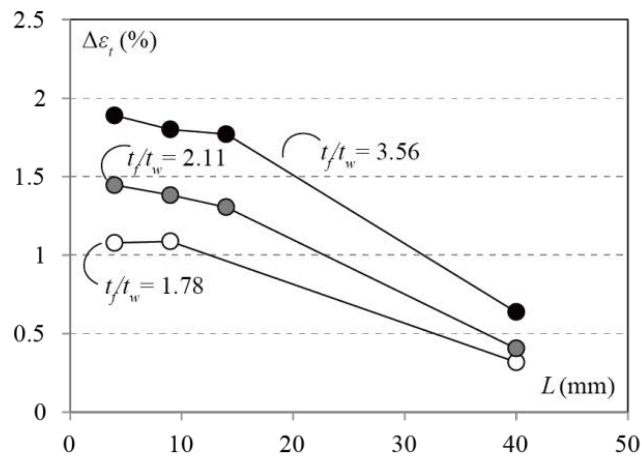
*: The shortest distance between D.H. and tip of welds



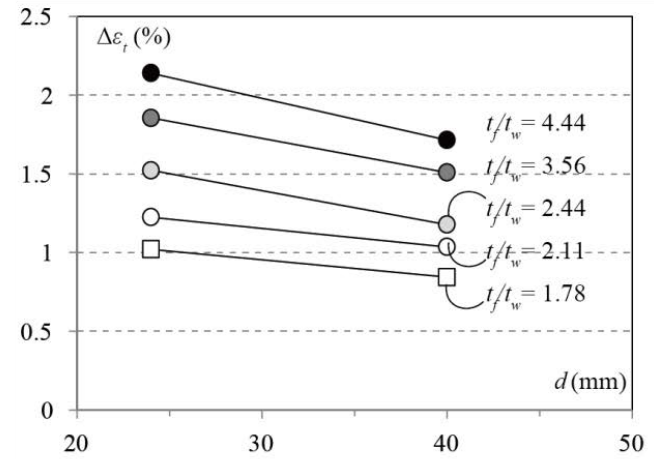
(a) Effect of flange-to-web thickness ratio



(b) Effect of thickness of web



(c) Effect of distance between DH and weld toe



(b) Effect of diameter of drain hole

Fig. 12 Effect of geometric parameters on the magnitude of tensile strain

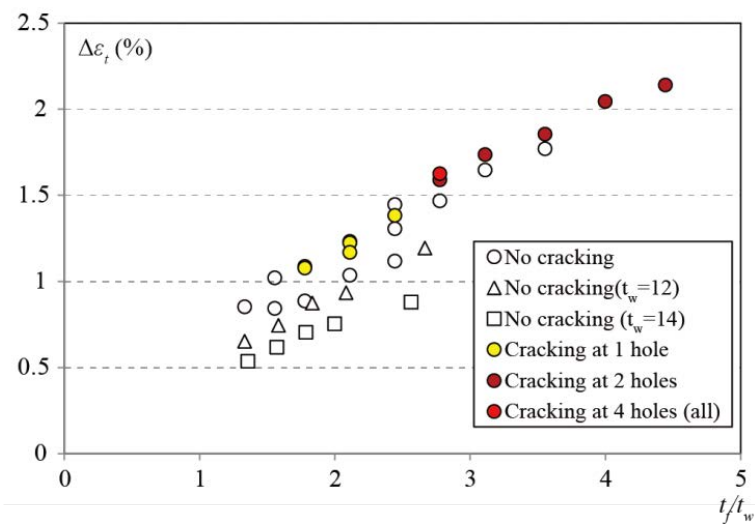


Fig. 13 Correlation between tensile strain and LMAC occurrences

Effect of Geometric Configuration on High-Mast Illumination Pole Demands During Galvanizing Process

Reza Nasouri¹, Kien Nguyen², Arturo Montoya¹, Adolfo Matamoros¹, Caroline Bennett², Jian Li², Thomas Kinstler³

¹ Department of Civil and Environmental Engineering, University of Texas at San Antonio, San Antonio, Texas

² Department of Civil, Environmental and Architectural Engineering, University of Kansas, Lawrence, Kansas.

³ GalvaScience LLC, Springville, Alabama.

Abstract:

Cracks that develop during galvanizing at the pole-to-base plate connection of High Mast Illumination Poles (HMIPs) are a major source of concern to fabricators and highway officials in the United States. Due to life-safety concerns, substantial resources are spent performing detailed inspections of welded connections, and financial losses are incurred every time a damaged connection is found. One of the most important causes of connection damage are thermally-induced deformations during the galvanizing process. A study was performed to evaluate the effects of HMIP geometric configuration on the critical stress and strain demands during galvanizing. HMIP configurations evaluated in the study had pole shapes, dimensions, and pole-to-base plate connection detailing used in the state of Texas. The main parameters of the study were base plate thickness, pole shaft wall thickness, and number of pole sides. Finite element models of pole-base plate assemblies were subjected to a temperature field representative of the galvanizing process and analyzed using coupled thermo-mechanical analysis. Deformations were computed while varying the position of the pole-base plate assemblies through a fixed-location temperature field, following a path that simulated four stages of the hot-dip galvanizing procedure: dipping, dwelling, extraction, and cooling. Results from the analyses showed that HMIP configuration had a significant effect on strain and stress demands during the simulated galvanizing process. Stress and strain demands were highest at locations near the pole-to-base plate connection. In models with the same pole thickness, smaller ratios of pole-to-base plate thickness corresponded to lower stress and strain demands at critical locations. In models with the same base plate thickness, stress and strain demands were inversely proportional to pole thickness, with stresses for 7.9 mm (5/16 in.) thick poles being higher than stresses for 12.7 mm (1/2 in.) thick poles. Stress and strain demands were found to be lower for poles having a circular shape than for multi-sided poles.

Introduction

Hot-dip galvanizing (HDG) is a protective coating process widely used to prevent corrosion in steel structures [1-6]. On occasion, incidents of cracking have occurred in steel structures during the galvanizing process. Such cracks require costly repairs and, if undetected, can trigger the premature failure of HMIPs placed in-service. In recent years many instances of fatigue failure of high-mast lighting poles have been reported, with documented cases of at least 10 high-mast structures that have collapsed and 60 that have been taken out of service. In most instances in-service fatigue cracks originated in the HMIP pole wall, at the weld toe of pole-to base plate connection [7-11].

While the root causes of these cracks remain poorly understood, some studies have related the formation of such cracks to thermally-induced deformations during the hot-dip galvanizing process [2, 8, 12]. Measuring deformations of HMIPs during galvanizing is not a trivial task because sensors must resist very high temperatures for the duration of the zinc bath, and can only provide localized information. Finite element modeling is an effective approach for analyzing and visualizing the behavior of structures under thermomechanical loading conditions. For example, Kleineck [13] developed a 3D thermomechanical FE model to simulate the effects of temperature during the galvanizing process of HMIPs. The FE model developed by Kleineck was calibrated using temperature and strain readings from thermocouples and strain gages attached to HMIPs during the galvanizing process. One of the main limitations of the model by

Kleineck is that it neglected many important parameters of the configuration of the HMIPs such as welded connections, the presence of a collar (backing ring), and the HMIP shape, which can critically affect the propensity to crack initiation.

Objective and Scope

The objective of this study was to investigate the effect of geometric parameters on thermally-induced strain and stress demands during the hot-dip galvanizing process. Parameters evaluated in the study were: base plate-to-pole thickness ratio, base plate thickness, pole thickness, and pole shaft shape. The steel material model used in the analyses included mechanical and temperature-related nonlinear behavior. Three-dimensional finite element models of HMIP subassemblies were subjected to temperature fields representative of the galvanizing process and analyzed using coupled temperature-displacement analysis with the commercial finite element software ABAQUS [14]. Analysis steps were broken into four different stages of galvanizing: dipping, dwelling, extraction, and cooling. Results from numerical simulations were used to evaluate the effect of shape parameters on the propensity to develop cracks during galvanizing. Calculated stresses/strains were solely thermally-induced, and were not superimposed on any residual stresses due to cold forming of pole facets (as appropriate), welding stresses, or loading induced due to lifting, buoyancy, or draining. Material properties were uniform throughout the models and did not consider variations in hardness or constitutive behavior.

Finite Element Model

Model Geometry

It is standard practice in the United States to manufacture the pole shaft component of HMIPs with either a multisided or round cross-section [15, 16]. Welded connection details are specified by each state Department of Transportation, which results in a few different types of connections used throughout the country. This study focuses on the standard connection detail specified by the Texas Department of Transportation, designated throughout as the "Texas Detail", shown in Figure 1. This connection detail includes a backing ring (or collar) placed externally to the pole shaft. A full penetration weld is used to attach the pole shaft and collar to the base plate, and a fillet weld is used to attach the top of the collar to the pole shaft (Fig. 1a).

Each FE model (Figure 1) includes seven different parts: (a) a pole shaft, (b) a base plate with 12 anchor bolt holes and a circular access manhole in the middle, (c) an external collar, (d) a full penetration weld, (e) a fillet weld, (f) an internal seal weld, and (g) a top plate.

FE models were classified in four groups. Group 1 had a 76 mm (3 in.) thick hollow base plate with a 1200 mm (47 in.) outer diameter and 560 mm (22 in.) inner diameter. This configuration had a twelve-sided pole with a length of 4.3 m (14 ft.) and a thickness of 8 mm (5/16 in.). The outer diameter of the pole was 830 mm (32-5/8 in.), and the pole was attached to the base plate using a full penetration weld. At the opposite end, a thinner 25mm (1 in.) plate with the same cross-section was used. The backing ring was 6 mm (1/4 in.) thick and 305 mm (12 in.) long, and like the pole shaft, had a twelve-sided shape. This group is referred to as the control or base group throughout this paper (Figure 1b). Group 2 had the same configuration as Group 1 with the exception of the pole thickness, which was 13 mm (1/2 in.). Group 3, had the same configuration as Group 1, with the exception of a 25 mm (1 in.) thick base plate, and was intended to evaluate the effect of base plate thickness on stress and strain demands. Group 4 had a pole with round shape. Figure 1b presents the different geometric configurations evaluated. The collar and weld parts, only shown for Group 1, had similar dimensions for all four groups.

The shape of the backing ring (collar) was adjusted to conform with the pole configuration of each group. The shape characteristics of each group are presented in Table 1. Groups 1 and 4 had the highest base plate-to-pole thickness ratio (9.5). Group 2 had the lowest base plate-to-pole thickness ratio (2.9), while Group 3 had a ratio of 5.9.

Material Properties

In the type of coupled temperature-displacement analyses used to simulate the hot-dip galvanizing procedure in this study, temperature and displacement fields are solved concurrently for each iteration. Temperature-dependent thermal (Figure 2a) and mechanical properties (Figure 2b), adopted from Peric et al. [17], were assumed to be the same for the weld and base metal (steel grade EN 10025-2: S355JR, US grade 50). The authors have successfully used the similar thermo-mechanical properties for studying the behavior of other steel components under thermally induced loads due to welding and galvanizing [18-20]. The yield strain and yield stress of steel at room temperature were $1700 \mu\epsilon$ and 345 MPa (50 ksi), respectively. Because the material model accounts for variations in material properties with temperature, these magnitudes become lower as temperature becomes higher.

Mesh

A 3-D mesh with 8-node reduced integration coupled temperature-displacement continuum elements, denoted as C3D8RT in ABAQUS, was used for all parts. Brick element size in the connection region was approximately $5 \times 5 \times 5$ mm ($0.2 \times 0.2 \times 0.2$ in.). For the mesh resolution used in the study each thermo-mechanical analysis was completed in approximately 10 days in the UTSA high performance computer cluster SHAMU.

Thermal Cycle

Nonlinear analyses were performed for the four groups of HMIPs evaluated. Each model was subject to a 900-second galvanizing sequence that included dipping (180 sec), dwelling (300 sec), extraction (360 sec), and cooling (60 sec).

Results and Discussion

Calibration of Heat Convection Coefficient

The heat convection coefficient (h_c) of steel in the molten zinc bath was an unknown parameter and significantly different values are reported in the literature. The heat convection coefficient adopted in this study was obtained by calibrating the calculated temperature field using experimental measurements reported by Kleineck [13], who recorded temperature variations in HMIP poles throughout the galvanizing process using thermocouple gages. An h_c value of $1500 \text{ W}/(\text{m}^2 \text{ K})$ was found to provide the best agreement between experimental data and simulation results in several calibration runs. An ABAQUS user subroutine designated "*Film*" was developed to mimic the galvanizing procedure. This subroutine defines the ambient temperature as a function of position. Figure 3 shows the surface temperature field distribution during the dipping stage of galvanizing (at 74 seconds from the start of the simulation) using the adopted heat convection coefficient.

Parameters related to the galvanizing process used in this study were chosen to be representative of industry practice and were kept constant in all simulations. The ambient temperature was set to $18 \text{ }^\circ\text{C}$ ($64 \text{ }^\circ\text{F}$) and the zinc bath temperature to $445 \text{ }^\circ\text{C}$ ($830 \text{ }^\circ\text{F}$). HMIPs were submerged in the molten zinc bath at an angle of 8 degrees with respect to horizontal and at a vertical speed of 22 mm/s (0.9 in./s). HMIPs were extracted from the molten zinc bath maintaining the angle of 8 degrees at a vertical speed of 11 mm/s (0.45 in./s)

Maximum Principal and von Mises Stress Fields

Figure 4 shows stress contours for the maximum principal and von Mises stress fields of the four groups, at a discrete time of 74 seconds after analysis initiation. At this time, within the dipping phase, the critical pole location coincided with the elevation of the zinc bath, which was found to be the condition that imposed the highest strain and stress demands in the connection. Von Mises stress (also known as maximum distortion energy criterion) gives an indication of when a ductile material (e.g. steel) begins to yield and provides a valuable metric to determine the potential for cracking. In structural elements stress demands are highest at locations where there are discontinuities in geometry (i.e. sharp corners), and at

the boundaries between components. In the models analyzed such locations include the interface between the base plate and pole shaft and bends along the length of multi-sided poles. Furthermore, these locations are more vulnerable to damage due to variations in hardness, residual stresses, and other discontinuities in material properties. For the purpose of comparing the potential for cracking of different configurations, stress and strain were extracted at 13 mm (1/2 in.) from the interface between the pole and the base. This location, identified by the circle in Figure 4, was found to correspond to the maximum demand during the thermal cycle.

The stress contours in Figure 4 show improved behavior for Groups 2 and 4, which indicates that reducing the base plate-to-pole thickness ratio and using poles with round shape are effective approaches to reduce stress demand. Although corners of multi-sided poles are locations where stress demands are higher, the peak demand for the round pole show that the location corresponding to the surface of the galvanizing bath will experience large stress demands regardless of shape. Between the two computed metrics, maximum principal stress resulted in higher and more localized demands than von Mises stress.

Stress histories at the critical location for the entire galvanizing process are shown in Figure 5, in the form of comparisons between the stress corresponding to each Group and the stress calculated with the control Group (1). A common trend was observed for all groups. There was a significant spike in stress when the pole was partially submerged during the dipping cycle (0 to 180 s), at the time when the surface of the zinc bath and the critical location in the pole had the same elevation. As the elevation of the surface of the zinc bath increased over the critical pole location, the magnitude of the stress decreased, and remained nearly constant during the dwell time (180 to 480 s). During extraction (480 to 840s), there was another significant increase in stress when the surface of the zinc bath coincided in elevation with the critical location in the pole. Stresses decreased during cooling, but this stage of the galvanizing cycle was omitted from Figure 5 because demands were found to be lower than in previous stages.

Figure 5(a) shows that, at the critical location during dipping, the model with a thicker base plate exceed the yield stress, while the model with a 25 mm-thick (1 in.) base plate maintained elastic behavior with a maximum demand of 320 MPa (46 ksi). Moreover, the Group 1 model had compressive stresses at the end of the dipping stage and the initial part of the dwelling stage, while the Group 2 model returned to a stress of zero.

The Group 2 model had negligible stresses at the critical location throughout most of the dwell time. Figure 5(b) shows a comparison between Group 1 and Group 3 models. The results show that during the dipping stage the stress demand at the critical location for Group 3 had a slightly lower peak than Group 1, and that the Group 3 model had a small tensile stress demand during most of the dwell time. Figure 5(c) shows that, among all the configurations evaluated, the round pole (Group 4) had the lowest peak demand during dipping and the highest tensile stress demand during extraction. Principal stresses shown in Figure 5 indicate that Groups 1 and 2 exceeded the yield point of steel at room temperature (345 MPa), while in configurations corresponding to Groups 3 and 4 the steel material remained in the linear elastic range for the entire galvanizing process.

A comparison between von Mises stress demands at the critical location of the different HMIP configurations are shown in Figure 6. The von Mises stress demands had similar trends to those observed for the maximum principal stress, with the main difference that two peaks in demand were observed during the dipping stage instead of one. The observed behavior during the dwelling and extraction stages were comparable to those observed in Figure 5.

Figure 7 shows the maximum principal and von Mises stress demands during the entire duration of the thermal cycle for each of the four groups. Among the four, the control model experienced the largest stress demands at the critical location and the round pole had the lowest. Although the relative magnitude of the stress demands was the same for Maximum Principal and Von Mises stresses (Group 1, Group 3, Group

2 and Group 4 in descending order), the difference between maximum magnitudes of the von Mises stress was smaller than the maximum principal stress.

Maximum Principal Strain

Comparisons between computed stresses have inherent limitations because the magnitude of the stress is limited by the yield surface of the material. Comparisons in terms of strain demands can offer a better measure of incursions into the nonlinear range of response, and some researchers have suggested that the potential of crack initiation during galvanizing may be related to inelastic deformation demands. Figure 8 shows the maximum principal strain demand at the critical location for each of the four HMIP groups. Values shown in Figure 8 represent the maximum demand over the length of the entire galvanizing process. The rank order of maximum strain demands in Figure 8 was the same as the stress demands shown in Figure 7, which was Group 1, Group 3, Group 2 and Group 4 in descending order. The ratio of Group 1 to Group 4 was higher for maximum principal strain (1.4) than it was for maximum principal stress (approximately 1.25), which confirms that strain measures show a larger difference for propensity to crack initiation than stress measures. The control model experienced the largest strain demands at the critical location, with a maximum strain of approximately 1680 $\mu\epsilon$, while the HMIP with the thinner base plate (25 mm) had a maximum principal strain demand of 1400 $\mu\epsilon$. Figure 8 shows that pole shape (12 sided vs round) had the largest effect on strain demand as indicated by a Group 1-to-Group 4 ratio of 1.4. Maximum strain demand increased proportionally to the ratio of plate-to-pole thickness. In 12-sided poles, changing the ratio of plate-to-pole thickness from 9.5 to 2.9 led to a decrease of approximately 17% (Group 1 to Group 2 ratio of 1.17), while changing the ratio from 9.5 to 5.9 led to a decrease of approximately 7% (Group 1 to Group 3 ratio of approximately 1.07). Changing the ratio of plate-to-pole thickness can be achieved by decreasing plate thickness or increasing pole thickness, both of which were found to be equally effective, although in practice there are limitations on how much pole thickness may be increased.

Equivalent Plastic Strain

Equivalent plastic strain (PEEQ) gives a cumulative measure of plastic strain in the HMIP throughout the entire simulation, including dipping, dwelling, extraction, and cooling. Unlike total strain, which increases and decreases throughout the simulation and includes thermal strains, plastic strain is a measure of inelastic mechanically-induced strain which may be the most closely related to material damage. The cumulative plastic strain at the end of the analyses is shown in Figure 9 for Groups 1 (control), 2 (change in plate thickness, and 4 (round pole). Using cumulative plastic strain as a measure of potential for crack initiation, the model with the highest propensity for cracking was the 12-sided pole with the highest base plate-to-pole thickness ratio (9.5). Propensity for damage was significantly lower for the round pole with a similarly high ratio of plate-to-pole thickness ratio (9.5). The lowest potential for cracking corresponded to the model with the lowest plate-to-pole thickness ratio of 2.9. According to this metric, the ratio of plate-to-pole thickness had a more significant effect on the propensity to develop cracks during galvanizing than pole shape, although changes in both parameters resulted in a large reduction in cumulative plastic strain. Furthermore, it is noted that the 12-sided pole with the thinner base plate had a base plate-to-pole thickness ratio of 2.9 while the round pole had a base plate-to-thickness ratio of 9.5, so a direct comparison between the two is not entirely objective. Based on the results presented in this paper, it is reasonable to expect that reduction in the base plate-to thickness ratio should have an equally beneficial effect on round poles as it does on 12-sided poles.

Conclusions

This study evaluated the effects of HMIP geometric configuration on the critical stress and strain demands during galvanizing. The results showed that maximum strain and stress demands occurred during the dipping stage, when the HMIP was partially submerged, at the elevation corresponding to the surface of the zinc bath. Stress and strain demands were highest for the 12-sided model with a base plate thickness of 76 mm, which had the largest base plate-to-pole thickness ratio (9.5). This was designated as the control or baseline model. A similar 12-sided configuration with the same pole thickness and the smallest base

plate thicknesses (base plate-to-pole thickness ratio of 2.9) had the lowest stress and strain demands among the 12-sided poles. A 12-sided configuration with the same base plate thickness as the control model but a thinner pole shaft (base plate-to-pole thickness ratio of 5.9) also had lower stress and strain demands than the control model, although higher than the model with base plate-to-pole thickness ratio of 2.9. The circular pole model had the lowest stress/strain demands, particularly during the dipping phase, with magnitudes considerably lower than those observed in the control model.

Results showed that in 12-sided poles with connection details employed by the Texas DOT, strain demands decreased inversely proportional to base plate-to-pole thickness ratio, so limiting the ratio of plate-to-pole thickness is likely to be an effective approach to reduce the potential for cracking due to thermal shock during galvanizing. Results also showed that an equally effective approach to reduce cracking during galvanizing would be to implement the use of round instead of multi-sided poles.

References

- [1] AASHTO, Standard specifications for structural supports for highway signs, luminaries, and traffic signals, American Association of State Highway and Transportation Officials (AASHTO), 2013.
- [2] T. Kinstler, GalvaScience LLC, Springville, AL (2005).
- [3] E. ISO, Hot dip galvanizing.
- [4] ASTM-A123, Pressed and Forged Steel Shapes, Plates, Bars, and Strip.
- [5] ASTM-A143, Standard Practice for Safeguarding Against Embrittlement of Hot-Dip Galvanized Structural Steel Products and Procedure for Detecting Embrittlement, ASTM International, 2014.
- [6] ASTM-A385, Standard Practice for Providing High-Quality Zinc Coatings (Hot-Dip).
- [7] S. Roy, Y. Park, R. Sause, J. Fisher, Fatigue resistance of pole-to-base plate connections in high level lighting structures, Structures Congress 2010, 2010, pp. 170-181.
- [8] C.S. Pool, Effect of galvanization on the fatigue strength of high mast illumination poles, 2010.
- [9] Y. Zhou, M. Dawood, B. Gencturk, Journal of Constructional Steel Research 138 (2017) 463-472.
- [10] A.G. Association, North America (2010).
- [11] A.G. Association, North America (2017).
- [12] T. Kinstler, Metalplate Galvanizing, Inc., Limited and Internal Circulation.
- [13] J.R. Kleineck, Galvanizing crack formation at base plate to shaft welds of high mast illumination poles, 2011.
- [14] A.V. Simulia, Dassault systemes (2013).
- [15] AASHTO, Standard Specifications for Structural Supports for Highway Signs, Luminaires, and Traffic Signals (6th Edition), with 2015 Interim Revisions, American Association of State Highway and Transportation Officials (AASHTO).
- [16] A.P. Stam, Fatigue Performance of Base Plate Connections Used in High Mast Lighting Towers, University of Texas at Austin, 2009.
- [17] M. Perić, Z. Tonković, A. Rodić, M. Surjak, I. Garašić, I. Boras, S. Švaić, Materials & Design 53 (2014) 1052-1063.
- [18] K. Nguyen, R. Nasouri, C. Bennett, A. Matamoros, J. Li, A. Montoya, Sensitivity of Predicted Temperature in a Fillet Weld T-Joint to Parameters Used in Welding Simulation with Prescribed Temperature Approach, Science in the Age of Experience, Chicago, IL, USA, 2017, pp. 1-16.
- [19] K. Nguyen, R. Nasouri, C. Bennett, A. Matamoros, J. Li, A. Montoya, Distortion of Steel Plate Girders due to Hot Dip Galvanizing, National Steel Bridge Alliance (NSBA) World Steel Bridge Symposium (WSBS) 2018, Baltimore, MD, 2018.
- [20] K. Nguyen, R. Nasouri, C. Bennett, A. Matamoros, J. Li, A. Montoya, Materials Performance and Characterization In press (2018).

Figures and Tables

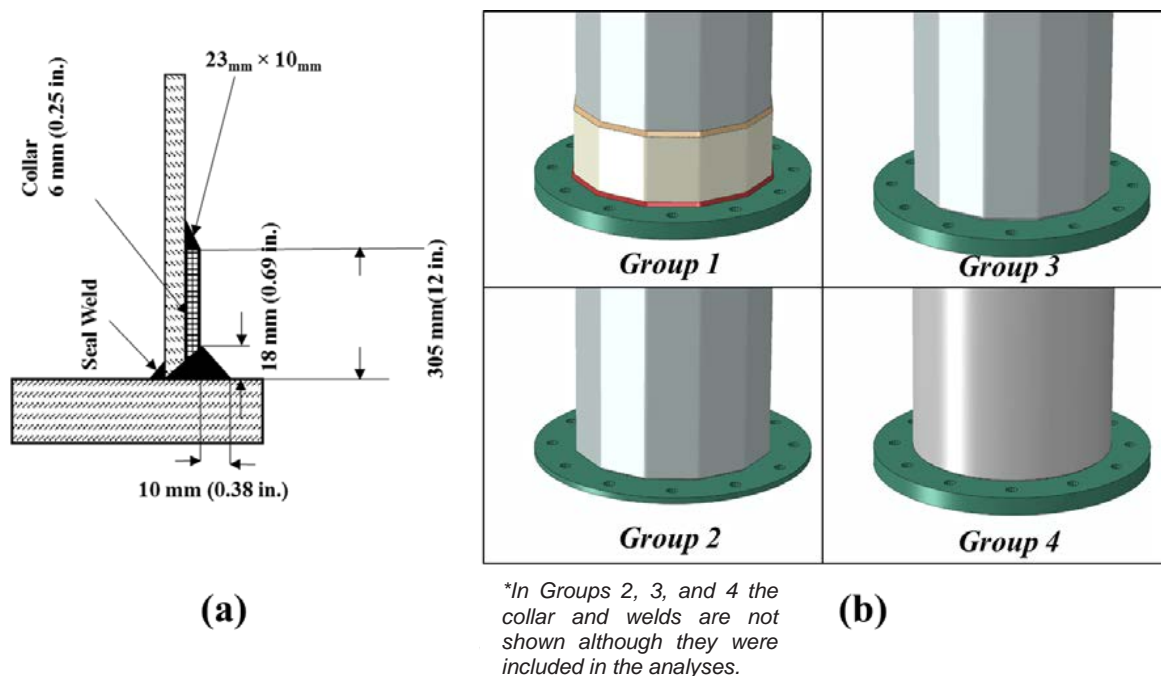
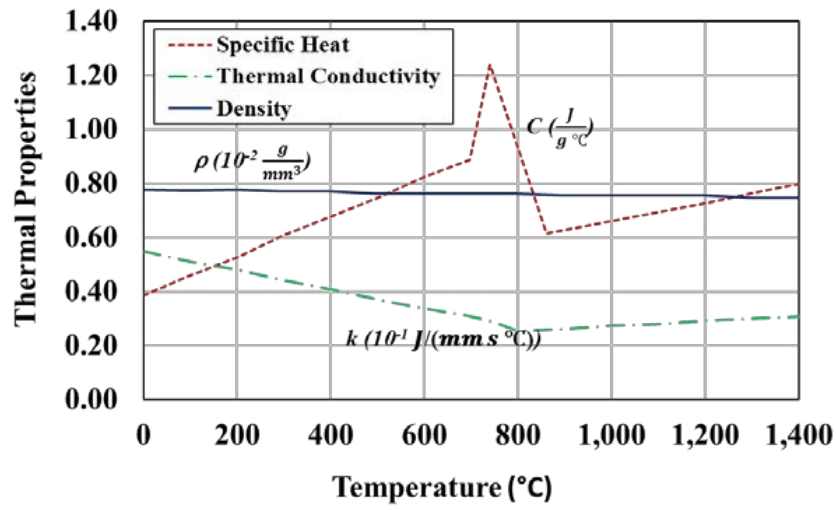
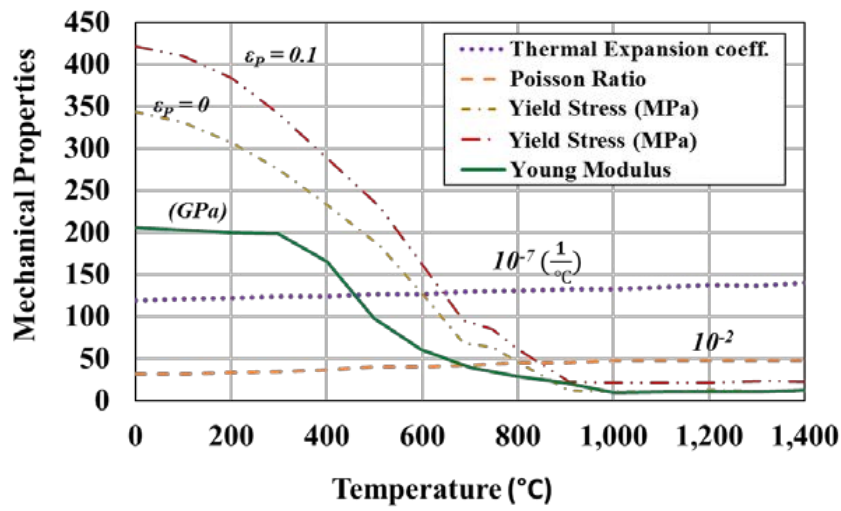


Figure 1.a) HMIP pole to base-plate connection detail specified by Texas DOT b) Groups of HMIP models showing geometric parameters evaluated in the study



(a)



(b)

Figure 2. Material Properties adopted from Peric et al. (2014); a) Thermal, b) Mechanical

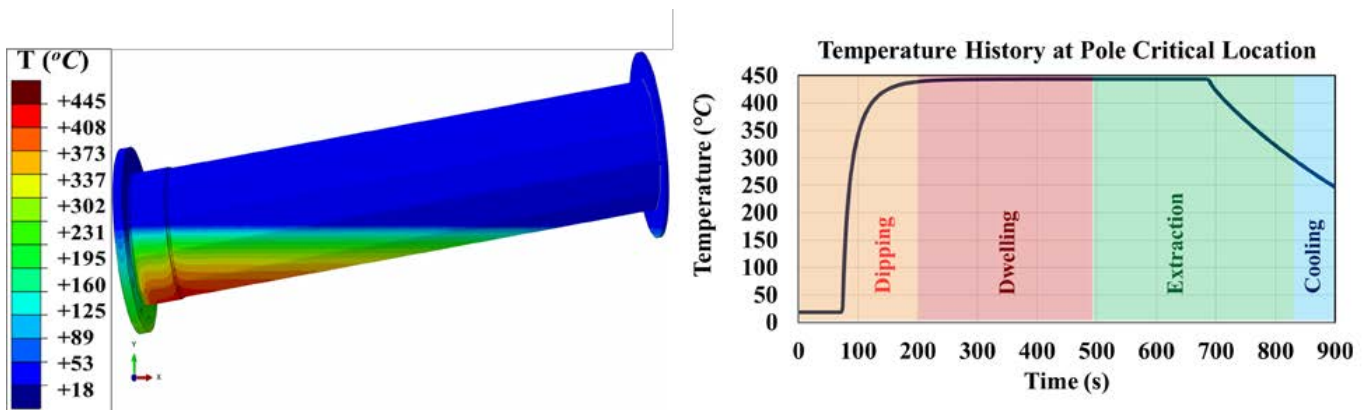


Figure 3. Temperature Distribution for Control Model at 74s

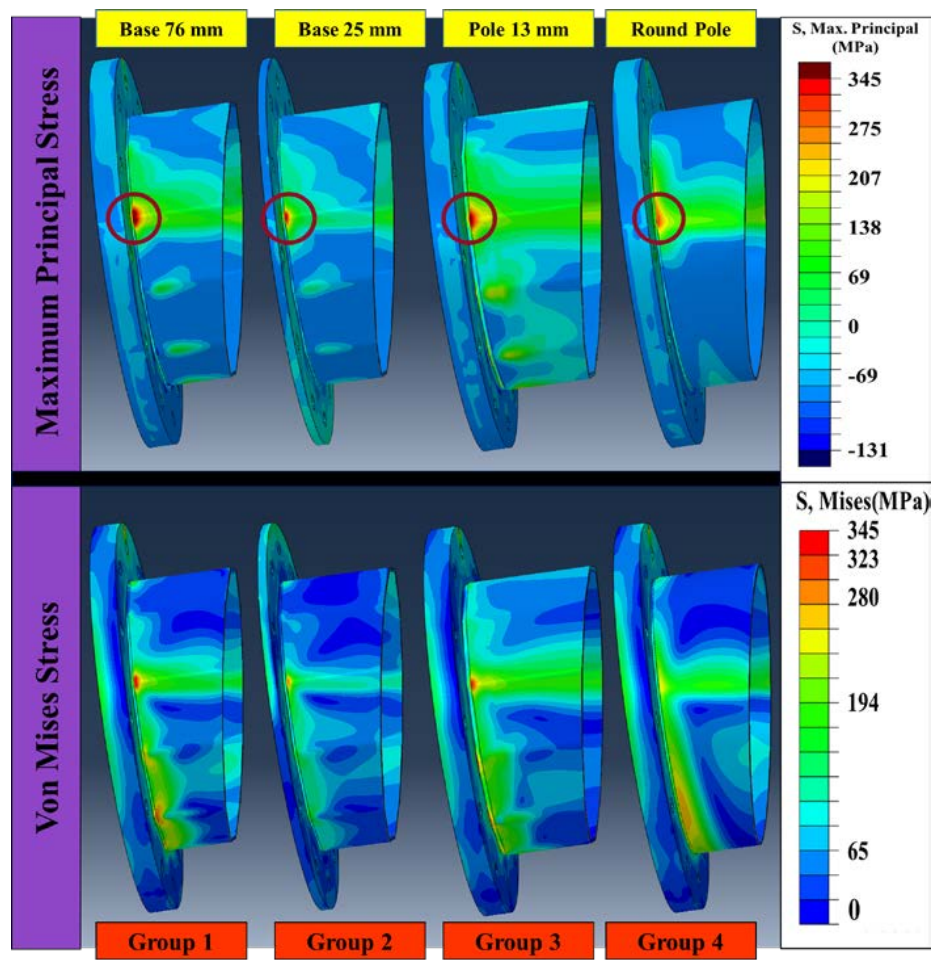


Figure 4. Contour plots for pole maximum principal and von Mises stress at 74s (collar not shown)

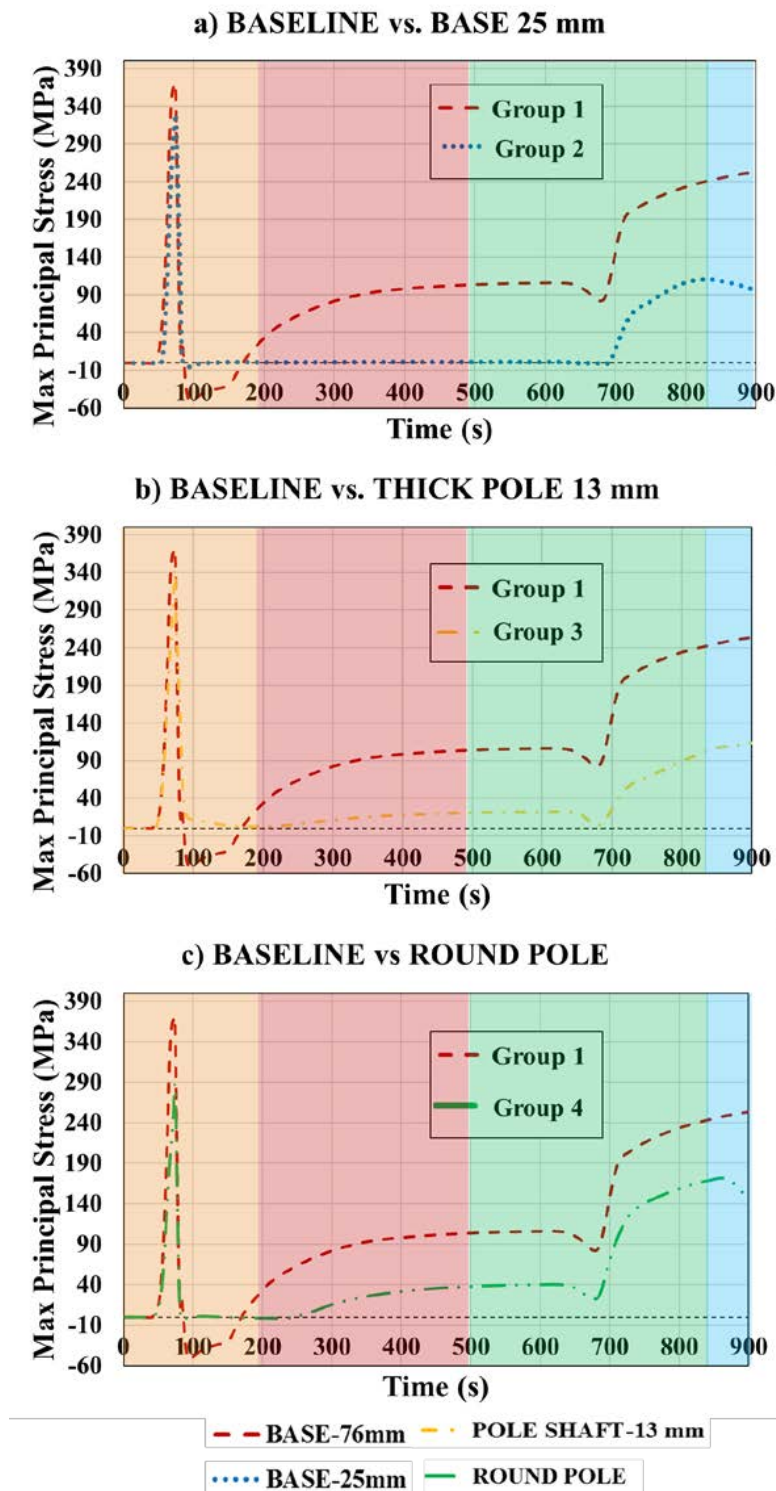


Figure 5. Comparison between maximum principal stress at critical pole location of control model and: a) 25 mm thick base plate model; b) 13 mm thick pole shaft model; c) round pole model

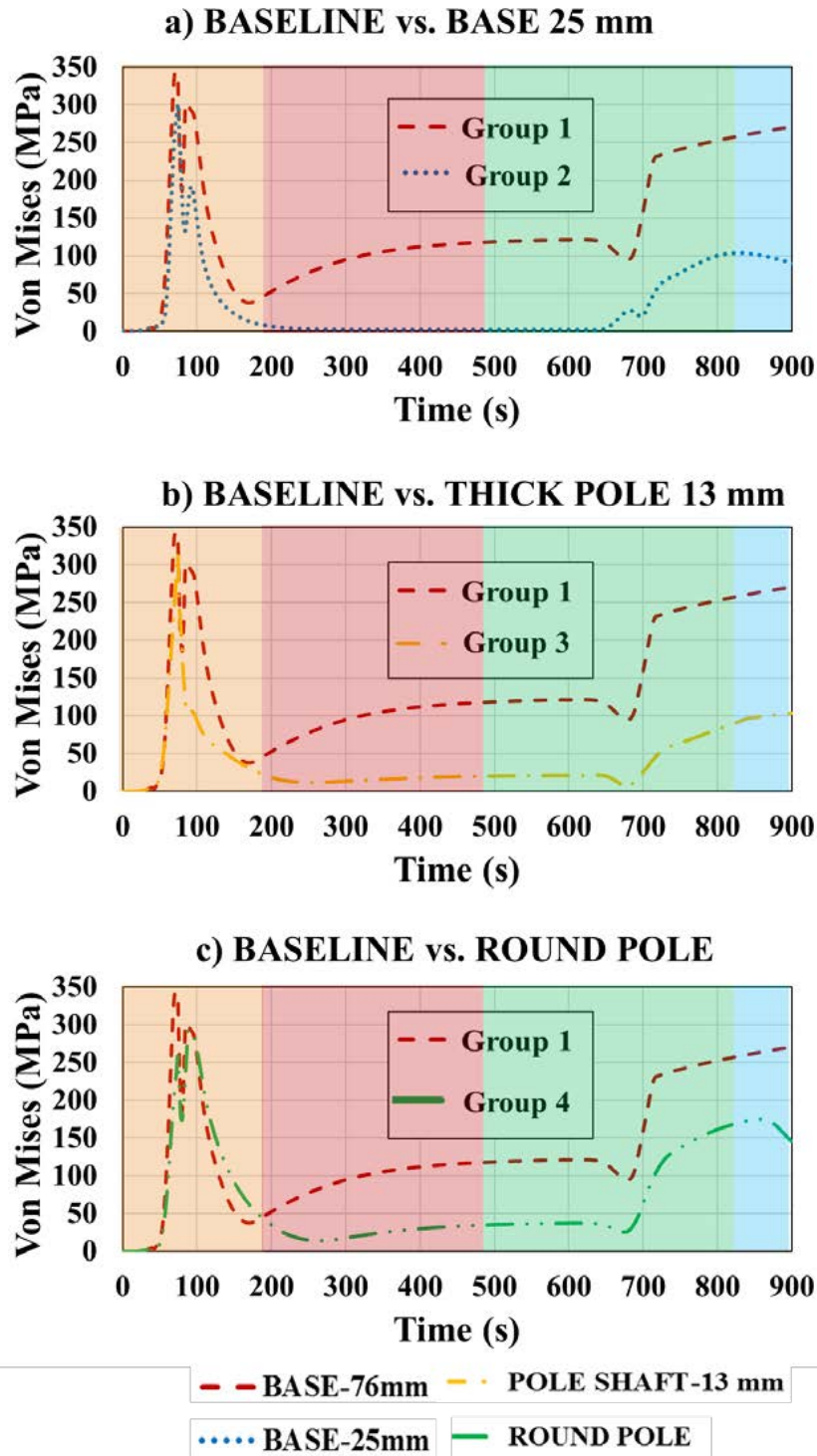


Figure 6. Comparison between von Mises Stress at critical pole location of control model and: a) 25 mm thick base plate model; b) 13 mm thick pole shaft model; c) round pole model

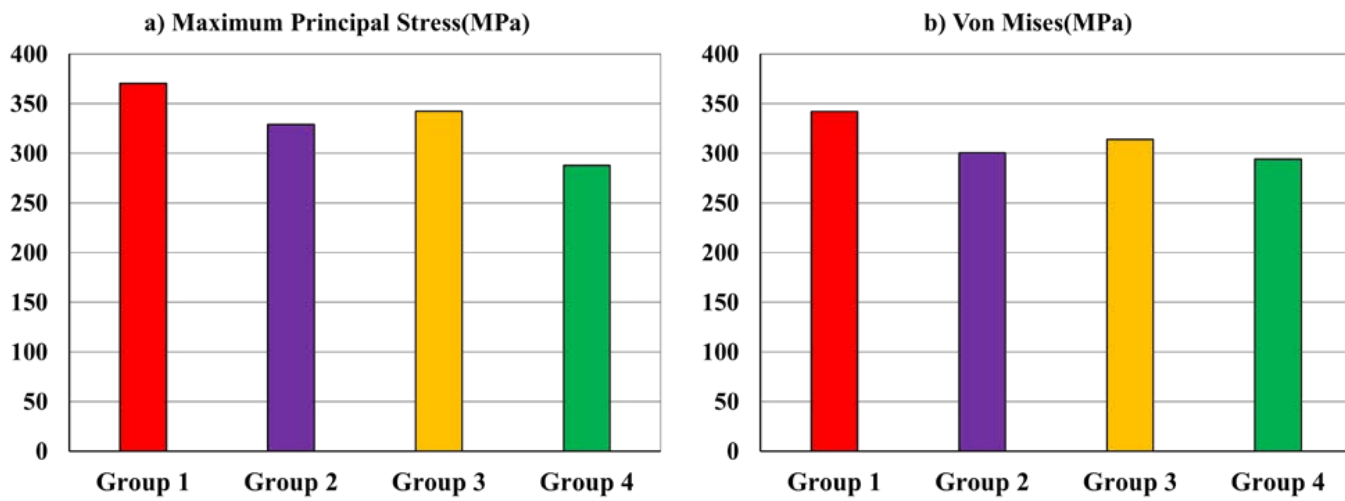


Figure 7. Maximum demand at critical pole location: a) maximum principal stress, and b) von Mises stress

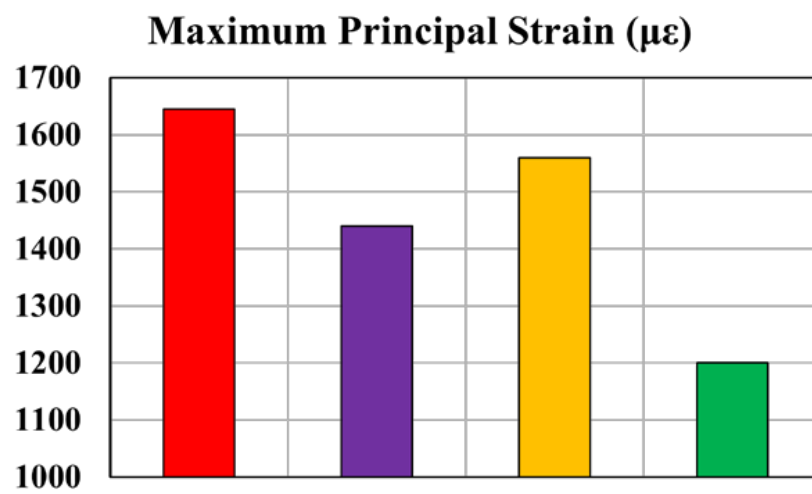
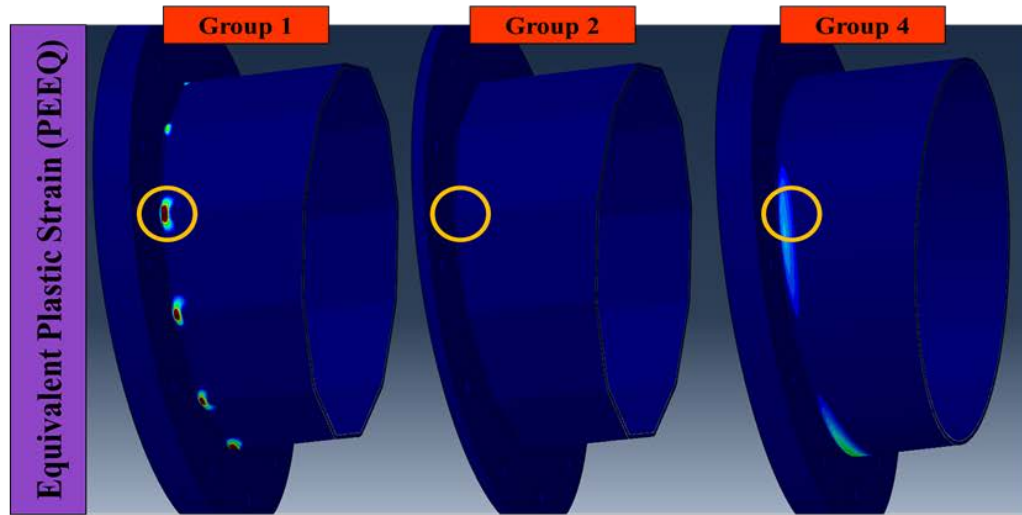
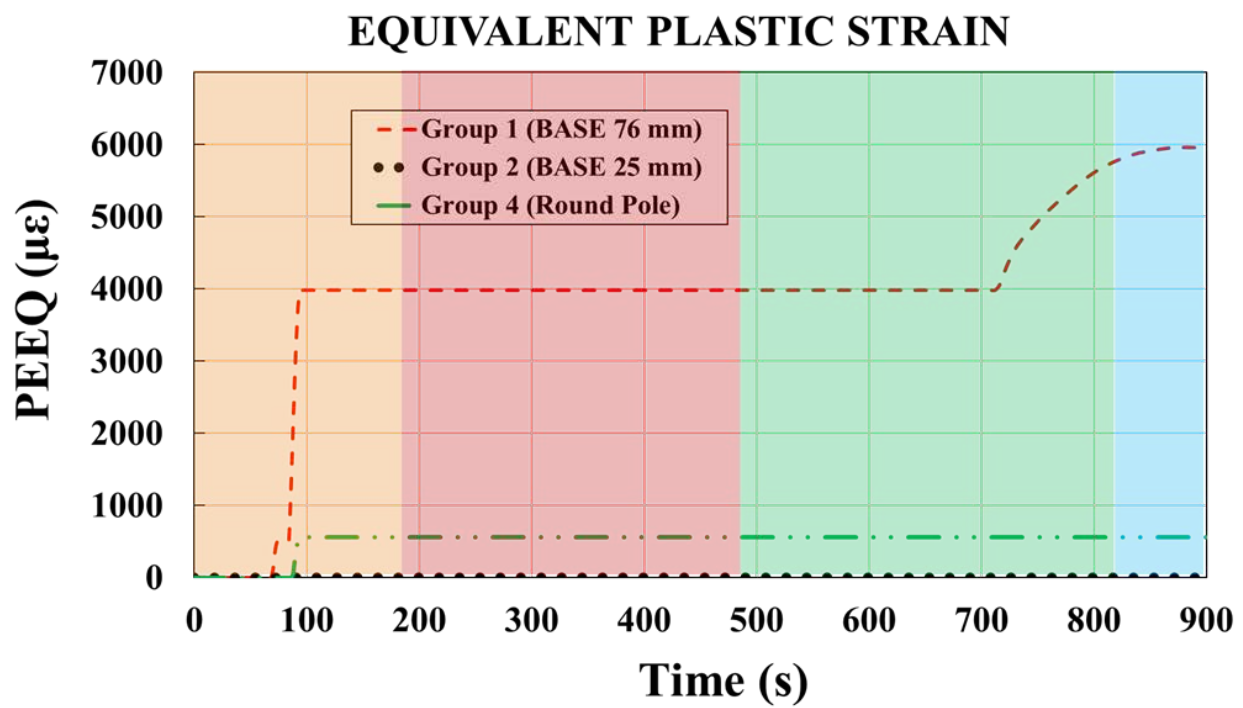


Figure 8. Maximum strain demand at critical pole location



(a)



(b)

Figure 9. a) PEEQ contour plot at the end of the simulation (collar not shown); b) Plastic strain history at critical pole location throughout the galvanizing process

Table 1. Shape parameters

Group	Target Parameter	Base Plate Thickness (mm)	Pole Thickness (mm)	Pole Shape	Plate-to-pole Thickness ratio
1	Control Model	76	8	12-Sided	9.5
2	Base Plate Thickness	23	8	12-Sided	2.9
3	Pole Wall Thickness	76	13	12-Sided	5.9
4	Pole Shape	76	8	Round	9.5

Author Biographies

Reza Nasouri, Ph.D. Candidate

Reza Nasouri is a Ph.D. candidate in Structural Engineering at the University of Texas at San Antonio (UTSA). His Focus is on “Mitigation of Weldment Cracking of Highway Steel Structures due to the Galvanizing Process”. He is also currently involved in developing a high-resolution model capable of simulating the response of bridge structures to hydrodynamic loads for hurricane design conditions. He received his M.S. degree in civil engineering from the University of Texas at San Antonio in 2015. Since 2017, Nasouri has been serving as the Public Relations Director of American Concrete Institute (ACI) Student Chapter at UTSA.

Kien Nguyen, Ph.D. Candidate

Kien Nguyen is currently a PhD candidate in Structural Engineering at the University of Kansas, USA. He spent four years working as a Design Engineer at Kirby Building Systems in Vietnam. He also worked as an adjunct lecturer during the same four years at Saigon Technology University after earning his BS (2008) and MS (2011) in Vietnam and South Korea, respectively. He is a registered Professional Engineer in the State of Missouri, USA.

Arturo Montoya, Ph.D.

Dr. Arturo Montoya is an Assistant Professor with a joint appointment between the Departments of Civil and Mechanical Engineering at the University of Texas at San Antonio. He obtained all his degrees in Civil Engineering from Columbia University: B.S. '07, M.S. '08, and Ph.D. '12. He also has a Bachelor's degree in Physics from St. Lawrence University. Dr. Montoya has a strong background in computational modeling in civil engineering applications and more than 10 years of experience in developing novel computational tools for assessing the integrity of aging structures, including corroded suspension bridge cables. He is a co-developer of the complex finite element method (ZFEM), a novel numerical tool for performing crack growth assessments under high temperature environments. In addition, Dr. Montoya has performed numerical analysis to evaluate the potential risk of hydrogen embrittlement of Zinc-Nickel coated high strength steel in the landing gears of aircrafts.

Dr. Montoya is a core leader of the Center for Simulation, Visualization and Real Time Prediction (SiViRT) at UTSA. In 2014, Dr. Montoya and his graduate student, Armando Gomez-Farias, were the recipient of the Zarem Award given by the American Institute of Aeronautics and Astronautics for the technical excellence demonstrated in their research work. In addition, he received the Mindlin Award (2012) and Henry Michel Award in Civil Engineering (2007) at Columbia University in recognition of a promising research career and superior achievement, respectively. Besides, Dr. Montoya dedicates time to be involved in synergistic activities, such as being a reviewer for academic journals.

Adolfo Matamoros, Ph.D., PE, F.ACI

Adolfo B. Matamoros is the Peter T. Flawn Professor and Assistant Chair in the Department of Civil and Environmental Engineering at the University of Texas at San Antonio, where he joined the faculty in 2014. Prior to UTSA, he worked for 15 years at the University of Kansas, in Lawrence, KS where he held the titles of Professor, Associate Chair for Undergraduate Studies, and Director of Laboratories. He received his MS and PhD degrees in civil engineering for the University of Illinois at Urbana-Champaign in 1994 and 1999, respectively, and the degree of Licenciado from the University of Costa Rica, in 1989.

Professor Matamoros is a Licensed Professional Engineer in the state of Texas, and is active in multiple professional organizations including the American Concrete Institute, the American Society of Civil Engineers, and the Earthquake Engineering Research Institute. He has chaired national technical committees such as the joint ACI/ASCE Committee 408 on Bond and Development of Reinforcement, and the ACI 423-445 ad-Hoc Committee on shear/anchorage failure in end regions of prestressed members. He is a voting member of ACI Committees 374, Seismic Resistant Design, 341, Earthquake-Resistant Concrete Bridges, 369, Seismic Repair and Rehabilitation, and 445, Shear and Torsion.

He is an expert on experimental stress analysis with 20 years of experience in structural testing. He has experience in testing of reduced-scale and full-scale specimens and components made with steel, concrete, composite materials, and adaptive materials both under pseudo-static and dynamic loading. In addition to his experience with experimental testing, he has worked on nonlinear finite element simulations of steel and reinforced concrete structures and has published several studies on the repair of damage due to fatigue in structural steel bridges.

Caroline Bennett, Ph.D., PE

Caroline Bennett received her B.S. (2002) and Ph.D. (2006) in Civil Engineering from the University of Cincinnati. She is an expert in the area of fatigue of steel structures and steel bridge engineering. She has served as the Principal Investigator on a number of research projects aimed at improving the fatigue performance of structures, including Transportation Pooled Fund study TPF-5(189), "Enhancement of Welded Steel Bridge Girders Susceptible to Distortion-Induced Fatigue." Professor Bennett was awarded the Robert Dexter Memorial Lecture for her work in the area of mitigating distortion-induced fatigue cracking. Dr. Bennett is an expert in performing both large- and small-scale experimental testing of steel structures and components and in performing sophisticated computational simulations using the finite element method. She has considerable experience performing and analyzing materials characterization work, including tension testing, tensile fatigue testing, and Charpy V-notch testing.

Caroline Bennett serves on a number of national professional organizations. She has served as an active member on Transportation Research Board Committees AFF20 "Committee on Steel Bridges," and AFF20(1) "Analysis of Steel Bridge Systems" since 2006. Dr. Bennett recently served as a member of the Technical Expert Task Group (TETG) for SHRP R19A, "Bridges for Service Life beyond 100 Years: Innovative Systems, Subsystems, and Components." She chaired the ASCE Committee on Fatigue and

Fracture from 2008-2011, and has served as an active member since 2006. Dr. Bennett has been an active participant in the ASCE Committees on Steel Bridges and Structural Members.

Jian Li, Ph.D.

Professor Jian Li holds a B.S. and M.S. in civil engineering (Harbin Institute of Technology 2005, 2007) and a Ph.D. in civil engineering (University of Illinois at Urbana-Champaign 2013). He joined the faculty of the Department of Civil, Environmental, and Architectural Engineering at The University of Kansas in 2013. Prior to coming to The University of Kansas, he was a graduate research assistant at the Smart Structures Technology Laboratory at the University of Illinois, where he worked on multiple National Science Foundation projects on developing wireless smart sensor networks for infrastructure monitoring and an integrated seismic risk assessment framework incorporating substructure hybrid simulation. He was one of the main contributors to the long-term deployment of the Jindo Bridge sensor network in South Korea, which is the world's largest wireless sensor network for infrastructure monitoring.

Dr. Li has research interests primarily in the area of structural dynamics and earthquake engineering, with particular emphasis on vibration-based structural health monitoring, wireless smart sensor networks, system identification, model updating, damage detection, substructure hybrid simulation, advanced fragility analysis, and seismic risk assessment and mitigation. He has 25 research publications including refereed Journal articles, conference papers, technical reports and magazine articles on these topics.

Dr. Li is a member of the Earthquake Engineering Research Institute (EERI), the Consortium of Universities for Research in Earthquake Engineering (CUREE), and the American Society for Engineering Educations (ASEE).

Thomas Kinstler

Thomas Kinstler has a B.S. in Chemistry from Fordham University, M.A. in Interdisciplinary Marketing from the University of Alabama, and an M.S. in Materials Engineering from the University of Alabama Birmingham. He has over forty years of experience in the Hot-Dip Galvanizing industry, metal processing and manufacturing. His experience includes plant design, machinery and process selection, plant start-up and plant process trouble-shooting, technical support, root cause analysis and evaluation. He has Six Sigma certification. Tom Kinstler retired as Vice President for Development and Technology for multinational Hot-Dip Galvanizing Company to pursue undergraduate Adjunct Teaching, Technical Consulting and Research.

Tom Kinstler chaired the technical committee which oversees Internationally-recognized ASTM galvanizing specifications (A05.13) for over a decade. Multiyear service on numerous other technical, and research-steering committees including American Galvanizers Association, American Iron and Steel Institute, and International Lead Zinc Research Organization. Hundreds of presentations, and seminars completed. He completed research and authored an often-cited technical paper on liquid-metal embrittlement of steels, selected and presented at the triennial International Galvanizing Conference (Intergalva 2006) in Naples, Italy (June 2006).

Tom Kinstler is a recognized expert in metal materials and corrosion. He had wide-ranging consulting clients and expert-witness assignments in materials litigations. He is widely recognized for success in technical Service, investigation, and support for galvanized manufactured products. He has world-wide collaborations and contacts related to Hot-Dip Galvanizing and extensive experience in methods of Materials Characterization from basic metallography to electron optic methods.

Session 6:

Bath Alloy Technology

Influence of alloying elements on galvanizing abnormalities with a special view on surface defects

Roger Pankert Boliden, (Sweden)

Introduction:

Use of alloyed Zinc-melts is quite common in general galvanizing. Many different bath compositions have been elaborated and proposed for general galvanizing during the last 3 decades.

Focus for all alloys has always been about coating thickness reduction on reactive steels.

With regard to new directives, the use of certain alloying is or will be restricted.

Nevertheless, alloying elements also change the physical properties of the liquid Zinc. The interaction of pretreatment and physical properties of the Zinc on certain galvanizing defects will be discussed and weighed.

Finally it will be summarized which alloying elements will have either positive or negative effect on galvanizing defects.

Challenges for Galvanizing:

Aside good corrosion resistance and correct surface aspects of the galvanized steel, galvanizers experience many challenges.

New steel compositions are penetrating the market. Product mix covers traditional Si-killed steels over newly penetrating Al-killed steels up to highly alloyed steels. All of them showing different microstructures (also related to cooling history) and internal oxidation affecting the wettability during galvanizing.

On top, increased use of flat products and welded steel beams are changing the habits.

Last but not least, removal of synthetic emulsions on cold rolled material is has led to enhanced pretreatment steps.

Generally observed surface defects are shown in **fig.1**

Most effects can be related mainly to 4 origins:

Excessive Zn-Fe-reaction,

Surface contamination on the steel,

Bad wettability of the steel by the liquid Zinc,

Iron-precipitations through composition or temperature changes

Excessive Zn-Fe-reaction has historically been related to the steel composition.

Mainly the Si and P-contents have been investigated. Very thick coatings are observed within a Si-content from 0,03 – 0,12%.

Schulz¹⁾ related coating growth on hydrogen effusion of Si-containing steels.

The Zinc-Iron-reaction:

The Zn-Fe reaction has been studied in depth by Horstmann²⁾

By immersing steel in liquid Zinc, the steel starts to dissolve and this Iron will start to compose first zeta-phase, which later converts to the compact delta-phase.

Horstmann studied the Iron dissolution in liquid Zinc and attributed the amount of Iron present in the different intermetallic phases.

With increasing temperature, the amount of Fe increase as expected.

From the binary phase diagram Zn-Fe it is known, that the destabilization of the zeta-phase starts at 480°C which here translates in an increased Fe-loss.

The amount of Fe bound in the different phases is given in **fig.2**

A second important result was, that the Fe contained in the zeta-phase will be less with increasing galvanizing temperature.

As more energy is available, the formation of the more stable delta-phase is promoted.

When related to the Si in the steel he made two interesting observations.

With increasing Si-content in the steel, the amount of dissolved Fe is increasing, and secondly, the enhanced Fe-dissolution starting for pure Fe at 480 °C (due to the destabilization of the zeta-phase) is shifted towards lower temperatures (**fig. 3**)!

Further Sebisty³⁾ observed, that for some steels with Silicon between 0,15 and 0,25%, the coating thickness is reduced if galvanizing temperature is increased from 450 to 465°C.

Micrographs show that again in this case the formation of the delta-phase is favored.

Zinc-Iron reaction in combination with wetting of the steel:

Zraggen & ass.⁴⁾ studied difficulties for galvanizing on laser cut edges.

Poor adherence of coatings are attributed to the formation of stable oxides which often can not be removed in the pickling step. Those oxides, -together with the structure less martensite (**fig.4**) create very brittle phases. Improvement is observed if oxides are removed (or in a wider sense if wettability by the Zn is improved).

Further the observed cauliflower like outburst on laser-cut edges are attributed to the fact that diffusion of Zn into Fe is dependent on the microstructure of the steel.

This is in line with Böttcher⁵⁾ who observed that Fe-diffusion is enhanced in tempered Martensit and or Perlit.

Additionally F. Nieth⁶⁾ examined the influence of surface contaminations on rough and grooved surfaces on drawn tubes. His observations can be summarized as follows:

Grooves on the surface are leading to overthickness, delta phase nearly disappears and zeta-phase outbursts are growing.. After annealing, the coating thickness goes down by 40%.

On the non annealed tubes, degreased and pickled tubes had a 20% lower coating thickness than just the pickled tubes

And last but not least, surface contaminations can be the origin of strong coating growth which was correlated to wetting behavior.

To summarize; Fe dissolution increases with Si- and P-contents in the steel but also with amount of martensite (cooling) and of dislocations (cold working).

If the amount of dissolved Fe per time-unit is substantial, it will mostly generate the Fe-poor zeta-phase and huge coating thickness will be observed.

Promoting the formation of a (compact) delta-phase will therefore reduce (local) overthickness.

Wettability also plays an important role, as any disturbances of the wetting of steel will generate different types of abnormalities.

To avoid /reduce many types of surface defects, a Zinc melt having a good wettability and favoring the delta-phase is therefore desirable.

Alloying elements:

Alloying Elements in a galvanizing bath⁷⁾ can be classified in (**fig 5**):
elements taking part in the Zinc-Iron-reaction such as Al and Ni
elements not taking part in the Zn-Fe-reaction such as Pb, Bi and Sn; which only affects the physical properties of the melt.

Elements reducing defects related to Zinc-Iron reaction

Surface defects related to excessive coating growth (**fig 6**), can mainly be related to zeta-phase outbursts on depressed delta-phase.

Aluminum is known to execute a sort of inhibition effect to coating growth of reactive steels. During the inhibition period, the attack on Fe is negligible and no Fe-Zn-compounds are formed⁸⁾ (A.R.P. Ghuman and J.I. Goldstein, Metallurgical Transactions, 3 (1971) 2903

Nickel is known for a compactation of intermetallic Zn-Fe-layers. Due to this compactation, Fe-diffusion towards the melt is reduced. Therefore, not only the total thickness of intermetallics is reduced, in addition to this, the relative growth of the delta-phase against the zeta-phase is enhanced.

Elements reducing defects related to physical properties of the melt

Surface defects related to physical properties (**fig.7**) of the liquid Zinc are related to a combination of viscosity, surface tension and wettability.

Recently in some countries, a tendency to Pb-free or Pb-poor Zn-bathes is ongoing.

Pb having been a very effective alloying element improving drainage of the Zinc as well as wettability and sinking of dross particles.

Potential substitutes for Pb are Sn and Bi.

Viscosity:

Viscosity of different Zn-melts have been extensively examined.

It has to be mentioned, that viscosity is measured under protective atmosphere (to exclude oxidation and contaminations) by using materials not reacting with liquid Zn.

It has been found that the influence of Sn and Bi as such is very low.

Nevertheless by comparing a huge amount of existing results, it can be concluded that at 450 °C related to Pb we can state following Pb-equivalent

$$\text{Pb-equivalent viscosity} = \text{Pb} + 2,5\text{Sn} + 2,5\text{Bi}$$

Surface tension

Also the surface tension is measured under protective atmosphere on materials not reacting with Zn.

Bi as a Pb-substitute is in use since end 90s⁹⁾ and concluded to have a huge positive influence. Compiling all available results, at 450 °C it can be stated that.

$$\text{Pb-equivalent surface tension} = \text{Pb} + 0,15\text{Sn} + 6\text{Bi}$$

Wettability

Neither viscosity, nor surface tension can describe the wetting-behavior in a galvanizing bath. Basically it is the wetting behavior describing best what is going on in a galvanizing bath. This, because the wetting behavior depends on surface conditions as cleanliness and roughness and also on the steel reactivity (reactive steels (high Si show better wetting behavior). Further, it would be expected that wetting behavior does improve with raising temperatures.

CRM in Liège developed a methodology to measure the wettability (**fig.8**)

By dipping a steel into liquid Zinc, first the surface of the liquid is pushed down. When wettability starts surface will be covered more and more by the liquid and because of capillary forces even ends at a level higher than the initial surface.

As a value for wettability, the time is taken till Θ reaches 90 °.

An example of results is given in **fig.9**.

The methodology gives explainable results and is in line with expected observations when galvanizing.

It has been found out, that wetting behavior increases up to 0,2% Bi; after that no further effect. Sn improves wettability up 1% and after this no further improvement.

Compiling all available results, at 450 °C it can be stated that.

$$\text{Pb-equivalent wettability} = \text{Pb} + 3\text{Sn} + 2\text{Bi}$$

Sure, wettability of the melt alone will not be a grant for defect-free galvanizing, but together with a highly performing pre-treatment; they can help to bring certain defects to a minimum.

Iron precipitations

Fe-solubility in liquid Zinc is strongly affected by temperature and (depending on the alloying element) on local concentrations¹⁰⁾.

Basically, all elements added into the Zinc to participate at the Zn-Fe-reaction have an influence on the Fe-solubility (see **fig. 10**).

In this example of a Ni-containing bath, a temperature drop of 10 °C can promote Fe-precipitations up to 70 g/t; an increase of the Ni-concentration by 0,06% will generate up to 60 g/t Fe-precipitations in the affected zone!

Those elements must therefore be added in a smooth way to avoid Fe precipitations which will combine with Zn to form small (floating) dross particles generating pimples on the galvanized steel.

Focus for the galvanizing practice:

Compiling all this together (**fig. 11**) with a special view on galvanizing abnormalities, we can conclude, that alloying elements can help, -together with a good pre-treatment to reduce surface defects.

Elements taking part in the Zinc-Fe-reaction will improve the situation with regard coating thickness abnormalities and homogeneity, and will help to get a shiny aspect. On the other hand, those elements can produce pimples if not added properly.

Elements as Pb, Bi and Sn have an influence on the physical properties of the liquid melt and can help to reduce all abnormalities related to a bad drainage.

References:

- 1) Schulz W-D, Schubert P and Thiele M: Proceedings Intergalva 2003
- 2) Horstmann D: Zum Ablauf der Eisen-Zink-Reaktion, GAV-Schrift 1991 pp 11-30
- 3) Sebisty JJ: 11 International Zinc Conference, Stresa 1973
- 4) Zraggen M, V Trzebiatowski, Duebendorf h and Haslinger A: Lasergeschnittene Bauteile – eine Herausforderung fuer Verzinker; JOT 4/01, 2001
- 5) Boetcher HJ: Moeglichkeiten zur Minderung der Eisen-Zink-Reaktion beim Feuerverzinken; Metall 38/9 pp 862-866
- 6) Nieth F: Einfluss verschiedener Oberflächenverunreinigungen des Stahls auf die Ausbildung von Zinkueberzuegen; GAV-Schrift 1980 pp 49-78
- 7) Pankert R: Workshop 7; Intergalva 2015
- 8) Ghuman ARP and Goldstein JI: Metallurgical Transactions 3 ,1971 p 2903
- 9) Gagne M: Proceedings Intergalva 1997
- 10) Pankert R: Proceedings Intergalva 2009

Figures:

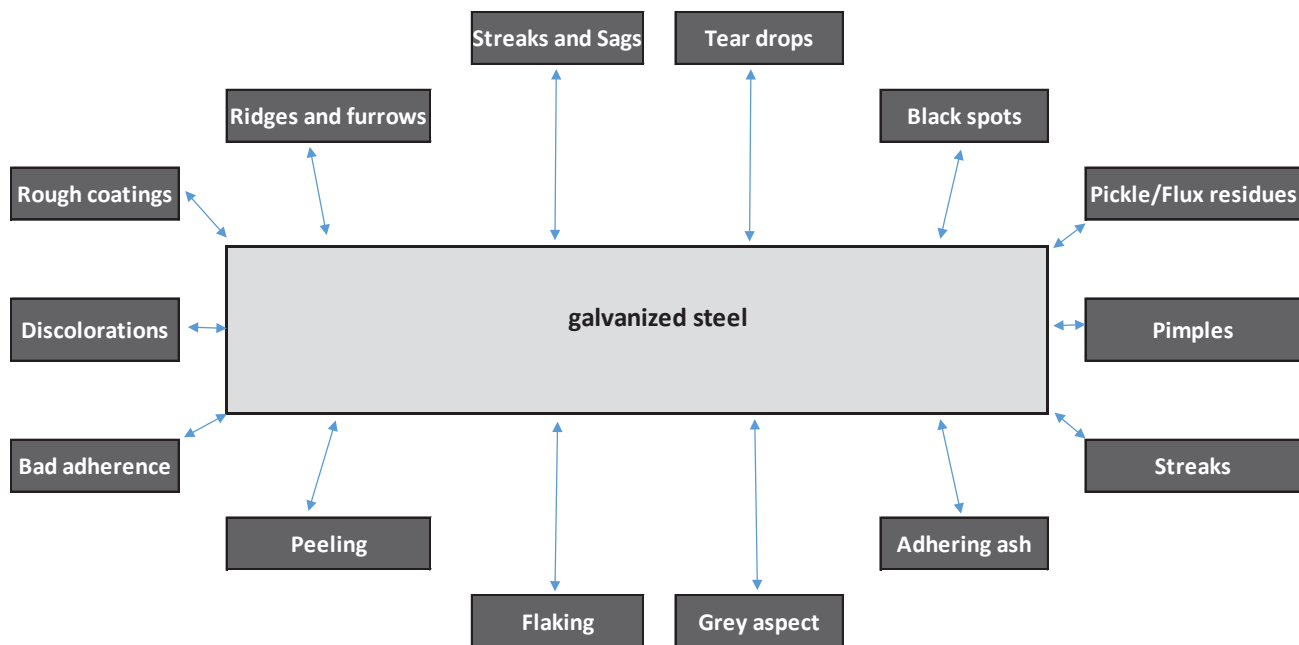


Fig. 1: Common galvanizing defects

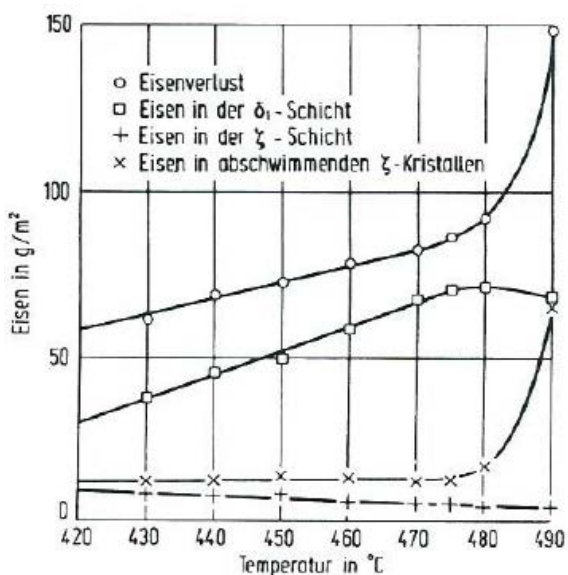


Fig. 2: Fe distribution in intermetallics (according Horstmann²⁾)

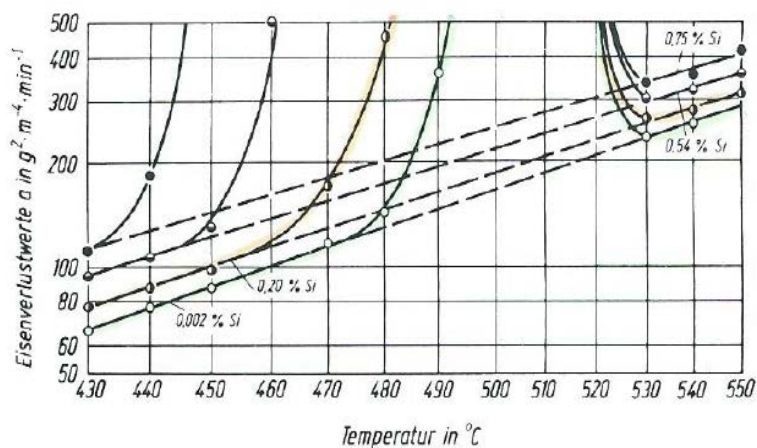


Fig. 3: Influence of Si on dissolved Fe (according Horstmann²⁾)

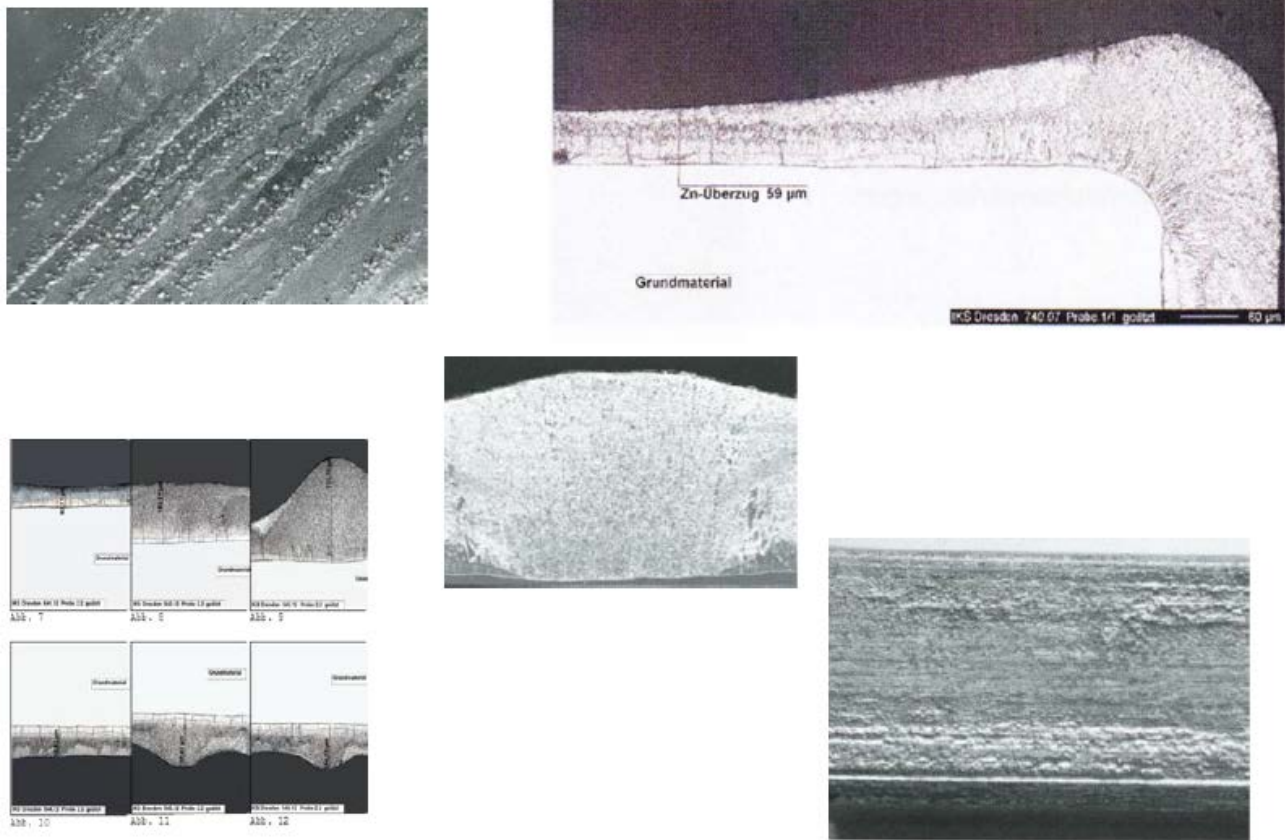


Fig 6: Typical defects related to (locally) excessive coating growth

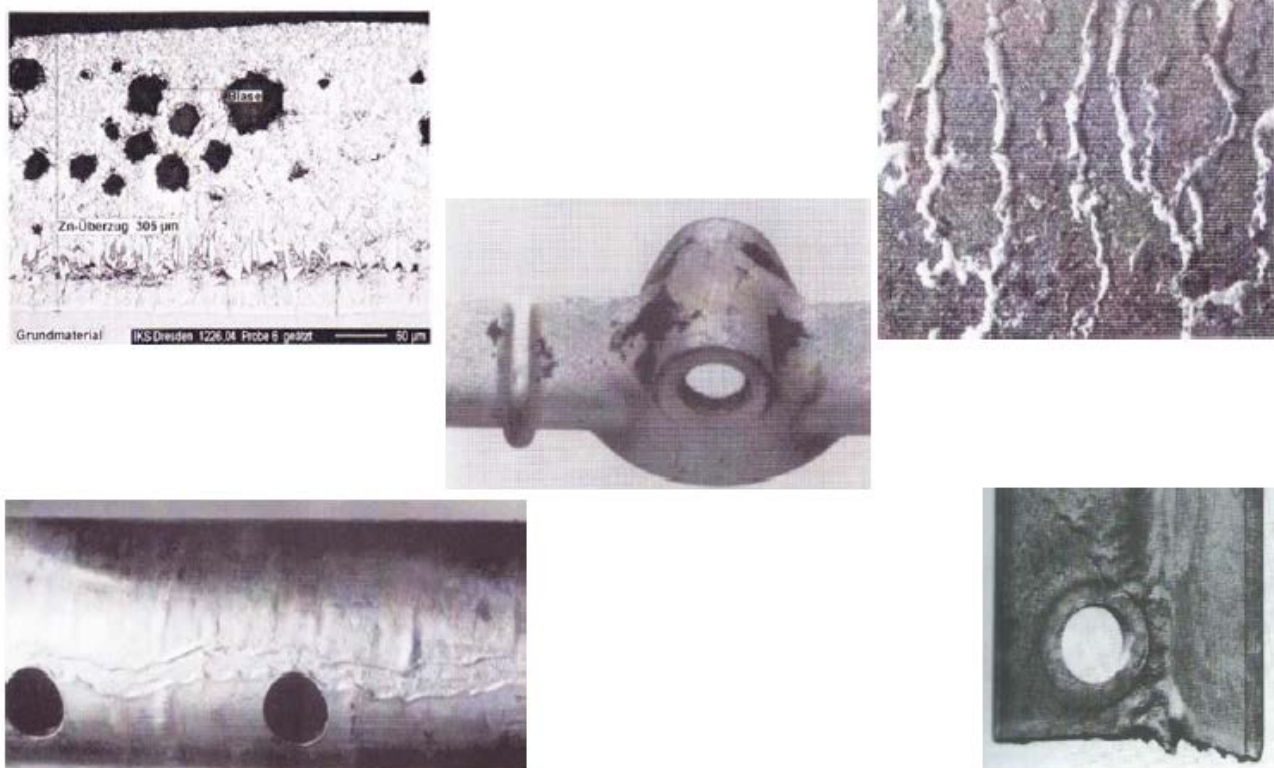


Fig 7: Typical defects related to physical properties of the melt

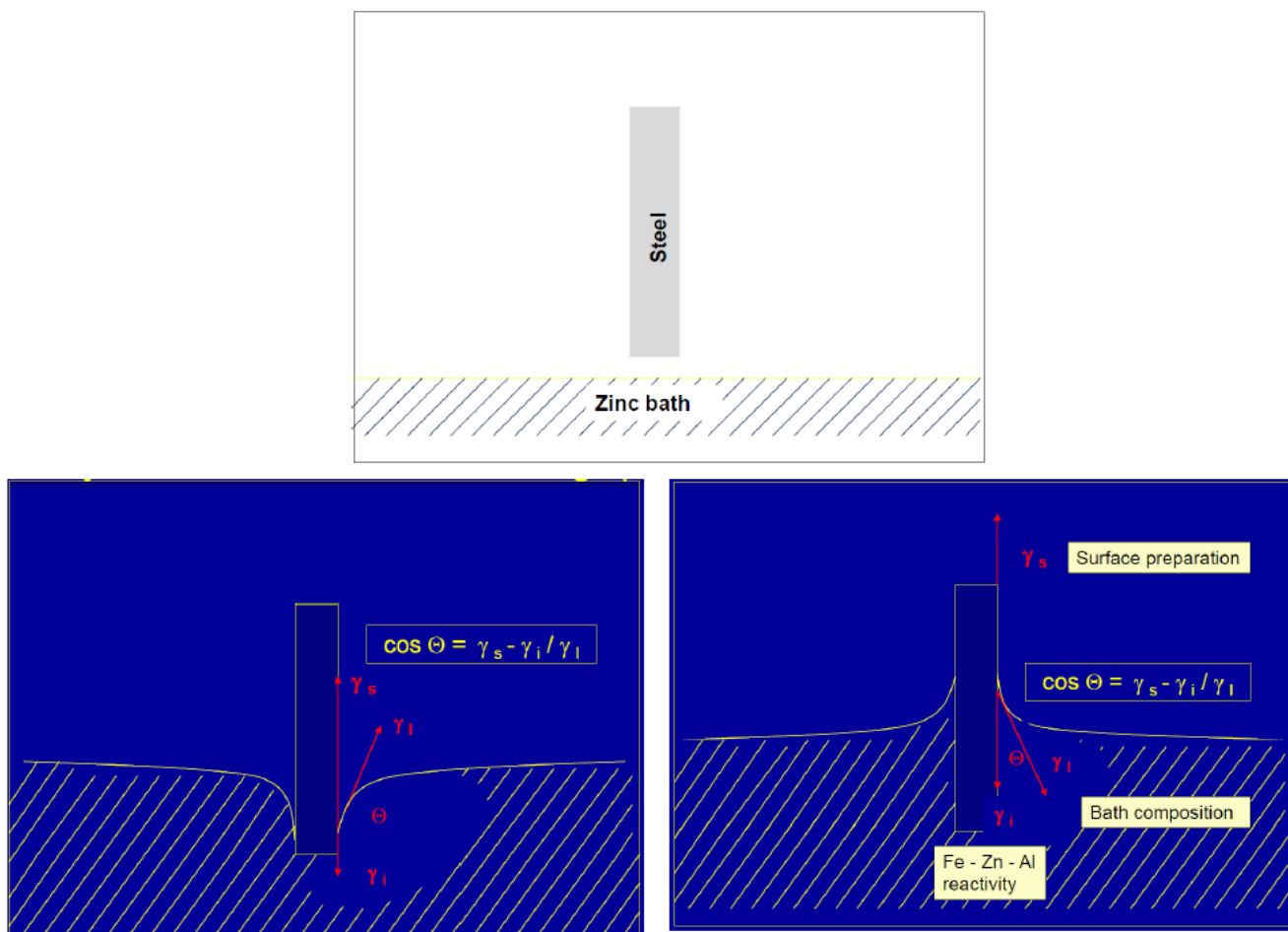


Fig 8: Wettability measurement by meniscograph (CRM)

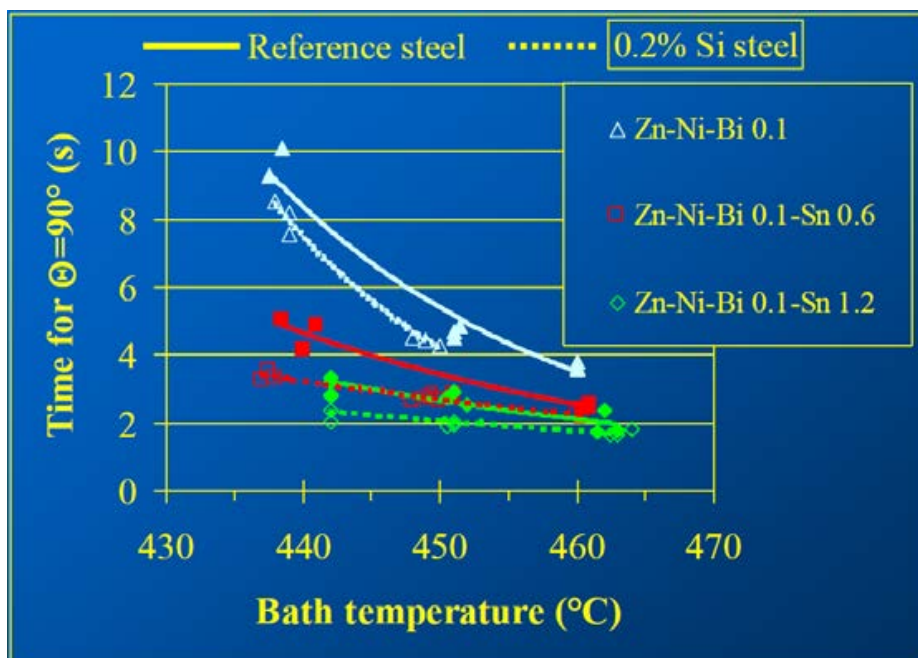


Fig 9: Some results obtained on a non reactive steel

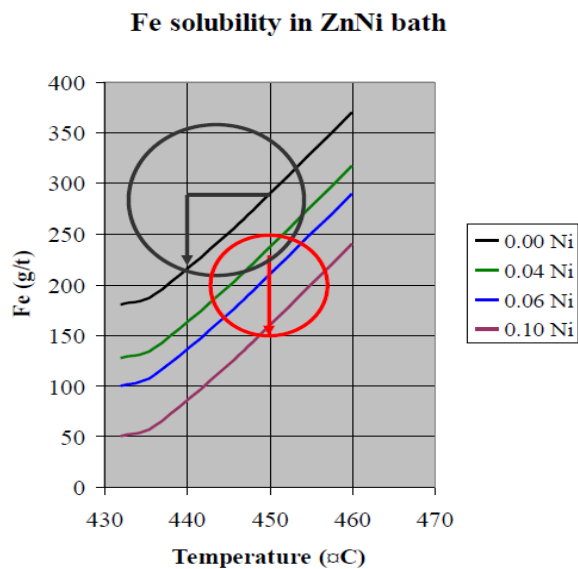


Fig 10: Fe-precipitations through temperature and concentration changes

Origin	defects and abnormalities													
Zn-Fe-reaction														
Surface contamination														
Physical properties Zn														
Fe-precipitations														
	Reduced coating thickness	Coating homogeneity	Black spots	Discolorations	Gray aspect	Ridges and furrows	Rough surface	Enhanced dross	Streaks and sags	Tear drops	Pickle and flux residues	Pimples	Bad adherence	Peeling / Flaking
Process														
Degreasing														
Rinsing														
Pickling														
Rinsing														
Fluxing														
Drying														
Zn-bath														
Al														
Ni														
Pb														
Bi														
Sn														

Fig 11: Influence of pre-treatment and Zinc-bath composition on galvanizing abnormalities

BISMUTH INFLUENCE IN DIFFERENT CONCENTRATIONS IN THICKNESS AND COATING MORPHOLOGY FOR HOT-DIP GALVANIZING PROCESS

Mariana Fornaciari Schaeffer¹

William Barbosa Borges²

Renato Cavalcanti de Albuquerque Tozin³

Pedro Ruf Pereira Viana⁴

1 Chemical Engineer, Bachelor, *Chemical Technician, Department of Chemistry/Environment, Brametal S.A, Linhares, Espírito Santo, Brazil.*

2 Materials Engineer, Bachelor, *Responsible Chemist, Department of Chemistry/Environment, Brametal S.A, Linhares, Espírito Santo, Brazil.*

3 Chemical Engineer, *Graduated, Department of Market Development, Votorantim Metais SA, São Paulo, Brazil.*

4 *Chemist, Metallurgical and and Materials PhD, COPPE/UFRJ, Rio de Janeiro, Brazil.*

Abstract

Angles were galvanized carbon steel in industrial scale in ten different zinc baths, each composed of various bismuth concentrations (0 ppm to 1160ppm). The tank which already made use of about 1.00% lead. The coatings obtained were studied by layer thickness and metallographic analysis using the software Fiji / ImageJ and images obtained by scanning electron microscopy (SEM). Variations in thickness were obtained and morphology of the coating and is not proportional to the increase in the bismuth concentration in the bath. Bismuth showed to be effective in reducing the thickness to the specimens galvanized in concentrations of 156, 255, 386 and above 837ppm bismuth, however was noticed a significant increase in coating thickness at concentrations between 610 ppm and bismuth 660ppm in the bath, and in the same concentration range was not clear formation of four typical phases of a galvanized coating (γ), δ), zeta (ζ) and eta (η)). Even in the largest concentration of bismuth in the zinc bath, was observed in fragments dispersed phase eta (η), possibly consisting of pure bismuth.

Keywords: Hot-dip galvanizing; Bismuth; Coating properties; Industrial test.

1 INTRODUCTION

The Hot Dip Galvanizing Process can be summarized as the immersion of a previously prepared and cleaned surface of a steel or cast iron substrate into a molten zinc dip in order to cover the substrate's surface with a corrosion resistant zinc coat.

It is during the immersion of the part into the galvanizing kettle that the coating formation takes place, in which a zinc-iron intermetallic layers are developed through diffusive phenomena and an external layer is produced at the moment the galvanized part is pulled out from the kettle [1, 2]. The coating layers, known as phases, are denominated as: gamma (γ), delta (δ), zeta (ζ) e eta (η). The zeta phase (ζ) is the first one formed. It has an approximate iron composition of 5.80% to 6.20%. It grows columnarly above the delta phase (δ)_and, depending on the iron saturation of the bath, zeta (ζ) crystals can be formed and get confined into the eta (η) phase. The second phase formed is the delta phase (δ), which also has a columnar morphology with an approximate iron composition of 7.00% to 12.00%. The gamma phase (γ), the thinnest and the closest to the steel's surface layer, has an approximate iron composition of 21.00% to 28.00%, being the last phase formed during the immersion. The outermost layer is the eta (η) layer, which is not formed through diffusion phenomena, and has a chemical composition similar to bath of molten zinc [3, 4, 5].

The hot dip galvanized coating thickness varies, it is in general between 75 and 125 micrometers [2]. To each type of galvanized there is a standardized specification in which the acceptable minimum average thicknesses are specified to avoid issues in galvanized steel usage [6, 7].

Thicknesses considerable above the standardized ones are not very well estimated. The intermetallic phases are hard, though brittle. Thicker layers may present weak adherence and peel off with certain easiness, furthermore, leading to a higher zinc consumption [8].

Many factors may influence the thickness and properties of the coating, among them, the elements added to the zinc bath [9, 10].

The addition of alloying elements to the zinc bath is up to the galvanizer, since the bath's composition is not less than 98% zinc; otherwise, the process is not classified as a hot dip galvanization process [7].

Aiming to improve or attribute some desirable characteristics to the galvanized coating or process, the addition of elements such as aluminum and lead are often made [2]. Recently, the addition of others elements such as bismuth has been made, in order to gather additional improvements to the hot dip galvanization process [8, 11].

Currently studies have shown that the bismuth can provide coating thickness reduction and better finishing due to higher efficiency on the molten zinc drainage from of the part. The bismuth has properties similar to that of lead, with the advantage of being non-toxic, thus a possible alternative to the replacement of lead in galvanization [12]. The bismuth has a low melting point (271.3°C) and in the molten, it is one of the metals, which display the lowest surface tensions (376 N/m), such characteristics favors the reduction of the surface tension of the zinc bath by the presence of bismuth in it [8, 13, 14, 15].

The surface tension reduction of the bath promoted by the bismuth enables a higher zinc drainage during the pulling out of the part from off the galvanizing kettle, what can shorten the thickness of the eta phase (η) coating layer. The combined effect of bismuth and lead in the bath can bring about better results [14].

In a laboratorial essay in which hot rolled steel sheets where galvanized, bismuth additions up to 1.00% to the bath decreased the coating thickness in average 18.29% in comparison to a bath without it; however, with a concentration of 2.00%, the reduction was less remarkable, being of 13.41%. The authors considered that the result could have been affected for some alteration of the galvanizing conditions and samples used. According to the authors, bismuth additions up to 2.00% did not altered the coating morphology, which was still composed of the four typical phases formed (gamma (γ) delta (δ), zeta (ζ) and eta (η)) [16].

However, the authors noticed in the micrographs taken, the presence of white dots in the upper part of the coating formed in the bath with a bismuth content above 1.00%. The white dots where seen in between the zeta (ζ) and outer eta (η) phases, likewise tiny inclusions. Through microanalysis, it was verified that such white dots were composed by pure bismuth. The bismuth was confined into the coating under the form of precipitates [16].

In another test performed in a pilot line, blackheart malleable cast iron samples were galvanized in twenty different zinc baths, each one composed of different combinations of the elements aluminum, nickel, tin and bismuth. It was verified that bismuth additions of 0.10% to the zinc bath interfered in the coating thickness, decreasing it. Nevertheless,

in the 0.06% bismuth bath, the coating formed was thick, with a higher amount of layers than the galvanized coatings formed in pure zinc baths and, around 17.40% larger than the ones attained in baths with 1.00% of lead addition [8].

Hence, the objective of this present study was to evaluate the influence of the different bismuth concentrations into the thickness and morphology of hot dip galvanized coatings, produced in an industrial line, employing a hot dip galvanizing kettle already containing a bath with a typical lead composition of 1%.

2 MATERIALS AND METHODS

Carbon steel angles manufactured according to ABNT NBR 7007 AR 415 and ASTM A572 G60 specifications were chosen as the research material. 110 angles with dimensions of 120x3x45mm and composition shown in Table 1, were pierced and cut off.

Elements	Concentration (%)
C	0,220
Mn	1,280
Si	0,260
P	0,016
S	0,023
Nb	0,002
Cu	0,190
Cr	0,060
Ni	0,050
Sn	0,025
Mo	0,006
V	0,022
Fe	Balance

Table 1 – Chemical composition of the samples.

The galvanization of the samples was performed in an industrial line of a steel industry specialized in the production of transmission towers. The hot dip galvanizing kettle had a 226-ton capacity of zinc (Figure 1).



Figure 1 – Hot dip galvanizing kettle used in the galvanization of the samples.

The zinc added to the kettle had a minimum purity of 99.99%. The kettle received small weekly additions of zinc-aluminum alloy 5.00% in order to improve the brightness of the galvanized part. It also had a lead content of approximately 1.14% of the bath's composition, which was intended to make the dross removal easier. For testing purposes, an alloy containing bismuth was added to the molten zinc bath. The alloy composition is displayed in Table 2.

Elements	Min (%)	Max (%)
Zn	97,800	100
Pb	-	0,020
Cd	-	0,003
Fe	-	0,005
Sn	-	0,005
Cu	-	0,003
Al	0,005	0,015
Bi	1,850	2,150

Table 2: Chemical composition of the zinc-bismuth alloy.

The essays and analysis carried out in this study were performed for ten different bath concentrations of bismuth, accordingly with Table 3.

Zinc Bath	1	2	3	4	5	6	7	8	9	10
ppm Bi	0	156	255	386	610	616	660	837	1030	1060

Table 3: Bismuth content variation of the ten baths analyzed.

The concentration of bismuth and other elements of the bath were confirmed through optical emission spectrometry (OES) analysis. The OES results shown in Table 4 corresponds to the average of three sampling measurements taken from the bath. Each sample was identified by the bismuth content of the hot dip galvanizing bath in which it was extracted.

Sample	Name	Cd%	Cu%	Fe%	Pb%	Ni%	Bi%	Al%	Zn%
1	0ppmBi	0,0004	0,0176	0,0300	1,0800	0,0007	<0,0010	<0,0010	98,8700
2	156ppmBi	0,0004	0,0171	0,0200	1,1500	0,0007	0,0156	<0,0010	98,8100
3	255ppmBi	0,0004	0,0173	0,0250	1,1300	0,0010	0,0255	<0,0010	98,8009
4	386ppmBi	0,0005	0,0176	0,0200	1,1200	0,0010	0,0386	<0,0010	98,8400
5	610ppmBi	0,0006	0,0175	0,0287	1,1200	0,0010	0,0610	<0,0010	98,8312
6	616ppmBi	0,0006	0,0170	0,0245	1,1000	0,0010	0,0616	<0,0010	98,8600
7	660ppmBi	0,0006	0,0172	0,0250	1,1000	0,0010	0,0660	<0,0010	98,8552
8	837ppmBi	0,0006	0,0169	0,0279	1,0500	0,0010	0,0837	<0,0010	98,9026
9	1030ppmBi	0,0005	0,0166	0,0267	1,0300	0,0010	0,1030	<0,0010	98,9242
10	1160ppmBi	0,0005	0,0164	0,0302	1,0700	0,0010	0,1160	<0,0010	98,8809

Table 4: Element content confirmation of the of the ten zinc baths studied.

The samples were galvanized accordingly to the usual process conditions of the hot dip galvanization plant. To each bath composition, eleven samples were galvanized. They were hooked into a steel holder and, moved with the assistance of a crane. The same conditions were held to all samples. Before the dipping into the molten zinc bath, the samples had their surfaces prepared.

The pretreatment of the samples began with a simultaneous degreasing/pickling bath with 15% of hydrochloric acid content under environment temperature for 15 minutes. After the degreasing/pickling step, the samples were sent to a washing tank where they were washed and afterwards conducted to another tank with flux, which contained a mixture of zinc chloride and ammonium chloride solutions around 60°C. The samples were kept soaked into the flux for 5 minutes. After fluxing, the samples were fixed into a transmission chain and were preheated in a drying tunnel at 70°C. After dried, they were immersed into the galvanizing kettle for 3 minutes in a temperature range of 448°C to 450°C.

Once immersed into the molten bath, the samples did not undergo any vibration. After that, they followed to a cooling bath containing a chromate based passivating solution and, stayed there for 2 minutes. Subsequently they were left to cool down at environment temperature.

The layer average thickness measurements of the samples, were attained throughout the treatment of the images, taken by scanning electron microscopy (SEM), with the Fiji/ImageJ software. With the Fiji/ImageJ software, the measurements of layer thickness were taken along the coating's transversal section and, were considered as the average of 20 measurements equally distributed. The measurements were focused on the total coating and eta phase (η) thickness, because, according to the literature, the eta phase would be,

In addition, with all images obtained by SEM analysis, it was not possible to visualize the phases present in the coating, as well as their morphologies, with an amplification between 2100 to 2400 times.

3 RESULTS AND DISCUSSION

The SEM image of the 0ppmBi sample is shown in Figure 2. For comparison purposes, it was considered as reference to the other samples with different bismuth concentrations. In Figure 2 it was possible to notice a typical galvanized coating, with the presence of the four stratified phases arising outwards from the steel surface. The shape of the phases was evident, enabling the phases to be easily distinguished. The first thin layer nearest to the steel's surface was possibly made of gamma (γ) phase. The next thicker layer, with a columnar morphology refers to delta phase (δ). The following phase, the thickest one, with long and large columns ending up in a needle like shape into the zinc bulk, is possibly zeta phase (ζ) and, the outermost layer, could be eta (η). The eta phase (η) had 13.13 μm of average thickness, sharing 16.60% of the total coating thickness.

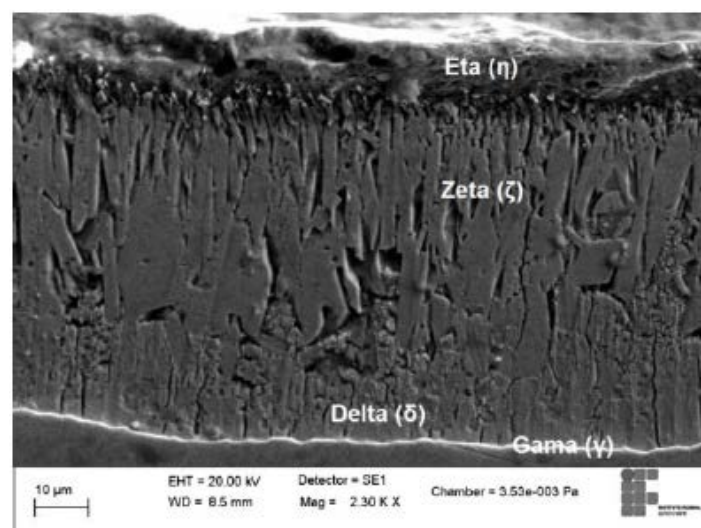


Figure 2: SEM image of the 0ppmBi sample coating with a 2300X amplification.

In the 156ppmBi, 255ppmBi e 386ppmBi samples, it was also possible to notice the presence of the four typical phases formed in hot dip galvanized coatings. In addition to that, a slight intermetallic phase's compaction along with an expressive thickness reduction of the eta phase (η) were observed. Such effects were remarkably manifested by the 386ppmBi sample, as can be seen in Figure 3. The total average thickness of the coating was 66.69 μ m and, the eta phase's (η) 6.44 μ m, representing 9.66% of the total coating thickness. The thickness reduction of sample 386ppmBi's coating was of 15.69% in comparison with the 0ppmBi sample.

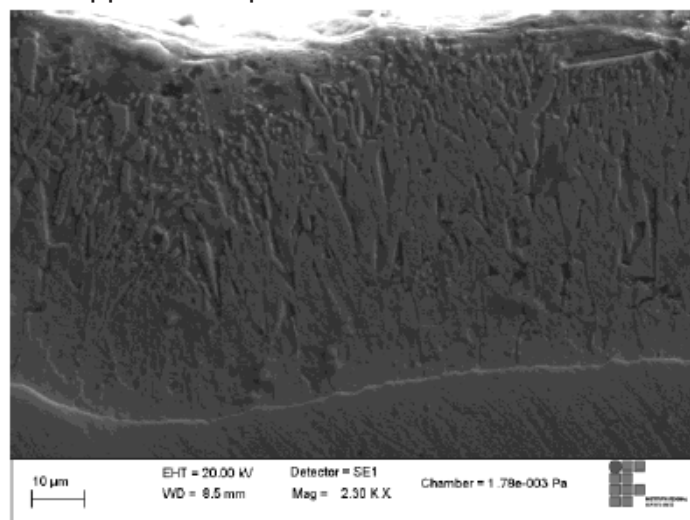


Figure 3: SEM image of the 386ppmBi sample coating with a 2300X amplification.

The 386ppmBi sample displayed a more compacter delta phase than the 0ppmBi sample. The zeta phase (ζ) exhibited short length and large width columns ending up in the eta phase (η) interface in a thin needle like shape with tiny crystals immersed into the eta phase (η) bulk. The eta phase (η) was depicted in good definition and 49.00% thinner. The bismuth possible decreased the superficial tension of the bath, facilitating the molten zinc drainage during the pulling out of the part from of the kettle, which lead to a smaller thickness of the most external coating phase, agreeing with the literature results [12, 14]. Also, the combined effect of lead-bismuth could have intensified the molten zinc drainage, even for those concentrations with low bismuth content [14]. However, the effect of reduction of the layer average thickness, as well as the formation of a typical layer structure were not kept with the bismuth concentration increasing. The 610ppmBi, 616ppmBi and 660ppmBi samples did not displayed the characteristic coating features. The most noticeable changes were behold by the 616ppmBi sample, which can be seen in Figure 4.

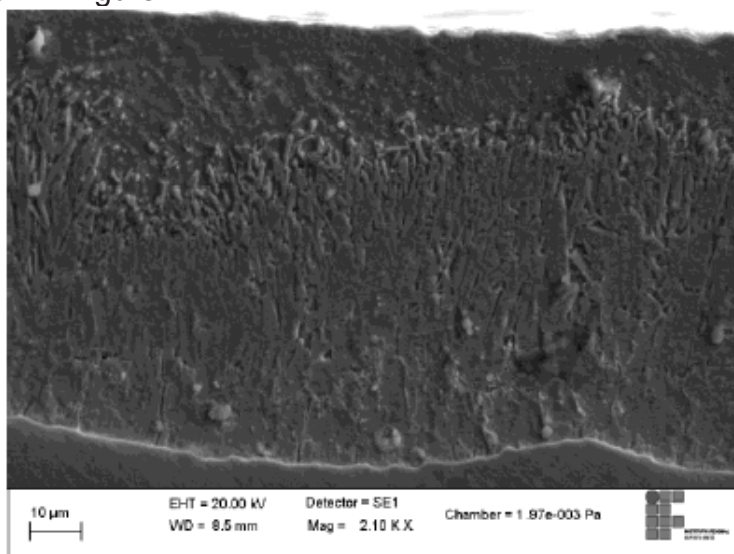


Figure 4: SEM image of the 616ppmBi sample coating with a 2100X amplification.

The delta phase (δ) was shown excessively thin, or virtually nonexistent and without definition with the zeta phase (ζ). There was not any remarkable columnar growing apparent on the zeta phase (ζ). It was thick with its outer limits highly fragmented with several small crystals scattered into the eta phase (η). The eta phase (η) was thick and easily discernable to the zeta phase (ζ). In those concentrations, it was noticed tiny light-colored fragments trapped inside the eta phase (η). Such fragments are uncommon in typical bismuth free coatings. Accordingly to the literature, bismuth concentrations up to 2.00% do not modify the coating morphology, allowing the formation of the typical four-phase structure [16]. Nevertheless, in the industrial test performed in this study, concentrations of around 600ppm produced irregular coatings, without clear definition between intermetallic phases.

The total average thickness of the 616ppmBi sample coating was 85.42 μ m, 7.99% thicker than the 0ppmBi sample coating. The eta phase (η) showed average thickness of 19.21 μ m, which represented a sharing of 22.49% of the total coating thickness. It was similarly verified in the literature, that a coating formed into a 0.006% bismuth bath exhibit considerably higher thickness in comparison with a coating galvanized into a 1.00% lead bath. The reason for such behavior was not found, however, a deeper study might be able to explain the reason of the bismuth concentration effect on the bath previously mentioned [8].

Analyzing the sample coatings with bismuth content above 837ppmBi, could be noticed the reappearance of the of the typical coating morphology, showing well distinguishable phases domain, even though, with an eta phase (η) extremely thick, as can be seen in the SEM image of the sample 1030ppmBi coating, shown in Figure 5. The average coating thickness of the eta phase (η) was 15.22 μ m, which represented 22.76% of the coating total thickness. The intermetallic layers were compacted.

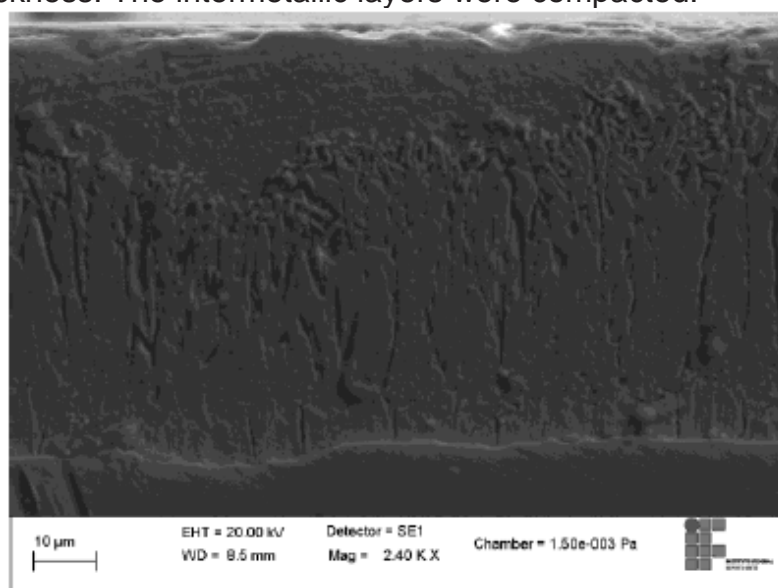


Figure 5: SEM image of the 1030ppmBi sample coating with a 2400X amplification.

The delta phase (δ) exhibited thin morphology with well-defined columnar shape, being clearly discernible from the zeta phase (ζ). The zeta phase (ζ) presented large length and short width columns meeting the eta phase (η) interface in a needle-like shape with small crystals scattered over it. The eta phase (η) was considerable thick and well defined in the region of interface with the zeta phase (ζ). It was also noticed an increase of the light-colored fragments and white dots dispersed into the bulk of the outmost phase of the coating, as depicted in Figure 6. In which some fragments were circled in eta phase (η) amplification of the 1030ppmBi sample.

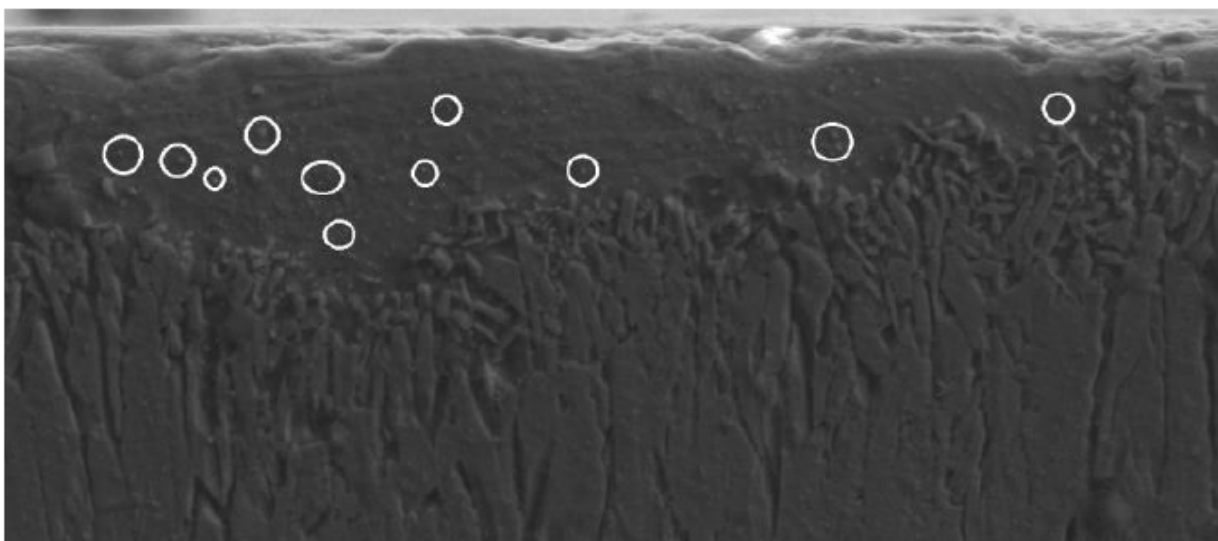


Figure 6: Eta phase (η) amplification of the 1030ppmBi sample coating.

The behavior found agreed with the one described in the literature, in which analyzing coatings containing bismuth, there was observed the presence of light-colored fragments into the eta phase (η), which were confirmed being composed basically by bismuth [16]. Thus, the white dots found in the coatings with bismuth content above 600ppmBi investigated in this study, were probably bismuth fragments.

In order to better visualize the influence of bismuth in the coating thickness, the average thicknesses of all samples analyzed in this study were plotted in Figure 7. All samples fulfilled the minimum thickness requisitions required by the standards [6 7].

The sum of the blue and red columns represent the coating total average thickness to each sample and, the percentage describe shows how much the eta phase (η) (red) and the intermetallic phases gamma (γ), delta (δ) and zeta (ζ) (blue) shares the total average thickness of the coating.

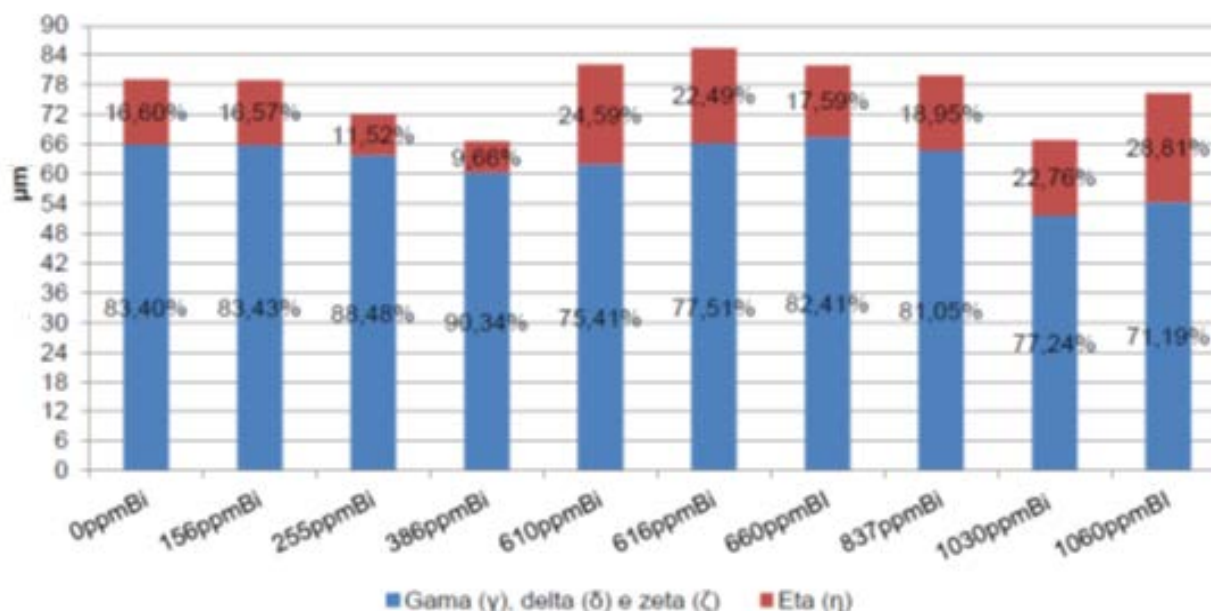


Figure 7: Coating average thickness of each sample.

4 CONCLUSION

It was confirmed that when bismuth is added into a hot dip galvanizing bath of an industrial line, it influences the thickness and morphology of the coating. Moreover, it was not observed any pattern behavior associated with the increasing of bismuth concentration in the bath. Up to the concentration of 386 ppmBi in the molten zinc kettle, the bismuth reduced the coating thickness, being the eta phase (η) reduction expressive, also, it was noticed the formation of a typical four-phase coating structure, being these four phases gamma (γ), delta (δ), zeta (ζ) e eta (η). Between the 610ppmBi and 660ppmBi bath concentrations, it was not clear the formation of the coating intermetallic phases. The bismuth started to interfere into the phase growing, making them thick and, additionally influenced the external eta phase (η). A deeper study could explain the reason why such concentrations of bismuth contribute to the achievement of anomalous coatings.

In concentrations above 837ppmBi, the external phase acquired was even thicker, however, the compacting of the intermetallic phases were very significantly, leading to a reduction of the total average thickness of the coating. It was noticeable the reappearance of the four-phase typical coating. Also, in the highest bismuth concentrations, it was seen several fragments into the coating eta phase (η), which possibly were bismuth under the form of inclusions.

4 REFERENCES

- 1 - Pannoni, FD. Princípios da Galvanização a Fogo. 2010 [acesso em 02 abr.2014]. Disponível em: <http://www.ztec.ind.br/pdf/principios/principios.pdf>.
- 2 - ABM – Associação Brasileira de Metais. Zincagem por imersão a quente. São Paulo: AMB, 1976.
- 3 - Rodrigues, JS. Estudo da Corrosão de Revestimentos de Zinco-Ligas Obtidos por Imersão a Quente Sobre Aços Baixo-Carbono. Dissertação (Mestrado em Engenharia) – Departamento de Metalurgia da Escola de Engenharia da Universidade Federal do Rio Grande do Sul, Porto Alegre, 2011.
- 4 - Associação Brasileira de Normas Técnicas. NBR 7414: Galvanização de produtos de aço ou ferro fundido por Imersão a quente – Terminologia. Rio de Janeiro, 2009.
- 5 - ICZ – Instituto de Metais Não Ferrosos. Galvanização por imersão a quente por processo contínuo versus galvanização geral (batelada). São Paulo, 2011.
- 6 - American Society for Testing and Materials. ASTM A123/A123M – 13: Standard Specification for Zinc (Hot-Dip Galvanized) Coatings on Iron and Steel Products. Estados Unidos, 2012.
- 7 - Associação Brasileira de Normas Técnicas. NBR 6323: Galvanização de produtos de aço ou ferro fundido – especificação. Rio de Janeiro, 2007.
- 8 - Lima, G. Influência da Adição de Diferentes Concentrações de Bismuto, Níquel, Estanho e Alumínio sobre a Espessura da Camada, Resistência à Corrosão e Brilho nos Revestimentos Galvanizados. 2007. Dissertação (Mestrado em Ciência e Engenharia de Materiais) – Centro de Ciências Tecnológicas da Universidade do Estado de Santa Catarina, Joinville, 2007.
- 9 - ICZ – Instituto de Metais Não Ferrosos. Guia de Galvanização por Imersão a Quente. ICZ: São Paulo, 2010.
- 10 - Sobrinho, PS. Vantagens do aço com maior vida útil. Siderurgia Brasil, São Paulo, ano 14, n.92, p. 40-41, 2013.
- 11 - Li, Z.; Su, X.; He, Y. 450°C isothermal section of the zn-fe-bi ternary phase diagram. Journal of Alloys and Compounds.v.462, p. 320-327, 2008.
- 12 - Fratesi, R.; Ruffini, N.; Malavolta, M. Contemporary use of Ni and Bi in hot dip galvanizing. Surface & Coatings Technology, v.157, p. 34-39, 2002.
- 13 - Aso, A.; Knewitz, F.; Martins, V. Influência do bismuto nas propriedades mecânicas do aço rápido AISI M2 sinterizado. Estudos Tecnológicos, v.5, n. 3, p. 421-430, 2009
- 14 - Gagné, M. Hot-dip galvanizing with zinc-bismuth alloys: after-fabrication. The Bulletin of the Bismuth Institute.v.72, 1998.
- 15 - Beguin, P; Bosschaerts, M; Dhaussy, D. Galveco: a solution for galvanizing reactive steel. The Bulletin of the Bismuth Institute.v.76, 2000.
- 16 - Pistofidis, N; Vourlias, G; Konidaris, S.The effect of bismuth on the structure of zinc hot-dip galvanized coatings. Materials Letters, v. 61, p. 994-997, 2006.

Lead-free and bismuth-containing zinc melts and kettles in hot-dip galvanizing

Jürgen Triebert*, Theresa Klein, Steffen Six
all Institut für Korrosionsschutz Dresden GmbH

*Project manager and contact

Summary

For many decades lead was used as a common alloying additive in hot-dip galvanizing at concentrations of 0.3 – 1.2 wt-% Pb for the reduction of the surface tension of the liquid zinc. However, lead and its chemical combinations are EU-classified as hazardous for health, toxic for reproduction and hazardous to the aquatic environment. A research project at IKS Dresden investigates the possibility of substitution of lead in zinc melts by bismuth. Bismuth and its chemical combinations are not hazardous for health or for the environment. Bismuth causes a much stronger decrease of the surface tension of the liquid zinc bath than lead. Compared to lead, a much lower concentration of bismuth is necessary in zinc melts. But in literature bismuth or rather bismuth in combination with tin is suspected to cause a faster attack on the intermetallic phases of iron and zinc on the kettle wall.

Within the research project several comprehensive long-term dipping tests were performed in a small zinc kettle at IKS Dresden (30 kg Zn) with different amounts of bismuth in zinc baths over a period of 6 - 14 weeks, respectively. The results clearly show that bismuth in zinc melts at concentrations of 0.15 to 4.5 wt-% Bi does not cause a faster attack on the intermetallic phases of iron and zinc on the kettle wall or on the steel of the kettle wall itself. Compared to lead-containing zinc melts bismuth even leads to an additional stabilisation of the intermetallic phases on the kettle wall.

In the tested lead-free and bismuth-containing zinc melts the achievable kettle service life should be comparable or higher than in previous conventional, lead-containing zinc baths. In the case of severe dosing mistakes during subsequent alloying of the zinc melt with Bi master alloys or pure Bi, as a result of which layers containing more bismuth are formed on the bottom of the kettle, the performed dipping tests show that at least in a period of approx. 10 weeks up to a Bi concentration of 4.5 wt-% (in regard to one test even > 60 wt-% Bi) no damage of the protective alloy phases occur on the kettle wall. The bismuth-containing zinc baths examined during the research project, thus, enable a secure (kettle breakthrough) and durable (kettle service life) hot-dip galvanizing process without the necessity of using lead.

Hot-dip galvanized steel sheets from lead-free zinc baths with bismuth concentrations of 0.15 and 0.25 wt-% Bi showed a very good appearance, a high adhesion and a very high mechanical resistance of the zinc coating at conventional film thicknesses.

Paper

For many decades lead was used as a common alloying additive in hot-dip galvanizing at concentrations of 0.3 – 1.2 wt-% Pb. The addition of lead has the following effects /1/:

- Reduction of the surface tension of the liquid zinc for the improvement of wetting of the dipped steel constructions (good results in hot-dip galvanizing)
- Protection of the kettle bottom by a liquid lead sump
- Simplified removal of dross from the kettle bottom.

However, lead and its chemical combinations are EU-classified as hazardous for health, toxic for reproduction and hazardous to the aquatic environment /2; 3/. Lead enriches on the surface of zinc coatings on steel

constructions with up to 5 wt-% Pb. During weathering of the zinc coatings lead combinations can be released into the environment.

An ongoing data collection by the German industry association Feuerverzinken e.V. /4/ for Germany showed, that for several years an increasing number of plants reduce the lead content in their melts:

2012

- Approx. 53 % of the German hot-dip galvanizing plants have a lead content of less than 0.3 wt-% in their melts, 47 % operate with a lead content of > 0.3 wt-%

2015

- Approx. 62 % of the German hot-dip galvanizing plants already operate with a lead content of less than 0.3 wt-% in their melts
- Approx. 20 % of the German hot-dip galvanizing plants reduced the lead content in their melts even under 0.03 wt-% by now.

The motivations for that are reasons of work safety and environmental protection. The following alternatives exist in regard to hot-dip galvanizing using lead-containing zinc melts:

1. Hot-dip galvanizing in lead-free and utterly unalloyed zinc melts (max. 0.06 % Ni and little Al) at respectively high surface tension of the zinc bath:
 - Poorer wetting of the parts to be galvanized, in case of difficult surface/surface preparation (roughness, mill scale residues...) possible galvanizing problems
 - Significantly higher efforts for the pre-treatment of the parts to be galvanized (degreasing, pickling, flux treatment)
2. Hot-dip galvanizing in a zinc melt alloyed with bismuth (Bi) as substitution for lead for comparably good wetting and covering of the parts to be galvanized; bismuth reduces the surface tension of liquid zinc approx. 4 to 5 times more effectively than lead /1/. Bismuth as well as its compounds are non-toxic, non-toxic for reproduction and not hazardous for the environment. The higher raw-material price for Bi or Bi master alloys compared to Pb (currently approx. factor 4.5 to 5) compensates by the significantly lower amount of Bi required for comparable zinc melts (approx. factor 4 to 5).

Until now, however, the following concerns/insecurities and restrictions using bismuth in zinc melts apply:

- Bismuth, in higher concentrations, promotes liquid metal embrittlement (LME), this, however, also applies for lead in higher concentrations. Thus, in the DAST guideline 022 for the hot-dip galvanizing of load-bearing building components the Bi content in zinc melts of zinc bath class 1 is limited to a maximum of 0.15 wt-% of Bi.
- Based on processing cases of damage in regard to several kettle breakthroughs the IKS proposed the theory /1/, that Bi-containing and/or Bi- and Sn-containing zinc melts attack the protective alloy phases of the zinc kettles (esp. the δ_1 -phase). They also decompose them and, consequently, can lead to increased steel ablation rates or reduced kettle service life or, in extreme cases, to kettle breakthroughs. The following figures illustrate this correlation.

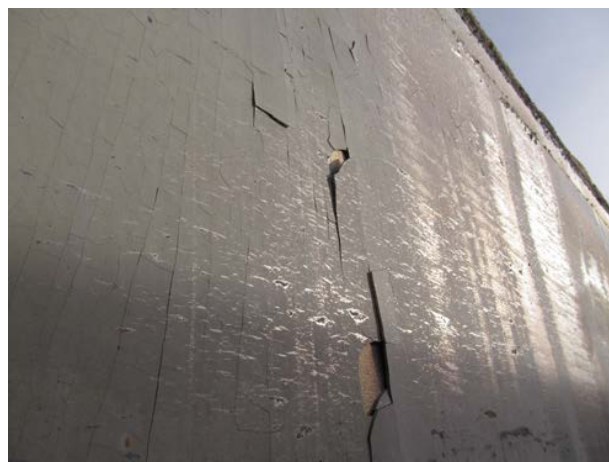


Figure 1: Discarded kettle after 10 years of operation; the Fe-Zn-alloy phases formed on the kettle wall, which protect the steel from the zinc melt, crack during cooling due to different coefficients of expansion of steel and hard zinc

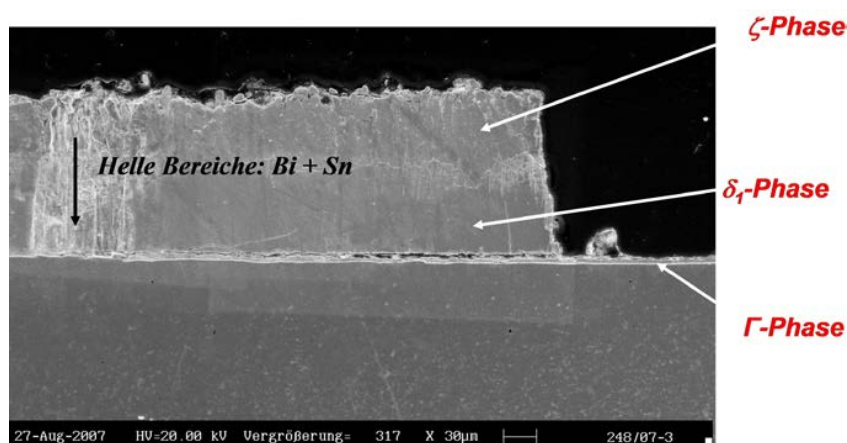


Figure 2: Bi and Sn (bright-coloured areas in the SEM image of the cross-section) from the melt of a kettle breakthrough with approx. 0,1% Bi and 1,0% Sn obviously attacked the Fe-Zn alloy phases of the kettle wall and led to its delamination /1/

Operating with lead-containing zinc melts, so far, normally results in a kettle service life between 6 to 10 years. The assumption, that Bi-containing and/or Bi- and Sn-containing zinc melts could attack the kettle walls of the steel kettles and significantly decrease their durability, resulted in a great uncertainty regarding the substitution of lead by bismuth in the hot-dip galvanization plants. A research project at IKS Dresden investigates the possibility of substitution of lead in zinc melts by bismuth. The objective of this research project is the development of a hot-dip galvanization method, which provides sufficient kettle service life for batch galvanizing in low-lead or lead-free as well as bismuth-containing zinc melts in steel kettles. The project should contain the following aspects:

- As much as possible, complete elimination of lead from the zinc melts and substitution by the non-toxic bismuth being unhazardous to the environment
- However, simultaneous guarantee of sufficient kettle service life with Pb-free and Bi-containing zinc melts.

Consequently, the central question of the research project is:

- Does bismuth, at least in higher concentrations (dosing mistakes, layer-formation in the kettle), really

attack the alloy layers of the galvanizing kettles and decreases their service life or does Bi increase the danger of kettle breakthroughs?

Within the research project several comprehensive long-term dipping tests were performed in a small zinc kettle at IKS Dresden (30 kg Zn) with different amounts of bismuth in zinc baths over a period of 6 - 14 weeks, respectively.



Figure 3: IKS Dresden hot-dip galvanizing kettle with control unit

The used steel test specimens ($90 \times 25 \times 10 \pm 0,05$ mm) have been prepared from components of real galvanizing kettle walls. They have been removed from discarded, large galvanizing kettles during kettle replacements (see figure 4). The kettle steels have been exactly characterized metallographically and analytically. In each case this was low-silicon steel with almost identical composition.

For the determination of the exact steel ablation rates in the dipping tests the dimensions of the steel test specimens, prepared with very low tolerances, were precisely measured prior to and after exposure in the different zinc melts by means of a calibrated digital calliper. For this, first, the formed zinc coatings were completely stripped after the dipping tests using urotropin-inhibited, 16% hydrochloric acid in accordance with DIN EN ISO 1460. Figure 5 shows the respective test specimens after the dipping tests.



Figure 4: One of the four galvanizing kettles, from which samples were taken for the research project. The arrow indicates one of the sampling locations in this kettle



Figure 5: Test specimens after a long-term dipping test in a zinc melt: Test specimens left with zinc coating, test specimens right after stripping of the coating with inhibited HCl for measuring (determination of thickness)

Test parameters for the long-term dipping tests:

- Use of a conventional Pb-containing reference zinc melt (0.8 wt-% Pb, Bi-free)
- Use of several lead-free zinc baths with different Bi-contents
- Dipping duration 6 to 14 weeks in each case
- Removal of two test specimens after 2, 4, 6, 10 and, if applicable, 14 weeks in each case
- Temperature of the zinc melt: $475 \pm 2^\circ\text{C}$ constant; continuous in-situ measurement/recording by means of two separate thermal elements in the zinc melt and additionally 2 x weekly by means of a calibrated external temperature sensor/measuring device
- Constant maintenance of the zinc bath/test specimens:
 - 2 to 3 x per week hard zinc removal and moving of the test specimens in the melt
 - In an interval of 1 to 2 weeks additional dosing of zinc and, if necessary, also of Bi, Pb and Ni (depending on the analysis of the melt)
 - In an interval of approx. 2 to 3 weeks melt analyses
- Composition of the zinc melts:
In general, the following were used:
 - High-purity zinc SHG 99,995% Zn
 - Fe-saturated zinc melts (Fe around 0.05 wt-%), Al-free
 - 0.05 wt-% Ni for the reduction of the film thickness in the sandelin and sebisty range
 - In regard to bismuth, to some extent, also significantly higher concentrations were used than would be regularly done in real zinc baths. This way the effect of possible severe dosing mistakes was to be simulated. Since it consistently occurs that galvanizing plants do not use the lead or bismuth master alloys for the make-up of the melt due to cost-saving reasons but use the pure metals, local overdosing of Bi is an important aspect to be absolutely considered in regard to the kettle service life.

Table 1: Composition of the zinc melts used in the research project, all in wt-%

Zinc bath	Bi	Pb	Fe	Ni
Reference	-	0,8	saturated (approx. 0,05)	0,05
Bismuth 0,15 (DASSt 022)	0,15	-	saturated (approx. 0,05)	0,05
Bismuth 0,25	0,25	-	saturated (approx. 0,05)	0,05
Bismuth 1,5	1,5	-	saturated (approx. 0,05)	0,05
Bismuth 4,5 (saturated with Bi-ump)	4,5	-	saturated (approx. 0,05)	0,05
Bismuth 0,15 + pure Bi in an alcove of the specimen	60 - 100	-	saturated (approx. 0,05)	0,05

Results of the research project

Figure 6, as an example, shows three typical developments for the determined steel ablation rates, on the one hand in a conventional, lead-containing and bismuth-free zinc melt with 0.8 wt-% Pb and 0.05 wt-% Ni, and on the other hand in Bi-containing and lead-free zinc melts.

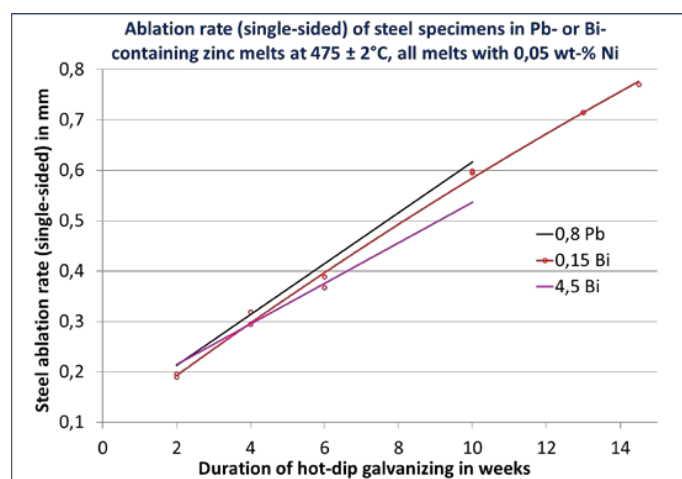


Figure 6: Ablation rate of the steel specimens in Pb- or Bi-containing zinc melts at 475 ± 2°C; the curves of steel in zinc melts with 0.25 % Bi and 1.5 % Bi (not shown here) range between the curves at 0.8 % Pb and 4.5 % Bi

The dipping tests, performed over several weeks in each case, in differently alloyed zinc melts clearly show that lead-free, Bi-alloyed zinc melts do not lead to higher steel ablation on the kettle walls than conventional, lead-containing and Bi-free zinc baths. The tendency is even towards lower steel ablation rates and, thus, longer kettle service life for Bi-containing zinc melts. This result, initially, contradicts the basic assumptions of the present research project, however, it shows that purely Bi-containing melts are uncritical in regard to kettle service life. This provides security when using such innovative, Bi-containing melts as substitution for conventional zinc baths with Pb.

After exposure of the test specimens during the dipping test, metallographic cross-section were prepared and examined in regard to the thickness of the formed Fe-Zn alloy layers using a light microscope. The formation of the Fe-Zn alloy phases on the steel is crucial for the protection of the zinc kettle from attacks by the zinc melt. The examinations show that the film thicknesses of the formed Fe-Zn alloy phases (see Table 2 and Figure 7) correlate exactly with the determined steel ablation rates (Figure 6). The higher the Bi content of the melt is, the higher are the film thicknesses of the protective inter-metallic phases Γ , Γ_1 and δ_1 on the steel as well. The thicknesses of these layers in the Pb-containing, Bi-free reference melt with 0.8 % Pb are significantly lower in each case after identical periods of exposure.

Table 2: Mean values of the thicknesses of the different Fe-Zn alloy phases, which formed on the test specimens in different zinc melts after different dipping periods, determined in the metallographic cross-section by means of a light microscope, all given in μm

Schmelze		0,8 Pb			
Legierungsphase		2 Wo	4 Wo	6 Wo	10 Wo
Γ		x	3	3	2
Γ_1		8	9	10	10
δ_1		1946	2165	2660	2826
ζ		68	62	74	82
Summe		2024	2239	2746	2920

Schmelze		0,25 Bi		
Legierungsphase		2 Wo	4 Wo	6 Wo
Γ		x	3	2
Γ_1		7	10	7
δ_1		1949	2404	2693
ζ		65	71	83
Summe		2021	2488	2785

Schmelze		4,5 Bi				Bi-Sumpf
Legierungsphase		2 Wo	4 Wo	6 Wo	10 Wo	4 Wo Zn + 2 Wo Sumpf
Γ		2	2	3	4	4
Γ_1		8	8	8	11	13
δ_1		2015	2764	3210	3857	3664
ζ		75	93	105	106	195
Summe		2100	2867	3326	3977	3875

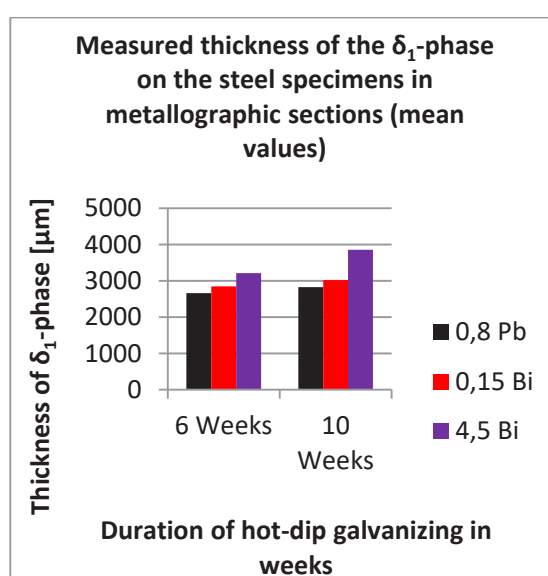


Figure 7: Thickness of the δ_1 -phase on the steel specimens after exposure in different zinc melts at $475 \pm 2^\circ\text{C}$; the δ_1 -phase protects the steel

The imaginable worst case using bismuth-containing zinc melts are severe dosing mistakes and the occurrence of layer formation in the zinc kettle when using pure Bi-metal for subsequent alloying of the zinc melts. The IKS does not recommend this type of subsequent alloying instead of using master alloys explicitly, however, some galvanizing plants practice it. In order to examine such a case, in two tests the effect of very high bismuth concentrations on the already formed Fe-Zn alloy layers of steel test specimens in zinc melts is investigated. In the first test steel test specimens have been exposed for 4 weeks in a Bi-saturated melt with 4.5 wt-% Bi, featuring a bismuth sump on the bottom of the kettle, for the formation of the alloy phases. Subsequently, the test specimens have been lowered into the Bi sump on the bottom of the kettle (> 60 wt-% Bi) for two weeks. After removal, these test specimens showed neither higher ablation rates than the reference test specimens in the lead-containing, bismuth-free melt, nor any damage of the alloy phases in the metallographic cross-section. In the second test the test piece prepared from low-silicon steel, shown in Figure 8, has been galvanized at $475 \pm 2^\circ\text{C}$ in a bismuth-containing melt, in accordance with DAST guideline 022, with 0.15 % Bi and 0.05 % Ni for 6 weeks for the formation of the alloy layers. Subsequently, pure Bi-metal was dosed into the alcove of the test specimen without entirely removing the test specimen from the melt (avoiding of crack formation in the alloy layers). After another 3 weeks of exposure to pure Bi in the inside at $475 \pm 2^\circ\text{C}$ the test specimen was removed, immediately emptied and quenched in water in order to largely inhibit any reactions after removing. Subsequently, the alloy phases inside the alcove and on the outside of the test specimen were analysed metallographically.



Figure 8: Test specimen for a test with pure bismuth in the alcove

During the light-microscopic and SEM/EDX examination of the respective metallographic cross-sections of this test the following was detected:

- On the inside of the test specimen, in the alcove, filled with 100 wt-% Bi significantly thicker Γ -, Γ_1 - and δ_1 -phases were detectable at the end of the test, than on the outside of the test specimen, which was merely exposed to the normal zinc melt with 0.15 % Bi
- The thickness of the protective δ_1 -phase (EDX line-scan analysis: 7 to 12% Fe) on the inside of the test specimen (in the alcove) was determined to be approx. 4000 μm
- In none of the different metallographic cross-sections of the inside and outside of the test specimen accumulations of bismuth in the δ_1 -phase or close to the steel (Γ -phases or interfaces between steel and Γ -phase or between Γ_1 - and δ_1 -phase, respectively) were found, the structure of the formed alloy layers was undisturbed and entirely normal
- In no location of the inner alcove area indications of a damage of Fe-Zn alloy phases, formed in the first 6 weeks in the zinc melt with 0,15 % Bi, caused by the pure bismuth were found.

Consequently, it appears to be confirmed that the range above the Zn-Bi miscibility gap of > 50 % in the zinc melt is relatively secure, at least in regard to the decrease of the wall thickness and for short-term periods. This

result, also, correlates with the results of the dipping tests and even supports them. However, the increased hazard to kettle wall steels caused by liquid metal embrittlement (LME) due to high bismuth concentrations shall be mentioned. Since kettles, however, nowadays are manufactured almost entirely strainlessly, this risk is limited to locations on the kettle in which e.g. the stabilization cylinders pressed into the sidewalls. This occurs mostly as a result of gas inclusions in building components and, thus, gas explosions in the kettle and wall expansions. The cylinders, however, are positioned mostly in centred height on the outside walls, but excessive Bi concentrations would accumulate on the bottom due to density. The hazard of LME on the kettle, consequently, is rather minor even for momentarily increased Bi-concentrations.

Additional dipping tests with cyclic temperature program

During the presentation of intermediate results at the 12th Korrosionsschutztag in Dresden 2016 hot-dip galvanizers noted that dipping tests at absolutely constant zinc bath temperatures do not sufficiently correspond to reality, since dipping of larger components/constructions coincides with significant temperature variations in the zinc melt. These cause thermal strains in the Fe-Zn alloy phases on the kettle wall. In addition, in reality occasionally occurs that due to powerfully heating burners after the drop of temperature (momentarily) the dangerous range between 490 - 530°C with high ablation rates is reached. This could also have influence on the structure and thickness of the protective alloy layers on the kettle walls. In two additional dipping tests with cyclic temperature program for the zinc melt and two differently alloyed melts it was attempted to accommodate this fact and to simulate the respective conditions. For this, the cyclic temperature program, illustrated in Figure 9, was used.

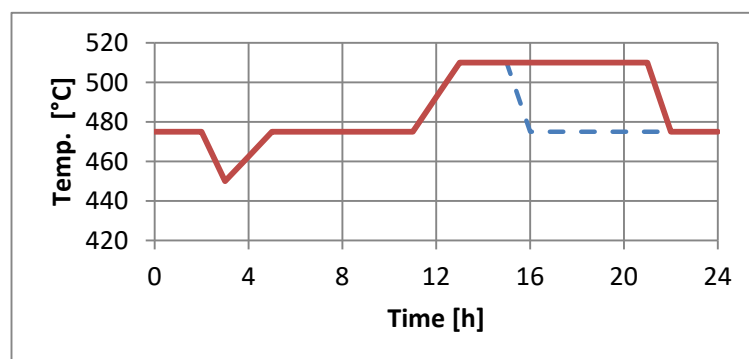


Figure 9: Cyclic temperature program for zinc melt over 24 h for two additional dipping tests

Again, the already described kettle steel test specimens were used. On the one hand they have been exposed in a conventional, lead-containing and bismuth-free zinc melt with 0.8 wt-% Pb and, on the other hand, in a lead-free, bismuth-containing zinc melt with 1.0 wt-% Bi for a period of 5 or 22 days (cycles), respectively. This test was evaluated gravimetrically by means of the weight loss of the test specimens after 5 or 22 days, respectively. After exposure, the zinc coatings of the test specimens were, again, first stripped using urotropin-inhibited hydrochloric acid. The weight loss was determined by means of a calibrated and adjusted analysis scale. The results are graphically illustrated in Figure 10.

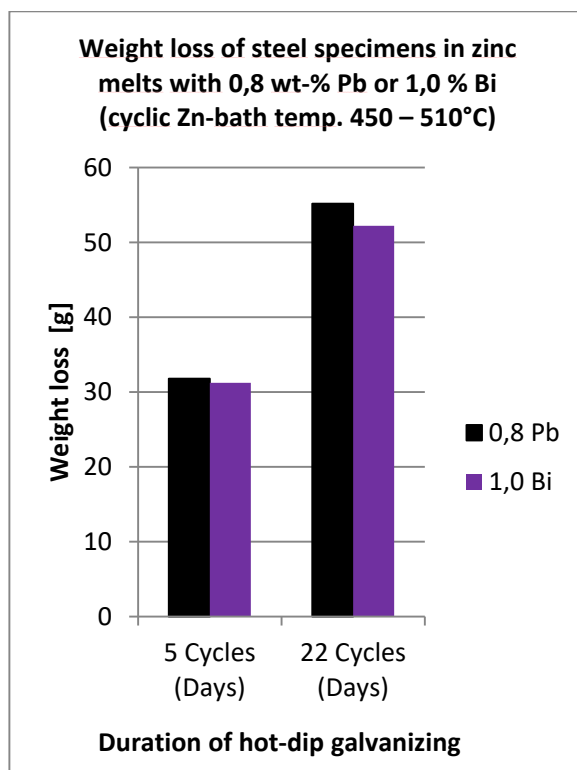


Figure 10: Results of both dipping tests with cyclic temperature program for the zinc melt

Even under these realistic conditions (great temperature variations in the zinc melt and significant excess of the limit of 490°C) the test specimens in the bismuth-containing zinc melt without lead showed slightly lower ablation rates than those test specimens in the lead-containing and bismuth-free reference melt. This also correlates again with the performed dipping tests. Bismuth-containing zinc melts, consequently, obviously do not lead to higher ablation rates on the kettle walls than conventional lead-containing zinc baths, even under great temperature variations in the zinc melt and while momentarily exceeding the 490°C limit.

Conclusion

- Bismuth is a suitable substitution for lead in zinc melts for hot-dip galvanizing.
- In contrast to lead bismuth does not form toxic compounds or compounds toxic to reproduction or is not, as metal, even classified in that respect, the lower dosing amount that is required (in regard to the surface tension of the zinc melt and the wetting/covering of the components to be galvanized) in comparison to lead compensates for its higher raw-material price.
- Bismuth in lead-free zinc melts with a concentration within the range of DAST guideline 022 ($\text{Bi} \leq 0.15$ wt-%) and also significantly above does not lead to increased kettle wall ablation rates and, thus, does not lead to decreased kettle service life or even to an increased danger of kettle wall breakthroughs.
- Bi-containing zinc melts (0.15 to 4.5 wt-% Bi) even show slightly lower steel ablation rates than conventional Pb-containing melts (0.8 wt-% Pb).
- The steel ablation rates determined during the dipping test correlate exactly with the film thicknesses of the formed Fe-Zn alloy layers on the test specimens, measured in the metallographic cross-section, which protect the steel substrate from attack by the zinc melt: The higher the Bi content of the melt, the higher the film thicknesses of the protective intermetallic phases Γ , Γ_1 and δ_1 on steel. The thicknesses

of these layers in the Pb-containing melt (0.8 wt-% Pb) are significantly lower in each case after identical periods of exposure.

- Quite probably tin in higher concentration is responsible for the kettle damages found in /1/ or the combined additional alloying of Sn + Bi or Sn + Pb.
- Sn + Bi as well as Sn + Pb form very low-melting eutectic compounds which can obviously penetrate and damage the Fe-Zn alloy phases.
- The critical Sn concentration for this is not known yet, so it is safer to refrain from adding Sn to Bi- or Pb-containing melts, or at least to operate below the limit of the DAST guideline 022 (≤ 0.1 wt-% Sn).
- The respective correlations between the kettle service life and the use of Sn-Bi- or Sn-Pb-alloyed zinc melts are to be subject of a planned follow-up project.

Table 3: Suitable compositions of zinc baths for secure and durable hot-dip galvanizing in the temperature range of 430 to 480°C

Alloy metal/ Type of zinc melt	Bi	Pb	Sn	Ni	Fe
Bi- and Pb- containing zinc melts	$\leq 0,15$ * $\leq 0,25$ **	0,1 - 1,15	$\leq 0,1$ * preferably tin- free	0,05 (0,00 - 0,06)	saturated (approx. 0,05)
Bi-containing and Pb-free zinc melts	$\leq 0,15$ * $\leq 0,25$ **	< 0,03	$\leq 0,1$ * preferably tin- free	0,05 (0,00 - 0,06)	saturated (approx. 0,05)

* Limit value in accordance with DAST guideline 022 (zinc bath class 1) for batch galvanizing of load-bearing building components

** For the reduction of the surface tension

In the zinc melts composed that way the achievable kettle service life should be comparable or higher than in previous conventional, lead-containing zinc baths. In the case of severe dosing mistakes during subsequent alloying of the zinc melt with Bi master alloys, as a result of which layers containing more bismuth are formed on the bottom of the kettle, the performed dipping tests show that at least in a period of approx. 10 weeks up to a Bi concentration of 4.5 wt-% (in regard to one test even > 60 wt-% Bi) no damage of the protective alloy phases occur on the kettle wall. The compositions of the zinc baths shown in Table 3, thus, enable a secure and durable (kettle service life) hot-dip galvanizing process without the necessity of using lead.

References

- /1/ Schulz, W.-D., Thiele, M. (2012) "Feuerverzinken von Stückgut", Leuze-Verlag, 2nd edition
- /2/ Regulation (EC) No 1272/2008 of the European Parliament and of the Council of 16 December 2008 on classification, labelling and packaging of substances and mixtures (CLP regulation)
- /3/ Meeting of the REACH committee on February 3/4, 2016 - Decision of the EU member states: Classification of lead in metallic form as toxic to reproduction category 1A (9. ATP of the CLP regulation)
- /4/ Personal information by the industrial association Feuerverzinken e.V.

Authors' Biography

Dr. Jürgen Triebert, born 1966, studied chemistry at the Technische Hochschule Leuna-Merseburg from 1987 to 1992 and earned his doctorate in 1997 at the Martin-Luther University Halle-Wittenberg. After working as head of laboratory in two different environment laboratories he is head of laboratory at the Institut für Korrosionsschutz Dresden GmbH since 2003 and is head of the Coatings and Analysis department since 2013. He is the manager of the research project and contact person for the presented subject.

Contact: Tel.: 0351 / 871-7118, E-Mail: juergen.triebert@iks-dresden.de

Dipl.-Ing. Theresa Klein, born 1990, has been working at the Institut für Korrosionsschutz Dresden GmbH (IKS) as a research assistant in the field of corrosion in water-bearing systems. In the context of her diploma thesis in chemical engineering at the TU Dresden she was previously involved in bringing into service the laboratory galvanization kettle at the IKS as well as in the tests regarding kettle service life during batch galvanizing.

Contact: Tel.: 0351 / 871-7116, E-Mail: theresa.klein@iks-dresden.de

Dipl.-Ing. Steffen Six, born 1965, studied manufacturing engineering at the TU Dresden from 1987 to 1992. After working at a planning office and as a research assistant at the TU Dresden in the field of mechanic joining technology for several years he has been working at the Institut für Korrosionsschutz Dresden GmbH as research assistant since 2011. During this time he handled different research projects in the field of hot-dip galvanizing. The focus of his research work is especially on layer-forming reactions from interactions of steel, zinc melts and technological boundary conditions.

Contact: Tel.: 0351 / 871-7120, E-Mail: steffen.six@iks-dresden.de

New Zinc-Aluminum-Magnesium Alloy Galvanizing Technology

Y Kiyokawa, Komagata Galvanizing Co LTD. (Japan)

Abstract

As Japan is surrounded by the sea, steel structures along the coastal areas are exposed by the sea-breeze and are severely corroded in a short period of time. In addition to this, in an area of heavy snowfall, a lot of anti-freeze agents which contains calcium chloride is sprayed on the road surface which makes the environment more and more corrosive. As a result, the maintenance cost of steel structures in this kind of area becomes very high. Zinc-aluminum alloy coating is well known as an excellent corrosion protector even in severe corrosive environments such as salt damage areas.

In Japan, some galvanizing plants produce zinc-aluminum alloy coating by using a two-bath system, but the efficiency is not satisfactory and the production is limited.

We developed new zinc-aluminum alloy galvanizing technology using a one-bath system. In this system, steel articles are dipped in to a special solution which contains aluminum powder after usual hot-dip galvanizing.

Zinc-aluminum alloy coating produced from this new technology results in excellent corrosion protection and the production cost is much lower than other methods.

This new technology was patented in Japan in 2016.

Introduction

JGA carried out the exposure test for 15 years to investigate the performance of zinc coating and zinc-aluminum alloy coating. The test samples were placed on the inspection passage of a bridge located approximately 200 m from the coast near the Itoigawa IC of the Hokuriku Expressway in Niigata Prefecture. This area is an extremely corrosive climate zone with intense seasonal winds from the sea in the winter. (Refer to Table 1.JGA news 76)

According to the results of the exposure tests conducted over the past 10 years, the general hot dip galvanized steel sheet is corroded with a weight of 465 g/m². On the other hand, it was found that the Zn-5%Al alloy galvanizing steel sheet is corroded with a weight of 141 g/m², and the Zn-5%Al-1%Mg alloy galvanizing steel sheet is corroded with a weight of 76 g/m².

These results indicate that the Zn-5%Al alloy galvanizing steel sheet has a three times higher corrosion resistance than the general hot dip galvanized steel sheet, and the Zn-5%Al-1%Mg alloy galvanizing steel sheet containing 1% Mg has twice the corrosion resistance. As a result, we obtained the result in which the corrosion resistance increased by about six times compared

to general hot dip galvanized steel sheets. It is worth mentioning that these results were confirmed in a severe corrosive environment.

In Japan, the two-bath-type Zn-Al alloy galvanizing technology was developed about 20 years ago, but this technology requires a conventional molten zinc bath and another Zn-Al alloy bath. For alloy baths, in particular, ceramic furnaces, which have excellent durability, are mainly used because conventional iron kettles are severely damaged in this kind of situation. However, the difficulty of changing equipment and the high investment cost for ceramic furnaces have been obstacles to spreading this technology.

We have studied the method of alloy coating by attaching metal powder immediately after withdrawing the article from the zinc bath in the galvanizing process. Although we initially attempted to attach Al powder, we proceeded to study the method of forming a Zn-Al-Mg alloy layer by also attaching Mg to produce a more corrosion-resistant alloy layer.

However, there were some problems.

One of the problems was the galvanizing temperature. Usually the galvanizing temperature for a small product is around 480°C to 500°C. But the melting points of Al and Mg are considerably higher, and it is hard to make alloy. In addition, there is a risk of ignition and explosion if we handle these powders at high temperatures and it makes extremely difficult to handle these fine metal powders.

Liquid projection Zn-Al-Mg

Figure 1 shows the three phase diagram of Zn, Al, and Mg.

The melting point of Zn is 419.58°C, Al is 660°C, and Mg is 650°C. On the other hand, when they are alloyed, the melting point of Al-Mg alloy decreases to 420°C, Zn-Al alloy to 400°C, Zn-Al-Mg alloy to 340°C, and Zn-Mg alloy to 340°C, which can be read from the figure. Of course, these figures vary depending on the allocation ratio.

We have searched for a method of conducting alloy galvanizing using these alloy powders. Initially, we mixed the metal powders with substances, such as a flux solution and silicone oil, and dipped the article into the mixture while stirring it. But we found a better solution. It is a new method of using a fluidized bed.

Fluidized bed equipment

Figure 2 is the basic fluidized bed equipment used for testing. We used alloy powder which has a particle diameter of around 40 μ to 120 μ. The powder tank and the lower air chamber are

partitioned with a metal mesh.

We used a mesh with an opening of 35 μ to 40 μ . We placed a punching metal under the mesh so that it could withstand the weight of the powders.

The fluidized bed is a method of sending compressed air from the bottom of a tank filled with alloy powders to liquefy the powders. As a result, an article withdrawn from the galvanizing bath can be easily immersed in the powder tank, enabling easier and more uniform product finishing than immersing in a liquid such as oil. The size of the powder tank is determined by the object to be galvanized. Since the air pressure varies with capacity, it should be controlled with a flow meter.

This method enables alloy galvanizing by adding a small tank filled with metal powders, no major equipment change is needed.

Although the melting point of the Al-Mg alloy is the highest among the above-listed alloys, we finally focused on experiments using the Al-Mg alloy powders, considering the already existing zinc coating and cost efficiency based on gravity capacity.

Galvanizing process

<Bolts and small products>

Pretreatment → Primary flux → Zinc galvanizing (60sec) → Centrifuge(1sec) → Secondary flux
→ Alloy galvanizing (alloy powder tank:3sec) → Cooling

Result of analysis

Table 2, are results of analysis by X-ray fluorescence analyzer, using Al-20%Mg alloy powder. In the test, the galvanizing temperature and dipping time were set to 500°C and 60 seconds, respectively, and the article is centrifuged for 1 second and dipped in the powder tank for 3 seconds. The difference from the existing Zn-Al-Mg alloy galvanizing is a thicker coating. In addition, the contents of Al and Mg are higher, although they vary a little depending on the composition. And some wrinkles can be seen on the matte surface, unlike general hot dip galvanizing.

Conclusion

Our Zn-Al-Mg alloy galvanizing method is a very new technology that has been almost completed this fiscal year. This technology can form sufficient alloy layers although they vary a little. Since the surface condition of this alloy galvanizing is inferior to that of the existing galvanizing, we will continuously make efforts to improve the quality. The corrosion resistance verification test is currently in progress, and we hope to develop the new alloy galvanizing with

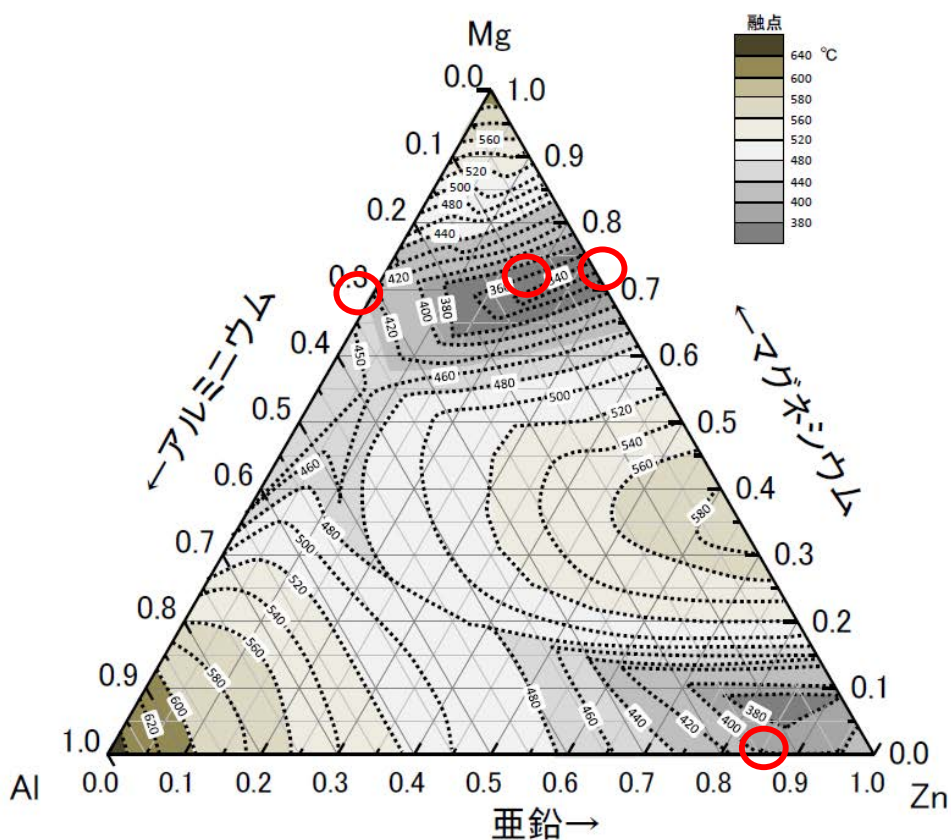
higher corrosion resistance. We believe that the new technology performances excellently in severe corrosive environments. We wish to express our gratitude for the cooperation of the Graduate School of Engineering, College of Engineering, Osaka Prefecture University, in developing this technology.

Table 1 The results of exposure tests

Exposure Period	Zn-1%Al	Zn-3%Al	Zn-5%Al	Zn-1%Al-1%Mg	Zn-3%Al-1%Mg	Zn-5%Al-1%Mg	Zn
1 year	10	4	5	5	4	4	20
2 years	22	12	10	10	9	9	48
3 years	80	20	20	14	17	26	108
5 years	138	86	55	48	54	11	259
10 years	361	256	150	141	102	76	465
15 years	n.a.	210	150	320	211	77	n.a.

(Refer to JGA news 76, 25p)

Figure 1 Liquid projection Zn-Al-Mg



- ① Al - Mg alloy
- ② Zn - Al alloy
- ③ Zn - Al - Mg alloy
- ④ Zn - Mg alloy

Figure 2 Fluidized bed equipment for testing

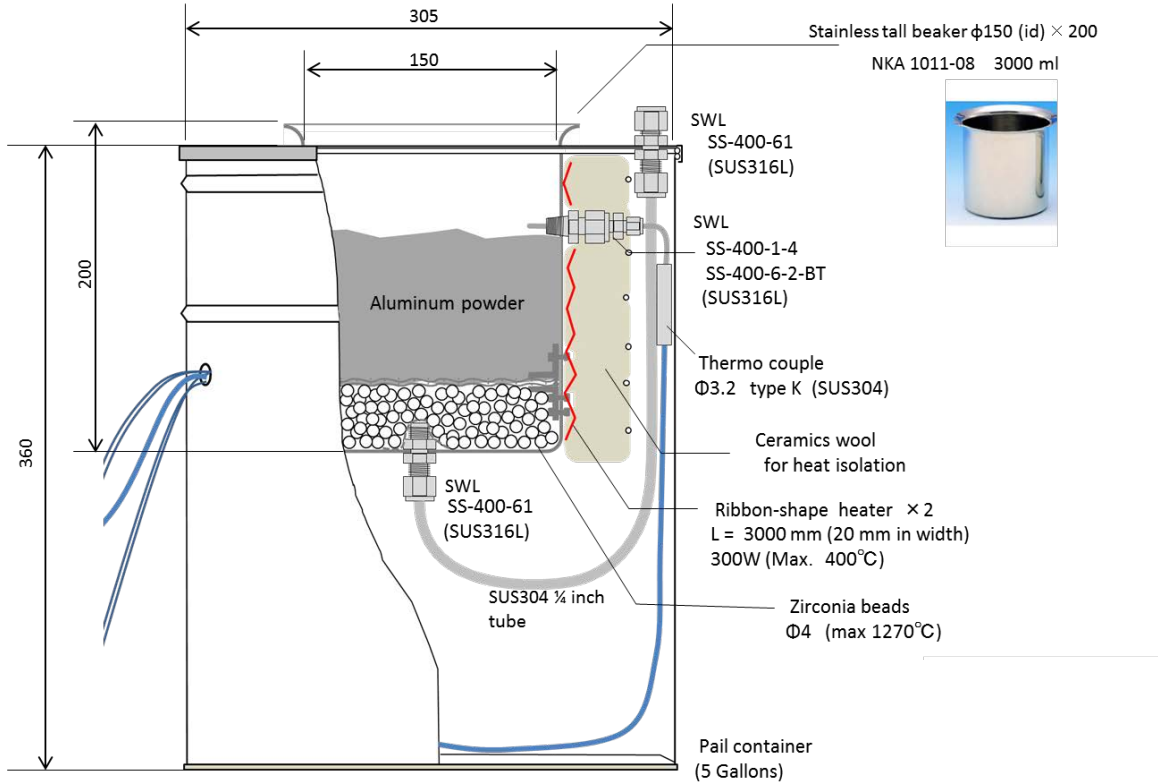
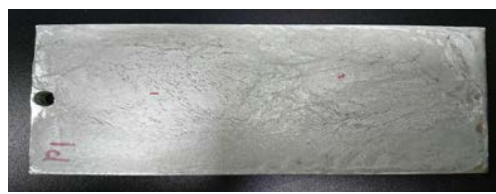


Table 2 Results of analysis by X-ray fluorescence analyzer

	80219-i-1		80303-p-1	
thickness	① 77.4 μ	② 108 μ	① 82 μ	② 63.1 μ
Zn	80.3075(\pm 0.0737)	83.5667(\pm 0.0761)	85.2122(\pm 0.0776)	83.5813(\pm 0.0758)
Fe	3.9801(\pm 0.0196)	2.6372(\pm 0.0161)	3.5578(\pm 0.0186)	2.7977(\pm 0.0165)
Sn	0.0467(\pm 0.0023)	0.0368(\pm 0.0023)	0.0305(\pm 0.0019)	0.0370(\pm 0.0020)
Bi	0.3177(\pm 0.0088)	0.3101(\pm 0.0090)	0.2887(\pm 0.0088)	0.2883(\pm 0.0087)
Pb	0.0000(\pm 0.0006)	0.0054(\pm 0.0048)	0.0071(\pm 0.0050)	0.0228(\pm 0.0051)
Cd	0.0011(\pm 0.0006)	0.0010(\pm 0.0007)	0.0015(\pm 0.0007)	0.0013(\pm 0.0006)
Al	10.6664(\pm 0.0753)	8.4349(\pm 0.0672)	8.1494(\pm 0.0669)	9.4604(\pm 0.0703)
Mg	4.6805(\pm 0.1215)	5.0080(\pm 0.1221)	2.7527(\pm 0.1061)	3.8111(\pm 0.1131)



Session 7:

Insights in Galvanizing for Architecture and Construction

Modern application of bath galvanized steel facades in architecture

Daniela Ridder M. Sc.
Prof. Dr.-Ing. Helmut Hachul
University of Applied Science and Arts Dortmund
Department Architecture
Teaching and research area architecture and metal construction

Sustainable building shells made of steel

Climate change is a current issue of the 21st century, caused by increased CO₂ emissions. Due to the required CO₂ reduction of the federal government, among other things in the building sector, building envelopes must meet ever higher requirements in the field of energy saving and recovery. [1] One goal is to have an approximately climate-neutral building stock by 2050. The concept is to reduce the heat requirement of existing buildings to 20% by 2020 and to build all new buildings as the lowest energy buildings. [2] The quality and the structural design of the building envelope play a decisive role here. For the calculation of the heating demand according to DIN V 18599: 2016-10, the transmission heat losses that are caused by temperature differences (inside / outside) have to be considered. [3] It is essential to ensure that the losses are minimized. Among other things, this can be reduced in rear-ventilated facades-systems by minimizing design-related thermal bridges. [4] Two solutions are conceivable for optimizing the substructure for rear-ventilated facades (RVF) according to DIN 18516-1: 2010 (German Industrie Standard). In the first approach, energy savings can be achieved by reducing wall brackets per square meter. The second approach is to conserve resources by reducing the material thickness of the support profiles to the lowest possible level.

Innovation of DIN 18516-1 (German Industrie Standard)

Rear-ventilated facades according to DIN 18516-1 [5] represent a constructive and building physics convincing solution for high-quality facades. The design possibility of the facade cladding of this system is very diverse. There is a wide range of materials that can be adapted to the individual design of the building and its surroundings. Artificial and natural stones, metals, glass and composite materials provide a high quality appearance. [6] The facade cladding takes over the rain and windproofness. Incidental moisture, e.g. Precipitation or use moisture is caused by convection, which is dissipated in the specified ventilation space and ensures a balanced indoor climate. [7] The feature of rear-ventilated facades is a multi-part structure. The primary structure is closed on the outside with a diffusion-open insulation. Main components of the substructure are wall brackets with thermal break and support profiles. The wall brackets are connected by anchoring elements to the primary structure. Fixed and floating points take up the longitudinal expansion of the materials, the connecting elements are to be adapted thereto. Outermost system situation form the clothing elements. An important feature is the ventilation space, which according to the standard has a minimum of 20 mm [5]. Substructures are divided into one-, two- and multi-part designs. In addition to the multi-part structure, effort and costs of the substructure increase, but this also increases the assets required to level uneven wall surfaces. The main area of application is solid construction. In addition to the established material for the substructure aluminum, the new version of DIN 18516-1 offers galvanized steel as the material for substructures and connecting elements [5]. Steel has good mechanical properties, so the use of bath galvanized steel promises great potential in terms of economy and sustainable use of resources [8].



Fig. 1: University of Düsseldorf, Chair of Business Administration, Economics, RVF-system
 Fig. 2: Roof and facade cladding made of bath galvanized expanded metal, roof substructure: bath galvanized steel

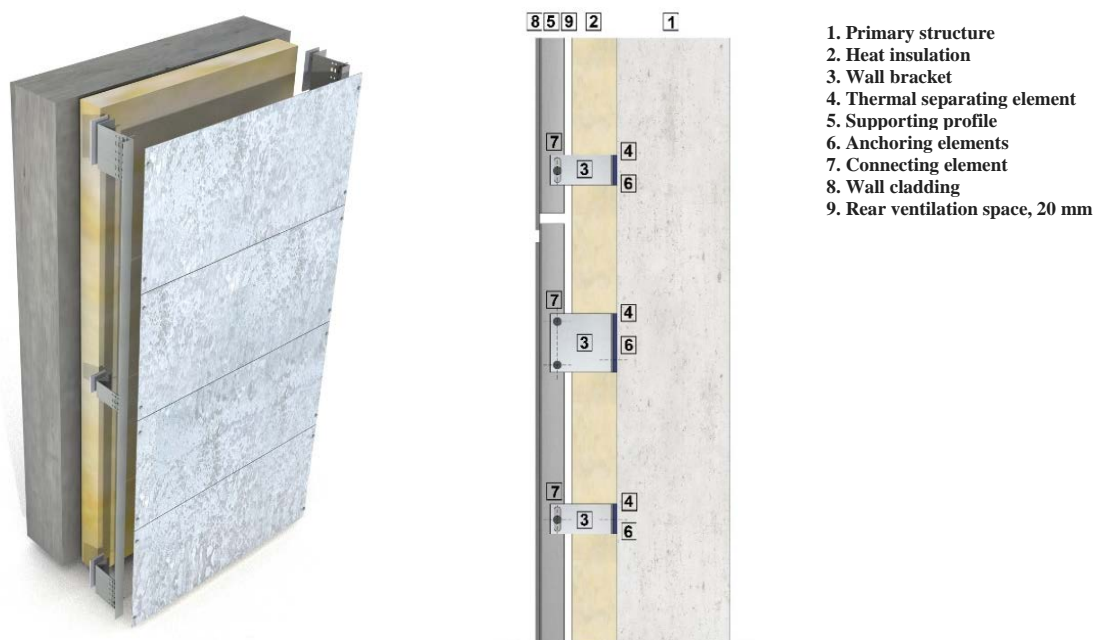


Fig. 3: Facade construction according to DIN 18516-1

RVF made of galvanized steels

Always more architects and builders are choosing bath galvanized facade cladding elements. The surface not only has an optically active liveliness through the so-called "zinc flower", which can be adjusted as alloys in steel such as silicon and phosphorus. In addition, this offers a durable and massive corrosion protection.

Folkwang University, Essen

In 2017, a new building of the Folkwang University of the Arts was built for students in Essen on the grounds of the Zeche Zollverein mine. The 140 m long building complex was placed with protrusions and recesses on the edge of the colliery area. The MGF architects from Stuttgart opted for a curtain rear-ventilated facade with 4 mm thick flat bath galvanized facade panels with a visible screw connection. [9] Continuous window bands characterize the floor space of the building. In addition, glass elements were used as impact protection flush with the facade level in front of the circumferential window bands, thus resulting in a flat, large building envelope. [10] The choice of facade element sizes seems arbitrary, but there are repetitions in the dimensions. In the base area, element sizes of approximately 134 cm x

87.5 and 66.5 cm x 134 cm result. A halving of the larger facade elements has taken place so that the center distances of about 66 cm of the substructure do not vary.



Fig. 4: Folkwang University, Essen, RVF- system, facade cladding made of bath galvanized steel sheet
 Fig. 5: Visible fastening of the facade cladding by facade drill screws, light reflections cause the zinc layer to gleam bronze in some places

Residential building, Oberweningen (Switzerland)

The two semi-detached impress with their striking facade surface. The artist Thomas Sonderegger designed an expressive building shell together with the L3P architects from Regensburg. The remarkable thing is the surface of the metallic building envelope. The artist achieved this through a 5 µm deep etch on the bath galvanized steel sheet surface. [11] At first glance, it is not clear that this is a bath galvanized building shell. The facade elements have been given a bronze color by the surface treatment. As a result, the polygenic structures seem to connect with the environment. The etched elements were used in the facade as well as in the roof area, resulting in a harmonious overall picture of the building design. The exact execution with respect to the etching of the zinc surface is not known, however, the protective corrosion layer is still guaranteed. [11]



Fig. 6: Residential building, Switzerland, RVF- system, facade cladding made of etched bath galvanized steel sheet
 Fig. 7: 5 µm deep etching on the bath galvanized steel sheet

Mensa Werner von Siemens School, Bochum

Completed in 2010, the expansion building on the site of the Werner von Siemens School in Bochum is one of the few known projects to date with a substructure made of bath galvanized steel. Architecture office Reiser und Partner from Bochum have designed this building as an independent two-storey building new construction planned on the existing school complex in 2008. In addition to a large cafeteria with associated infrastructure areas, there are also four classrooms in the 25 m x 14.50 m large building. [12] The facade area is 440 m² and was provided with large-format 1500 mm x 2695 mm, piece-galvanized cladding sheets with a material thickness of 3 mm, which are connected as a visible screw with the substructure. At different times of day and the associated incidence of light, the surface of the galvanized cladding elements always gets a different appearance. This gives it a liveliness, but at the

same time forms a calm and harmonious facade look. [13] The joint width is 5 mm and is an essential part of the planning and execution to absorb the resulting length expansion of the material so that no damage. The necessary external insulation is concealed by a back-sided placement of piece-galvanized flat steel in the area of the vertical joints. However, these do not have any supporting function. On the other hand, the vertical joints are closed by the vertically laid support profiles of the substructures. [12] The wall structure complies with DIN 18516. The primary structure consists of a 240 mm reinforced concrete construction which defines the cubature of the building. On the outside wall side of the primary construction, a 120 mm non-combustible insulation is fixed. The pierced by the anchored to the primary structure wall bracket. The substructure consisting of wall bracket and support profiles are in the form of an L-profile and are made of 3 mm bath galvanized steel. With regard to the execution of substructures, there are pages on the part of architects and facade planners keep in mind when using galvanized substructures. To date, the building described no defects or damage known. Even the protective corrosion layer of the facade elements could withstand the everyday life of the school grounds and the weather. A measurement according to DIN EN ISO 1461 in January 2018 showed an average layer thickness of 57.4 μm . This is significantly above the minimum value of 55 μm for steel components specified in the standard ($\geq 1,5\text{mm} - \leq 3\text{mm}$). [14] Externally also no corrosion is evident at connection points.



Fig. 8: Cafeteria - Werner von Siemensschule, Bochum, R VF- system, substructure made of galvanized steel

Fig. 9: Fastening the bath galvanized facade cladding with facade screws, back cover of the joints

Substructures made of galvanized steel

Influence of the wall bracket on the U-value of the wall

The individual wall brackets are fixed at fixed intervals according to statics on the primary structure, in most cases this is designed as a solid wall made of reinforced concrete. For the most part, the choice of wall bracket is based on the material aluminum. Due to the typical structure of the R VF-system, piercing points of the wall brackets are created by the thermal insulation. The mineral wool insulation and aluminum wall brackets have very different thermal conductivities, therefore the heat dissipation in the area of the wall brackets are significantly increased and three-dimensional (selective) thermal bridges are created. [8] A figure shows a picture of a R VF facade with substructure made of U-profiles with a cladding facade made of coated aluminum and mineral thermal insulation. The substructure consists of 3,00 mm thick aluminum wall brackets. In the area of the exit point of the metal by the thermal insulation significant temperature differences can be seen. At this point, a temperature of 0,9 ° C (measuring point M1) is to be read and measured on the surface of the thermal insulation -3,4 ° C (measuring point M6). The determined temperature values over the course of the wall bracket towards the facade cladding show that the surface temperature decreases again (M2: -2,2 ° C, M3: -1,8 ° C, M4: -2,6 ° C M5: -3,0 ° C). This shows that there is a weak spot in the system at the exit point of the wall

bracket due to the thermal insulation. Here are strong temperature differences and thus it comes in these areas of the wall structure to significant heat loss.

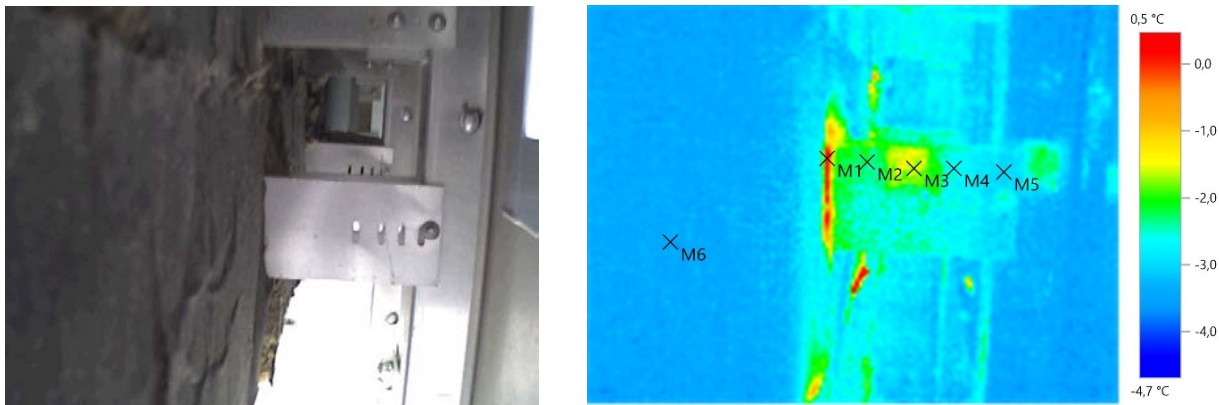


Fig. 10: Thermography image; piercing points of the U-wall bracket due to the mineral thermal insulation (Date: 27.02.2018, outdoor temperature -13 C °)

The heat losses described must be taken into account in the calculation of the heat balance of the buildings above the U-value (heat transfer coefficients). To determine the heating requirement of a building, a thermal bridging loss coefficient χ -value (point thermal bridging loss coefficient) in W/K according to DIN EN ISO 10211-1 for three-dimensional thermal bridges is determined and multiplied to the U-value of the undisturbed wall. [15] The determination of the loss coefficient is very complex, since here the different installation of wall brackets per m² and the number must be included in the different areas of the facade. By means of simulation, the value for the point-specific heat transfer coefficient can be defined. [8]

One solution option to minimize heat losses is to compensate for the losses to be taken into account under EnEV 2014 by means of greater thermal insulation. In order for the minimum requirement of the EnEV 2014 (U-value $\leq 0,24$ W / m²K [16]) to be achieved or to comply with the passive house standard (U-value $\leq 0,15$ W / m²K [17]), this would have to be increased significantly [18]. This approach strongly neglects aspects of sustainability and resource conservation. Another approach for improving the U-value in the RVF wall component is to select a material for the wall holder with a low thermal conductivity. Potential wall mounts made of alternative materials such as stainless steel, stainless steel-aluminum combinations, glass fiber reinforced plastic (GFRP) or GFRP-aluminum combinations improve the problem of three-dimensional thermal bridges. Critical factors of the improved materials, however, are construction-relevant issues such as fire behavior and economy. Marketable GFRP wall mounts with the material PA66 have fire protection classes B1 (flame retardant) [19] [20]. The use of GFRP wall brackets is therefore limited to building heights of up to 22 m. For this purpose, the Landesbauordnung NRW (NRW state building regulations) prescribe flame-retardant (B1) substructures for use. For building heights over 22 m, building material class A1 or A2 is mandatory for the substructure (non-flammable). [21] Furthermore, design-related, stiffening transverse ribs of the GRP console can make even heat treatment problems more difficult. Furthermore, there is a wall bracket made of aluminum and glass fiber reinforced plastic (polyamide, EN AW-6063 T66). The plastic bar is positioned in the area of thermal insulation due to its low thermal conductivity. [22] Another development of a wall holder is made of steel. This system consists of a long system dowel (acts as a wall holder) anchored in the primary structure. The dowel is offered in the materials stainless steel (A4) and galvanized steel. Support profiles and system connectors in both variants are made of aluminum [23]. For the reasons mentioned, the comparison of current aluminum wall brackets and support profiles with new variants made of both galvanized steel is a good idea. This material has a significantly lower thermal conductivity than aluminum and a much better fire behavior than plastic. An application of steel substructures with a melting point of 1536 ° C (for example structural steel S235 JR) [24] is to be regarded as a great advantage, since the melting point of aluminum at about 659 ° C [25], the GFRP material (polyamide PA 66) with > 260 ° C [26] significantly lower.



Fig. 11: Wall bracket made of GFRP; (Polyamide, EN AW-6063 T66); Support profile made of aluminum
 Fig. 12: Wall bracket, system anchor made of stainless steel A4 or galvanized steel, system connector and support profile made of aluminum

An investigation provides initial results for improving the heat transfer through the use of steels [27]. Based on a reference wall with a classic RVF wall construction; load-bearing solid wall, external mineral thermal insulation, rear ventilation level 20 mm, curtain aluminum cladding. With identical construction of the substructure, the materials aluminum, bath galvanized steel and stainless steel were compared. Only the replacement of materials with different coefficients of thermal conductivity in the wall bracket area shows a significant difference in the comparison of the results of the thermal conductivity coefficient (U-value). The aluminum wall brackets compared to wall brackets made of galvanized steel and stainless steel have low losses.

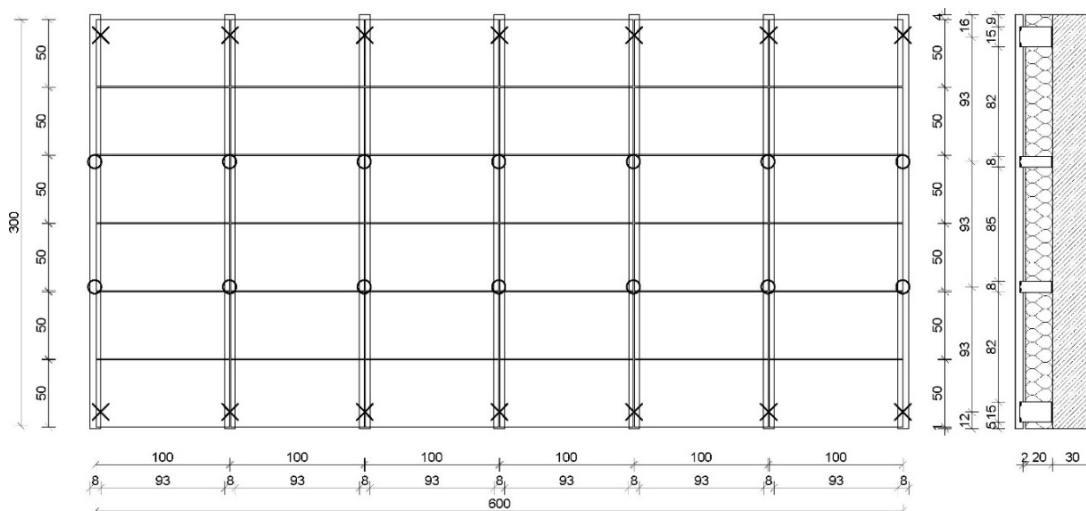


Fig. 13: Reference wall surface 18m², 28 L-wall bracket (fixed and sliding points), L-supporting profiles, thickness of thermal insulation 200mm - λ 0.033; thermal calculation of losses due to different bracket materials

Wall bracket and supporting profile Aluminum EN AW 6060	Wall bracket and supporting profile bath galvanized steel S235	Wall bracket and supporting profile stainless steel V2A
Thermal bridge loss coefficient with thermal separator: wall bracket h=138 mm, χ -value = 0,0455 W/K [27]	Thermal bridge loss coefficient with thermal separator: wall bracket h=138 mm, χ -value = 0,189 W/K [27]	Thermal bridge loss coefficient with thermal separator: wall bracket h=138 mm, χ -value = 0,00735 W/K [27]
heat transition coefficient undisturbed wall (without wall bracket) = 0,197 W/m²K	heat transition coefficient undisturbed wall (without wall bracket) = 0,197 W/m²K	heat transition coefficient undisturbed wall (without wall bracket) = 0,197 W/m²K
Total heat transition coefficient U=0,27 W/m²K	Total heat transition coefficient U=0,23 W/m²K	Total heat transition coefficient U=0,21 W/m²K

Tab. 1: Comparison of the substructure material between aluminum, bath galvanized steel and stainless steel using a reference wall surface

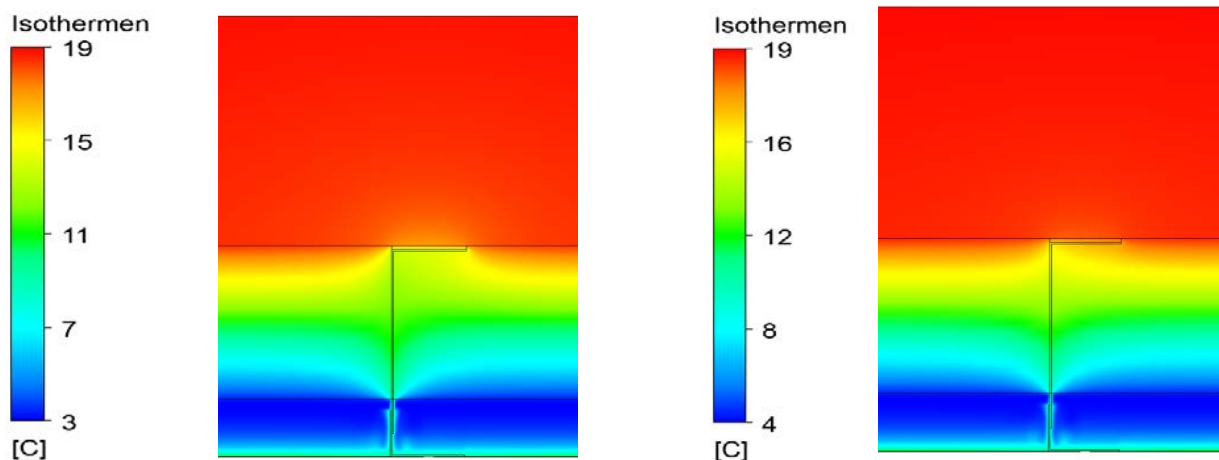


Fig. 14: Isothermal processes - left: wall bracket aluminum EN AW6060, right: wall bracket steel S235, structure of facade: above – primary structure, middle – heat insulation with wall bracket, below - cladding

Resource optimization through substitution

In 2014, Prof. Dr.-Ing. H. Hachul and the Institut Feuerverzinken (German Institute of bath galvanizing) jointly supervised a master thesis at the University of Applied Sciences and Arts, Department of architecture + metal construction. This scientific preliminary study describes the subject of bath galvanized steel substructures ("New possibilities and application examples of Substructures made of galvanized steel", authors: Michael Heinemann M. Sc. and Daniela Ridder M. Sc.). [28] The positive aspects identified here for the potential supplementation of bath galvanized steel profiles in the area of RVF give reason for a deeper investigation. In addition to the fundamentally better mechanical characteristics (reference aluminum), the focus here was on general manufacturability for piece galvanizing thin steel profiles, for which there were no results so far. In addition, a first classification of relevant substructures was carried out, including amongst other things in the items multi-part, material, clothing material, form of clothing, type of fixation and loads introduced. To prove the resource efficiency is amongst other things the investigation for the smaller dimensioning of wall brackets and support profiles necessary. For this purpose, a rough calculation was carried out in order to estimate a static upgrade. The comparison of a 1mm thick steel profile versus an equivalent aluminum counterpart showed that steel has a lower utilization because steel has a higher cutoff stress and modulus of elasticity [29]. Added to this was the question of whether the quality (quality, layer thickness) of the corrosion protection layer of the steel deteriorated. It was assumed that the profiles heated in the molten zinc to 440 ° C - 460 ° C [30] would deform. It could be proven that no deformations occurred on the components (material quality S235 in the material thicknesses 0.75mm / 1.00mm / 1.5mm / 3.00mm). The measurements of the protective zinc layer of the thinner components also corresponded to DIN EN ISO 1461. However, the positive results are limited by the short component length of the specimens of only 700mm. Practical are supporting profile lengths 2000-6000mm. The measurements of the protective zinc layer of the thinner components corresponded to DIN EN ISO 1461 [14]. The measurements of the profiles were determined with a calibrated measuring device. It has been shown that the average values are even higher than the required minimum layer thicknesses [28].

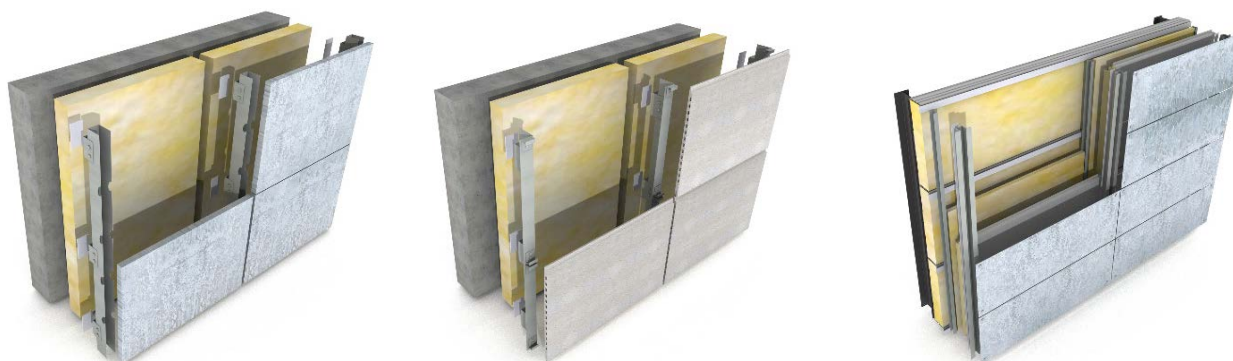
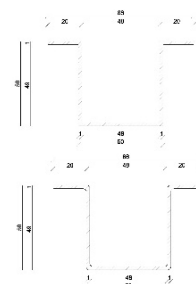


Fig. 15: left: two-part substructure, U-wall bracket, U- supporting profile, concealed mounting, hook-in cassettes, middle: multi-part substructure, L-wall bracket, L- supporting profile, clamps, heavy facade cladding made of ceramic right: lightweight steel construction with steel cassettes, hybrid construction, substructure (hat profile) on sandwich element

Calculation of two span beam		Wind load
Hat profile Steel d=1mm; L=1m		0,78 kN
Hat profile Aluminum d=1mm; L=1m		0,78 kN

Load-bearing capacity [I _y]		Load capacity
Steel	0,15 cm ⁴	15 %
Aluminum	0,21 cm ⁴	21 %



Tab. 2: Rough dimensioning of two aluminum and steel hat profiles, right picture: sketch of the calculated hat supporting profile, above: aluminum, below: steel

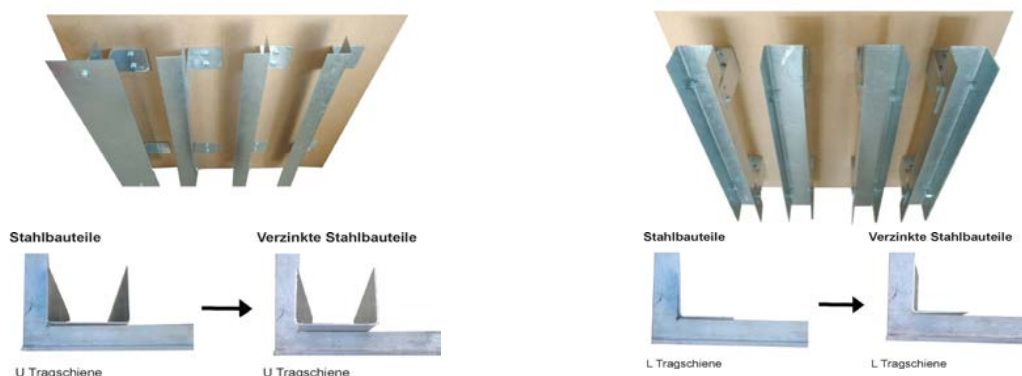


Fig. 16: Test specimen: left bath galvanized U-profiles, right L-profiles, piece-galvanized specimens, t = 0.75 / 1.00mm / 1.50mm / 3.00mm. Facade versions U-supporting in U-bracket (left), L-profile in (right) L-wall bracket, the joints were made with metric screws

Steel parts and their thicknesses	Average layer thicknesses (minimum value) µm Measurement of the prototypes	Average layer thicknesses (minimum value) µm DIN EN ISO 1461	
Comparison of the average zinc layer thicknesses on the U-profile			
3 mm	55,5	≥1,5mm-≤3mm	55
1,5 mm	56,2	≥1,5mm-≤3mm	55
1,0 mm	57,4	<1,5mm	45
0,75 mm	58,7	<1,5mm	45
Comparison of the average zinc layer thicknesses on the L-profile			
3 mm	58,8	≥1,5mm-≤3mm	55
1,5 mm	57,9	≥1,5mm-≤3mm	55
1,0 mm	74,5	<1,5mm	45
0,75 mm	61,4	<1,5mm	45

Tab. 3: Comparison of the average zinc layer thicknesses on the L- and U-profiles

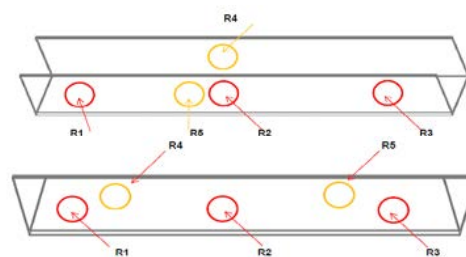


Fig. 17: Measurement of the zinc layer is placed vertically by placing the probe on the galvanized component, position of the standardized measuring points / reference areas R1-5 (top U-profile, below L-profile) for the determination of the average zinc layer thicknesses

Further research approach

An addition to previous substructure systems through the use of bath galvanized steels according to DIN 18516-1 appears to be interesting and promising both for the level of the supporting profiles and for the level of the wall brackets. Previously executed buildings are individual solutions, a scientific level of analysis is missing. A systematic investigation is imperative to verify the potential benefits of the construction, including: Energy saving, resource efficiency, economy, sustainability, durability and practicality. The intended research results therefore represent a significant expansion in the level of knowledge in the field of the use of bath galvanized steel for substructures. Overall, the project is to prove that substructures made of bath galvanized steels according to DIN EN ISO 1461 [14] due to economic, structural-physical advantages, higher stiffness and better energy and resource efficiency represent an important innovation for RVF-constructions according to DIN 18516-1.

Acknowledgements

To get this work done, I have received expert support from many people who have contributed to the content of this work. At this point I would like to thank all those who have contributed to the success of this research work through their professional and personal support. My biggest thanks go to Prof. Dr.-Ing. Helmut Hachul and Prof. Dr.-Ing. Thorsten Weimar for her willingness to supervise and support the dissertation project. Likewise, I would like to thank Mr. Dipl.-Ing. Mark Huckshold, Dipl.-Ing. P. Düren-Rost, Dipl.-Kff. Holger Glinde and Udo Geczi for the invitation to Intergalva 2018. I am very pleased to be able to present the topic of my dissertation in the context of the event by means of a lecture and a scientific publication. I would also like to thank Prof. Dr.-Ing. Marius Geller, Dipl.-Ing. Norbert Kluck and Pascal Legran from the Department of Mechanical Engineering of the University of Applied Sciences Dortmund who supported me in the field of thermal simulation and provided me with results and images.

References

- [1] Bundesministerium für Wirtschaft und Energie (BMWi) -Energieeffizienzstrategie für Gebäude, November 2015
- [2] Bade, M., Umweltbundesamt, Der Weg zum Klimaneutralen Gebäudebestand, 2013, November
https://www.umweltbundesamt.de/sites/default/files/medien/378/publikationen/hgp_gebaeudesanierung_final_04.11.2014.pdf, Datum: 23.03.2018
- [3] DIN V 18599:2016, Energetische Bewertung von Gebäuden, Berechnung des Nutz-, End- und Primärenergiebedarfs für Heizung, Kühlung, Lüftung, Trinkwarmwasser und Beleuchtung, Beuth Verlag
- [4] Schmieder, M. und Huber, J., Fassade 2/2014, Wärmebrücken bei VHF: Herausforderungen, Berechnungen und Vermeidungen
- [5] DIN 18516-1, (2010), Deutsche Norm Außenwandbekleidung hinterlüftet, Berlin, Beuth Verlag GmbH, DIN Deutsches Institut für Normung e.V., S. 139
- [6] Holl, C., (2007). Metallfassaden, München, Deutsche Verlagsanstalt München
- [7] Fachverband-vorgehängte-hinterlüftete-Fassaden, (November 2014), Gestaltung – Technik – Wirtschaftlichkeit – Nachhaltigkeit, http://www.fvhf.de/Fassadenbilder/docs/Prospekte/FVHF_Fassaden_Imagebroschuere.pdf, Berlin: FVHF
- [8] Schneider, K. J., Bautabellen für Architekten, 23. Auflage, März 2018
- [9] Meinig, M., industrieBAU- architektur, technik, management, Bauen für Forschung und Entwicklung, Von der Zeche Inspiriert, (1|2018)
- [10] Kraft, M., Roszak, M., und Radosch, T., Feuer Trutz Magazin 2. 2017, Baulicher Brandschutz
- [11] Institut Feuerverzinken, Feuerverzinken Special, Fachzeitschrift Fassaden, Experimentelles Novum - Getrenntes Doppelhaus mit geätzter, feuerverzinkter Fassade, 2012
- [12] Godau, D. (08. 2012) Werner von Siemens Schule in Bochum, Ernst & Sohn Hrsg., Innovative Fassadentechnik
- [13] Glinde, H. (06/2011), Metallbau – Das Fachmagazin, Datum 05.04.2018, Neuer Glanz für den Schultag, http://www.metallbau-online.info/artikel/mb_2011-06_Feuerverzinkte_Fassade_1184850.html
- [14] DIN EN ISO 1461:2009-10, Durch Feuerverzinken auf Stahl aufgetragene Zinküberzüge (Stückverzinken) - Anforderungen und Prüfungen (ISO 1461:2009); Deutsche Fassung EN ISO 1461:2009
- [15] DIN 10211:2018-03, Wärmebrücken im Hochbau - Wärmeströme und Oberflächentemperaturen - Detaillierte Berechnungen (ISO 10211:2017); Deutsche Fassung EN ISO 10211:2017, Beuth Verlag
- [16] EnEV 2014, Anlage 3 Nr. 7, Anforderungen Tab. 1, <http://www.enev-online.de>, Datum 08.02.2018
- [17] Passivhaus Institut, Qualitätsanforderungen an Passivhäuser, Datum: 08.02.2018
- [18] Kühnert, T. und Hruby, J., Innovative Fassadentechnik, Ernst und Sohn, April 2015, VHF mit geringerem U-Wert- (k)ein Widerspruch
- [19] Broschüre Systea, Wandkonsole Tekofix
(http://systea.systems/fileadmin/systea/downloads/180326_SYSTEA_Wandbock_4-Seiter_RZ_WEB.pdf) Datum: 05.04.2018
- [20] DIN 4102-1, Brandverhalten von Baustoffen und Bauteilen - Teil 1: Baustoffe; Begriffe, Anforderungen und Prüfungen, Beuth Verlag
- [21] LBO Landesbauordnung NRW, MBO Musterbauordnung, Tabelle: Gebäudeklassen
- [22] Fa. Hilti Deutschland AG, Innovative Fassadentechnik, Ernst & Sohn Hrsg., Wandhalter für die Unterkonstruktion hinterlüfteter Fassaden: keine Wärmebrücken – sicherer Halt, April 2016
- [23] Fa. BWM Dübel und Montagetechnik GmbH, Broschüre, BWM Konstruktion, Wandhalter ATK 601 Neu, file:///C:/Users/PC/AppData/Local/Temp/ATK-601-NEU_v2.pdf
- [24] Dillinger, J., Dobler, H.-D., Doll, W. und Escherich, W., Metalltechnik Grundbildung, Europa Lehrmittel, Auflage 7 - 2014, S.137

- [25] Fischer, U. (2011), Tabellenbuch Metall, Auflage 45, Haan-Gruiten, Europa Lehrmittel Verlag, S. 112
- [26] DIBt-Zulassung-Nr. Z-10.9.-459, Antragsteller Maas Profile GmbH, Geltungsdauer 17.Juni 2013 – 17. Juni 2018 (Datum:05.04.2018), S. 20
- [27] Legran, P., Fachhochschule Dortmund, Prof. Dr. M. Geller, D. Ridder M. Sc., Simulation von vorgehängten hinterlüfteten Fassadensystemen mit unterschiedlichen Unterkonstruktionen zur Bewertung der Einsparungen hinsichtlich Wärmeverluste und Materialbeanspruchung
- [28] Heinemann, M. und Ridder, D., Fachhochschule Dortmund, Dipl.-Ing. P. Düren-Rost, Dipl.-Kff. Holger Glinde, Prof. Dr.-Ing. H. Hachul, Neue Möglichkeiten und Anwendungsbeispiele von Unterkonstruktionen aus feuerverzinktem Stahl, September 2014
- [29] Kraus, F., Tabellen zur Tragwerkslehre, 12. Auflage, 2014, Verlag Rudolf Müller GmbH & Co. KG
- [30] Institut Feuerverzinken GmbH, Arbeitsblatt A2-Verfahrensablauf beim Feuerverzinken nach DIN EN ISO 1461 <http://www.feuverzinken.com/wissen/arbeitshilfen/arbeitsblaetter/a-korrosionsschutz-feuverzinken/a2-verfahrensablauf-beim-stueckverzinken/?type=333>, Datum: 05.04.2018

Figure references

- Fig. 1-5: Ridder, D., Fachhochschule Dortmund, Fachbereich Architektur
- Fig. 8-13: Ridder, D., Fachhochschule Dortmund, Fachbereich Architektur
- Fig. 6-7: Hachul, H., Fachhochschule Dortmund, Fachbereich Architektur
- Fig. 14: Legaran, P., Fachhochschule Dortmund, Fachbereich Maschinenbau
- Fig. 15-17: Heinemann, M. und Ridder, D., Fachhochschule Dortmund, Fachbereich Architektur

A bright future for hot dip galvanized steel in the circular economy

Bruno Dursin
Zinkinfo Benelux

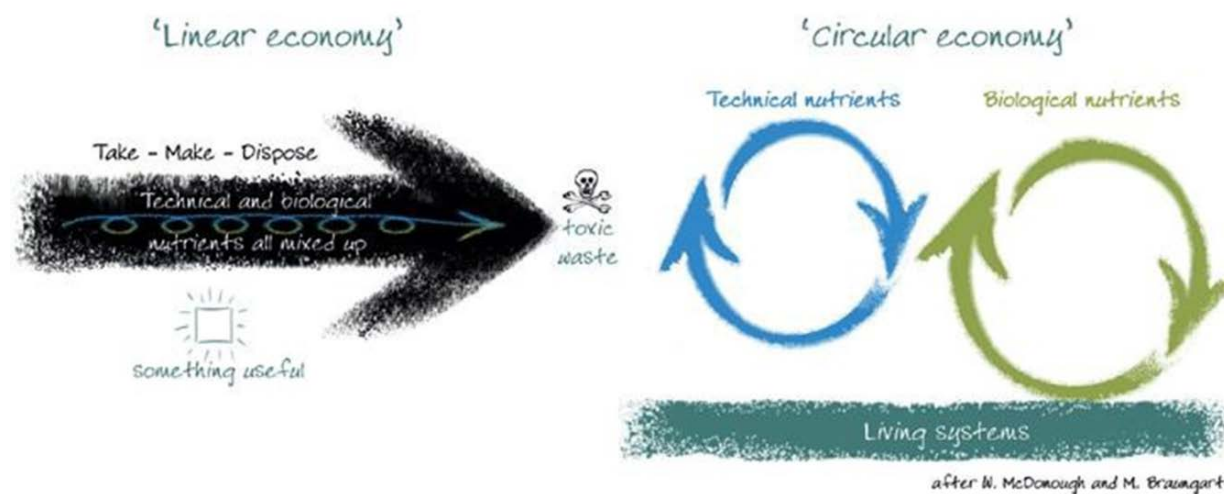
“Earth is a community to which we belong and not a commodity for us to exploit”

I admit, it sounds a bit provocative. But maybe we need a bit of provocation in order to create a switch of mind. My story is mainly based on the Dutch example, but I am convinced that the phenomena and principles of Circular Economy will spread gradually over the entire globe.

The Dutch economy is doing well. And the building industry is benefitting from it. But on the one hand we can see how many office buildings remain vacant, while on the other hand new ones are constantly being built. Seems a bit weird to me. And in a way it could have been avoided. If we had thought and designed according to a circular model. But that's going to change, if not for the sole fact that society expects us to use sparingly the resources that Mother Nature is offering us. Circular economy is the future.

Let's start with some basics: what does 'circular economy' actually mean? I would use the following definition:

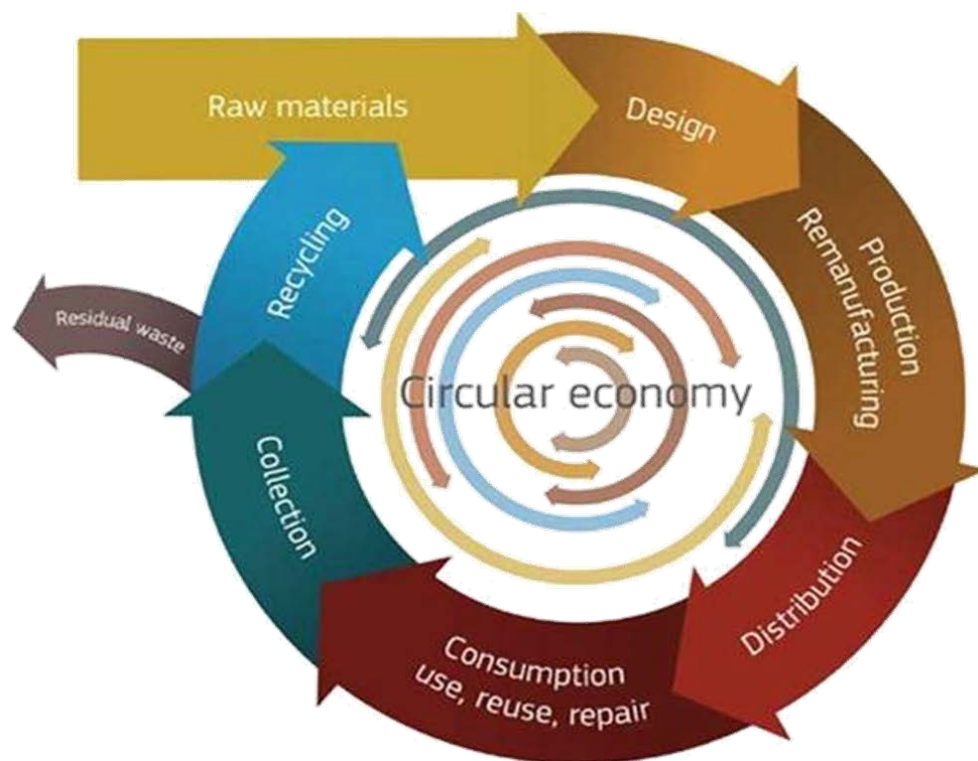
The circular economy is a move from linear business models, in which products are manufactured from raw materials and then discarded at the end of their useful lives, to circular business models where intelligent design leads to products or their parts being repaired, reused, returned and recycled. (1)



A circular economy aims to rebuild capital, whether it is financial, manufacturing, human, social or natural. This approach enhances the flow of goods and services. The concept of the circular economy drives optimal resource efficiency. It makes sure that resources are efficiently allocated to products and services in such a way as to maximize the economic well-being of everyone. In addition, products need to be designed to be durable, easy to repair and, ultimately, to be recycled. The cost

of reusing, repairing or remanufacturing products has to be competitive to encourage these practices. Simply replacing a product with a new one should no longer be the norm.

A circular economy ensures that value is maintained within a product when it reaches the end of its useful life while at the same time reducing or eliminating waste. This idea is fundamental to the triple-bottom –line concept of sustainability, which focuses on the interplay between environmental, social and economic factors.

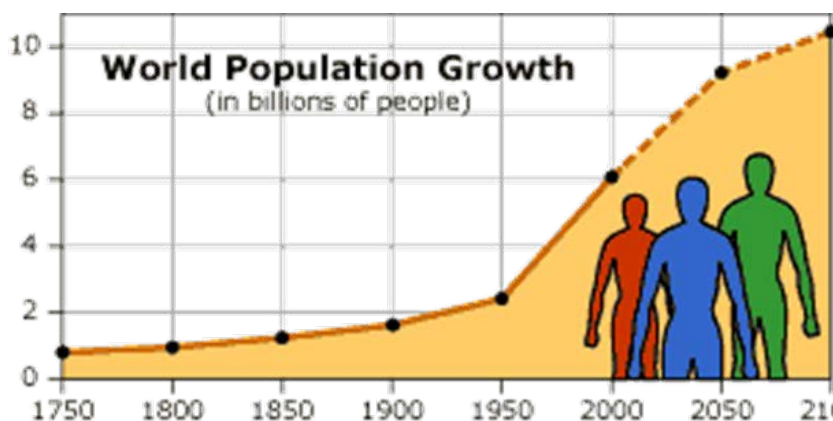


(Source: Bouke Bonnema – Tata Steel)

Without a life cycle approach , it is impossible to have a genuine circular economy.

Why is the European Commission pushing towards a circular economy? (2)

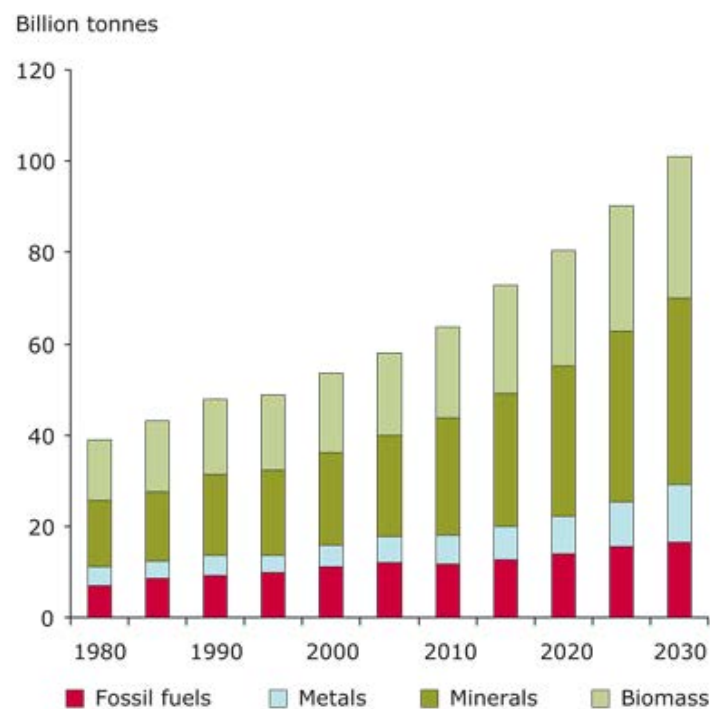
- world population growth puts increasing pressure on authorities to act.



(Source: Bauke Bonnema – Tata Steel)

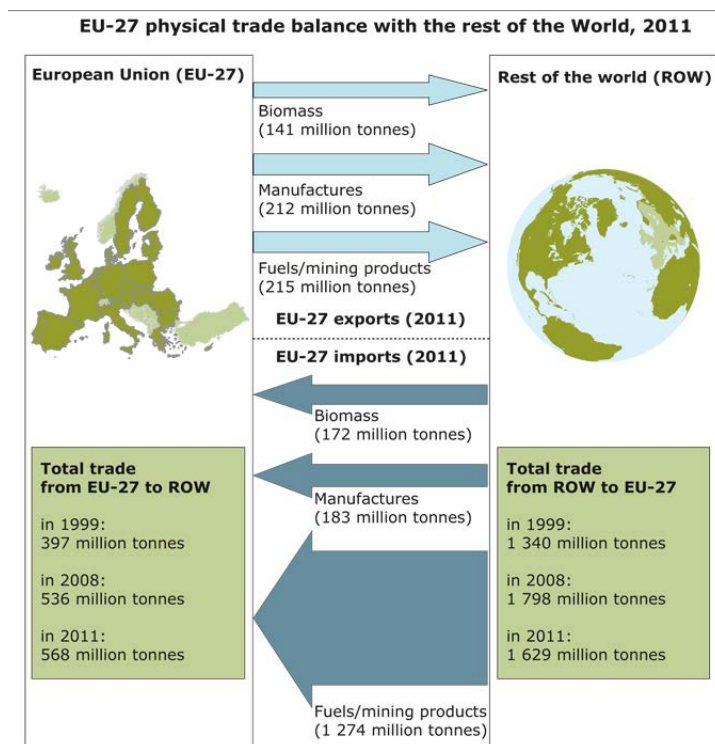
- Europe wants to invest in supply security, and at current speed of consumption we are jeopardizing this goal.

Global resource extraction 1980–2030, by category



Source: SERI et al., 2009.

- We wear a huge responsibility for future generations, so striving for sustainability has become a moral duty.
- Europe wants to capitalize on the huge potential in financial-economic, social and environmental benefits of the circular economy.
- Today, Europa is strongly dependent on the import of natural resources (90% is coming from non-EU members). This is a major strategic risk that has to be reduced.



Source: Eurostat Comext statistics.

Opportunities & threats

The transition from a linear towards a circular economy offers a number of direct and indirect benefits:

- Cost reduction the EU 380-630 billion €/year (Ellen MacArthur Foundation)
- 7 billion/year in the Netherlands (TNO)
- Saving 2.9 – 3.7 trillion \$ in 2030 worldwide through increasing resource efficiency (McKinsey, 2011)
- Supply security
- Development of new knowledge
- Boost innovation
- Creation of new (industrial) activities

On the other hand, we encounter a number of obstacles in our strive to change from linear -> circular.

- institutional (vested interests)
- Organizational (no coordination)
- Legal (legislation slows down innovation)
- Economical (current focus on existing business models)
- Technical (today innovations are mainly aimed at production growth)

What about the building industry?

Why is construction a priority area for a circular economy? The impact is huge, we can achieve quick wins if we focus on construction.

Construction sector represents :

- 40% of material use
- 50% CO2 emissions
- 20% water use
- 25% all transport

In simple terms, circular construction means: building the LEGO way. From the beginning you start thinking about how to design a building in order to be able to dismantle easily its components at the end of the buildings' lifetime. In order to reuse them or give them back to nature. It's the opposite to what we have been doing for ages using the linear building model. In this model resources are being transformed into building products and components, that are being demolished at the end of the lifetime of the building and send to the landfill. In the best case scenario they are recycled (steel), sometimes they are down-cycled (concrete) but often it's a pure waste of value. Not to mention the environmental damage.... (3)

Another way of building

Builders will have to change their way of thinking:

- Design flexible and adaptable buildings, that provide basic functions for a long period, but at the same time can be adapted.
- Design in a 're-functionable' way. At design stage take into account future new functions and new users for a building.
- Make sure that components are re-usable and design the building accordingly.
- Use resources with a high residual value: so preferably steel instead of concrete because steel is easily dismantlable and can get a premier second life. For concrete, this is much less feasible unless smart components are designed that are re-usable. Beware, the concrete lobby is working very hard on this subject, f.e. re-usable elements for facades.

The Dutch Government has developed a clear vision and a roadmap towards a fully circular building environment in 2050. The roadmap is defined: (4)

- In 2030 all public procurements will be 'circular'.
- Leading up to this, all public enquiries will be circular by 2023.
- Drastic reduction of CO² consumption in the building sector. 50% reduction by 2030 en 100% reduction by 2050.
- By the end of 2020 a decision on a mandatory 'material – ID'. The Government will define a system that will allow a transparent listing of materials and resources used in the construction of a building.
- Temporary subsidisation of circular business models. Temporary financial support will be provided in order to develop these models.
- Development of a uniform methodology for circularity through pilot projects.

- Integrate circularity in government’s standards. In 2018, the Dutch government will start a program for research on this subject.
- International positioning and collaboration. The Netherlands are working closely together with neighboring countries towards a circular building economy in North-Western Europe.
- In 2021, circular building will constitute an integral part of the school curriculum.
- The creation of a knowledge institution.

In practice

A circular economy aims at reusing materials in the most valuable way. So, first of all we should try to reuse the complete product/building component. If this is not achievable, we should reuse parts of it and at least we should reuse the resources/raw materials. Producers of building materials and designers play a crucial role if we want to move towards a circular building environment.

The R’s in the circular economy

The available literature offers different approaches or sequences but this is the most commonly used one:



(Source: Jacqueline Kramer – Utrecht Sustainability Institute)

Recycling: almost the last step.

There’s a logic behind this scheme. What are the shortest circles that you can close as an organization? Where can your company have the highest impact? Maybe you have noticed that recycling is one of the last steps in the order of priority. Obviously, because it’s energy consuming and because in most cases (but not for steel!) there’s a loss of quality (down-cycling). There are many

chances and opportunities for our economy - including job opportunities – before we opt for recycling.

Refuse

Before buying a product, before extracting a resource, before producing a component or a packaging, we should always ask ourselves: do we really, really need it? Anything that can prevent the use of resources is worth thinking about.

Reduce

Can we reduce the amount of raw materials used in the production of building products?

Reuse

Reuse building products again after the end of lifetime of the building, in order to reintegrate them in new building projects.

Repair

In a circular economy, there will be a shift from a product-based economy towards a service-based economy. Repair/maintenance will be a part of it. This is not new but it will become increasingly important. We should try to limit the distance between the repair shop and the user, in order to limit the environmental impact. Moreover, this will stimulate local economy and increase the ease of use for the end user.

Refurbish

Retrofitting used products like ink cartridges or tablets. The second-hand market will grow inevitably.

Remanufacture

New products are created from (parts of) old ones. This counts as well for overhauling. Overhauling means checking and, if necessary, repairing engines and machines. The engine is technically speaking restored to good condition by overhauling it. The engine is hereby disassembled and cleaned. Worn parts are replaced by new ones. The automotive industry is a compelling example which has been doing this for years now.

Repurpose

Re-using a product for another purpose; it is already a commonplace in the world of design. Repurposing means recovering components for re-use if the product itself has become virtually useless.

Recycle

Processing and re-use of materials. In the Netherlands, recycling percentages are high in comparison to other countries in Europe and elsewhere. As stated earlier, this is one of the final steps in a circular economy.

Recover

This is the last 'solution' in the circular economy. Separating building components for energy recovery during incineration. Incineration without energy recovery and sending waste materials to landfill are absolutely 'not done' in a circular economy.

Redesign

Personally, I would like to add this one, and rank it between reduce and reuse. In a circular economy we must design products in a different way. Design in view of a longer service life, modular design enabling easy replacement of components, smart packaging, use of sustainable materials. This is a major aspect of the circular economy. The biggest profit will already be made if, at design stage, we take into account repairability, reuse or recyclability.

Shift from waste market to raw materials market

The principle of a waste market is dumping and combusting. In a raw materials market, we are returning (building) waste as a raw material to the cycle.

The role assignment in the waste market is different to the one in a raw materials market. Waste processing is mainly done by large companies and waste collection is mostly in public hands. In a raw materials market, specialized innovative companies become producers of raw materials and energy. Municipalities control a high-quality closed circuit through their procurement policy.

From raw materials recycling to closed circuit

A shift from a linear economy to a circular one means that products should be designed to be a raw material after their use. This requires a collaboration with partners in the entire chain or even in new chains. The major task is to collectively develop circular raw materials chains (in stead of only recycling existing waste flows)

A closed circuit of building waste and demolition waste creates added value:

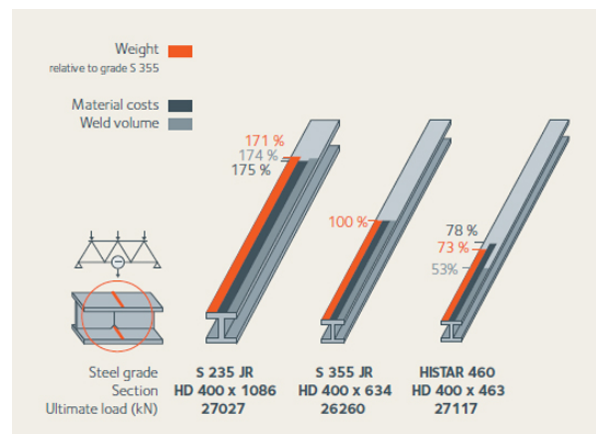
- efficiency improvement in the demolition and building process
- cost reductions
- new jobs
- environmental benefit

This can only be achieved if consortia of companies are formed who collaborate and if new financial arrangements are developed that make this business model more profitable.

'The steel case' (5)

How does steel fit in the 10 R's and where lies its competitive advantage over competing materials ?

REDUCE: Reducing the weight of products, and therefore the amount of material used, is key to the circular economy . Through investments in research, technology and good planning, steelmakers have over the past 50 years drastically reduced the amount of raw materials and energy required to make steel. In addition, the steel industry is actively promoting and developing the use of high - strength and advanced high-strength steel grades in many applications. These grades contribute to the lightweighting of applications, from wind turbines to construction panels and automobiles, as less steel is needed to provide the same strength and functionality.



(Source: ArcelorMittal)

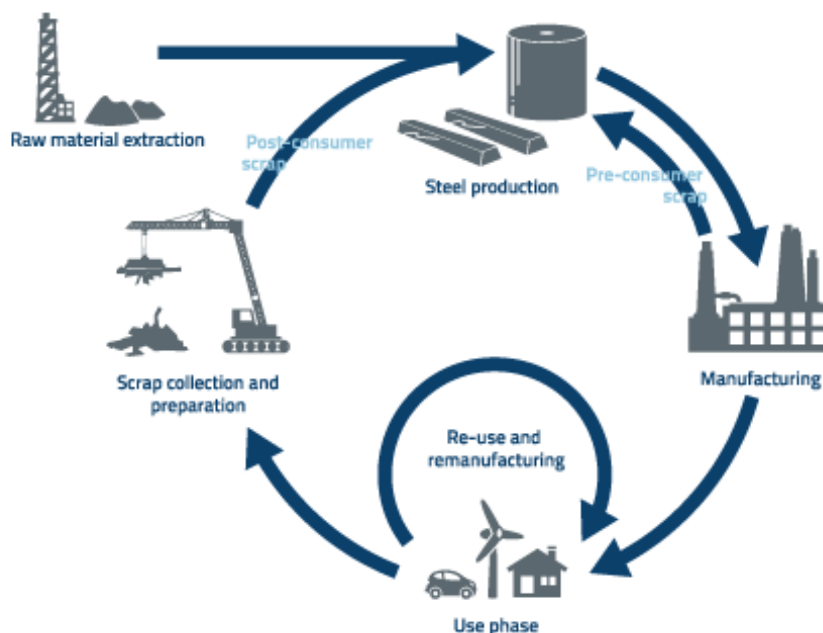
REUSE : Because of its durability, steel can be reused or repurposed in many ways, with or without remanufacturing. This already occurs with automotive components, buildings, train rails and many other applications. Reuse of steel is not limited to its original application; repurposing dates back to ancient times (turning swords into ploughshares). Reuse occurs in sectors where it is technically possible without reducing safety, mechanical properties and/ or warranties. Rates of reuse will increase as eco- design, design for reuse and recycling, and resource efficiency become more commonplace.

REMANUFACTURE: Many steel products, such as automotive engines and wind turbines, can be remanufactured for reuse to take advantage of the durability of steel components . Remanufacturing restores durable used products to like-new condition. It differs from repair, which is a process limited to making the product operational, as opposed to thorough disassembly and restoration with the possible inclusion of new parts.

RECYCLE : Recycling has been carried out in the steel industry since steel was first made. Steel is 100% recyclable and can be recycled over and over again to create new steel products in a closed material loop. Recycled steel maintains the inherent properties of the original steel. The magnetic property of steel ensures easy and affordable recovery for recycling from almost any waste stream while the high value of steel scrap guarantees the economic viability of recycling. Today, steel is the most recycled material in the world. Over 650 Mt of steel are recycled annually, including pre- and post-consumer scrap.

ONCE PRODUCED, STEEL IS AN ETERNAL SOURCE FOR FUTURE GENERATIONS

Source: EUROFER



In a well-structured circular economy, the steel industry has significant competitive advantages over competing materials. The steel industry continues to further integrate these advantages into its operations in order to highlight the benefits of steel to those people making decisions on material choices. Co-operation from the whole production chain is necessary to ensure that reused or remanufactured products have the same properties as new steels.

KIVI oongres Tata Steel Slide 18

Steel in the circular economy



(Source: Bauke Bonnema – Tata Steel)

What about Hot-dip Galvanizing?

Undoubtedly, batch hot-dip galvanizing has many arguments that strengthens 'the steel case' with regards to circular building.

- REUSE: if designers want to integrate reusable steel elements in the structural part of a building, they should use hot-dip galvanizing as the ideal coating system. HDG steel will not suffer from demounting and remounting activities as opposed to painted steel which will need to be repainted or at least repaired. Moreover, HDG offers longer lifetime expectations to steel than other coating systems, which allows frequent reuse of the material.
- REPAIR: although batch HDG requires few maintenance compared to other coating systems, it is easily repairable if needed. Many techniques exist to repair damaged parts and they readily available on the market.
- RECYCLE: zinc is recycled from most of its applications again and again without any loss in quality. In this respect zinc differs from many other synthetic materials for which recycling leads to a lower quality (downcycling) or for which energetic recovery is the only way to make further use of a product after the use phase.

Conclusions

- A shift from linear to circular economy is inevitable and has already started.
- A useful model can be developed based on the 10 R's
- Collaboration at early stage between the partners within the construction chain is crucial.
- Role of the industry: design and manufacture products for circular use
- Role of the authorities:
 - o initiate (through circular sourcing),
 - o stimulate innovation
 - o facilitate bottom-up initiatives (repairshops, etc.)
 - o adapt regulation
- Steel has a strong case and HDG can strengthen the arguments pro-steel in the debate.
 - o easily demountable and remountable
 - o suited for designing prefabricated elements
 - o the highest % of recyclability compared with concrete or wood.
 - o HDG ensures low maintenance cost -> interesting for investors
 - o HDG steel: very limited or no repairs required before reuse
 - o HDG steel: excellent TLCC compared to other painted steel.

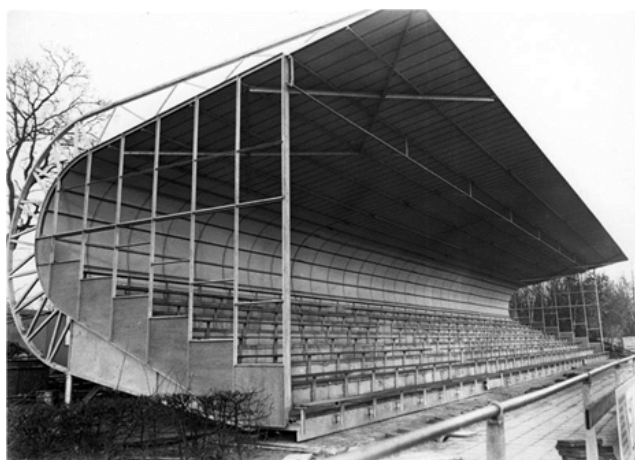
Case studies

1) Grandstand in Gramsbergen (2013) (6)



(Source: Zinkinfo Benelux , Maité Thyssen)

An existing Elasco stand was saved from the sledgehammer thanks to the enthusiasm and decisiveness of one man in particular. In summer 2011, Harry Haverkotte, former board member of SV Gramsbergen, heard that their neighbours from Hoogeveen would move to a new sports park. He bought the main grandstand for €7,000 which included the cost of disassembly. The stand was originally built in 1976. Back then, the board of Hoogeveen awarded the construction for f 139,200. If you would convert this to euro's and take the current purchasing power into account, you would arrive at an amount of ca. €163,000.



(Source: VV Hoogeveen)

Within two years, a wonderful 32m long stand arose from the ground. Eventually, the stand only cost €35,000 while a new building would have at least cost € 200.000. Everything was re-used, apart from the bolts and nuts and the old wooden boards. The boards were replaced by new chairs. The only paintwork that had to be done was on the inside of the roofing.



(Source : SV Gramsbergen, Harry Haverkotte)

The excellent state of the galvanized steel immediately caught the eye during its disassembling. Just to be clear, we are talking about an outer structure that has spent 40 years out in the weather. The galvanized steel was in perfect state, nothing had to be sprayed or regalvanized. Zinkinfo has performed measurements on the steel in 2015. The zinc coating still totals more than 100 μm . In our view, the stand can still last at least 50 years.

2) The Greenhouse – Utrecht (2018) (7)

In 2014, Cepezed was commissioned to convert the former Knoop Barracks in Utrecht into a modern government office complex. The Central Government Real Estate Agency (Rijksvastgoedbedrijf) requested, as part of the project, a solution for the space between the barracks and the neighbouring Rabobank head office. As a definitive use for this location does not have to be determined until fifteen years from now, a temporary function was sought to liven up the site, which otherwise would remain unused. Cepezed developed a plan whose function and architecture would both be based on circularity.



(Source: Cepezed)

The Green House houses a ‘circular’ hotel/catering concept plus conference facilities. True to the principles of circularity, the entire building (including its Stelcon plate foundation and prefab concrete blocks) can be disassembled. In fifteen years, it can be taken apart and rebuilt at another site. Re-use also played an important part in the choice of materials for the project.

The two-layer pavilion was designed as a generic construction kit with a disassemblable steel frame comprised of hot-dip galvanised profiles. The dimensions were derived from those of the smoked-glass facade cladding of the former barracks – the cladding was re-used for the building’s second skin and the pavilion’s small greenhouse.

The Glass House’s circularity can also be found in the fact that the right floor was selected for the right location. Pavement stones from an old quay in Tiel were employed for the ground floor in place of the usual poured floor. They lie on a compacted layer of sand with floor heating. The floor in the second layer consists of prefabricated timber elements. For the roof, light perforated steel plate, filled with insulation, was opted for.



(Source: Cepezed)

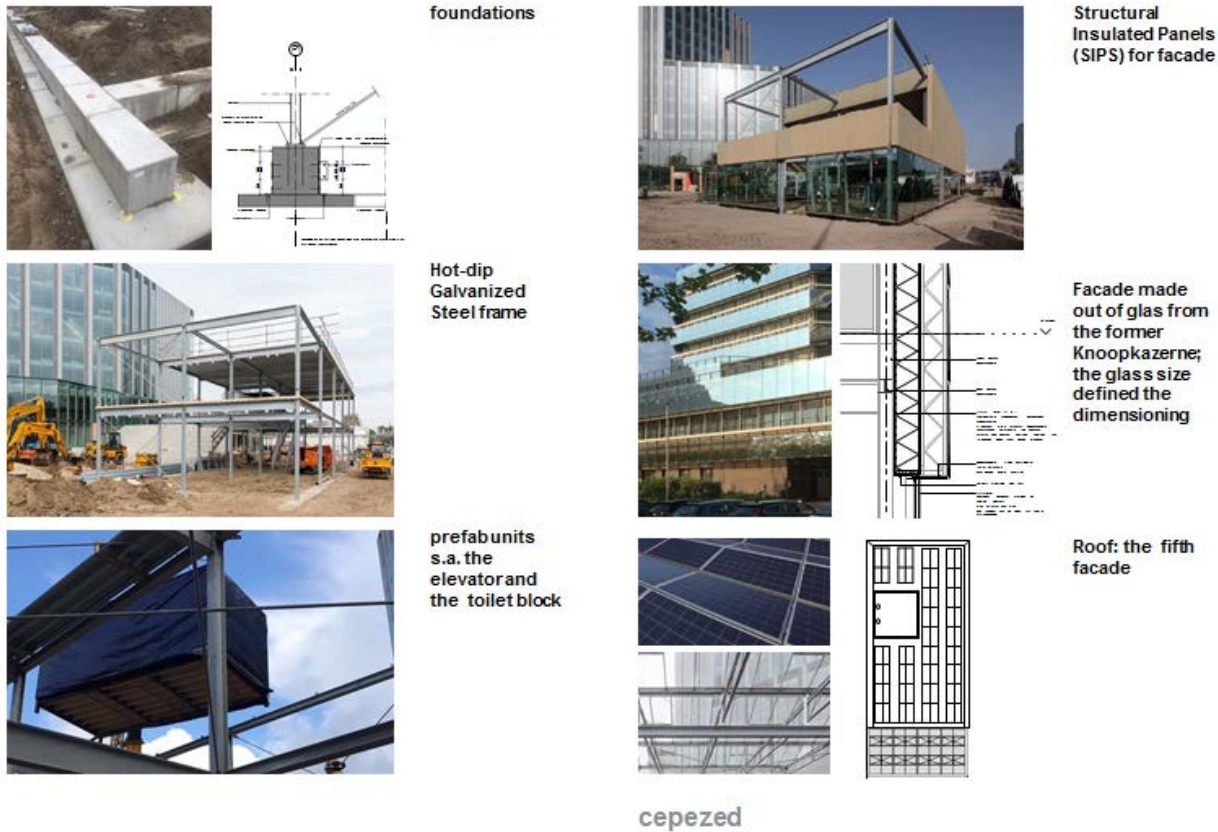
The eighty-square-metre vertical-farming greenhouse is located in the second layer, beside the conference rooms. Here, vegetables and herbs are grown for the restaurant. A mezzanine in the pavilion renders the (publicly accessible) greenhouse clearly visible from the restaurant below. Large green walls also substantially contribute to the overall feel of The Green House. The pavilion's roof is filled with solar panels.

The Green House features a 'first': a plugless kitchen in which meals are prepared without the use of electricity, but, rather, with energy-efficient ovens heated with renewable fuels. Much of the furnishings were found by means of urban mining; the new furniture was made using re-cycled materials.

Motivation for the use of hot-dip galvanised steel for The Green House

The circular pavilion The Green House, is to remain at its present location in Utrecht for a limited period. Following this initial use, it will take up a new function at a new location. The design's relocatability is facilitated by a modular and reassemblable construction system, featuring a steel main load-bearing construction. Owing to their high degree of precision, steel components are easy to take apart and put together again. A special feature of the steel frame of The Green House is its square grid, with which multiple building configurations are possible with one-and-the-same construction kit.

circular building elements



(Source: Cepezed)

Both the pavilion’s structure and steel profiles are fully visible. In terms of appearance, the hot-dip galvanised steel underscores perfectly the bold character of The Green House and the urban-farming greenhouse. After all, hot-dip galvanised steel is often used in farmhouse construction.

Additionally, hot-dip galvanisation lends itself well to disassembly and reassembly, as the coating will not be damaged through work or transport.

In devising a self-contained circular business case, the submitters also searched for sustainable materials that were as economically advantageous as possible. **Hot-dip galvanised steel has a good price/quality ratio and is an excellent choice in terms of sustainability, as well.**

3) Temporary Car Park Morspoort – Leiden (2012)



(Source: Continental Car Parks)

The winning proposal of a competition to design a temporary parking garage in Leiden, the Netherlands. The building fits into its urban planning setting at the edge of the city centre, facing the 'Morspoort'. The parking floors have been divided up in a readily accessible way, with parking places that are easy to turn into, and are furnished with clear signals and signs. The façade is partly transparent, allowing a view out onto the surroundings. In addition, a minimum number of slim columns have been used, in order not to block sight lines and to provide a feeling of safety. The parking garage contains 410 parking places, but the building is very compact, allowing the existing stands of trees along the road to be retained.

The garage is situated facing the western gate to the city, the 'Morspoort', and will be operated by the municipality over the next 10 years. This period could possibly be extended for a flexible period of 10 years, with regard to structure and management. ultimately, the ground has to be made available again for urban development. The use of recyclable materials means the building is easy to remove.

Hot-dipped galvanized steel

The entire structure of the car park is made of hot dip galvanized steel elements: columns, beams (high grade steel), cross members, fences... Hot dip galvanized steel proved to be perfect choice for a car park that had to be easily demountable afterwards. HDG doesn't require periodic maintenance and after demounting/remounting it will need few or no after-treatment. The self-healing effect of the zinc layer ensures a second life to the steel structure. Steel offers a lightweight solution allowing a design with slender columns. And as we all know, slenderness means more daylight into the building.

References

- (1) + (5) Brochure "Steel in the circular economy. A life cycle perspective © World Steel Association, 2015. www.worldsteel.org
- (2) Jacqueline Kramer – Utrecht Sustainability Institute : "From a linear towards a circular economy" www.usi.nl
- (3) Nederland circulair ! : E-book: " maak je bouwproject circulair" www.circulairondernemen.nl
- (4) Transitieteam Circulaire Bouweconomie: Transitieagenda 2018-2023
- (6) Zinkinfo Benelux , Elasco – Duurzaam sporterfgoed , 2015
- (7) Cepezed - The Greenhouse, 2018 www.cepezed.nl
- (8) Paul de Ruiter Architects, Parkeergarage Centrum Morspoort, 2012

Session 9:

Galvanizing Meets Market Demands

Application of Galvanized Steel for the Construction of Utility

Tunnels in China

Qifu ZHANG

*(NEL of Advanced Coating Technology for Metals, China Iron & Steel Research Institute Group, Beijing 100081, China
China Galvanizers Association, Beijing 100081, China)*

Abstract: The underground utility tunnel is an important part of smart cities, and its construction is also a key measure to promote urbanization in China. At present, the utility tunnels in China are mainly concrete structures. During the construction process, the traffic and the surrounding environment would be affected due to the excavated road. It needs a long construction period, and the later maintenance is very difficult. This article proposes to apply the galvanized corrugated steel structures in underground utility tunnels to achieve the goal of easing steel overcapacity and improving the construction of municipal facilities. It can also reduce costs to the greatest degree while ensuring its mechanical performance and corrosion resistance.

Keywords: utility tunnel, galvanizing, corrugated steel

1. Introduction

The underground utility tunnel can house a full range of electric power, water, communications, gas, heating lines, and other public services, and it is a new model to effectively solve the contradictions in urban infrastructure construction. According to the “Guiding Opinions of the General Office of the State Council on Promoting the Construction of Urban Underground Integrated Utility Tunnel (No.61[2015] of the State Council)”, a complete system of utility tunnels will be built by 2020 to achieve high-quality urban planning in China.

At present, most of the present tunnels are prefabricated concrete and cast-in-place utility tunnels, which have some shortcomings such as high cost and long construction period. Relatively speaking, the advantages of corrugated steel utility tunnels are prominent. Corrugated steel utility tunnels are made of the steel plates with a thickness of 1.6 ~ 12mm, they are machined by cold rolling in the factory and quickly fabricated together at the construction site. As early as 1945, a corrugated steel utility tunnel was built in Jena, former East Germany. It adopted the anti-corrosion method of hot-dip galvanizing and has been used for more than 72 years. In 1991, a single-cabin corrugated steel utility tunnel with a length of 3 km was built in the industrial park in Kassel, Hessen, Germany, which included pipelines for water supply, heat, electricity, communications, and sewage. And it has been used for more than 26 years. The corrugated steel utility tunnels have an unparalleled superiority to the concrete utility tunnels and can play an active guiding role in the construction of urban utility tunnels. In May 2017, the 50-meter test section of the prefabricated steel utility tunnel was built in Hengshui City, Hebei Province, China, and it has passed the evaluation and acceptance.

2. Advantages of Corrugated Steel Utility Tunnels

With the rapid advancement of underground utility tunnel construction, the market space of the corrugated steel utility tunnel has been greatly expanded, which has also become a rare opportunity for iron and steel enterprises to solve the problems of overcapacity. Compared with traditional prefabricated concrete utility tunnels and cast-in-place utility tunnels, the prominent advantages of corrugated steel utility tunnels are mainly manifested in the following aspects:

1) Lower Cost

The utility tunnel consists of tunnel body and pipelines. According to the trial version of national standards on investment, it is estimated that the underground utility tunnels will cost about 56-131 million yuan (considering only the construction costs of the tunnel body), as shown in Table 1. Taking into account the total length of the utility tunnels in China, the total investment would be 1.6-3.2 trillion yuan. Based on the actual measurement in the test section of Hebei, the total cost of the corrugated steel utility tunnel was reduced by 10% to 20% compared with the traditional concrete structure, which means that it can save nearly 10 million yuan per kilometer.

Taking the 4×3.5m reinforced concrete utility tunnel as an example, the construction cost is about 80 million yuan per kilometer, while the construction cost of ϕ 4.5m corrugated steel structure is about 60 to 70 million yuan per kilometer, and it can fully meet the demands. In addition, the steel can be 100% recycled, with obvious advantages in the cost. Through calculations, the cost advantage of the steel structure becomes more obvious if the utility tunnel is longer than 20km, and the longer the utility tunnel, the more obvious the price advantage.

Table 1 Construction Costs of Underground Utility Tunnels in China

Type of Utility Tunnel	Construction Cost (million yuan/Km)
10-20 (single-cabin)	56
20-35 (single-cabin)	68
20-35 (double-cabin)	79
35-45 (double-cabin)	110
35-45 (triple-cabin)	119
35-45 (quadruple-cabin)	131

2) Short Construction Period

The construction of traditional cast-in-place concrete utility tunnels is restricted by technology and climate, and has a greater impact on surrounding traffic and environment. The corrugated steel utility tunnel adopts integrated corrugated steel pipe (diameter<3m) or assembled corrugated steel plate, it can be processed and produced in the factory and assembled on-site, as shown in Fig.1, the construction period can be shortened by 30%-50 % comparing with the cast-in-place concrete structure. It is very suitable for projects requiring short-term construction such as emergency repairs.



Fig.1 Assembly Corrugated Steel Utility Tunnel

3) High Safety

The traditional cast-in-place concrete utility tunnel is a long-distance linear structure, which requires uneven settlement along the way and longitudinal deformation coordination ability. Assembled corrugated steel utility tunnel adopts corrugated steel plates (pipes) with light weight and strong flexibility, which can better adapt to various geological environment and conditions. According to the

theoretical determination, the weight of the steel utility tunnel is only one-third of the concrete structure. Compared with traditional reinforced concrete materials, steel components are mostly standard parts formed by production lines. They are assembled on the construction site and have obvious advantages such as uniform material quality, strong stability, and convenient transportation and assembly, making it easy to fully develop the quality control of the projects.

4) Long Service Life

The construction quality of the traditional concrete utility tunnel is greatly affected by the construction environment, construction technology and management level, and the quality is difficult to control. However, most of the steel utility tunnels are large-section thin-walled structures, assembled steel utility tunnels are produced in batches by the factory, and the product quality is easy to detect and control. Reliable quality and long service life can be achieved through multiple preservatives. Theoretical calculations show that the corrugated steel utility tunnel can prolong the service life by 20%, and its main body structure can serve as long as 120 years.

5) Environmentally Friendly

The construction of the reinforced concrete utility tunnel has an obvious impact on the urban environment. And it needs a huge amount of materials and a long construction period. While the corrugated steel utility tunnel has obvious advantages such as less dust, less noise and high assembly speed, which can greatly reduce the adverse effects on the appearance and transportation of the city. In addition, it can reduce the amount of natural materials such as cement, gravel, sand, protect the environment, and reduce the carbon footprint. Therefore, the construction of the corrugated steel utility tunnel is conducive to building a better environment.

6) Promoting Related Industrial Chain

The production of corrugated steel utility tunnels depends on the implementation of imported and upgraded technologies and equipment on the basis of traditional steel structure processing, the construction of prefabricated production lines in the updated fields, complex and sophisticated hot-dip galvanizing, spraying operations. It requires a large amount of local resources, thus increases employment opportunities and upgrades the skills of workers. It not only avoids the long-standing phenomena of “zip road” and “city spider net”, but also has a positive significance in resolving excess steel production capacity in China. If corrugated steel utility tunnels are used, nearly 4,000 tons of steel are consumed per kilometre, and the initial planning of the utility tunnel is not less than 50 kilometers according to the reference data. The steel consumption in the construction of tunnel body alone is about 200,000 tons. This data is of great appeal to local governments, especially those local governments who need to resolve the huge pressure on steel overcapacity. Therefore, the construction of steel utility tunnels can be regarded as a major advantage in economic restructuring.

3. Construction of Utility Tunnels in China

The utility tunnel, as a major capital investment in urban development, should be considered in the broad context of the urban planning strategy. The underground utility tunnel will not only promote the urbanization, but also will stimulate investment. In May 2017, the "13th Five-Year Plan for the Municipal Infrastructure Construction in Nationwide Cities" issued by the State Council required that more than 8,000 km of underground pipelines should be constructed by 2020.

3.1 Types of the Utility Tunnels in China

With the continuous improvement of urbanization, underground pipelines are more and more complicated. According to statistics, the incidence of underground pipeline accidents throughout the country is as high as 5.6 times per day, and the direct economic loss caused by ground excavation is

nearly 200 billion yuan every year. Therefore, it is necessary to build reasonable utility tunnels. According to the nature of the included pipelines, it can be divided into trunk utility tunnel, branch utility tunnel and cable utility tunnel; according to the number of cabins, it can be divided into single-cabin utility tunnel, double-cabin utility tunnel and multi-cabin utility tunnel; and in terms of the construction method, it can be divided into the open-cut method, cut-and-cover method and shield-driven method. In addition, the sectional shapes of utility tunnels can be rectangular, circular, tubular, pyriform and so on. For concrete utility tunnels, their sections are mainly rectangular and circular, as shown in Fig.2. Based on the research of J.H. Wang, the rectangular section is adopted for shallow utility tunnels, while the circular section is adopted for deep ones; for corrugated steel utility tunnels, their section is not likely to be rectangular, for example, the section of the corrugated steel utility tunnel in Hebei is pyriform, as shown in Fig.3.

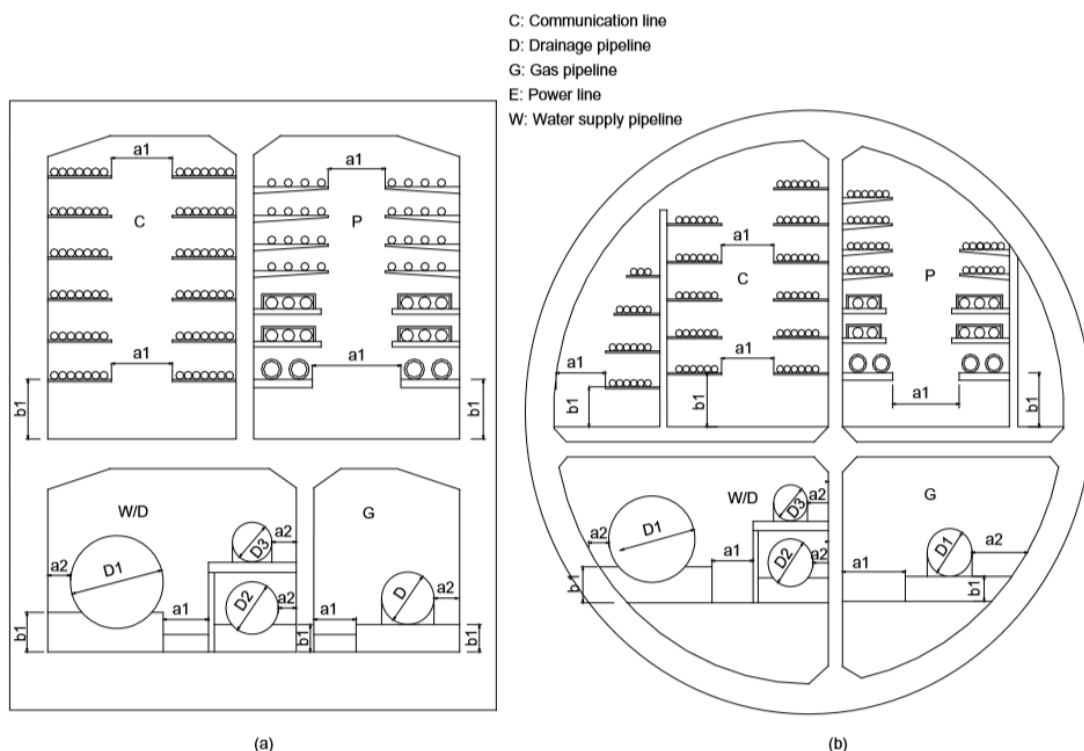


Fig.2 Diagram of Utility Tunnels

(a) rectangular section type; (b) circular section type



Fig.3 Corrugated Steel Utility Tunnel in Hebei

In order to promote the sustainable and healthy development of the construction industry, the State Council has proposed the promotion of prefabricated building structures. The vigorous development of fabricated building structures is conducive for the promotion of industrial restructuring and upgrading, and is in line with the concept of energy conservation and high efficiency. The research and

development of the corrugated steel utility tunnel is precisely in line with the strategic orientation of the prefabricated building structures. The prefabricated steel utility tunnel is a novel system made of galvanized corrugated steel plates (pipes) fastened with high-strength bolts, load-bearing ring beams and assembled brackets mounted internally, combined with external anti-corrosive coatings, high-tech waterproofing means and internal fire-resistant cloths.

3.2 Application of Galvanized Steel in Utility Tunnels

The steel utility tunnels emerged relatively late in China. In May 2017, China's first fabricated corrugated steel utility tunnel was built in Hengshui City, Hebei Province. The utility tunnel has a total length of 1.8km, an internal net height of 4.8m and a net width of 6.5m. It is a double-cabin utility tunnel, and the pipelines in this utility tunnel include power, communication, heat, sewage, water supply, and reclaimed water. The 50-meter experimental demonstration section of the fabricated corrugated steel utility tunnel fully complies with the requirements of the Technical Code for Urban Utility Tunnel Engineering (GB50838-2015), Technical Specifications for Corrugated Steel Utility Tunnel Engineering (DB13(J)T 225-2017) and related specifications.

In addition to the fabricated corrugated steel utility tunnel in Hebei, steel utility tunnels have also been built in Qinghai, Heilongjiang and Shandong, as shown in Fig. 4. The construction of utility tunnels in Haidong, Qinghai will reach 79.33 kilometers by 2020, with a total investment of 5 billion yuan. Zhengping Group is building the first all-steel utility tunnel in the northwestern region.



Fig.4 Corrugated Steel Utility Tunnels

3.3 Prospect of Galvanized Steel in Utility Tunnels

With the implementation of the “Go globally” and the “Belt and Road Initiative”, the national infrastructure construction along the Belt and Road is on the rise. The batch export of corrugated steel utility tunnels can not only greatly transfer China’s excess steel production capacity, but also realize all-round and multi-level interconnection and interoperability with countries along the Belt and Road relying on the successful output of complete sets of equipment and technology. In addition, according to "2018-2022 In-depth Research and Investment Forecast Report of China’s Urban Underground Utility Tunnel Construction" released by CIConsulting: At this stage, the construction of urban utility tunnel is just in a pilot phase in our country, but it is also the most favorable opportunity for the large-scale development of urban utility tunnels, the underground pipelines for water supply, drainage, gas supply and heating in our country have already exceeded 1.48 million kilometers and it is at the peak of construction and urban renewal now. Based on the research of Chao Yang, the trend of the utility tunnel construction in China is shown in Fig.5.

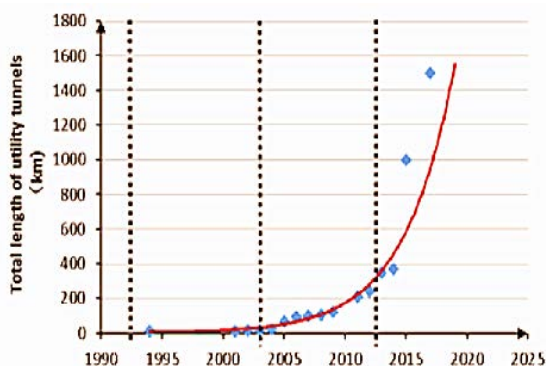


Fig.5 Growth Curve of Utility Tunnels in China

According to the requirements of the “Technical Specifications for Corrugated Steel Utility Tunnel Engineering” implemented on June 1, 2015, the design life of the underground utility tunnel is 100 years, and the life expectancy of hot-dip galvanized corrugated steel utility tunnels recommended by the US AISI standard and AASHOTO standard is 37.5 to 78 years. Though it has been proven that hot-dip galvanized steel with 600g/m² zinc coating has a service life of more than 75 years, and some studies indicate that hot-dip galvanizing and flexible ceramics or bitumen can provide the underground utility tunnel with a service life over 100 years. Utility tunnels are always placed underground, they are subject to a hot and humid environment that is a fertile ground for corrosion of steel, which could lead to potential failure and collapse of the tunnel. It is still necessary to adjust the process to enhance the corrosion resistance of the steel structure.

In February 2016, the State Council issued the “Opinions on Resolving the Excess Production Capacity in the Iron and Steel Industry to Achieve Extricate Development”, proposing to reduce the steel production capacity by 100-150 million tons in 3-5 years. As the anti-corrosion technology of buried steel products is gradually maturing, it already has the foundation of a large-scale promotion of the steel utility tunnel. On April 1, 2017, Xiong'an New Area was officially established, which brings a huge market for steel utility tunnels, and it is taken as an example to analyze the market of utility tunnels in China. Compared with other cities, the Xiong'an New Area is built from scratch, and the cost of laying an underground pipe gallery utility tunnel is lower and the resistance is smaller. As shown in Table 2, the Xiong'an New Area's long-term investment on utility tunnel may reach 100 billion yuan.

Table2 Market Prospect of Underground Utility Tunnels in Xiong'an New Area

	Coverage area (km ²)	Distance (km)	Unit price (billion yuan/km ²)	Market size (billion yuan)
Initially	100	26-46	0.12	3.12-5.52
Medium-term	200	52-92	0.12	6.24-11.04
Long-term	2000	520-920	0.12	62.4-110.4

In accordance with the annual construction length of 2000 km, the unit cost of 80-120 million yuan/km (the current unit cost is about 0.8 billion yuan/km), the market of underground utility tunnel is about 1600-240 billion yuan per year, the investment of underground utility tunnel during the "13th Five-Year" period is about 640-960 billion yuan. Using the corrugated steel utility tunnel can resolve the contradictions and pressures of local government on investments to a considerable extent. And the PPP mode will become the main method in the trillion-scale market for solving the long-term investment in the underground utility tunnel.

Currently, most corrugated steel utility tunnels adopt hot dip galvanized coating as the basic coating. Generally, hot-dip galvanized coatings have a service life of 25 to 50 years and most of the coatings can serve more than 40 years. However, in underground and acidic or alkaline environments, hot-dip galvanized coatings will quickly corrode and are generally not recommended to be used in underground environments, an over-wrapped protective coating also plays an important role. In most instances, hot dip galvanizing and other external anti-corrosion coatings are jointly used in the corrugated steel utility tunnel engineering. It has both superior mechanical properties and chemical resistance of polymer materials. And it can perfectly meet the requirements of anti-corrosion for underground utility tunnels.

4. Conclusions

Corrugated steel utility tunnel is expected to replace the traditional reinforced concrete utility tunnels, which has become the general trend of development. The main conclusions of this paper are as follows:

- 1) China is in a period of rapid development of urbanization, the construction of underground infrastructure is lagging behind, but the construction of underground utility tunnels is facing an unprecedented opportunity for development;
- 2) In recent years, many policies and measures have been promulgated by Chinese government to vigorously promote the construction of underground utility tunnels, thus solving the problems of urban construction and steel overcapacity;
- 3) Hot-galvanized corrugated steel utility tunnel has begun to develop and being applied in China, which will greatly promote the development of urbanization;
- 4) There is not enough relevant standards and specifications for corrugated galvanized steel used in utility tunnels, which needs all of us to make greater efforts.

References

- [1] No.61[2015] Guiding Opinions of the General Office of the State Council on Promoting the Construction of Urban Underground Integrated Utility Tunnel
- [2] State Council: 13th Five-Year Plan for the Municipal Infrastructure Construction in Nationwide Cities
- [3] Jianhong Wang, Atushi Koizumi, Xinrong Liu. Advancing sustainable urban development in China[J]. Municipal Engineer, 2008, 3-10.
- [4] DB13(J)T 225-2017 Technical Specifications for Corrugated Steel Utility Tunnel Engineering
- [5] GB50838-2015 Technical Code for Urban Utility Tunnel Engineering
- [6] CIConsulting: 2018-2022 In-depth Research and Investment Forecast Report of China's Urban Underground Utility Tunnel Construction
- [7] Chao Yang, Fang Leping. Discussion on the development of underground utility tunnels in China[J]. Procedia Engineering, 2016, 540-548.
- [8] State Council: Opinions on Resolving the Excess Production Capacity in the Iron and Steel Industry to Achieve Extricate Development

Beyond construction – galvanizing in transport and other applications

H Glinde, Industrieverband Feuerverzinken (Germany)

Approximately 50 percent of all batch galvanized steel in Germany is used in the construction industry. Beside that the transport and automotive sector and mechanical engineering are with more than 10 percent of the tonnage other important markets for batch galvanizing in Germany.

Galvanizing for the automotive industry - a short historical review

Until the 1970ies corrosion had been a big problem for the automotive industry. Rusty cars were all around. If things went well, ten years without any repairing by welding were possible. If it was bad, then the end could come after six years. A lack of corrosion protection in combination with poor steel qualities ensured that even most cars from the premium segment had to be repaired by welding after 10 years.

In 1975 Porsche found a solution. The 911 became the first production car to receive a continuously galvanized body (Image 1). For that reason Porsche was able to offer a six-year warranty against rust, which was extended later even to ten years. The galvanized bodywork improved not only the life time, but also the safety of the vehicle, because the measure maintains the overall stiffness and crash safety of the body despite aging vehicle.

Ten years later in 1985 Audi started the mass production of what they called „complete galvanized“ cars using a mix of continuously hot dip galvanized and electro plated parts. Even the cars were not batch galvanized, galvanizing was seen as the only proper way to protect steel against rust. The fact that Audi did a huge global advertising campaign (Image 2) brought the message that galvanizing is the best protection against rust into everybody's mind. Galvanizing became for the automotive industry the super-hero for corrosion protection. Many other car producers started offering galvanized cars.

A few car producers like Talbot Matra, Renault, Lotus and BMW introduced batch galvanized chassis for some models, e.g. the BMW Z1 (Image 3). In addition to that batch galvanizing became in fashion within the growing classic car restoration scene, which was very often a nightmare for galvanizers, because batch galvanizing of car bodies that are not designed for galvanizing made a lot of problems. Nevertheless there are many classic cars on the road that had been batch galvanized during the restoration process. Examples are Porsche 914, Volkswagen Beetle (Image 4) or Alfa Romeo Spider. Even a book based on a masterthesis had been written about batch galvanizing of classic cars (Image 5). As a positive result of that batch galvanized chassis parts are available as small series aftermarket parts for classic cars like Citroen 2 CV or Landrover models until today.

Galvanizing for transport and automotive - today's situation

Today in Germany the main markets for batch galvanizing in the automotive industry are:

- production of components for cars,
- chassis and other components for light commercial vehicles
- chassis and other components for car trailers
- chassis and other components for truck trailers

Production of batch galvanized components for cars

Numerous car manufacturers are increasingly reducing the steel thickness of bodywork with the aim of saving weight and costs. As a result, the underbodies of the cars must be reinforced by stabilizers to achieve the necessary stiffness. While corrosion is not anymore a problem for bodywork, there is today still existing a corrosion problem for underbody components. Some car producers try to solve it by using paint systems, whereas the German premium car producers BMW and Mercedes Benz are using batch galvanized underbody components in mostly all car models. These components are usually stabilizing parts and landing gear parts. An example are galvanized landing gear components for the BMW M6 (Image 6). With regard to the high production numbers of BMW and Mercedes Benz it is clear that even „light“ batch galvanized parts represent a high tonnage for the German batch galvanizing industry. Batch galvanizing is for underbody parts the most efficient solution, because of its robustness and resistence against heat from the exhaust pipe.

Production of chassis and other components for light commercial vehicles

Light commercial vehicle is the official EU-term for a vehicle with a gross vehicle weight of up to 3.5 tonnes. Typical Light commercial vehicles are for example Mercedes Sprinter, Volkswagen Transporter, Iveco Daily or Ford Transit. More than 2,1 million units of Light commercial vehicles had been produced within the European Union in 2016. Most of them are sold directly as standard products to the costumers. A very small share, which is a high five digit number, is modified by spezialized vehicle construction companies. These spezialized vehicle construction companies are often linked to the big Light commercial vehicles Producers by Partner-Programs and a lot of these modified vehicles can be ordered on the selling platforms of the Light commercial vehicles Producers. Typical modifications are Platform vehicles and car transporters, refrigerated box constructions, Sales vehicles, Horse transporters, Boxbodies, Minibuses, Money and Valuables transporters or Motorhomes. For many of these modiflicated Light commercial vehicles galvanized chassis are used (Image 7). Big vehicle construction companies like AL-KO are producing up to 9000 chassis per year.

Chassis and other components for car trailers

Trailers for cars and light commercial vehicle are limited to 3,500 kg permissible maximum mass. There is a big variety of trailers availbale with different numbers of axles and for a lot of purposes. Examples are vehicle trailers, Live stock trailers, tipper trailers, commercial trailers, boat trailers and caravans. According to the german trailer association more than 200.000 units of trailers limited to 3,500 kg permissible maximum mass are produced per year. The majority of these trailers have a batch galvanized chassis. Some trailers producer also offer duplex-coated models, e.g. boat trailers for premium motor or sailing yachts. In addition to that batch galvanized steel is used for a lot of other components e.g. profiles for load platforms or tail boards, frames for tippers, jockey wheels etc.

Chassis and other components for truck trailers

Corrosion has been an undeniable problem for commercial vehicles for decades. Snow, rain, dew salts and highway stone as permanent stress factors left their mark on the truck semi-trailers after just a few years. The robust hot-dip galvanizing offered an effective alternative, but was an extremely challenging task for the vehicle designers. Although galvanizing had proved its worth as corrosion protection for car trailers for decades, galvanizing of truck trailers was considered technically challenging for a long time. Hot dip galvanized truck trailers could only be found as rare single solutions. The situation changed abruptly, when radical construction design changes allowed the market leader Schmitz Cargobull to galvanize its truck trailers, creating a revolution in the industry with a hot-dip galvanized chassis (Image 8). Numerous other manufacturers then also switched their production to corrosion protection by batch galvanizing. Some manufacturers went the wrong way and changed from wet painting to solutions like cathodic dip painting to improve the corrosion protection performance of their trailer. Corrosion protection was for some years the central issue in the competition between the manufacturers of truck trailers. Today even former opponents rely on the corrosion protection by hot-dip galvanizing. Some truck trailer producers give their costumers the possibility to choose between painted or batch galvanized chassis.

Typical products of the trucktrailer business are curtainsiders, box body trailers, flatbed semitrailers, container trailer and tipper. More than two thirds of the western european trucktrailer market is served by german producers. The market leader with a share of 33 percent is Schmitz Cargobull, a german company that is mainly focussed on the production of trailers with batch galvanized chassis. Other bigger german companies, that offer batch galvanized trailer chassis are the Humbaur/Kögel-Group, Sommer and Fliegl. Many other small truck trailer producer in Germany offer galvanized trailers as well. In addition to that a lot of other bigger and smaller components like bumpers, stakes, ramps, sparewheelcarrier are batch galvanized.

Other applications

There are in Germany many other applications beyond the construction industry where batch galvanized steel is used, mostly for components for mechanical engineering products. Cranes, special machinery and vehicles for use in agriculture, forestry and construction or vehicle cleaning technology for cars and trucks are a only few examples for that (Image 9).

Outlook and conclusion

Although the use of batch galvanizing in the automotive sector has lead to a largely disappearance of corrosion, there is still need for action. Untill today electroplated galvanized components are in use that get rust after a short time. Coated components also show corroding phenomena at edges and in the welding areas. If continuous galvanized components are used, edgeband rust is preprogrammed. The ban of the use of chromium (VI) increases the demand of reliable corrosion protection systems as well. So from a corrosion protection point of view there is even now a really big additional potential for batch galvanizing in the automotive sector.

New chances for galvanizing will be offered by the change to electro mobility, that will be expected for the next years. Electromobiles will have no traditional gearbox. For that reason the space of the engine bay must be closed by additional underbody components and/or be stabilized. The weight of electro mobiles is higher than the weight of traditional cars. This will make additional stabilizing components necessary. Electromobiles will produce less heat. The positive drying effect by traditional motor heat with regard to corrosion protection will not exist anymore. The strength of corrosion protection becomes more important. Batch galvanizing can offer solutions for electromobiles.

Biography:

Holger Glinde holds a degree in business administration and is been working as the head of marketing and business administration for more than 2 decades for the Industrieverband Feuerverzinken, which is the German Galvanizers Association. Since 2007 he is Editor-in-Chief of the International Journal of Hot Dip Galvanizing and since 2012 Chairman of the Marketing Committee of the European General Galvanizers Association (EGGA).

Images:



Image 1: In 1975 Porsche started producing the 911 model with a continuously galvanized body. (Image: Porsche AG)

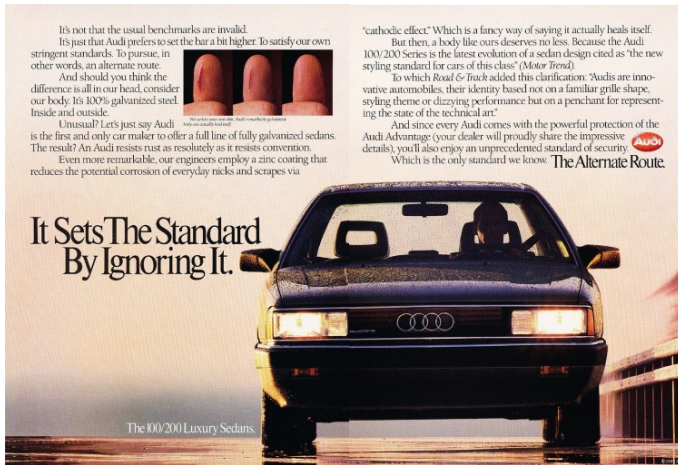


Image 2: Audi did a huge global advertising campaign and brought the message that galvanizing is the best protection against rust into everybody's mind. (Image: Audi AG)

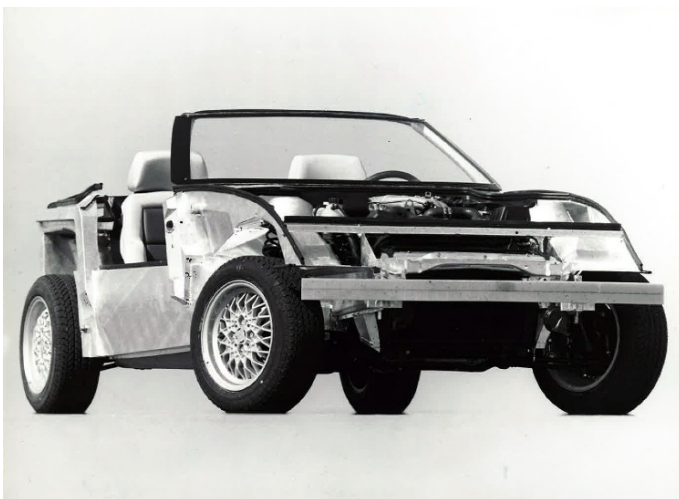


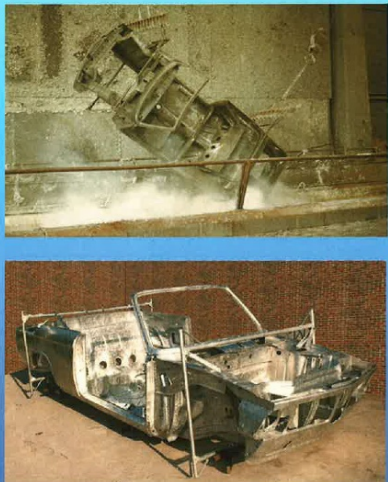
Image 3: The BMW Z1 has a very complex batch galvanized chassis. (Image: BMW AG)



Image 4: Restored Volkswagen Beetle with batch galvanized body. (Image: Institut Feuerverzinken)

Korrosionsschutz von Automobilkarosserien durch Feuerverzinken

Emil F. Rohrer



Basiert auf der Diplomarbeit:
Optimale konstruktive Gestaltung von Kraftfahrzeugkarosserien zum Feuerverzinken in Tauchbädern am Beispiel eines BMW 1600-2 Cabriolets

Image 5: E Rohrer wrote a book about galvanizing of classic cars.



Image 6: Batch galvanized landing gear component of the BMW M6. (Image: BMW AG)



Image 7: Chassis-production in the AL-KO-Factory. (Image: AL-KO)



Image 8: Schmitz Cargobull is producing batch galvanized truck trailer chassis for more than 15 years. (Image: Schmitz Cargobull)



Image 9: Special machinery for use in construction like the Zemmler screening station are using batch galvanized components. (Image: Zemmler)

DURABILITY DESIGN USING GALVANIZED REINFORCEMENT

Peter Golding - Galvanizers Association Australia

Frank Papworth, Building and Construction, Research and Consulting (BCRC)

Abstract:

Durability design using carbonation and chloride models continues to gain favour as a means of assessing requirements for specific projects and to assess the benefits of different materials. Models in international codes are based on full probability analysis or by using partial factors derived from full probability analysis. In both cases the precision of the analysis is dependent on the accuracy of the distributions used for the key input variables. The paper discusses this with specific reference to critical chloride level (C_c) for corrosion initiation.

Use in practice has shown galvanized reinforcement adds significantly to longevity of structures. This is discussed. However, there is a lack of information on C_c for galvanized reinforcement, the key parameter responsible for the performance improvement. The paper shows the design life improvement expected from galvanized reinforcement assuming the 2-3 times improvement in C_c found in limited research but notes that a better-defined distribution for C_c of galvanized reinforcement is required.

Keywords: Galvanized reinforcement, corrosion, marine, carbonation, modelling, critical chloride level.

1. Introduction

The rust that forms on reinforcement in concrete is expansive and causes cracking and spalling of the concrete as well as loss of the reinforcement diameter. The cost of repair can exceed the cost of original construction even excluding the operational costs. When operational costs include public costs, repairs can cost many times the cost of original construction. Robert Courland [1], contrasts longevity of modern concrete with that of Roman structures, noting that 'our ignorance' in durability design has led to repair and rebuilding costs of trillions of dollars in USA alone to be paid by future generations. But in assessing reinforcement corrosion financial costs are not all that matters. Modern society and its codes now recognise that equally important are environmental and safety costs. The increasing rate of corrosion induced damage since the 1970's, and a growing awareness of the importance of sustainability in construction has led to a ground swell in defining appropriate durability design processes.

Service life design of reinforced concrete was a major development introduced in the International Federation for Structural Concrete (*fib*) Model Code 2010 [2] and will become an even more integral part of the Model Code 2020. MC 2010 introduced for the first time the concepts of consequence-based reliabilities in durability design and design life models for chloride ingress and carbonation. These approaches were developed in conjunction with ISO 16204 [3] and are becoming the central planks of durability design worldwide.

Extensive as MC2010 is on durability design it does not give any guidance on galvanized reinforcement noting only, "*The following special types of steel that show enhanced corrosion protection properties can be used: galvanized steels, epoxy coated steels and stainless steels.*" Use of reinforcement with a high resistance to corrosion has the potential to reduce the impost of reinforcement corrosion by orders of magnitude.

This paper investigates the new service life design processes in *fib* Model Codes in regards the potential benefits of using galvanized reinforcement and highlights the research required to overcome 'our ignorance' of parameters required to design appropriately.

2. The Reinforcement Corrosion Process

A commonly accepted theory for the corrosion activation of steel in concrete is described below. A passive oxide film forms on the surface of steel or zinc in concrete. If the passive film breaks down, then corrosion rates can be high.

2.1 Chlorides

Chloride ions at sufficient dosage break down the passive film while hydroxyl ion from the cement continue to build it. Only when the chloride to hydroxyl ion ratio is high enough, known as the critical chloride level, C_c , does the passive layer break down and corrosion commence. The hydroxyl ions derive from the cement. As cement content is known and the hydroxyl ion content is not, it is common to refer to C_c as a function of the cement content.

The hydroxyl ions determine the pH of the concrete. A change in pH from 13.5 to 12.5 would indicate a 10-fold reduction in the hydroxyl ion content and indicate a similar reduction in C_c . This level of pH change would not be detected in a normal carbonation tests using phenolphthalein which only indicates a change in pH at a pH of approximately 9.5.

The principle benefit of using galvanized reinforcement is that it has a higher C_c than normal steel. In this paper the critical chloride for galvanized rebar is referred to as C_{CG} .

2.2 Carbonation

When carbonation of concrete occurs, there is a drop in pH such that when fully carbonated the pH of the concrete drops to below 9. At a pH of 9 conventional reinforcement will corrode but galvanizing does not.

3. Early History of Assessment of Galvanized Reinforcement in Concrete

Galvanized reinforcement has been used in concrete for well over 50 years. Guides produced in 1970 and 1981 [4,5] provide extensive information on field experience and laboratory tests that validates the use of galvanized reinforcement. Unfortunately, other research using accelerated tests overcame the key performance benefit of using galvanized reinforcement in marine exposures.

3.1 Field Experience

Use of galvanized reinforcement in marine exposures is less extensive than it should be as many specifiers, even durability engineers, often reject its use due to the bad impressions created by inappropriate accelerated tests in the 1970's. However, there are many examples of its successful use in a wide range of exposures. While these conclusively prove vastly improved corrosion resistance they do not provide a design approach.

3.1.1 Coastal Exposures

In coastal exposures there are many examples of successful use from around the world. Some of these have been reported by Yeomans [27].

Bermuda pioneered galvanized reinforcement use in hot saline environments for a number of critical structures in the 1950's. This proved extremely successful. The 1953 Longbird bridge is a prime example. In 1981 [5] an assessment showed no deterioration of the galvanizing even though the chloride level at the reinforcement was 1.2 wt% cement, i.e. three times C_c often quoted for conventional reinforcement. The reduced maintenance cost of structures using galvanized reinforcement compared to conventional reinforcement led the Bermuda government to use galvanized reinforcement in all structures in a \$300 million infrastructure program in the 1990's [6].

The Sydney Opera House, completed in 1975, is one of the world's most recognizable and iconic buildings. Situated on Sydney Harbour, recognized as a severe coastal exposure, its distinctive roof comprises sets of interlocking vaulted 'shells'. Each post-tensioned shell is faced with pre-cast segments rising to a central ridge beam. Galvanized mesh was exclusively used in the manufacture of these precast segments to provide long-term corrosion protection and to minimise the risk of cracking and rust staining of the gleaming white ceramic cladding tiles. After nearly 50 years exposure to salt spray and high humidity, the sail panels have shown no signs of deterioration although cover was low to minimize weight.

3.1.2 *Marine Exposures*

An example of this construction method is the Townsville marina which employs a high-density polystyrene flotation cell encased in a reinforced concrete shell. All reinforcement was hot dip galvanized. After more than 20 years operation, the marina was redesigned in 2008. All cells were removed and inspected. Though several black steel reinforced elements around the marina needed to be replaced, the galvanized reinforced flotation cells were in such good condition that all of them were re-located in the new layout of the marina.

Galvanized reinforcement has been widely used in many docks, jetties, pontoons and buoys. Examples include the Onimichi Pier in Japan, the Lillholmens Pontoon Bridge in Finland and the Lamma Island Pier in Hong Kong.

3.1.3 *Industrial Exposures*

Galvanized steel reinforcement was used in the construction of linings for three deep water ocean outfall tunnels at North Head, Bondi and Malabar in Sydney. The tunnels were bored through coastal cliffs and the seabed to about 3 km offshore. The tunnels were lined with a combination of precast panels and in-situ concrete, all of which were galvanized reinforced for long-term corrosion protection.

3.1.4 *Carbonation Exposures*

In carbonation environments galvanized reinforcements use is common place. A perfect example of the benefits of galvanized reinforcement is in precast parapets on bridges where it is used to allow low covers and more attractive and lightweight units.

Others uses include the precast elements of important buildings, such as the Parliaments of Australia and New Zealand, the Bahai Lotus Temple in India and other buildings and structures where thin elements are an architectural feature.

The corrosion resistance of galvanizing in carbonated concrete is generally accepted and the paper does not discuss performance assessment for carbonated concrete.

3.2 *Accelerated Tests*

A constant problem with accelerated tests, deemed a necessity to determine the performance of materials that can give over 100 years' service life, is assurance that the results are representative of the mechanisms that provide the long life. Galvanized steel reinforcement used in marine exposures delays the corrosion initiation phase but may reduce the propagation period due to the high chloride level at the bars surface once corrosion commences. The overall life is however considerably extended under normal circumstances. Accelerated tests that reduce the initiation period, for example by increasing the surface chloride level and reducing the cover, such that the propagation period is dominant in the tests can totally mask galvanizing performance. Accelerated tests should be specifically developed to provide a reasonable distinction of performance for the parameter being measured, i.e. in this case increased critical chloride level.

The alternative to accelerated tests is to measure the key performance parameters directly, in this case the critical chloride level, and to use modelling to determine the impact on design life. This is a preferred approach as it enables performance assessment in a wide range of exposures.

3.3 *Conclusions*

There is strong evidence of the improved performance of galvanized reinforcing to resist corrosion to marine exposures. However, inappropriate accelerated tests have sometimes left a poor impression of galvanized reinforcements performance. Accelerated testing should be defined to measure performance of reinforcement in a meaningful way. However, a test to at least measure the relative critical chloride level of different steels is required. This would need to reflect the imperfections and chemistry variations in concrete that cause the wide critical chloride level for conventional reinforcement.

4. *fib* Durability Design Guidance

fib has various guidance notes on durability design of reinforced concrete. *fib* Bulletin 49 [7] is a technical document on reinforcement durability, including galvanized reinforcement, but does not give appropriate guidance on durability design. MC2010 [8], based on *fib* Bulletin 34 [9], introduces modelling but gives no information on galvanized reinforcement. Since the introduction of MC2010, *fib* Commission 8 on Durability Design (COM8) has developed guides on how to use the models [10,11] for conventional reinforcement but galvanized reinforcement has not featured.

4.1 *fib* Bulletin 49

fib Bulletin 49 provides a guide to galvanized reinforcement production, properties, potential damage and deterioration, bond and applicable codes. This and other references (12, 13) provide a starting point for a durability design guide in that the influence of production, damage, initial reactions and required properties can be assessed.

The relatively new process of in-line or continuous galvanizing provides a 50 µm thick layer of pure zinc, with improved ductility and greater uniformity, and the IZA claim (14) enhances the reinforcement protection even though the galvanizing thickness is less than the traditional batch galvanizing process. The distinction between the two galvanizing processes means a change to project specifications is needed and modelling parameters for both processes is required.

4.2 Durability Modelling to MC2010

Reinforcement in new concrete can be taken to not corrode because of a dense oxide layer that forms on the bar due to the reactions between steel and concrete in uncontaminated concrete. This layer is called the passive layer. Over time chlorides or carbon dioxide may penetrate through the concrete covering the reinforcement and break down the passive layer. This is called depassivation. After depassivation the reinforcement will corrode at a certain rate and rust typically forms on the bar surface. Rust occupies more space than the original steel and as the degree of rust increases it causes a bursting pressure that is eventually sufficient to crack the concrete.

The underlying simple design life model (Figure 1) that is used universally in durability design is that proposed by Tutti (29). In this model the life of a structure can be designated in two parts:

- A first phase, commonly referred to as T_0 , is taken as the time it takes for a chloride or carbonation corrosion activation front to reach the reinforcement.
- A second phase, commonly referred to as T_1 , is the time from the start of reinforcement corrosion to the time at which unacceptable damage occurs.

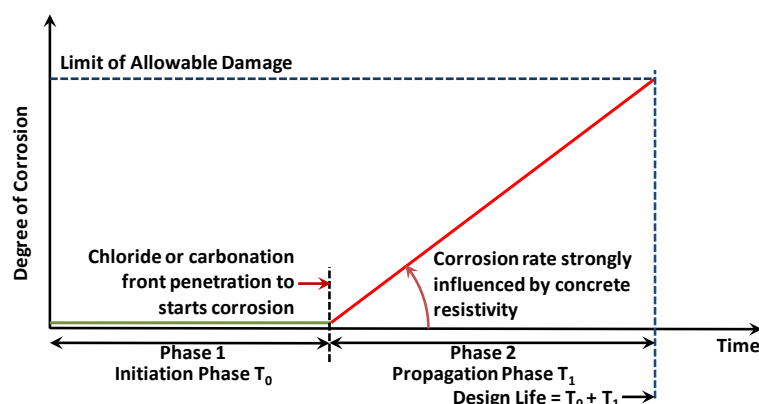


Figure 1 Tutti's Model for Design Life

While the Tutti model is a useful explanation of the design life assessment process a more complex version is required for a detailed assessment involving phase 2, such as the *fib* model (Figure 2).

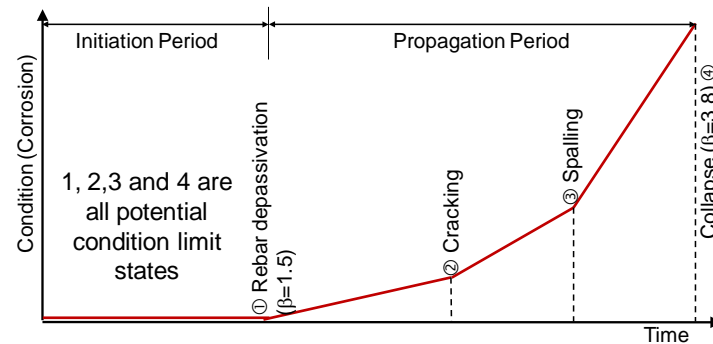


Figure 2 fib Model Code Design Life Model

A limit state is any defined point in the structures life. It can be performance or prescriptive based. The end of phase 1 is often defined as the 'limit state of depassivation'. There are various stages of deterioration. With reinforcement corrosion these are defined by *fib* Model Code 2010 as depassivation, cracking, spalling or collapse and any might be the appropriate limit state provided the appropriate reliability is established.

Mathematical models for calculating the time to corrosion initiation due to carbonation and chloride penetration are given in *fib* Model Code 2010. The models are empirical and only apply to situations that are like those from which the models were developed. However, that gives a broad scope.

In many exposures where carbonation occurs, for example in buildings, the concrete is so dry that the corrosion rate is negligible and phase 2 can be much longer than the design life. Although recognising that there are no agreed models to determine phase 2 *fib* Model code notes "To support corrosion of the reinforcement a certain level of humidity is needed. For structural elements solely exposed to a relatively dry indoor environment a limit state 'depassivation' may not be relevant as no significant corrosion will develop". Conversely for concrete exposed to rain or higher humidity's the corrosion rate in carbonated concrete can be high, particularly where the concrete is designed for low exposures. This high corrosion rate is apparent in old internal elements that become exposed to rain as the structure becomes dilapidated (e.g. broken window and collapsing roofs).

Discussing chloride models *fib* Model Code 2010 notes "As with carbonation there are no available models with broad international consensus available for predicting the length of the corrosion period till cracking, spalling or collapse of the structure occurs when this Model Code was published. For this reason, service life designs are normally based on the limit state of depassivation (reaching a critical chloride concentration at the rebar surface)." Efforts are being made to provide a propagation period in Model Code 2020.

Hence the Model Code recognises that for carbonation there are legitimate reasons for considering a phase 2 for conventional reinforcement, at least in dry environments, but for chlorides no such reasons are proposed. There will be a residual phase 2 until corrosion induced cracking occurs, but whether this should be considered, given *fib*'s views, is ultimately the owners judgement on risk.

ISO 16204 gives a basic limit state function for durability design of the propagation period but notes "At the time of publishing this international standard, no time-dependent model with general international consensus is available for this deterioration process. The time span from initiation to cracking may be estimated from existing structures where the concrete composition, execution and exposure conditions have been similar to those expected for the structure considered."

In view of the above for durability design in marine situations where galvanized reinforcement would typically be used the propagation period is not currently considered and service life would be based on the initiation period alone.

4.2.1 Verification methods

fib Model Code on Service life Design (9) provides four methods of durability verification. These methods are discussed below along with what is needed for galvanized reinforcement.

Deemed to Satisfy - This is where experience has shown that compliance with a certain set of parameters will provide the reliability sought at the end of the design life. National Codes typically provide durability requirements as cement system, water to cement ratio and cover for normal reinforcement. Unfortunately, as concrete materials change with time experience is proving unreliable and modelling is becoming the new arbiter of what is acceptable.

Avoidance of Deterioration - In this case the item causing an unacceptably low reliability of reinforcement corrosion would be replaced by something that would not. Galvanized reinforcement in concrete that might carbonate and be in a damp environment is an ideal example.

Full probability analysis – This is the preferred approach to modelling as it incorporates all the model variables as distributions and give reliability at the end of the design life. However, the approach is let down by the lack of data and precision on the variable distributions. Critical chloride level for galvanized reinforcement is one such factor. While the characteristic values for normal reinforcement and galvanized reinforcement are often stated as being 0.4 wt% and 1.0 wt% cement respectively there is little data on the critical chloride level distribution for galvanized reinforcement.

Partial factor approach - The development of partial factors for the corrosion models is dependent on having reasonable data for the model input variable distributions to calculate the partial factors. The partial factors are then bound to be more conservative than a full probabilistic analysis because they encompass a wide range of situations. In any event the key for durability design is to have a reasonable and agreed distribution of the key variables, i.e. critical chloride level for galvanized rebar.

Notably the use of the corrosion models in discrete form is not included in *fib* Bulletin 34 (9).

4.2.2 Reliability

Reliability is a well-recognised term used in structural design and simply expresses the fact that a higher reliability (lower likelihood of failure) is required where the consequence of failure is higher. Use of this term in structural codes for durability design was first introduced in Model Code 2010. Reliability requirements of 1.5 and 3.8 are applied to the limit states of depassivation and collapse respectively (Figure 2Figure 5). However, reliability should be based on consequence of failure. Required reliability at depassivation may be higher if the criteria are used as a proxy for some other condition or lower in certain robust structures with no economic consequences of deterioration.

It is now becoming apparent that in some circumstances a durability failure could have very high consequences and hence a much lower probability of failure at the end of design life than the 5% to 10% often assumed for corrosion induced serviceability failures. Allowing for an ultimate limit state (ULS) reliability might push up cover requirements by 30%. This may have unacceptable cost consequences or cracking issues that could be overcome by maintaining cover and using galvanized reinforcement.

4.2.3 Robustness

Model Code 2010 defines robustness as “*the ability of a structure subject to accidental or exceptional loadings to sustain local damage to some structural components without experiencing a disproportionate degree of overall distress or collapse.*” This is primarily related to structural design but could also be applied to durability design where instead of exceptional loading the durability equivalent of exceptional exposures could apply, for example:

- poor workmanship leading to poor concrete quality and high ingress rates
- water exposure on carbonated concrete inside buildings
- basement designed for internal exposures but are exposed to run off with de-icing salts
- industrial plants subject to process waters not included in the design assumptions

Galvanized reinforcement with higher corrosion resistance may provide robustness due to its ability to resist unexpected overload from chlorides.

4.2.4 Chloride Model

The chloride ingress in model Code 2010 (Table 1) has only one variable that is affected by the change of reinforcement (C_c) and hence the only thing preventing use of the *fib* model for design using galvanized reinforcement is this development of this factor. Although there is anecdotal information of the higher C_c for galvanized reinforcement (C_{CG}) compared to normal steel there are no distributions provided and it is often not clear whether quoted values for C_{CG} are means or characteristics values. Also, quoted values are for a single case of laboratory concrete and not representative of values found in field concrete.

Table 1 Inputs for the Chloride Diffusion Model of a Coastal Structure

Parameter		Unit	Distribution Type	Mean μ	Std Dev σ	a	b
D_{RCM}	Chloride Migration Coef.	$10^{-12} \text{ m}^2/\text{s}$	Normal (Gauss)	8.5	2.4	-	-
t_0	Age of Samples at Test	Days	Constant	28	-	-	-
$C_{s,\Delta x}$	Surface Chloride Level	wt.-%/c	Lognormal	0.8	0.27	-	-
α	Aging Coefficient	-	Beta	0.65	0.12	0	1.0
T	Initiation period	Years	Constant	80	-	-	-
T_{ref}	Test Temperature (23°C)	K	Constant	296	-	-	-
T_{real}	Temp. Exposure Site (16°C)	K	Normal	289	5	-	-
b_e	Temp. Coefficient Exponent	-	Normal	4800	700	-	-
Δx	Convection zone depth	mm	Constant	0	-	-	-
C_C	Critical Chloride Level	wt.-%/c	Beta	0.60	0.15	0.2	2.0
C_{nom}	Cover (measured)	mm	Normal (Gauss)	38.8	7.3	-	-

If it is assumed that the mean C_{CG} is three times that of conventional reinforcement, then the relative performance can be assessed using mean values for the variables for a reliability of 0 (Table 2).

Table 2 Assessment for Requirements for 50 yr Service Life & Reliability 0 (7-day curing)

Reinforcement	Coastal Structure				Marine Structure			
	Norm.	Galv.	Norm.	Galv.	Norm.	Galv.	Norm.	Galv.
Cement type	Type III B		Type 1		Type III B		Type 1	
w/c ratio	0.45				0.38			
Cover (mm)	45				65			
Diffusion Coefficient ($\times 10^{-12} \text{ m}^2/\text{sec}^2$)	4.0		8.3		2.5		6.8	
Aging Coefficient [11]	0.65				0.4		0.3	
Base Chloride Level (wt% cem.)	0.23				0.12			
Surface Chloride Level (wt% cem.)	3.0		2.0		5.5		4.5	
Allowable increase in chlorides	0.37				1.68			
Temperature (°C)	25							
Critical Chloride Level (wt% cem.)	0.6	1.8	0.6	1.8	0.6	1.8	0.6	1.8
Est. time to Depassivation (years)	@250	>250	42	>250	97	>250	11	62
Cover 50 years to Depassivation (mm)	33	<20	50	<20	53	33	>75	50

Bearing in mind that Table 2 only applies to elements with a reliability of 0 (for example, a robust marine deck soffit) and only assumes the higher mean critical chloride level, the galvanized reinforcement might provide the following advantages:

Marine Structures

- Ability to use type 1 cement at acceptable covers. This could be useful in remote sites with only a Type 1 cement silo available.

Coastal Structures

- Galvanized reinforcement provides a significantly higher reliability than normal steel when using Type I cement. This would be important for operationally critical elements such as crane beams or architecturally important building. Although Type III B cement does meet the requirements low early age strength can be an issue.

Coastal and Marine

- Significant reductions in cover when using Type 1 or Type III B cements. This could provide significant cost benefits by reducing weight on bridges and buildings. This has a cost and sustainability benefit.

4.2.5 Carbonation Model

The Model Code 2010 is based on the time it takes for a carbonation front to reach the reinforcement. Because galvanized reinforcement does not depassivate in carbonated concrete the model tells us that galvanized reinforcement has a virtually indefinite life. This has the following benefits:

- a) In high carbonation exposures such as vehicle tunnels, enclosed carparks, some industrial areas and some atmospheric areas with high exhaust level carbon dioxide levels can be 2 to 3 times

that of normal atmospheres. In such cases the normal cover requirements in codes are likely to be inadequate. In tunnels reduced covers relative to current codes might translate to reduced thicknesses and less excavation, providing potentially significant cost savings.

- b) The minimum cover specified in codes is often not achieved because the codes underestimate the distribution of cover expected in practice. *fib* 34 suggests adding 10 mm to minimum cover to allow for cover variance for carbonation modelling. With the advent of methods that can rapidly scan for in situ cover, the frequency of post pour cover checking is increasing. The frequencies of *reported* cover failures are therefore increasing leading to large expense on some projects for measuring covers, measuring the concrete's carbonation resistance and modelling of the residual life to try and justify low covers [28]. Galvanized rebar would provide assurance of durability at significantly lower covers.

4.3 *fib* Bulletin 76

fib 76 provides further background to full probabilistic modelling and gives a reliability analysis of deemed to satisfy provisions in several national codes. It shows that not all codes give adequate reliability. A major issue is the use of Type 1 cements for chloride exposures. Use of fly ash and slag provide higher performance concrete for marine exposure but this can increase construction cost due to slow early strength development. No assessment is given for galvanized reinforcement, but this would be helpful as it may provide the reliability required even using Ordinary Portland Cement.

4.4 *fib* TG8.3 Model Sensitivity Analysis

The report for this analysis has been written and is currently under review. It shows the sensitivity of the chloride and carbonation models. It considers all the input variables. Of key interest for the use of galvanized reinforcement is the chloride activation level that will initiate corrosion. The critical chloride distribution is wide because corrosion activation for normal reinforcement depends very much on voids around the reinforcement. If the sensitivity to voids is reduced with galvanized reinforcement the critical chloride distribution might be a lot tighter and the chloride activation level apparently higher.

5. Sustainability

Guy Keulemans [13] notes *"Concrete is the third-largest contributor to carbon dioxide emissions, after automobiles and coal-fuelled power plants. Cement manufacturing alone is responsible for roughly 5% of global CO₂ emissions. Concrete also makes up the largest proportion of construction and demolition waste, and represents about a third of all landfill waste. ... The world needs to reduce its concrete production, but this will not be possible without building longer-lasting structures ... The collapsed civilisations of the past show us the consequences of short-term thinking. We should focus on building structures that stand the test of time – lest we end up with hulking, derelict artefacts that are no more fit for their original purpose than the statues of Easter Island."*

Richard Weyers [30] reported for the American Galvanizers Association on the life cycle costs of various rebar options (epoxy, galvanized and stainless), comparing their performance in chloride contaminated bridge decks with differing crack densities in Virginia, USA. Present costs for galvanized rebar were reported as well below both epoxy and stainless, and *"with higher Cl levels the galvanized steel total present costs and life-cycle costs would eventually approach that of stainless steel, while the epoxy-coated rebar total costs and life cycle costs would be far in excess of stainless steel. ... stainless steel rebar can really only be considered if a completely maintenance-free life is required for more than 100 years, regardless of cost."*

The requirement to drastically reduce the cost to the environment of our infrastructure due to climate change requires a step change in thinking, one that increases the life of our structures. Galvanized rebar has the potential to significantly increase the life of concrete structures in environments where climate change is likely to have the most effect – those coastal regions likely to suffer from rising seas, and those regions not currently affected, becoming affected as they suffer from changing climate.

A 2010 CSIRO report [26] on climate change indicated a likely increase of up to 3.5% in chloride induced corrosion initiation around the coasts of Australia, with the west coast of Western Australian and the east coast of New South Wales up to the border with Queensland at most risk due to the relatively higher increase in temperature to 2100 in those areas. It recommends that *"potential impacts of climate change and adaptation options to respond to the impacts should also be taken into*

account in the planning of concrete structures such as bridges and port infrastructures which are crucial to national and local economy as well as communities.”

6. Critical Chloride Content (C_c)

Values for C_c for conventional, galvanized and stainless steels abound.

6.1 Conventional Reinforcement

C_c from laboratory and field experiments in marine atmospheric zones was studied by Meira [17]. Average total chloride threshold varied in a range between 0.88 and 1.58 (% cement weight) for laboratory and field exposure experiments, respectively. C_c from field exposure experiments were lower than those obtained from wetting and drying cycles in a laboratory environment, which seems to follow a similar general tendency of other published data. This difference can be explained by aspects that make depassivation easier for outdoor experiments and are mainly connected with environmental interaction, like deeper concrete carbonation and more suitable moisture and oxygen contents for starting corrosion.

Angst (18, 19) reviewed the published C_c from laboratory conditions and outdoor exposure conditions. He reported that the published results scatter in a wide range from 0.02 to 3.08% total chloride by weight of binder. C_c was influenced by many factors and varied with time. Major influences were the quality of the steel-concrete interface, the potential of the steel and the pH of the pore solution. He concluded that C_c is dominated by the nature of the steel-concrete interface and the concrete pH at the interface. For example, in areas of poor compaction or reduced pH due to carbonation, C_c will be lower.

Frederiksen (20) studied chloride ingress in various ways to build an engineering approach to estimate C_c values in different environments. The reason given was that “no procedure yet exists which has proven to be scientifically correct for the evaluation of long term threshold levels.” Frederiksen proposed that for marine splash zones and atmospheric marine and de-icing salt zones C_c be 0.6% and 0.3% by weight of cement for GP and 20% fly ash concretes respectively.

Alonso [21] reviewed published data and found a wide range of C_c (Figure 3). Whilst there are cases of high C_c it is important to note that corrosion activation can occur at very low chloride levels. This spectrum of results is likely to be wider when a large range of structures are considered, but the range is high within one structure.

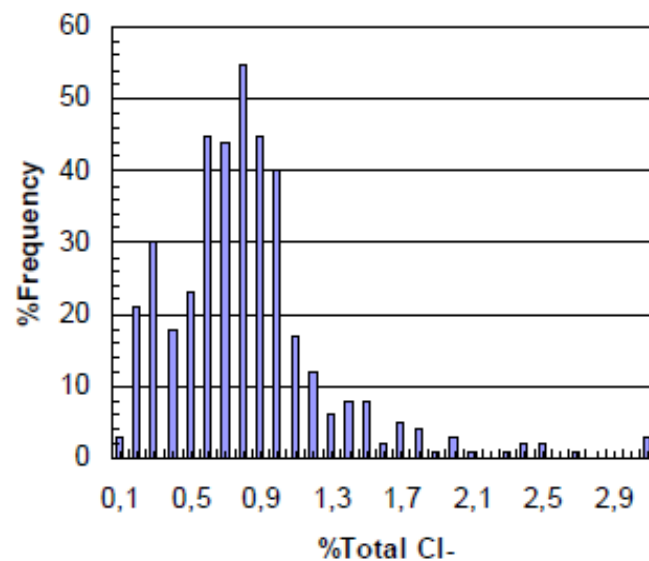


Figure 3 Histogram of the Total Chloride Threshold (% wt of cement) from the Values Published

Markeset [22] describes a method to measure critical chloride content in real structures by installing corrosion sensors (this method has yet to find acceptance in the general literature although it shows promise). Fourteen measurements (not sufficient to be taken as statistically representative but interesting none the less) on a 37 years old quay gave a variation in C_c that are compared with Browne’s data (Table 3). The corrosion sensors measure the time to depassivation while Browne’s

measurements were based on visual inspection of the reinforcement for rust. This would account for the higher values suggested by Browne. However, at the negligible risk level required for assessment, C_c is similar at 0.4 % by wt of cement.

Table 3 Critical Chloride Content (% weight of cement)

Probability/risk of corrosion	Critical Chloride Content	
	According to Browne	Norwegian quay ¹
Negligible	<0.4	<0.4
Possible	0.4-1.0	0.4-0.7
Probable	1.0-2.0	0.7-1.3
Certain	>2.0	>1.3

¹ Assuming 350 kg cement/m³ and density 2350 kg/m³

Markeset also showed a lognormal distribution gave the best fit to the measurements, giving a mean value for C_c of 0.77% weight of cement and a coefficient of variation equal to 32% (Figure 4). The lower C_c given by *fib* will reflect a distribution for multiple structures instead of one but at the 5% failure level C_c of the two distributions are similar, i.e. 0.35 wt% cement for *fib* and 0.43 wt% cement for Markeset.

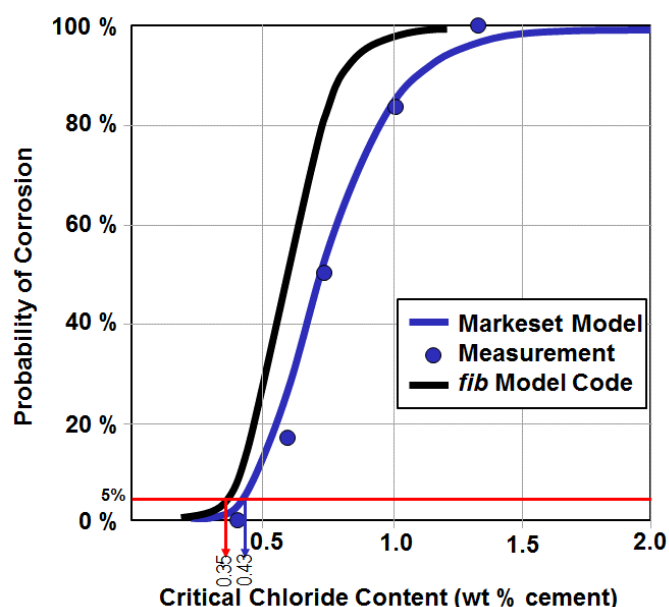


Figure 4 Markeset’s Critical Chloride Content compared with statistical model according to *fib* Model Code for Service Life Design (Bulletin 34)

Life-365 [15] provides guidance on the chloride threshold as follows: “The actual relationship between corrosion and chloride content is likely to be influenced by a whole range of parameters ... At this time there are no clearly defined relationships that can easily be incorporated into a simple service life model. Consequently, Life-365 does assume a single chloride threshold value (C_t).... In selecting an appropriate value for C_t , reference was made to the work of Glass and Buenfeld (1995) who presented a comprehensive review of the literature on this topic. they concluded that “Without further work no improvement can be made to the suggested chloride threshold levels of 0.4 for buildings exposed to a temperate European climate and 0.2 wt% binder for structures exposed to a more aggressive environment.” Other saline exposures might have a different distribution.

Clearly there is no fixed value for C_c and several factors are known to affect the critical chloride content (Figure 5). Because it is generally considered too difficult to be precise about C_c ’s distribution for a structure, a distribution applicable to all structures is generally used in modelling.

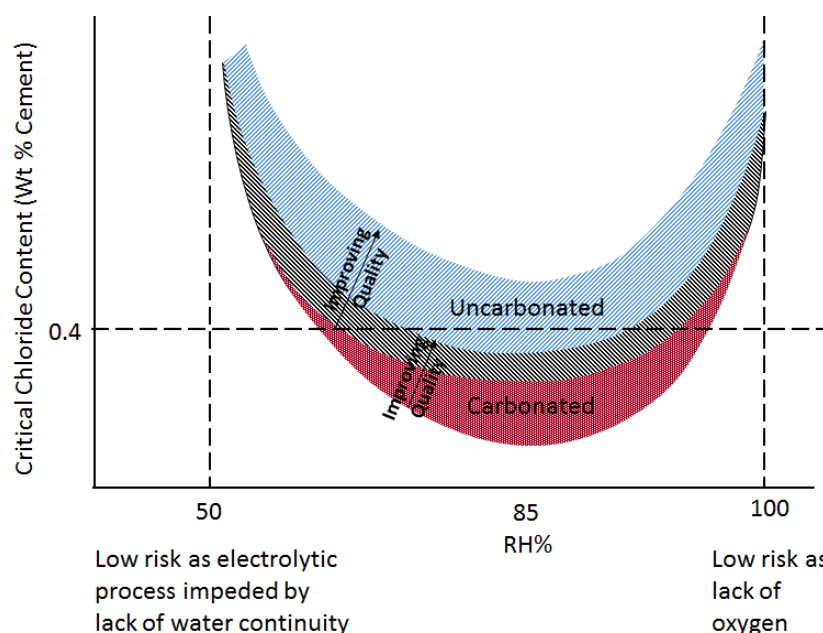


Figure 5 Critical Chloride Content (7)

When modelling design life *fib* Model Code 34 [9] is the most authoritative document as it forms the foundation for *fib* Model Code 2010 [2] and ISO 16204 (3). *fib* 34 notes that C_c can be taken to have a beta distribution with mean value of 0.6 and standard deviation of 0.15 wt% binder and the lower characteristic value is therefore around 0.35 wt% binder (Figure 4).

There is no single agreed method to determine C_c and researchers have tested for it in a diverse number of ways. This variation in test procedures accounts in part for why there is such a wide range in the published C_c values.

When an anode forms in one location due to chloride ingress the electrical potential of the bar changes and a current flow from the anode to the cathode occurs. Developing anodes can be detected in laboratory samples where the test set-up allows for the continuous measurement of potentials and current flow. When corrosion is detected then the chloride profile can be measured and the level of chloride at the reinforcement assessed from the profile. The chloride content at time of activation is one of the measures used as the C_c .

Although the test method described above has been used frequently in research to get an indication of C_c levels of a certain system, no test has been agreed for doing this because of a failure to attain consistent results with any of the test methods. This is even though the tests are undertaken in ideal laboratory conditions with the ability to locate electrodes in the ideal locations.

Identification of C_c on old structures is complicated for a few reasons:

- 1) When an anode forms it polarises surrounding steel such that it only corrodes at a higher chloride level. Testing such areas would give unrealistically high C_c .
- 2) Chloride ions move under the influence of the corrosion current towards the anode. Hence an area that is corroding will have higher chloride levels than those needed to establish the corrosion.
- 3) Wherever concrete is tested it will not be known when a bar started to corrode or how long it will be until it corrodes. Hence establishing C_c , assuming there was an agreed criterion for corrosion initiation, would require sufficient sites close to the point of corrosion. This is unlikely to be manageable on an existing structure.

Bamforth (23) notes that *"The point at which corrosion begins is not well defined in absolute terms. The threshold value is often determined by electrochemical measurements of steel embedded in concrete or mortar using the change in either half-cell potential or corrosion rate as the indicator. In a recent study of reinforced concrete blocks exposed to UK coastal conditions different threshold levels were observed using the different techniques. Based on half-cell potential measurements the chloride threshold was 0.3-0.4% wt. of cement ... but when assessed on the basis of corrosion rate this value was in excess of 1%."* The author goes on to suggest an alternative approach to establish C_c which

would give yet a different value. He concludes that *“Clearly the method of test must be considered when defining the threshold value.”* This may be due to the lack of a universal correlation between corrosion rate and potential.

Bamforth also notes that curing has been found to affect the threshold values. He reports work which showed the C_C increased from 0.139 wt% sample to 0.212 wt% sample when curing was lifted from 3 days to 14 days. This is likely to be one of the reasons for a high variability within a structure.

Silva [24] research on C_C led to the following conclusions:

- 1) the large scatter of C_C means it is almost impossible to define appropriate criteria for service life design.
- 2) the main reasons for the scatter are the number of parameters which influence corrosion initiation (e.g. binder type, water-binder ratio, type of steel, etc.) and the different methods used in the experiments.
- 3) along the steel, differences in the moisture content and oxygen availability, concentration of aggressive species and metallurgical properties are likely to create electrochemical inhomogeneity. These differences between more cathodic and anodic regions favour the chloride migration along the interface to the anode regions and the high concentrated chloride ions facilitate the dissolution of the passive film and finally initiate pitting corrosion.

6.2 Galvanized Reinforcement

The extensive research on C_C content for conventional reinforcement has shown a wide range of influences. Hence a wide distribution has been defined for use in modelling. While there has been significant testing done on the C_C for galvanized steel, no-one has yet produced a distribution for use in full probabilistic design. The current array of quoted values suggests a wide distribution exists, but this distribution has not been yet established to cater for all structures.

COM8 has instigated a working party to consider how galvanized reinforcement should be considered in MC2020. The brief for this group notes:

“Other references provide evidence as to how galvanized bars have performed in service. Of less use are accelerated time to corrosion damage tests. Some data is available for chloride activation levels and it may be possible to use this to help develop a critical chloride level (threshold) distribution.

Regardless of thickness the galvanizing breaks down quickly once the corrosion activation levels are reached and the ensuing corrosion rate of the underlying reinforcement will be rapid once this occurs due to the high chloride levels. This means galvanizing thickness may not be critical as it is only present to increase the activation level and hence extend the initiation time, and the propagation period may be small due to the high chloride levels.

One issue of establishing the critical chloride level for a concrete is that the quality variations found in real structures is difficult to simulate in laboratory tests. It may be that the distribution needs to be established on real structures. Much of the data available for normal reinforcement was developed in that way.

7. Summary

Intuitive assessments of the data available for galvanized reinforcement indicates that higher reliability, lower cover, increased life and more sustainable outcomes compared to normal reinforcement are possible for the design of both marine and coastal concrete structures. Research is required to develop a distribution of the critical chloride level for use in full probabilistic design. An opportunity exists for the galvanizing industry to influence the creation of galvanized steel service life design models in *fib* design guidance. The potential for growth is significant and the increased use of galvanized steel in this application would likely open new batch and continuous galvanized reinforcement opportunities.

References

1. Courland R. "Concrete Planet" Prometheus Books, New York 2011
2. *fib* Bulletin 65 and 66, Model Code for Concrete Structures 2010 – Final draft, Volume 1 and 2, Lausanne, Switzerland, 2012
3. ISO 16204 "Durability - Service Life design of Concrete Structures." International Standards Organisation, Geneva, Switzerland. 2012
4. "Galvanized Reinforcement for Concrete" International Lead and Zinc Research Organisation Inc, New York 1970
5. "Galvanized Reinforcement for Concrete – II" International Lead and Zinc Research Organisation Inc, New York 1981
6. Allan N.D. "The Bermuda Experience: Leading the way on Galvanized Reinforcement" Yeomans S.R. 'Galvanized Steel Reinforcement in Concrete' Elsevier 2004
7. *fib* Bulletin 49 "Corrosion protection of reinforcing steels." Lausanne, 2009
8. *fib* Bulletin 65 and 66 "Model Code 2010Vol 1 & 2" Lausanne, 2012
9. *fib* Bulletin 34, Model Code for Service Life Design, Lausanne, Switzerland, 2006
10. *fib* draft report "Operational document to support Service Life Design". To be published late 2018
11. *fib* Bulletin 76 "Benchmarking of deemed-to-satisfy provisions in standards: Durability of reinforced concrete structures exposed to chlorides."
12. Yeomans S.R. "Galvanized Steel Reinforcement in Concrete." Elsevier, Amsterdam, 2004.
13. *fib* Bulletin 53, Structural Concrete Textbook on Behaviour, Design and Performance. Volume 3, 2010. Reprint of values from CEB Design Guide 1992
14. "Continuous Galvanized Rebar", International Zinc Association, 2015 <https://www.zinc.org/CGR/> (accessed 28 May 2018)
15. Life-365 "Life-365™ Service Life Prediction Model™." Version 2.1. Life-365 Consortium II 2012
16. Keulemans G. "The problem with reinforced concrete." The conversation. Online articles from UNSW, 2016
17. Meira G.R., Andrade C., Vilar E.O. and Nery K.D., "Analysis of chloride threshold from laboratory and field experiments in marine atmosphere zone", *Construction and Building Materials* 55 (2014) 289-298.
18. Angst U., Vennesland O., "Critical Chloride Content in Reinforced Concrete - State of the Art." Concrete Repair, Rehabilitation and Retrofitting II. Taylor and Francis. London, 2009
19. Angst U. and Vennesland Ø., "Critical chloride content – State of the art", SINTEF Report No. SBF BK A07037, December 2007.
20. Frederiksen J.M., "Chloride threshold values for service life design", RILEM Workshop in Paris, September 2000.
21. Alonso M.C., "Chloride threshold values in the literature", COIN Workshop on "Critical chloride content in reinforced concrete", Trondheim, 5-6 June 2008.
22. Markeset G., "Critical chloride content and its influence on service life predictions", COIN Workshop on "Critical chloride content in reinforced concrete", Trondheim, 5-6 June 2008.
23. Bamforth P.B "Enhancing Reinforced Concrete Durability". Concrete Society Technical Report 61. Camberly, UK 2004.
24. Silva N., "Chloride induced corrosion of reinforcement steel in concrete – Threshold values and ion distributions at the concrete-steel interface", Doctoral Thesis, Chalmers University of Technology, Sweden, 2013.
25. HB84 "Guide to Concrete Repair and Protection" Guide to Concrete Repair and Protection" Australian Standards, Sydney 2006

26. Wang, X., Nguyen, M., Stewart, M. G., Syme, M., Leitch, A. (2010). Analysis of Climate Change Impacts on the Deterioration of Concrete Infrastructure – Synthesis Report. Published by CSIRO, Canberra. ISBN978 0 643 10364 1
27. “International Zinc Association Workshops, China, June 2007 and other private communications”
28. Papworth F., and C. Gehlen C. “National and international code based deterministic and full probabilistic modelling to describe reliability of various Australasian marine structures.” Performance-based approaches for concrete structures, *fib* Symposium, Cape Town’, Nov 2016
29. Tuutti K. “Corrosion of Steel in Concrete. CBI Research. Stockholm. 1982
30. Weyers R.E. “Virginia bridge deck service life performance and associated costs: influence of reinforcing steel type.” International Zinc Association, North Carolina, 2017

About the Authors

Mr. Papworth gained his M.I.C.E. through concrete durability research. Over the last 35 years his durability consulting has continued in areas such as inspection, repair, non-destructive testing, silica fume, steel fibres, thermal analysis, crack control, durability plans and chemical attack. As Managing Consultant for BCRC he has been responsible for the durability design of some of Australia’s largest projects. Mr. Papworth was Chairman of the Concrete Institute of Australia committee on concrete durability from 2010 to 2015, is Chair of the International Federation for Structural Concrete (*fib*) Commission 8 “Concrete Durability” and is joint chair of *fib* AG4, an action group dealing with durability design in Model Code 2020. In 2014 he was awarded the Mohan Malhotra prize for services to Concrete Durability.

Mr. Golding gained his MBA and BEng (Mech., Hons) from the University of Adelaide and has worked in the steel industry in Australia for nearly 30 years in manufacturing, marketing and general management roles. He was the lead writer of the Australian and New Zealand HDG Inspectors Course and co-authored the ASI publication “Design and Detailing for Corrosion Protection of Steel Structures”. Mr. Golding is a member of seven Australian Standards committees, including BD-084 (Steel Reinforcing and Prestressing Materials) and MT-014 (Corrosion of Metals). Since 2011 he has been the CEO of the Galvanizers Association of Australia.

Session 10:

Practical Experience & Market Opportunities with Galvanized Rebar

Hot-dip galvanized reinforcing steel - better prospects for applications in Germany

Robert Adams - Technical University of Kaiserslautern, Department of civil engineering
Prof. Dr.-Ing. Wolfgang Breit - Institute of Construction Material Technology

Abstract

On the basis of the regulations that apply in reinforced concrete construction the hot-dip galvanizing of reinforcing steel represents an additional measure to increase the durability, especially in the case of corrosive attack as a consequence of carbonation and/or the action of chlorides. Unlike the situation abroad the use of hot-dip galvanized reinforcing steel has not so far become widespread in Germany.

One of the reasons for this is that its application is currently regulated through a general building inspectorate approval. Because of the lack of established knowledge this imposes constraints that, de facto, form an obstacle to greater spread of the use of hot-dip galvanized reinforcing steel. Marketing is also made more difficult by the fact that the additional benefits cannot currently be quantified.

As part of the AiF research project IGF 499 "Growth of technology and safety in the application of hot-dip galvanized reinforcing steel for establishing a sustainable market position in reinforced concrete construction" the intention is to develop the basic principles to open up the potential that the hot-dip galvanized reinforcing steel offers for improving the durability of reinforced concrete components and for opening up new market sectors for the producers and downstream processors of the reinforcement for reinforced concrete.

An important result of the research project is that it has become possible to estimate the risk of liquid metal assisted stress cracking and to give a recommendation for the minimum bending roller diameter to be used for the procedure of bending the reinforcing steel before galvanizing that has not so far been covered by the regulations in Germany. For oscillating stresses this has proved just as effective as ungalvanized steels or steels that were galvanized before bending. In spite of this a diminution of the long-term fatigue strength, as is currently specified in the approval, still seems to be reasonable.

On the basis of the results the processing temperature for bending can be lowered to a lower limit of -20 °C without any negative effect on the mechanical properties of ungalvanized and galvanized steel. Reinforcing rods that were galvanized before bending can be re-bent under building site conditions.

The investigations carried out into the corrosion behaviour in carbonated concrete support the recommendation for a reduction of the concrete cover in the XC exposure class. With chloride stressing, corresponding to the XD and XS exposure classes, increased corrosion rates were only detected above a chloride content of 1 mass % relative to the cement content. In contrast to ungalvanized reinforcing steel no macro element formation could be detected in samples with active corrosion areas. A coating/inhibitor that prevents the evolution of hydrogen in fresh concrete was also developed during the work that was carried out.

1. Introduction

On the basis of the regulations that apply in reinforced concrete construction the hot-dip galvanizing of reinforcing steel represents an additional measure for increasing the durability.

Advantages can be expected, especially with corrosion stressing as a result of carbonation and/or the action of chloride in exposed positions and in areas with increased risk of corrosion, such as at joints or in positions and components at risk of cracking.

Unlike the situation abroad the use of hot-dip galvanized reinforcing steel has not so far become widespread in Germany.

Its application is currently regulated in Germany through a general building inspectorate approval from the DIBt (German Institute for Building Technology) with approval number Z-1.4-165 [1]. Because of the lack of established knowledge this imposes constraints that, de facto, form an obstacle to greater spread of the use of hot-dip galvanized reinforcing steel

As part of the AiF research project IGF 499 "Growth of technology and safety in the application of hot-dip galvanized reinforcing steel for establishing a sustainable market position in reinforced concrete construction" the intention is to develop the basic principles to open up the potential that the hot-dip galvanized reinforcing steel offers for improving the durability of reinforced concrete components and for opening up new market sectors for the producers and downstream processors of reinforcement for reinforced concrete.

Participating in the project were the Faculty of Building and Construction Materials, Technical University of Kaiserslautern (FWB), the Federal Institute for Materials Research and Testing, Darmstadt, at Darmstadt Technical University(MPA-DA) and the Federal Institute for Materials Research and Testing, Berlin (BAM).

One of the aims of the project was to establish verified application limits for the processing of hot-dip galvanized reinforcing steels by the procedures of "bending after galvanizing" and "bending before galvanizing" with respect to permissible bending parameters and the influence of galvanizing on fatigue properties. Another aim was to identify the passivation reaction during concreting (evolution of hydrogen) in connection with the introduction of low-chromate cements and to determine the corrosion behaviour of galvanized reinforcing steels with respect to the advance of corrosion and the useful life.

Fig. 1 provides an overview of the research objectives and the areas of responsibility of the participating research establishments.

This paper presents the results of the research project from the sub-areas of materials technology and manufacturing technology, in which particular attention is paid to the procedure not previously covered in Germany of "bending before galvanizing", the influence of galvanizing on the fatigue strength and bending at low temperatures.

1. Choice of materials and test programme

The following materials and diameters were used in the research project:

- B500B, Tempcore steel, diameters 10 mm, 16 mm and 25 mm

- B500B, coil material (WR), diameter 14 mm
- B500A, coil material (KR), diameter 10 mm

This selection covers the great majority (> 95 %) of the types of steel currently available in Germany/Europe and the most common diameters.

The samples were galvanized either before bending (here and below Procedure A) or after bending (here and below Procedure B) in accordance with the intended focal points of the investigation.

The zinc bath compositions corresponded to the specifications given in the DAST guideline 022 "Hot-dip galvanizing of load-bearing steel components" [3]. The samples were galvanized in accordance with the specification IFG FV 2014, issued on 1st December 2014, mentioned in the approval.

For determination of the application limits it was necessary to establish adequate ductility of the materials being investigated. This was characterized by the parameters, determined with the aid of tensile tests, of extension at peak load A_{gt} , of the yield point to tensile strength ratio R_m/R_e , and the behaviour in the re-bending test based on DIN EN 15630-1. The bending parameters, namely degree of deformation (d_{br}/d_{St}) and bending temperature, were varied systematically in several stages during the bending/re-bending tests. The rate of bending and the bending angles were also varied in 2 stages. The assessment was based on the criterion given in DIN 488 whereby after the test the sample must not exhibit any fractures or cracks that are visible to a person with normal or corrected eyesight. In order to check whether cracks in the layer of zinc extended into the base material the zinc layer had to be removed from the hot-dip galvanized samples. This was carried out in the area of the deformed bending zone after the re-bending through 20 ° using the method described in DIN EN ISO 1460 "Metallic zinc coating by hot-dip galvanizing on ferrous materials – gravimetric method for determining the mass per unit area".

The remaining properties of the samples after they had been completely straightened and then aged again were determined in the tensile test based on DIN EN ISO 15630-1. Non-contact measurement of the uniform elongation under peak load A_{gt} was carried out with an optical position sensor.

The mechanical and technological properties of samples that had been bent through 180 °, aged, load-free, for 15 minutes in a molten salt bath at 450 °C and then fully bent back, were determined in the tensile test to assess the possible age-hardening susceptibility of the reinforcing steel during the galvanizing process and the influence of plastic deformation caused by the bending. Straight bars (black material) were also aged for 15 minutes in the molten salt bath and their mechanical and technological properties were determined in the tensile test.

Tensile tests and creep tests were carried out in molten zinc to identify relevant bending parameters and assess the risk of liquid metal assisted cracking/embrittlement (LMAC, LME) during galvanizing after previous bending.

Loops that had been bent through 180 ° were immersed in Class 1 molten zinc (as specified in DAST Guidelines 022) at 450 °C and opened out in the tensile tests at a constant traversing rate of 0.05 mm/sec so that the nominal stress and the opening at failure could be determined. This generated additional stresses that went beyond the internal stresses and the thermal stresses occurring during

the galvanizing. These induced LMAC damage and enabled differences to be identified with respect to the influence of the bending temperature and the bending roller diameter used for producing the samples.

For the creep tests samples that had been bent through 180 ° were tested for the typical galvanizing duration of about 15 minutes in molten zinc at 0 MPa (load-free ageing), 50 MPa, 100 MPa and 200 MPa. The background to these investigations was the question about the additional stress at which crack growth occurs. Light-microscopy investigations were then carried out on longitudinal ground sections to check whether and to what extent cracks are formed.

Internal stress measurements were also carried out on bent samples at intervals of 1 mm across the cross-section from the inside of the bend to the outside of the bend to assess the possible danger of liquid metal assisted cracking (LMAC).

Transfer of these results to larger diameters was achieved by numerical comparison calculations. The material laws needed for the numerical calculation were determined through the true expansion curve. The calculations were carried out using the Abaqus program. The investigations into the influence of galvanizing on the fatigue strength were carried out on samples bent through 180 ° that were either ungalvanized or galvanized following the procedures “bending after galvanizing” and “bending before galvanizing” and on straight samples.

Fig. 2 shows the test programme and the basic sequences of the investigations that were carried out

3. Results

3.1 Initial characterization

The steels included in the investigation were first submitted to thorough initial characterization in the ungalvanized and galvanized states and assessed for possible risks with respect to the danger of LMAC and bending at low temperatures.

The **chemical compositions** of the samples met the requirements of DIN 488. With respect to the relevant silicon content for galvanizing, the materials B500B 10 mm and B500B 14 mm lay in the high silicon range (Si > 0.25 mass %). All the other materials were located in the Sebisty range.

The Tempcore materials exhibited a tempering microstructure in the edge region while in the core there was a ferritic-perlitic **microstructure**. The coil material was ferritic-perlitic throughout.

The measurements carried out on the ribbed surfaces show that these are reduced by the galvanizing. This effect was most marked with the coil materials B500B 10 mm and B500B 14 mm that were first straightened before the galvanizing.

At the same time as the microscopic investigations the **thickness of the zinc layer** on the samples was determined by the gravimetric method described in DIN EN ISO 1460. The measured zinc layer thicknesses lay at the upper limit of the range covered by the approval or even above it.

Damage to the zinc layer in the form of cracking or even flaking occurred during the bending of the samples, depending on the bending roller diameter. The investigations into the bending behaviour at low temperatures showed that the intensity is also aggravated by decreasing temperatures.

The **mechanical properties** of the steels investigated met the requirements of DIN 488.

Comparatively severe scattering was observed with the B500B 10 mm material, which can be attributed to the production and rolling processes for the Tempcore steel.

Because of the temperature effects during the galvanizing process the B500A 10 mm and B500B 14 mm coil materials used in the investigation still exhibited a **flow range** with a pronounced yield stress R_{eH} after the hot-dip galvanizing. The yield stress and tensile strength were not significantly affected by the galvanizing process, as is shown by comparison of the characteristic values determined on ungalvanized and galvanized samples based on the actual cross-sectional areas.

Fatigue tests were carried out on straight, ungalvanized, samples and samples galvanized by Procedure A (galvanizing – bending) complying with DIN EN ISO 15630-1 to determine the fatigue strength of the Tempcore B500B 10 mm material at the load levels 35 kN, 30 kN and 25 kN with a test frequency of 15 Hz in the pulsating tensile stress range. These showed lower numbers of cycles for the galvanized samples than for the ungalvanized samples

Other fatigue tests with Tempcore B500B 10 mm samples and B500A 10 mm coil material complying with the requirements of DIN 488 showed that the requirements for 25 % diminution specified in the approval and standard were achieved by both materials.

The **re-bending trials** that were carried out showed that the occurrence of cracks on the surface during re-bending through 20 ° is prevented with a minimum bending roller diameter of $4 \times d_{St}$. Diminution by one step would be possible with the B500B 10 mm and B500B 14 mm materials in the ungalvanized state. Test series with the QT 25 material showed that there was also a reserve when processing with the minimum bending roller diameter of $7 \times d_{St}$ specified in the standard.

Tests were carried out with the B500B 10 mm and B500A 10 mm materials for the bending parameters that are important in the context of the research project, namely bending angle, bending roller diameter, bending temperature, bending rate and rib orientation, in which these influencing variables were varied in several stages. The particular intention was to investigate whether any systematic differences in the properties remaining after the bending occur in a temperature range down to -20 °C for the usual bending shapes, namely angles (90 °) and loops (180 °).

In each case the samples that had been fully bent back failed in the tensile test outside the fully bent-back bending zone; the requirements of DIN 488 were fulfilled with respect to the yield strength, the tensile strength and the A_{gt} . The A_{gt} measurements in the bending zone region proved that even in these highly stressed zones there is still a residual ductility. No clear relationships could be deduced from the investigations that were carried out.

More extensive investigations in the context of the tensile tests in Class 1 molten zinc (in accordance with DAST Guideline 022) at 450 °C showed that the bending temperature had no influence on the

result and the bending roller diameter had a definite influence. As far as the roller diameter was concerned it could be deduced that the maximum tolerable stresses fall as the diameter becomes smaller and at the same time the stress maxima are displaced toward smaller openings. When compared with the B500A 10 mm material the B500B 10 mm material could generally tolerate less opening (at the maximum stress) and less nominal stress and, because of the greater hardness at the edges, was clearly more vulnerable to LMAC damage.

The progress of the hardness with depth in unbent samples corresponded to the respective material microstructures. With the bent samples the bending caused somewhat higher values in the outer region than in the unbent region.

The load-free ageing tests in a molten salt bath at 450 °C that were carried out to assess a possible **age-hardening susceptibility** showed that only the bent samples of the B500B 16 mm exhibited a slight ageing effect. None of the other materials showed any ageing effects.

3.2 The “bending before galvanizing” procedure

3.2.1 Potential danger of LMAC

The various materials (black material) were bent through 90 ° as specified in the standard with different bending roller diameters to assess the possible danger with respect to liquid metal assisted cracking (LMAC) and for the numerical simulation. The internal stresses were then determined at intervals of 1 mm across the cross-section from inside of the bend to the outside.

With all the materials there were tensile stresses in the range from 200 MPa to 300 MPa at the inside of the bends and compression stresses of a similar order of magnitude at the outside of the bends. In some cases there were strongly marked local stress maxima at the transition through zero.

Internal stress measurements were carried out in the same way on samples that had been bent through 180 ° and produced by Procedures A and B for comparison with ungalvanized samples to check the possible influence of the galvanizing process on the internal stresses.

The basic behaviour pattern of the internal stresses was as expected. A significantly marked reduction in the stress maxima was observed in the samples produced by Procedure B when compared with the ungalvanized samples and the samples produced by Procedure A. The decrease in the internal stresses can be attributed to the hot-dip galvanizing and has already been verified in [4]. The internal stresses were reduced by about 100 MPa (about 33 %) with the B500B 16 mm material and by about 200 MPa (about 45 %) with the B500B 14 mm material.

To assess the potential danger with respect to liquid metal assisted cracking eight samples of the B500B 10 mm material that had been bent through 180 ° with each of the bending roller diameters of 40 mm and 50 mm were tested in the creep test for the typical galvanizing duration of about 15 minutes in molten zinc at 0 MPa (load-free ageing), 50 MPa, 100 MPa and 200 MPa and then examined for any cracking by light-microscopy on longitudinal ground sections.

The results of the creep rupture tests on the samples with additional loads of 200 MPa and 100 MPa are shown by way of example in **Fig. 3**. Every one of the curves had a bend and no cracking was visible from shapes of the curves. The influence of creep, caused by the effect of heat and the load stage chosen for the test, was apparent in the samples with the additional load of 200 MPa. For the samples loaded at 100 MPa there was equilibrium between the externally applied nominal stress and the restoring forces in the sample. Beyond a certain point the opening remained constant with time. In the tests carried out there were no significant differences between the samples bent with the 40 mm and the 50 mm rollers with respect to their curve shapes.

Metallographic investigations were carried out with half the aged samples. Re-bending tests up to 20 ° in accordance with DIN EN ISO 15630-1 were carried out on the rest of the samples, which were then also submitted to metallographic examination.

It was found that even before the reverse bending virtually all the samples investigated exhibited initial LMAC damage starting from the rib feet. After the re-bending through 20 ° the damage tended to be more strongly marked due to the mechanical stress applied but, apart from one case, ran only a few millimetres into the base material. Fig. 4 and Fig. 5 show examples of the metallographic results. From **Fig. 4** in particular it emerges that the cracks start at the rib feet and are significantly enlarged after the re-bending (**Fig. 5**).

This means that for the tests described there was clearly a discrepancy between the experimental test curves and the metallographic evaluations. For all the samples, regardless of the bending roller diameter and the additional stress applied, no signs of cracking were apparent from the loading curves in contrast to the metallographic findings described above.

3.2.2 Permissible bending roller diameters

For the investigations into bending using Procedure B, angles and loops were produced at room temperature with a bending rate of 10 rpm and then galvanized using the materials B500B 10 mm, B500A 10 mm, B500B 14 mm and B500B 16 mm. The laboratory could not re-bend the loops bent with B500B 25 mm material so only angles were produced and galvanized with this material.

The following **Table 1** summarizes the sample shapes produced and the bending roller diameters used.

During the investigations the samples were first aged and then re-bent through 20 °. The zinc layer exhibited cracks in all cases so the zinc layer was removed from the samples at the bend using the procedure described in DIN EN ISO 1460 to establish whether the cracks extended into the base material. The samples were then completely straightened, aged and tested in the tensile test.

Provided no fracture or detectable gaping cracks had occurred during the straightening, samples with incipient cracks were also tested in the tensile test. Based on DIN 15630-1 it was assumed that a "superficial ductile crack" is allowed to occur at the base of ribs and is not to be considered a fault if the depth is not greater than the width of the crack.

The materials investigated exhibited differing behaviour with respect to the cracking.

In contrast to the other materials some of the samples of the B500B 14 mm material bent with a bending roller diameter $d_{Br} = 50$ mm exhibited brittle fractures during re-bending through 20° . On the other hand, the samples bent with a bending roller diameter $d_{Br} = 85$ mm remained apparently free from cracks both during the re-bending and during the straightening; no brittle fractures occurred.

Local defects in the material microstructure were suspected of being the possible cause of this phenomenon that only occurred in isolated cases. Microscopic investigations showed that the crack starts from flaws in the microstructure and there are areas with brittle separation fractures as well as areas with ductile fractures in the cross-sectional area.

The loops and angles of B500B 16 mm material bent with a bending roller diameter $d_{Br} = 60$ mm mainly failed during re-bending through 20° as a result of gaping cracks that started from the rib feet and ran on into the base area and that widened further with increasing bending. This cracking occurred in virtually all the angle and loop samples tested. However, the cracking behaviour can be described as ductile.

3.2.3 Evaluation of the results

The minimum bending roller diameters (bold, shaded in grey) shown in **Table 2** can be specified on the basis of the investigations carried out.

This is based on the fact that, up to a limiting diameter of 16 mm, deformation for corrective reasons or as a result of outside interference cannot be absolutely ruled out under construction site conditions. For this reason the samples must not exhibit any incipient cracks in the base material with this type of stressing as the corrosion protection is then nullified even if the mechanical properties are not apparently impaired by the cracks. In the context of the investigations that have been carried out adequate safety is established by the (incipient) crack-free behaviour of the sample during re-bending through 20° .

The given limiting diameters can be regarded as recommendations for galvanizing by Procedure B (bending before galvanizing).

Even if the B500A 10 mm material can, according to the tests that were carried out, be bent with a bending roller diameter of 40 mm it is recommended for practical construction reasons that a minimum bending roller diameter of $6 \times d_{St}$ is specified for all bar diameters up to 14 mm.

Because cracking cannot definitely be ruled out when B500B 16 mm is re-bent with a bending roller diameter of 100 mm a minimum bending roller diameter of $8 \times d_{St}$ is recommended for this material. Regardless of the galvanizing a bending roller diameter of $d_{Br} = 7 \times d_{St}$ represents the lower limit for bar diameters $d_{St} \geq 20$ mm. Re-bending of these bar diameters seems to be virtually ruled out under construction site conditions.

Also for practical construction reasons it is therefore recommended that a minimum bending roller diameter of $8 \times d_{St}$ is specified for all bar diameters ≥ 16 mm if the samples are to be bent through an angle $\geq 90^\circ$.

Basically, however, the results also leave the option open of proving the functionality of smaller bending roller diameters in individual cases while taking the above-mentioned principles into account.

3.3 Influence of galvanizing on fatigue strength

Loops of the B500B 10 mm material that had been bent through 180 ° at room temperature were used for investigating the fatigue behaviour. Comparative fatigue tests were then carried out under identical test conditions on samples galvanized by Procedures A and B and on ungalvanized samples. The results of the fatigue tests are shown in **Figs. 6 to 8** as Wöhler curves.

Basically, the results lie at comparable levels. Closer inspection shows that there are slight differences. For example, the fatigue strength stress $\delta_{B50\%}$ is 168 MPa for the ungalvanized samples, 189 MPa for Procedure A and 191 MPa for Procedure B. There is no detectable reduction of the fatigue strength of samples produced by Procedure B when compared with those produced by Procedure A.

One explanation could be the diminution of internal stresses due to the galvanizing [4]. This was confirmed by the investigations carried out as part of the initial characterization. The samples produced by Procedure B (bending – galvanizing) exhibited a significant reduction in internal stresses when compared with ungalvanized samples and those produced by Procedure A (galvanizing – bending). Due to the high heat input the internal tensile stress are relieved during the galvanizing so that cracks could in fact be present but, because of the reduced internal tensile stresses at the inner radius of the bend, not to the extent that would have been expected.

This hypothesis is supported by metallographic examination of samples that passed the test without fracture. The cracks in the sample from Procedure A are as equally strongly marked as in the ungalvanized sample tested at identical load levels (**Fig. 9**). The cracks in the sample produced by Procedure B are significantly deeper for a somewhat higher load level. It is also clear that here again all the cracks start from the rib feet (**Fig. 10**).

Fracture face investigations under a scanning electron microscope showed the typical features of fatigue fractures.

A combination of internal tensile stresses combined with notches resulting from the manufacturing process that act as crack-initiating points at the rib feet can be perceived as the cause of the cracks.

Bearing in mind the chosen method of testing, Procedure B should be evaluated as not critical with regard to the Wöhler curves.

On the other hand, with unbent reinforcing steel there is a reduction in fatigue strength with galvanized samples when compared with ungalvanized samples, regardless of the material. At comparable load levels the hot-dip galvanized samples achieved fewer load cycles. However, the B500A 10 mm and B500B 10 mm material samples tested achieved the requirements for a 25 % diminution scheduled in the approval and the standard.

3.4 Bending at low temperatures

According to DIN EN 1992-1-1 (EC2) and the associated national application regulations DIN EN 1992-1-1/NA D and DIN EN 13670 the requisite security against damage to the reinforcement and the concrete when processing reinforcing steel into reinforcing elements is achieved with DIN 1045-3 (NA to DIN 13670) by limiting the bend radii, by the guidelines of the reinforcement regulations and by limiting the bending temperature.

DIN EN 13670 permits bending at temperatures below -5 °C provided that this is designated in the construction documents and that additional precautionary measures are observed but the German application regulation DIN 1045-3 restricts the permissible bending temperature to a lower limit of -5 °C.

For the enterprises that process reinforcing steel – bending operations, placing operations, raw construction work companies – extending the temperature range down to a lower limit of -20 °C offers the advantage that the risk of downtime due to excessively low temperatures is practically ruled out.

For this reason the research project also examined whether the bending temperature for ungalvanized and galvanized reinforcing steel can be lowered without impairing the steel properties.

The investigations were carried out on ungalvanized reinforcing steel and on reinforcing steel that had been galvanized by Procedure A “galvanizing before bending”.

The samples for testing at room temperature were stored in the laboratory climatic chamber at 20 ± 2 °C. The samples at controlled temperatures were stored overnight in a freezer chest at the intended temperature plus a safety margin of about 2 K, transported to the bending machine in a container filled with coolant and bent promptly after removal from the coolant. This procedure ensured that the samples had the intended temperatures.

Ungalvanized samples were tested at the temperature stages of room temperature, -5 °C and -20 °C. The initial tests indicated that no negative results were to be expected so the samples produced by the procedure “galvanizing before bending” were only tested at the temperature stages of room temperature and -20 °C. In view of the recommendation in DIN 1045-3 that the rate of bending should be suitably reduced at bending temperatures between 0 °C and -5 °C some individual test series were also carried out at a bending rate of 20 rpm.

No brittle fractures and no cracking occurred in the bending tests during the bending. When the samples had warmed up again to room temperature in air they were aged at 100 °C. After cooling to room temperature at about ≥ 20 °C they were bent back, examined for cracking and finally completely straightened. The tensile tests to establish the remaining properties were carried out after renewed ageing.

No fractures occurred in the bending zone with the samples investigated. The A_{gt} values showed that a residual ductility was still present in the bending zones. $R_{p0.2}$ values lay above the nominal value of the yield strength of 500 N/m².

As a whole it was established that all the steel samples tested after being completely straightened fulfilled the requirements of DIN 488 for the characteristic mechanical values. The results gave no indication of any clearly recognizable systematic influence of the bending temperature and/or bending rate.

The results obtained indicate that bending at low temperatures down to -20 °C is basically possible with bending roller diameters $\geq 4 \times d_{St}$ for bar diameters $d_{St} \leq 16\text{ mm}$ and $\geq 7 \times d_{St}$ for bar diameters $d_{St} \geq 16\text{ mm}$ without impairing the material properties.

3.5 Re-bending under construction site conditions

Re-bending of reinforcing bars with a diameter $\leq 14\text{ mm}$ under construction site conditions is covered in Germany by DIN EN 1992-1-1/NA D and the DBV Code of Practice "Re-bending of reinforcing steel and requirements with regard to protective boxes in accordance with Eurocode 2", January 2011.

The results obtained in the tensile tests during the investigations carried out on fully re-bent samples support the conclusion that the steel samples investigated have reserves of ductility with respect to the stated limit for bending roller diameters of $6 \times d_{St}$. However, there are also important questions about the fatigue strength in this application so a more comprehensive recommendation is not possible.

In the same way as was shown with the investigations for bending at low temperatures the bending properties of the samples galvanized by Procedure A behave like the ungalvanized steel samples. Damage to the galvanizing is to be expected with full re-bending. This should be repaired as necessary to preserve the corrosion protection.

The microscopic investigations that were carried out showed that the samples produced by Procedure B exhibit microcracks in the area of the rib feet even in the undeformed state before the re-bending. In view of the danger of cracking that exists with uncontrolled re-bending under construction site conditions it is recommended that systematic re-bending should not be permitted with these types of steel.

3.6 Corrosion properties

The investigations into corrosion behaviour that were carried out in carbonated concrete support the recommendation for a reduction in the concrete cover for exposure class XC. Increased corrosion rates during exposure to chlorides, corresponding to exposure classes XD and XS, were only found above a chloride content of 1 mass % relative to the cement content. In contrast to ungalvanized reinforcing steel no macro element formation was detected in samples with active corrosion areas. A coating/inhibitor that prevents the evolution of hydrogen in fresh concrete was also successfully developed during the work that was carried out.

Detailed information can be found in the contribution to the conference by the project partner BAM.

4 Outlook

Unlike the situation in Germany, where only very few projects, such as parts of the Chancellery building (Berlin), parts of the new museum in Nürnberg and the bridge edge beams of an autobahn

bridge on the BAB A99 (Bavaria), have been carried out so far with hot-dip galvanized reinforcement, hot-dip galvanized reinforcing steel is used significantly more frequently abroad with great success due to the simplified application and implementation regulations.

Against the background of the experience that is already available abroad with the practical use of hot-dip galvanized reinforcement it can be assumed that, because of its potential, this method of construction will also open up a larger area of application in Germany if the results obtained in this projects are successfully introduced into building practice and the regulations are quickly adapted to the state of the art with regard to the aim of establishing Procedure B.

Acknowledgements

- Badische Stahlwerke GmbH
- Baustahl-Armierungsgesellschaft Mannheim mbH
- Hipercon Forschungsschwerpunkt TUK
- Institut Feuerverzinken GmbH
- Institut für Stahlbetonbewehrung e.V.
- ZINKPOWER Willi Kopf GmbH & Co. KG

References

- [1] Deutsches Institut für Bautechnik, Allgemeine bauaufsichtliche Zulassung Z-1.4-165, Feuerverzinkte Betonstähle, Berlin, 2014
- [2] AIF, Technologie- und Sicherheitszuwachs bei der Anwendung von feuerverzinktem Betonstahl zum Ausbau einer nachhaltigen Marktposition im Stahlbetonbau, Abschlussbericht, Forschungsvorhaben IGF 499 ZN/1
- [3] Deutscher Ausschuss für Stahlbau: DAST-Richtlinie 022, Feuerverzinken von Stahlbauteilen, 2009
- [4] Körber, D.: Einflussgrößen auf die flüssigmetallinduzierte Spannungsrisskorrosion beim Feuerverzinken. Dissertation, 2013, TU Darmstadt 2013

Figures and tables

Unresolved issues – areas of responsibility

MPA Darmstadt

Materials technology

- Risk of liquid metal assisted cracking (LMAC)
- Influence of galvanizing on fatigue strength

FWB, TUK

Production technology

- galvanizing after bending
- bending at temperatures down to -20 °C
- Re-bending under construction site conditions

Research objectives

1. Experimental and numerical determination of verified and scientifically based application limits

- after the galvanizing
- before the galvanizing

of bent reinforcing steel

BAM

Corrosion protection

- reactions and interactions between zinc and fresh concrete
- inhibiting the reactions (chromate reducer)
- Corrosion behaviour during the action of chlorides and carbonation

2. Identifying the passivation reaction during concreting (evolution of hydrogen)

3. Determining the corrosion behaviour of galvanized reinforcing steel with respect to the advance of corrosion and the useful life

Figure 1: Issues, areas of responsibility and research objectives

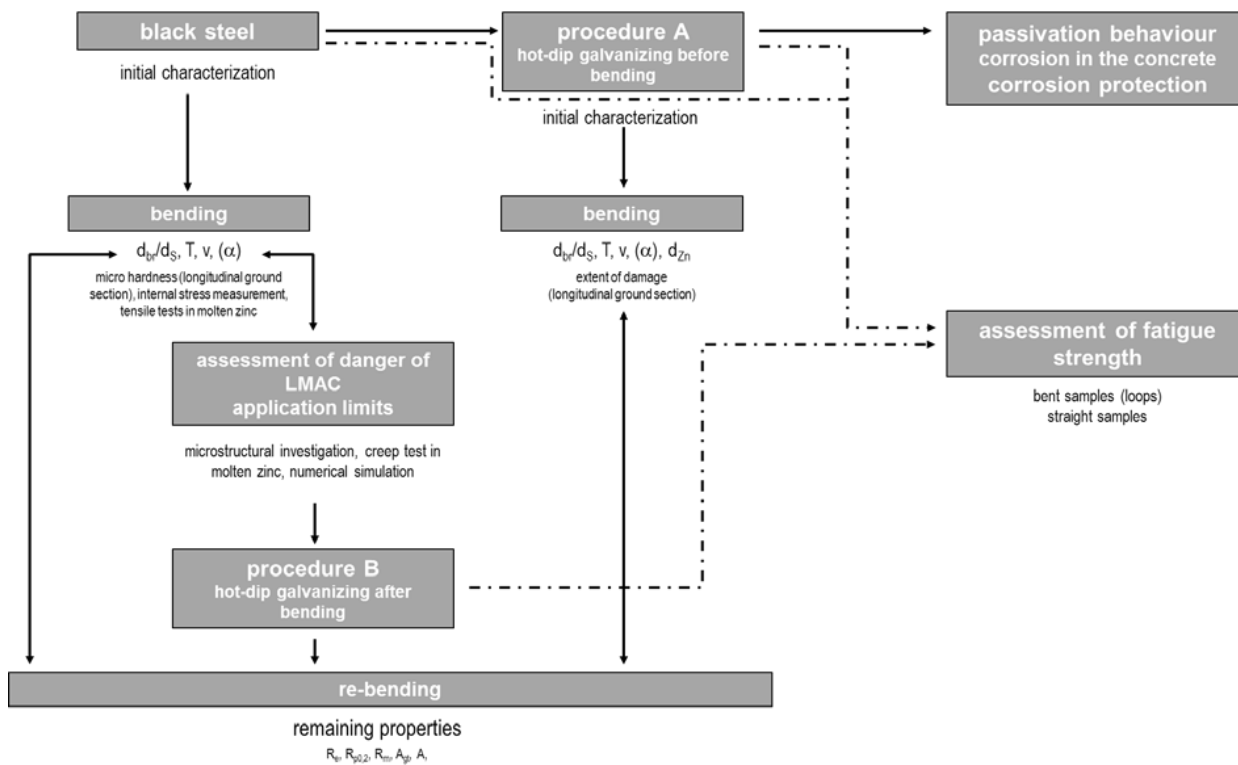


Figure 2: Test programme/project structure

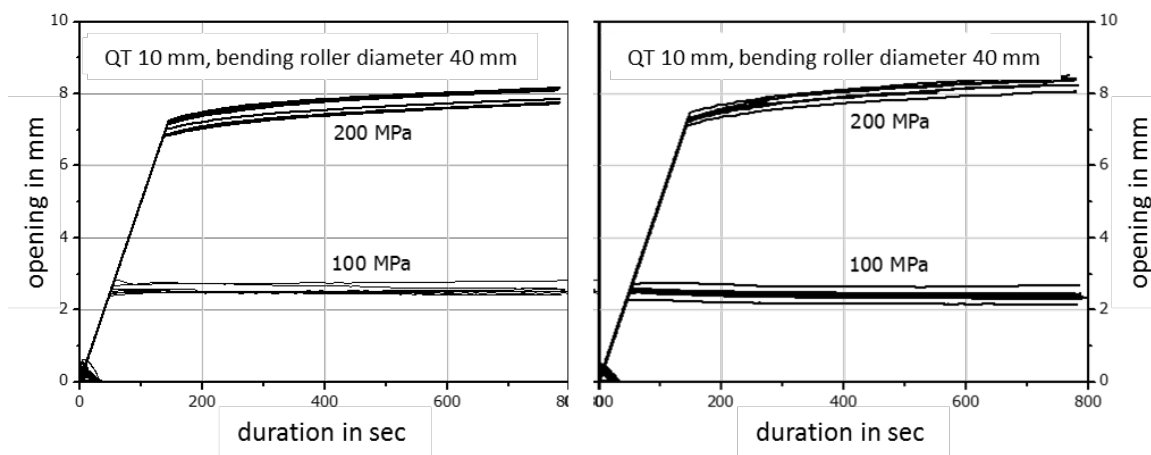


Figure 3: Results of the creep rupture tests, material B500B 10 mm [2]

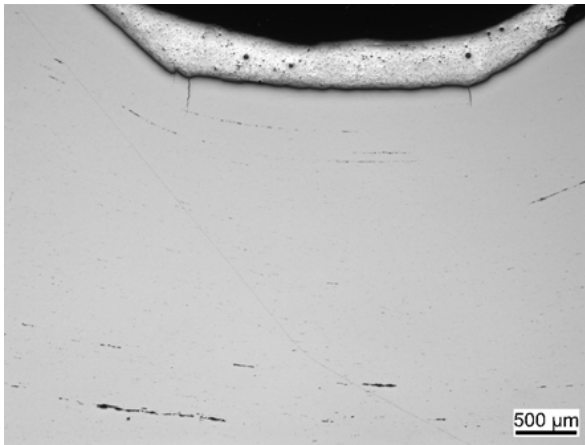


Figure 4: Material B500B 10 mm, $d_{Br} = 50$ mm, $\sigma_{nenn} = 50$ MPa, example of cracks before the re-bending (20 °) [2]

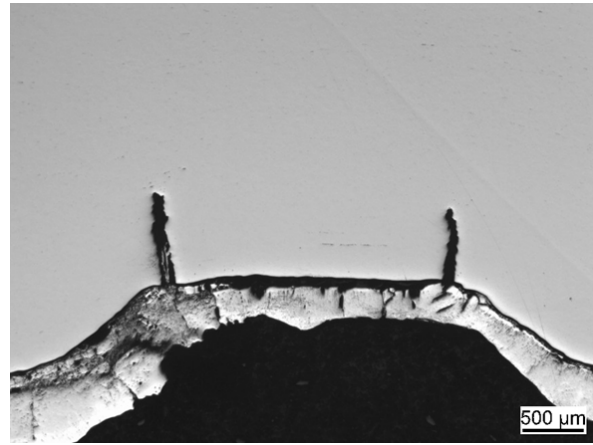


Figure 5: Material B500B 10mm, $d_{Br} = 50$ mm, $\sigma_{nenn} = 50$ MPa, example of cracks after the re-bending (20 °) [2]

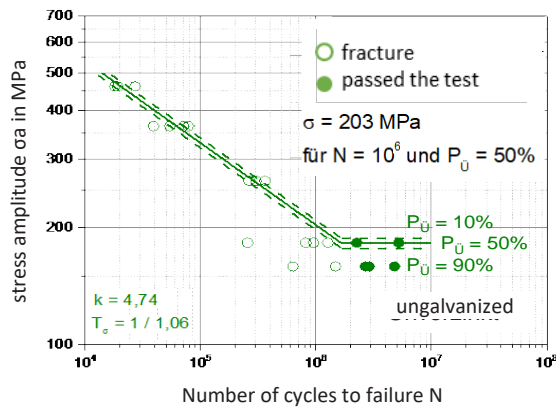


Figure 6: Wöhler curves of the ungalvanized samples (loops) [2]

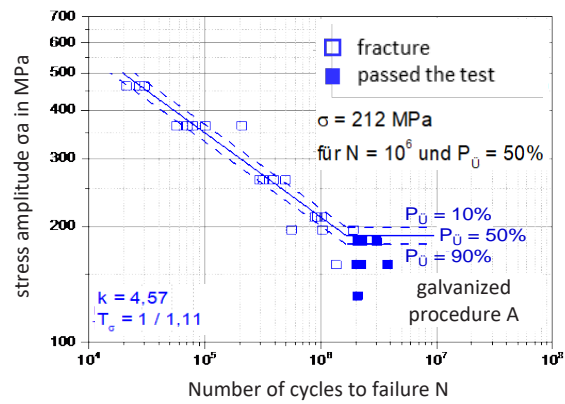


Figure 7: Wöhler curves of the samples galvanized by Procedure A (galvanizing – bending) (loops) [2]

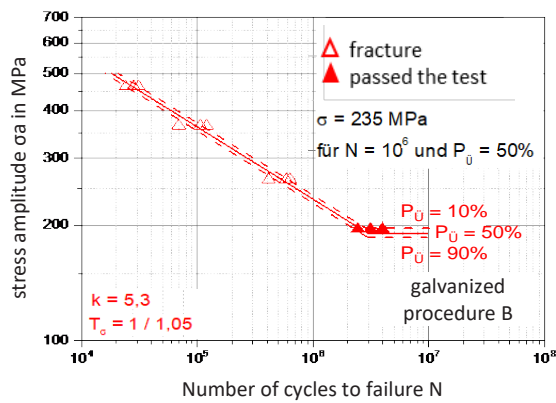


Figure 8: Wöhler curves of the samples galvanized by Procedure B (bending – galvanizing) (loops) [2]



Figure 9: Metallographic findings for samples that had passed the test without fracture – ungalvanized (left) and galvanized using Procedure A (galvanizing – bending) (right) [2]

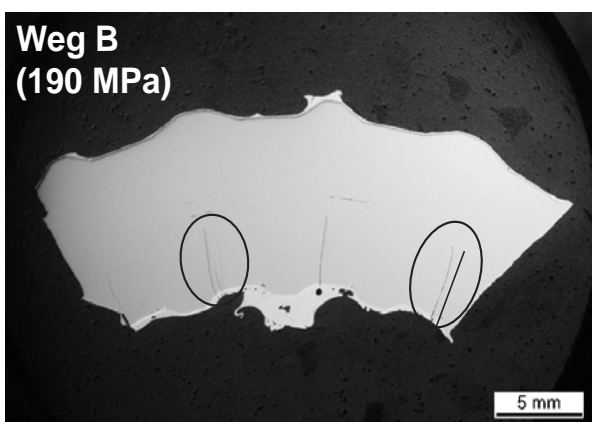


Figure 10: Metallographic findings of a sample that has passed the test without fracture – galvanized using Procedure B [2]

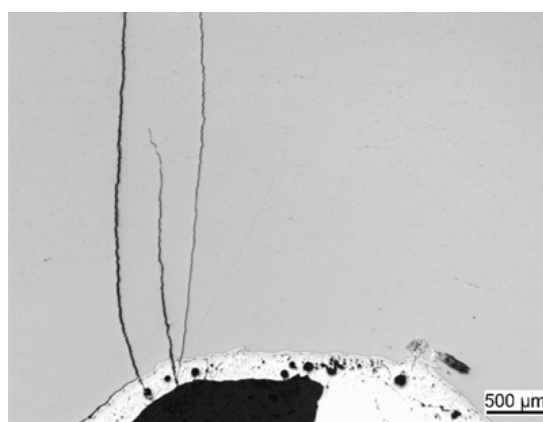


Figure 11: Detail from Fig. 10 [2]

Table 1: Sample shapes for samples galvanized by Procedure B (bending – galvanizing)

Material	Bending shape		Bending roller diameter		
			4 x d _{St}	6 x d _{St}	8 x d _{St}
B500B 10	angle	loop	40	60	85
B500A 10	angle	loop	40	60	85
B500B 14	angle	loop	50	85	100
B500B 16	angle	loop	60	100	135
				7 x d _{St}	8 x d _{St}
B500B 25	angle		160	185	200

Table 2: Permissible bending roller diameter for the “bending before galvanizing” procedure

Material	Bending shape		Bending roller diameter		
			4 d _{St}	6 d _{St}	8 d _{St}
B500B 10	angle	loop	40	60	85
B500A 10	angle	loop	40	60	85
B500B 14	angle	loop	50	85	100
B500B 16	angle		60	100	135
				7 d_{St}	8 d_{St}
B500B 25	angle		160	185	200

Abbreviations

d _{St}	bar diameter
d _{br}	bending roller diameter
T	temperature
R _{eH}	yield strength
R _{p0,2}	0.2 % proof strength
A _{gt}	extension at peak load
LMAC	liquid metal assisted cracking

Author Biography

Robert Adams

Studied Construction Engineering, Political and Educational Sciences at the Technical University of Kaiserslautern. Since 1988 he has been a member of the scientific staff in the Faculty of Building Construction Materials.

Wolfgang Breit

Studied civil engineering at the Aachen University of Technology. From 1990 to 1997 he was a member of the scientific staff at the Institute for Building Research at Aachen University of Technology (ibac) where he obtained his doctorate in 1997. From 1997 to 2007 he was senior engineer in the concrete technology department of the Research Institute of the Cement Industry in Düsseldorf.

Since 2007 he has been head of the Faculty of Building Construction Materials at the Technical University of Kaiserslautern where, since 2008, he has also been senior director of the Materials Testing Office.

He is also a member of the DAfStb (German Committee for Structural Concrete), Berlin, the DBV (German Association for Concrete Technology and Construction Engineering), Berlin, the DVGW (German Association for the Gas and Water Industries), Bonn, the VDB (Association of German Concrete Engineers), Düsseldorf, the IK-Bau (North Rhine-Westphalia Chamber of Building Engineers), Düsseldorf, the FBF (ibac Association for Promoting Building Research), Aachen, and a co-worker on a large number of bodies and committees that set the standards and regulations, such as CEN, DIN DAfStb, DVGW, DWA and VMPA.

Corrosion Behaviour of Galvanized Reinforcement in Chloride Containing Mortar and Carbonated Mortar

Gino Ebell, Andreas Burkert and Jürgen Mietz

Bundesanstalt für Materialforschung und -prüfung (BAM), 7.6 Corrosion and Corrosion Protection, 12205 Berlin, Germany

Abstract The corrosion behavior of galvanized steel in chloride containing and in carbonated concrete is different from the corrosion behavior of reinforcement made of carbon steel. In case of galvanized reinforcement in chloride containing concrete structures the potential drop and the typical pitting corrosion as in the case of normal carbon steel reinforcement do not occur. The corrosion behavior of galvanized reinforcement in carbonated concrete is mainly influenced by the lower pH-value of carbonated concrete. To describe the influence of chlorides in concrete structures and a lower pH-value on the corrosion activity of galvanized reinforcement, different electrochemical measurements were made. The anodic and cathodic partial reaction were investigated by galvanostatic pulse measurements and potentiodynamic measurements. Especially the galvanostatic pulse measurements can describe the influence of the lower pH-value by the anodic polarization resistance with a polarization time of 20 sec. . The influence of the chloride content on the corrosion behavior will be described by potential current curves and the determined corrosion rate by Tafel plots. Additionally, corrosion current measurements were performed, coupled with potential measurements, between galvanized steel in chloride containing and chloride free concrete as well as in carbonated and non-carbonated concrete. Normally, the potential measurements are an indicator to localize the anodic and cathodic parts of a macro system. In both cases the results are different to the well known potential ranges of corroding carbon steel reinforcement. The results are a part of the Industrial Collective Research (IGF) project No. 499 which was supported by the AiF [1].

Keywords

Hot dip galvanized steel, reinforcing steel, zinc, cement, concrete, carbonated concrete, chloride containing concrete, electrochemical measurements, polarization

Introduction

The durability limitation of reinforced concrete buildings is based on the corrosion durability of the embedded reinforcement. The durability of the reinforcement can be shortened by two kinds of external attacks, the carbonation of the concrete or by chloride attack. The reinforcement is normally protected against corrosion by the high alkaline pore solution and against the outer environments by the concrete cover. In case of carbonated concrete, the pH-value of the concrete pore solution is less than 8.6, and the corrosion protection of carbon steel is not stable anymore [2, 3]. Corrosion of galvanized steel in carbonated concrete is different from the corrosion of reinforcement made of carbon steel. This is based on the corrosion mechanism of galvanized steel in dependence of the pH-value of carbonated concrete. Also in chloride containing concrete structures, which are reinforced with hot dip galvanized rebars, a classical formation of a macro-element cell was not observed.

Experimental

Test parameters

The concrete design was in accordance with DIN EN 1766 and contains 345 kg/m³ CEM I 42,5 R Portland cement, the w/c-ratio was set to 0.50 and the maximum gravel size was about 4 mm.

The used kind of specimen was designed in preliminary investigations and is shown in Figure 1. A commercial type of reinforcing steel was used, ribbed bars (BSt 500 S) with a diameter of 10 mm and welded wires for the electron conduction to the outer area. The concrete cover is about 15 mm. The used spacers are made out of mortar with the same concrete mixture as the specimen.

The mean zinc layer thickness of the hot dip galvanized specimens was about 140 μm.

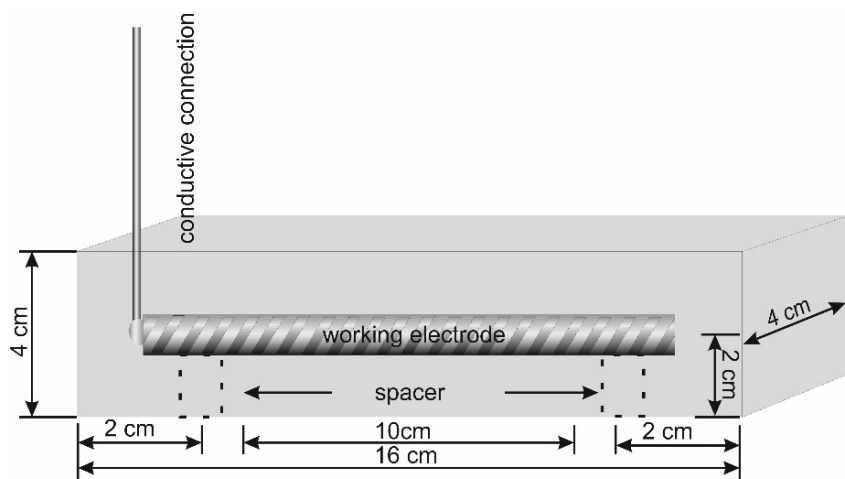


Figure 1: specimen design

Carbonation of concrete specimens

The carbonation process of concrete specimens with a high cement content like in our specimens, needs a high CO₂ concentration inside the specimen containment to proceed the carbonation process in a short time. Therefore, we designed a carbon dioxide flow cell as shown in Figure 2. The atmospheric conditions inside the cell are 100 % carbon dioxide and a relative humidity of about 60 %. Before the carbonation process was started, the specimens were dried inside an oven at 80°C for 5h.

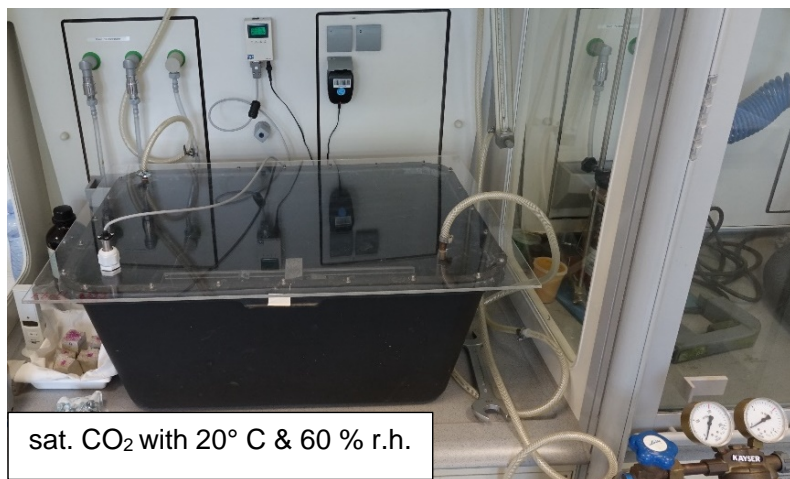


Figure 2: carbonation chamber for accelerated carbonation processes

Chloride admixtures of concrete specimens

The chloride content of the specimen was carried out by an admixture of sodium chloride during the fresh concrete manufacturing. We produced specimen with an addition of 0.2, 0.4, 1.0 and 2.0 M. % of chloride content, based to the cement weight of the concrete mixture.

Electrochemical investigations

To describe the influence of a lower pH-value on the corrosion activity of hot dip galvanized reinforcement, different electrochemical measurements were made. The anodic and cathodic partial reactions were investigated by galvanostatic pulse measurements and potentiodynamic measurements. Especially the galvanostatic pulse measurements can describe the influence of the lower pH-value by the anodic polarization resistance with a polarization time of 20 sec. [4, 5]. Additionally, corrosion current measurements were performed, coupled with potential measurements, between galvanized steel in carbonated and non-carbonated concrete and also potentiodynamic polarization measurements. The setup for the electrochemical polarization investigations is shown in Figure 3.

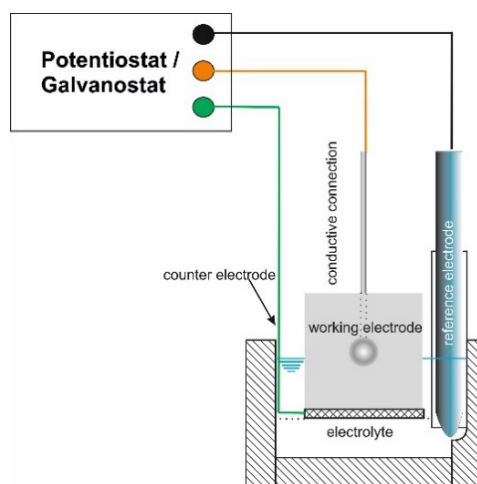


Figure 3: three electrode-setup for electrochemical measurements

The measurement setups for the potential and element current measurements are shown in Figure 4. On the left side of figure 4 the setup for carbonated specimens under dry conditions with an electrolyte gel as conductive electrolyte is shown. On the right side of figure 4 the electrolyte is changed; for the chloride containing specimens and for another series of carbonated specimen, the conductive electrolyte connection is performed by water.

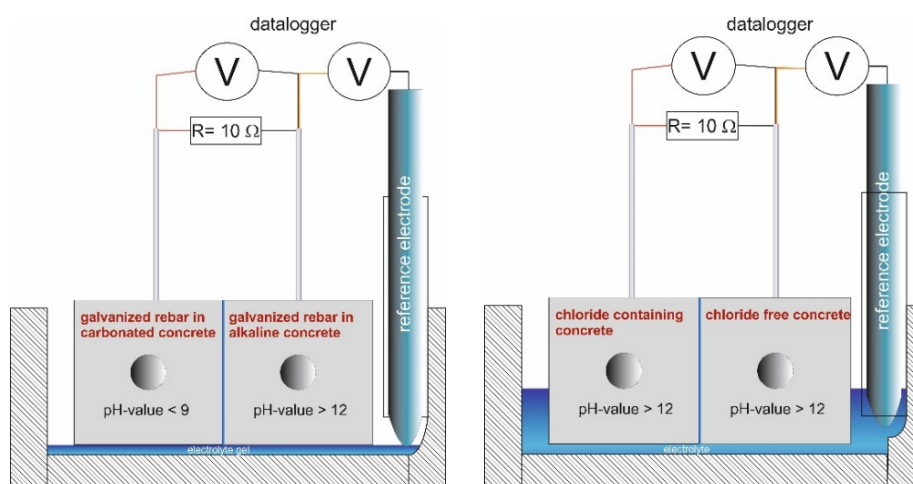


Figure 4: setup for electrochemical potential and current measurements

Results and discussion

Galvanized reinforcement in carbonated concrete

The following results are based on studies of corrosion elements consisting of hot-dip galvanized reinforcing steel in carbonated mortars and hot-dip galvanized rebar in alkaline mortars. Figure 5 shows an example of the progress of carbonation. The non-carbonated area is visualized by applying a phenolphthalein solution.

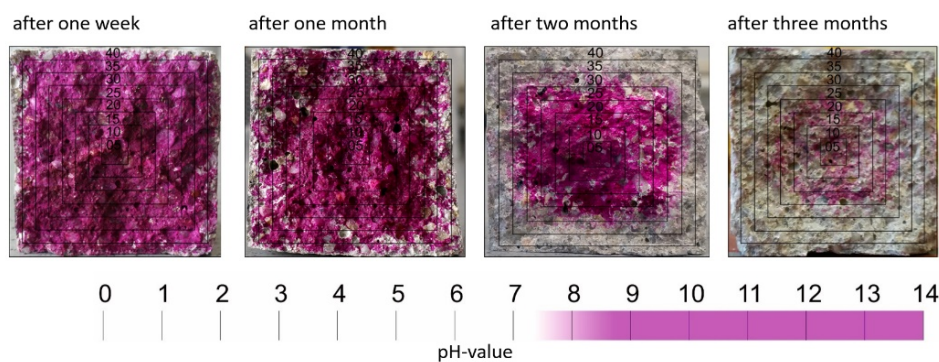


Figure 5: example for the carbonation depth of accelerated carbonation process

For the simulation of the exposure class XC1 (dry) an electrolyte gel was used, for the exposure class XC1 (wet) - XC4 an electrolytic coupling by water was used. The free corrosion potentials of the series with electrolyte gel show significant potential differences, between the carbonated and non-carbonated specimen of each pair, at the beginning of the measurement, Figure 6 left. The measured free corrosion potentials of the carbonated samples are up to 425 mV more negative than those of the alkaline samples. The series, which has been electrolytically connected by water, has a maximum potential difference of 70 mV and is in a range comparable to the carbonated samples of the gel series (Figure 6 right).

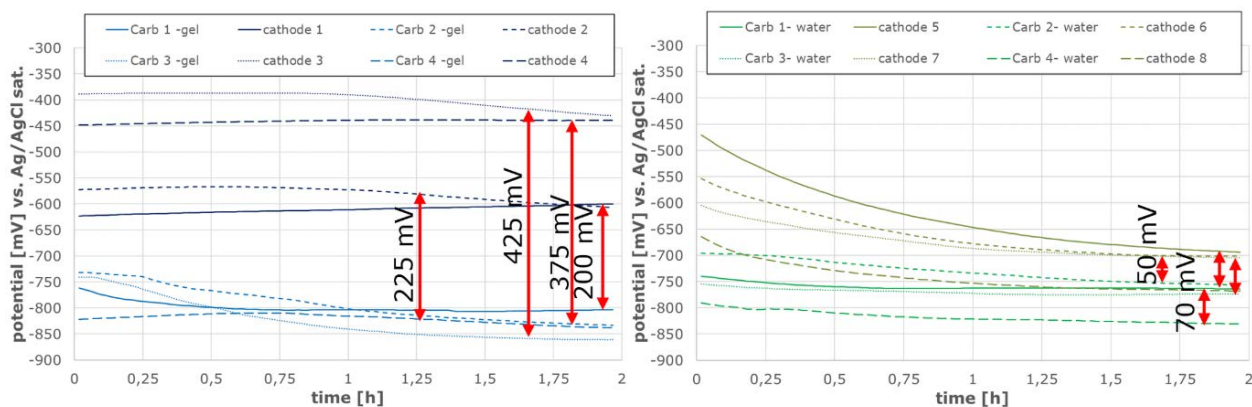


Figure 6:left: free corrosion potential of the gel series; right: free corrosion potential of the water series

Due to the electric-connection between the paired specimens, both series showed a potential drop down to a potential range in which the cathodic partial reaction occurs with the evolution of hydrogen (Figure 7 left and Figure 8 left). Comparing the measured element currents of both series, the gel series has significantly higher element currents at the initiation phase, Figure 7 right and Figure 8 right. This is based on the higher potential difference of the free corrosion potentials. After about 500 hours, the element current in both series is in the range of 0 or negative. That means, that between carbonated and non-carbonated areas no significant element current exists. Different as in case of carbon steel reinforcement, where the carbonated area forms the anode of a macro-element system, the galvanized rebar in carbonated concrete forms the cathode of the macro-element system.

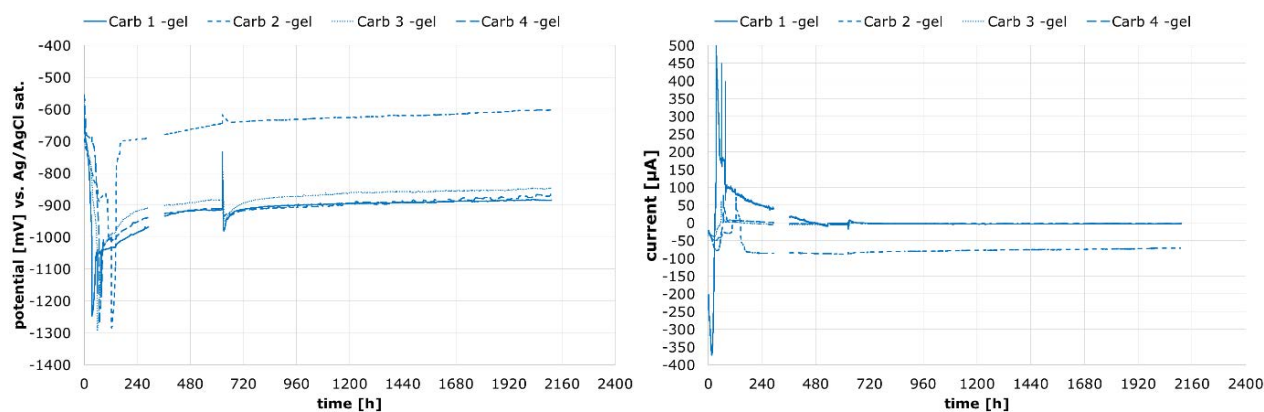


Figure 7: left: corrosion potential of the gel coupled specimens; right: corrosion current of the gel coupled specimens

At the end of the measurement, both series show a scattering of the corrosion potentials, the measured potentials are between -600 mV and -900 mV.

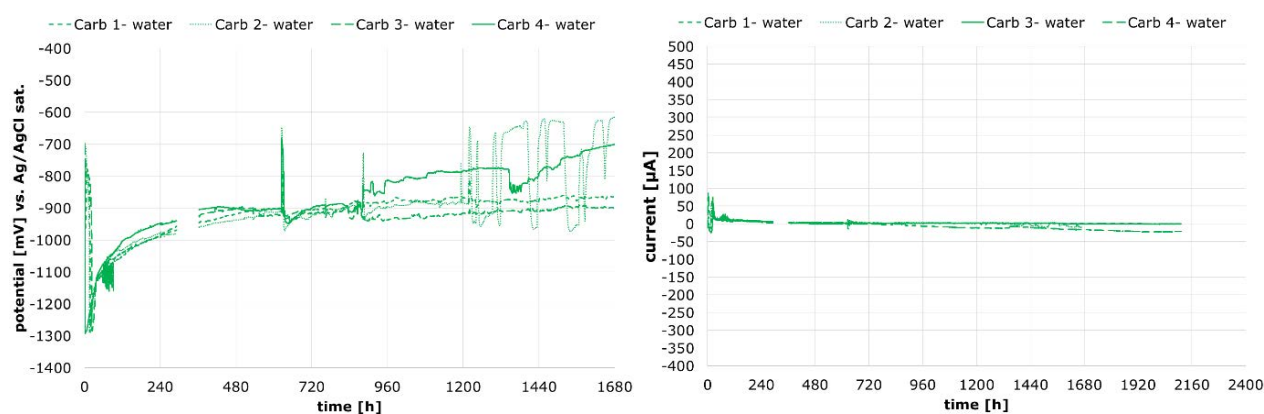


Figure 8: left: corrosion potential of the water coupled specimens; right: corrosion current of the water coupled specimens

The subsequent galvanostatic and potentiodynamic measurements of the carbonated and alkaline specimens were performed after completion of the element current measurements.

The self-corrosion rate was determined by means of current-potential curves, they are shown in Table 1. Considering the determined results for carbonated, water-saturated samples and a minimum zinc layer thickness of 85 μm a period of approx. 49 years until complete removal of zinc by corrosion was calculated. The time until the carbonation depth reach the embedded reinforcement must be considered. For example, if a concrete cover of 15 mm is carbonated after approx. 15 years and a corrosion rate of about 2.0 $\mu\text{m/a}$ is assumed according to [6], the residual zinc layer thickness is approx. 55 μm . This results in a useful life of about 45 to 55 years (water-saturated or moist gel). However, it can be assumed that the self-corrosion rate in alkaline concrete is further reduced within the period of time until the pH-value of about 8.6 is reached. On the one hand, this is due to the progression of the passive layer formation and, on the other hand, to the lowering of the pH-values below 12.4, which results in a reduction of the self-corrosion rate.

Table 1: self-corrosion rate of carbonated series

specimen	corrosion current [μA]	current density [mA/m^2]	corrosion rate (self- corrosion) [$\mu\text{m}/\text{a}$]
Carb.- gel	2,7	0,82	1,23
Carb.- water	3,8	1,15	1,72
Alka.- gel	8,0	2,43	3,63
Alka.- water	25,0	7,59	11,37

Galvanized reinforcement in chloride containing concrete

The following results are based on investigations of corrosion elements consisting of hot-dip galvanized reinforcing steel in chloride-containing mortars and hot-dip galvanized reinforcing steel in chloride-free mortars. The free corrosion potential of the specimens was recorded over a period of 432 hours at the first measurement period, at the second measurement period the free corrosion potential was measured over 1580 h. At the beginning of the first measurement campaign, the average free corrosion potential was around 700 mV. After 5 to 20 h a potential drop occurred at almost all specimens to levels where the cathodic partial reaction occurs under formation of hydrogen [6], Figure 9 left. The free corrosion potential at the beginning of the second measurement campaign depends on the chloride content. With increasing chloride contents the potential increase too, Figure 9 right.

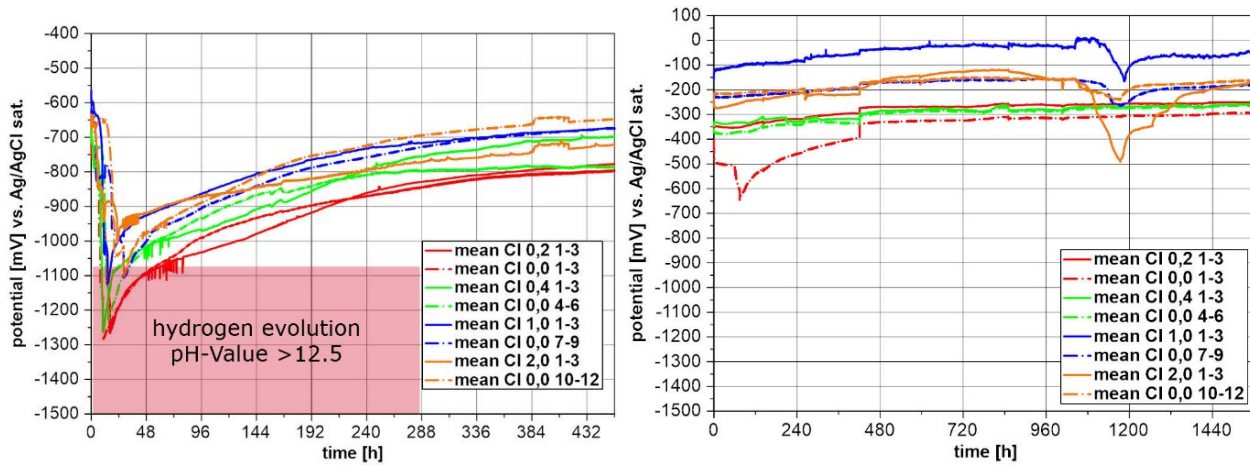


Figure 9: free corrosion potential of measurement campaign one (left) and two (right)

After the free corrosion potential measurement, the specimens were electrically conductive connected. Regardless to the chloride load, all samples show identical corrosion potentials at starting the element current measurement of about -700 mV vs. a saturated Ag/AgCl reference electrode. In the first measuring campaign, the corrosion potentials and currents were measured over a period of 1680 h (70 days). In the second measurement campaign the measurement takes 2400 h (100 days). Between the two measurement campaigns the specimens were decoupled for different electrochemically polarization measurements. In case of these two campaigns we did not show the results from the potential and current measurements in detail, the main information is shown by the measured charge for each coupled specimen pair and campaign.

Figure 10 show the measured charge over the time period of 1680 h at the left side and the measured charge from the second measurement campaign at the right side.

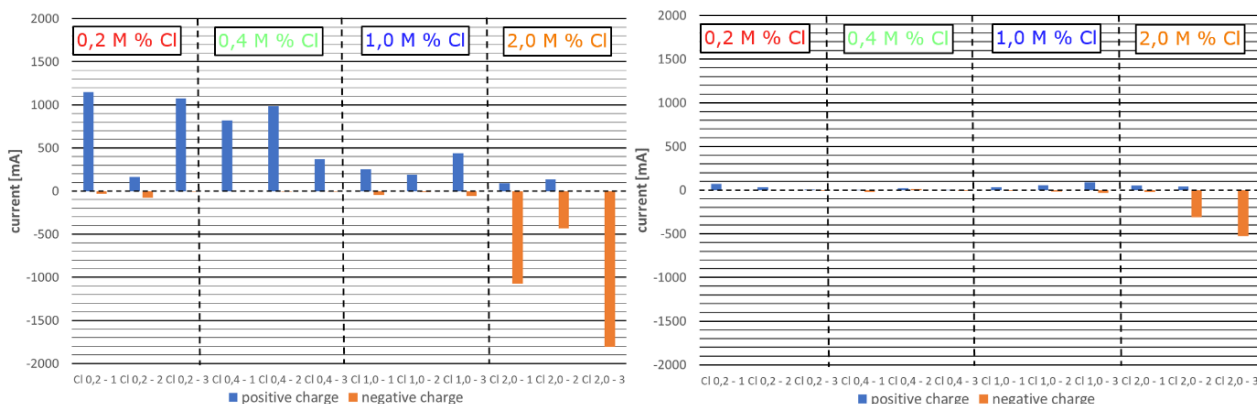


Figure 10: calculated charge of the measured element current from campaign one left and campaign two right

The corrosion currents were also determined from current-potential curves. The calculated corrosion current densities and the resulting corrosion rates can be taken from Table 2.

Table 2: self-corrosion rate of chloride containing series

specimen	self-corrosion current [μA]	current density [mA/m^2]	corrosion rate [$\mu\text{m}/\text{a}$]
CI 0,2	4,5	1,36	2,04
CI 0,4	4,6	1,39	2,09
CI 1,0	15,0	4,55	6,80
CI 2,0	20,0	6,06	9,07

Table 3 lists the corrosion currents from self-corrosion and element current, so that the expected corrosion rates could be calculated.

Table 3: self-corrosion rate combined with element-corrosion rate of chloride containing series

specimen	self-corrosion and element current [μA]	current density [mA/m^2]	corrosion rate [$\mu\text{m}/\text{a}$]
CI 0,2	4,5 + 0,5	1,51	2,27
CI 0,4	4,6 + 0,1	1,42	2,14
CI 1,0	15,0 + 0,5	4,70	7,02
CI 2,0	20,0 + 0,0	6,06	9,07

Considering the determined corrosion rates for 1 M. % chloride content and a minimum zinc layer thickness of 85 μm , a period of approx. 12 years would be enough for a complete removal of the zinc layer. However, depending on the diffusion migration resistance of the concrete, an already reduced zinc layer thickness can be assumed until the chloride content of 1 M.% is reached. This results in an effective increase of the total service life. For example, to reach a chloride content of approx. 1 M.% 25 years of service life would be needed and a residual zinc layer thickness of approx. 35 μm can be given. This zinc layer contributes to a service life gain of then 5 years. The gain in service life refers here to the initiation of a possible pitting corrosion process at the steel substrate. Studies in [7] have shown that a chloride content of 0.4 M.% chloride does not necessarily lead to pitting corrosion at non-galvanized reinforcing steels.

Conclusion

Investigations in carbonated concrete confirmed a clear advantage of hot-dip galvanized reinforcing steel over non-galvanized reinforcing steels. Here, a decrease in the corrosion rate of zinc due to carbonation could be observed. Based on a minimum zinc layer thickness of 85 μm , a service life of 45 - 55 years results regardless of the concrete cover thickness. Considering a zinc layer thicknesses of 140 μm to 160 μm , determined on the investigated ribbed concrete steels, a service live of 70 to 90 years results.

Based on the results, it can be recommended to include the following information and meaningful formulations in the regulations (Eurocode, national annex, building supervisory approvals). If hot-dip galvanized reinforcing steel is used, the concrete cover can be reduced in the exposure classes XC, according to DIN EN 1992-1-1 [8] to 10 mm as shown in Table 4.

Table 4: example for the reduction of concrete cover thickness in exposure classes XC

Exposure class	Environment	Informative examples where exposure classes may occur	Indicative minimum strength class	$C_{\text{min,dur}}$	$\Delta C_{\text{dur,Zn}}$
XC1	Dry or permanently wet	Concrete inside buildings with low air humidity / Concrete permanently submerged in water	0	10	10
XC2	Wet, rarely dry	Concrete surfaces subject to long-term water contact / Many foundations	C25/30	20	10
XC3	Moderate humidity	Concrete inside buildings with moderate or high air humidity / External concrete sheltered from rain	C30/37	20	10
XC4	Cyclic wet and dry	Concrete surfaces subject to water contact, not within exposure class XC2	C35/45	25	10

If the components are exposed to exposure classes XS or XD, hot-dip galvanizing also provides additional protection. In contrast to the use of non-galvanized reinforcing steel, there are no pitting corrosion due to chlorides at galvanized reinforcing steels in concrete. The investigated specimens of chloride-containing mortar, show a significant increase in the corrosion rate only above 1 M.% chloride content, based on the cement weight. At 0.2 and 0.4 M.%, no chloride-related corrosion phenomena could be detected on the hot-dip galvanized reinforcing steel. Thus, with a sufficient zinc layer thickness and a chloride content of < 1 M. % in the concrete, an increase in service life of several years can be achieved. In contrast to non-galvanized concrete steels with active corrosion areas, no macro-element formation was found on specimens containing chloride when hot-dip galvanized reinforcing steels were used. However, a reduction of the concrete cover for exposure classes XD and XS cannot be recommended.

Acknowledgement

This work was supported by the German Federal Ministry for Economic Affairs and Energy via the Industrial Collective Research (IGF) program of the AiF (IGF project 499) [1].

- [1] **Breit, W.; Oechsner, M.; Burkert, A.; Ebell, G.; Adams, R.; Hoche, H.; Körber, D.,** *Technologie- und Sicherheitszuwachs bei der Anwendung von feuerverzinktem Betonstahl zum Ausbau einer nachhaltigen Marktposition im Stahlbetonbau*, 2017.
- [2] **Nürnberg, Ulf:** *Korrosion und Korrosionsschutz im Bauwesen*, Band 1, Grundlagen, Betonbau, Wiesbaden; Berlin: Bauverlag GmbH 1995
- [3] **Nürnberg, Ulf,** *Verhalten feuerverzinkter Bewehrungsstähle in alkalischem Beton unter Berücksichtigung des Alkali- und Chromatgehaltes der verwendeten Zemente - Zusammenfassung des bekannten Wissens -*, GAV- Bericht 155, Gemeinschaftsausschuss Verzinken e. v., Düsseldorf, 2007.

- [4] **Andrade, C. und Alonso, C.**, *Test methods for on-site corrosion rate measurement of steel reinforcement in concrete by means of the polarization resistance method*, In: Materials and Structures 37, 623-643, 2004/11/01, (2004)
- [5] **Metikoš-Huković, M. und Zevnik, C.**, *Determination of Polarization resistance and corrosion rate by using pulse method, polarization curves and AAS*, In: Materials and Corrosion 33, 661-668, (1982)
- [6] **Burkert, A., Ebell, G. und Lehmann, J.**, "Einfluss chromatreduzierter Zemente auf die Ausbildung der Verbundzone Stahl/Beton bei Verwendung feuerverzinkter Bauteile," 52. DAFStb-Forschungskolloquium. p.^pp. 272-282.
- [7] **Beck, M.**, "Zur Entwicklung der Eigenkorrosion von Stahl in Beton," RWTH-Aachen, Aachen, 2010
- [8] **DIN DIN EN 1992-1-1** 2011. *Eurocode 2: Bemessung und Konstruktion von Stahlbeton- und*

Spannbetontragwerken –

Teil 1-1: Allgemeine Bemessungsregeln und Regeln für den Hochbau;

Deutsche Fassung EN 1992-1-1:2004 + AC:2010, (2011).

Session 11:

Sustainability and Environment

Integration of a kettle cover in the zinc bath enclosure

F Nerat, KVK KOERNER Chemieanlagenbau G.m.b.H (Austria)

Abstract

Energy saving is an important point in hot dip galvanizing plants. During the production period waste heat from combustion air is recovered to be used for tank heating and/or heating of a dryer. If furnace is in idle mode, more than 95% of energy loss is via zinc surface of kettle. Therefore kettles are covered if there is no production in order to reduce energy consumption.

It depends very much on management and operators, how the covering of kettles is being managed.

Cover manipulation can be more or less complicated depending on the location of the cover storage. Nevertheless it needs time to bring the cover to the kettle and it is a safety issue.

This paper presents a special execution of zinc bath enclosure, where the kettle cover is integrated in the enclosure and works as a window and in the same time can be used as kettle cover.

Very quick manipulation is possible and enables operators to close the kettle also during short non galvanizing periods. Huge energy saving and cost reduction can be achieved.

This patented integrated kettle cover system can be realized in new kettle enclosures and can also be retrofitted to existing zinc bath enclosures.

Energy consumption in hot dip galvanizing plants

Modern Hot dip galvanizing plants consume a lot of energy. Environmental protection requires filter systems for zinc dust, scrubbers for aggressive fumes, tanks heating but also, crane systems, hall heating, ventilation requires a lot of energy.

But far the highest consumption of energy comes from the furnace.

This is the part of the plant, that is focussed now in this presentation.

In the following investigations we are considering a furnace with 13 m length, 1,8 m wide and 3,2 m deep and a production value of approx 10t/h.

These figures are commonly used and they are the basis of following considerations.

We are considering modern designs of furnaces, which means furnaces with furnace enclosure. We do not consider systems with lateral fume extraction channels, which will cause much higher energy consumption.

Energy is needed to keep the zinc at the target level of approx 450°C, to cover energy loss due to furnace casing (depending on the quality of furnace insulation) and due to energy consumption by galvanizing steel (heating the steel up from approx 80°C (if dryer is operated) up to 450°C, (zinc consumption approx 5-6%). and loss of energy via zinc surface.

There are different operating conditions, that we are considering. The different operating conditions are full operation, idle with kettle not covered and idle kettle covered.

At full production the required energy is approx 1400 kW whereas only 4% is needed for furnace casing, approx 55% is required for material heating and zinc consumption, and the rest of approx. 41% is energy loss via the surface of zinc surface.

At periods, where no material is galvanized, but kettle is not covered, the energy consumption is approx 620 kW whereas 9% is for heat loss of furnace and 91% is energy loss via zinc surface of kettle.

If the kettle is covered the energy consumption is approx. 65 kW. Only 14% of this consumption comes from zinc surface, because of zinc kettle cover, and the rest of 86% is energy loss for the furnace.

It is obvious, that covering the kettle saves a lot of energy – approx 550kW in our example)

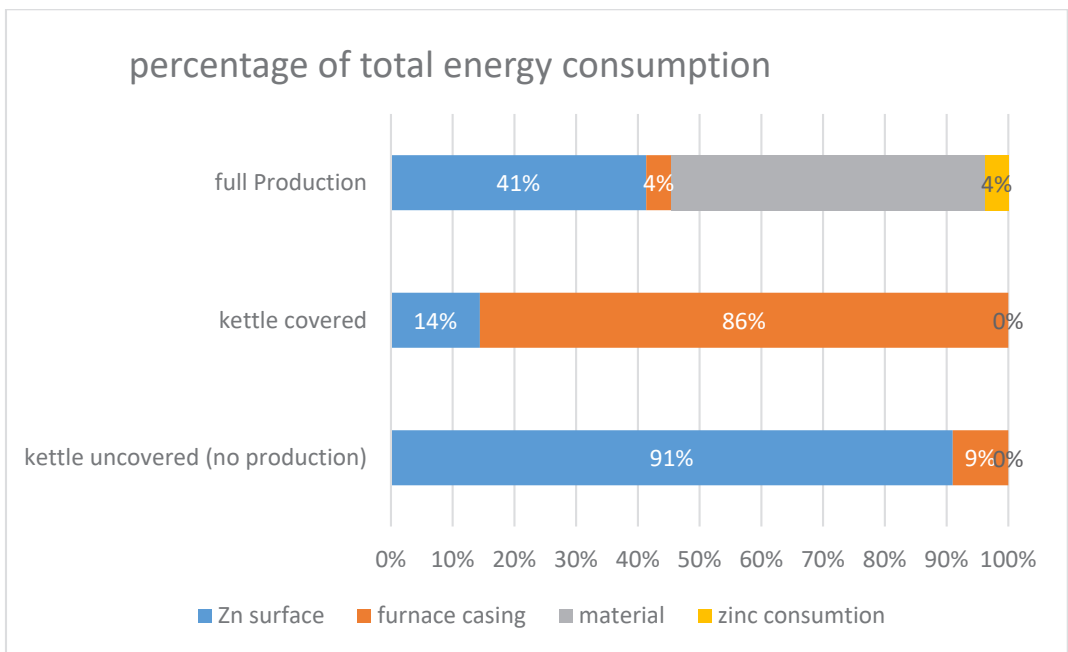


Figure 1: Percentage of energy consumption on furnace

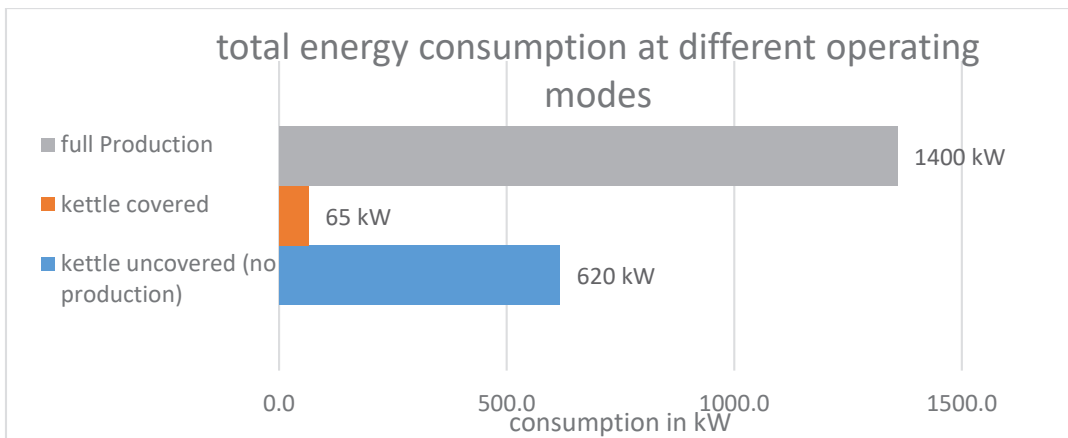


Figure 2: Total energy consumption at different operating modes

So it makes sense to cover the kettle as much as possible, if there is no galvanizing. Almost all galvanizers have kettle covers and they also use them at non operation periods.

Kettle covers are stored more or less near the kettle and are manipulated by means of crane systems or fork lifts. Some covers, especially for bigger kettles are consisting of several pieces.

Moving the covers at end of the shifts and before starting the production requires certain time and energy consumption is high at that time. (see figure 3)

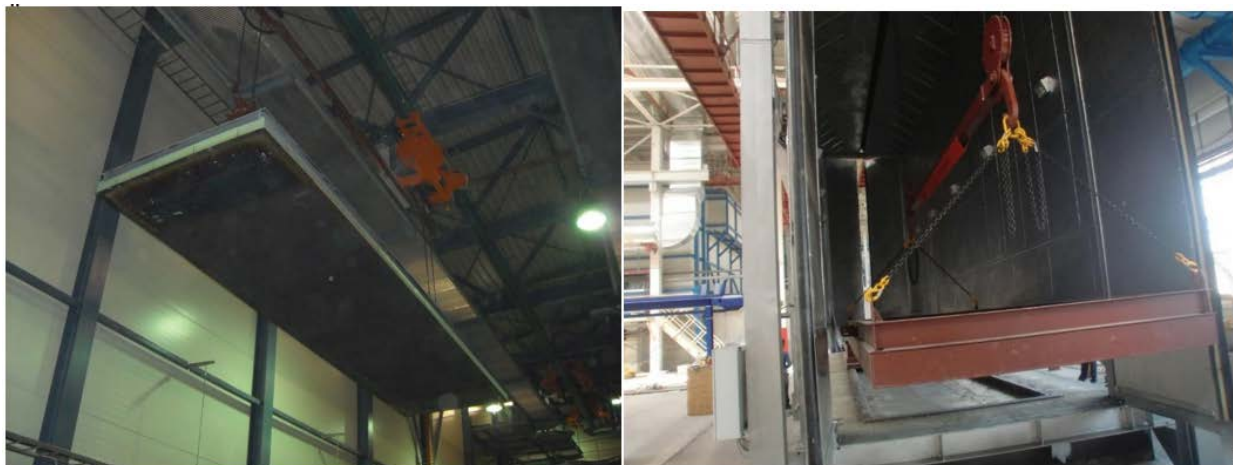


Figure 3: Manipulating a normal zinc bath cover by cranes

Integrated kettle cover, technical execution

It was the goal to create a solution, where the kettles can be covered very quickly and also during short production breaks during the day.

There have been different basic requirements in the design:

- Simple and robust design
- Easy to be operated
- Safety
- For new plants and for retrofitting
- Reasonable price

The final result was a cover, which is integrated in the zinc furnace enclosure and works in the same way as lateral door of the enclosure and as kettle cover.

There are different layout options for material flow in HDG plants. In the following explanation we are considering a kettle which is placed in a way, that material is moved longitudinal direction. This is the fact in almost all modern plants (L-shape, loop systems or other special solutions)

At the zinc bath enclosure there are windows on both lateral sides in order to enable operators to clean the zinc surface after immersing the material into the zinc.

In our solution, we modified one of the two windows in a way, that it is wide enough to cover the kettle after it is hinged from vertical position to horizontal. This cover does not have windows, since the operators can stand on the other side during the dipping process and can watch the dipping process.

The cover needs to be insulated and is designed in a way, that operators can walk on it, once it is layed down on the kettle. This enables easy cleaning of the inner side of the enclosure.

For principle system see figure 4.

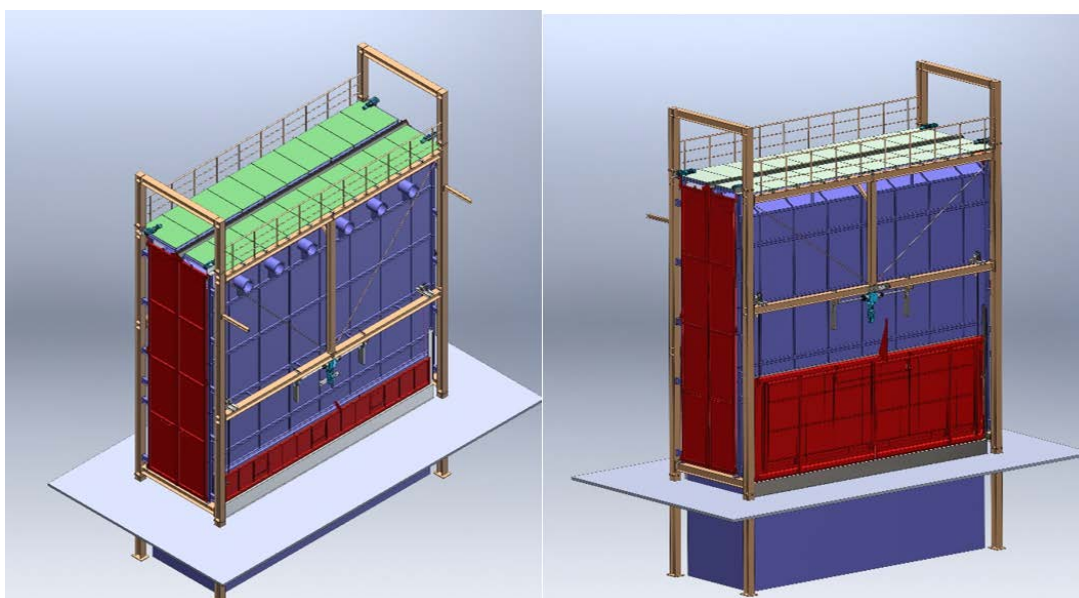


Figure 4: Zinc bath enclosure left view normal window, right view integrated cover(window)

The lifting device for the cover is very similar to the lifting device of the window. No additional units are necessary. We are also using the same lifting equipment (ropes, chains or belts)

During normal working time the window and the cover are operated exactly in the same way. They are closed during immersion and are lifted approx one metre up for the cleaning process.

If the cover needs to be layed down on the kettle, the chains are moved more than the closing position of the window and by means of a special kinematic the door hinges by 90° and closes the kettle.

This requires less than one minute and can be done easily by the operator at any time, he wants.

If the break is over, the chains are lifting the cover again until it has reached the upright position. This is the position of the closed window. Pulling further the cover lifts up and works as a normal window.

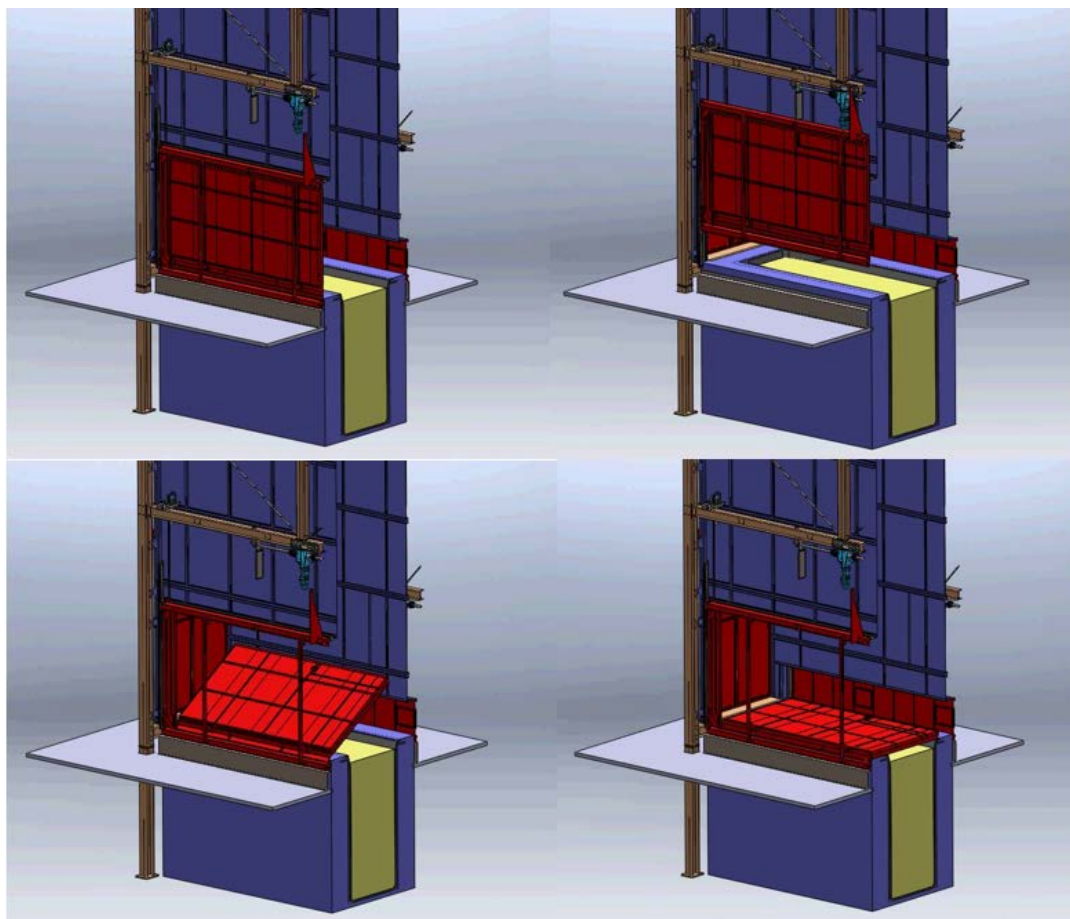


Figure 5: Shows different positions of the integrated cover/window



Figure 6: Shows a test run for an integrated cover to be retrofitted in an existing installation

Integrated kettle cover, economical aspects

As mentioned above, the energy saving by covering the kettle during non galvanizing periods is huge. With this integrated cover it is possible to cover the kettle not only after the shifts, but also, if there are short breaks during the day. If the material cannot be feeded to the plant as necessary material needs longer in pretreatment and dryer, it is easy and quick to cover the kettle by pushing a button. So also for short breaks energy can be saved. If there is a break of only 12 min, nobody would cover the furnace. With this device kettle can be covered for approx.10 minutes

Lets consider above mentioned furnace with 13 m length, 1,8 m width and 3,2 m depth.

Energy saving with covered kettle is approx 550 kW.

At production start and production end, there can be approx 0,5 hours less open kettle time , because there is no more manipulation of the cover. During short breaks kettle can be covered. Considering 0,5 hours per shift means 1,5 h. So every day there is an additional saving due to covered kettle of 2 hours or more.

For 320 working days per year and 2 hours for each working day means 640 hours per year, where kettle can be covered longer than in traditional plants.

The annual additional energy saving is approx 352.000 kWh. Considering a price per kWh of approx 0,04 Euros there is an annual saving of approx EUR 14.000,--

There are some more other aspects that needs to be considered if an integrated kettle cover is used. It is difficult to find a cost value for these positions, but there is some saving also there.

There is no more space required for storing the standard cover, no additional cranes or fork lifts are necessary, no personnel needed for the manipulation of the cover.

It is also the safety aspect that will give a huge advantage, since no crane or fork lift handling is necessary.

And finally there is a cost saving, because no standard kettle cover is necessary.

Economic investigation shows, that for new installations the additional investment pays back within approx 1,5 years.

For retrofitting an existing plant the ROI is at approx 4 years, since there is a bigger investment in adapting the steel structures (see table 1).

Table 1

	new installation	Retrofitting
additional investment	40.000,00 €	
new integrated kettle cover module		75.000,00 €
saving for no standard kettle cover needed	-20.000,00 €	-20.000,00 €
steel work for adapting the existing enclosure		depending on existing design
other savings (man power, crane usage, storage area etc.)	not considered	not considered
total invest	20.000,00 €	55.000,00 €
annual saving approx	14.000,00 €	14.000,00 €
ROI approx	1,5 years	4 years

Conclusion

Since the biggest loss of energy is via the zinc surface, covering a zinc kettle, if no galvanizing is done, is the easiest way to save energy cost.

Normally there is a separate zinc furnace cover in use, that has to be stored somewhere and needs to be moved from storage place to the furnace.

This manipulation requires manpower, crane or forklift usage and is always a safety issue.

There is a new kind of zinc furnace cover, which is integrated in the zinc bath enclosure. This special design makes sure, that the cover has 2 different functions. It is working as a normal lateral window of the zinc bath enclosure, which is opened for cleaning the zinc furnace after material is immersed into the zinc. Before the next dip the window is closed again, like at a normal enclosure.

If there is a production break (pause, no material available, delays in the pretreatment or dryer etc) the window can be lowered further by means of the normal lifting device and is hinged onto the furnace. So it is possible to cover the furnace quickly and a lot of energy can be saved.

It makes it possible to cover the furnace also during short bakes, where a normal cover never would be used.

Advantages of the integrated cover:

- Huge energy saving compared to standard covers
- Saving of man power cost
- Less space required because no cover storage is necessary
- No separate crane or forklift necessary
- Very save operation without cranes
- For new installations
- For retrofitting existing enclosures
- Short ROI period

Author`s Biography

NAME Fritz NERAT

ORGANISATION

KVK KOERNER
Austria

Fritz NERAT studied mechanical engineering at technological University in GRAZ

He started his career at ANDRITZ AG as project manager for paper machines.

In October 1994 he entered KVK KOERNER as a sales engineer.

During the following years KVK KOERNER developed the encapsulated pretreatment according the KVK system. Today the encapsulated pretreatment plant is state of the art for modern hot dip galvanizing plants.

Since 2007 Fritz Nerat is managing director at KVK KOERNER and responsible for all technical, technological and sales aspects.

He covers several patents in the field of the encapsulated pretreatment system and of the integrated zinc furnace cover

Reducing emissions and immissions in pre-treatment plants caused by hydrochloric acid

From J.Kader, Stockmeier Chemie

Why is reduction of acid fumes important?

Acid fumes attack plants by metal corrosion, are dangerous for the environment and harm workers health.

Pickling as it can be (HCl about 100 g/l) with iron (Fe⁺⁺):



Background to hydrochloric acid

What is the reason that the use of hydrochloric acid will lead to problems?
 Hydrochloric acid is a solution based on the gas HCl !

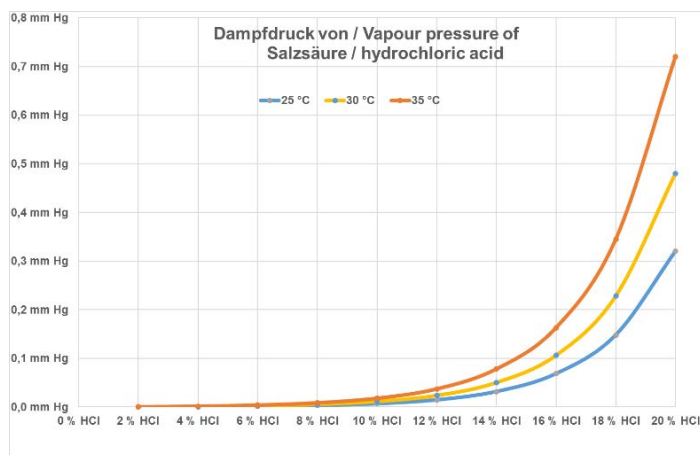
Wikipedia* is telling the true story:

The compound hydrogen chloride has the chemical formula HCl and as such is a hydrogen halide. At room temperature, it is a colorless gas, which forms white fumes of hydrochloric acid upon contact with atmospheric water vapor. Hydrogen chloride gas and hydrochloric acid are important in technology and industry. Hydrochloric acid, the aqueous solution of hydrogen chloride, is also commonly given the formula HCl.

A lot of problems are caused by the gaseous behaviour.

* source: https://en.wikipedia.org/wiki/Hydrogen_chloride [2018/05]

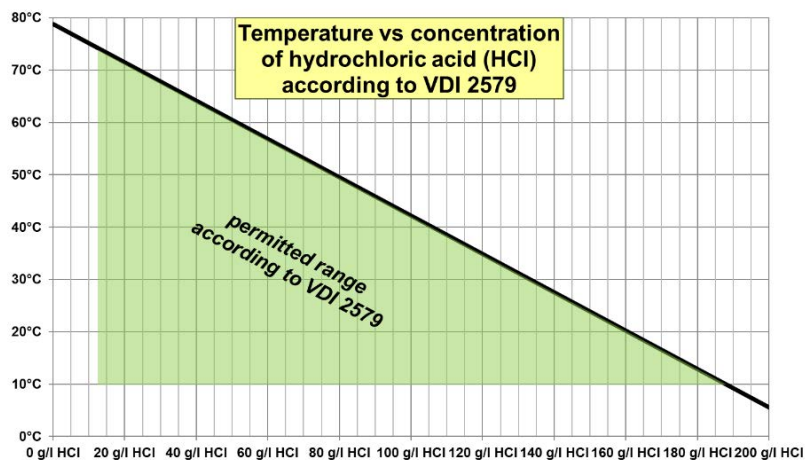
Temperature and concentration influences outgassing:



High concentration & high temperature
 → more vapours (= emission)

Low emission means:
 max. 160 g/l HCl at 20°C
 max. 135 g/l HCl at 30°C

This behaviour was leading to the recommendation in VDI 2579 "Guideline to control emissions from HDG plants"



Use of hydrochloric acid (HCl)

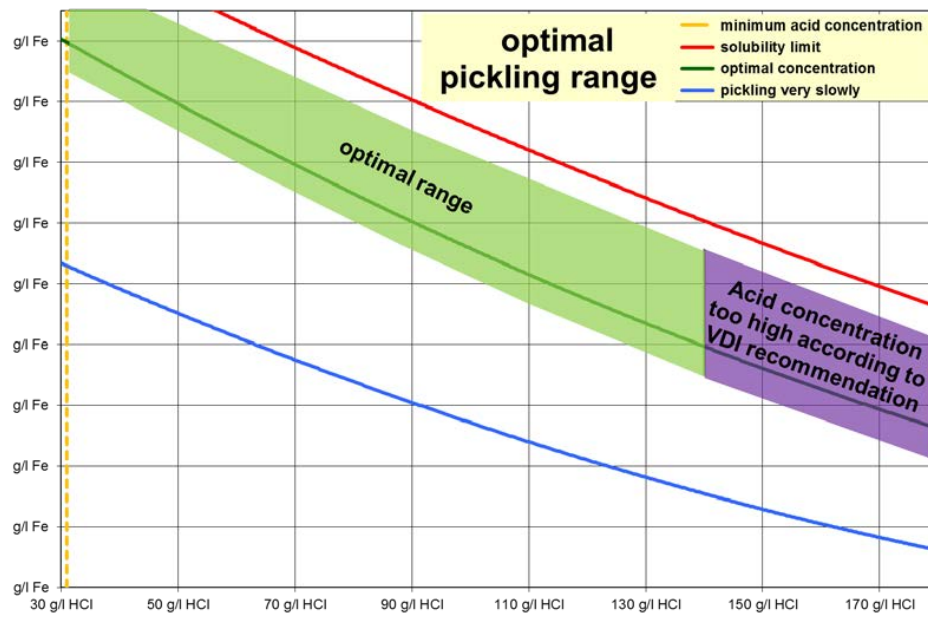
Faster pickling is possible at higher temperature and high concentration of hydrochloric acid.

To minimize emission you have to follow two simple rules:

- 1) Follow the optimal concentration range but avoid too high concentration of acid.

The gaseous behavior of HCl will cause you to respect the maximum concentration. Outgassing can be reduced a bit, but it can be avoided only by covering.

Pickling optimum for hydrochloric acid

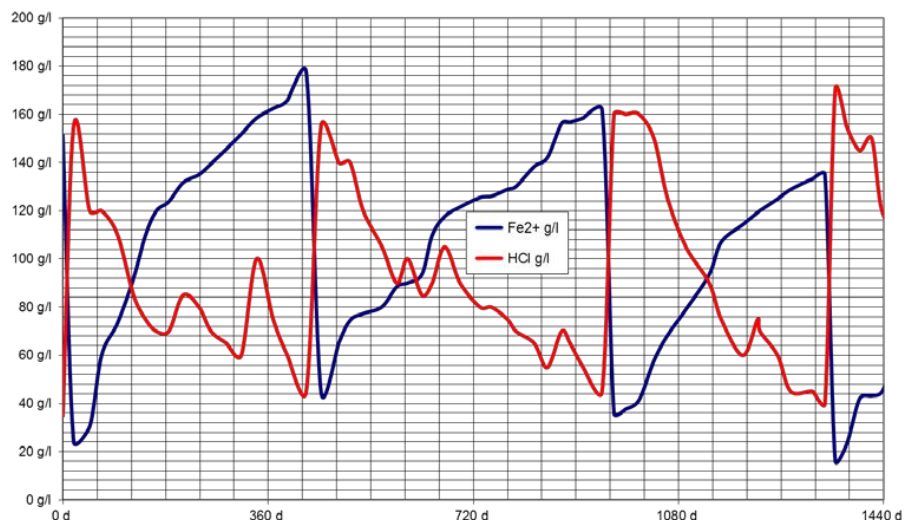


Pickling based on hydrochloric acid has to be changed at approx. 150 -180 g/l iron. If you are working at 20°C or less you should make up the acid with max. 160 g/l HCl.

Recommendation to reach the optimum relation between acid and iron:

Use old acid (partially change). Start with approx. 50 g/l iron.

Example see graph. →.



To minimize emission you have to follow two simple rules:

2) Use proper additives to minimize emission of HCl aerosols.

Aerosol formation can be controlled by influencing size and amount of H₂ bubbles, which will carry out hydrochloric acid (drops and gas).

As well, the pickling performance can be adjusted.

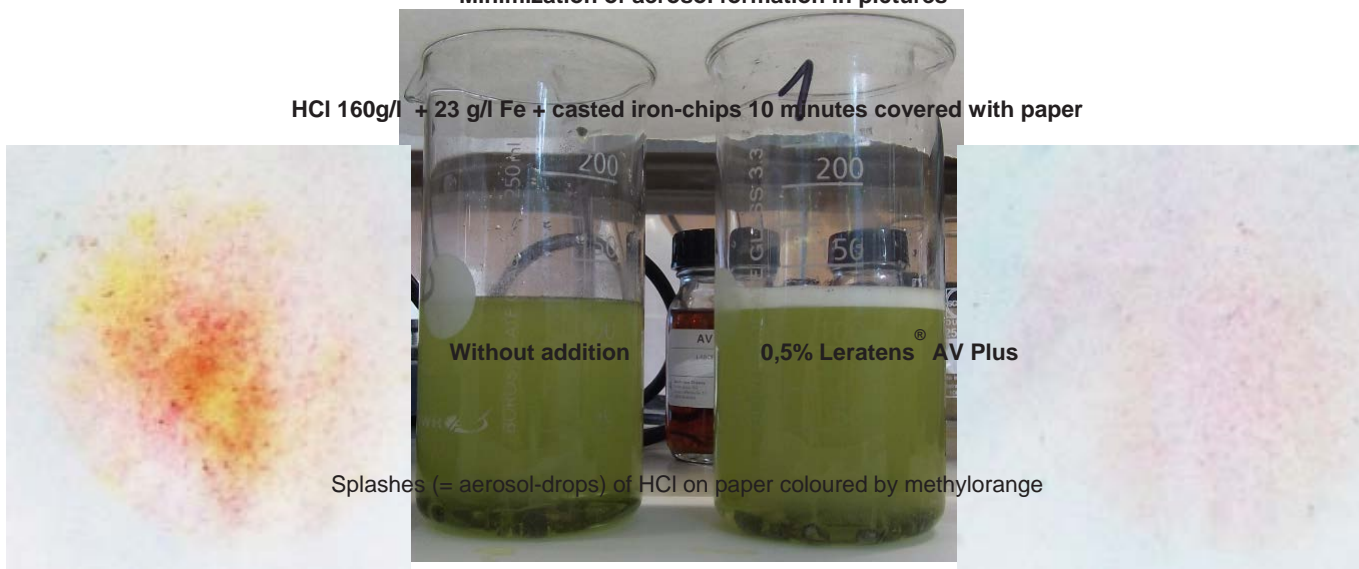
A proper additive can reduce vapour & mist from HCl by:

- ✓ Minimizing aerosol formation
- ✓ Inhibition of iron dissolving from bright steel
- ✓ Reduction of gas formation out of hydrochloric acid

All these points are leading to reduction of aerosols and outgassing of acid

There are as well advantages for plant life, environment & workers health

✓ **Minimization of aerosol formation in pictures**



Gas- formation in HCl 140g/l + 80 g/l Fe pickling steel-sheets

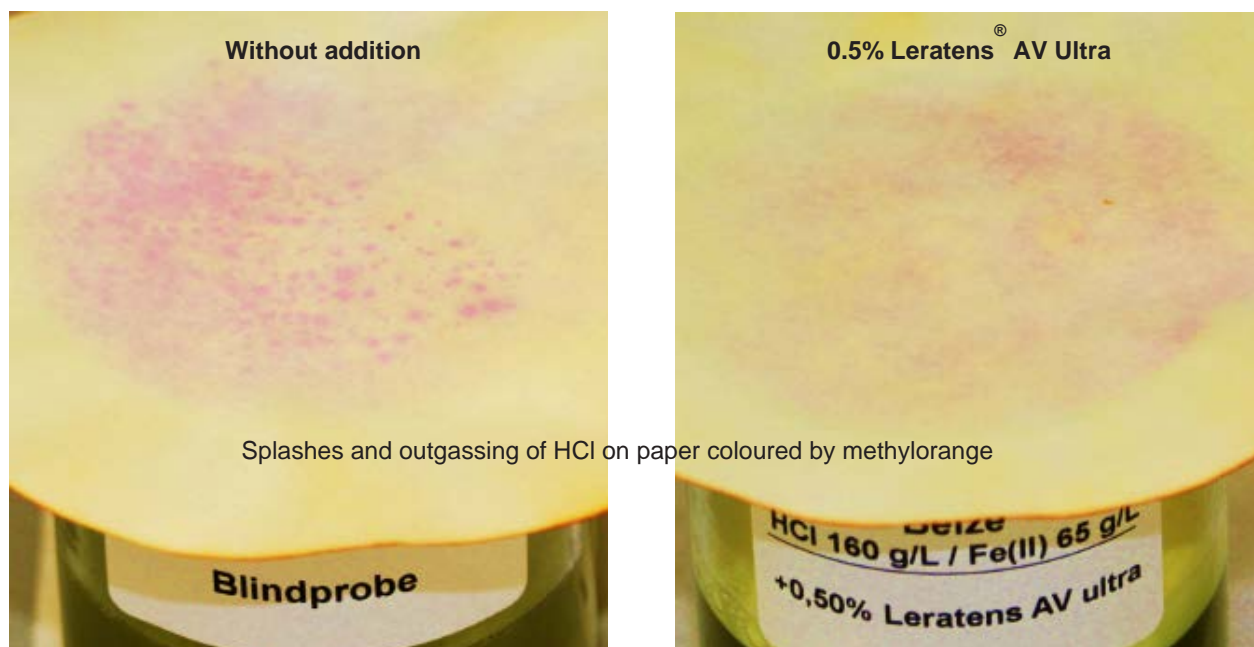


✓ Inhibition of iron dissolved during pickling in pictures



✓ outgassing of pickling acid in pictures

Test in HCl 160 g/l + iron 65 g/l pickling casted iron chips



outgassing of pickling acid is reduced by addition of additive

Proper additives will additionally:

- ✓ accelerate pickling effect by penetrating mill scale
- ✓ optimize pickling effectivity by degreasing effects
- ✓ reduce carry out pickling solution by reduced surface tension

Some additives are as well able to

- ✓ prevent against flotations in pickling acid

✓ **Flotation on pickling baths in pictures**



All these points are leading to:

Reduction of aerosols & outgassing and savings in acid

There are as well advantages for

Quality, plant life, environment & workers health

Pickling in HCl are there any useful alternatives?

The PICKLING is used to remove oxides (mill scale, corrosion).

Organic contaminations like oil have to be removed by degreasing.

Here is the point to ask which acid should be taken.

Very common is the use of HCl.

But this acid causes the most problems, because HCl is a gas.

Using sulphuric acid instead of hydrochloric acid will lead to other problems:

- ➔ pickling performance at low temperature is worse than HCl
up to about 60°C is necessary to hold pickling times short
- ➔ sulphuric acid leaves often black layer
- ➔ maximum iron concentration is approx. 120 g/l (HCl 180 g/l)

Other acids are too expensive, too dangerous or too weak.

Therefore most galvanizers are using hydrochloric acid.

Avoiding pickling – is there any possibility?

In the pre-treatment nearly all installations are using at least one pickling solution to remove oxides.

To avoid pickling there is only ONE alternative:

BLASTING

But:

- ➔ blasting will need a lot of energy
- ➔ the surface has to be free of oil
 - if not, blasting can carry the oil into the surface
- ➔ it is not easy to use, especially at bigger parts
 - hollow sections and pipes/tubes can hardly be treated inside
- ➔ it will roughen the surface
 - zinc-pickup will be higher than usual

Therefore blasting today is sometimes used for small parts like screws but not common in use.

Conclusion:

Hydrochloric acid seems to be the best suitable acid for the pickling process.
On the other hand, hydrochloric acid will produce emissions.

Reduction of emissions is necessary to save your plant, workers health, and the environment.

Knowledge about the chemical and physical behaviour is useful.
It is possible to minimize emission and optimize pickling performance.

**Poor pickling means
poor conditions for the galvanizing process**

Effective recovery of HCl and metals from pickling solutions by cutting-edge membrane technologies

R. Gueccia, S. Randazzo*, A. Culcasi, A. Cipollina, G. Micale

Dipartimento di Ingegneria Chimica, Gestionale, Informatica, Meccanica, Università di Palermo – Viale delle Scienze ed.6, 90128 Palermo, Italy

*Corresponding Author. E-mail: serena.randazzo@unipa.it

INTRODUCTION

The pickling process is an essential step in the hot-dip galvanizing process. It is performed by immersing manufactured steel pieces in acid baths in order to dissolve the oxidized layers. During the pickling process, acid attacks metal oxides on the surface, dissolving them in the pickling bath. Thus, the efficiency of the pickling liquor decreases due to the accumulation of metal salts and the consumption of free acid in the solution. When hydrochloric acid is used, ferrous chloride is produced during the pickling treatment, reaching concentrations up to 250 g/l, while the acid concentration decreases by 75-85%. A pickling bath in this condition is considered spent [1] due to the very low pickling rate, hence it needs to be replaced. In common industrial practice, part of the exhausted solution is withdrawn and replaced with fresh acid or with a more concentrate solution to prolong the pickling bath life, while spent solution is disposed as a waste.

Disposal of the spent pickling solution strongly affects the hot-dip galvanizing industries footprint and costs, thus the recovery of acid is one of the most beneficial steps to reduce the environmental and economic impact. In particular, continuous regeneration of pickling solutions can enhance pickling rate and process performance, but also reduce industrial wastewater disposal and chemicals consumption. The recovery and recycling of valuable compounds (e.g. acid, metals and water) can be accomplished by coupling two cutting-edge membrane technologies: diffusion dialysis (DD) and membrane distillation (MD) [2,3]. Membrane techniques are considered simple, effective and sustainable [1] and can be easily scaled from small to medium size installations.

In the present work, a case study is presented, relevant to the hot-dip galvanizing plant of TecnoZinco (Palermo, Italy). The site has a capacity of 20,000 tons per year of treated steel. Starting from an accurate data mining, a Process Flow Diagram (PFD) of an integrated process that provides a continuous regeneration of pickling solution is proposed, within the framework of the EU-funded ReWaCEM project (www.rewacem.eu), with the final aim of building

a pilot plant to be installed and operated in real environment.

A steady state process simulator for the integrated process has been developed, aiming to design, analyze and predict performance of the pilot unit. A parametric analysis of the model is performed varying hydrochloric acid in the stream going out from the pickling tank. Results presents the perspective operation of such plant, indicating the technical feasibility of the novel developed process.

HOT-DIP GALVANIZING PROCESS AT TECNOZINCO PLANT– MAIN ASPECTS

Hot-dip galvanizing process includes several steps. Following the pathway shown in Fig. 1, the manufactured steel is first degreased in a bath under action of surfactants, then is transferred in a pickling tank, washed in a rinsing tank and put in a fluxing bath before drying and galvanizing. The fluxing solution contains zinc chloride to protect the manufactured steel before the immersion in the molten zinc bath and ammonium chloride to catalyse zinc covering.

Pickling process is performed by immersing manufactured steel in hydrochloric acid (HCl) bath. The acid dissolves the oxidized layers of the manufactured steel leading to the formation of iron(II) chloride in the pickling solution. The kinetic of these reactions is strongly affected by the presence of the acid molecules and also by the iron ions concentration. A specific relationship between the acid and the iron concentration for optimal pickling operation is reported in the literature as the *Kleingarn Curve* (Fig. 2). As a consequence, controlling acid and iron concentrations within the tank increases pickling rate compared to replacing the entire spent acid bath with fresh acid. Note that, the composition of some samples from Tecnozinc pickling baths is reported as an example in the graph (Fig. 2).

Tecnozinc facility uses 7 pickling bathes containing in total more than 350 m³ of acid pickling solution. The acid consumption is approximately 160-240 ton per year. Bathes can be grouped in three classes according to the "pickling power", i.e. highly effective pickling (HCl 120-160 g/L, Fe 50-80 g/L - area A in Fig. 2), intermediate effective pickling (HCl 80-120 g/L, Fe 80-150 g/L - area B in Fig. 2) and poorly effective pickling (HCl 20-80 g/L, Fe 150-180 g/L - area C in Fig. 2). Based on periodical analysis

of free acidity and iron content, HCl and Fe concentrations are varied to reach the optimal pickling rate by spilling part of the solution and subsequent replenishing.

Besides iron ions, also zinc is present in the pickling tanks of hot-dip galvanizing plants where goods and winches used for pieces handling are often covered of zinc. Therefore, the pickling process generates a waste acid stream of approximately 300 ton per year, characterized by high concentrations of heavy metals, namely iron (150-180 g/L) and zinc (10-30 g/L). Disposal costs incurred by Tecnozinco include transportation to a far waste treatment plant in northern Italy.

INTEGRATED PROCESS DESCRIPTION

The proposed integrated process aims at synergically merging DD and MD processes to keep HCl and iron concentrations in the pickling tank at the optimum concentrations. The Process Flow Diagram is shown in Figure 3. Starting from the pickling tank, the outgoing stream, named *Waste Acid solution (WAS)*, after a pre-treatment, is sent to the Diffusion Dialysis unit (in the retentate side) in which the recovery of the acid occurs. Here, the acid stream is separated from the metal ions due to the anionic exchange membrane. In fact, due to the positive charge of the membrane, the transport of chlorides is permitted. However, also H^+ ions can diffuse through the anionic membrane, despite own positive charge, for their little dimension and do to the tunneling mechanism [3,4]. Conversely, other positive charged ions, iron and zinc cations for instance, are rejected because of the electrostatic repulsion. Therefore, the acid is recovered in the diffusate side of the DD unit and separation from salts occurs. Nevertheless, as reported in literature and as observed in our research investigation campaign, iron and zinc can pass through the membrane, reaching leakage percentage of 5-10% for iron and up to 50-60% for zinc [4].

The stream enriched in acid, named *Recovered Acid Solution (RAS)* is sent to the MD unit, where the acid is concentrated. Membrane Distillation achieves the concentration of acid due to water evaporation. In fact, it is a process in which a microporous hydrophobic membrane separates two aqueous solutions at different temperature and composition. The driving force for MD is the partial pressure difference induced by the temperature and composition of the layers adjacent to the membrane [2]. This specific membrane rejects water and permits steam passage, thus water can be recovered once the steam condenses directly in the solution (*Permeate* stream) in the cold compartment. In MD, also some HCl is transported through the membrane [2]. The *Permeate* stream from MD is

sent to the DD unit (in the diffusate side), after the addition of a *Process Water (PW)* stream, necessary to reach the desired flow rates inside DD unit. This stream is named *Draw Solution (DS)*. The stream outing from MD concentrated in acid, the *Recovered Pickling Solution (RPS)*, is sent to the pickling tank.

The other stream coming out from the DD unit in the retentate side, called *Metals Rich Brine (MRB)*, is an acid stream enriched in iron and zinc chlorides. In order to compensate the acid lost here and the acid reacted in the pickling process, a *Make-Up (MU)* of fresh acid is added in the pickling bath.

Even the metals are recovered in the proposed integrated process. In fact, the *Metals Rich Brine (MRB)* stream is sent to a Reactive Precipitation unit in which the acid is neutralized and, at the same time, the iron is recovered as hydroxide by precipitation with ammonia. The addition of hydrogen peroxide in the reactive precipitation process is needed to oxidize Fe^{2+} to Fe^{3+} .

The stream generated from this step, after separation of solids by filtration, is sent to a Brine Membrane Distillation unit. Here, distillate water and a more concentrated ammonium and zinc chloride solution are produced which can be used, the first as process water, the latter in the fluxing bath of the pickling plant.

As previously mentioned, the pilot-scale unit will be installed at Tecnozinco, where also a recovery of waste heat (necessary for the MD operation) is foreseen for enhancing the process sustainability.

MODELING OF THE INTEGRATED PROCESS

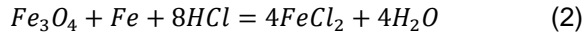
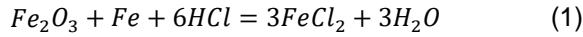
A mathematical model able to design and predict the integrated system operations was developed and implemented in an Excel spread sheet with Macros in Visual Basic language.

Data Mining

The first step of the modelling activity was to fix parameters and operative conditions of the pickling process. Looking at Figure 3, the streams took into account to start the modelling activity were the inlets of manufactured steel, acid make-up, entrainment from the previous step of degreasing and the outlets of entrainment, water evaporation and HCl gas emission. The main important information was the consumption of the acid per ton of steel manufacturing. In order to estimate this value, two possible options were possible: using kinetics data from literature or collecting information from historical statistics of the company. In this work, the latter was selected as starting point. Moreover, fixing a time frame of 1 year, real data from Tecnozinco have been collected regarding the bath pickling volume, the quantity of manufacturing steel, acid make-up, the starting bath composition and the quantity of exhausted solution disposed. Other data, such as

inlet and outlet entrainment volumetric flow rates were derived from work experience. All these information allowed the closure of the pickling overall mass balance, estimating the water evaporation rate.

The calculations were figured out by considering Eq. (1-2) as the main chemical pickling reactions when corrosion inhibitors are used [5]:



It was assumed that the reaction (1) accounts for the 20% and the reaction (2) for the 80% of the acid consumption according to the scale composition [6]. Thereafter, conversion rates of species involved in the pickling process were calculated by adopting the following expression:

$$w_i = k_i * w_s \quad (3)$$

where w_i and w_s are mass flow rates [ton/h] of the i -component and of the manufactured steel, respectively, and k_i is the kinetic constant of the i -component. k_i values were evaluated under the assumption of a complete stoichiometric conversion of the reagents.

Model assumptions

In order to develop the mathematical model the following hypotheses were assumed:

1. The process is modelled in steady state conditions;
2. The amount of steel manufactured is fixed;
3. The pickling bath and the reactive precipitator are considered as a CSTR reactors;
4. The ratio between the DD inlet volumetric flow rates is fixed to 1;
5. The minimum ΔC driving force between HCl concentrations of the retentate and diffusate streams in the DD unit is fixed at 3 g/L;
6. The pH of the outlet stream of the reactive precipitator is fixed at 4;
7. The Metals Sludge exiting the precipitation reactor contains 35% of the total solution outgoing from the reactive precipitator.

Pickling tank

The streams related to the pickling tank are: *Waste Acid Solution*, *Acid Make-Up*, *Process Water* (Fig. 3).

The pickling batch is modelled as a continuous perfectly-mixed reactor. As a result, the volumetric flow rate coming from the pickling bath is calculated by the Equation 4.

$$F_{WAS} = \frac{k_{Fe} \cdot w_s + w_{Fe}^{DD} + w_{Fe}^{entr,in}}{C_{Fe}} \quad (4)$$

where F_{WAS} is the *Waste Acid Solution* volumetric flow rate [lt/h], k_{Fe} is the iron production constant, w_s is the manufactured steel mass flow rate [ton/h], w_{Fe}^{DD} is the iron mass flow rate [kg/h] recovered by the Diffusion dialysis process and $w_{Fe}^{entr,in}$ is the iron flow rate inlet in the pickling bath with the entrainment stream from the rinsing tank [kg/h]. C_{Fe} represents the optimal iron concentration on the basis of the linear regression of the so-called Kleingarn Curve (see Fig. 2), reported in Eq. 5:

$$C_{Fe} = -0,8333 \cdot C_{HCl} + 200 \quad (5)$$

To evaluate the process streams mass density, the model developed by M. Laliberté et al. was adopted [7]. As a consequence of the assumptions 1 and 3, the *Waste Acid Solution* composition is constant during the process and it is equal to the composition inside the pickling tank.

The mass flow rate of the acid *Make-Up* stream is calculated by the following equation

$$w_{HCl}^{MU} = w_{HCl}^{MRB} + k_{HCl} \cdot w_s + w_{HCl}^{entr,out} \quad (6)$$

where w_{HCl}^{MU} , w_{HCl}^{MRB} and $w_{HCl}^{entr,out}$ are the hydrochloric acid mass flow rate [kg/h] of the *Make-Up*, *Metals Rich Brine* and *Entrainment,out* streams, respectively. $k_{HCl} \cdot w_s$ term concerns the HCl flow rate reacted in the pickling process [kg/h]. The *Make-Up* stream is necessary within the pickling bath to compensate the hydrochloric acid outlet from the diffusion dialysis unit in the *Metals Rich Brine* stream. The *Entrainment,out* stream is dragged by the transfer of the manufacturing steel from the pickling tank to the rinsing tank.

The *Process Water* stream is evaluated by performing a global mass balance using the entire integrated system as computing volume (Eq. 7).

$$w_{tot}^{pw} = w_{tot}^{MRB} + w_{entr,out} + w_{evap} - w_{tot}^{MU} - k_{oxides} \cdot w_s - w_{entr,in} \quad (7)$$

where

w_{tot}^{pw} , w_{tot}^{MRB} , $w_{entr,out}$, w_{evap} , w_{tot}^{MU} and $w_{entr,in}$ are the water mass flow rate [kg/h] in the *Process Water* incoming into the system, in the *Metals Rich Brine*, in the *Entrainment,out*, in the evaporation, in the *Make-Up*, and in the *Entrainment,in* streams, respectively. $k_{oxides} \cdot w_s$ term concerns the oxides mass flow rate inlet within the manufactured steel in the pickling tank [kg/h].

Diffusion Dialysis unit

Concerning the Diffusion Dialysis unit, the other streams that have to be characterized for the

integrated process design are: *Recovered Acid Solution, Draw Solution, Metal Rich Brine* (Fig. 3). Main balances used in this section derived from the results obtained from an experimental campaign carried out by some of co-authors [10]. Experiments were performed with a DD laboratory test-rig, where a Fumatech FAD-type Anionic Exchange Membrane (AEM) was adopted, in order to collect information for calibrating/validating the model before using it for design purposes.

The hydrochloric acid recovery was obtained by using Eq. 8.

$$w_{HCl}^{DD} = A \cdot PM_{HCl} [P_{j,HCl} \cdot (C_{HCl,mol}^R - C_{HCl,mol}^D) + U_s \cdot (C_{Fe,mol}^R - C_{Fe,mol}^D)] \quad (8)$$

where w_{HCl}^{DD} is the mass flow rate of hydrochloric acid [kg/h] passing from the retentate to the diffusate side of the DD unit, A is the membrane area [m²], $P_{j,HCl}$ is the membrane permeability to the hydrochloric acid [m/h], U_s is the further permeability to the passage of acid due to the presence of the corresponding anion salt [m/h], $C_{HCl,mol}^R$, $C_{HCl,mol}^D$ and $C_{Fe,mol}^R$, $C_{Fe,mol}^D$ are the average concentrations of hydrochloric acid and iron in the retentate and in diffusate side [mol/l], respectively. The expression for $P_{j,HCl}$ and U_s was derived experimentally [8] and it is reported in Eq. 9 and 10.

$$P_{j,HCl} = 1.16 \cdot 10^{-3} C_{HCl,mol}^R{}^3 - 6.95 \cdot 10^{-3} C_{HCl,mol}^R{}^2 + 1.48 \cdot 10^{-2} C_{HCl,mol}^R + 2.38 \cdot 10^{-3} \quad (9)$$

$$U_s = 1.09 \cdot 10^{-2} C_{HCl,mol}^R + 2.18 \cdot 10^{-3} \quad (10)$$

Despite the anionic exchange membrane rejects in theory all iron ions, a small passage of iron chloride is observed [4,8]. Therefore, salt diffusion through the AEM membrane was considered by using Eq. 11.

$$w_{Fe}^{DD} = A \cdot P_{j,Fe} \cdot PM_{Fe} (C_{Fe,mol}^R - C_{Fe,mol}^D) \quad (11)$$

where w_{Fe}^{DD} is the iron mass flow rate [kg/h] passing from the retentate to the diffusate side of the DD unit, A is the membrane area [m²], $P_{j,Fe}$ is the membrane permeability to the FeCl₂ [m/h], $C_{Fe,mol}^R$ and $C_{Fe,mol}^D$ are the iron average concentrations in the retentate and in the diffusate side [mol/l], respectively. The expression for $P_{j,Fe}$ was derived experimentally [8] and it is reported in Eq. 12.

$$P_{j,Fe} = -6.73 \cdot 10^{-5} C_{Fe,mol}^2 + 4.21 \cdot 10^{-4} C_{Fe,mol} + 1.08 \cdot 10^{-4} \quad (12)$$

in which $C_{Fe,mol}$ is the average iron molar concentration [mol/l] in the retentate side of the DD unit.

Concerning the zinc passage, similar considerations were accomplished by using a

leakage percentage of 35% derived from the experimental campaign carried out [8].

Two contributions for the water passage are considered: the osmotic and the drag fluxes through the membrane. The osmotic flux J_{osm} is calculated by Eq. 13.

$$J_{osm} = R \cdot T \cdot P_w \cdot \rho_w \cdot (2 \cdot \Delta C_{HCl,mol}^{av} + 3 \cdot \Delta C_{Fe,mol}^{av} + 3 \cdot \Delta C_{Zn,mol}^{av}) \quad (13)$$

where R is the gas constant [lt bar/(K mol)], T is the average temperature [K], P_w is the water permeability [lt/(m² h bar)], ρ_w is the water density (kg/dm³), $\Delta C_{HCl,mol}^{av}$, $\Delta C_{Fe,mol}^{av}$ and $\Delta C_{Zn,mol}^{av}$ are the average concentration difference [mol/lt] in the DD of the HCl, Fe and Zn respectively. The expression for P_w was derived experimentally:

$$P_w = 6.1 \cdot 10^{-3} C_{HCl,mol}^R + 2.2 \cdot 10^{-2} \quad (14)$$

in which $C_{HCl,mol}^R$ is the average hydrochloric acid molar concentration [mol/lt] in the retentate side of the DD unit. The drag flux J_{drag} is calculated according to the following equation:

$$J_{drag} = \left(7 \cdot \frac{w_{HCl}^{DD}}{MM_{HCl}} + 18 \cdot \frac{w_{FeCl_2}^{DD}}{MA_{FeCl_2}} + 18 \cdot \frac{w_{ZnCl_2}^{DD}}{MA_{ZnCl_2}} \right) \cdot MM_{H_2O} \quad (15)$$

where w_{HCl}^{DD} , $w_{FeCl_2}^{DD}$ and $w_{ZnCl_2}^{DD}$ are the HCl, FeCl₂ and ZnCl₂ mass flow rates [kg/h] passing through the DD membrane, MM_{HCl} and MM_{H_2O} are the HCl and H₂O mole masses [g/mol] and MA_{Fe} is the iron atomic mass [g/mol].

Finally, the overall mass balance for DD unit is reported in Eq. 16.

$$w_{tot}^{DS} + w_{tot}^{WAS} = w_{tot}^{MRB} + w_{tot}^{RAS} \quad (16)$$

where w_{tot}^{DS} , w_{tot}^{WAS} , w_{tot}^{MRB} and w_{tot}^{RAS} are the total mass flow rates of the *Draw Solution, Waste Acid Solution, Metals Rich Brine* and *Recovered Acid Solution* streams [kg/h].

Membrane Distillation unit

With regard to Membrane Distillation unit, the streams to be characterized are: *Recovered Pickling Solution, Permeate* (see Figure 3).

The fluxes of water and HCl in the vapour phase passed through the membrane are derived from simulations carried out by another research partner within the ReWaCEM consortium. The values of J_i [kg/(h·m²)] used in the model are extrapolated from simulation results. Specifically, J_{water} is 3.0-3.1 kg/(h·m²) and J_{HCl} is 0.06-0.12 kg/(h·m²) for the acid concentrations considered in this work.

The overall mass balance for the Membrane Distillation unit is reported in Eq. (17):

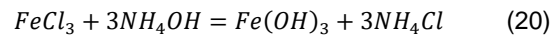
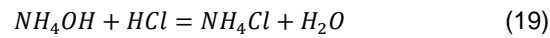
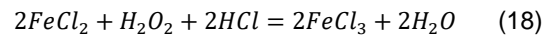
$$w_{tot}^{RAS} = w_{tot}^{RPS} + w_{tot}^{MD} \quad (17)$$

where w_{tot}^{RAS} , w_{tot}^{RPS} and w_{tot}^{MD} are the total mass flow rates of the *Recovered Acid Solution*, *Recovered Pickling Solution* and *Membrane Distillation Permeate* streams [kg/h].

Reactive Precipitation stage

The Reactive Precipitation unit is modelled considering the complete iron precipitation from the solution in the form of iron hydroxide by adding ammonia/water solution (30% w/w). Since the iron in solution is mainly present in the reduced form, especially due to the strong acid conditions, oxidizing is necessary to obtain a high pure iron hydroxide precipitate, free of zinc. In fact, pH precipitation of zinc hydroxide is very similar to iron(II) hydroxide, but higher than iron(III) hydroxide enough to obtain the precipitation of only iron(III) at an operating pH range of 3-4. A 35% of drag solution was considered in the precipitated.

The following reactions are considered in the reactive precipitation process:



The hydrogen peroxide mass flow rate is calculated according to the following expression:

$$w_{H_2O_2}^{Ox} = \frac{w_{Fe}^{MRB} \cdot MM_{H_2O_2}}{2 \cdot MM_{Fe}} \quad (21)$$

where $w_{H_2O_2}^{Ox}$ and w_{Fe}^{MRB} are the mass flow rate [kg/h] of the hydrogen peroxide and iron in the *MRB* stream, $MM_{H_2O_2}$ and MM_{Fe} are the mole mass [g/mol] of H_2O_2 and Fe, respectively.

The mass flow rate of the alkaline reactant is computed using the relation:

$$w_{NH_4OH}^{Alk} = \left[(10^{-pH_{in}} - 10^{-pH_{fin}}) \cdot F_{tot} + 2 \cdot \frac{C_{Fe^{2+}} \cdot F_{tot}}{MM_{Fe}} \right] \cdot MM_{NH_4OH} \quad (22)$$

where $w_{NH_4OH}^{Alk}$ is the reactant mass flow rate [kg/h], pH_{in} and pH_{out} are the initial and final pH of the solution, F_{tot} is the volumetric flow rate [lt/h], $C_{Fe^{2+}}$ is the iron concentration [g/lt], MM_{Fe} and MM_{NH_4OH} are the iron and NH_4OH mole mass [g/mol].

Regarding the *Metals Sludge (MS)* calculations, the following equations are used:

$$w_{H_2O}^{MS} = \left[(10^{pH_{in}} - 10^{pH_{fin}}) \cdot F_{MRB} \cdot MM_{H_2O} + w_{H_2O}^{MRB} + w_{H_2O}^{alk} \right] \cdot \alpha \quad (23)$$

$$w_{HCl}^{MS} = \left[w_{HCl}^{MRB} - (10^{pH_{in}} - 10^{pH_{fin}}) \cdot F_{MRB} \cdot MM_{HCl} \right] \cdot \alpha \quad (24)$$

$$w_{Cl}^{MS} = \alpha \cdot w_{Cl}^{MRB} + (w_{HCl}^{MRB} - w_{HCl}^{MS} - w_{HCl}^{out}) \cdot \frac{MA_{Cl} \cdot \alpha}{MM_{HCl}}$$

(25)

$$w_{NH_4^+}^{MS} = w_{NH_4OH}^{alk} \cdot \alpha \cdot \frac{MA_{NH_4^+}}{MM_{NH_4OH}} \quad (26)$$

$$w_{OH^-}^{MS} = \frac{3 \cdot C_{Fe^{3+}}^{MRB} \cdot F_{MRB} \cdot MM_{OH}}{MA_{Fe}} \quad (27)$$

where $w_{H_2O}^{MS}$, $w_{H_2O}^{MRB}$ and $w_{H_2O}^{alk}$, w_{HCl}^{MS} and w_{HCl}^{MRB} , w_{Cl}^{MS} , w_{Cl}^{MRB} and w_{HCl}^{out} , $w_{NH_4^+}^{MS}$ and $w_{NH_4OH}^{alk}$, $w_{OH^-}^{MS}$ are the mass flow rates [kg/h] of water, HCl, chloride ions, ammonium cations, ammonium hydroxide and hydroxyl ions in the *Metals Sludge*, *Metals Rich Brine*, Alkaline reactant and out from the reactive precipitator streams respectively, pH_{in} and pH_{fin} are the initial and final pH of the solution, F_{MRB} is the *MRB* volumetric flow rate [lt/h], MM_{H_2O} , MM_{HCl} , MA_{Cl} , $MM_{NH_4^+}$, MM_{NH_4OH} , MM_{OH^-} and MM_{Fe} are the component molar mass [g/mol], α is the fixed drag solution percentage and $C_{Fe^{3+}}^{MRB}$ is the iron concentration in *Metals Rich Brine*.

For the characterisation of the reactive precipitator outlet solution, $1-\alpha$ is used. This stream is carried to the *Brine MD* where water is recovered and then, added to the *Process Water*. The *Brine MD* is designed considering that a maximum allowable ammonium chloride concentration of 350 g/lt in the *MD* outlet stream is permitted due to the salt solubility limit.

RESULTS OF THE MODEL

A parametric analysis of the model was performed varying the main process parameter, specifically the outlet hydrochloric acid concentration in the *Waste Acid Solution* from the pickling tank. In particular, three case-studies have been considered by fixing the HCl concentration in the pickling bath to 80, 100 and 120 g/lt and imposing the corresponding iron concentration from the Kleingarn curve. Results were obtained considering constant values of the evaporation flux and inlet/outlet entrainment rate in the pickling tank.

Process streams flow rates

The flow rate of all the considered streams increases as the HCl concentration in the *Waste Acid Solution* increases from 80 to 120 g/lt, as shown in Figure 4.

Waste Acid Solution flow rate increases from 13.2 to 18.0 lt/h as the iron concentration decreases according to the pickling curve (see Eq. 4). Also the *Recovered Acid Solution* flow rate increases, from 13.6 to 19.0 lt/h, because higher is the *Draw Solution* due to the assumption of $WAS/DS = 1$. Moreover, for this assumption, also the *Process Water* flow rate raises, from 7.6 to 11.6 lt/h, due to the closure of the overall mass balance.

Another important parameter involved in the model process is the inlet of *Acid Make-up* in the pickling tank, necessary to restore the HCl consumed in the pickling reactions and lost in *Metal Rich Brine* stream. Considering that HCl consumed in the pickling tank is constant as manufacturing steel inlet is constant, the variation of the *Make-Up* volumetric flow rate mainly depends on the different quantity of HCl in the *Metals Rich Brine* stream. Thus, as *MRB* flow rate increases from 12.9 to 17.0 lt/h, also the *MU* stream increases (6.4-6.7 lt/h).

Finally, considering the assumption of steady-state operating mode, the higher is the *WAS* flow rate, the higher is the *Recovered Pickling Solution* (8.8 to 12.7 lt/h) due to the closure of the pickling unit mass balance.

Definitely, for a waste acid solution stream to be treated of 13-18 lt/h, about 6.5 lt/h of *Acid Make-Up* are required to keep the HCl concentration constant at the optimal condition in the pickling tank.

HCl and Fe concentrations

Varying HCl concentration in the *WAS*, clearly, influences acid and iron concentrations along process units. In the pickling stage, where optimal conditions are set accordingly to the Kleingarn curve, a growing HCl in *WAS* concentration leads to iron concentration decreasing. In the *RAS*, and consequently, in the *RPS*, C_{Fe} trend is increasing mainly due to the increase of the membrane area (Fig. 5a). In fact, this value raises from 0.8 to 1.5 m² due to the requirement meeting of the $\Delta C_{min-d} = 3$ g/lt.

For what concern the HCl, the higher is the concentration in *WAS* (80-120 g/lt), the higher is in the *RAS* (71.6-110.5 g/lt) as a higher acid flow rate through the membrane is observed (0.9-1.9 kg/h). Consequently, also the acid reintroduced in the pickling tank in the *RPS* stream is increased (100.5-146.6 g/lt, Fig. 5a).

Similar considerations can be done for the *DS* stream, where the HCl concentration increases due to the higher acid flow rate through the membrane in the MD unit (0.09-0.24 kg/h).

In the *MRB*, HCl and Fe concentrations depend on the components passage through the membrane in DD unit and, as a consequence, the increasing trend of the acid and the decreasing trend of the iron in the *WAS* are found also in the *MRB* (Fig. 5b).

Recovery Ratio

The acid recovery ratio *RR* that occurs in the Diffusion Dialysis unit is calculated by the following equation:

$$RR (\%) = \frac{F_{HCl,d}^{out} - F_{HCl,d}^{in}}{F_{HCl,r}^{in}} \times 100 \quad (28)$$

where $F_{HCl,d}$ and $F_{HCl,r}$ are the hydrochloric acid molar flow rate of the diffusate and retentate solutions and the apexes *in* and *out* indicate the inlet and outlet from the DD channel, respectively. The Recovery Ratio slightly increases from 80 to 86% due to an increment of the HCl flux through the membrane (1.12-1.26 kg/h·m²).

Reactive precipitation stage

The oxidant and alkaline reactants volumetric flow rates are correlated to the iron content in the reactive precipitation unit inlet stream (*Metal Rich Brine*). As the HCl increases in the *WAS*, considering the Fe concentration decreasing and the *MRB* volumetric flow rate increment, a higher mass flow rate of iron has to precipitate (1.68-1.71 kg/h). As a consequence, as shown in Table 1, higher reagents consumptions, i.e. hydrogen peroxide and ammonium hydroxide solutions, are required. Moreover, an increasing iron content leads to higher *Metals sludge* flow rates.

Concerning the Brine Membrane distillation, as shown in Table 2, the MD inlet volume flow rate increases (12.5-15.4 lt/h) as the *Metals Rich Brine* flow rate increases. On the other hand, NH₄Cl concentration decreases (188-160 g/lt) due to a dilution effect for the *MRB* flow rate increment. As expected, Brine MD outlet streams flow rates raise as the inlet MD increases. The values reported in Table 2 are calculated by imposing the maximum allowable ammonium chloride concentration of 350 g/lt, as stated above.

Definitely, for a waste acid solution stream to be treated of 13-18 lt/h, about 3.2 lt/h of hydrogen peroxide and about 4.5 lt/h of ammonium hydroxide solutions are required to obtain about 3.2 kg/h of iron(III) hydroxide product. In addition, the water permeate stream recovered from the Brine MD of about 7 lt/h can contribute for the 70% to the process water stream required in the Demo.

CONCLUSIONS

This work focuses on a novel approach for the recovery and optimisation of pickling solutions for hot-dip galvanising plants, with a specific focus on a case study relevant to the hot-dip galvanizing plant of TecnoZinco (Palermo, Italy). The simulation tool, design and operational sensitivity analysis of a demonstration pilot plant to be installed within the EU-funded ReWaCEM project activities (www.rewacem.eu) is presented. Starting from an accurate data mining, a Process Flow Diagram (PFD) of an integrated process for continuous regeneration of pickling solutions is proposed and analysed by the purposely implemented process simulator. The parametric analysis shows the effect of increasing the hydrochloric acid concentration in

the *Waste Acid Solution* on the main streams of the process. All operational parameters are monitored, including HCl and Fe concentrations, performance indicators and membrane area requirements.

A high acid recovery (higher than 80%) is obtained in the DD, while keeping a low iron leakage (below 3-5%). Even if a make-up of fresh acid is still necessary in the integrated process, it is reduced of 10% compared to that currently required in the plant. The advantage of the reactive precipitation stage relies in the obtainment of pure iron hydroxide as by-product. Moreover, the concentrated solution exiting from the final MD unit can be reused in the fluxing baths of the pickling plant thus further integrating the whole process with savings in chemicals and process water. Successful operation of the integrated process will allow to avoid the standard periodic steps of withdrawing and refilling pickling baths at the same time guaranteed the pickling operation under optimal conditions, thus reducing pickling time and enhancing the overall system effectiveness.

ACKNOWLEDGMENTS

This work has been funded by EU within the ReWaCEM project (Resource recovery from industrial waste water by cutting edge membrane technologies) – Horizon 2020 program, Grant Agreement no. 723729. www.rewacem.eu

REFERENCES

- [1] Regel–Rosocka, M. (2010) Journal of Hazardous Materials, 177, 57-69
- [2] Tomaszewska, M., Gryta, M., Morawski, A.W. (2001) Separation and Purification Technology, 22-23, 591-600
- [3] Luo, J., Wu, C., Xu, T., Wu, Y. (2011) Journal of Membrane Science, 366, 1-16
- [4] Xu, J., Lu, S., Fu, D. (2009) Journal of Hazardous Materials, 165, 832-837
- [5] Jatuphaksamphan, Y., Phinichka, N., Prapakorn, K. and Supradist, M. (2010) Journal of Metals, Materials and Minerals, 20(1), 33-39
- [6] Campano, B.R. The Kleingarn Regenerated Spent Acid at Increasing Ferrous (Fe^{+2}) and Ferric (Fe^{+3}) Chloride Content, <https://www.finishing.com/library/campano/kleingarn.pdf>
- [7] Lalibertè, M. and Cooper, W. E. (2004) Journal of Chemical & Engineering Data, 49, 1141-1151
- [8] Gueccia, R., Randazzo, S., Chillura Martino, D., Cipollina, A. and Micale, G., Experimental investigation and modelling of diffusion dialysis for HCl recovery from waste pickling solution, in preparation

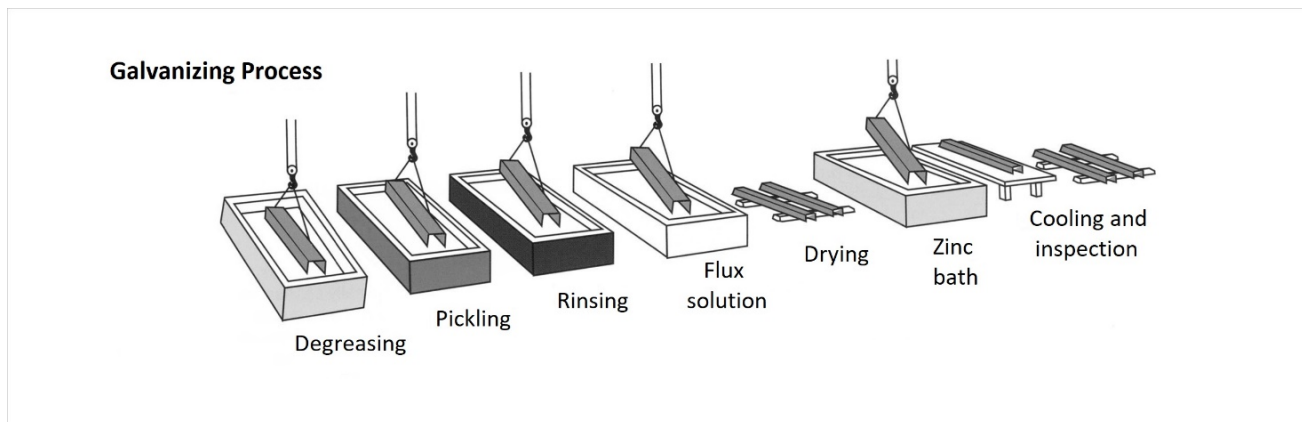


Figure 1. Hot-dip galvanizing process steps at Tecnozinco plant

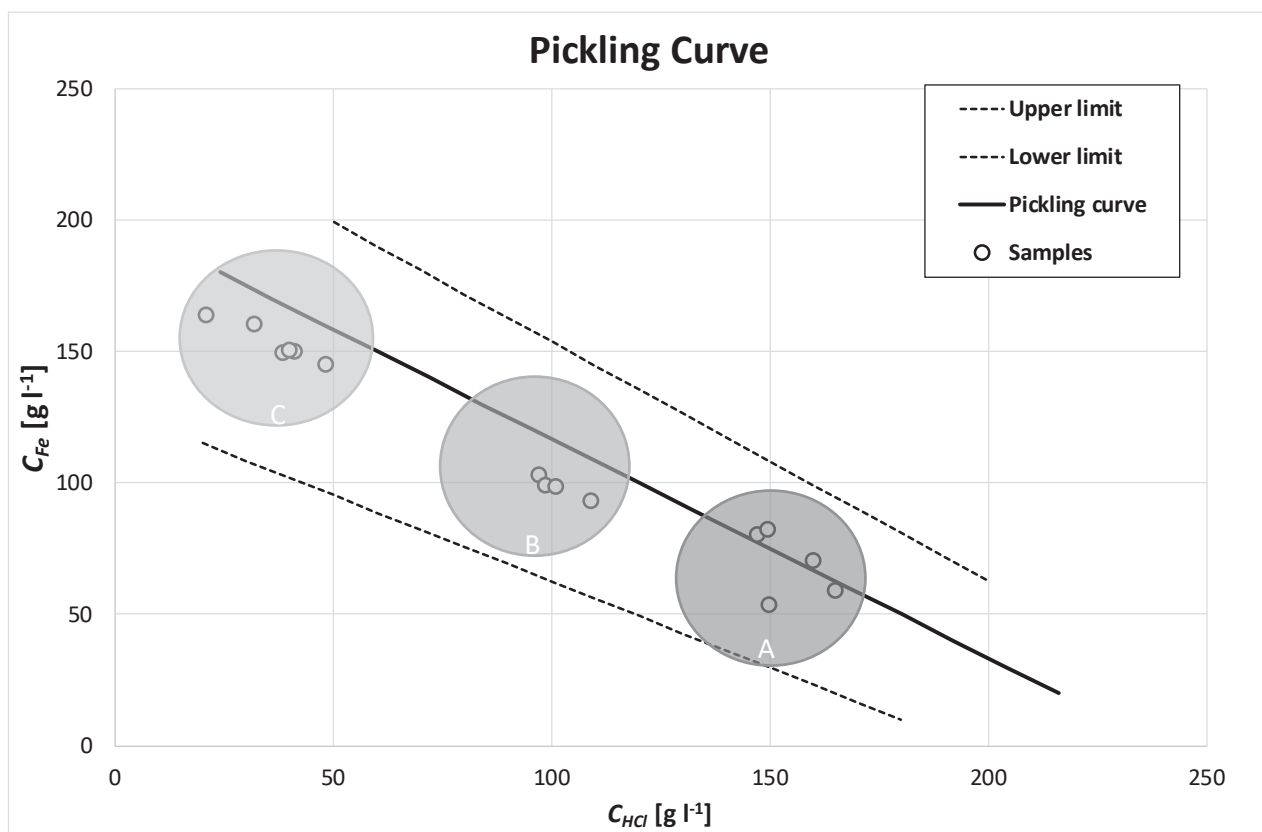


Figure 2. Kleingarn curve. Fe concentration vs. HCl concentration is reported. (—) represents the optimum pickling line; (- - -) delimited the pickling active region. Tecnozinco recent sample compositions are also reported in the figure.

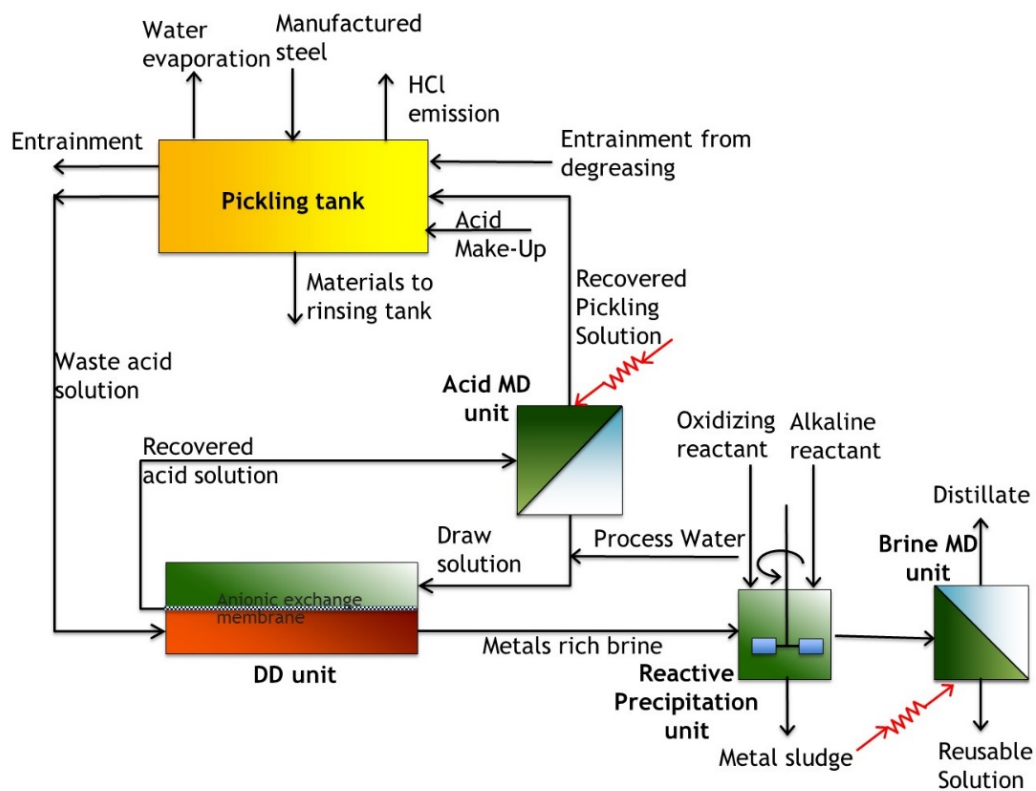


Figure 3. Process Flow Diagram (PFD) of the membrane integrated process for HCl and metals recovery

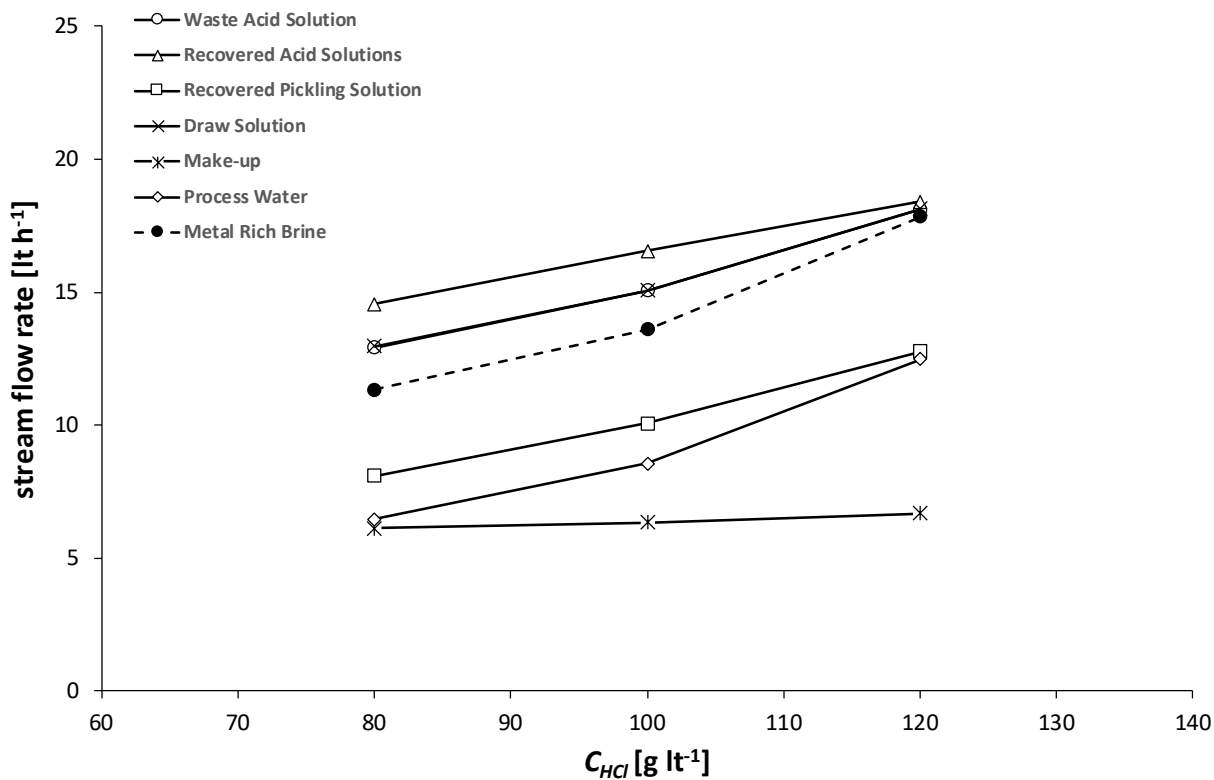
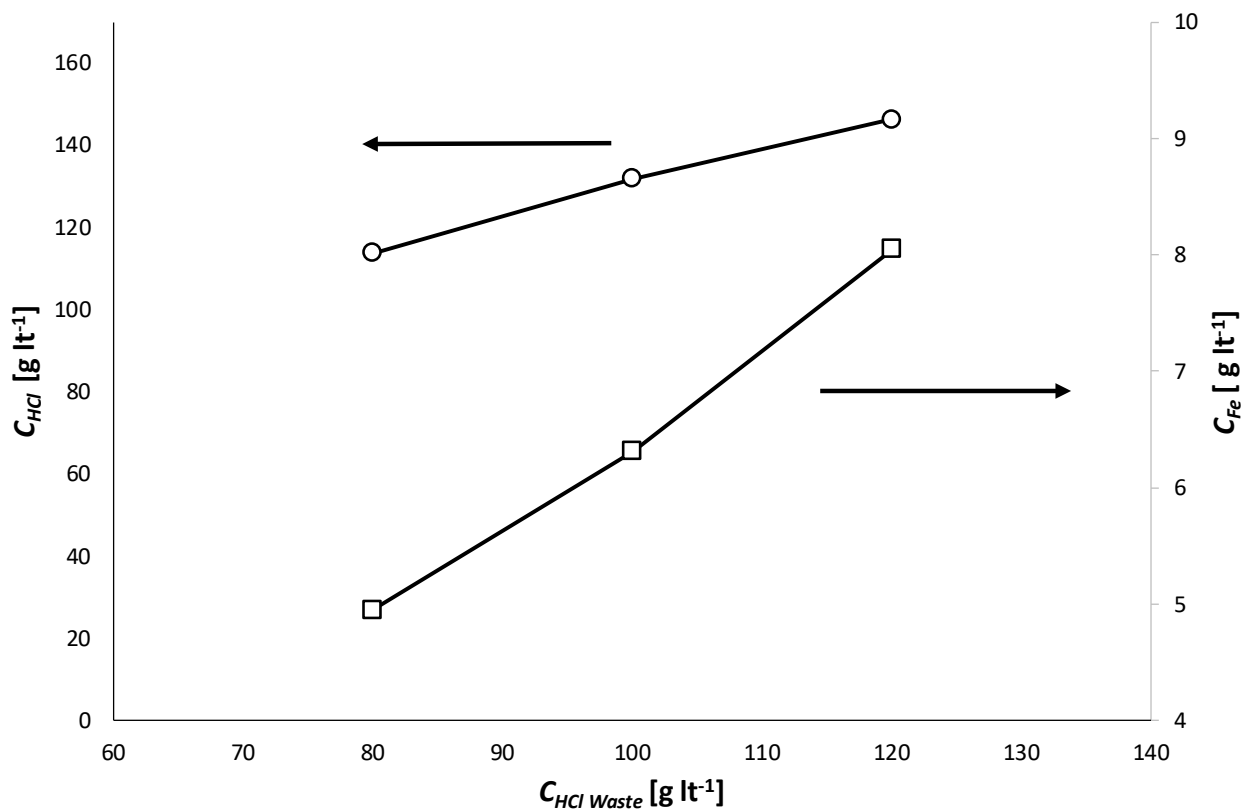
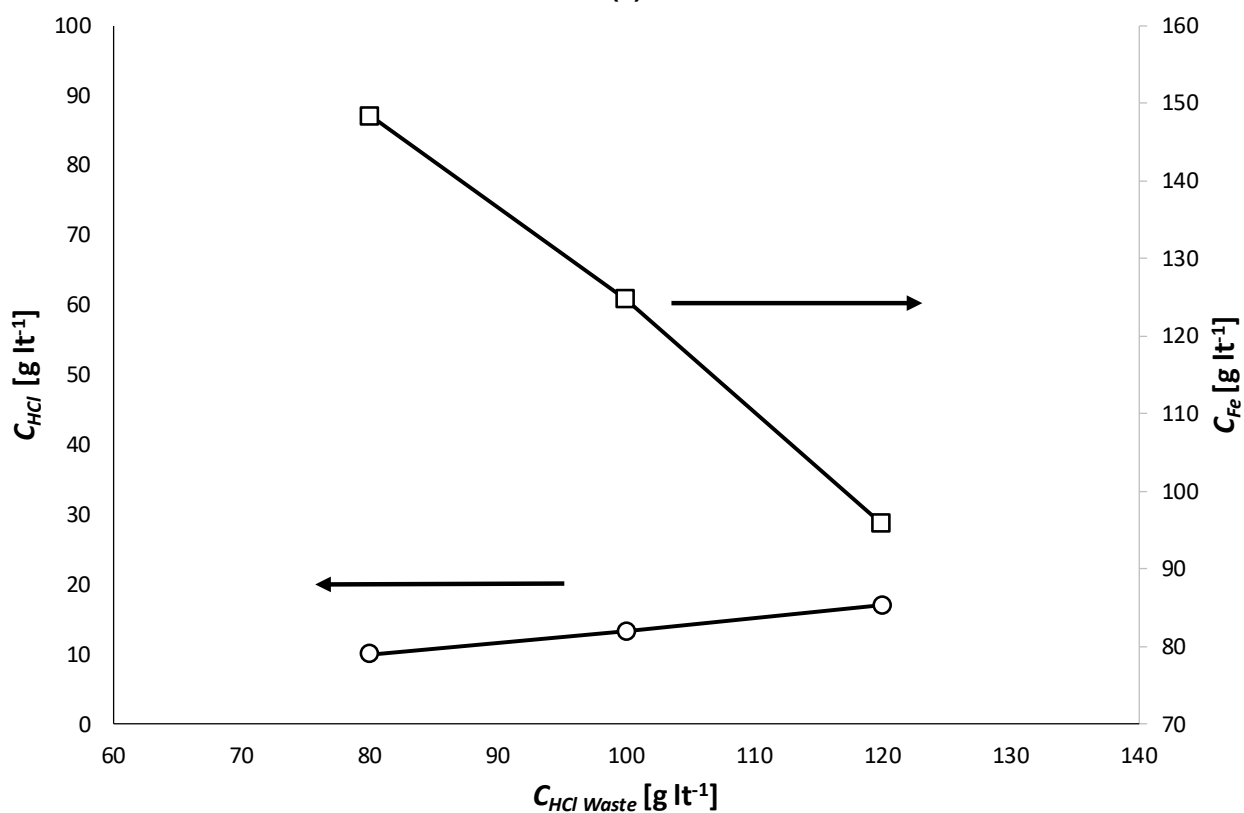


Figure 4. Waste Acid Solution, Recovered Acid Solution, Recovered Pickling Solution, Acid Make-Up and Process Water flow rates as a function of C_{HCl} in the Waste Acid Solution. $WAS/DS = 1$; $\Delta C_{min-r-d}$ in DD = 3 g/L. Evaporated flux and inlet and outlet entrainment solutions are constant.



(a)



(b)

Figure 5. HCl and Fe concentration in the *Recovered Pickling Solution* (a) and in the *Metal Rich Brine* (b) as a function of C_{HCl} in the *Waste Acid Solution*. $WAS/DS = 1$; $\Delta C_{min-r-d}$ in $DD = 3\ g/L$.

Table 1. Main streams flow rates as a function of C_{HCl} in the reactive precipitation stage (pH of the outlet stream = 4, drag solution in precipitate = 35%)

		$C_{\text{HCl,waste}} \text{ [g/t]}$		
		80	100	120
Oxidant	$W_{\text{tot}} \text{ [kg/h]}$	3.1	3.2	3.2
Alkaline reactant	$W_{\text{tot}} \text{ [kg/h]}$	4.4	4.5	4.6
Metals sludge	$W_{\text{tot}} \text{ [kg/h]}$	10.3	11.2	12.0

Table 2. Main streams flow rates as a function of C_{HCl} in the Brine-MD

	$C_{\text{HCl,waste}} \text{ [g/t]}$	$Q \text{ [lt/h]}$	$C_{\text{NH}_4\text{Cl}} \text{ [g/t]}$	$\rho \text{ [g/lt]}$
Inlet MD	80	12.5	188	1060
	100	14.1	168	1053
	120	15.4	160	1050
Outlet MD	80	6.7	350	1103
	100	6.8	350	1103
	120	7.1	350	1103
Permeate	80	5.6	0	1000
	100	7.2	0	1000
	120	8.2	0	1000

AUTHOR BIOGRAPHY

Serena Randazzo held a PhD in Nuclear, Chemical and Safety Technologies with a thesis on water treatment and electrochemical oxidation in 2011 at the University of Palermo. She worked for some years in the R&D division of a big Italian company producing lead-acid batteries. Since 2014 she is back as a PostDoc at the University of Palermo working on systems for the treatment and recovery of specific industrial wastewaters, generated by pickling process. In these years, she worked on design and construction of a small-scale pilot plant of pyrohydrolysis aiming at regenerating hydrochloric acid and producing valuable products to be installed in a hot-dip galvanizing plant in Italy within P.O. F.E.S.R. Sicilia 2007/2013 "Green Waste" project.

Since 2016 she is working on design and construction of a small-scale pilot plant adopting membrane technologies with the aim of recover hydrochloric acid and metals as valuable products to be installed in a hot-dip galvanizing plant in Italy within EU funded ReWaCEM project.

Session 12:

**Corrosion protection
performance of zinc and
zinc alloy coatings**

Atmospheric exposure of carbon and galvanized steel with different duplex systems at Oil & Gas Company – Brazil

Mr. Ricardo Suplicy Goes, Engineer, Executive Manager of ICZ	Non-Ferrous Metals Institute, São Paulo-Brazil
Mr. Marcelo Schultz	Corrosion Consultant, Petrobras, Brazil
Ms. Renata Yuriko Ogura	Galvanizer Armco Staco
Mr. Paulo Cesar Maziero Tiano	Galvanizer Marangoni Maretti
Mr. Celso Gnecco	Paint Company Sherwin-Williams
Prof., PhD Idalina Vieira Aoki (Chem. Eng. Dept - Polytechnic School	University of São Paulo.

ABSTRACT

This paper intends to: (1) Demonstrate the performance of Duplex System (painted galvanized steel) in the marine coast of Northeast Brazil. (2) Evaluate different options of coated systems: Epoxy Isocyanate + Epoxy Polyamide + PU; Epoxy Amine (Damp Tolerant) + Epoxy Polyamide + PU; Epoxy Polyamide + Epoxy Polyamide + PU; Epoxy Amine + PU; Epoxy Amine Micaceous Iron Oxide + PU; DTM Acrylic Water Base and Powder Coating. (3) Evaluate different options of surface pretreatment (sweep blast; sulfursilane). (4) To outline for Oil & Gas companies that they may expect higher anticorrosion performance by using Duplex System (painted galvanized steel) more frequently in the marine coast environment, hence demonstrating its superior performance.

These field tests, of two-year term (2014-2016), were held by Hot Dip Galvanized companies (ICZ members), a paint manufacturer and an Oil & Gas company. Those results intend to indicate which of these systems can be used in Oil & Gas companies to improve and obtain higher performance of carbon steel.

KEYWORDS: Duplex System, Hot Dip Galvanized, Performance.

INTRODUCTION:

This paper was conducted by the Brazilian ICZ – Non-Ferrous Metals Institute, its galvanizer members and partner companies, to attend your vision, which is:

- To lead and support the sectors of zinc, nickel and lead metals in the development and dissemination of their applications and sustainable use in Brazil.

AIM:

To outline for Oil & Gas companies that they may expect higher anticorrosion performance by using Duplex System (painted galvanized steel) more frequently in the marine coast environment, hence demonstrating its superior performance.

TEST DESIGN:

Performance comparisons, through corrosion rates, exposing 236 (199+37) samples in marine coast area:

- Uncoated carbon steel (30);
- Uncoated galvanized carbon steel (33);
- Uncoated Zinc Thermal Sprayed carbon steel (03);
- Coated carbon steel (48);

- Duplex System (painted galvanized carbon steel) (81) (including 03 not passive with chromate);
- Duplex System: (painted with surface pretreatment based on sulfursilane) (02);
- Duplex System: (painted with surface pretreatment based on hybrid coating with silanes) (02);
- Uncoated Galvanized screws (20);
- Uncoated Galvanized wire (01);
- Black (04) rebars / Galvanized (04) rebars;
- Black rebars embedded in concrete (08) /galvanized rebars (08) embedded in concrete;

Coating Systems:

- Epoxy Isocyanate + Epoxy Polyamide + PU;
- Epoxy Amine (Damp Tolerant) + Epoxy Polyamide + PU;
- Epoxy Polyamide + Epoxy Polyamide + PU;
- Epoxy Amine + PU;
- Epoxy Amine Micaceous Iron Oxide + PU;
- DTM Acrylic Water Base;
- Powder Coating.

Substrates

- Carbon Steel;
- HDG Steel
- Thermal Spraying
- Galvanized Screws
- Galvanized Wires
- Galvanized/Black Rebar

Surface Pretreatment

- Sweep Blast
- Degreased
- Scotch-Brite
- Sulfursilane
- Hybrid (Silane)
- Not Passivated with chromate

TERM / ANALYSES PERIOD:

Term: 02 years (NOV 2014 – DEC 2016):

Inspections:

- Visual Aspects: During two years in all the inspections, every 3 months;
- E_{corr} (corrosion potential) (V) - Only for rebars embedded in concrete: Every 3, 6 months and after the first and second year;
- Weight loss measurement: After 6 months, one and two years;
- Corrosion rate determination: After 6 months, one and two years;
- Pull-off Adhesion Test: After two years of exposure

LOCATION / ENVIRONMENT FEATURES:

We chose the area of Northeast Brazil, located in Sergipe state, Aracaju city, Atalaia beach, Latitude of Atalaia: -10.9880; Longitude of Atalaia: -37.0534.

We expect to confirm the C5 category in the test area. By the Brazilian ABNT NBR 14643 standard, it may be observed a zinc corrosion rate of 4.2 to 8.4 micrometers per year. In contrast, carbon steel features a corrosion rate of 80 to 200 micrometers per year in the C5 category.

We have defined two places for the tests. One by the beach and the second is about 500 meters to the inland, because in this area we have the presence of flare – SO₂ (Sulfur Dioxide), considered an atmospheric contaminant.

The annual environment features are:

Average temperature: 22°-30° Celsius;

Average Relative Humidity: 60%;

Precipitation: 52–334 mm;
 Wind Speed: 08-15 km/h – east;
 Chlorides Analyses: Ongoing (ASTM G140 Standard Test Method for Determining Atmospheric Chloride Deposition Rate by Wet Candle Method).

OVERVIEW:

SAMPLES ON BEACH AREA:

An overview of the samples on the beach is shown in figure 01 of appendix "Figures".

Samples: 15 (fifteen) samples of carbon steel.

On each "sample" is written the type of material and the time to take out for inspection and/or analysis.
 See figure 02 in the appendix "Figures".

Samples: 15 (fifteen) samples of uncoated galvanized (HDG-Hot Dip Galvanized) carbon steel.

On each "sample" is written the type of material and the time to take out for analysis.
 See the figure 03 in the appendix "Figures".

PANEL 1: 44 (forty-four) samples of coated steel (16), Duplex System (27) and uncoated Zinc Thermal Sprayed (01).

On each "sample" is written the ICZ code identification of type of material. All the samples of this panel were taken out after the first year of exposure for analysis in laboratory.
 See figure 04 in the appendix "Figures".

PANEL 2: 46 (forty-six) samples of coated steel (16), Duplex System (29) and uncoated Zinc Thermal Sprayed (01).

On each "sample" is written the ICZ code identification of type of material. All the samples of this panel were taken out after two years for analysis in laboratory.
 See figure 05 in the appendix "Figures".

PANEL 3: 49 (forty-nine) samples of coated steel (16), Duplex System (29) and uncoated Zinc Thermal Sprayed (01); 03 Uncoated HDG steel.

On each "sample" is written the ICZ code identification of type of material. All the samples of this panel were taken out after two years for analysis in laboratory. This panel was planned to take out its samples after three years.
 See figure 06 in the appendix "Figures".

Uncoated Galvanized screws (20):

- 20 carbon steel screws exposure on the beach:
- They will be analysed after the third year.
- See the figure 07 in the appendix "Figures".

Uncoated Galvanized wire (01):

- 10 meters of galvanized wire exposure on the beach:
- They will be analysed after the third year.
- See the figure 08 in the appendix "Figures".

Black (04) rebars / Galvanized (04) rebars:

- Black and galvanized rebars are not embedded in concrete on the beach.
- See the figure 09 in the appendix "Figures".

Black rebars embedded in concrete (08) /galvanized rebars (12) embedded in concrete:

Black and galvanized rebars embedded in concrete on the beach.

- pH in the wet concrete used is 12.5:

Reactions between galvanized reinforcement bars and concrete are only of concern during the initial curing stages of the concrete. The initial stages of curing include the time when the concrete mix is still wet. During this time, the pH of the concrete is very alkaline with a pH of approximately 12.5. The wet concrete reacts with the zinc to form hydroxyzincates ($\text{Ca} [\text{Zn} (\text{OI}-\text{OH} \times 2 \text{H}_2\text{O})$), which protects the zinc from further corrosion, but can evolve hydrogen gas. Excessive Hydrogen evolution during curing results in a more tenuous interface between the galvanized steel and the concrete, thus reducing the bond strength. Using concrete mixes with extremely high pH's may increase these reactions to unacceptable levels. Wet concrete mixes with a pH of over 13.3 have shown to significantly increase the reactions between concrete and galvanized rebar and should be avoided if possible without chromates.

- The concrete used presented the concentration of Cr(III) in the samples ranged from 10.9 to 88.0 mg kg⁻¹, which ensures that the reactions between the galvanized rebar and concrete are limited.
- Water/cement ratio:

The aim is to analyse the evaluating the effect of varying the water/cement ratio on the adherence between galvanized steel rebars and the concrete in which these are embedded.

Water/cement ratio used:

With 0.4 water/cement ratio:

- 06 (six) in the black rebars;
- 09 (nine) in the galvanized rebars;

With 0.6 water/cement ratio:

- 02 (two) in the black rebars;
- 03 (three) in the galvanized rebars;

SAMPLES ON INLAND AREA:

Samples: 15 (fifteen) samples of carbon steel.

On each "sample" is written the type of material and the time to take out for analyses.

See figure 10 in the appendix "Figures".

Samples: 15 (fifteen) samples of uncoated galvanized (HDG-Hot Dip Galvanized) carbon steel.

On each "sample" is written the type of material and the time to take out for analyses.

See figure 10 in the appendix "Figures".

IDENTIFICATION OF SAMPLES WITH LAMINATED TAGS:

All the samples are identified for the ICZ management.

See figure 11 in the appendix "Figures".

SCANNED SAMPLES:

Samples of carbon steel and galvanized steel (HDG) were scanned before their exposure in both sites.

The aim is to register the aspect of exposed samples by scanned images to evaluate the performance of the zinc coating on the carbon steel. See figure 12 in the appendix "Figures".

FINAL ANALYSES AFTER TWO YEARS.

The Carbon Steel samples on the beach area.

The carbon steel samples of panel A, located in the region of UPGN, 500 meters from the beach, ICZ 01.03, 01.04 and 01.05 were withdrawn after 12 months and the samples ICZ 01.06 (see figure 13) to 01.15 after 24 months of exposure for laboratory analysis.

Table 1 shows all the results of corrosion rate in terms of mass gain, r_{gm} , mass loss, r_{corr} , and loss of equivalent thickness for the carbon steel samples exposed in the UPGN on panel A.

The average of mass loss, r_{corr} , was between 174.6 g/m² year (1st year) and 140.7 g/m² year (2nd year) shown in table 1, allows to classify the category of aggressiveness of the UPGN environment as **C2 – low aggression**.

The carbon steel samples of the B panel located 50 meters from the beach, ICZ 01.18, 01.19 and 01.20 were withdrawn with 12 months and the samples ICZ 01.21 to 01.30, after 24 months of exposure for laboratory analysis.

The average mass loss, r_{corr} , was between 460.0 g/m².year (1st year) and 576.2 g/m².year (2nd year) shown in table 2, and allows to classify the category of the environment near the beach as **C4 – high aggression**. It should be emphasized that according to ISO 9223 standard what is worth noting is the classification obtained after 12 months of exposure.

In the carbon steel sample ICZ. 01.22, figure 14, it the appearance is showed after 24 months of exposure in the site 50 m from the beach.

See Tables 1 and 2 in the appendix "Tables" and figure 13 and 14 in the appendix "Figures".

The Galvanized Steel samples on the beach area.

The same laboratory analyses were carried out after 01 and 02 years of exposure for the galvanized steel samples.

Table 3 – Results of corrosion rate for the galvanized steel samples exposed in the UPGN panel C. The samples ICZ 02.03 and 02.04 were exposed for 1 year and the samples 02.05 to 02.10 have been exposed for 02 years.

The average mass loss rate, r_{corr} , was between 12.6 g/m².year (1st year) and 10.4 g/m².year (2nd year), shown in table 3, allows to classify the category of aggressiveness of the UPGN environment as **C3 – medium aggression**.

In the galvanized steel sample ICZ 03.02, figure 15, it is showed after 24 months of exposure in UPGN, with 0, 5mm incision.

Table 4 – Results of corrosion speed for the galvanized carbon steel samples exposed on the beach panel D. The samples ICZ 02.11, 02.12 and 02.13 were exposed for 1 year. The sample ICZ 02.15 (figure 16) for 2 years.

The average mass loss, r_{corr} , was between 31.4 g/m².year (1st year) and 35.0 g/m².year (2nd year), shown in table 4, after 12 months, allow to classify the category of the environment near the beach as **C5 – very high aggression**.

The aggressiveness measured by galvanized steel did not coincide with the aggressiveness classified with the carbon steel samples, having been larger. It must be emphasized that in the ISO 9223 standard, zinc refers to rolled zinc plates and, in this work, it is zinc applied by hot immersion, which has a different microstructure, that makes it more active and it shows a slightly larger corrosion rate. It is worth noting that the thickness loss rate of carbon steel is ten times greater than the loss of galvanized steel thickness to the same level of middle aggressiveness. The results of corrosion rate after two years of exposure led to the same aggressive classification after one year of exposure according to ISO 9223 standard. This shows the consistency of the results obtained in the project.

The galvanized carbon steel with incision of 0.5 mm sample, ICZ 03.05 (Figure 17), exposed after 2 years, shows no sign of corrosion products from the carbon steel substrate, proving the corrosion protection provided by the hot-dip zinc coating. It is clear the higher aggressiveness of the environment near the beach when compared to the environment within the UPGN. These results reinforce the classifications obtained for the aggressiveness of the two environments with the hot galvanized samples, according to ISO 9223, being C3 to the UPGN and C5 near the beach. Samples with incision reveal the power of protection provided by the zinc anodic coating to steel, even in the presence of a defect.

See tables 03 and 04 in the appendix "Tables" and figures 15, 16 and 17 in the appendix "Figures".

Coated Carbon Steel samples.

After two years of exposure, it can be said that the best paint systems for carbon steel were the systems 4 (ICZ 125 – figures 18A and 18B) and System 2 (ICZ95) of the Sherwin Williams and the System 2 (ICZ23) of the Marangoni, in that order.

The figures 18A and 18B, a sample with incision, shows an initial of corrosion in the steel. See in the appendix "Figures".

After two years of exposure, the painted carbon steel samples were evaluated according to ISO 4628-8 and the results of the evaluation were gathered in table 05.

The evaluation of the samples exposed for two years revealed that Marangoni Systems 1, 2 and 3, System 2 and SW 4 system are the best for carbon steel. It took into account the corroded area, as the delamination area was the same for all the painted carbon steel samples. The worst systems were system 1, System 5 and system 3.

All coated systems are described in appendix "Samples - Field Tests - Atalaia Beach - ICZ Petrobras".

The Duplex System samples on the beach area.

After two years of exposure of the samples, it is noted that all the samples painted on galvanized steel present excellent aspect in the region of the incision, superior to the samples painted on carbon steel.

The Marangoni System 2 (ICZ47 – Figures 19A and 19B) and Sherwin Williams Systems 3 (ICZ104 – Figures 20A and 20B), 4 (ICZ119 - Figures 21A and 21B) and 5 (ICZ134 - Figures 22A and 22B) showed better performance for galvanized steel. It should be highlighted the excellent performance of the electrostatic painting made by Trifer (ICZ65 - Figures 23A and 23B).

Another point to be highlighted was the best performance of the Sherwin Williams system 7 (ICZ145) when with silane hybrid pretreatment. The sample treated with Sulfossilane (Sherwin Williams system 6 (ICZ 143)) did not perform well.

After two years of exposure, the painted hot-dip galvanized samples (duplex system) and without incision show excellent aspect (see table 06) and all were classified according to ASTM D610 with classification between 10 and 9S or 9P. This reveals the excellent performance and absence of pores in the paint systems applied on hot-dip galvanized steel. Even after two years of exposure, it is still impossible to distinguish between the paint systems, showing the superiority of the duplex system compared to the paint systems applied directly on carbon steel.

It was observed that the Duplex System did not show any sign of red corrosion.

See tables 05 and 06 in appendix "Tables". See all figures in the appendix "Figures".

After two years of exposure, the hot dip galvanized and the coated carbon steel samples were classified as to the degree of corrosion and delaminated area around the incision with the use of a chisel for the removal the paint and using the ISO 4628-8 standard and an image treatment software the ImageJ1.5i and the results are gathered in table 38. The results after two years of exposure show that all the Sherwin Williams paint systems presented very good results in addition to electrostatic painting. The Marangoni systems did not have such a good result for galvanized steel, presenting better performance for carbon steel. Pretreatment with Sulfossilane worsened the result obtained for the SW 3 painting system. With a hybrid pretreatment (silanes based on epoxy) has not altered the good quality of the system 3 and can be an alternative to the light blasting of hot dip galvanized.

The uncoated galvanized wire samples in the beach area.

It was analyzed only by visual inspection. After 09 months of exposure it was observed the presence of red corrosion in the frontal area to the sea was observed by the action of the sea Breeze/winds. See figure 24 in the appendix "Figures".

The uncoated galvanized screws samples in the beach area.

The general aspect of the screws shows that after two years, there are spots with red corrosion (attack on the substrate), but this occurred mainly in the screw thread region, because in this region, the thickness of the zinc coating is not homogeneous and therefore does not provide so effective protection for the thread region. The head of the screws always presents better aspect, but some show greater attack in the region that was directly facing the wind. See figure 25 in the appendix "Figures".

Rebar embedded in concrete:

Samples of Rebar embedded in concrete on the beach area:

Visual analyzes

After two years of exposure, the performance of the samples was analyzed with black steel rebar (P), zinc metallized (M) and hot-dip galvanized steel rebar (G). The influence of the water/cement ratio of 0.4 and 0.6 on corrosion behavior was also analyzed.

Black rebar

For the samples P4 (ratio 0.4) and P5 (ratio w/c 0.6), the black rebar, which was completely embedded in the concrete, the advance of the corrosion was between 1.5 to 2.0 cm. No difference in the advance of corrosion was reported as a function of the water cement ratio. It is showed in figure 26 in the appendix "figures".

Metallized rebar

There is no advance of corrosion in rebar metallized with zinc. It is showed in the figure 27 of the samples M4 in the appendix "figures".

Hot-dip galvanized steel rebar

There is no advance of corrosion in Hot-dip galvanized steel rebar. No difference in the advance of corrosion was reported as a function of the water cement ratio. It is showed in figure 29 for the sample G6 (w/c ratio 0.6) in the appendix "figures".

Potential Measurements

Potential measurements were carried out in 8 samples embedded in concrete (4 galvanized rebar and 4 blacks). The rebars have 300 mm long embedded in concrete and 100 mm (total 400 mm) exposed to the environment.

According to ASTM C 876 values smaller than -350 mv (i.e.-400 MV, -500 MV) already indicate 90% likelihood of corrosion occurring. For values between -200 MV and -350 MV, the corrosion process is uncertain. For values greater than -200 MV (i.e.-150 mv, -100mV) the likelihood of corrosion is very low.

According to table 07- Measurements of corrosion potential of the rebar embedded in concrete against the reference electrode of Cu/CuSO₄ exposed near the beach of Atalaia, SE, we can observe that, in two years of exposure, over time the values of black rebar potential became more positive, for example from -330 mV to -207 mV, indicating the passive state of the steel embedded in concrete.

The same occurred for the hot dip galvanized steel rebar, for example from -745 mV to -577 mV, indicating that these also were passive in the concrete by the formation of calcium hydroxyzincate.

See table 07 in the appendix "Tables".

FINAL CONSIDERATIONS:

After two years of exposure at the beach of Atalaia, Sergipe, northeast of Brazil, the samples with duplex system, painted hot dip galvanized steel, showed huge good performance compared to painted carbon steel samples, since they did not present the occurrence of red corrosion.

The results allowed to conclude on the best pretreatments of the galvanized steel samples that are the light blasted, the degreasing or the use of hybrid pretreatment (silanes based on epoxy).

The best paint systems for hot dip galvanized steel were the System 1 and 3 of the Sherwin Williams. The worst were the Marangoni system 3 and Sherwin Williams System 2. The Marangoni systems did not have such a good result for galvanized steel, presenting better performance for Carbon steel.

The samples of galvanized steel rebar embedded in concrete, by visual analysis, did not present any advance of corrosion while the rebar in carbon steel presented the advance of the corrosion.

The potential values of the carbon steel and galvanized steel rebar embedded in the concrete in relation to the Cu/CuSO₄ reference electrode allowed to evaluate that after two years, both are still in a passive situation.

ACKNOWLEDGEMENTS

I would like to express the deepest appreciation to all authors. This project would not have been possible without the help of them: Marcelo Schultz, Genaro Zanon, Renata Yukiro Ogura, Paulo Cesar Maziero Tiano, Celso Gnecco and Professor Idalina Vieira Aoki.

I would like to thank everyone who has worked in this project, dedicating time, materials and knowledge to make it happen.

REFERENCE STANDARDS:

- ABNT NBR 6209:2007 - Atmospheric Corrosion - Metallic Material – Outdoor Test;
- ASTM D1014-09: 2009 - Standard Practice for Conducting Exterior Exposure Tests of Paints and Coatings on Metal Substrates;
- ABNT NBR 6210:2008 - Atmospheric corrosion - Metallic materials - Preparing, cleaning and determination of corrosion rate of specimens in corrosion Tests;
- ISO 9223: 2012 - Corrosion of metals and alloys - Corrosivity of atmospheres - Classification, determination and estimation);
- ISO 9226: 2012 - Corrosion of metals and alloys - Corrosivity of atmospheres -- Determination of corrosion rate of standard specimens for the evaluation of corrosivity;
- ABNT NBR 14643:2001 - Atmospheric corrosion - Classification of corrosivity of atmospheres;
- ISO 12944 - 1 to 6 - Paints and varnishes - Corrosion protection of steel structures by protective paint systems - Part 2:1998 Classification of environments / Part 5: 2007 Protective paint systems
- ABNT NBR 15877 - Pull-off adhesion test
- ISO 4624: 2002 Paints and varnishes - Pull-off test for adhesion.
- ISO 4628-8 Assessment of degree of delamination and corrosion around a scribe or other artificial defect
- ASTM C876 - 09 - Standard Test Method for Corrosion Potentials of Uncoated Reinforcing Steel in Concrete
- ASTM D4541 - 02 Standard Test Method for Pull-Off Strength of Coatings Using Portable Adhesion Testers

ICZ - INSTITUTO DE METAIS NÃO FERROSOS

São Paulo, April 13th, 2018

ICZ PAPER INTERGALVA 2018 - APPENDIX – TABLES

Title: Field Tests of Duplex System at O&G Company in Brazil

Affiliation/Company: Paper ICZ – Non-Ferrous Metals Institute

Table 1: Results of corrosion rate in terms of mass gain, r_{gm} , mass loss, r_{corr} , and loss of equivalent thickness for the carbon steel samples exposed in the UPGN on panel A.

Sample	r_{gm} (mg/m ² . day)	r_{corr} (mg/m ² . day)	r_{corr} Avera- -ge	r_{corr} (g/m ² . year	r_{corr} avera ge	DP	Loss of thickness					
							m/year	0.024	24.05	Avera- ge (μ m/ye- -ar)	SD standa rd deviat ion	Catego- ry
ICZ.01.01	285.0	518.6		189.3			2.40E-05	0.024	23.89			
ICZ.01.02	279.0	515.0	516.8	188.0	188.6	0.9	2.38E-05	0.024	24.08	24.0	0.1	C2
ICZ.01.03	287.7	519.3		189.5			2.408E-05	0.021	20.73			
ICZ.01.04	263.1	446.9		163.1			2.073E-05	0.022	21.76			
ICZ.01.05	283.8	469.2	478.4	171.3	174.6	13.5	2.176E-05	0.0175	17.54	22.19	1.72	C2
ICZ.01.06	-36.55	378.10		138.01			1.754E-05	0.0169	16.87			
ICZ.01.07	163.16	363.70		132.75			1.687E-05	0.0176	17.55			
ICZ.01.08	161.41	378.51		138.16			1.755E-05	0.0184	18.38			
ICZ.01.09	164.04	396.32		144.66			1.838E-05	0.0175	17.47			
ICZ.01.10	158.41	376.76		137.52			1.747E-05	0.0169	16.94			
ICZ.01.11	158.65	365.21		133.30			1.694E-05	0.0185	18.48			
ICZ.01.12	142.93	398.44		145.43			1.848E-05	0.0198	19.80			
ICZ.01.13	162.02	427.00		155.85			1.98E-05	0.0176	17.61			
ICZ.01.14	156.30	379.65		138.57			1.761E-05	0.0182	18.15			
ICZ.01.15	162.05	391.37	385.5	142.85	140.7	6.8	1.815E-05	0.0182	18.15	17.88	0.87	C2

ICZ - INSTITUTO DE METAIS NÃO FERROSOS

Table 2 – Results of corrosion rate for the carbon steel samples exposed on the beach panel B. The samples 16 and 17 (by 6meses) and samples 18, 19 and 20 (for 1 year) and samples 21 to 30, for two years.

sample	r_{gm} (mg/m 2.day)	r_{corr} (mg/m 2.day)	r_{corr} average	r_{corr} (g/m ² .y ear)	r_{corr} avera ge	SD stand ard devia tion	Loss of thickness					Aggress iveness catego ry
							m/year	mm/ year	µm/ year	Avera ge	SD	
ICZ.01.16	445.2	1113.8		406.5			5.17E-05	0.052	51.66			
ICZ.01.17	444.4	1119.2	1116.5	408.5	407.5	1.4	5.19E-05	0.052	51.91	51.8	0.2	C4
ICZ.01.18	504.6	1337.0		488.0			6.201E-05	0.062	62.01			
ICZ.01.19	456.2	1180.3		430.8			5.474E-05	0.055	54.74			
ICZ.01.20	572.8	1263.4	1260.3	461.1	460.0	28.6	5.859E-05	0.059	58.59	58.4	3.6	C4
ICZ.01.21	-234.4	1419.2		518.00			6.582E-05	0.0658	65.82			
ICZ.01.22	-342.4	1654.9		604.03			7.675E-05	0.0768	76.75			
ICZ.01.23	-283.4	1595.7		582.41			7.4E-05	0.0740	74.00			
ICZ.01.24	-305.4	1767.2		645.03			8.196E-05	0.0820	81.96			
ICZ.01.25	-170.5	1608.7		587.16			7.461E-05	0.0746	74.61			
ICZ.01.26	-214.4	1726.9		630.33			8.009E-05	0.0801	80.09			
ICZ.01.27	-283.3	1643.6		599.93			7.623E-05	0.0762	76.23			
ICZ.01.28	-206.9	1455.3		531.20			6.75E-05	0.0675	67.50			
ICZ.01.29	-25.5	1576.0		575.23			7.309E-05	0.0731	73.09			
ICZ.01.30	-169.0	1337.9	1578.5	488.3	576.2	49.8	6.205E-05	0.0621	62.05	73.21	6.3	C4

ICZ - INSTITUTO DE METAIS NÃO FERROSOS

Table 3 – Results of corrosion rate for the galvanized steel samples exposed in the UPGN panel C. The samples ICZ 02.03 and 02.04 were exposed for 1 year and the samples 02.05 to 02.10 form exposed for 02 years.

Sample	r_{gm} (mg/m ² .day)	r_{corr} (mg/m ² .day)	r_{corr} average	r_{corr} (g/m ² .year)	r_{corr} Average	SD stand ard devia tion	Loss of thickness				SD	Class
							m/ year	mm/ye ar	μm/ year	Avera -ge		
ICZ.02.01	mirror											
ICZ.02.02	29.2	38.6		14.1			1,98 E-06	0.002	1.98			
ICZ.02.03	34.3	25.8		9.4			1.32 E-06	0.001	1.32			
ICZ.02.04	35.4	38.8	34.4	14.2	12.6	2.7	1.99 E-06	0.002	1.99	1.76	0.4	C3
ICZ.02.05	36.8	37.3		13.6			1.91 E-06	0.0019	1.91			
ICZ.02.06	38.3	30.1		11.0			1.54 E-06	0.0015	1.54			
ICZ.02.07	24.1	21.3		7.8			1.09 E-06	0.0011	1.09			
ICZ.02.08	41.6	30.8		11.3			1.58 E-06	0.0016	1.58			
ICZ.02.09	38.9	25.4		9.3			1.30 E-06	0.0013	1.30			
ICZ.02.10	37.7	26.4	28.5	9.7	10.4	2.00	1.35 E-06	0.0014	1.35	1.46	0.28	C3

ICZ - INSTITUTO DE METAIS NÃO FERROSOS

Table 4 – Results of corrosion rate for the galvanized carbon steel samples exposed on the beach panel D. The samples ICZ 02.11, 02.12 and 02.13 were exposed for 1 year. The sample ICZ 02.15 (figure 16) for 2 years.

Sample	Γ_{gm} (mg/m ² .day)	Γ_{corr} (mg/m ² .day)	Γ_{corr} Average	Γ_{corr} (g/m ² .year)	Γ_{corr} Average	SD	Loss of thickness					Class
							m/year	mm/year	μ m/year	Average	SD standard deviation	
ICZ.02.11	78.9	87.5		31.9			4.5E-06	0.0045	4.47			
ICZ.02.12	73.5	76.1		27.8			3.9E-06	0.0039	3.89			
ICZ.02.13	73.6	94.4	86.0	34.5	31.4	3.4	4.8E-06	0.005	4.83	4.40	0.5	C5
ICZ.02.14	59.5	110.9		40.49			5.7E-06	0.0057	5.67			
ICZ.02.15	76.3	74.2		27.06			3.8E-06	0.0038	3.79			
ICZ.02.16	78.2	101.7		37.10			5.2E-06	0.0052	5.20			
ICZ.02.17	82.9	88.1		32.14			4.5E-06	0.0045	4.50			
ICZ.02.18	92.8	101.9		37.21			5.2E-06	0.0052	5.21			
ICZ.02.19	144.9	99.2	96.0	36.21	35.0	4.7	5.1E-06	0.0051	5.07	4.91	0.66	C5

Table 05 – Degree of attack of the painted carbon steel samples, with incision, by ISO 4628-8 standard, using an image J 1.5i software for image treatment and obtaining the attacked or detached area of the film, after two years of exposure on the beach.

Sample	Paint System/treatment	Absolute corroded Area (cm ²)	Absolute delaminated area	Degree of attack by ISO 4628-8	Degree of delamination by ISO 4628-8
ICZ 20	Marangoni – sist. 1	3.687	16.838	G3	G5
ICZ21	Marangoni – sist. 1	3.067	6.847	G3	G5
ICZ 23	Marangoni – sist. 2	3.941	19.151	G4	G5
ICZ24	Marangoni – sist. 2	2.558	6.593	G3	G5
ICZ 26	Marangoni – sist. 3	2.749	10.394	G3	G5
ICZ27	Marangoni – sist. 3	3.593	11.484	G3	G5
ICZ 80	SW sist. 1	10.147	33.59	G5	G5
ICZ81	SW sist. 1	12.702	24.736	G5	G5
ICZ 95	SW sist. 2	5.041	10.62	G4	G5
ICZ96	SW sist. 2	2.815	9.208	G3	G5
ICZ 110	SW sist. 3	9.066	15.153	G5	G5
ICZ111	SW sist. 3	11.876	26.733	G5	G5
ICZ 125	SW sist. 4	1.780	6.341	G2	G5
ICZ126	SW sist. 4	1.90	6.576	G2	G5
ICZ 140	SW sist. 5	10.016	26.690	G5	G5
ICZ141	SW sist. 5	8.454	23.595	G5	G5

ICZ - INSTITUTO DE METAIS NÃO FERROSOS

Table 06 - Attack degree according to ASTM D610 of the samples galvanized and painted after two years of exposure on the beach Atalaia.

Sample	Paint System/treatment	Attack degree by ASTM D610
ICZ 29	Marangoni – sist. 1/ Armco without passivation	10
ICZ 32	Marangoni – sist. 2/Armco without passivation	10
ICZ 35	Marangoni – sist. 3/Armco without passivation	10
ICZ 38	Marangoni – sist. 1/Marangoni passivated	10
ICZ 41	Marangoni – sist. 1/Marangoni without passivation	10
ICZ 53	Marangoni – sist. 1/ Marangoni Thermal spray	10
ICZ 56	Trifer – electrostatic / Trifer	9P
ICZ 62	Trifer – electrostatic / Armco without passivation	9P
ICZ 68	SW sist 1 / Armco GJ	10
ICZ 71	SW sist 1 / Armco GD	10
ICZ 83	SW sist 2 / Armco GJ	9S near edge
ICZ 86	SW sist 2 / Armco GD	9P
ICZ 98	SW sist 3 / Armco GJ	10
ICZ 101	SW sist 3 / Armco GD	10/9S
ICZ 113	SW sist 4 / Armco GJ	9S
ICZ 116	SW sist 4 / Armco GD	10
ICZ 128	SW sist 5 / Armco GJ	10
ICZ 131	SW sist 5 / Armco GD	9S
ICZ142	SW sist. 1/Armco washed + sulfossilane	9P
ICZ144	SW sist. /Armco washed + hybrid	10

ICZ - INSTITUTO DE METAIS NÃO FERROSOS

Table 07 - Measures of corrosion potential of the rebar embedded in concrete against the reference electrode of Cu/CuSO₄ exposed to the edge of the beach of Atalaia.

Local	Item	Sample	Ratio water/cement	Day of measure (mV)			
				05.03.15	09.07.15	24.09.15	10.12.15
Beach	1	Galvanized rebar G (0) (4º LE de frente)	0.6	-786	-897	-675	-689
				-788			
	2	Galvanized rebar (3º LE de frente)	0.4	-793	-789	-759	-535
				-793			
	3	Galvanized rebar (2º LE de frente)	0.4	-745	-817	-558	-577
				-746			
	4	Galvanized rebar (1º LE de frente)	0.4	-770	-824	-727	-747
				-771			
5	Black rebar (4º LE de frente)	0.4	-401	-388	-307	-299	
			-402				
6	Black rebar (3º LE de frente)	0.4	-368	-327	-209	-213	
			-369				
7	Black rebar (2º LE de frente)	0.4	-396	-357	-234	-230	
			-397				
8	Black rebar - P (0) (1º LE de frente)	0.6	-330	-291	-236	-207	
			-331				

ICZ - INSTITUTO DE METAIS NÃO FERROSOS

São Paulo, April 13th, 2018

ICZ PAPER INTERGALVA 2018 - APPENDIX – FIGURES

Title: Field Tests of Duplex System at O&G Company in Brazil

Affiliation/Company: Paper ICZ – Non-Ferrous Metals Institute

Figure 01:

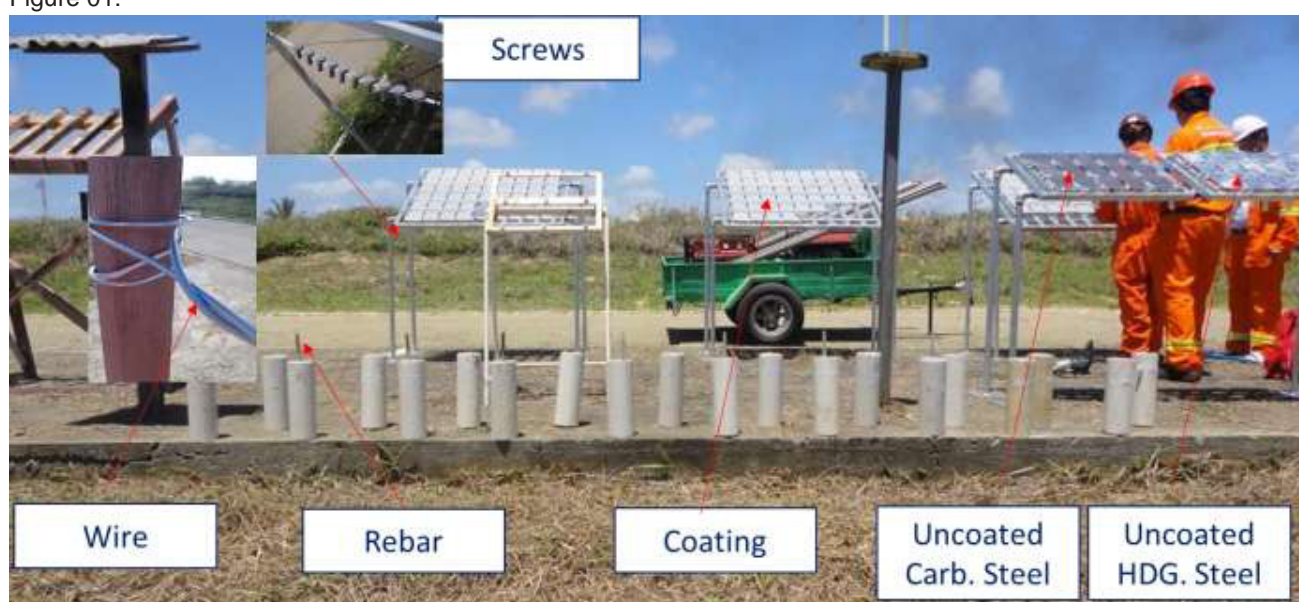


Figure 02:

PANEL B - BEACH AREA - 15 SAMPLES OF CARBON STEEL				
ICZ 01.16 Steel Carbon 6 MONTHS	ICZ 01.19 Steel Carbon 1º YEAR	ICZ 01.22 Steel Carbon 18 MONTHS	ICZ 01.25 Steel Carbon 2º YEAR	ICZ 01.28 Steel Carbon 3º YEAR
ICZ 01.17 Steel Carbon 6 MONTHS	ICZ 01.20 Steel Carbon 1º YEAR	ICZ 01.23 Steel Carbon 2º YEAR	ICZ 01.26 Steel Carbon 30 MONTHS	ICZ 01.29 Steel Carbon 3º YEAR
ICZ 01.18 Steel Carbon 1º YEAR	ICZ 01.21 Steel Carbon 18 MONTHS	ICZ 01.24 Steel Carbon 2º YEAR	ICZ 01.27 Steel Carbon 30 MONTHS	ICZ 01.30 Steel Carbon 3º YEAR

ICZ - INSTITUTO DE METAIS NÃO FERROSOS

Figure 03:

PANEL D - BEACH - 15 SAMPLES OF HDG STEEL				
ICZ 02.11 HDG STEEL 1º YEAR	ICZ 02.14 HDG STEEL 2º YEAR	ICZ 02.17 HDG STEEL 3º YEAR	ICZ 03.05 HDG Steel +Incision 0.5 mm 1º YEAR	ICZ 04.05 HDG steel+Incision 2.0 mm 1º YEAR
ICZ 02.12 HDG STEEL 1º YEAR	ICZ 02.15 HDG STEEL 2º YEAR	ICZ 02.18 HDG STEEL 3º YEAR	ICZ 03.06 HDG Steel +Incision 0.5 mm 2º YEAR	ICZ 04.06 HDG steel+Incision 2.0 mm 2º YEAR
ICZ 02.13 HDG STEEL 1º YEAR	ICZ 02.16 HDG STEEL 2º YEAR	ICZ 02.19 HDG STEEL 3º YEAR	ICZ 03.07 HDG Steel +Incision 0.5 mm 3º YEAR	ICZ 04.07 HDG steel+Incision 2.0 mm 3º YEAR

Figure 04:

PANEL 1 - BEACH - 44 SAMPLES of Coated Steel(16); Duplex System(27); Zinc Thermal Sprayed(01)								
ICZ 10	ICZ 13	ICZ 16	ICZ 19	ICZ 22	ICZ 25	ICZ 28	ICZ 31	ICZ 34
ICZ 40	ICZ 43	ICZ 46	ICZ 49	ICZ 52	ICZ 55	ICZ 58	ICZ 61	ICZ 64
ICZ 70	ICZ 73	ICZ 76	ICZ 79	ICZ 82	ICZ 85	ICZ 88	ICZ 91	ICZ 94
ICZ 100	ICZ 103	ICZ 106	ICZ 109	ICZ 112	ICZ 115	ICZ 118	ICZ 121	ICZ 124
ICZ 130	ICZ 133	ICZ 136	ICZ 139					
ICZ 37	ICZ 67	ICZ 97	ICZ 127					



Figure 05:

PANEL 2 - BEACH - 46 SAMPLES of Coated Steel(16); Duplex System(29); Zinc Thermal Sprayed(01)								
ICZ 11	ICZ 14	ICZ 17	ICZ 20	ICZ 23	ICZ 26	ICZ 29	ICZ 32	ICZ 35
ICZ 41	ICZ 44	ICZ 47	ICZ 50	ICZ 53	ICZ 56	ICZ 59	ICZ 62	ICZ 65
ICZ 71	ICZ 74	ICZ 77	ICZ 80	ICZ 83	ICZ 86	ICZ 89	ICZ 92	ICZ 95
ICZ 101	ICZ 104	ICZ 107	ICZ 110	ICZ 113	ICZ 116	ICZ 119	ICZ 122	ICZ 125
ICZ 131	ICZ 134	ICZ 137	ICZ 140	ICZ 142	ICZ 144			
ICZ 38	ICZ 68	ICZ 98	ICZ 128					



ICZ - INSTITUTO DE METAIS NÃO FERROSOS

Figure 06:

PANEL 3 - BEACH - 49 SAMPLES of Coated Steel(16); Duplex System(29); Zinc Thermal Sprayed(01); 03 Uncoated HDG steel.									
ICZ 12	ICZ 15	ICZ 18	ICZ 21	ICZ 24	ICZ 27	ICZ 30	ICZ 33	ICZ 36	ICZ 39
ICZ 42	ICZ 45	ICZ 48	ICZ 51	ICZ 54	ICZ 57	ICZ 60	ICZ 63	ICZ 66	ICZ 69
ICZ 72	ICZ 75	ICZ 78	ICZ 81	ICZ 84	ICZ 87	ICZ 90	ICZ 93	ICZ 96	ICZ 99
ICZ 102	ICZ 105	ICZ 108	ICZ 111	ICZ 114	ICZ 117	ICZ 120	ICZ 123	ICZ 126	ICZ 129
ICZ 132	ICZ 135	ICZ 138	ICZ 141	ICZ 143	ICZ 145	ICZ 02.01	ICZ 03.01	ICZ 04.01	



Figure 07:



Figure 08:



ICZ - INSTITUTO DE METAIS NÃO FERROSOS

Figure 09:



Figure 10:



ICZ - INSTITUTO DE METAIS NÃO FERROSOS

Figure 11:



Figure 12:



ICZ - INSTITUTO DE METAIS NÃO FERROSOS

Figure 13:



Figure 13



Figure 14



Figure 15:



Figure 16

ICZ - INSTITUTO DE METAIS NÃO FERROSOS



Figure 17



Figure 18A



Figure 18B

ICZ - INSTITUTO DE METAIS NÃO FERROSOS



Figure 19A



Figure 19B



Figure 20A



Figure 20B

ICZ - INSTITUTO DE METAIS NÃO FERROSOS



Figure 21A

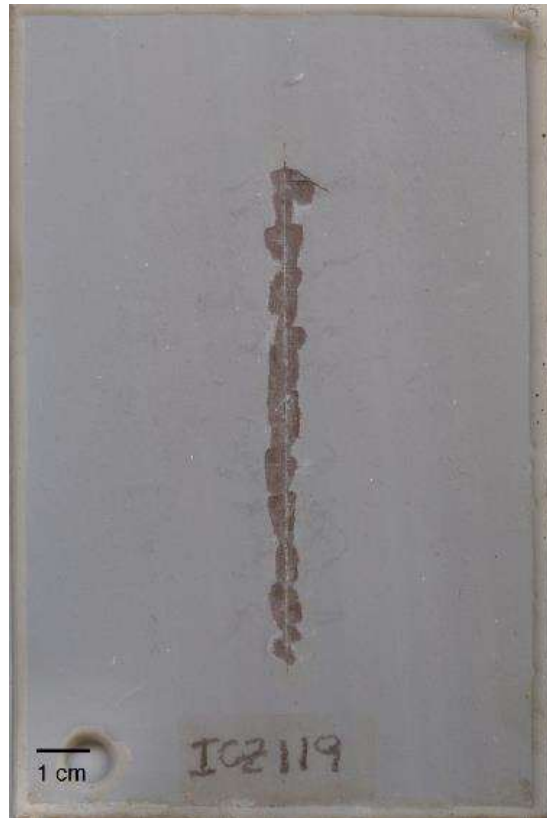


Figure 21B



Figure 22A



Figure 22B

ICZ - INSTITUTO DE METAIS NÃO FERROSOS



Figure 23A



Figure 23B



Figure 24

ICZ - INSTITUTO DE METAIS NÃO FERROSOS



Figure 25

ICZ - INSTITUTO DE METAIS NÃO FERROSOS



Figure 26



Figure 27

ICZ - INSTITUTO DE METAIS NÃO FERROSOS



Figure 28



Figure 29

ICZ PAPER INTERGALVA 2018 - APPENDIX – Samples - Field Tests - Atalaia Beach - ICZ Petrobras
 Title: Field Tests of Duplex System at O&G Company in Brazil
 Affiliation/Company: Paper ICZ – Non-Ferrous Metals Institute

DUPLEX SYSTEM PERFORMANCE TESTS									
Samples planning for field tests - Atalaia Beach - Sergipe									
Item	Samples	Supplier	INTERNAL CODE	ICZ EXTERNAL CODE	ABNT NBR STANDARD	Quantity			
						Minimum number of samples per material	Type of paint (systems)	Sub Total	Total with "135 of mirrors".
						-	15	199	268
1	Carbon steel	Armco Staco		ICZ 01.01 à ICZ 01.30	ISO 8501-1 blasted carbon steel SA2.5	3		30	1
2	Hot dip galvanized carbon steel	Armco Staco		ICZ 02.01 à ICZ 02.19		3	-	19	1
3	Hot dip galvanized carbon steel with longitudinal incision of 0.5 mm of thickness	Armco Staco		ICZ 03.01 à ICZ 03.07		3	-	7	1
4	Hot dip galvanized carbon steel with longitudinal incision of 2.0 mm of thickness	Armco Staco		ICZ 04.01 à ICZ 04.07		3	-	7	1

PINTURA PELA MARANGONI									
5	Coated carbon steel by MARANGONI	Marangoni	Goniwater IN DTM F140+Goniwater IN Enamel	ICZ 10	ISO 8501-1-blasted carbon steel SA2.5	3	3	9	18
			Goniwater IN DTM F140+Goniwater IN Enamel	ICZ 11					
			Goniwater IN DTM F140+Goniwater IN Enamel	ICZ 12					
			Goniwater IN DTM F140+Goniwater IN DTM F228	ICZ 13					
			Goniwater IN DTM F140+Goniwater IN DTM F228	ICZ 14					
			Goniwater IN DTM F140+Goniwater IN DTM F228	ICZ 15					
			Goniwater IN DTM F228	ICZ 16					
			Goniwater IN DTM F228	ICZ 17					
6	Hot dip galvanized carbon steel with longitudinal incision of 0.5 mm of thickness by MARANGONI	Marangoni	Goniwater IN DTM F140+Goniwater IN Enamel	ICZ 19	ISO 8501-1-blasted carbon steel SA2.5	3	3	9	18
			Goniwater IN DTM F140+Goniwater IN Enamel	ICZ 20					
			Goniwater IN DTM F140+Goniwater IN Enamel	ICZ 21					
			Goniwater IN DTM F140+Goniwater IN DTM F228	ICZ 22					
			Goniwater IN DTM F140+Goniwater IN DTM F228	ICZ 23					
			Goniwater IN DTM F140+Goniwater IN DTM F228	ICZ 24					
			Goniwater IN DTM F228	ICZ 25					
			Goniwater IN DTM F228	ICZ 26					
7	Hot dip galvanized carbon steel by Armco Staco (A.S) and coated (duplex system) by MARANGONI	Marangoni	Goniwater IN DTM F140+Goniwater IN Enamel	ICZ 28	11297	3	3	9	18
			Goniwater IN DTM F140+Goniwater IN Enamel	ICZ 29					
			Goniwater IN DTM F140+Goniwater IN Enamel	ICZ 30					
			Goniwater IN DTM F140+Goniwater IN DTM F228	ICZ 31					
			Goniwater IN DTM F140+Goniwater IN DTM F228	ICZ 32					
			Goniwater IN DTM F140+Goniwater IN DTM F228	ICZ 33					
			Goniwater IN DTM F228	ICZ 34					
			Goniwater IN DTM F228	ICZ 35					
8	Hot dip galvanized carbon steel by MARANGONI and coated (duplex system) by MARANGONI	Marangoni	Goniwater IN DTM F140+Goniwater IN Enamel	ICZ 37	11298	3	1	3	6
			Goniwater IN DTM F140+Goniwater IN Enamel	ICZ 38					
			Goniwater IN DTM F140+Goniwater IN Enamel	ICZ 39					
9	Hot dip galvanized carbon steel by MARANGONI, not passivated and coated (duplex system) by MARANGONI	Marangoni	Goniwater IN DTM F140+Goniwater IN Enamel	ICZ 40	11299	3	1	3	6
			Goniwater IN DTM F140+Goniwater IN Enamel	ICZ 41					
			Goniwater IN DTM F140+Goniwater IN Enamel	ICZ 42					
10	Hot dip galvanized carbon steel and coated (duplex system) with longitudinal incision of 0.5 mm of thickness by MARANGONI	Marangoni	Goniwater IN DTM F140+Goniwater IN Enamel	ICZ 43	11297 / 10253	3	3	9	18
			Goniwater IN DTM F140+Goniwater IN Enamel	ICZ 44					
			Goniwater IN DTM F140+Goniwater IN Enamel	ICZ 45					
			Goniwater IN DTM F140+Goniwater IN DTM F228	ICZ 46					
			Goniwater IN DTM F140+Goniwater IN DTM F228	ICZ 47					
			Goniwater IN DTM F140+Goniwater IN DTM F228	ICZ 48					
			Goniwater IN DTM F228	ICZ 49					
			Goniwater IN DTM F228	ICZ 50					
11	Thermal Spray coated carbon steel and coated by the MARANGONI	Marangoni	Goniwater IN DTM F140+Goniwater IN Enamel	ICZ 52		3	1	3	6
			Goniwater IN DTM F140+Goniwater IN Enamel	ICZ 53					
			Goniwater IN DTM F140+Goniwater IN Enamel	ICZ 54					

COATED BY TRIFER									
12	Hot dip galvanized carbon steel and coated (duplex system) by Trifer	Trifer	Electrostatic powder coating.	ICZ 55	11297	3	1	3	6
				ICZ 56					
				ICZ 57					
13	Hot dip galvanized carbon steel by Trifer and coated (duplex system) by Trifer with longitudinal incision	Trifer	Electrostatic powder coating.	ICZ 58	11298	3	1	3	6
				ICZ 59					
				ICZ 60					
14	Hot dip galvanized carbon steel and coated (duplex system) by Trifer	Trifer	Electrostatic powder coating.	ICZ 61	11297 / 10253	3	1	3	6
				ICZ 62					
				ICZ 63					
15	Hot dip galvanized carbon steel and coated (duplex system) by Trifer with longitudinal incision	Trifer	Electrostatic powder coating.	ICZ 64	11298 / 10253	3	1	3	6
				ICZ 65					
				ICZ 66					

SYSTEM 01 SHERWIN - WILLIAMS TOTAL						3	5	15	30
16	Hot dip galvanized carbon steel blasted and coated (duplex system) (GB)	Sherwin - Williams	System 01: PRIMER: 1 d Epoxy-isocyanate (N-2198) (25 µm); INTERM.: 1 d Epoxy-polyamide (N-2628) (175 µm); Finish: 2 d polyurethane (N-2677) (60 µm) Thickness Total: 320 µm	ICZ 67	1				
				ICZ 68	1				
				ICZ 69	1				
	hot dip galvanized carbon steel (SCOTCH BRITE) brushed, DEGREASED and coated (duplex) (GD)	Sherwin - Williams	System 01: PRIMER: 1 d Epoxy-isocyanate (N-2198) (25 µm); INTERM.: 1 d Epoxy-polyamide (N-2628) (175 µm); Finish: 2 d polyurethane (N-2677) (60 µm) Thickness Total: 320 µm	ICZ 70	1				
				ICZ 71	1				
				ICZ 72	1				
	Hot dip galvanized carbon steel, blasted, coated (duplex system) and with LONGITUDINAL INCISION of 0.5 mm (GBI)	Sherwin - Williams	System 01: PRIMER: 1 d Epoxy-isocyanate (N-2198) (25 µm); INTERM.: 1 d Epoxy-polyamide (N-2628) (175 µm); Finish: 2 d polyurethane (N-2677) (60 µm) Thickness Total: 320 µm	ICZ 73	1				
				ICZ 74	1				
				ICZ 75	1				
	Blasted carbon steel and coated (CS)	Sherwin - Williams	System 01: PRIMER: 1 d Epoxy-isocyanate (N-2198) (25 µm); INTERM.: 1 d Epoxy-polyamide (N-2628) (175 µm); Finish: 2 d polyurethane (N-2677) (60 µm) Thickness Total: 320 µm	ICZ 76	1				
				ICZ 77	1				
				ICZ 78	1				
	Blasted carbon steel and coated with LONGITUDINAL INCISION of 0.5 mm of thickness (CSI)	Sherwin - Williams	System 01: PRIMER: 1 d Epoxy-isocyanate (N-2198) (25 µm); INTERM.: 1 d Epoxy-polyamide (N-2628) (175 µm); Finish: 2 d polyurethane (N-2677) (60 µm) Thickness Total: 320 µm	ICZ 79	1				
				ICZ 80	1				
				ICZ 81	1				
SYSTEM 02 SHERWIN - WILLIAMS TOTAL						3	5	15	30
17	Hot dip galvanized carbon steel blasted and coated (duplex system) (GB)	Sherwin - Williams	System 02 PRIMER: 1 d/AMINE Epoxy Primer grey (25 µm); INTERMEDIATE: no; Finishing: 1 d 2Poliuretano (N-2677) (70 µm thickness: 95 µm)	Total	ICZ 82	1			
					ICZ 83	1			
					ICZ 84	1			
	hot dip galvanized carbon steel (SCOTCH BRITE) brushed, DEGREASED and coated (duplex) (GD)	Sherwin - Williams	System 02 PRIMER: 1 d/AMINE Epoxy Primer grey (25 µm); INTERMEDIATE: no; Finishing: 1 d 2Poliuretano (N-2677) (70 µm thickness: 95 µm)	Total	ICZ 85	1			
					ICZ 86	1			
					ICZ 87	1			
	Hot dip galvanized carbon steel, blasted, coated (duplex system) and with LONGITUDINAL INCISION of 0.5 mm (GBI)	Sherwin - Williams	System 02 PRIMER: 1 d/AMINE Epoxy Primer grey (25 µm); INTERMEDIATE: no; Finishing: 1 d 2Poliuretano (N-2677) (70 µm thickness: 95 µm)	Total	ICZ 88	1			
					ICZ 89	1			
					ICZ 90	1			
	Blasted carbon steel and coated (CS)	Sherwin - Williams	System 02 PRIMER: 1 d/AMINE Epoxy Primer grey (25 µm); INTERMEDIATE: no; Finishing: 1 d 2Poliuretano (N-2677) (70 µm thickness: 95 µm)	Total	ICZ 91	1			
					ICZ 92	1			
					ICZ 93	1			
	Blasted carbon steel and coated with LONGITUDINAL INCISION of 0.5 mm of thickness (CSI)	Sherwin - Williams	System 02 PRIMER: 1 d/AMINE Epoxy Primer grey (25 µm); INTERMEDIATE: no; Finishing: 1 d 2Poliuretano (N-2677) (70 µm thickness: 95 µm)	Total	ICZ 94	1			
					ICZ 95	1			
					ICZ 96	1			

SYSTEM 03 SHERWIN - WILLIAMS TOTAL						3	5	15	30
18	Hot dip galvanized carbon steel blasted and coated (duplex system) (GB)	Sherwin - Williams	System 03: PRIMER: 1 d Damp Tolerant Epoxy (N-2680) (150 µm); INTERMEDIATE: 1 d Epoxy-polyamide (N-2628) (100 µm); Finish: Polyurethane 1 d (N-2677) (70 µm) Thickness Total: 320 µm	ICZ 97	1				
				ICZ 98	1				
				ICZ 99	1				
	hot dip galvanized carbon steel (SCOTCH BRITE) brushed, DEGREASED and coated (duplex) (GD)	Sherwin - Williams	System 03: PRIMER: 1 d Damp Tolerant Epoxy (N-2680) (150 µm); INTERMEDIATE: 1 d Epoxy-polyamide (N-2628) (100 µm); Finish: Polyurethane 1 d (N-2677) (70 µm) Thickness Total: 320 µm	ICZ 100	1				
				ICZ 101	1				
				ICZ 102	1				
	Hot dip galvanized carbon steel, blasted, coated (duplex system) and with LONGITUDINAL INCISION of 0.5 mm (GBI)	Sherwin - Williams	System 03: PRIMER: 1 d Damp Tolerant Epoxy (N-2680) (150 µm); INTERMEDIATE: 1 d Epoxy-polyamide (N-2628) (100 µm); Finish: Polyurethane 1 d (N-2677) (70 µm) Thickness Total: 320 µm	ICZ 103	1				
				ICZ 104	1				
				ICZ 105	1				
	Blasted carbon steel and coated (CS)	Sherwin - Williams	System 03: PRIMER: 1 d Damp Tolerant Epoxy (N-2680) (150 µm); INTERMEDIATE: 1 d Epoxy-polyamide (N-2628) (100 µm); Finish: Polyurethane 1 d (N-2677) (70 µm) Thickness Total: 320 µm	ICZ 106	1				
				ICZ 107	1				
				ICZ 108	1				
	Blasted carbon steel and coated with LONGITUDINAL INCISION of 0.5 mm of thickness (CSI)	Sherwin - Williams	System 03: PRIMER: 1 d Damp Tolerant Epoxy (N-2680) (150 µm); INTERMEDIATE: 1 d Epoxy-polyamide (N-2628) (100 µm); Finish: Polyurethane 1 d (N-2677) (70 µm) Thickness Total: 320 µm	ICZ 109	1				
				ICZ 110	1				
				ICZ 111	1				
SYSTEM 04 SHERWIN - WILLIAMS TOTAL						3	5	15	30
19	Hot dip galvanized carbon steel blasted and coated (duplex system) (GB)	Sherwin - Williams	System 04 PRIMER: 1 d Epoxy Micaceous Iron oxide (100 µm); INTERMEDIATE: no; Finish: Polyurethane 1 d (N-2677) (70 µm) Thickness Total: 170 µm	ICZ 112	1				
				ICZ 113	1				
				ICZ 114	1				
	hot dip galvanized carbon steel (SCOTCH BRITE) brushed, DEGREASED and coated (duplex) (GD)	Sherwin - Williams	System 04 PRIMER: 1 d Epoxy Micaceous Iron oxide (100 µm); INTERMEDIATE: no; Finish: Polyurethane 1 d (N-2677) (70 µm) Thickness Total: 170 µm	ICZ 115	1				
				ICZ 116	1				
				ICZ 117	1				
	Hot dip galvanized carbon steel, blasted, coated (duplex system) and with LONGITUDINAL INCISION of 0.5 mm (GBI)	Sherwin - Williams	System 04 PRIMER: 1 d Epoxy Micaceous Iron oxide (100 µm); INTERMEDIATE: no; Finish: Polyurethane 1 d (N-2677) (70 µm) Thickness Total: 170 µm	ICZ 118	1				
				ICZ 119	1				
				ICZ 120	1				
	Blasted carbon steel and coated (CS)	Sherwin - Williams	System 04 PRIMER: 1 d Epoxy Micaceous Iron oxide (100 µm); INTERMEDIATE: no; Finish: Polyurethane 1 d (N-2677) (70 µm) Thickness Total: 170 µm	ICZ 121	1				
				ICZ 122	1				
				ICZ 123	1				
	Blasted carbon steel and coated with LONGITUDINAL INCISION of 0.5 mm of thickness (CSI)	Sherwin - Williams	System 04 PRIMER: 1 d Epoxy Micaceous Iron oxide (100 µm); INTERMEDIATE: no; Finish: Polyurethane 1 d (N-2677) (70 µm) Thickness Total: 170 µm	ICZ 124	1				
				ICZ 125	1				
				ICZ 126	1				

SYSTEM 05 SHERWIN - WILLIAMS TOTAL						3	5	15	30
20	Hot dip galvanized carbon steel blasted and coated (duplex system) (GB)	Sherwin - Williams	System 05: 1 Epoxy Polyamide PRIMER: d (50 µm); INTERMEDIATE: 1 d Polyamide Epoxy (200 µm); Finish: Polyurethane 1 d (N-2677) (70 µm) Thickness Total: 320 µm	ICZ 127	1				
				ICZ 128	1				
				ICZ 129	1				
	hot dip galvanized carbon steel (SCOTCH BRITE) brushed, DEGREASED and coated (duplex) (GD)	Sherwin - Williams	System 05: 1 Epoxy Polyamide PRIMER: d (50 µm); INTERMEDIATE: 1 d Polyamide Epoxy (200 µm); Finish: Polyurethane 1 d (N-2677) (70 µm) Thickness Total: 320 µm	ICZ 130	1				
				ICZ 131	1				
				ICZ 132	1				
	Hot dip galvanized carbon steel, blasted, coated (duplex system) and with LONGITUDINAL INCISION of 0.5 mm (GBI)	Sherwin - Williams	System 05: 1 Epoxy Polyamide PRIMER: d (50 µm); INTERMEDIATE: 1 d Polyamide Epoxy (200 µm); Finish: Polyurethane 1 d (N-2677) (70 µm) Thickness Total: 320 µm	ICZ 133	1				
				ICZ 134	1				
				ICZ 135	1				
	Blasted carbon steel and coated (CS)	Sherwin - Williams	System 05: 1 Epoxy Polyamide PRIMER: d (50 µm); INTERMEDIATE: 1 d Polyamide Epoxy (200 µm); Finish: Polyurethane 1 d (N-2677) (70 µm) Thickness Total: 320 µm	ICZ 136	1				
				ICZ 137	1				
				ICZ 138	1				
	Blasted carbon steel and coated with LONGITUDINAL INCISION of 0.5 mm of thickness (CSI)	Sherwin - Williams	System 05: 1 Epoxy Polyamide PRIMER: d (50 µm); INTERMEDIATE: 1 d Polyamide Epoxy (200 µm); Finish: Polyurethane 1 d (N-2677) (70 µm) Thickness Total: 320 µm	ICZ 139	1				
				ICZ 140	1				
				ICZ 141	1				
SYSTEM 06 SHERWIN - WILLIAMS TOTAL						2	1	2	0
21	Hot dip galvanized carbon steel treated with SULFOSSILANE-based pretreatment SO42- (sulphate tetrahydrate + Silanes (4 molecules of sulfur) and coated.	Sherwin - Williams	System 06: PRIMER: 1 d Damp Tolerant Epoxy (N-2680) (150 µm); INTERMEDIATE: 1 d Epoxy-polyamide (N-2628) (100 µm); Finish: Polyurethane 1 d (N-2677) (70 µm) Thickness Total: 320 µm	ICZ 142	1				
	Hot dip galvanized carbon steel treated with SULFOSSILANE-based pretreatment SO42- (sulphate tetrahydrate + Silanes (4 molecules of sulfur) and coated. with LONGITUDINAL INCISION of 0.5 mm of thickness	Sherwin - Williams	System 06: PRIMER: 1 d Damp Tolerant Epoxy (N-2680) (150 µm); INTERMEDIATE: 1 d Epoxy-polyamide (N-2628) (100 µm); Finish: Polyurethane 1 d (N-2677) (70 µm) Thickness Total: 320 µm	ICZ 143	1				

SYSTEM 07 SHERWIN - WILLIAMS TOTAL						2	1	2	0
22	Hot dip galvanized carbon steel treated with a pretreatment with hybrid (silanes based on epoxy). Note: there's a Silane that is much more resilient and has thickness of 1 micron, painted.	Sherwin - Williams	System 07: PRIMER: 1 d Damp Tolerant Epoxy (N-2680) (150 µm); INTERMEDIATE: 1 d Epoxy-polyamide (N-2628) (100 µm); Finish: Polyurethane 1 d (N-2677) (70 µm) Thickness Total: 320 µm	ICZ 144	2680	1			
	hot dip galvanized carbon steel treated with a pretreatment with hybrid (Silanes based on Epoxy). Note: Ther is Silanes but is much more resistant and has thickness of 1 micron, painted with longitudinal incision of 0.5 mm.	Sherwin - Williams	System 07: PRIMER: 1 d Damp Tolerant Epoxy (N-2680) (150 µm); INTERMEDIATE: 1 d Epoxy-polyamide (N-2628) (100 µm); Finish: Polyurethane 1 d (N-2677) (70 µm) Thickness Total: 320 µm	ICZ 145		1			
SUMMARY OF AMOUNT OF SAMPLES BY SUPPLIER			Armco	63					
			Marangoni	45					
			Trifer	12					
			Sherwin-Williams	79					
			Total	199					

Durability determination of bridge constructions protected by hot dip galvanized coatings

Dipl.-Ing. (FH), IWE Peter Lebelt

Institut für Korrosionsschutz Dresden GmbH, peter.lebelt@iks-dresden.de

Dr.-Ing. Jörg Gehrke

Institut für Korrosionsschutz Dresden GmbH, joerg.gehrke@iks-dresden.de

Abstract:

In Germany and Europe pollution has been reduced systematically by stricter legal regulation with the determination of lower emission limit values in the past decades. Due to reduced pollution lower corrosivity and, thus, higher durability of zinc coatings in natural atmosphere were expected. Ordered by the Gemeinschaftsausschuss Verzinken e.V. (GAV) and directed by the Institut für Korrosionsschutz Dresden GmbH (IKS Dresden GmbH) exposure tests with standardized corrosion test specimens in accordance with ISO 9226 [1] on six selected road bridges in Germany were initiated in May 2011. The objectives were to determine the current atmospheric corrosivity and to gain information on the long-term corrosion behaviour of zinc coatings, in order to safeguard their application as maintenance-free corrosion protection system for dynamically loaded bridge constructions [2].

Introduction

The corrosive stress on steel constructions in natural atmosphere is caused to a large extent by the presence of an electrolyte (e.g. condensation water, precipitation, splash water) as well as simultaneous oxygen supply and the exposure duration of both of these components at a given temperature. Further, salts, sulphur dioxide and dust have additional accelerating effects on corrosion. For this reason steel constructions are protected from weathering conditions by corrosion protection systems. In case the electrolyte is absent or present in solid form at low temperatures, the atmospheric corrosion is disrupted. Removing the oxidant oxygen leads to disruption of the atmospheric corrosion reaction only in gas-tight spaces (e.g. box girders being hermetically sealed by welding). The absence of accelerating corrosion stimulants also has positive effects of decreased corrosion rates.

Between 1990 and 2015, according to information by the German Federal Environmental Agency, a significant decrease of exposure of pollutants in the atmosphere was detected [3] (see Figure 1). Due to decreased exposure of NO_x by 58,9%, SO₂ by 93,6% and NH₃ by 4,3% in the atmosphere in 2015 related to 100% in 1990, generally, an improvement of the air quality and, thus, a reduction of the corrosive stress can be assumed.

The improvement of the air quality becomes clear, as follows, by the decrease of the sulphur dioxide concentration within 10 years. While in 1990 an annual average concentration of sulphur dioxide of >175 µg/m³ was determined, already 10 years later the concentration of only 19 µg/m³ as maximum average value was determined in a German measuring station [4]. For the determination of current annual average values of the sulphur dioxide concentration in the atmosphere the German Federal Environmental Agency provided the data of daily measuring values of a one-year measuring period for four randomly selected measuring stations in Germany for a research project. The following Table 1 gives the annual average values calculated from this data. The continuing decrease of the sulphur dioxide concentration in comparison to the preceding years is clearly detectable.

Especially the decrease of the sulphur dioxide concentration has a positive effect on the corrosive stress, since sulphur dioxide is responsible for so-called "acid rain". The presence of sulphur dioxide leads to accelerated corrosion reactions for structural steel as well as for zinc. Is the electrolyte (rain, dew, fog) lacking this chemical compound corrosion activity decreases and with it the corrosion rate as well. The sulphur dioxide content also has direct influence on the determination of the corrosivity category, since it is included in the calculation of the corrosion rate in accordance with DIN EN ISO 9223 [5] as parameter P_d.

Another important influencing parameter for the corrosivity is the chloride concentration, which is also included in the calculation of the corrosion rate as parameter S_d in accordance with DIN EN ISO 9223 [5]. The atmospheric influence, however, is limited to coastal regions, since the chloride concentration quickly decreases [6] with increasing distance to the coast, measured in the Netherlands, see Table 2. Regarding

the influence of non-natural sources, such as road salt, the influence of the chloride concentration shall definitely be considered.

In terms of corrosion protection of atmospherically stressed steel components hot-dip galvanizing has proved itself under mainly static loading. A durability of several decades without maintenance and repair is normal. In regard to many hot-dip galvanized constructions the durability of the hot-dip galvanized coating reaches the service life of the construction without any required repair of the corrosion protection system zinc coating. Compared to commercial organic corrosion protection systems, which according to experience have to be maintained and renewed in intervals of 25 to 35 years, hot-dip galvanized coatings can be a very economic measure of corrosion protection in consideration of the service life of steel constructions [7].

Ordered by the Gemeinschaftsausschuss Verzinken e.V. (GAV) and directed by the Institut für Korrosionsschutz Dresden GmbH (IKS Dresden GmbH) exposure tests with standardized corrosion test specimens in accordance with ISO 9226 on six selected road bridges in Germany were initiated in May 2011 for the examination of the current corrosivity of the atmosphere and its further development [8].

Determination of the corrosivity category of the atmosphere on road bridges

For the determination of the current corrosivity category of the atmosphere standard test specimens/spirals in accordance with ISO 9226 made of unalloyed steel (Cu: 0,03-0,1%; P: < 0,07%; rest: Fe), zinc with 99,99%, copper with 99,5%, aluminium with 99,5% and additional hot-dip galvanized steel wire were exposed on six selected bridge constructions in Germany by the IKS Dresden GmbH. The exposure locations are listed in Table 3.

In regard to the site selection it was attempted to consider as many load categories as possible. Thus, for example, an agricultural road bridge over motorway A4 between the junctions Gera-Leumnitz and Ronneburg with expected de-icing salt spray as well as a motorway bridge on A93 between Kiefersfelden and Kufstein over the Inn river with expected bedwing/condensation were selected. Three corrosion test specimens were positioned in each of two characteristic areas on the bottom sides of the bridges of every construction. The exposure sites for the selected bridges are illustrated in Figure 2 to Figure 7 [2].

The test specimens were exposed in the centre of the bridge, at the abutment or in correspondence with relevant cardinal points under the bridges and protected from direct precipitation. Figure 8, as an example, shows the exposure of the used test specimens on the agricultural road bridge BW 142Ü2 over motorway A4 in the centre at the support between the lanes.

The corrosion rates for zinc determined after the first year of exposure on the one hand served for the determination of the corrosivity categories on the respective construction and on the other hand as basis for the calculation of the forecast curve for the theoretically possible durability of the hot-dip galvanized coating on steel. The zinc spirals of the corrosion test specimens, naturally weathered for two and five years, were used for the examination of the forecast curve and the determined corrosivity category for zinc.

In the following Table 4 the corrosion rates and corrosivity categories on the bridge constructions determined after the first year of natural weathering are compared for zinc, separated according to exposure site 1 and 2.

In Table 5 the corrosivity categories of zinc determined on bridge undersides in the context of a BAST (Federal Highway Research Institute) - study from 1983 [9] are compared to the corrosivity categories determined in 2012. For this comparison the highest determined corrosion rate of two measuring sites of a bridge from 2012 was used.

In Table 5 a distinct decrease of the measured corrosion of zinc compared to 1983 is detectable. The corrosion decreased to half has the effect that the corrosivity categories on the atmosphere for the four comparable bridges from 1983 are lower up to one category in 2012. However, the results show, too, that an improvement of the macroclimate (less pollutants in the atmosphere) has only minor or no improving effects on the stresses caused by corrosion, if simultaneously a local additional stress, such as road salt, interferes (microclimate). In consequence, the road salt in the spray caused by traffic on the agricultural road bridge over motorway A4 led to a higher corrosivity than the rural, natural environment would have suggested. In Table 6 the covering mass per unit area of the ions measured on the base plates of the corrosion test specimens are compared to the exposure sites on 3 characteristic bridges [2].

The evaluation of the found salt covering gave the following results:

- Rader Hochbrücke: The base plate of site 1 in approx. 60 m height above the Kiel Canal shows a higher salt covering than the base plate of site 2 at a distance of 500 m on the abutment
- Agricultural road bridge over A4: The base plate of site 1 on the west side (weather side) shows a lower salt covering than the base plate of site 2 on the east side. On both base plates ammonium ions were detected, the origin of which cannot be certainly clarified. The deposition is possible from residues of the diesel additive AdBlue (ammonia slip) or from fertilization in agriculture.
- Innbrücke in Kiefersfelden: The base plate of site 1 above the agricultural road shows a higher salt covering than the base plate of site 2 above the Inn river.

The salt covering correlates with the determined corrosivity categories. The higher the salt covering on the base plate was the higher was the determined corrosivity category as well. That for similar salt covering not the same corrosivity category on the different bridges can be detected is attributed to the different climatic conditions (wetting duration, temperature) in the respective bridge location.

Forecast on the durability of hot-dip galvanized coatings

An extended corrosion protection effect is to be expected principally for all corrosion protection systems with the decrease of pollutants in the atmosphere. The reduction of the corrosivity, however, has an especially positive effect on zinc coatings with an extended durability forecast, since the coatings are removed more slowly by corrosion. While in 1983 corrosivity categories of C4 and C3 were still determined, today corrosivity categories of C3 and C2 can be measured on the same constructions. The assessment in regard to the zinc corrosion as declining (non-linear) corrosion behaviour is possible, in accordance with DIN EN ISO 9224 [10], up to a service life of 100 years. The forecast coating thicknesses for the corrosivity categories C2 to C5 are given in Table 7.

Assuming corrosivity category C4 and the evaluation in accordance with declining corrosion behaviour of the zinc coating arithmetically a zinc film thickness of approx. 113 μm to 225 μm would be required for the intended service life of 100 years. Now, based on the highest determined zinc corrosion rate on the examined bridges of 3,6 μm (agricultural road bridge over motorway A4 in Thuringia) after the first year of exposure as the basis for the precise declining extrapolation, for a thickness of the zinc coating of 152 μm ($t^b = 42,267$, Table 3; zinc; B1) to 201 μm ($t^b = 55,719$, Table 3; zinc; B2) a theoretical durability of 100 years results.

Comparison between forecast and measured zinc corrosion

Further measuring of the corrosion rate on corrosion test specimens allowed for the comparison of the calculated forecast curve for the theoretical continuing zinc corrosion from the first year of exposure with the actually determined values after two and five years of natural weathering. The results are illustrated in Figure 9 to Figure 14 for the six bridge constructions.

Based on the results it can be verified that the frequently used linear approach for the interpretation of the corrosion behaviour of zinc coatings, by multiplication of the years of exposure with the loss by corrosion of the first year of exposure, is an utterly conservative approach and falls short of the detected declining corrosion behaviour of zinc coatings.

Summary

The examinations in regard to the current corrosivities in Germany verify that the atmospheric pollution significantly decreased compared to 1983 and that the corrosion protection of structural steel by means of hot-dip galvanized coatings is theoretically feasible for the service life of 100 years and practicable without significant additional time and effort. Exposure tests on a bridge over a motorway show, that corrosivity category C4 shall be assumed under the predominant microclimate present there. Based on the exposed test specimens it can be shown that durabilities of 100 years can be reached with zinc film thicknesses of >200 μm , which are common for structural steel. The frequently used approach of the linear corrosive removal for the interpretation of the durability of zinc coatings, from the loss by corrosion of the first year of exposure, is utterly conservative and falls short of the actual declining corrosion behaviour and, thus, of the extended durability.

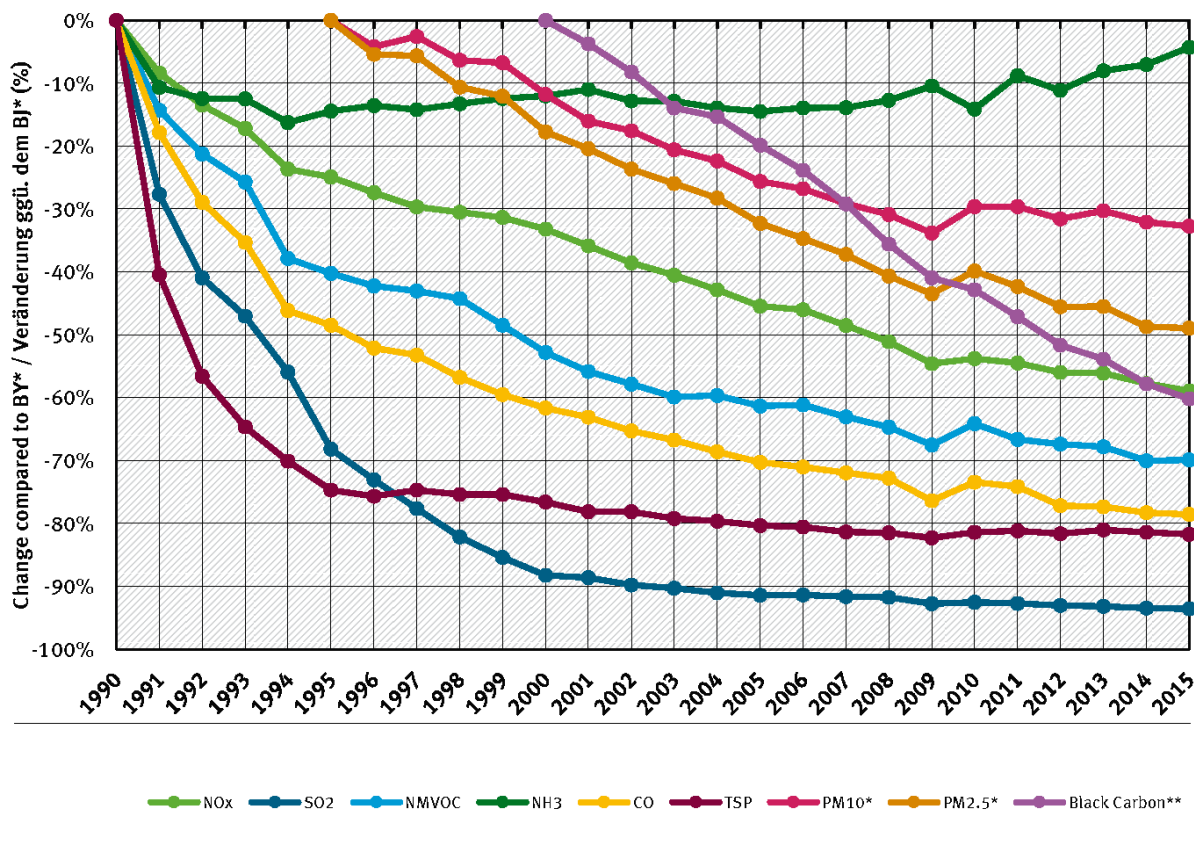
Acknowledgements

The results were determined in the context of an industrial research project in cooperation with the Gemeinschaftsausschuss Verzinken e.V. (GAV) and an AiF-IGF research project titled: "Feuerverzinken im Stahl- und Verbundbrückenbau" (FOSTA P835, IGF-No. 351/ZBG) of the Research Association for Steel Application (Forschungsvereinigung Stahlanwendung e.V. - FOSTA) in cooperation with the Gemeinschaftsausschuss Verzinken e.V. (GAV) and the Deutscher Ausschuß für Stahlbau (DASt) by order of the Federal Ministry for Economic Affairs and Energy. We would like to thank these institutions for their support and sponsorship.

Bibliography

- [1] ISO 9226, *Corrosion of metals and alloys - Corrosivity of atmospheres - Determination of corrosion rate of standard specimens for the evaluation of corrosivity*, Berlin: Beuth Verlag, 1992.
- [2] D. Ungermann, D. Rademacher, M. Oechsner, R. Landgrebe, J. Adelman, F. Simonsen, S. Friedrich and P. Lebelt, "Feuerverzinken im Stahl- und Verbundbrückenbau, IGF-No. 351/ZBG, FOSTA P835," Düsseldorf, 2014.
- [3] Umweltbundesamt, "Trend der Luftschadstoff-Emissionen," [Online]. Available: <https://www.umweltbundesamt.de/themen/luft/emissionen-von-luftschadstoffen/trend-der-luftschadstoff-emissionen>. [Accessed 28 März 2018].
- [4] Umweltbundesamt, "Historische Karten der Luftbelastung seit 1985," [Online]. Available: www.umweltbundesamt.de/themen/luft/daten-karten/entwicklung-der-luftqualitaet#textpart-4. [Accessed 28 März 2018].
- [5] DIN EN ISO 9223, *Korrosion von Metallen und Legierungen – Korrosivität von Atmosphären – Klassifizierung, Bestimmung und Abschätzung*, Berlin: Beuth Verlag GmbH, 05/2012.
- [6] *Merkblatt 400: „Korrosionsverhalten von feuerverzinktem Stahl“*, Düsseldorf: Stahl-Informations-Zentrum, ISSN 0175-2006, 6. Auflage 2001.
- [7] U. Kuhlmann, P. Maier, T. Ummenhofer, T. Zinke, M. Fischer and S. Schneider, "Untersuchung zur Nachhaltigkeitsberechnung von feuerverzinkten Stahlbrücken", vol. Heft B 112, Bundesanstalt für Straßenwesen, Ed., Bergisch Gladbach: Fachverlag NW in der Carl Schünemann Verlag GmbH, Februar 2015.
- [8] P. Lebelt and J. Gehrke, "GAV-Bericht 167: Korrosionsverhalten von Zink in natürlicher Atmosphäre," Gemeinschaftsausschuss Verzinken e.V., Düsseldorf, 2018.
- [9] Bundesanstalt für Straßenwesen, "Salzablagerungen auf Korrosionsschutzbeschichtungen an Brückenuntersichten, Heft 405," Typo-Druck- & Verlagsgesellschaft mbH, Bonn, 1983.
- [10] DIN EN ISO 9224, *Korrosion von Metallen und Legierungen - Korrosivität von Atmosphären - Anhaltswerte für die Korrosivitätskategorien*, Berlin: Beuth Verlag GmbH, 2012.

Figures and tables



* Base Year (BY) 1990, 1995 for PM10/PM2.5 / Basisjahr (BJ) 1990, 1995 für Feinstaub
 ** Black Carbon emissions from 2000 / Black Carbon Emissionen erst ab 2000

Quelle: German Emission Inventory (03.01.2017)

Figure 1: Emission trends of air pollutants for Germany [3]

Table 1: Annual average value SO₂, measuring period: 2015-07-01 to 2016-07-07

Selected measuring station in Germany	Average SO ₂ concentration
Datteln-Hagem, North Rhine-Westphalia	2,51 µg/m ³
Dresden Winkelmannstr., Saxony	3,11 µg/m ³
Zinnwald, Saxony	4,78 µg/m ³
Garz (Rügen), Mecklenburg-West Pomerania	0,79 µg/m ³

Table 2: Chloride content in rainwater in dependence of the distance to the sea

Distance from the coast in km	0,4	2,3	5,6	48	86
Chloride content in mg/l	16	9	7	4	3

Table 3: Selected bridge constructions for measuring the corrosivity category

Construction name	Federal state	Road/highway	Bridge over...
Rader Hochbrücke	Schleswig-Holstein	A7	Kiel Canal
Putlitz-Brücke	Berlin	Urban road	Road/railway
Müglitztalbrücke	Saxony	A17	Watercourse/road/railway
Agricultural road bridge	Thuringia	Field access	Federal motorway A4
Innbrücke	Bavaria	A93	Watercourse
Donaubrücke	Bavaria	A3	Watercourse

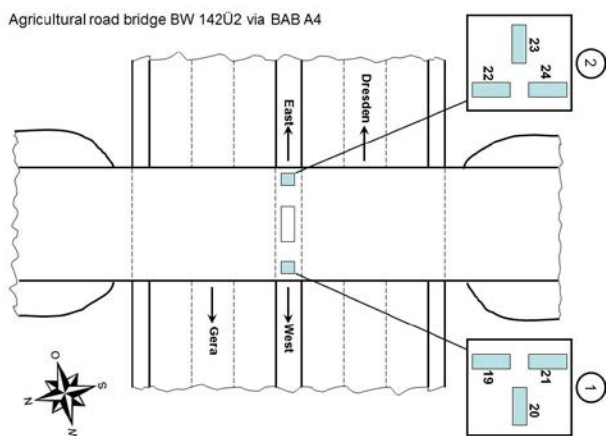


Figure 2: Position of test specimen at BW 142Ü2 bridge via BAB A4

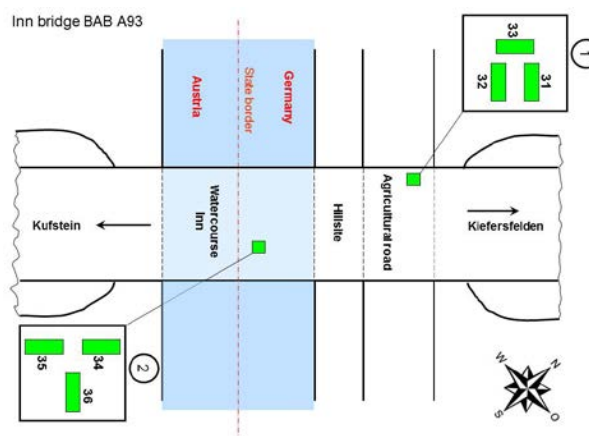


Figure 3: Position of test specimen Innbrücke BAB A93 near Kiefersfelden

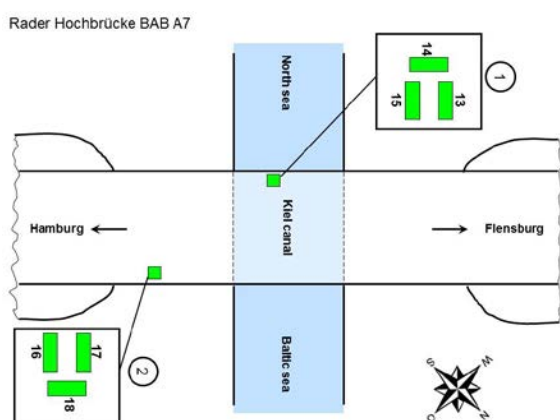


Figure 4: Position of test specimen Rader Hochbrücke BAB A7 near Rendsburg

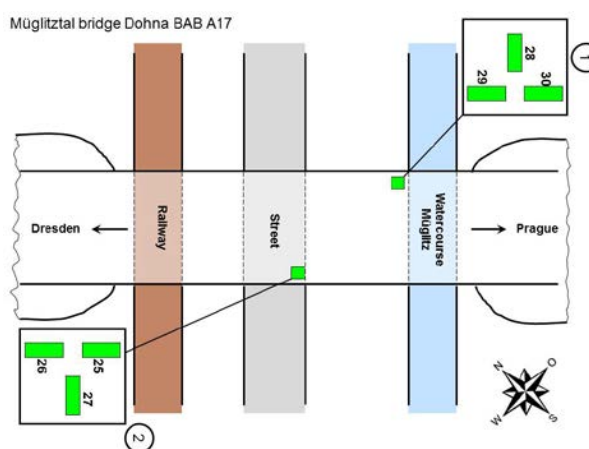


Figure 5: Position of test specimen Müglitztalbrücke BAB A17 near Heidenau

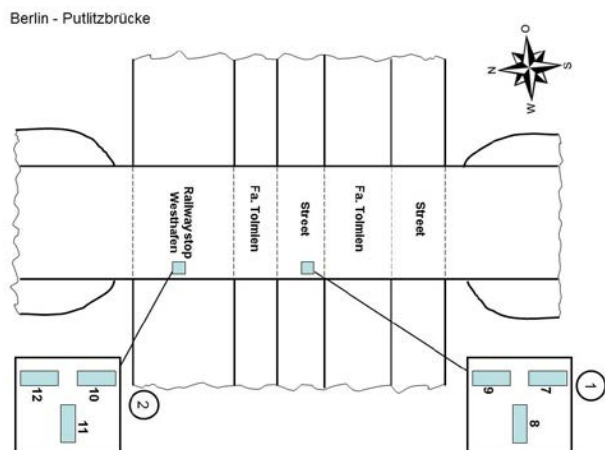


Figure 6: Position of test specimen Putlitzbrücke in Berlin

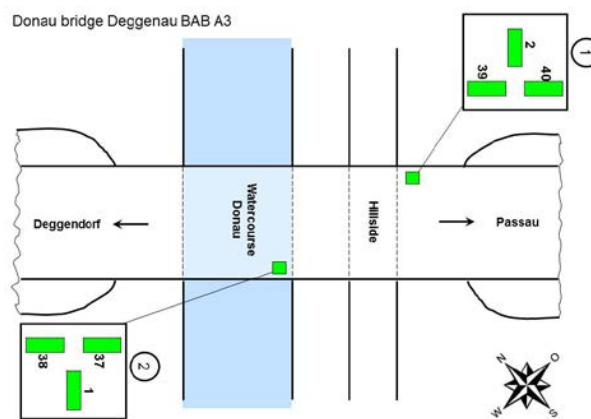


Figure 7: Position of test specimen Donaubrücke BAB A3 near Deggendorf (Deggenau)



Figure 8: Exposed test specimens on bridge over motorway A4 in Thuringia

Table 4: Corrosion rate and corrosivity category in 2012 after the 1st year of exposure

Bridge location	Zinc corrosion rate and corrosivity on exposure site 1	Zinc corrosion rate and corrosivity on exposure site 2
A4 agricultural road bridge BW 142Ü2 over motorway	2,65 µm/a / C4	3,6 µm/a / C4
Putlitzbrücke in Berlin over urban railway stop Westhafen	0,62 µm/a / C2	0,74 µm/a / C3
A7 "Hochbrücke Rader-Insel" near Rendsburg	1,31 µm/a / C3	1,7 µm/a / C3
A17 Bridge over Müglitz valley near Heidenau	0,48 µm/a / C2	0,65 µm/a / C2
A93 Bridge over the Inn river near Kiefersfelden	0,9 µm/a / C3	0,44 µm/a / C2
A3 Donaubrücke near Deggenau	0,54 µm/a / C2	0,62 µm/a / C2

Table 5: Corrosion rate and corrosivity category in comparison after the 1st year of exposure

Bridge location	Zinc corrosion rate / corrosivity category in 1983	Zinc corrosion rate / corrosivity category in 2012	Change of corrosivity category in 2012 compared to 1983
A4 agricultural road bridge BW 142U2 over motorway	No data	3,6 µm/a / C4	n/a
Putlitzbrücke in Berlin over urban railway stop Westhafen	2,7 µm/a / C4	0,74 µm/a / C3	Less
A7 "Hochbrücke Rader-Insel" near Rendsburg	2,4 µm/a / C4	1,7 µm/a / C3	Less
A17 Bridge over Müglitz valley near Heidenau	No data	0,65 µm/a / C2	n/a
A93 Bridge over the Inn river near Kiefersfelden	1,1 µm/a / C3	0,9 µm/a / C3	Less
A3 Donaubrücke near Deggenau	1,1 µm/a / C3	0,62 µm/a / C2	Less

Table 6: Determined salt covering on base plates of the test specimens exposed for one year

Ion concentration in the solution	No. of test specimen Rader Hochbrücke A7		No. of test specimen agricultural road bridge A4		No. of test specimen Innbrücke Kiefersfelden A93	
	Site 1	Site 2	Site 1	Site 2	Site 1	Site 2
Chloride in [mg/m ²]	843,1	343,1	718,44	1365,25	94,48	15,16
Nitrite in [mg/m ²]	<0,89	<0,93	<0,84	<1,74	0,85	<0,93
Nitrate in [mg/m ²]	<1,78	3,81	5,9	8,52	6,26	<1,86
Sulphate in [mg/m ²]	126,15	95,77	116,37	141,74	38,89	<1,86
Sodium in [mg/m ²]	511,72	247,33	693,14	719,15	112,89	11,44
Potassium in [mg/m ²]	20,17	29,94	4,22	<4,35	9,58	<4,65
Ammonium in [mg/m ²]	<0,89	<0,93	15,85	29,48	<0,95	<4,65
Magnesium in [mg/m ²]	13,24	<0,93	<0,84	<0,87	<0,95	<0,93
Calcium in [mg/m ²]	46,82	11,99	31,62	38,35	28,65	<4,65

< ... Element content lower than the detection limit given by numerical value

Table 7: Theoretically required thickness of zinc coating calculated in accordance with DIN EN ISO 9224 by means of the values from Table B.1

Corrosivity category	Zinc corrosion rate first 10 years r_{av} in µm/a		Zinc corrosion rate subsequent years stationary r_{lin} in µm/a		Theoretically required thickness of zinc coating for 100 years in µm	
	Min.	Max.	Min.	Max.	Min.	Max.
C2	0,07	0,5	0,05	0,4	5	41
C3	0,5	1,4	0,4	1,1	41	113
C4	1,4	2,7	1,1	2,2	113	225
C5	2,7	5,5	2,2	4,4	225	451

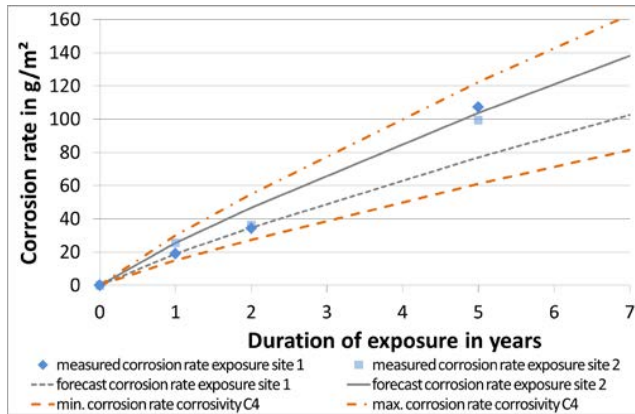


Figure 9: Zinc corrosion rate at agricultural road bridge BW 142Ü2 via BAB A4

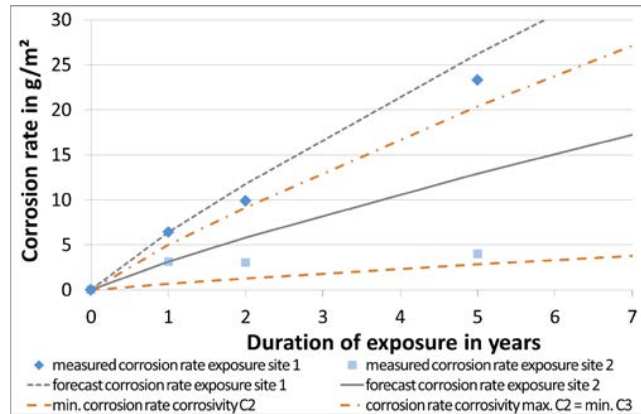


Figure 10: Zinc corrosion rate at Innbrücke BAB A93 near Kiefersfelden

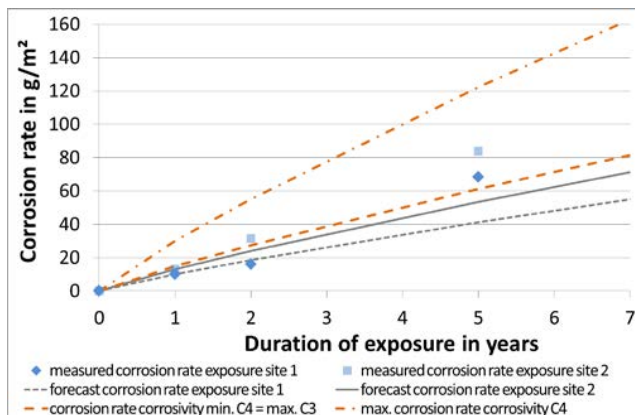


Figure 11: Zinc corrosion rate at Rader Hochbrücke BAB A7 near Rendsburg

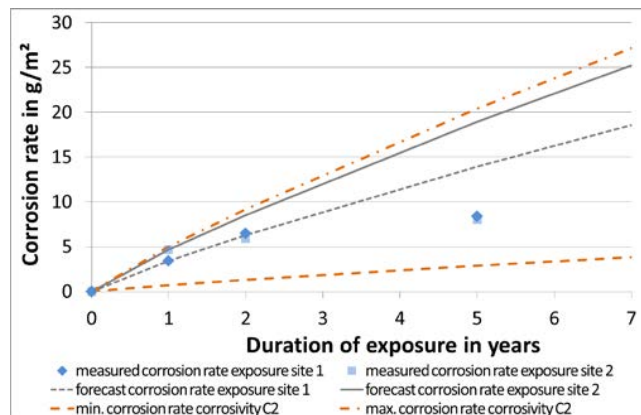


Figure 12: Zinc corrosion rate at Müglitztalbrücke BAB A17 near Heidenau

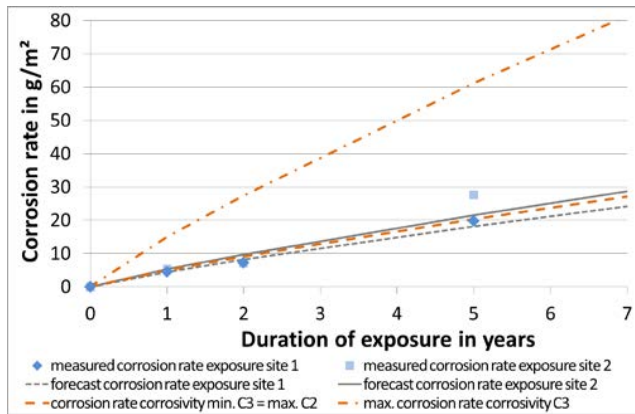


Figure 13: Zinc corrosion rate at Putlitzbrücke in Berlin

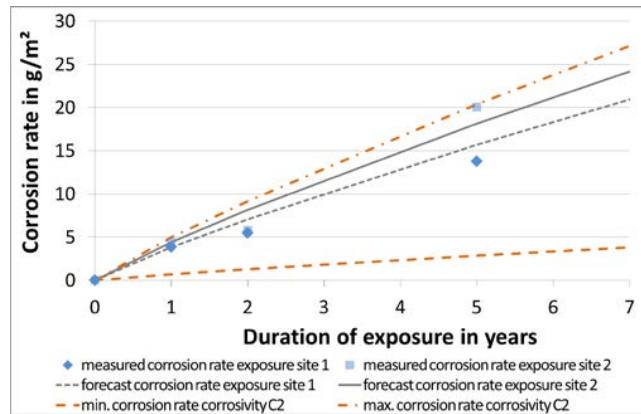


Figure 14: Zinc corrosion rate at Donaubrücke BAB A3 near Deggendorf (Deggenau)

Author Biographies

Peter Lebelt

Mr. Peter Lebelt, born in 1980, graduated in March 2006 from the University of Applied Sciences Mittweida with a degree to Dipl.-Ing. (FH) in the special field of surface and materials technology. In April 2007, he graduated as International Welding Engineer (IWE). Since March 2006, Mr. Lebelt has been working at the Institut für Korrosionsschutz Dresden GmbH as a research employee in the department of corrosion protection and process engineering. The focus of his work are scientific topics on joining technology, bonding technology, corrosion protection with organic coatings and zinc coatings, weathering steel and corrosivity of natural corrosion media. In addition, he is responsible for quality assurance site supervision and damage assessment in corrosion protection.

Dr. Jörg Gehrke

Dr.-Ing. Jörg Gehrke, born in 1967, graduated in 1995 from the Technical University Dresden with a degree to Dipl.-Ing. in the special field of machine engineering. In April 2000, he earned his doctorate in engineer science at the Technical University Dresden. Since November 2000, Dr.-Ing. Gehrke has been working at the Institut für Korrosionsschutz Dresden GmbH and since January 2006 he is heading the department of corrosion protection and process engineering. Since July 2015, Dr.-Ing. Gehrke has been working even as a publicly appointed and sworn expert for corrosion protection in steel, metal and vehicle construction.

Corrosion investigations on zinc coatings by using gel-type electrolytes

Martin Babutzka ¹, Andreas Burkert ¹, Andreas Heyn ²

¹ Bundesanstalt für Materialforschung und -prüfung (BAM), Berlin, Germany

² Otto von Guericke University Magdeburg, Magdeburg, Germany

Abstract

A new approach to the assessment of the corrosion behaviour of zinc coatings under atmospheric conditions can be achieved using gel-type electrolytes as an alternative to standard aqueous test electrolytes. Gel-type electrolytes allow minimally invasive corrosion investigations on zinc coatings. They also provide the possibility to carry out corrosion investigations onsite. By using gel-type electrolytes corrosion-relevant characteristic values such as corrosion currents and polarization resistances can be determined. These allow to describe the formation and the stability of the formed corrosion product layers under various climatic conditions. With this knowledge, a prediction of the zinc coating life cycle is possible. In this contribution, the value of gel-type electrolytes for corrosion research on zinc coatings is presented.

Problems with corrosion testing of zinc coatings

Recently, a significantly accelerated development of new zinc coating systems and alloys to ensure corrosion protection has been observed. This development is driven by the need for cost-effective but very efficient coatings in terms of corrosion protection that have to be as thin as possible. Zinc coatings provide a long life cycle, but corrosion protection is only ensured if a protective cover layer consisting of corrosion products in the form of zinc oxides, hydroxides and carbonates had the possibility to form itself on the surface through reactions with substances from the surrounding environment. Their formation and dissolution kinetics determine the consumption and the degradation of the coating under conditions of use and are therefore of crucial importance for the durability of the corrosion protection. New zinc coating systems are frequently developed by the automotive industry. The developers of new protection systems must always demonstrate the comparability with known systems in terms of the expected properties and the duration of protection. For this purpose, in the development phase primarily short-term chamber tests utilizing artificial climates are used. However, these chamber tests do not provide any reliable statements on the durability of a zinc coating and always use excessive test parameters to achieve the shortest possible test periods. Protective layers of corrosion products, which are crucial for the durability of a zinc coating, are destroyed during testing under these severe conditions (elevated temperature, highly concentrated salt solutions, excessive humidification periods) or cannot be formed. Corrosion conditions and corrosion phenomena are generated by sharpening the test conditions that often have no relevance under practical and realistic operating conditions [1]. Many of the current trends in zinc development are also attracting attention in other sectors, such as construction and civil engineering. The question arises again as to what corrosion performance the coating systems have regarding the specific requirements in these industries. A functionality of the corrosion protection over a period of 50 years and longer is needed. Currently available short-term tests are already a major problem when assessing much shorter periods of protection. This problem is increased for longer-term forecasts. In particular, a suitable test method for determining the durability of newly developed zinc coating systems is not yet available. Since there is no long-term experience of corrosion behaviour and topcoats for such alloys, only multi-year exposure tests under real climatic conditions can provide insights into the corrosion behaviour under durability aspects, which considerably impairs the introduction and approval of new products. Emanating from the issues that were described regarding efficient corrosion testing and investigation of zinc coatings there is the demand for a test method that has the following properties or can clarify the following questions:

- non-destructive or minimally invasive testing,
- description of natural formation, reformation and degradation of protective layers of corrosion products on the zinc surface,
- determination of corrosion relevant specific values that describe the current corrosion protection ability of the layer,
- comparison of the corrosion protection ability of different zinc coating systems,
- prediction of the life cycle of protective zinc coatings in dependence of the degradation.

Use of gel-type electrolytes for corrosion investigations as a new approach

The use of electrochemical test methods is a promising and successfully applied approach for many applications. Electrochemical investigations enable the determination of corrosion-relevant characteristic values and a characteristic description of the corrosion system or the principles of a corrosion mechanism with high accuracy and reproducibility. Nevertheless, problems arise in the case of zinc coatings, since the protective cover layers consisting of corrosion products are often only stable for a short time under the influence of the aqueous test electrolyte that is needed for corrosion testing. Cover layers often rebuild themselves regarding their composition or dissolve as a result of the contact with the aqueous test electrolyte. Therefore, the layers often cannot be measured in their initial state. The use of gel-type electrolytes for electrochemical laboratory investigations offers an alternative and a new test approach. This type of electrolyte consists of an electrolytically conductive polymerized mass of agar, which can be brought into a desired permanent shape. Gel-type electrolytes form a thin moisture film at the interface gel/zinc due to the syneresis effect (a phase separation of a two-phase system). By means of an electrochemical instrumentation with electrodes, it is possible to determine parameters and relevant values, such as polarization resistances and corrosion currents that provide the possibility to investigate the formation of the protective layers and their stability. The determined characteristic values allow a differentiation of various coatings and coating systems and can describe the current protective ability of the protective layers [2]. Testing with gel-type electrolytes is minimally invasive, since the naturally formed protective layers are only slightly influenced by the moisture film of the gel-type electrolyte. It has already been demonstrated on the example of galvanized zinc that gel-type electrolytes influence the protective layers significantly less than comparable aqueous testing electrolytes [2-4]. Dissolution of the protective layers is even almost completely inhibited due to the diffusion conditions in the gel-type electrolyte. Despite the advantages described, the use of gel-type electrolytes in corrosion research and testing is not yet widespread. However, successful applications in the area of quality assurance [5-7] and corrosion monitoring [4] show the potential of this novel testing approach.

Experimental setup and preparation of specimen

Sample sheets made of pure zinc (99.5 wt.-% Zn) with a sheet thickness of 0.8 mm were used for the investigations. Firstly, the sheets were cleaned and degreased. Secondly, samples were pickled in an ultrasonic bath with an 1 M sodium hydroxide solution for 5 minutes, rinsed with ethanol and dried under a warm airflow to remove the existing protective layers that formed under undefined conditions and to activate the sample surfaces. Thus, all samples had the same initial conditions for further investigations.

In a first series of experiments, the influence of the type of test electrolyte had to be clarified. For this purpose, the activated sample sheets were stored under the following climatic conditions and removed after 120 days for measurement to enable the formation of a protective layer consisting of zinc corrosion products:

- constantly at 96 % r. H. in a closed vessel at room temperature,
- exposure to city atmosphere in Berlin (rain and temperature changes possible).

The samples were electrochemically analyzed after exposure and in the activated state. Table 1 summarizes the two types of electrolyte that were used for the electrochemical studies.

Type A was an agar-based circular gel pad with a diameter of 19 mm and a pad thickness of 3 mm. This results in a theoretical electrolyte volume of 0.9 ml for the gel pad. The area of measurement for the gel pad was 2.84 cm². For the preparation of the gel pads a defined amount of high-purity agar powder was solved in demineralized water and then polymerized at elevated temperature. After this procedure, the gel pads had a gelatinous consistency, a dense surface with no macroscopically detectable porosity and could be brought to the dimensions desired for the test. The principle of the measurement with a gel pad is illustrated in Figure 1. The aqueous electrolyte (type B) was a 0.1 M sodium chloride solution which is used as a typical electrolyte for corrosion testing on a laboratory scale. Both types of electrolyte had a comparable electrolytic conductivity of 0.004 Ω⁻¹cm⁻¹ and 0.003 Ω⁻¹cm⁻¹, respectively. A counter electrode (CE) and a saturated Ag/AgCl electrode as reference electrode (RE) were used for all investigations. The sample acted as the working electrode (WE). The measurements using the aqueous electrolyte were carried out with the aid of a test cell attached to the surface resulting in an area of measurement of 3.14 cm² and an electrolyte volume of 6.3 ml.

At first, the corrosion potential was observed and recorded over a period of 10 minutes using the respective type of electrolyte. Subsequently, dynamic polarization was carried out to determine current density-potential curves in a potential range of -50 mV to +50 mV in relation to the corrosion potential. Polarization was performed at a polarization rate of 1 mV/s in anodic direction. In a potential range with a slight deviation from the free corrosion potential E_{cor} (± 10 mV vs. E_{cor}), linear polarization resistances (R_p) were subsequently determined as characteristic values for the current protective ability of the cover layers.

In a second series of experiments, the formation of protective layers on pure zinc samples in dependency of the exposure time was investigated. Activated samples were stored under the following conditions:

- constantly 96 % r. H. in a closed vessel at room temperature,
- constantly 33 % r. H. in a closed vessel at room temperature,
- exposure to city atmosphere.

At defined times, the samples were taken out, polarization resistances were determined and the samples were then placed back into the vessels or exposed to city atmosphere. The gel-type electrolyte (electrolyte type A from Table 1) and the corresponding measurement setup (Figure 1) were used for the measurements. Corrosion current densities (i_{cor}) were calculated from the polarization resistances as a characteristic value for the dissolution kinetics of the protective layers using the following relationship:

$$i_{cor} = \frac{B}{R_p} \quad (1)$$

A simplified value of 15 mV was assumed for B_{Zinc} . A Potentiostat/Galvanostat Interface 1000 from Gamry Instruments was used for all electrochemical experiments. In each case at least three measurements were performed. Deviations are not shown below as they were within a reasonable range of ± 10 % of the mean value. All electrochemical studies were performed at room temperature.

Comparison of gel-type and aqueous electrolyte at the example of pure zinc

Figure 2 shows the appearance and wettability of the sample surfaces by means of a drop of water after activating the surface and after 120 days of exposure. In the activated state no cover layer can be seen on the surface by visual examination and the sample shows a good wettability. After 120 days at a constant humidity of 96 % r. H. a shimmering white layer of corrosion products had formed on the surface, which was visible to the naked eye only under favourable light. However, the cover layer can be detected based on the worse wettability. When exposed to city atmosphere with possible rain and temperature changes an easily visible and dense surface layer of corrosion products had formed on the surface, which differed from the other two states due to its better wettability.

The following section illustrates how these surface states behave electrochemically as a function of the test electrolyte. Figure 3 shows a representative potential curve per sample state over a period of 10 minutes beginning from the first contact of the sample surface with the electrolyte. The potential measurement shows typical potential ranges for a pure zinc surface, but different trends depending on the surface state and the type of electrolyte. When using the gel pad as a test electrolyte, the potential curves provide a steady potential without potential drops or an excessive potential drift over the entire measuring period. Due to the formation of the protective layers, the samples exposed to different conditions for 120 days provide a potential that is more positive than the activated sample by a value of 150 mV. The sample states "active"/"protective cover layer" can thus be easily distinguished by means of gel pad. A distinction of the two sample states exposed for 120 days is not possible based on the potential value alone. For this purpose, an additional kinetic characteristic value (corrosion current density, polarization resistance) is required. When using a 0.1 M NaCl solution as test electrolyte, the potentials are closer to each other and differ only in a range of 50 mV. Thus, the different surface states are difficult to differentiate based on the potential. A peculiarity is provided at the potential curve of the sample that was stored in a closed vessel with a constant humidity of 96% r. H. After approximately 6 minutes of contact with the aqueous test electrolyte, the potential breaks down steadily and shifts in the cathodic direction. This trend could be observed in all measurements at this surface condition and is a first indication that contact with an aqueous electrolyte can strongly influence the formed surface layer and even destroy it.

This assumption is confirmed by polarization measurements. These show the differences in the electrochemical behaviour of the three different surface states after 10 minutes of potential measurement. Representative current density-potential curves and mean values of the determined polarization resistances are shown in Figure 4. The curves and the location of the free corrosion potentials differ depending on the electrolyte used and the surface condition. The use of the gel pad inhibits ongoing corrosion reactions in comparison to the aqueous electrolyte, regardless of the surface state. This is caused by the thin moisture film and the inhibited diffusion conditions in the gel pad. In contrast, in the case of an aqueous test electrolyte with its comparatively much larger electrolyte volume and the good diffusion conditions, the metal dissolution can take place more uninhibitedly. As a result, protective cover layers can degrade under the influence of an aqueous test electrolyte and are also able to dissolve. The determined linear polarization resistances as specific characteristic values allow a quick overview of the current condition of the protective cover layers. The gel pads confirm the assumptions regarding the different surface conditions. A clear gradation of the stability of the protective layers is provided, that formed after 120 days. Samples exposed to city atmosphere provide the most stable layer ($255 \text{ k}\Omega\text{cm}^2$). A comparatively low resistance value of $13 \text{ k}\Omega\text{cm}^2$ is measured at the activated surface, which is characteristic for this state. In contrast, when using the aqueous electrolyte, polarization resistances are much lower. As already assumed after the potential measurements, the zinc surface after 120 days at constantly 96% r. H. is in an active state with a low polarization resistance, resulting from the dissolution of the cover layer under the influence of the aqueous test electrolyte.

Investigation of protective layer formation on a surface of pure zinc

The foregoing studies have shown that gel-type electrolytes affect naturally formed zinc layers less than a typical aqueous test electrolyte for laboratory use. Gel-type electrolytes are minimally invasive and thus allow a description of the formation of the protective layers under atmospheric conditions, which would not be possible using aqueous electrolytes. Figure 5 illustrates the formation and stabilization of protective layers under various environmental conditions (constant low humidity, high humidity, outdoor exposure) on an activated pure zinc surface over a period of 91 days. The initially high corrosion current density present at an activated surface decreases strongly for all sample states within the first 14 days. The formation of protective cover layers from different zinc corrosion products on the surfaces is the reason for this behaviour. These inhibit further active dissolution of the surface. After about 21 days, the corrosion current densities set to a relatively constant level. This depends on the properties and the stability of the formed cover layers. Under constant environmental conditions, differences in the height of the measured corrosion current density are observed. Thus, at lower humidity (constantly 33 % r. H.) a higher current density is observed than at constantly high humidity (96 % r. H.), as a less stable top layer has formed. Nevertheless, the measured corrosion current density is comparatively high even with constantly high humidity. Accordingly, a constant high level of humidity on its own is not sufficient for the formation of a permanently stable covering layer in the case of pure zinc. The formation of protective layers under outdoor exposure takes place under different conditions. Due to temperature changes, irrigation and the change of wet and dry cycles, a stable layer of zinc corrosion products can be formed, that strongly inhibits the further dissolution. This is reflected in the lower current density values.

Conclusions

In this article, different states of pure zinc samples were investigated and compared with regard to their corrosion behaviour using an agar-based gel-type electrolyte and a 0.1 M NaCl solution. The results provided conclusions on the stability of the cover layers under the influence of the respective type of test electrolyte. By use of gel pads, it was possible to measure with minimal invasiveness under the given conditions and to determine reliable characteristic corrosion relevant values. In contrast, the use of an aqueous electrolyte typical for corrosion tests in laboratories had a greater influence on the cover layers on zinc surfaces and in one case also led to the dissolution of the cover layer. By applying the new test method, the protective layer formation of zinc under constant climate (low and high humidity) and outdoor exposure in city atmosphere could be observed and reconstructed. There were differences in the formation and the stability of the cover layers as a function of the atmospheric conditions. The positive properties of the gel-type electrolyte as a test device encourages further investigations into usability and application limits in corrosion research and testing. With this new test approach galvanized samples under different climatic conditions can be examined and evaluated.

References

- [1] Burkert, A, Heyn, A, Müller, T. (2013) Tagungsband zur GfKORR-Jahrestagung 2013, 10-16
- [2] Babutzka, M, Heyn, A. (2016) Werkstoffe und werkstofftechnische Anwendungen Band 59: 18. Werkstofftechnisches Kolloquium der TU Chemnitz, 313-323
- [3] Babutzka, M, Heyn, A. (2016) EUROCORR 2016-Conference Proceedings, paper P-56097
- [4] Cano, E, Crespo, A, Lafuente, D, Ramirez Barat, B. (2014) Electrochemical Communications, 41, 16-19
- [5] German Patent-No. 10 2010 037 775: Auflage für den Nachweis von korrosionsempfindlichen Metalloberflächen und Verfahren zum Nachweis von korrosionsempfindlichen Metalloberflächen. 08.05.2014
- [6] Detektion korrosionsempfindlicher Oberflächen nichtrostender Stähle durch die Verarbeiter, Abschlussbericht zum AiF-Forschungsvorhaben IGF-Nr. 17136 N/1, 2014
- [7] Burkert, A, Klapper, H. S., Lehmann, J. (2013) Materials and Corrosion, 64, 675-682

Tables and Figures

Table 1: used types of electrolytes and their composition

variation	type of electrolyte	composition
A	gel-type electrolyte	polymerized agar solution with 260 ppm chloride
B	aqueous electrolyte	0.1 M sodium chloride solution (~3540 ppm chloride)

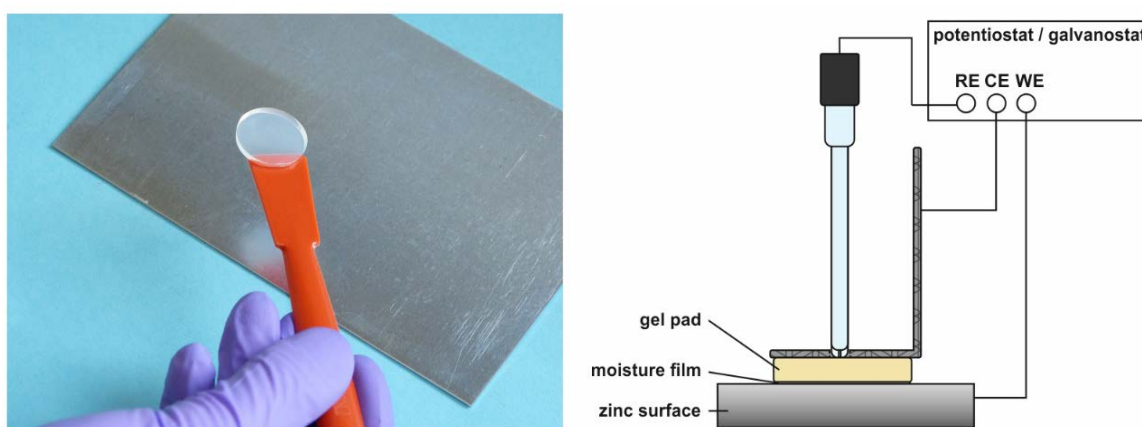


Figure 1: principle of measurement using a gel-type electrolyte, to the left: gel pad before application to the surface, to the right: measurement setup when using gel-type electrolytes

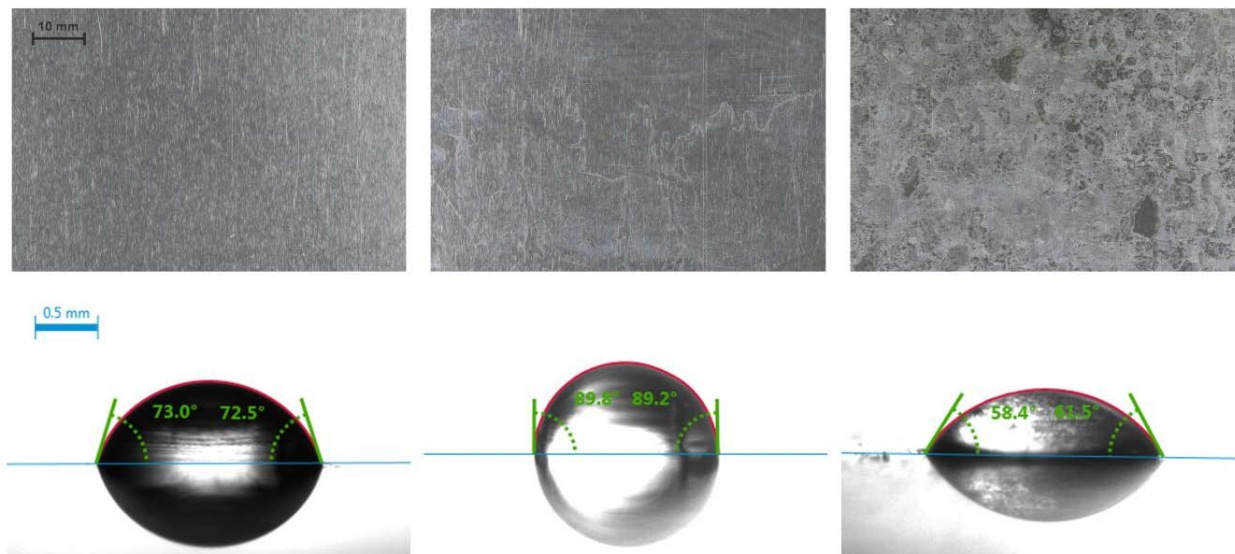


Figure 2: Appearance and wettability of the surface of pure zinc, wettability determined by contact angle method on a lying water drop, to the left: activated surface, middle: 120 days at constantly 96 % r. H., to the right: 120 days of exposure to city atmosphere

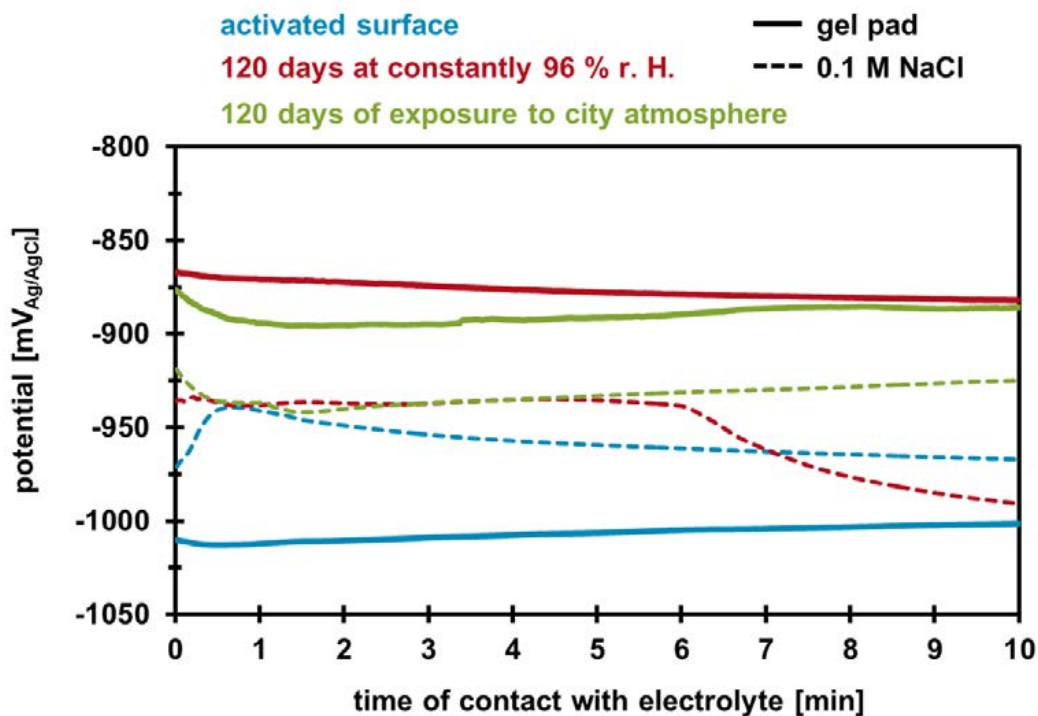


Figure 3: Potential curves of pure zinc with an activated surface and protective layers formed under different atmospheric conditions by variation of the type of test electrolyte

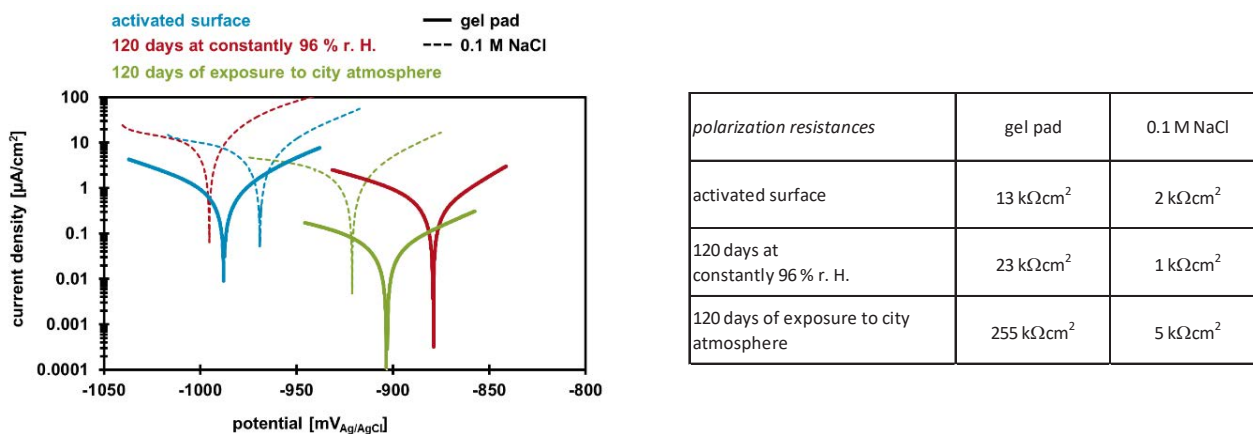


Figure 4: Mean values of polarization resistances and current density-potential curves of pure zinc with different surface states by variation of the type of test electrolyte

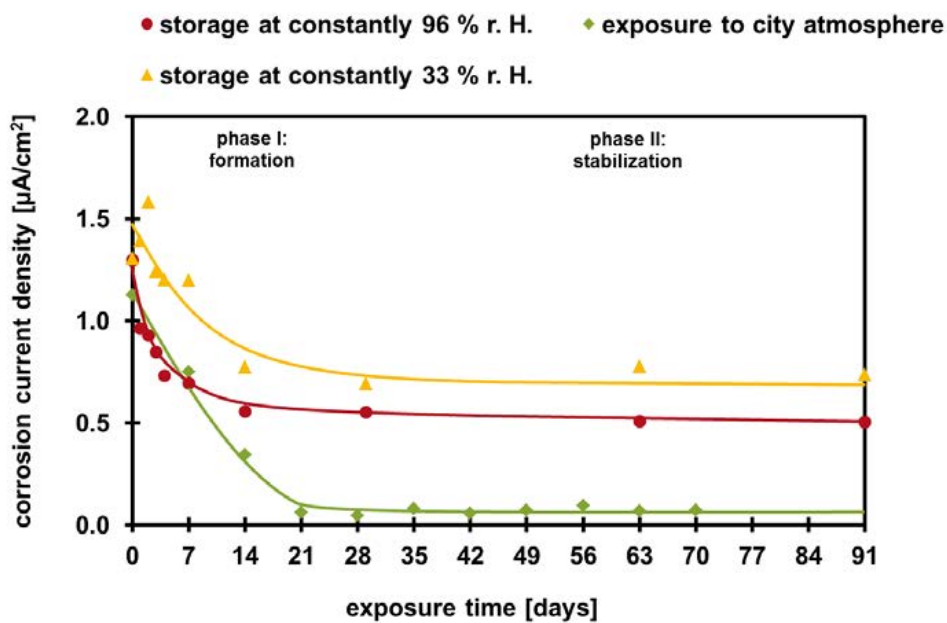


Figure 5: Decrease of corrosion current density as a result of protective layer formation under different atmospheric conditions by using gel-type electrolytes

Author Biography

Martin Babutzka

Born in 1988 * 2013 Master in Mechanical Engineering at the Otto von Guericke University Magdeburg/Germany * since 2013 PhD student at Otto von Guericke University Magdeburg * since 2014 scientific staff at the Bundesanstalt für Materialforschung und -prüfung in Berlin/Germany in Division 7.6 "Corrosion and Corrosion Protection"

Andreas Burkert

Born in 1965 * Dipl.-Ing. in Materials Engineering at TU Magdeburg/Germany * PhD 1999 at Otto von Guericke University Magdeburg/Germany * PostDoc at Bundesanstalt für Materialforschung und -prüfung in Berlin/Germany 2000 * 2005-2012 Head of working group „Corrosion behaviour of high-alloyed steel“ at BAM in Berlin * since 2013 head of Division 7.6 "Corrosion and Corrosion Protection"

Andreas Heyn

Born in 1968 * Dipl.-Ing. in Materials Engineering at TU Magdeburg/Germany * PhD 2004 at Otto von Guericke University Magdeburg/Germany * junior professor for "Corrosion and Corrosion Protection" at Otto von Guericke University Magdeburg/Germany and Bundesanstalt für Materialforschung und -prüfung in Berlin/Germany 2008-2014 * since 2014 teaching assignment for „Corrosion and Corrosion Protection at Otto von Guericke University Magdeburg/Germany * since 2015 freelancing in the area of corrosion diagnostics

Corrosion behaviour of zinc-chromium alloys for batch hot dip galvanizing

Prof. R. Feser

University of Applied Science South Westphalia, Iserlohn, Germany, feser.r@fh-swf.de

Abstract

Corrosion resistance of galvanized steel can be improved by the alloying element Cr. The newly developed zinc alloy should have a lower rate of corrosion under atmospheric conditions than the alloys currently used. The alloying elements should not lead to a deterioration of galvanizing behavior of reactive steels, but if possible allow a layer thickness reduction. Simultaneously, the usual process steps of hot-dip galvanizing should remain unchanged.

For the investigations samples of Sebisty steel were galvanized in zinc alloys with 1% and 2% Cr. All zinc alloys contained 0.5% Pb and were saturated with iron. The immersion time and the galvanizing temperature varied. The corrosion behavior was characterized by different tests. The electrochemical investigations do show no significant differences of the new zinc alloys in comparison to the commercial ones, due to the fact, that protective layers could not be formed in the electrolyte within short times. But atmospheric corrosion tests showed a significant improvement of corrosion resistance by alloying the zinc bath with Cr. Further corrosion tests in climate chambers verify the results of atmospheric corrosion tests. The zinc layers which occurred at the steel surface were characterized by metallographic cross section, a reduction of the layer thickness could be observed in dependence of galvanizing conditions.

Introduction

Steel still represents the metal which is used mainly for the construction of buildings, vehicles and industrial facilities. Particularly for the use under atmospheric conditions in which the component is directly exposed to rain or salt water, steel must be protected from corrosive attack. Corrosion of steel would be associated with a material loss which leads to structural weakening and would therefore possibly lead to a collapse of the structure. Organic coatings, which are a conventional corrosion protection, have the disadvantage that they are easily damaged and must be repaired regularly. Hot-dip galvanized structures are characterized by long service life of corrosion protection and require no further maintenance work [1].

The corrosion rate of zinc to atmosphere is less than 1 $\mu\text{m/a}$ and is therefore extremely low. During corrosion, a part of the zinc is incorporated in the top layer on the surface, another part is a so-called run-off to the environment of the construction [2].

Although the oxides/hydroxides of zinc are non-toxic, there are efforts to reduce zinc run-off into the environment. This can only be realized by developing new alloys which have a lower run-off rate. The reducing of the run-off rate can be achieved by changing the alloy composition, because the run-off rate depends on both the corrosion rate and the solubility of the zinc compounds which are formed. A reduced rate of corrosion of the zinc alloys would have the advantage that, firstly, the service life would rise at constant layer thickness or in case of lower coating thickness the same corrosion protection would be offered as in much thicker zinc coatings. In both cases, a reduction of zinc consumption will occur, so that conservation of the resource of the metals zinc and iron could be realized, while the entry of zinc would be lowered into the environment. In addition, extending the service life of steel structures can be achieved by the use of hot-dip galvanized steels, thus the resource steel will be protected.

New alloys for hot dip galvanizing therefore constitute a contribution to the sustainable use of materials that must be re-established under high energy expenditure otherwise. Furthermore, galvanized components can relatively quickly show white rust if a freshly galvanized surface is covered with water (during storage in the galvanizing or the customer). In these cases it would be advantageous if the white rust formation slows down. But the usual freshly galvanized coatings show a high susceptibility to white rust.

The developments of alloys in galvanizing had the aim of controlling the layer thickness of reactive steels in recent years. These steels showed uncontrolled growth of the layer, which resulted in coating layers of several 100 μm . The alloying elements aluminum and tin reduce the layer growth in thickness but cause increased problems in the pretreatment of the components, on the other hand it may lead to liquid metal induced stress corrosion cracking [3, 4, 5, 6]

Because the minimum coating thickness on normal steel with 80 μm is sufficient to offer good corrosion protection for decades. The reducing of corrosion rate of zinc alloy in recent years was not of interest. The influence of alloying elements on the corrosion resistance of zinc was mainly studied for the case of electrodeposited coatings, because the layer thickness is only a few microns. Galvanic zinc coatings are usually very thin and therefore an increased corrosion resistance is needed, otherwise red rust will appear very early. On continuously galvanized sheet material, the influence of alloying elements was studied, since these alloys also show a thinner coating than the batch galvanized materials.

Experimental

It was necessary to examine if the corrosion resistance of typically produced alloys can be improved for hot-dip galvanizing by the alloying element Cr. A new zinc alloy should be developed for batch galvanizing by the alloying of chromium to molten zinc. The newly developed zinc alloy should have a lower rate of corrosion under atmospheric conditions than the alloys currently used. The alloying elements should not lead to a deterioration of galvanizing behavior of reactive steels, but if possible allow a layer thickness reduction. Simultaneously, the usual process steps of hot-dip galvanizing should remain unchanged.

In this work different zinc baths with Cr as alloying element were prepared. Here, the concentrations were varied between 1% and 2% Cr shown in table 1. The alloying elements were melted with the zinc

together and solved by steering. All melts contained 0.5% Pb and iron saturation. In the various melts a steel S355 JN+2, which composition is given in table 2 below, was hot-dip galvanized.

The sample geometry was 10 cm x 10 cm x 4 mm. The immersion times were varied in the range of 3 – 10 min. Also dipping temperatures were preferably varied between 430 °C and 480 °C. The pretreatment of the steel samples was carried out in a conventional way by alkaline degreasing, etching in inhibited HCl and fluxing in ZnCl₂/NH₄Cl-containing flux bath with subsequent drying. The cooling of the galvanized samples was carried out in air. For characterization different tests like constant climate test, outdoor weathering with determination of the run-off rate, made of a cross section to characterize the phase structure and the film thickness, exposure tests in NaCl, adhesion tests and recording of slow current density-potential curves were performed.

Results

Zinc alloys with Cr as alloying element for hot dip galvanizing

The hot-dip galvanized steel sheets containing ZnCr-alloys showed a more brilliant surface on hot-dip galvanized coatings than by conventional alloys. Here, the gloss increased with increasing Cr content. However, a rise of the melting point of zinc alloy by alloying with Cr was noticeable during galvanizing. This problem could be counteracted by increasing the galvanizing temperature to achieve a sufficiently low viscosity of the molten zinc to produce a smooth layer surface. The galvanizing temperature of 450 °C seems to be high enough for a good layer formation and low enough not to attack the galvanizing kettle.

The preparation of the zinc-chromium alloy was carried out by the addition of Cr-powder (for the addition of 1% Cr) and Cr-particles (diameter 1-2 mm for the addition of 2% Cr) to the zinc melt. The solubility process was carried out by stirring by hand over 5 days at 600 °C. The preparation of ZnCr melt with 1% Cr was difficult because of floating chromium powder, which meant that in the zinc alloy about 0.39% Cr could be brought into solution, which about 0.14% Cr in the hot-galvanizing could be recovered. By using particulate chromium for 2% Cr alloys zinc melt 0.46% could be brought about into solution and about 0.22% Cr could be detected in the hot-galvanizing.

The layer thicknesses of hot dip galvanized coatings was determined by metallographic cross sections and using a light microscope. Also the various phases of the produced layers could be examined by etching. The layers showed a decrease in thickness with increasing temperature. The examination showed a layer thickness-reducing effect by the addition of Cr. This effect was higher in layers with 2% Cr than in layers with 1% Cr. Here, the thickness could be reduced to 70 µm – 80 µm and showed a layer thickness reduction of 34% at a galvanizing temperature of 450 °C and a galvanizing time of 10 min. Lower galvanizing times and lower galvanizing temperatures led to higher layer thicknesses due to rougher surfaces by the already mentioned increase of the melting point of the alloy. The coating thicknesses are shown in *Fig. 1*.

The chromium containing hot dip galvanizing layers formed δ -, ζ - and η -phases which are clearly visible. For the 1% Cr containing zinc layers, more frequently the incorporation of chromium particles in the η -phase can be found, especially occurring at low galvanizing temperatures, which resulted in local higher film thicknesses. This could not be observed in the layers with 2% Cr, where chromium particles were used, thus leading to lower layer thicknesses. The exemplary layer structure for a hot-dip galvanizing coating at a galvanizing temperature of 450 °C and a galvanizing time of 10 min, 2% Cr was added to the zinc bath, is shown in *Fig. 2*.

Exposed to constant climate test as well as in outdoor exposure the Cr-containing alloy layers achieved excellent results. In constant climate test, the white rust formation in alloys with 1% Cr was reduced by 17% and in alloys with 2% Cr it was reduced by 28% compared to galvanized coatings without Cr. To illustrate this behavior, a diagram with selected graphs is shown in *Fig. 3*. The corrosion resistance in outdoor weathering could be significantly increased by the addition of Cr. After 1000 h exposure a reduction of 95% by the addition of 1% Cr was achieved, compared to conventional hot-dip galvanized samples. Moreover the metallic gloss of the surface was retained. This suggests that by using these zinc alloys in the practice, a subsequent passivation of the surface could no longer be necessary. Therefore cost savings would be possible.

The determination of the run-off rate of zinc, based on collected rainwater, had no effect on the run-off of zinc by the addition of Cr. Here, calculated from the dissolved zinc ion removal rates were approximately $0.3 \mu\text{m/a}$, regardless of the presence of chromium. Even after a 3-week exposure of chromium-containing hot-dip galvanized samples in 0.1 mol/l NaCl solution no influence by chromium on the zinc dissolution could be found. These calculated corrosion rates, based on the dissolved zinc ion, were $10 \mu\text{m/a}$ and thus comparable to chrome-free hot dip galvanizing coatings.

The adhesive strengths of chromium-containing hot dip galvanizing layers were determined by adhesive test. Here in each case a double determination was carried out to show a trend. For a statistical analysis of the measurements, however, the measurements are not sufficient. However, it could be shown that the adhesive strength tends to be higher with chromium-containing hot dip galvanizing coatings than in a conventional hot-dip galvanizing layer with an average of 5 MPa . The chromium-containing hot dip galvanizing coatings could go up to 15 MPa , partially even greater than 20 MPa . The results of the samples with 1% and 2% Cr were comparable. In addition, it was noted that the bond strength tends to decrease with increasing galvanizing time. The fracture pattern showed mostly cohesive failures in the hot-dip galvanizing layer, but also in adhesion between the galvanizing layer and glue. The results of adhesive strength measurements are shown in *Fig. 4*.

Electrochemical measurements were carried out by the recording of current density-potential curves. The corrosion current densities determined from the current density-potential curves tended to be lower for chrome containing alloys than with pure zinc, however, they were subject to a certain fluctuation. Nevertheless, by alloying of 2% Cr the corrosion current density could be reduced by 55% compared to pure zinc and by 25% in comparison with a conventional hot-dip galvanizing layer. The positive effect of constant climate test and outdoor weathering could not be shown with this measuring method due to the absence of protective layer formation. The current density-potential curves are shown in *Fig. 5* and *6*.

The distribution of elements over the layer thickness was analyzed by GDOES analysis. It came out that the chromium preferably accumulates 1/3 of the layer thickness below the surface layer. The maximum of chromium alloys with 1% Cr is 0.64% and in alloys with 2% Cr it is 0.7%. The results are consistent with mapping images from SEM. This results suggests that the corrosion protection will increase with the removal of the layer during weathering. First recordings of current density potential curves on grinded or pre-weathered chromium layers seem to confirm this hypothesis. An exemplary graph for GDOES analysis for an alloy with 1% Cr, 0.5% Pb, iron saturation, and immersion temperature of $450 \text{ }^\circ\text{C}$ and immersion time of 10 min is given in *Fig. 7*.

Conclusions

The aim of this work was the development of a new hot-dip galvanizing coating by alloying the anticorrosion enhancing element Cr. The newly developed alloy should be more resistant against corrosion in comparison to alloys already used and also ensuring a controlled layer thickness growth on reactive steels. Preferably, a layer thickness-reducing effect by the added alloying elements should appear. There should be no change in the conventional pre-treatment.

This project showed a clear improvement in the corrosion resistance of galvanized coatings by alloying with Cr. Especially by alloying with Cr a big improvement of the corrosion resistance could be achieved in the constant climate test and the outdoor weathering. Reducing the formation of white rust in constant climate test at a 2% Cr containing zinc alloy was up to 28% after an exposure time of 24 h. Also interesting is the strong gloss of the film, which also remained in the weathering so that additional passivation layers wouldn't be necessary. The reduction of the layer thickness by 34% is positive. The fact that chromium enriched in about 1/3 of the layer thickness below the surface layer indicates that the corrosion protection increases with the lifetime.

Nevertheless, for the industrial use of these newly developed alloys for hot-dip galvanizing further investigation and optimization will be needed. The project shows the high potential of the alloying element Cr for hot dip galvanizing very well.

Acknowledgements

The financial support of BMWi is greatly acknowledged. The project was performed as an IGF project (Vorhaben-Nr. 17836 N) of GAV (Gemeinschaftsausschuss Verzinken e.V.)

References

- [1] Schulz, W.-D.; Thiele, Marc; Feuerverzinken von Stückgut Eugen G. Leuze Verlag, Bad Saulgau (2007)
- [2] Van Eijnsbergen, J.F.H.; Duplex Systems, Elsevier, Amsterdam, (1994), S. 45ff
- [3] Katzung, W., Schulz, W.-D.; Zum Feuerverzinken von Stahlkonstruktionen – Ursachen und Lösungsvorschläge zum Problem der Rissbildung. Stahlbau 74 (2005), Heft 4
- [4] Feldmann, M. et al; Ermittlung der Rissanfälligkeit von Baustählen beim Stückverzinken. MP Materials Testing 49 (2007) 5, 223-231
- [5] Feldmann, M., Pinger, Th. et al; Analyse der Einflüsse auf die Rissbildung infolge Flüssigmetallversprödung beim Feuerverzinken Stahlbau 77 (2008), Heft 1
- [6] Feser, R., Schnier, K.; Haarmann, S.; Influence of aluminium to liquid metal embrittlement, Proceedings Eurocorr 2011, Stockholm, Schweden

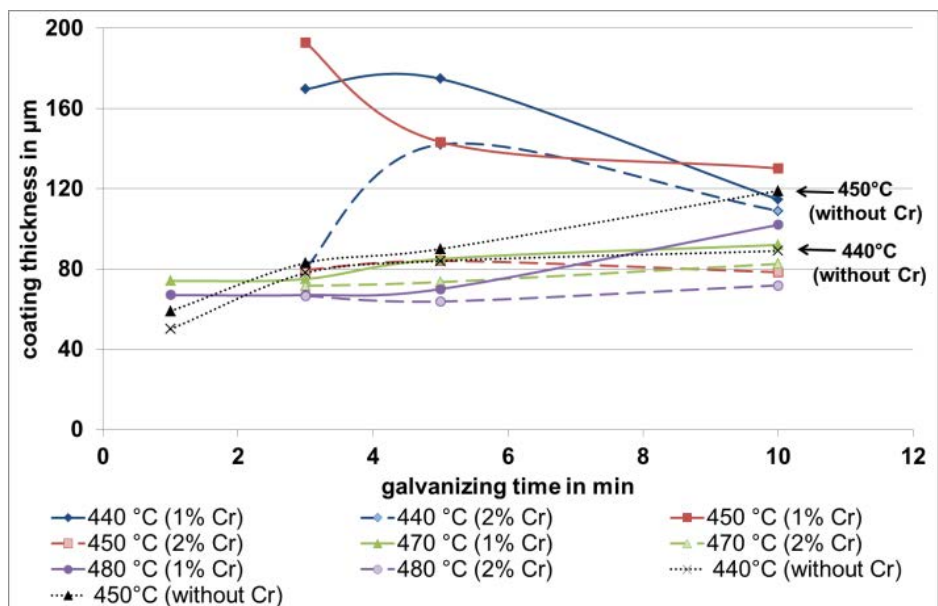


Figure 1: Coating thicknesses of hot dip galvanized coatings with different Cr contents, determined by light microscopy on metallographic cross sections

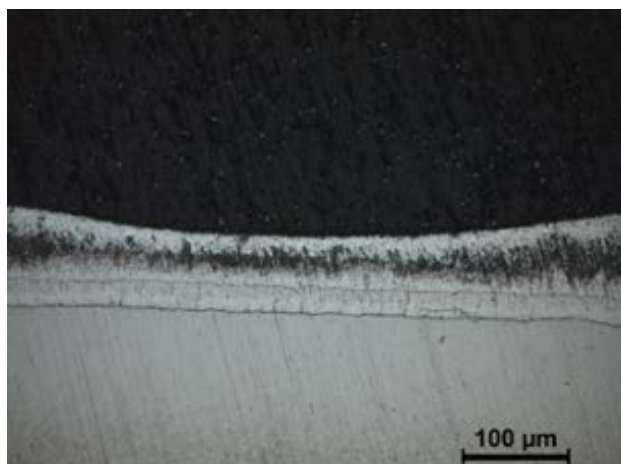


Figure 2: Metallographic cross section of hot-dip galvanized coating containing 2% Cr, 0.5% Pb, iron saturated; galvanizing temperature 450 °C, galvanizing time 10 min

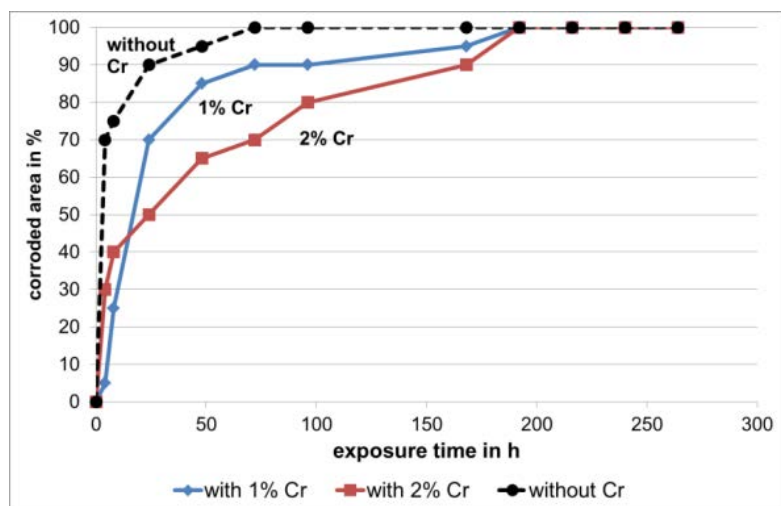


Figure 3: Exposure of Cr-containing hot dip galvanizing coatings in constant climate test over a period of 2 weeks (contained 0.5% Pb, iron saturation and different Cr concentrations); simplified representation, which results from a variety of measurements

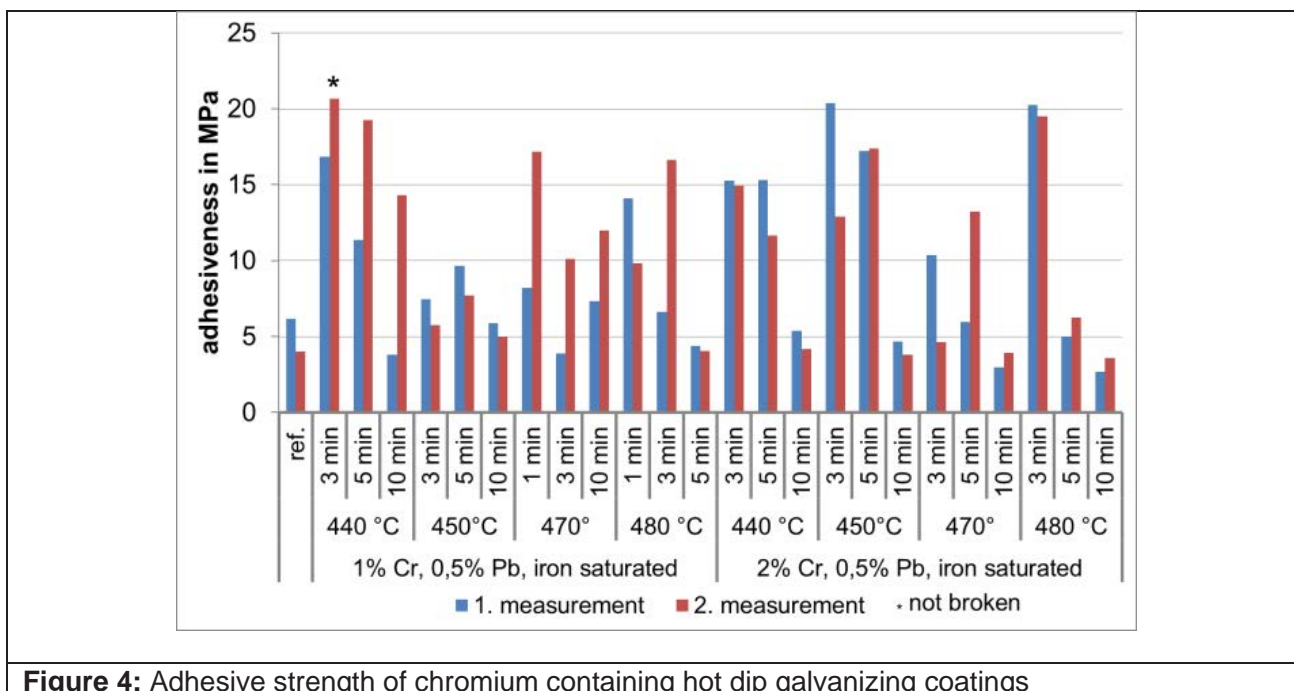


Figure 4: Adhesive strength of chromium containing hot dip galvanizing coatings

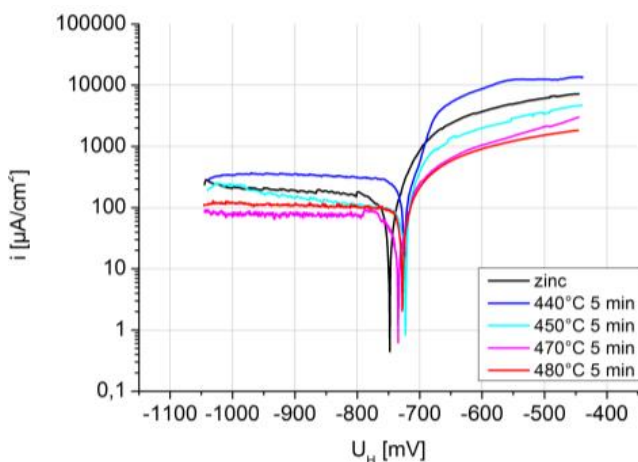


Figure 5: Current density-potential curves of 1% chromium containing hot dip galvanizing layers

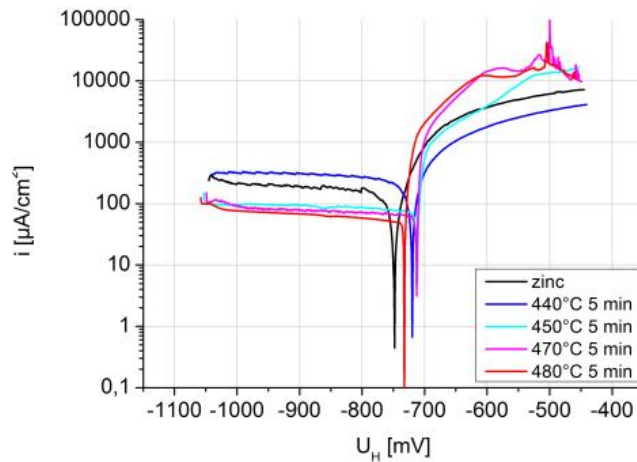


Figure 6: Current density-potential curves of 2% chromium containing hot dip galvanizing layers

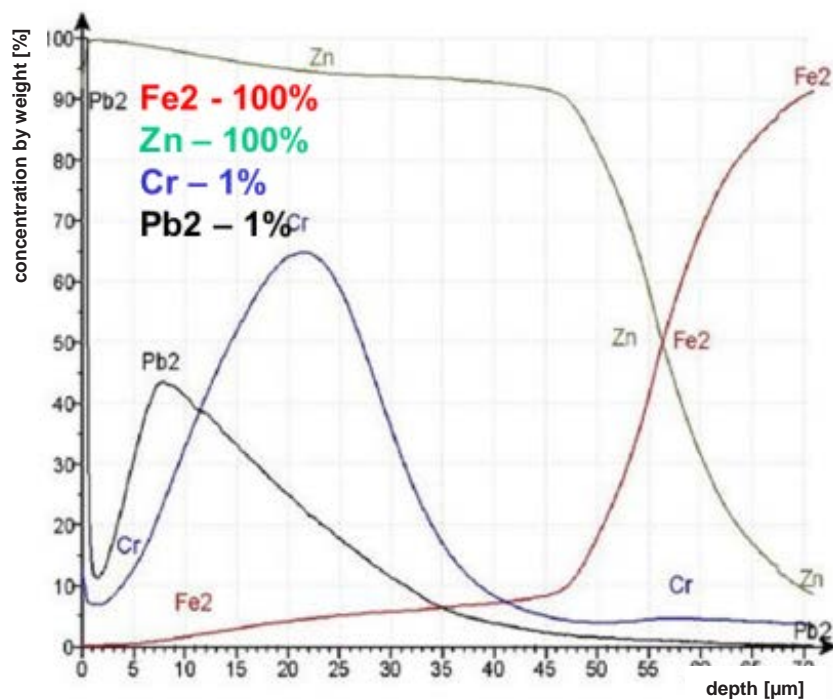


Figure 7: GDOES analysis of a zinc alloy containing 1% Cr, 0.5% Pb, iron saturated; galvanizing temperature 450 °C, galvanizing time 10 min

Table 1: Composition of the used zinc alloy, indicating the concentrations of the dosed alloying elements

Concentrations of the alloy elements in %			
Cr	Pb	Fe	Zn
1	0.5	saturated	rest
2	0.5	saturated	rest

Table 2: Alloy composition of the used structural steel S355J2+N according to analysis certificate

Alloy composition in %						
C	Si	Mn	P	S	Al	Cr
0.15	0.18	1.39	0.014	0.005	0.043	0.04
Cu	Mo	N	Nb	Ni	Ti	V
0.10	0.01	0.003	0.02	0.07	0.002	0.01